ACTA CHIMICA

ACADEMIAE SCIENTIARUM HUNGARICAE

TOMUS 68 FASCICULI 1—2

AKADÉMIAI KIADÓ, BUDAPEST

1971

ACTA CHIM. ACAD. SCI. HUNG.

ACTA CHIMICA

A MAGYAR TUDOMÁNYOS AKADÉMIA KÉMIAI TUDOMÁNYOK OSZTÁLYÁNAK IDEGEN NYELVŰ KÖZLEMÉNYEI

Az Acta Chimica német, angol, francia és orosz nyelven közöl értekezéseket a kémiai tudományok köréből.

Az Acta Chimica változó terjedelmű füzetekben jelenik meg, egy-egy kötet négy füzetből áll. Évente átlag négy kötet jelenik meg.

A közlésre szánt kéziratok a szerkesztőség címére (Budapest 112/91 Műegyetem) küldendők.

Ugyanerre a címre küldendő minden szerkesztőségi levelezés. A szerkesztőség kéziratokat nem ad vissza.

Megrendelhető a belföld számára az „Akadémiai Kiadó"-nál (Budapest V., Alkotmány utca 21. Bankszámla 05-915-111-46), a külföld számára pedig a „Kultúra" Könyv- és Hírlap Külkereskedelmi Vállalatnál (Budapest I., Fő utca 32. Bankszámla: 43-790-057-181) vagy annak külföldi képviseleteinél és bizományosainál.

Die Acta Chimica veröffentlichen Abhandlungen aus dem Bereiche der chemischen Wissenschaften in deutscher, englischer, französischer und russischer Sprache.

Die Acta Chimica erscheinen in Heften wechselnden Umfanges. Vier Hefte bilden einen Band. Jährlich erscheinen 4 Bände.

Die zur Veröffentlichung bestimmten Manuskripte sind an folgende Adresse zu senden:

Acta Chimica
Budapest 112/91 Műegyetem

An die gleiche Anschrift ist auch jede für die Redaktion bestimmte Korrespondenz zu richten. Abonnementspreis pro Band: $ 16.00.

Bestellbar bei dem Buch- und Zeitungs-Außenhandels-Unternehmen »*Kultúra*« (Budapest I., Fő utca 32. Bankkonto No. 43-790-057-181) oder bei seinen Auslandsvertretungen und Kommissionären.

ACTA CHIMICA

ACADEMIAE SCIENTIARUM HUNGARICAE

TOMUS 68

AKADÉMIAI KIADÓ, BUDAPEST

1971

ACTA CHIMICA

TOMUS 68

Fasciculi 1—2: 1971
Fasciculus 3: 1971
Fasciculus 4: 1971

INDEX

Acta Chimica Academiae Scientiarum Hungaricae, Tomus 68 (1—2), pp. 1—9 (1971)

DETERMINATION OF SMALL QUANTITIES OF EUROPIUM

M. FÁBIÁN-MOHAI, E. UPOR and GY. NAGY

(Mecsek Ore Mining Company, Pécs)

Received December 15, 1969

A method has been developed for the determination of small amounts of europium. Two of the three variations are based on the luminescence described by POLUEKTOV; however, selective sodium amalgam separation of europium has made possible the use of Arsenazo III reagent for the determination of the europium content of samples containing high quantities of rare earths.

Interfering contaminations are separated by oxalate precipitation and extraction of rare earths with dibutylphosphoric acid followed by re-extraction under special conditions.

The following sensitivities were obtained for the three methods: $1 \cdot 10^{-5}\%$ (fusion, luminescense), $2 \cdot 10^{-4}\%$ (*o*-phenanthroline + atophane) and $1 \cdot 10^{-3}\%$ (Arsenazo III).

After accomplishment of the described separations the obtained solution is suitable for any of the three types of analysis. These methods are suitable for the determination of the europium content of monacite, apatite, various rocks and compounds of rare earths.

Introduction

Besides neutron activation analysis and emission spectrometry, luminescent methods have also been developed for the determination of small quantities of europium [1—7]. Most of these results were published by POLUEKTOV *et al.* In their first paper [2] they reported the luminescence of europium in $SrCl_2$—NaCl mixtures fused in the reducing part of a gas flame. An analytical method for mixed oxides of rare earths is based on this experience. Europium is extracted with 0.25% sodium amalgam from a 0.5 *M* sodium citrate solution. According to the cited paper, complete separation is obtained from other rare earths, and samarium remains in the aqueous phase quantitatively; only europium and sodium will interchange in the amalgam. Several papers deal with the luminescence of solutions or suspensions of complexes formed in the presence of two chelating agents. β-diketones or other chelating agents (thenoyltrifluoroacetone, quinoline derivatives) and bases containing N atoms (*o*-phenanthroline, pyridine derivatives) are suitable chelating agents to produce compounds capable of excitation.

Samarium and terbium also show luminescence under similar conditions, and the other rare earths — depending on the electron structure — will enhance or decrease the intensity. Ions with changing valence and the transition metal ions have strong quenching effect.

The object of our work was the development of a method (or methods) for the determination of europium in minerals and various chemical intermediates or products containing rare earths. Since the amalgam method proposed by POLUEKTOV afforded a possibility for the selective separation of europium from other rare earths, determination of europium by means of its reaction with Arsenazo III could also be considered. Its preliminary condition is the complete separation of europium from the rare earths which are present in concentrations higher by 3—4 orders of magnitude. For the separation of the rare earths from other ions, we intended to use the conventional method developed for the determination of the total quantity of rare earths: oxalate precipitation, extraction with dibutylphosphoric acid and re-extraction after the addition of TBP [8].

Extraction of europium with sodium amalgam

The following factors had to be studied before development of the required method:

(1) efficiency of extraction and re-extraction of europium,

(2) effect of pH on the extraction,

(3) selectivity of the separation.

In the experiments, labelled ^{152}Eu and ^{153}Sm species were determined by measurement of the γ-activity or with Arsenazo III.

The experimental procedure was the following:

5 ml of sodium citrate solution was added to the acid solution containing the ions to be analyzed, which was then neutralized with 10% potassium hydroxide solution in the presence of phenolphtalein, and the volume was made up to 10 ml. The solution was shaken together with 1 ml of 0.25% sodium amalgam in a separatory funnel for 1 min, and after separation of the phases the amalgam containing the europium was washed with 0.5 *M* sodium citrate solution. After this, the amalgam was separated and dried from adhering water by means of filter paper strips, then decomposed by boiling with 5 ml of 2 *N* HCl solution. The determination was carried out in the aqueous phase.

The results obtained for the separation of europium are listed in Table I. As can be seen, the loss of europium during the procedure (two extractions, washing the amalgam twice and its decomposition with hydrochloric acid) is lower than 2% until obtaining the final solution. These values were found to be constant in the pH range between 8 and 12. Thus the adjustment of the correct pH value makes no difficulty during the extraction.

Extraction of the other rare earths was studied under identical conditions (two extractions and two washings). The results are given in Table II. Neither in this case do changes of the pH between 8 and 12 affect the efficiency of the extraction, *i.e.* the separation of europium from the other rare earths.

(Some difficulty was encountered because of the europium content of the chemicals used. After detection of the presence of europium by luminescence, this was removed from the solutions by means of a single amalgam extraction, and in the following work, such solutions were used as the starting material. The ^{153}Sm preparation was not radiochemically pure, either; its ^{152}Eu contamination was detected by γ-spectrometry and removed as described above).

Table I

Extraction of europium with 0.25% sodium amalgam

	Loss of europium, %
Extraction with 1 ml of amalgam	0.6
Extraction with 4×1 ml of amalgam	0.2
Washing with 2×20 ml of washing liquid	0.4
After re-extraction, in the amalgam	1.4

Table II

Extraction of rare earths with sodium amalgam

Rare earths added (mg)	Rare earths found (μg)
10 mg La + 10 mg Ce	<0.5
10 mg Y + 10 mg Yb + 10 mg Ho + + 10 mg Er	<0.5
10 mg Nd + 10 mg Pr + 10 mg Tm + + 10 mg Gd	<0.5
10 mg Sm	<0.5

Tables I and II indicate that the selectivity of the separation procedure makes possible the measurement of europium with Arsenazo III reagent, even in the presence of 3—4 orders of magnitude higher quantities of other rare earths. In addition to this, the possibility of determination by luminescence was also considered. This latter method is suitable for obtaining approximate analyses and for the analysis of samples of extremely low europium content.

Determination of europium with Arsenazo III reagent

Before the use of Arsenazo III as a reagent, we had to check whether the solution obtained by decomposition of the amalgam gives a proper medium for photometric measurements or not. According to our investigations, the mercury present in the aqueous phase does not interfere with the determina-

tion. It is, however, a well-known fact that in the slightly acid medium used for determination of the rare earths, sodium ions will also increase the light absorption of Arsenazo III at the wavelength used for the measurement (652 nm). It was found that perfectly identical sodium contents could not be ensured during the preparation of the amalgam. Thus, sodium ions appearing in the aqueous phase after decomposition of the amalgam could have a varying influence on the light absorption. Another possible error was due to the fact that the activity of the amalgam decreases on storage; use of an old preparation for extraction may result in 5—10% loss of europium. In order to eliminate both sources of error, the method of using an external standard was employed. Simultaneously with the analysis of the sample, a known quantity (10 μg) of europium was extracted with amalgam and measured in identical manner; arithmetic proportion was then used for calculation of the result.

Procedure

Reagents

NaOH, analytical grade, solid and 1 *N* solution;
HCl, analytical grade; conc., 8 *N*, 6 *N*, 2 *N* and 0.1 *N* solutions;
H_2O_2, analytical grade;
$H_2C_2O_4$, analytical grade;
Di-*n*-butylphosphoric acid (HDBP), 0.2 *M* solution in gasoline, prepared according to [9];
TBP, pss.;
0.25% sodium amalgam;
1 *M* sodium citrate solution;
0.1% Arsenazo III solution. The reagent was prepared according to [10] and calcium was removed by passing the solution through a cation exchange resin in H-form.
Sodium hexametaphosphate solution of 1 g/l concentration.
Europium stock solution of 10 mg/l concentration was made by dissolving Eu_2O_3 of spectral purity in HCl.

Maximum 1 g of the sample to be examined is weighed out (the actual value depending on the expected europium content). If the sample is soluble in acids, it is boiled with 20—30 ml of conc. HCl and a few drops of H_2O_2, then the solution is concentrated to small volume. When the sample is insoluble in acids, it is fused with sodium hydroxide in a nickel or iron crucible, and the melt dissolved in hot water. The hydroxide precipitate is filtered off and washed back into the beaker. In both cases this is followed by precipitation of the rare earth with oxalate (in the analysis of the rare earth compounds this is unnecessary), here amalgam extraction is the first step. When the total quantity of rare earths and calcium is less than 50 mg in the sample, a $CaCl_2$ solution equal to 50 mg Ca^{2+} should be added. The solution is boiled and 5 g of oxalic acid is added to precipitate the rare earths and calcium. In order to prevent precipitation of the titanium compounds present, a few millilitres of H_2O_2 are added. The pH of the solution adjusted to 2, the mixture is allowed to stand overnight. The precipitate is then filtered off, washed with hot water and ignited at 6—700 °C in a porcelain or platinum crucible. The residue is dissolved in a small amount of 1 : 1 HCl in a beaker. If the sample contains CeO_2, a few drops of H_2O_2 should be added to promote dissolution. The solution is concentrated to a small volume, neutralized with 1 *N* NaOH, then 2.0 ml of 1.0 *N* HCl solution is added, and the volume made up to 20 ml with distilled water. In order to reduce Fe^{3+} ions present in trace quantities, some ascorbic acid is added, then the rare earths are extracted by shaking with 20 ml of 0.2 *M* HDBP solution for half a minute in a separatory funnel. The organic phase is washed with 3×10 ml of 0.1 *N* HCl solution to minimize the extraction of calcium ions.

(The rare earth content of the solution to be extracted should be less than 50 mg. Partial precipitation of the corresponding complexes may occur when their quantity is higher than

20 mg. However, this precipitate will remain in the organic phase, and no loss will occur if the phases are separated carefully. During re-extraction the precipitate is dissolved. and the rare earths get into the aqueous phase without loss.)

In order to ensure re-extraction of the rare earths, 5 ml TBP solution is added to the organic phase. The produced conditions make possible the transfer of rare earths into the aqueous phase by shaking with 2×20 ml of 8 *N* HCl solution, without loss. The combined aqueous phases are evaporated to a small volume to remove most of the hydrochloric acid, and the residue is transferred into a measuring flask of 25—100 ml volume, depending on the europium content.

Maximum 5.0 ml of the solution — the actual amount depending on the europium content — is pipetted into a separatory funnel, then 5 ml of 1 *N* sodium citrate solution and one drop phenolphtalein indicator solution are added, the solution neutralized with 10% KOH, and the volume made up to 10.0 ml, when necessary. Europium is extracted by shaking with 2×1.5 ml of 0.25% sodium amalgam for 1 min. The aqueous phase is discarded and adhering water drops are removed with filter paper strips. The amalgam is washed with 2×10 ml of sodium citrate solution, transferred into a small beaker and decomposed by the addition of 5 ml of 2 *N* HCl solution and subsequent heating. The two phases are separated, and the aqueous phase containing the europium ions is neutralized with 1 *N* sodium hydroxide solution. After the addition of 1.5 ml of 0.1 *N* HCl, the solution is transferred into a 50 ml measuring flask. 2.0 ml of Arsenazo III solution is added and the volume is made up to the mark with distilled water.

The light absorption of the solution is measured by a spectrophotometer at 652 nm wavelength, in 5 cm layer thickness. Distilled water is used as reference. After recording the measured value, 2 drops of sodium hexametaphosphate solution are added to the solution in the cell, mixed, and the absorption of the mixture is again determined. The light absorption of the europium complex is obtained as the difference of the two measured values.

Simultaneously with the analysis of the sample, the amalgam extraction and determination of 10 μg of europium is also carried out. Arithmethical proportion calculation is used to obtain the result from the extinction values.

The sensitivity of the method is about $1 \cdot 10^{-3}$%. It is suitable for the analysis of apatite, monacite and various industrial products containing rare earths.

Determination of europium by means of the luminescence of its novatophane and o-phenanthroline complexes

As mentioned in the introduction, in solutions or suspensions of certain mixed complexes europium shows luminescence in ultraviolet light. The relatively high sensitivity is due to the fact that the organic part of the molecule transmits some of the excited energy to the central atom, europium. Other rare earth ions which have no 4f electrons (La, Y), or have their 4*f* orbitals saturated (Lu), and those where there are great energy differences between the ground and excited states (Gd, Tb) also show luminescence under certain conditions. Though they show no luminescence in the *o*-phenanthroline + atophane system, the loss of their excitation energy does not occur in a perfectly non-radiating manner, but the energy is partially transmitted to the europium present, resulting in an enhanced luminescence of the latter. The complexes of the other lanthanides also absorb light, however, they are deactivated by radiation-free transitions and this decreases the luminescence of europium [3].

Theoretically, limited compensation of these interferences is possible by the internal standard method in the case of objective measurements; however, the change in luminescence can be two orders of magnitude, and this

may result in very high errors in the determination. According to POLUEKTOV, samarium also shows luminescence under conditions identical with those used in the determination of europium. This interference can be eliminated by spectrofluorometry, utilizing the difference in their spectra, however, such an instrument is not always available. Owing to these facts, the use of the above-described sodium amalgam separation is recommended.

POLUEKTOV suggested various complex systems for the determination of europium by luminescence [4]. Of these, the above-mentioned combination of *o*-phenanthroline and atophane (2-phenylquinoline-4-carboxylic acid) was chosen. The only modification was the use of novatophane (2-phenylquinoline-4-carboxylic acid methyl ester). In the preliminary experiments an analytical UV lamp was used to achieve excitation, and evaluation was carried out visually.

As suggested by POLUEKTOV, the composition of the solution was the following: europium stock solution +0.5 ml of 40% urotropine solution +0.1 ml of 1% gelatine solution +0.5 ml of 0.5% novatophane + 0.7 ml of 1% *o*-phenanthroline; the volume of the mixture was made up to 5.0 ml with distilled water.

Our preliminary experiments indicated a sensitivity lower than that obtained by POLUEKTOV with the use of atophane. Under the given conditions, 1 μg of europium showed a very slight pink luminescence only. As mentioned above, POLUEKTOV reported the interference of some ions with the determination of europium, by decreasing or increasing its luminescence [4]. This latter effect was utilized for improving the sensitivity. Gadolinium was found to be the most suitable for this sensibilizing action, since our investigations confirmed its highest enhancing effect on the luminescence of europium. In the presence of 200 μg gadolinium the luminescence of even 0.1 μg europium can easily be detected. However, the desired effect can only be obtained in the absence of rare earths decreasing the luminescence. Thus in the presence of 50 μg Gd and 50 μg of Er (Nd, Tm, Dy), the luminescence of 2 μg europium cannot be noticed. 2 μg of europium in the presence of 300 μg Gd and 25 μg Er shows no stronger luminescence, than 0.2 μg of Eu in the absence of Er. According to these results, the amalgam separation is essential.

The hydrochloric acid solution obtained on decomposition of the amalgam does not affect the intensity of luminescence, thus this step does not interfere the analytical procedure; the stock solution obtained by the above-described HDBP extraction followed by amalgam extraction, is suitable for the determination by luminescence as well as by reaction with Arsenazo III. The addition of 200 μg of Gd is recommended to improve the sensitivity of the determination.

A reference series is prepared containing 0.0, 0.1, 0.2, 0.3, 0.5 and 1.0 μg of europium, and 200 μg portions of Gd are also added.

The method is suitable for the analysis of apatite, monacite and other materials containing rare earths. Considering that the lowest limit of detection of the luminescence is 0.1 μg of europium, and a maximum 50 mg of rare earths can be removed by the above described HDBP extraction, the sensitivity of the method is $2 \cdot 10^{-4}\%$ (if no stock solution is prepared, but the whole sample is used). In the case of samples of higher Eu content, the preparation of a stock solution is, of course, recommended. The method is suitable for rapid routine measurements in process control.

The error of the measurement is lower than $\pm 30\%$, even at visual evaluation. Other methods of evaluation, *e.g.* the use of the luminescent device of the Pulfrich photometer, are also possible. Increased accuracy can be obtained by the use of objective measuring methods such as spectrofluorometry.

Luminescent determination of europium in $SrCl_2$—NaCl melt

According to POLUEKTOV [2], 0.02 μg of europium can be detected as the minimum quantity in 200 mg of $SrCl_2$–NaCl melt (1 : 1 mixture). This luminescence is due to the excitation of Eu^{2+}, thus in fusing, proper conditions should be provided for the reduction of Eu^{3+}.

The sensitivity of the luminescence reported by POLUEKTOV was promising for the development of a method suitable for the analysis of rocks of average composition. (The average europium content of the Earth's crust is $1.2 \cdot 10^{-4}\%$ [1]). It was also our purpose to utilize this sensitivity for the development of a rapid, approximate method of lower accuracy.

First of all the experiments of POLUEKTOV were repeated. The stock solutions of europium (0.0, 0.005, 0.01, 0.02, 0.05 μg) were placed in glass evaporating dishes, and after the addition of 1.0 ml of a 25 mg/ml $SrCl_2$ solution and 1.0 ml of a 25 mg/ml NaCl solution, the mixture was evaporated to dryness in a sand bath and the residue collected. It was pressed to form a pellet, then fused in propane–butane gas flame, taking care to cool the melt in the internal sphere of the flame, ensuring reduction. The luminescence of 0.005 μg of europium in 50 mg of melt can easily be detected, thus the sensitivity obtained was the same as that reported by POLUEKTOV.

The luminescence observed in melts of other alkali and alkali-earth metal chlorides was also studied, but a decrease in sensitivity was observed in each case.

Effects of the conditions of fusing were also investigated. In order to obtain a shining pellet of strong and uniform luminescence, it should be cooled in the inner sphere of the flame by gradually reducing the air flow after fusing. Thus the melt solidifies within a few seconds. Pellets produced by means of

a spirit-lamp are slightly stained but they have uniform luminescence. Very poor luminescence is obtained in pellets prepared in ovens where no reducing atmosphere is provided.

The quenching effect of iron is significant; 10 μg of Fe decreases the luminescence to one-tenth of the original value. If no oxalate precipitation is required to provide separation from metals other than rare earths in the course of the analysis, iron can be removed during the HDBP extraction and re-extraction with HCl, after the addition of TBP. These separations are unnecessary when rare earth compounds are analyzed instead of rocks or other samples of complex composition. High amounts of iron, which would give rise to interference, are removed by extraction with 20% gasoline solution of TBP from 6 *N* HCl medium. The aqueous solution containing the europium is evaporated to dryness to remove the hydrochloric acid, with subsequent evaporation to dryness together with the fuse-mixture. (As the preliminary separation methods have been reported in detail and the luminescent measurement is described above repeated discussion of the procedure is unnecessary.)

With the use of an internal standard, the error of the measurement is less than $\pm 30\%$, even at low concentrations and visual evaluation.

Evaluation of the developed methods

It is a common advantage to all three methods that the analyses can be carried out equally well on the stock solutions obtained by the separation methods described. This makes possible the analysis of samples with widely varying europium contents and also the checking of the results to a certain extent. Since the analysis can be combined with the photometric determina-

Table III

Europium content of some samples, determined according to the described methods

Sample	Europium content (ppm)		
	Arsenazo III.	*o*-Phenanthroline + novatophane	$SrCl_2$—NaCl melt
Monacite	45	50	45—50
Wastes of production of trisodium phosphate			
1.	154	130	—
2.	140	120	—
3.	120	110	—
Apatite	46	53	—
Sm_2O_3 of 99% purity (Sojuzhimexport)	300	—	—
Y_2O_3 (Auer-Remy)	10	—	—

tion of the sum of rare earths [8] and the cerium content [11], its time requirement is not too high.

No standard samples were available for checking the methods. Therefore, the accuracy was checked by means of the stock solutions and internal standards. The above data referring to the error of the method were obtained in this manner.

Some samples were analyzed according to more than one method. The results are summarized in Table III.

REFERENCES

1. RJABCHIKOV, D. I., RJABUHIN, V. A.: Analiticheskaya himija redkozemelnih elementovi Ittria. Izd. Nauka, Moscow, 1966
2. POLUEKTOV, N. S., NYIKONOVA, M. P.: Redkozemelnie elementi. p. 208. Izd. A. N. USSR. 1959
3. KONONENKO, L. I., LAUER, R. S., POLUEKTOV, N. S.: Zh. Anal. Him. **18,** 1468 (1963)
4. POLUEKTOV, N. S., VITKUN, R. A., KONONENKO, L. I.: Ukr. Him. Zh. **30,** 629 (1964)
5. ALBERTI, G., MASSUCCI, A. M.: Anal. Chem. **38,** 214 (1966)
6. MELENTYEVA, E. V., POLUEKTOV, N. S., KONONENKO, L. I.: Zh. Anal. Him. **22,** 187 (1967)
7. MELENTYEVA, E. V., TISCHENKO, M. A., POLUEKTOV, N. S.: Sovremennye metodi himicheskogo i spectralnovo analiza materialov. p. 207. Izd. Metallurgia, 1967
8. MOHAI, M., UPOR, E.: Magy. Kém. Foly. **74,** 270 (1968)
9. UPOR, E.: Magy. Kém. Foly. **73,** 479 (1967)
10. UPOR, E., JURCSIK, I., MOHAI, M.: Acta Chim. Acad. Sci. Hung. **37,** 1 (1965)
11. MOHAI, M., UPOR, E.: Magy. Kém. Foly. **73,** 484 (1967)

Magda FÁBIÁN-MOHAI; Pécs III., 39-es Dandár út 4,
Endre UPOR; Pécs III., 39-es Dandár út 3.
Gyula NAGY; Pécs III., Páfrány u. 27.

Acta Chimica Academiae Scientiarum Hungaricae, Tomus 68 (1—2), pp. 11—19 (1971)

PREPARATION AND STUDY OF $CaSO_4$: Mn SUITABLE FOR DOSIMETRY

I. KÁSA, I. PORUBSZKY and L. KISS*, **

*(Department of Applied Chemistry, Technical University, Budapest and *National F. Joliot Curie Radiobiological and Radiohygiene Research Institute, Budapest)*

Received December 16, 1969

A study was made of the preparative conditions of manganese-activated calcium sulfate phosphors suitable for dosimetry and their effect on the thermoluminescent properties. Under the studied experimental preparative conditions, the optimum method of introduction of the activator was determined. The most favourable properties were possessed by those phosphors in which the introduction of the activator took place in acidic medium before the separation of the calcium sulfate. From a study of the effect of the heating atmosphere on the sensitivity, it was found that (since manganese ions oxidized to a valency state higher than two are responsible for the lower sensitivities of the samples heated in air), inasmuch as these oxidized manganese ions were subsequently reduced to divalent manganese and removed, the light intensity and sensitivity of the samples prepared in an atmosphere of air closely approached or reached the corresponding data of the samples prepared in the reducing atmosphere. In every sample the γ-ray dose is measured linearly in the examined region (10^{-2}—10^{2} R).

Introduction

The dosimetric application of thermoluminescent phosphors is becoming more and more widespread. Of the phosphors used, especially in measurements of very small doses, an important place is occupied by manganese-activated calcium sulfate. From the beginning of the 1950's numerous methods have been reported for the preparation of thermoluminescent phosphors suitable for dosimetry: calcium sulfate activated with manganese, samarium, or more recently dysprosium [1—14].

The modifications of calcium sulfate which contain water of crystallization ($CaSO_4 \cdot 2\ H_2O$ and $CaSO_4 \cdot 1/2\ H_2O$) do not possess thermoluminescent properties, whereas the anhydrous modification luminesces strongly. During the preparation, the formation of this modification must be strived for and at the same time the activator ion, in a suitable amount and form, must be built into the crystal lattice. This is most easily achieved by heating a mixture of the activator and calcium sulfate containing water of crystallization at a temperature of 900—1000 °C. HOFFMANN [1] prepared the $CaSO_4$: Mn phosphor as long ago as 1897 in this manner. LYMAN [2] observed that a manganese(II) sulfate content of between 0.2 and 17% does not affect the luminescent properties of the phosphor.

** Present address: Hungarian Dairy Experimental Institute, Mosonmagyaróvár — Budapest)

WATANABE [3] modified the procedure by mixing the sulfates with dilute sulfuric acid. After evaporation to dryness, the mixture was heated at 1000 °C. In this way the sensitivity of the phosphor increased significantly because sulfuric acid, by virtue of its dehydrating property, promotes the conversion of the dihydrate ($CaSO_4 \cdot 2\ H_2O$) to the anhydrous form ($CaSO_4$). PETER [4] showed that if the phosphor is heated in an argon atmosphere, then a further increase of the sensitivity may be observed since the oxidation of manganese(II) ions to ions of a higher valency state is prevented.

MAYER [5] carried out the formation of the anhydrite crystal structure with concentrated sulfuric acid at 300 °C where the excess sulfuric acid is removed. MEDLIN [6] modified the procedure in as much as the activator ion is precipitated together with calcium sulfate from a solution of calcium chloride by the addition of concentrated sulfuric acid.

The procedure of BJÄRNGARD [7] is to a certain extent a combination of the previous methods. $CaSO_4 \cdot 2\ H_2O$ of analytical purity and 1 mole% of $MnSO_4 \cdot H_2O$ are mixed with 25% sulfuric acid, and the mixture allowed to stand at room temperature for 16 hours. The water is removed at 80—90 °C and the acid at 250—300 °C, and the dry material is heated at 900 °C for 45 minutes in a reducing atmosphere ($N_2 + SO_2$).

A preparative method differing from the above was reported by SPURNY [8] and by others [9, 10]. The essence of this is that the $CaSO_4$: Mn is formed in a sodium chloride melt during slow cooling (ca. 40 °C per hour) from 1000 °C. Initial composition: a mixture of ignited calcium sulfate with sodium chloride and manganese(II)sulfate in a ratio of 4.5 : 4.5 : 1. The content of incorporated activator is less than 1%.

The exchange of the manganese activator for samarium does not improve the dosimetric properties [11].

Today, for the measurement of very small doses of 20—40μR [19], in nearly all cases $CaSO_4$: Mn is the thermoluminescent phosphor used.

In this work we deal with the effect exerted on the relative sensitivity and linearity of the phosphor by the mode of introduction of the activator, its concentration, the temperature of heating, and the subsequent reduction to manganese(II) and removal of manganese ions oxidized in the case of samples heated in the air.

We have already reported in several publications and lectures on the application in medical radiology of the $CaSO_4$: Mn phosphors prepared by us [15—17].

Experimental

1. Preparation of the stock solutions

A stock solution of calcium chloride was used for the preparation of the $CaSO_4$: Mn phosphors. This was prepared by dissolving calcium oxide of analytical purity in hydrochloric acid of analytical purity.

A $CaSO_4$: Mn phosphor of suitable quality can be prepared from chemicals of analytical purity with no further purification [3, 7]. In calcium oxide of analytical purity, the specifications (Ref. [18] p. 660) permit greater iron and heavy metal contents than in the other analytically pure chemicals used by us (H_2SO_4, $MnSO_4.4\,H_2O$, HCl) (Ref. [18] pp. 764, 846 and 1058). Since iron has a well-known luminescence quenching effect the calcium chloride solution was purified.

The slightly acidic solution (after oxidation with hydrogen peroxide) was made alkaline with calcium hydroxide paste, after about half an hour's stirring the suspension was filtered, and the filtered solution was used for the preparation of some of the phosphors (samples 1—3). In the following, this will be called solution A. During this purification operation the iron content of the solution decreased significantly, from 0.015% to below 0.005%.

The following operation was performed on part of the calcium chloride solution prepared in the previous manner: calcium sulfate was separated from the calcium chloride solution with a little sulfuric acid. After half an hour's stirring the solution was filtered and the filtrate used for the preparation of further phosphor samples (samples 4, 4a, 4b, 5, 5a, 5b). In the following this will be referred to as solution B.

The Ca^{2+} contents of solutions A and B were determined.

2. Activation of the samples

The samples were activated as follows.

Sample 1: An amount of manganese (II) sulfate activator corresponding to 1 mole% was dissolved in dilute (~30%) sulfuric acid. To this solution was added an amount of solution A almost equivalent to the sulfuric acid. (In samples 1—5 the excess sulfuric acid was less than 0.5%.)

Sample 2: The previous procedure was repeated with the difference that before the addition of solution A to the acidic manganese (II) sulfate solution the reductant hydroxylamine hydrochloride was added too.

Sample 3: The reductant hydroxylamine hydrochloride was dissolved in solution A and then an amount of manganese (II) sulfate corresponding to 1 mole% was precipitated with sulfuric acid.

Sample 4: This was the same as sample 1 but the solution B was used.

In order to study the effect of the activator concentration, the preparation of sample 4 was repeated using 0.5 mole% (sample 4a) and 1.5 mole% (sample 4b) of manganese (II) sulfate too.

Sample 5: This was the same as sample 3 with the difference that solution B was used.

After the separation of calcium sulfate the samples were evaporated to dryness on a steam-bath.

Sample 6: In this case, after the precipitation of calcium sulfate the suspension was evaporated to dryness on a steam-bath. The residue was kept at 340 °C for 3 hours, and after this, manganese (II) sulfate corresponding to 1 mole% was added to it.

3. Heating and after-treatment of the samples

The thermal treatment of the samples was performed in two ways. Half of the samples were heated in an atmosphere of air, the other half in an argon + sulfur dioxide atmosphere. The first 5 samples were treated at 900 °C. The material corresponding to the composition of sample 5 was also heated in a sulfur dioxide-containing argon atmosphere at 950 °C (sample 5a) and at 1000 °C (sample 5b).

Sample 6 was heated in reference [6] at 1050 °C both in air and sulfur dioxide-argon atmospheres.

For all the samples, half of the phosphors heated in air were after-treated, the purpose of which was the reduction and removal of oxidized manganese ions to manganese (II). The after-treatment was performed by boiling in a weak hydrochloric acid solution containing hydroxylamine hydrochloride. The samples were washed by decantation until chloride could no longer be detected with $AgNO_3$, then filtered and dried in a drying-oven at 120 °C.

In the case of the sample 1 phosphors prepared in the reducing atmosphere, the after-treatment was carried out to decide whether a further increase of sensitivity could be observed.

4. Excitation of the phosphors

The irradiation for the heating curves was carried out with γ-irradiation from Cs-137 (E_γ = 662 keV). To facilitate comparison of the heating curves, the samples were irradiated in all cases with 1 R, and measurements were begun exactly 1 hour after the irradiation. The ready phosphors were measured into polyethylene packets and the irradiation performed in these. An amount of the irradiated phosphor, corresponding to the experimentally determined saturation layer thickness, was taken in a 20 mm diameter nickel tray and so placed in the measuring apparatus.

In the study of the photomultiplier current-dose relation (linearity), γ-irradiation was carried out with Co-60 ($\bar{E}_\gamma$ = 1.225 MeV).

5. Measurement of the thermoluminescent emission

The measurement of the irradiated powders was performed with the help of the experimental TLD evaluating apparatus made in the Frederic Joliot-Curie Radiobiological and Radiohygiene Research Institute. The heating curves were recorded with a heating rate of 26 °C per minute.

Results and discussion

The heating curves of the $CaSO_4$: Mn samples prepared by the different procedures described in the experimental part are shown in Figs 1—8.

Some of the more important parameters of sample preparation, the intensity maxima (I_m) of the heating curves, and the temperatures relating to these (T_m) are given in Table I.

The results show that the values of T_m, in agreement with the literature data, fluctuate about 100 °C. The decrease of the activator concentration results in the decrease of T_m (Fig. 7).

From the values of I_m it is evident that the phosphors of highest light intensity, *i.e.* the most sensitivity ones, are those where the activator was introduced in an acidic medium (samples 1 and 4; Figs 1 and 4).

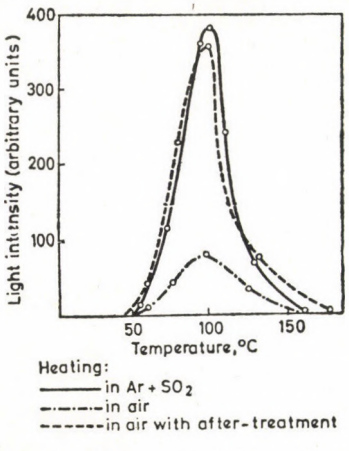

Fig. 1. Heating curves of $CaSO_4$: Mn samples no. 1

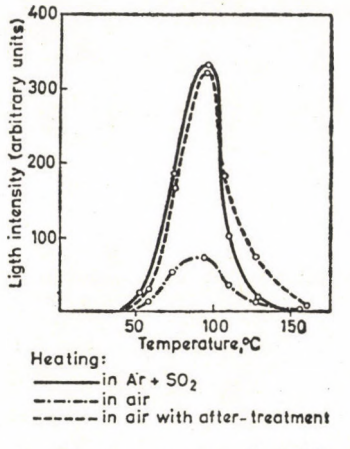

Fig. 2. Heating curves of $CaSO_4$: Mn samples no. 2

If the introduction of the activator does not take place simultaneously with the formation of calcium sulfate but substantially later (as in sample 6), then the sensitivity is significantly decreased (Fig. 6).

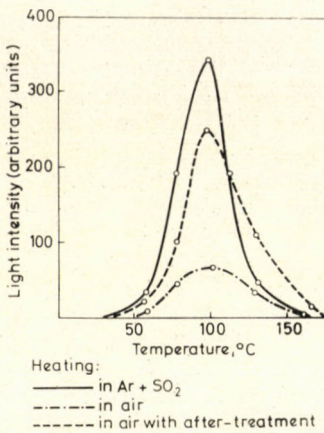

Fig. 3. Heating curves of $CaSO_4$: Mn samples no. 3

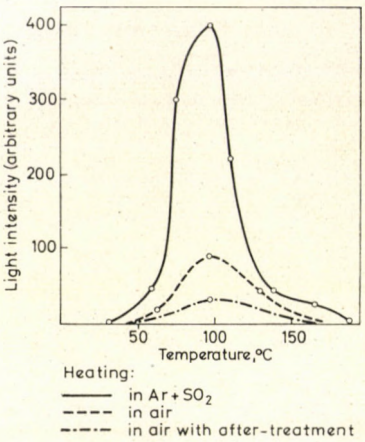

Fig. 4. Heating curves of $CaSO_4$: Mn samples no. 4

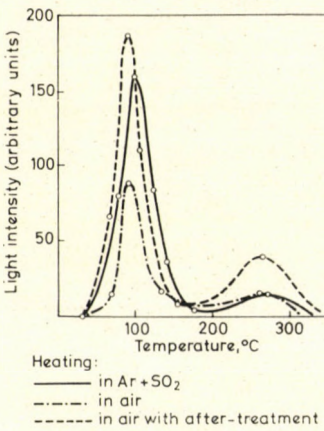

Fig. 5. Heating curves of $CaSO_4$: Mn samples no. 5

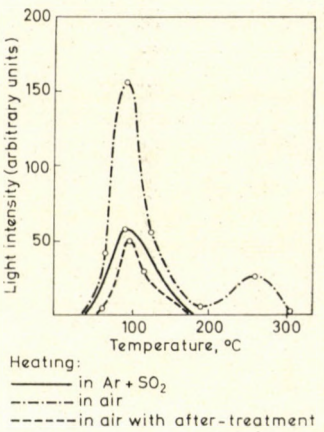

Fig. 6. Heating curves of $CaSO_4$: Mn samples no. 6

The separately added reductant does not increase the light intensity, but rather decreases it by about 15% (sample 2; Fig. 2).

A comparison of the measured data for samples 1 and 4 (Table I) shows that the second purification operation does not affect the light intensity substantially, increasing it by only about 3—4%.

The variation of the heating temperature between 900 and 1000 °C does not cause any significant differences (Fig. 8). It should be mentioned here that in the case of heating at 900 °C for sample 5 a new intensity peak is found at

about 265 °C; with heating at a higher temperature this disappears (Fig. 8). If the thermoluminescence dosimeter evaluation is made on the basis of the light intensity relating to T_m (peak height measurement), then use of phosphors possessing a single peak gives more accurate results, but the presence of more peaks makes possible the repeated evaluation of the dosimeter [20].

The decrease of the activator concentration from 1 mole% to 0.5 mole% brings about the decrease not only of T_m but also of the light intensity, by

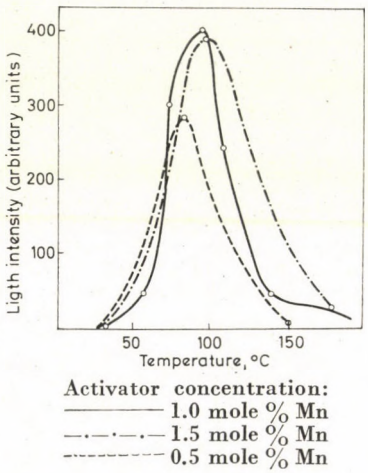

Fig. 7. Heating curves of samples containing different amounts of activator

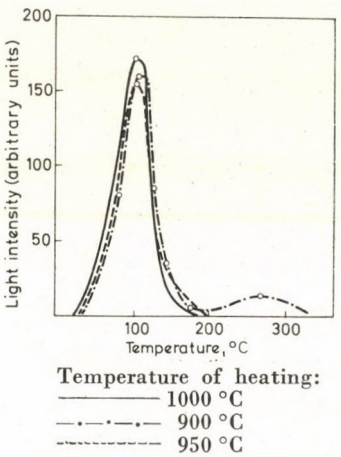

Fig. 8. Heating curves of samples heated at different temperatures

about 30%. At the same time, increase of the activator concentration to 1.5 mole% does not cause a substantial change (Fig. 7).

For the samples heated in an atmosphere of air, after-treatment is accompanied in all cases by a significant sensitivity increase (Table I). Even for the samples heated in the reducing atmosphere, a small increase of sensitivity (a few per cent) occurs as a result of after-treatment (sample 1).

During the after-treatment a decrease of the manganese content can be observed. The analyses showed that in the case of a 1 mole% manganese(II) sulfate initial activator content this decrease is about 30% of the original manganese content. That is, under our experimental conditions the activator content of the prepared $CaSO_4$: Mn is about 0.7%; this is the built-in amount that cannot be removed during the after-treatment. This result is in agreement with those of MAYER [5] and SPURNY [8]. Their preparative methods both differ substantially from our own, but nevertheless MAYER and SPURNY report concentration values of about 0.5% and less than 1%, respectively, for the incorporated manganese content. If its oxidation is prevented, the presence of not built-in activator has no substantial effect on the luminescence properties. This is the explanation of the observation of LYMAN [2]. At the

Table I

The intensity maxima (I_{max}) and the corresponding temperature maxima (T_{max}) of the heating curves of $CaSO_4$: Mn samples prepared in different ways

Sample number	Heating		Activator conc. mole %	After-treatment	I_{max} (arbitrary units)	T_{max} °C
	atmosphere	temperature °C				
	reducing	900	1	—	385	101
1	reducing	900	1	+	395	100
	air	900	1	—	80	98
	air	900	1	+	360	98
	reducing	900	1	—	330	94
2	air	900	1	—	70	94
	air	900	1	+	325	94
	reducing	900	1	—	345	96
3	air	900	1	—	65	102
	air	900	1	+	250	96
	reducing	900	1	—	400	96
4	air	900	1	—	30	96
	air	900	1	+	90	96
4a	reducing	900	0.5	—	285	85
4b	reducing	900	1.5	—	385	100
	reducing	900	1	—	160	101
5	air	900	1	—	77	96
	air	900	1	+	185	96
5a	reducing	950	1	—	155	100
5b	reducing	1000	1	—	170	102
	reducing	1050	1	—	56	92
6	air	1050	1	—	50	96
	air	1050	1	+	155	96

same time, the removal of the not built-in manganese activator in the case of the $CaSO_4$: Mn phosphor used for dosimetry is an essential step, even if (not being oxidized) it does not affect the luminescence properties, since because of its atomic number ($Z = 25$), it further impairs the otherwise not too favourable energy dependence of the phosphor. In our case, however, the sensitivity increases to several times that before treatment and this makes possible the preparation in an air atmosphere of phosphors of such sensitivity and light intensity that, without after-treatment, would have been possible to achieve only in a reducing atmosphere. Derivatographic measurements [21] have shown that a sample after-treated and dried at room temperature does not contain water of crystallization.

After-treatment has further advantages. The homogeneity of an after-treated sample is greater, and its adhering power and hygroscopicity less than those of a sample not after-treated. These advantages are fairly significant in practical application.

With thermoluminescent phosphors as dosimeters, evaluation can be carried out in two ways [20].

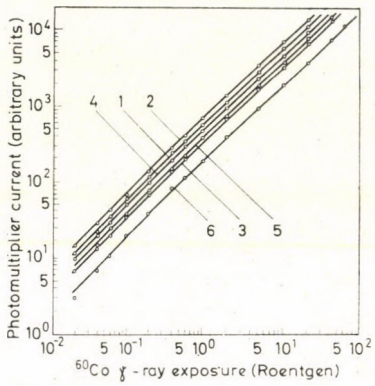

Fig. 9. Photomultiplier current-dose relation (linearity) of samples prepared in a reducing atmosphere

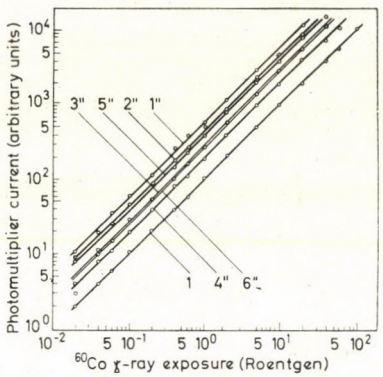

Fig. 10. Photomultiplier current-dose relation (linearity) of samples prepared in an atmosphere of air. ("After treated samples)

In the one case the area under the heating curve is measured (integral measurement); this area is proportional to the irradiation dose.

In the other case the peak maximum of the heating curve is measured (peak height measurement); under the given experimental conditions this too is proportional to the amount of irradiation.

An important requirement in both methods is that the direct proportionality between I_m, the area under the measured curve, and the extent of irradiation, should cover as large a measurement range as possible.

Thermoluminescent dosimeters can be used in a range of 4—8 orders of magnitude in general ($\sim 10^{-3}$—10^5 R) depending on the phosphor and the evaluation apparatus, and for the individual phosphors the direct proportionality (linearity) exists almost in the same scale.

Depending on the sensitivities of the individual samples, with the experimental TLD evaluation apparatus used by us measurements could be made in a scale of about 4 orders of magnitude (10^{-2}—10^2 R) (Figs 9 and 10). The results show that in the examined range, for samples heated in both the reducing atmosphere (Fig. 9) and in air (Fig. 10), the proportionality does exist. (In Fig. 10, of the samples not after-treated, only the data for sample 1 are given.)

Here the important fact must be pointed out that the after-treated samples too maintain their linearity over the entire examined range (Fig. 10) and, as already mentioned, their sensitivity too increases substantially (4—6 times) compared to that of those not after-treated (Fig. 10, curves 1 and 1").

With the given evaluation apparatus it was not possible to determine either the upper or the lower limit of the linearity of the measurement region without its modification. It may be presumed that if measured with a more sensitive evaluation apparatus with a larger measurement range, the linearity would be found to exist over an even larger interval in both directions, but particularly in the direction of the upper measurement region.

REFERENCES

1. HOFFMANN, M. W.: Ann. Phys. **60,** 269 (1897)
2. LYMAN, T.: Phys. Rev. **48,** 149 (1935)
3. WATANABE, K.: Phys. Rev. **83,** 785 (1951)
4. PETER, H.: Atomkernenergie **5,** 453 (1960)
5. MAYER, U.: Naturwiss. **43,** 79 (1956)
6. MEDLIN, W. L.: J. Phys. Chem. Solids **18,** 238 (1961)
7. BJÄRNGARD, B.: Aktiebolaget Atomenergie Report. Stockholm, Sweden, AE—109 (1963)
8. SPURNY, Z.: Kernenergie **5,** 611 (1962)
9. ARKHANGELSKAYA, V. A., VAYNBERG, B. I., RASUMOVA, T. K.: Opt. i Spektr. **4,** 681 (1958)
10. NOSENKO, B. M., REVZIN, L. S., YASKOLKO, V. YA.: Zh. Techn. Fiz. (Soviet) **26,** 2046 (1956)
11. SVARC, K. K., GRANT, Z. A.: Termoluminescentnaya Dozimetriya, Izdatyelstvo Zinatne, Riga, 1968
12. KRASNAYA, A. R., NOSENKO, B. M., REZVIN, L. S., YASKOLKO, V. YA.: Atomnaya Energ. **10,** 630 (1961)
13. WITZMANN, H., HERZOG, G., WUNTKE, K.: Z. Phys. Chem. **225,** 325 (1964)
14. MEJDAHL, V.: Health Phys. **18,** 164 (1970)
15. TÖRÖK, I., BOROS, L., KÁSA, I.: Lecture I. Gemeinsame Tagung der Österreichischen Verbandes für Strahlenschutz und der Ungarischen Strahlenschutzgruppe der Eötvös Loránd Physikalischen Gesellschaft. Wien, 23—25 April, 1969
16. TÖRÖK, I., BOROS, L., KÁSA, I.: Lecture II. Gemeinsame Tagung der Österreichischen Verbandes für Strahlenschutz und der Ungarischen Strahlenschutzgruppe der Eötvös Loránd Physikalischen Gesellschaft. Wien, 23—25 April, 1969
17. TÖRÖK, I., BOROS, L.: Strahlentherapie, Heft 12 (1969)
18. KOLOS, E.: Vegyszervizsgálat (Chemical Analysis). Műszaki Könyvkiadó, Budapest, 1969
19. ATTIX, F. H.: NRL Report 6145 Sept. 18 (1964)
20. SCHAYES, M.: Belgian Technical Week, Budapest, November 10—18, 1969
21. PAULIK, F., PAULIK, J., ERDEY, L.: Z. anal. Chem. **160,** 241 (1958)

Imre KÁSA
Iván PORUBSZKY
Lajos KISS
Budapest XI., Egry J. u. 20.

Acta Chimica Academiae Scientiarum Hungaricae, Tomus 68 (1—2), p. 21—27 (1971)

THERMODYNAMICS OF THE GAS PHASE REACTION OF TRICHLOROSILANE WITH VINYLCHLORIDE AT HIGH TEMPERATURES

D. KNAUSZ

(Department of General and Inorganic Chemistry, Eötvös Loránd University, Budapest)

Received December 16, 1969

Using the equilibrium constant for the reaction of trichlorosilane with vinylchloride, the heat of formation of vinyltrichlorosilane was determined. This value was found to be consistent with other data available in the literature on formation heats of similar substances. Values of the equilibrium constant were calculated for several temperatures. Data were obtained on the average reaction heat and the average change of entropy in the temperature interval of 600—821 K.

In a recent paper [1] the kinetic study of the reaction

$$Cl_3SiH + CH_2 = CHCl \rightleftharpoons CH_2 = CHSiCl_3 + HCl \qquad (1)$$

carried out in the gas phase, at atmospheric pressure, in a flow system, at 548 °C was described. According to the results, this reaction is of the second order and leads to equilibrium.

From the kinetic data given in Ref. [1], the equilibrium constant of reaction (1) is calculated: $K_p = 2.27$, at 548 °C.

The equilibrium constant and the thermodynamic characteristics of components taking part in the reaction are connected by the following well-known relationship:

$$R \ln K_p = -\left[\Delta\left(\frac{G^0 - H_0^0}{T}\right) + \frac{\Delta H_0^0}{T}\right] \qquad (2)$$

where: R is the universal gas constant, K_p the equilibrium constant (in pressure units), $\Delta\left(\frac{G^0 - H_0^0}{T}\right)$ the reduced free enthalpy difference between the reactants and products, ΔH_0^0 the heat of the hypothetic gas reaction taking place at 0 K. Using the above given value of the equilibrium constant by means of expression (2), the heat of formation at the absolute zero can be calculated for any reacting component provided that the heats of formation of all the remaining components taking part in the reaction as well as the $\left(\frac{G^0 - H_0^0}{T}\right)$ values for each component are known. In the case of reaction (1), the data

necessary for the calculations are known for all the components except vinylchlorosilane. These data are collected in Table I.

The $\left(\frac{G^0 - H_0^0}{T}\right)$ values of vinyltrichlorosilane can be calculated by quantum-statistical methods from spectroscopic and stereochemical data for this compound [8]. Thus the heat content, reduced free enthalpy, entropy and con-

Table I

Data used for the calculation of the heat of formation of vinyltrichlorosilane

Compound	$(\Delta H_f^0)_0$		$-\left(\frac{(G^0 - H_0^0)}{T}\right)$
	kcal/mole	Reference	Reference
HCl	− 21.984	[2]	[2]
$HSiCl_3$	−125.6	*a*, *b*,*c*	[3]
CH_2—CHCl	7.011	*c*, *d*	[6]

a calculated from the heat of hydrolysis given by WOLF [4], using WISE's value [5] for amorphous SiO_2: $[(\Delta H_f^0)_{298}\ SiO_{2(amorph.)}] = -215.9$ kcal/mole
b $[(\Delta H_f^0)_{298} HSiCl_{3(g)}] = -126.8$ kcal/mole
c Value obtained from Eq. (3)
d $[(\Delta H^0)_{298} C_2H_3Cl_{(g)}] = 5.2$ kcal/mole [7]

stant pressure heat capacity were calculated (using a rigid rotator, harmonic oscillator approximation) for the ideal gas state and 1 atm pressure. For the model outlined above statistical thermodynamics give the following relationships:

$$H - H_0^0 = 4RT + E_{\text{vibr}} \tag{3}$$

$$\frac{G^0 - H_0^0}{T} = R\left(-\frac{3}{2}\ln M - 4\ln T - \frac{1}{2}\ln I_A I_B I_C + \right.$$

$$\left. + \ln p + \ln \sigma - 129.520\right) + \left(\frac{F}{T}\right)_{\text{vibr}} \tag{4}$$

$$S = R\left(\frac{3}{2}\ln M + 4\ln T + \frac{1}{2}\ln I_A I_B I_C - \ln p - \ln \sigma + 133.520\right) + S_{\text{vibr}} \tag{5}$$

$$C_p = 4R + C_{\text{vibr}} \tag{6}$$

The values corresponding to the vibrational frequencies were determined as follows:

$$E_{\text{vibr}} = R \sum_i \frac{1}{e^{\frac{h\nu_i}{kT}} - 1} \cdot \frac{h\nu_i}{k} \tag{7}$$

$$\left(\frac{F}{T}\right)_{\text{vibr}} = R \sum_i \ln\left(1 - e^{-\frac{h\nu_i}{kT}}\right) \tag{8}$$

$$S_{\text{vibr}} = R \sum_i \frac{\frac{h\nu_i}{kT}}{e^{\frac{h\nu_i}{kT}} - 1} - R \sum_i \ln\left(1 - e^{-\frac{h\nu_i}{kT}}\right) \tag{9}$$

$$C_{\text{vibr}} = R \sum_i \frac{\left(\frac{h\nu_i}{kT}\right)^2 e^{\frac{h\nu_i}{kT}}}{\left(e^{\frac{h\nu_i}{kT}} - 1\right)^2} \tag{10}$$

where: R is the universal gas constant, T the temperature, M the molecular weight of the compound, $I_A I_B I_C$ the moment of inertia of the molecule, p the pressure, σ a symmetry number, h the Planck constant, k the Boltzmann constant and ν_i are the vibrational frequencies.

The Hirschfelder formula [9] was used to calculate the moment of inertia:

$$I_A I_B I_C = \begin{vmatrix} A & -F & -E \\ -F & B & -D \\ -E & -D & C \end{vmatrix} \tag{11}$$

where the meaning of notations is:

$$A = \sum_i m_i (y_i^2 + z_i^2) - \frac{1}{M}\left(\sum_i m_i y_i\right)^2 - \frac{1}{M}\left(\sum_i m_i z_i\right)^2 \tag{12}$$

$$B = \sum_i m_i (x_i^2 + z_i^2) - \frac{1}{M}\left(\sum_i m_i x_i\right)^2 - \frac{1}{M}\left(\sum_i m_i z_i\right)^2 \tag{13}$$

$$C = \sum_i m_i (y_i^2 + x_i^2) - \frac{1}{M}\left(\sum_i m_i y_i\right)^2 - \frac{1}{M}\left(\sum_i m_i x_i\right)^2 \tag{14}$$

$$D = \sum_i m_i y_i z_i - \frac{1}{M}\left(\sum_i m_i y_i\right)\left(\sum_i m_i z_i\right) \tag{15}$$

$$E = \sum_i m_i x_i z_i - \frac{1}{M}\left(\sum_i m_i x_i\right)\left(\sum_i m_i z_i\right) \tag{16}$$

$$F = \sum_i m_i x_i y_i - \frac{1}{M}\left(\sum_i m_i x_i\right)\left(\sum_i m_i y_i\right) \tag{17}$$

In the above expressions m_i stands for the mass of the i-th atom in the molecule, $M = \sum_i m_i$ is the mass of the molecule, x_i, y_i, z_i are the rectangular coordinates of the i-th atom in the molecule.

The stereochemical data of the molecule were taken from the paper by VILKOV *et al.* [10]. Thus the moment of inertia $I_A I_B I_C = 1.09749 \times 10^{-113}$ g^3cm^6, the molecular weight is 161.491, and the symmetry number is 1. The vibrational frequency values were taken from SHULL's paper [11]. The total translational, rotational and vibrational values are shown in Table II.

Table II

Thermodynamic characteristics of vinyltrichlorosilane in the ideal gas state, at 1 atm pressure (cal. $K^{-1} \cdot mole^{-1}$)

T (K)	$\frac{H^0 - H_0^0}{T}$	$-\frac{(G^0 - H_0^0)}{T}$	S	C_p
100	10.69	51.83	54.57	15.03
200	14.76	60.53	75.29	22.20
273.15	17.31	65.52	82.83	26.16
298.15	18.10	67.07	85.16	27.31
300	18.38	67.21	85.58	27.40
400	19.97	72.80	92.77	32.37
500	23.34	77.74	101.08	34.18
600	25.29	82.03	107.31	36.40
700	27.05	86.42	113.46	38.07
800	28 52	89.93	118.45	39.72
821.15	28.72	90.69	119.41	39.90
900	29.84	92.37	122.21	40.86
1000	30.99	96.57	127.56	41.87

Using the data given above, the heat of formation of vinyltrichlorosilane at the absolute zero was calculated by means of Eq. (2). Since the $\left(\frac{G^0 - H_0^0}{T_0}\right)$ values are generally tabulated at intervals of 100 K, the $\Delta \frac{G_0 - H_0^0}{T_0}$ value for 548 °C was determined by interpolation. The heat of formation of vinyltrichlorosilane at 0 K was found to be $(\Delta H_f^0)_0 = -104.7$ kcal/mole. The standard heat of formation was calculated from this value using the equation:

$$(\Delta H_f^0)_T = [(H_T^0 - H_0^0) + (\Delta H_f^0)_0]_c - \Sigma (H_T^0 - H_0^0)_e \qquad (18)$$

where

$(\Delta H_f^0)_T$ is the normal heat of formation of the compound at 298 K;
$(\Delta H_f^0)_0$ is the normal heat of formation of the compound at 0 K;
H_T^0 is the enthalpy of the compound or element at 298 K;
H_0^0 is the enthalpy of the compound or element at 0 K;

subscripts c and e refer to the compound and the elements forming this compound, respectively. On the basis of these calculations we obtain the following

value for the normal heat of formation of vinyltrichlorosilane: $(\Delta H_f^0)_0 = -106.9$ kcal/mole.

The method of calculating the heat of formation of molecules from the bond increments, using additivity rules, is widely known. These increments are related to the bond dissociation energies. Recently similar bond-additivity rules were applied for a systematization of the heats of formation of silicon compounds. O'NEAL and RING [12] have calculated the heat of formation of silicon compounds using a simple bond-additivity method. VAN DALEN *et al.* [13] have calculated the heats of formation of methylsilanes, chlorosilanes and methylchlorosilanes (of general formula X_nSiY_{4-n}, where n is the bond number for ligand X, 4-n is the same for ligand Y) from the following equation:

$$\Delta H_f^0(X_nSiY_{4-n}) = na(Si-X) + (4-n)a(Si-Y) + n(4-n)i(X, Y) \quad (19)$$

where $a(Si-X)$ and $a(Si-Y)$ are proportional parts of the ΔH_f^0 values of the SiX_4 and SiY_4 molecules, respectively; $i(X, Y)$ is a bond-influence term expressing the deviation from the additivity rule.

These bond-additivity rules, too permit to calculate the heat of formation of vinyltrichlorosilane and to compare it with the value obtained above. Thus, using a simple additivity rule, this value is $(\Delta H_f^0)_{298} = -101.5$ kcal/mole. By means of Eq. (19) we get for the difference between the 'influence' terms of the vinyl (hydrogen and vinyl) chloro groups:

$$i(CH_2CH,\ H) - i(CH_2CH,\ Cl) = 1.8$$

Besides the heat of formation of vinyltrichlorosilane determined earlier the following values were used as basic data in the calculations:

$$[(\Delta H_f^0)_{298}CH_2CHSiH_{3(g)}] = -1 \text{ kcal/mole} \quad [12, 14]$$

$$[(\Delta H_f^0)_{298}SiCl_{4(g)}] = -161.2 \text{ kcal/mole}^*$$

$$[(\Delta H_f^0)_{298}SiH_{4(g)}] = -27.0 \text{ kcal/mole}^{**}$$

The value for $i(CH_3, H) - i(CH_3, Cl)$ is 2.1, according to van DALEN's work [13]. Since bond 'influencing' occurs as a secondary effect, the agreement of the above data is satisfactory. This agreement proves the consistency of in this paper obtained value of the heat of vinyltrichlorosilane formation with other known data.

* Calculated from the heat of hydrolysis given by WOLF [4], using WISE's value [5] for amorphous SiO_2: $[(\Delta H_f^0)_{298}SiO_{2(amorph)}] = -215.9$ kcal/mole.

** This value was obtained, using the combustion heat data given by FEHER *et al.* [15] and that obtained for amorphous SiO_2 by WISE [5] $[(\Delta H_f^0)_{298}SiO_{2(amorph)} = -215.9$ kcal/mole.

On the basis of the results on vinyltrichlorosilane and Eq. (2), new information can be obtained for the equilibrium established in Ref. [1]. Therefore, the values for the equilibrium constant were calculated for temperatures different from those used in the experiments. The results are summarized in Table III.

Table III

Equilibrium constants of reaction (1) at different temperatures

T (K)	K_p
400	1.71×10^2
600	9.03
800	2.52
1000	1.15

In our earlier paper [16] it was noted, that the expedient temperature range for kinetic measurements is 400—550 °C, since below 400 °C the reaction rate is too low, while above 550 °C the following side reaction takes place besides main process (1):

$$Cl_3SiH + CH_2 = CHCl \rightarrow SiCl_4 + CH_2 = CH_2 \tag{20}$$

On the basis of our results referring to the temperature range suitable for kinetic measurements some other important thermodynamic characteristics can be determined: the average heat of the reaction and the average entropy change can be calculated as follows:

$$\lg K = -\frac{\Delta H^0}{4.576\,T} + \frac{\Delta S^0}{4.576} \tag{21}$$

where

ΔH^0 is the average heat of the reaction

ΔS^0 is the average entropy change accompanying the reaction.

The calculations were performed for the temperature range 327—548 °C (600—821 K) which is wider than the above mentioned interval, because data necessary for the calculations are available at steps of 100 K. These calculations yielded $\Delta H^0 = -6.3$/kcal for the average reaction heat and $\Delta S^0 = -6.2$/kcal/K for the average entropy change.

REFERENCES

1. Lengyel, B., Knausz, D., Székely, T., Telegdy, L.: Acta Chim. Acad. Sci. Hung. **64**, 155 (1970)
2. Karapetyants, M. H.: Chemical Thermodynamics (in Hungarian) p. 453. Akadémiai Kiadó, Budapest, 1951

3. Shaulov, Yu. H., Korobov, V. V., Golosova, R. M., Volkov, V. L.: Zh. Fiz. Khim. **40,** 1893 (1966)
4. Wolf, E.: Z. Anorg. Allgem. Chem. **313,** 228 (1961)
5. Wise, S. S.: U. S. At. Energy Comm. ANL 6472 71, (1962) Wise, S. S., Margrave, J. L.: J. Phys. Chem. **67,** 815 (1963)
6. Richards, R. E.: J. Chem. Soc. **1948,** 1931
7. Jochi, R. M., Zwolinski, B. J.: J. Polymer Sci. Pt B **3,** 779 (1965)
8. Godnew, L. N.: Berechnung thermodynamischer Funktionen aus Moleküldaten. VEB Deutscher Verlag der Wissenschaften, Berlin, 1963
9. Hirschfelder, J. O.: J. Chem. Phys. **8,** 431 (1940)
10. Vilkov, V. L., Mastrykov, V. S., Akusin, P. A.: Zh. Strukt. Khim. **5,** 183 (1964)
11. Shull, E. R. Thursack, R. A., Birdsall, C. M.: J. Chem. Phys. **24,** 147 (1956)
12. O'Neal, H. E., Ring, M. A.: Inorg. Chem. **5,** 435 (1966)
13. van Dalen, M. J., van den Berg, P. J.: J. Organometal. Chem. **16,** 381 (1969)
14. Tannenbaum, S.: J. Am. Chem. Soc. **76,** 1027 (1954)
15. Feher, F., Jansen, G., Rohmer, H.: Angew. Chem. **75,** 859 (1963)
Feher, F., Jansen, G., Rohmer, H.: Z. Anorg. Allgem. Chem. **329,** 31 (1964)
16. Knausz, D., Gömöry, P., Telegdy, L.: Annales Univ. Sci. Budapest, Sec. Chim. **8,** 71 (1966)

Dezső Knausz; Budapest VIII., Múzeum krt. 6—8.

Acta Chimica Academiae Scientiarum Hungaricae, Tomus 68 (1—2), pp. 29—38 (1971)

INVESTIGATION OF ADSORPTION PHENOMENA ON PLATINIZED PLATINUM ELECTRODES BY TRACER METHODS, V

THE POTENTIAL DEPENDENCE OF CHLORIDE ION ADSORPTION

GY. HORÁNYI, J. SOLT and F. NAGY

(Central Research Institute for Chemistry of the Hungarian Academy of Sciences, Budapest)

Received November 4, 1969

1. The adsorption of chloride ions on a platinum electrode in a 1.0 *N* solution of perchloric acid as supporting electrolyte has been studied by means of tracer techniques.

2. The potential dependence of the adsorption of chloride ions varies with the state of the electrode: on freshly prepared or regenerated electrodes, adsorption occurs in two distinct steps which coalesce upon aging of the electrode.

There are many papers in the literature in which the specific adsorption of halide ions is discussed. Among these the studies reported by BALASHOVA [1] deserve special mention.

In this paper as an extension of studies formerly described, we wish to direct attention to some phenomena, not yet mentioned in the literature, relating to the potential dependence of chloride ion adsorption.

Experimental

In the study of the adsorption of chloride ions the isotope ^{36}Cl, which emits β-radiation ($E_{max} = 0.716$ MeV), was used. The measurements were carried out in an apparatus already described [2], the technique used in the experiments was essentially the same as that employed in the cases of sulfuric and acetic acid.

In the present study, too, the supporting electrolyte was 1.0 *N* perchloric acid which ensured that enrichment in the double layer due to electrostatic forces was negligible.

Results

There is a characteristic difference between experimental results obtained with freshly prepared electrodes and with electrodes previously used. This difference was primarily in the character of the potential dependence of adsorption, and not in the adsorption capacity.

The concentration of hydrochloric acid was varied within the limits of 10^{-5} and 10^{-2} mole/l and the potential dependence was studied between 0 and 800 mV. The potentials are those with respect to that of a hydrogen electrode at 1 atm in 1.0 *N* perchloric acid.

The potential dependence of adsorption on electrodes previously used exhibits the features reported in numerous publications. This is shown in Fig. 1, where the concentration of hydrochloric acid is 1.3×10^{-4} mole/l. In essence, the shape of the curve is not affected by the potential at which the measurement is started, *i.e.* no hysteresis is in evidence.

The curves obtained with freshly prepared electrodes after cathodic regeneration differ significantly from those for the preceding case. This is shown in Fig. 2. In this instance the shape of the curve depends on the direction followed during measurement (*cf.* Fig. 3), *i.e.* there is a characteristic hysteresis effect in the potential dependence of adsorption. In Fig. 3, Curve 1 was recorded with potentials increasing from 0 to 800 mV, while Curve 2 with potentials changing in the reverse direction.

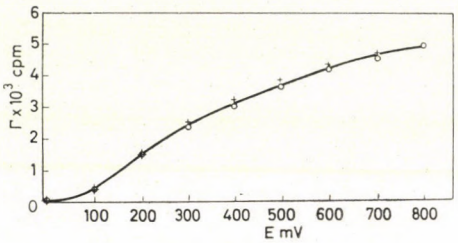

Fig. 1. The potential dependence of adsorption on an electrode previously used, at 1.3×10^{-4} mole/l HCl

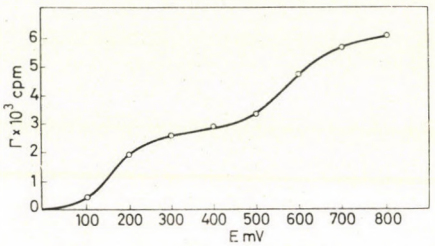

Fig. 2. The potential dependence of adsorption on a freshly prepared electrode

If the potential interval between 0 and 800 mV is repeatedly covered in both directions, the curve shown in Fig. 2 will gradually change that in Fig. 1. This process is shown in Fig. 4. The numbers marking the individual curves indicate their order of succession. In the case of freshly prepared or regenerated electrodes, two characteristic sections can be distinguished in the potential dependence of adsorption (*cf.* Fig. 2). On the corresponding derivative $\left(\frac{d\Gamma}{dE}\right)$ curve (*cf.* Fig. 5), these two sections become very distinctly separated. This phenomenon is observed in quite a wide concentration range. Fig. 6 shows the potential dependence of adsorption, respectively, for 1.3×10^{-5} (Curve 1), 2.6×10^{-5} (Curve 2), 1.3×10^{-4} (Curve 3), and 1.3×10^{-3} (Curve 4) mole/l HCl.

The accurate determination of the concentration dependence of adsorption on a given electrode is difficult due to aging and slow transformation of the electrode. The comparison of results obtained with various electrodes is limited by uncertainties involved in the determinations of surface areas.

It is necessary to perform measurements in a sufficiently wide potential range at a given concentration to obtain information concerning the state of

the electrode. For, as we have seen, the character of the potential dependence of adsorption reflects the changes that have occurred in the state of the electrode, and upon going to another concentration, the electrode should first be regenerated. Measurements at several, especially low, concentrations with the same electrode are time-consuming, and during this the electrode may be subject to more or less important changes.

With all these uncertainties in mind, not more than the character of the concentration dependence of adsorption can be deduced from Fig. 6.

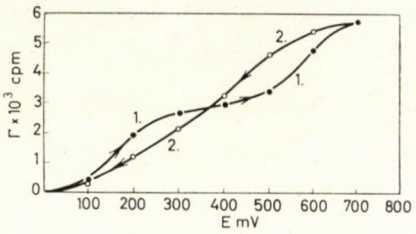

Fig. 3. Adsorption hysteresis
Curve 1: potential changed from 0 towards 800 mV;
Curve 2: potential changed from 800 to 0 Vm

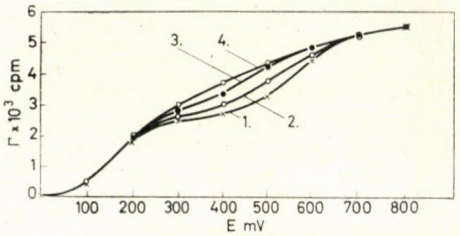

Fig. 4. The potential dependence of adsorption, changing with the number of measureents

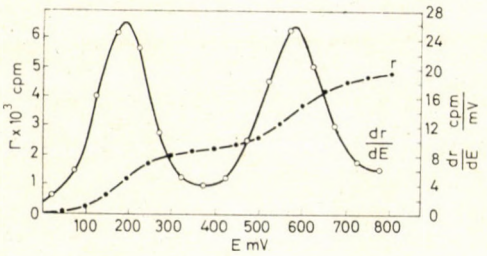

Fig. 5. Two sections the potential dependence of adsorption (Γ curve) illustrated by a $\frac{d\Gamma}{dE}$ curve

In studying potential dependence of adsorption, the situation is more favourable.

We have arrived at the conclusion that the dependence of adsorption on the concentration and electrode potential can be expressed, as a first approximation, by

$$\Gamma = A \cdot F(c)f(E) \tag{1}$$

which means that the adsorbed amount can be described as the product of two functions each of one variable. Factors which characterize the state and quality of the surface are incorporated in constant A. The magnitude of these factors changes with time even for a given electrode. The study of the adsorp-

tion of sulfuric acid [3] suggested an adsorption isotherm essentially identical with that described by Eq. (1). For sulfuric acid we have found that at a given potential a limiting adsorption is attained by a gradual increase of concentration and that this limit is a function of the electrode potential. We formulated this by stating that the maximum coverage, Γ_0, is a function of the electrode potential.

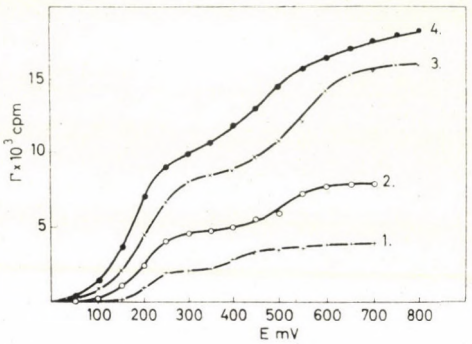

Fig. 6. The potential dependence of adsorption at various concentrations. Curve 1 at 1.3×10^{-5}, Curve 2 at 2.6×10^{-5}, Curve 3 at 1.3×10^{-4} and Curve 4 at 1.3×10^{-3} mole/l of hydrochloric acid

If we accept Eq. (1) as valid for the case of chloride ion adsorption, then the curves for the same concentration (c = constant) can be transformed one into another by dividing the Γ values pertinent to one curve by the adsorbed amount Γ_h pertinent to an arbitrary electrode potential E_h. The relative values thus obtained are denoted by Γ_r:

$$\Gamma_r = \frac{\Gamma}{\Gamma_h} = \frac{f(E)}{f(E_h)} \tag{2}$$

Thus Γ_r is independent of the concentration and A. With $E_h = 700$ mV as the basis of reference, the Γ_r values calculated from results of measurements on a freshly regenerated electrode immersed in hydrochloric acid solutions of various concentrations are collected in Table I.

Fig. 7 is a graphical representation of these data with the boundary curves that include the data.

At first sight, the area defined by the boundary curves seems to be too large. However, considering that as the relative error in any of the data measured is a few per cent, Eq. (1) may be accepted as suitable, at least as a first approximation, for the description of the observed phenomena. At a constant concentration an average curve can be drawn through the area between the boundary curves.This curve gives the generalized potential dependence of adsorption.

Table I*

E mV \ *c* mole/l	2.6×10^{-5}	1.3×10^{-4}	2.6×10^{-4}	6.5×10^{-4}	6.5×10^{-4}	1.3×10^{-3}	1.3×10^{-3}	2.6×10^{-3}	6.5×10^{-3}
50	0.012	0.010	0.017	0.016	0.032	0.029	0.027	0.026	0.017
100	0.038	0.050	0 050	0.056	0.122	0.086	0.110	0.060	0.079
150	0.138	0.134	0.175	0.350	0.271	0.219	0.275	0.166	0.210
200	0.300	0.285	0.309	0.270	0.420	0.371	0.423	0.333	0.342
250	0.519	0.430	0.425	0.388	0.495	0.438	0.492	0.411	0.421
300	0.595	0.524	0.489	0.450	0.516	0.486	0.508	0.465	0.465
350	0.629	0.560	0.513	0.472	0.526	0.514	0.529	0.500	0.491
400	0.637	0.584	0.554	0.494	0.537	0.533	0.540	0.517	0.517
450	0.694	0.632	0.612	0.528	0.569	0.572	0.566	0.552	0.553
500	0.756	0.698	0.714	0.584	0.649	0.638	0.640	0.605	0.605
550	0.918	0.795	0.802	0.686	0.787	0.724	0.777	0.710	0.702
600	0.975	0.926	0.833	0.820	0.910	0.847	0.900	0.865	0.833
650	0.978	0.966	0.947	0.933	0.968	0.933	0.952	0.947	0.929
700	1.000	1.000	1.000	1.000	1.000	1.000	1.000	1.000	1.000
750	1.000	1.050	1.030	1.010	1.040		1.040		
800		1.070	1.065	1.080	1.075		1.075		

* Where concentrations are the same, the data refer to different electrodes.

In order to obtain the generalized potential dependence in analytical form the fact is utilized that the increase in adsorption as a function of the electrode potential, occurs in two sharply distinguished phases, and the analytical form of the functions which describe these phases is similar.

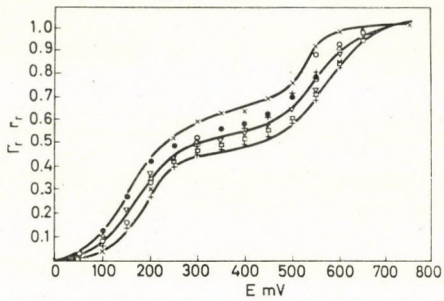

Fig. 7. Boundary curves and average values for the data in Table I

The analogy with the adsorption of hydrogen suggests

$$\Gamma_r = \frac{\Gamma^0 10^{b(E-E_0)}}{1+10^{b(E-E_0)}} \tag{3}$$

as a suitable equation for the description of the two phases mentioned. In Eq. (3), Γ^0, b, and E_0 are constants. Thus the curve composed of two sections can be expressed by the equation

$$\Gamma_r = \frac{\Gamma_1^0 10^{b_1(E-E_{01})}}{1+10^{b_1(E-E_{01})}} + \frac{\Gamma_2^0 10^{b_2(E-E_{02})}}{1+10^{b_2(E-E_{02})}} \tag{4}$$

that contains six unknown constants, and only the knowledge of these allows it to be compared with experimental results. Values for E_{01} and E_{02} can be determined from the inflexion points of the Γ_r *vs.* E curves, or from the maxima of the derivative curves since E_{01} and E_{02} are sufficiently apart. For the determination of b_1 the fact can be utilized that for potentials $E \ll E_{01}$, the approximate relationship

$$\Gamma_r \approx \Gamma_1^0 10^{b_1(E-E_{01})} \tag{5}$$

is valid. The logarithmic form of Eq. (5) corresponds to a straight line the slope of which is b_1. In order to determine b_1, we recorded the initial section of Γ_r *vs.* E curves on various electrodes for small steps of potential. These experiments are summarized in Fig. 8a, which shows that, in fact, the lg Γ_r *vs.* E presentation produces straight lines in conformity to Eqs (4) and (5), and

that, due to the scatter in the individual series of data, these lines are not identical but only parallel.

The determination of Γ_1^0 can be carried out using the correlation

$$\frac{1}{\Gamma_r} = \frac{10^{-b_1(E-E_{01})}}{\Gamma_1^0} + \frac{1}{\Gamma_1^0} \tag{6}$$

which is valid for such potentials where the second term of Eq. (4) is still negligible. If $\frac{1}{\Gamma_r}$ is plotted as the function of $10^{-b_1(E-E_{01})}$, a straight line should result, the slope or the intercept of which is suitable for the calculation of Γ_1^0. The

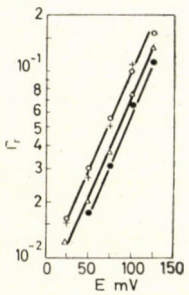

Fig. 8a. Initial section of the lg Γ_r *vs.* E curves for the determination of b_1

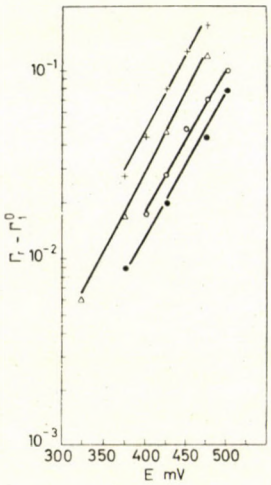

Fig. 8b. Initial section of the lg $(\Gamma_r^0 - \Gamma_1^0)$ *vs.* E curves for the determination of b_2

simplest way of obtaining the values for Γ_1^0 and Γ_2^0 is direct determination from the curves. It follows from Eq. (4) that in the points of inflexion ($E = E_{01}$ and $E = E_{02}$) that $\Gamma_r(E_{01}) = \frac{\Gamma_1^0}{2}$, and $\Gamma_r(E_{02}) = \Gamma_1^0 + \frac{\Gamma_2^0}{2}$, since $E_{01} \ll E_{02}$. If Γ_1^0 is known, b_2 can be calculated. If $E \gg E_{01}$, Eq. (4) assumes the form

$$\Gamma_r = \Gamma_1^0 + \frac{\Gamma_2^0 10^{b_2(E-E_{02})}}{1 + 10^{b_2(E-E_{02})}} \tag{7}$$

which, after treatment similar to that outlined for b_1, yields the value for b_2. In Fig. 8b the $\lg(\Gamma_r - \Gamma_1^0)$ *vs.* E plots are shown. These straight lines are also parallel which seems to support the correctness of the method and gives access to values of the constant b_2. Table II summarizes the values of the constants pertaining to the average curve in Fig. 7, the values for Γ_r^c calculated from these, and also the $\bar{\Gamma}_r$ values of the average curve.

Table IIa

	1	2
Γ_0	0.515	0.515
b	$\frac{1}{90}$ mV^{-1}	$\frac{1}{120}$ mV^{-1}
E_0	175 mV	550 mV

Table IIb

E, mV	Γ_r^c	$\overline{\Gamma_r}$	E, mV	Γ_r^c	$\overline{\Gamma_r}$
50	0.020	0.020	450	0.576	0.586
100	0.066	0.072	500	0.656	0.654
150	0.178	0.192	550	0.771	0.778
200	0.336	0.338	600	0.886	0.883
250	0.450	0.447	650	0.963	0.951
300	0.500	0.500	700	1.000	1.000
350	0.520	0.527	750	1.018	1.028
400	0.539	0.546			

The solid curve in Fig. 9 corresponds to Γ_r^c, and the points represent values of $\overline{\Gamma_r}$.

On the basis of the foregoing we think that Eq. (4) is acceptable as a good approximation for the adsorption of chloride ions.

As far as the interpretation of this correlation is concerned, several ideas can be put forward already about the origin of the two sections. It is possible that the two sections correspond to adsorption on various types of adsorption sites, but it is also possible that they indicate totally different adsorption processes which occur at the same sites. It is highly probable that adsorption is accompanied by some degree of charge transfer. Adsorption after the addition of hydrochloric acid to the cell is accompanied by a positive current pulse on an electrode potentiostatically adjusted to 500 mV and immersed in a 1.0 N solution of perchloric acid, as shown by Curve b in Fig. 10. For comparison, there with the effect caused by sulfuric acid is shown by curve a. The latter effect is significantly weaker.

For the interpretation of the adsorption mechanism only such a theory is acceptable from which it follows that the number of active sites available for adsorption is a function of the electrode potential. Formally, for instance,

we may suppose that an equilibrium process

$$nA + ze^- \rightleftharpoons NA^{*\frac{z}{n}-} \tag{8}$$

occurs, involving charge transfer between sites considered active and inactive from the point of view of adsorption. Here z is the number of charges; A represents inactive and A^* active sites; n is the stoichiometric factor.

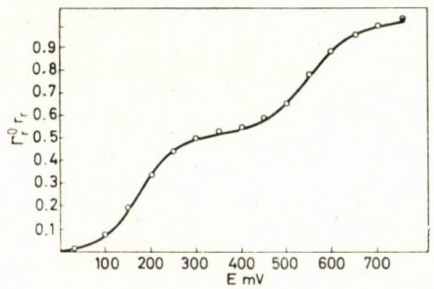

Fig. 9. Comparison of calculated (solid curve), and average values (points) obtained from the curve of averages

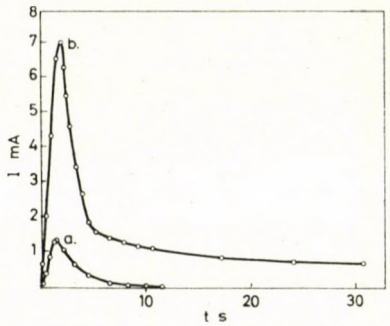

Fig. 10. Current pulse at 500 mV which accompanies the adsorption of *a)* sulfuric acid, and *b)* hydrochloric acid

For this equilibrium it is possible to write

$$E = E_0 + n\frac{RT}{zF}\ln\frac{N_A^*}{N_a - N_A^*} \tag{9}$$

where $N_A{}^*$ is the number of the active sites, and N_a is that of all the sites. Rearrangement of Eq. (9) gives

$$N_{A^*} = N_a \frac{e^{\frac{zF}{nRT}(E-E_0)}}{1 + e^{\frac{zF}{nRT}(E-E_0)}} \tag{10}$$

which essentially corresponds to Eq. (3). As mentioned before, the two sections observed experimentally could be attributed to two different kinds of active sites characterized by different values of E_0, z, and n. The process of aging could then be interpreted as a structural rearrangement accompanied by the convergence of potentials E_0 towards each other. In spite of this the agreement between Eqs (10) and (3) can only be considered formal due to the lack of further evidence therefore further studies are needed for the elucidation of the adsorption mechanism.

REFERENCES

1. BALASHOVA, N. A.: Use of radio-active isotopes in electrochemical studies. Doctoral thesis (in Russian), Moscow, 1966
2. SOLT, J., HORÁNYI, GY., NAGY, F.: Magy. Kém. Foly. **73,** 414 (1967)
HORÁNYI, GY., SOLT, J., NAGY, F.: Magy. Kém. Foly. **73,** 561 (1967)
3. NAGY, F., SOLT, J., HORÁNYI, GY.: Magy. Kém. Foly. **75**, 530 (1969)

György HORÁNYI
János SOLT
Ferenc NAGY

Budapest II., Pusztaszeri út 59—67.

Acta Chimica Academiae Scientiarum Hungaricae, Tomus 68 (1—2), pp. 39—46 (1971)

INVESTIGATION OF ADSORPTION PHENOMENA ON PLATINIZED PLATINUM ELECTRODES BY TRACER METHODS, VI

THE ROLE OF ADSORPTION EQUILIBRIA IN HETEROGENEOUS CATALYTIC HYDROGENATION CARRIED OUT IN AQUEOUS MEDIA

GY. HORÁNYI, J. SOLT and F. NAGY

(Central Research Institute for Chemistry of the Hungarian Academy of Sciences, Budapest)

Received November 24, 1969

On the basis of concrete examples, it has been shown that, contrary to prevailing views, during catalytic hydrogenation and electrohydrogenation in an aqueous media, no adsorption equilibrium of the substrate can be postulated. Accordingly, the concepts about the kinetics of these reactions need revision. In this context some general considerations have been put forward.

In studies of heterogeneous catalysis it is the changes in the bulk concentration which furnish the basis for conclusions concerning the reactions which occur at the phase boundaries. It is necessary to make certain more or less justified assumptions, to pave the way of inferences about concentrations at the interface, drawn from concentration data proper to the bulk of the respective phases.

So, in a great number of papers about heterogeneous catalytic hydrogenation, it is assumed that both the adsorption steps preceding reaction and the corresponding desorption process are rapid, consequently, an adsorption equilibrium involving all the components which take part in the reaction is maintained [1].

The assumption of an equilibrium is of principal significance since only such an equilibrium allows, using the adsorption isotherms, to make on estimate of the surface concentrations on the basis of concentrations measured in the homogeneous phases. In what follows we propose to show that in numerous cases it is not justified to suppose that an adsorption pre-equilibrium is maintained during hydrogenations carried out on platinum in aqueous media at room temperature.

1. Problem of the existence of an adsorption equilibrium

Questions concerning the adsorption of organic compounds on platinum surfaces from aqueous media are discussed by the steadily expanding literature of electrosorption [2].

However, the literature data concerning the adsorption equilibrium of such compounds are contradictory. The adsorption of ethylene and benzene

representatives of the unsaturated and aromatic class of compounds, on platinum, has been extensively studied by BOCKRIS *et al.* [3]. According to these authors, adsorption from aqueous media involves the following equilibrium:

$$S_o + n(H_2O)_a \rightleftharpoons n(H_2O)_o + S_a \qquad (1)$$

where S stands for the substrate, and subscripts *o* and *a* refer to the solution and the adsorption phase, respectively. From the equilibrium constants reported by the authors, it follows that at room temperature saturation is reached already at rather low concentrations (10^{-6} to 10^{-5} mole/l) of the adsorbate.

The equilibrium constant does not indicate, however, the magnitude of the rate constants of adsorption and desorption, though it is obvious that if a reaction occurs, it will be the absolute values of these rate constants which will determine whether or not an adsorption pre-equlibrium can be assumed.

Our observations up to now seem to suggest that for a rather wide variety of adsorbates the rate of the overall adsorption process is determined by the rate of diffusion [2], *i.e.* the rate of adsorption is high or at least higher than that of diffusion.

However, little is known about the rate of desorption. This rate can be studied, by means of tracers, following the exchange adsorbed molecules either so that molecules in the adsorbed phase or those in the solution are labelled with ^{14}C.

Many experiments have been carried out by both methods; in what follows a number of concrete experiments will serve as examples illustrating our observations.

2. Study of desorption rates

The apparatus previously described [4] was used. As shown in an earlier paper [5], in the present method the adsorption of labelled species is recorded directly, by measuring the radiation that arrives from the surface. In the experiments to be discussed here, we proceeded as follows. The electrode immersed in a 1.0 *N* solution of perchloric acid was adjusted to such a potential at which no reaction of the adsorbed species occurs, *i.e.* neither oxidation nor hydrogenation should be expected. Then the adsorbate, labelled with ^{14}C, was added to the system. After the adsorbed amount (c.p.m.) had attained a constant level, the inactive component was added in large excess at the time indicated by an arrow on the curve. In this case, in view that the overall specific activity of the adsorbed species is reduced by two or three orders of magnitude, possible further adsorption escapes observation: thus it is un-

equivocally the desorption process that is being followed, and the decrease in the counts per minute gives the rate of desorption.

The desorption rates of acetone and phenylacetic acid are shown in Figs 1 and 2, respectively. In the way described, acetone was added at 300 mV, while phenylacetic acid at 400 mV, to the system. Had a true dynamic adsorption–desorption equilibrium in fact existed, a decrease of c.p.m. should have occurred at any potential at a rate corresponding to the rate of desorption until the c.p.m. coming from the surface did not fall below 1% of the original value.

However, as shown by the Figures, an appreciable exchange of the labelled component occurs only at such potentials ($E \leq 200$ mV) where hydro-

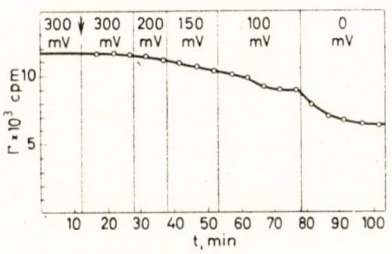

Fig. 1. Desorption rate of acetone at various electrode potentials

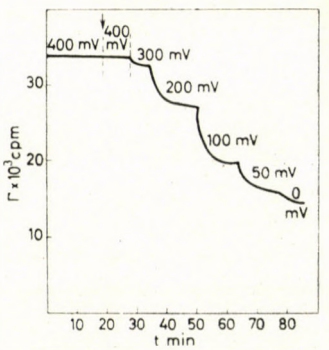

Fig. 2. Desorption rate of phenylacetic acid at various electrode potentials

genation also has to be taken into account. It is remarkable that the exchange rate decreases significantly within a relatively short time at each potential, and further exchange is observed only when the potential is shifted towards more negative values. The rate of hydrogenation, referred to 1 cm^2 of the geometrical surface, at potentials more negative than 100 mV, is in the mA range, consequently, if the active component adsorbed on the surface were completely removable by reaction, the half-life of the observed decrease in c. p. m. should be in the order of seconds. The observed picture contradicts this, thus the interpretation of the phenomenon requires further assumptions, *e.g.* that of a heterogeneous surface. If only one desorption or reaction rate constant is operative the c.p.m. would decrease exponentially with time.

For a comparison, Figs 3 and 4 show the exchange of acetic and hydrochloric acids, followed in exactly the same way as that of acetone and phenylacetic acid. Both acetic acid and hydrochloric acid (or chloride ions) exhibit significant specific adsorption. For labelling ^{14}C and ^{36}Cl were used.

In these cases the exchange is very rapid already at the starting potentials and is practically complete within a short time.

The comparison of Figs 1 and 2 with Figs 3 and 4 unequivocally shows that, apart from rapid responses to changes of potential, the desorption rate of acetone and phenylacetic acid is very low.

Owing also to these low rates of desorption, the occurrence of an adsorption equilibrium cannot be accepted without reserve. Obviously, a slow reac-

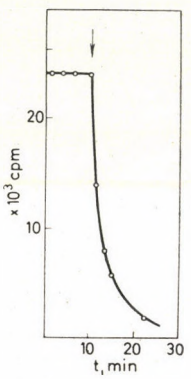

Fig. 3. Desorption of acetic acid at 700 mV

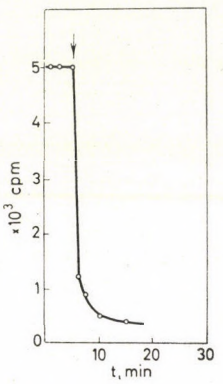

Fig. 4. Desorption of hydrochloric acid at 400 mV

tion which occurs at a rate proportional to the coverage, may suggest the apparent existence of an adsorption isotherm.

In the steady state, the following expression can be written for the reaction rate

$$w = k_A c(1 - \Theta_s) = k_r \Theta_s \tag{2}$$

where k_A is the rate constant of adsorption, k_r is the rate constant of the reaction, and Θ_s is the stationary coverage by the adsorbed species.

Rearrangement of Eq. (2) produces a relationship between concentration and coverage that has the form of the Langmuir isotherm, *viz.*

$$\Theta_s = \frac{\frac{k_A}{k_r} c}{1 + \frac{k_A}{k_r} c} \tag{3}$$

At any rate it can be concluded from what has been said that at appreciable rates of hydrogenation no adsorption pre-equilibria seem possible irrespective of whether or not adsorption equilibria as such do exist.

3. Connection between the adsorption of hydrogen and substrate

As found in former experiments [6], in the presence of unsaturated compounds the adsorption of hydrogen decreases: thus a displacement effect in adsorption was postulated. In the presence of acetone (Fig. 5) and phenylacetic acid (Fig. 6) these adsorbates do not interfere with the adsorption of hydrogen, as witnessed by the hydrogen adsorption section ($E < 300$ mV)

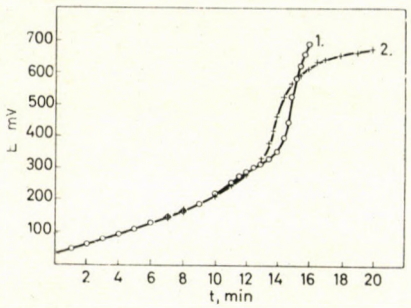

Fig. 5. Galvanostatic charging curves: 1. in the supporting electrolyte (1.0 *N* perchloric acid); 2. after addition of 10^{-2} mole/l of acetone

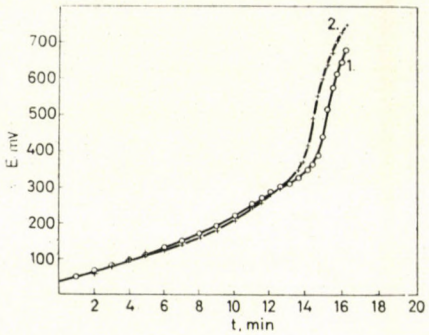

Fig. 6. Galvanostatic charging curves: 1. in the supporting electrolyte (1.0 *N* perchloric acid); 2. after addition of 10^{-2} mole/l of phenylacetic acid

of the charging curves. In these cases the adsorption of hydrogen and substrate are independent of each other, thus it may be supposed that different active centers are involved in the adsorption of the two components.

4. Aging of the electrode and permanent adsorption

In desorption experiments we have seen that part of the adsorbed substance is not removed even during hydrogenation reaction. Thus this fraction must be regarded as permanently adsorbed.

The permanently adsorbed fraction cannot be removed but by vigorous oxidation, as shown for phenylacetic acid in Fig. 7. In this case after the adsorption of labelled phenylacetic acid, a large excess of the inactive compound was added to the system and hydrogenation started. After allowing the fraction permanently adsorbed at 0 mV, *i.e.* the part not removed during reaction, to become constant, the potential of the electrode was shifted, by means of a potentiostat, towards positive values. As shown in Fig. 7, a significant diminution of the permanently adsorbed fraction did not begin below 700 mV.

This explains the role of anodic regeneration used in the case of electrohydrogenation. At the same time some light is shed upon the cause of the aging processes. According to our experimental findings, the amount of per-

manently adsorbed fraction changes in time, roughly in parallel with the aging of the electrode, *i.e.* the catalyst.

Accordingly, aging in this case is due to irreversible adsorption of the molecule perhaps accompanied by bond fission rather than to adsorption of impurities.

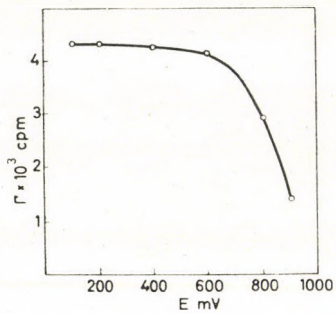

Fig. 7. The removal of the permanently adsorbed fraction of phenylacetic acid at positive potentials

5. Kinetics of electrohydrogenation

According to what has been found, only unidirectional processes (adsorption, reaction) of the substance seem to exist.

In the steady state the rate of electrohydrogenation at a given potential is described by

$$w = k_D (c_0 - c_f) = k_A c_f (1 - \Theta_s - \Theta_M) = k_r \Theta_s \tag{4}$$

where k_D, k_A and k_r are the rate constants of diffusion, adsorption and the reaction, respectively, c_0 and c_f are concentration of the reactant in the solution and at the electrode surface, respectively. Θ_s and Θ_M are steady-state coverage by the mobile and the permanent fraction, respectively. Rate constant k_r includes the potential dependence of the rate and the dependence of the rate on hydrogen adsorption or activity. If there is no diffusion control, then $c_f \approx c_0$, and the stationary coverage by the mobile fraction is

$$\Theta_s = \frac{1 - \Theta_M}{1 + \dfrac{k_r}{k_A c_0}} \tag{5}$$

and the reaction rate is

$$w = \frac{k_r (1 - \Theta_M)}{1 + \dfrac{k_r}{k_A c_0}} \tag{6}$$

As pointed out when the adsorption equilibrium was discussed, rate equation (6) is identical in form with that for a process involving adsorption pre-equilibrium described by a Langmuir-type isotherm.

In the literature generally this mechanism is accepted when a rate equation of type (6) is applicable.

This was the case *e.g.* in a recent communication [7] about the interpretation of phenomena observed during the hydrogenation of acetone in acid media. Our experimental findings, and what has been said here, seem clearly to demonstrate that in that case no pre-equilibrium is possible, thus the authors must have formed an erroneous concept about the mechanism.

Depending on the value of the term $\frac{k_r}{k_A c_0}$, Eq. (6) may assume various forms, *viz.*

a) if $k_r \gg k_A c_0$,

$$\Theta_s \approx \frac{k_A c_0}{k_r}(1 - \Theta_M) \tag{7}$$

and

$$w \approx k_A c(1 - \Theta_M);$$

b) if $k_r \ll k_A c_0$,

$$\Theta_s \approx 1 - \Theta_M \tag{8}$$

and

$$w \approx k_r(1 - \Theta_M).$$

The electrohydrogenation of acetone also furnishes an example for case (7), as has been shown in a previous communication [8]. There when varying the electrode potential, a limiting current unaffected by stirring or by the electrode potential was attained at a given acetone concentration, for k_r is a function of the potential. In such cases the reduced limiting current clearly reflects the aging of the electrode, or the increase of Θ_M.

The case defined by Eq. (8) has been discussed in former communications [9]. In such cases the reaction rate is a function of k_r only and is governed by the electrode potential alone.

Much more complicated correlations emerge when all three steps have to be considered simultaneo ısly. Then

$$w = \frac{k_A k_D c_0 + k_r k_D + k_A(1 - \Theta_M)}{2k_A} \pm$$

$$\pm \frac{\sqrt{[k_A k_D c_0 + k_r k_D + k_A(1-\Theta_M)]^2 - 4k_r k_A [k_A k_D c_0 (1-\Theta_M)]}}{2k_A}$$

Here we wish to note that the ratio of adsorption to mass transport by diffusion depends very much on the quality of the electrode surface. Mass

transport by diffusion is proportional to the geometrical surface area while in adsorption processes the true surface is involved. Thus the adsorption rates per cm^2 of the geometrical surface include also the roughness factor. In consequence, through changes of the roughness factor it is possible to affect substantially the ratio of the rates of the various steps. Thus it may happen that in the case of the same reaction, at one time diffusion and at another time adsorption or reaction is rate-limiting, depending on the magnitude of the roughness factor.

In summary, we may state that under the conditions of heterogeneous catalytic hydrogenation in aqueous media, in the cases studied and for the class of compounds used as models, an adsorption pre-equilibrium of the substrate cannot be assumed, and there are doubts that an adsorption equilibrium can exist at all. Accordingly, the concepts about the kinetics of heterogeneous catalytic reactions of the above types of compounds seem to need some modifications. General points of view pertinent to this question have been put forward in this paper.

REFERENCES

1. SOKOLSKY, D. V.: Gidrirovanie v rastvorach. Alma-Ata, 1962
2. GILEADI, E.: Electrosorption. New York, Plenum Press, 1967
   DAMASKIN, B. B. et al.: Adsorbtsia organicheskikh soedinenii na elektordakh. Moskow, 1968
3. GILEADI, E., RUBIN, B., BOCKRIS, J. O'.M.: J. Phys. Chem. **69,** 3335 (1965)
   BOCKRIS, J. O' M.: J. Phys. Chem. **70,** 1207 (1966)
4. SOLT, J., HORÁNYI, GY., NAGY, F.: Magy. Kém. Foly. **73,** 414 (1967)
5. HORÁNYI, GY., SOLT, J., NAGY, F.: Magy. Kém. Foly. **73,** 561 (1967)
   SOLT, J., HORÁNYI, GY., NAGY, F.: Magy. Kém. Foly. **74,** 52 (1968)
6. HORÁNYI, GY., SOLT, J., NAGY, F.: Magy. Kém. Foly. **75,** 539 (1969)
7. HEMPTINNE, X. de, SCHUNCK, K.: Trans. Faraday Soc. **65,** 591 (1969)
8. HORÁNYI, GY., SOLT, J., SZABÓ, S., NAGY, F.: Magy. Kém. Foly. **76,** 333 (1970)
9. NAGY, F., TELCS, I., HORÁNYI, GY.: Acta Chim. Acad. Sci. Hung. **37,** 295 (1963)

György HORÁNYI
János SOLT
Ferenc NAGY

Budapest II., Pusztaszeri út 59—67.

Acta Chimica Academiae Scientiarum Hungaricae, Tomus 68 (1—2), pp. 47—59 (1971)

INVESTIGATION OF THE ELECTROCHEMICAL PROPERTIES OF SOME AMINOAZOBENZENE DERIVATIVES, I

THE ELECTROCHEMICAL REDUCTION MECHANISM OF 4-AMINOAZOBENZENE, 2,4-DIAMINOAZOBENZENE AND 4'-ETHOXY-2,4-DIAMINOAZOBENZENE

L. Ladányi, M. Vajda* and Gy. Vámos

*(Institute of Inorganic and Analytical Chemistry, L. Eötvös University, Budapest and *Institute of Organic Chemistry, L. Eötvös University, Budapest)*

Received November 14, 1969

The mechanism of the electrochemical reduction of some derivatives of aminoazobenzene (4-aminoazobenzene (**I**), 2,4-diaminoazobenzene (**II**) and 4'-ethoxy-2,4-diaminoazobenzene (**III**) was investigated using voltammetric, constant potential electrolytic, and UV-visible spectrophotometric methods. It was found that the overall two-electron reduction of the azo group is a two-step process. It proceeds through an intermediate formed from the azo group by addition of one electron either with an ECE mechanism or through a disproportionation step. Further disproportionation of the hydrazo group leads to an overall four-electron reduction. The examination of the electrochemical properties of the aromatic amines formed (1,2,4-triaminobenzene and 1,4-phenylenediamine) made it possible to elucidate details of the reduction mechanism.

Introduction

The investigation of the electroreduction of 4-aminoazobenzene (**I**), 2,4-diaminoazobenzene ('chrisoidine', **II**) and 4'-ethoxy-2,4-diaminoazobenzene ('*p*-ethoxychrisoidine', **III**) was prompted firstly by the great differences between the behaviour of these compounds and that of the very thoroughly studied azobenzene–hydrazobenzene system [1, 2, 3] and secondly by the hope that the study of the electrochemical properties of these compounds will assist in the more profound understanding of their function as indicators.

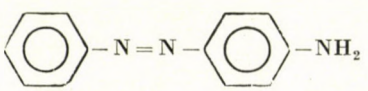

I

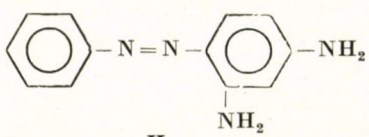

II

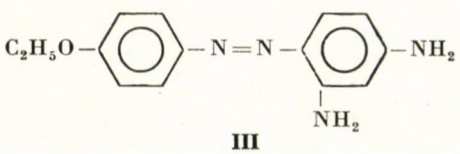

III

Experimental

Materials

4-aminoazobenzene (Fluka), Chrisoidine. HCl, *p*-Ethoxy-chrisoidine.HCl (Michrome), 1,2-diamino-4-nitrobenzene (EGA Chemie KG) were used as supplied.

The buffers used were prepared according to CLARK and LUBBS (pH 1.0—2.0) and BRITTON—ROBINSON (pH 2—12). Oxygen was removed by high purity nitrogen (specified purity 99.995% N_2, Budapest Oxygen Works). All solutions were prepared with bidistilled water.

Polarographic maxima were suppressed by a freshly prepared gelatine solution.

Instrumentation

Voltammograms were recorded with a Radiometer PO-4-g polarograph and a Metrohm E 446 IR compensator, using the usual three-electrode system and a water-jacketed cell. The temperature was kept constant at 25.0 ± 0.1 °C. Electrode potentials were measured against a saturated calomel electrode with an accuracy of ± 5 mV.

The working electrodes used were paraffin-impregnated spectroscopic graphite [4] (rod-form), carbon paste [5] and the dropping mercury electrode. Constant potential electrolyses were performed on a stirred mercury pool and a platinum spiral separated by a fritted glass disc.

pH values were measured with an accuracy of ± 0.01 pH unit (RADELKIS OP-205 Precision pH-Meter).

Absorption spectra were recorded on a UNICAM SP 700 instrument using 1 mm infrasil cells.

Preparation of solutions

Stock solutions of the compounds under investigation were prepared in 96% alcohol. Aliquots were diluted to given volumes with the appropriate buffer and the pH values measured. In a given series of experiments, the alcohol and depolarizer concentration were kept constant.

Results

1. Preliminary investigation

The cyclic voltammogram of **I** on a carbon paste electrode is shown in Fig. 1. **II** and **III** gave qualitatively similar voltammograms. As the figure shows, the wave obtained in the first cathodic cycle (wave *A*) is completely irreversible. At more positive potentials, on the other hand, a reversible redox system (*B*, *C*) can be seen which appears only after the first cathodic sweep. Further cycles show no new data.

For the purpose of identifying the type of current causing the waves, peak-current (i_p) *vs.* square root of scan rate ($V^{1/2}$) diagrams were plotted. These gave straight lines in the region of 0.1—0.8 V/min. This fact [6], the temperature coefficient, and the dependence of the limiting current on mercury pressure at the DME (see Table I) show that the waves are diffusion-controlled.

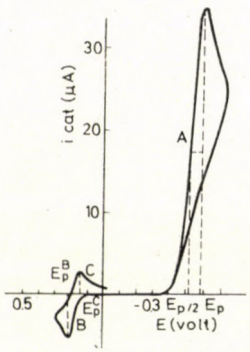

Fig. 1. Cyclic voltammetry of **I** on a carbon paste electrode. $C^\circ = 5.00 \times 10^{-5}$ *M*; pH = 6.21; scan rate 0.8 V/min; $C_{\text{alcohol}} = 10.0\%$ *v/v*

2. *pH-Dependence of the cyclic voltammetric curves*

E_p *vs.* pH values of the first cathodic wave (*A*) are shown in Figs 2, 3 and 4.

The E_p *vs.* pH plot of **I** is a straight line, while those of **II** and **III** show two breaks on the graph giving three straight sections with slopes of 0.06, 0.03 and 0.06 V/pH, respectively. The second break corresponds to the pK_2 value in the case of **II** [7]. No pK_a data for **III** were found in the literature.

It is noteworthy that $E_{p/2} - E_p$ values for the waves *A* are 57 ± 5 mV throughout the whole pH-range studied in the case of **II** and **III** and up to pH = 4.4 in the case of **I**.

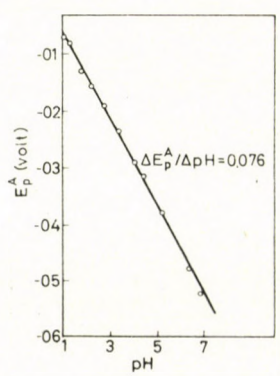

Fig. 2. Peak potential *vs.* pH diagram for **I** on a paraffin-impregnated graphite. $C^\circ = 5.00 \times 10^{-5}$ *M*; $C_{\text{alcohol}} = 5.0\%$ *v/v*; scan rate: 0.1 V/min

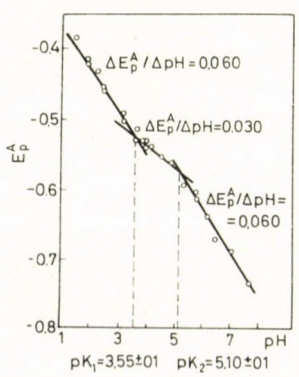

Fig. 3. Peak potential *vs.* pH diagram for **II** on a carbon paste electrode. $C^\circ = 4.00 \times 10^{-4}$ *M*; $C_{\text{alcohol}} = 20.0\%$ *v/v*; scan rate = 0.8 V/min

Using an impregnated graphite electrode we succeeded to obtain the E_p *vs.* pH diagram of the wave *B* of chrisoidine (**II**) (Fig. 5). The fairly flat peaks and therefore ill-defined potentials made it impossible to construct this function with sufficient precision in the case of the other two compounds.

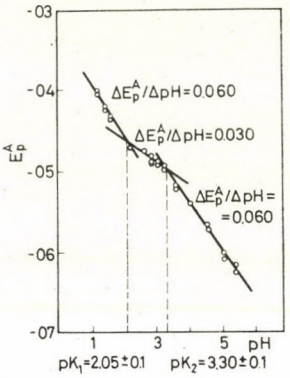

Fig. 4. Peak potential *vs.* pH diagram for **III** on a carbon paste electrode. $C^\circ = 4\times10^{-4}$ *M*; $C_{alcohol}$ = 20.0% *v/v*; scan rate = 0.8 V/min

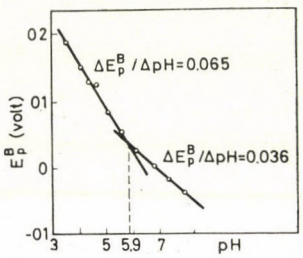

Fig. 5. Peak potential *vs.* pH diagram for Wave *B* of **II** on a paraffin-impregnated graphite electrode $C^\circ = 5.00\times10^{-5}$ *M*; $C_{alcohol}$ = 5.0% *v/v*; scan rate = 0.8 V/min

2. Polarography, constant potential reduction, coulometry

All three compounds are reducible at the DME in a single step. Their polarographic behaviour is summarized in Table I.

Table I

D. C. polarography of some azo compounds

pH = 3.80; Temperature: 25 ± 0.1°C; $m^{2/3}\cdot t^{1/6} = 2.951$ $mg^{2/3}$ $sec^{-1/2}$; $C = 1.00\times10^{-3}$ *M*; h = 78.2 cm

Compound	I^*	$E_{1/2}$ V	$\frac{\log i_d}{\log h}$	temp. coeff. of i_d (% °C) temp. range: 20—40 °C	log. plot anal. ($C=5\times10^{-4}$ *M*) $\log\frac{i_d-i}{i}=f(E)$ (V/log unit)	$i_d=f(C)$ function (conc. range: 10^{-3}—10^{-4})
4-aminoazobenzene(II)	5.09	−0.353	0.45	2.44	0.058	linear
2,4'-diaminoazobenzene (II)	4.42	−0.354	0.50	1.76	0.058	linear
4-ethoxy-2,4-diamino-azobenzene(III)	3.82	−0.406	0.50	1.75	0.057	linear

* Diffusion current constant
$I = i_d/m^{2/3}t^{1/6}C$
($\mu A/mg^{2/3}sec^{-1/2}mM$)

All three compounds were reduced potentiostatically on a stirred mercury cathode on the limiting current section of the polarographic wave ($E = -0.90$ V). The reduction was accomplished in discrete periods. (The time for one period corresponded with the time necessary for the filling of the H_2—N_2 gas coulometer [8]). After the reduction was interrupted, a polarogram was recorded. Constant potential reduction was resumed as soon as the

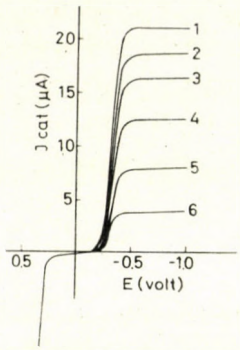

Fig. 6. Current-voltage curves (2—6) obtained during the *CP* reduction of **I** on a DME. Curve 1: polarogram obtained before electrolysis. $C^\circ = 1.00 \times 10^{-3}$ *M*; $C_{alcohol} = 20.0\%$ *v/v*

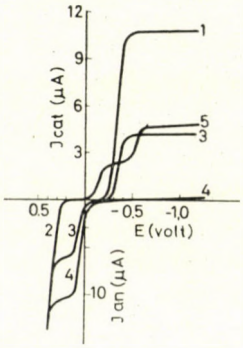

Fig. 7. Current voltage curves (DME) obtained during the *CP* electrolysis of **II**. $C^\circ = 1.00 \times 10^{-3}$ *M*; $C_{alcohol} = 20\%$ *v/v*. 1: cathodic scan before electrolysis. 2: anodic scan before electrolysis (mercury dissolution curve), 3: curve obtained during the *CP* reduction (see Section 3 in Table II), 4: curve obtained after completion of the *CP* reduction, 5: curve obtained after completion of the re-oxidation of the reduced product

polarogram was taken. We computed the amount of charge passed during the reduction of the amount of depolarizer reduced in each period (from the difference of the polarographic wave heights and the data obtained by coulometry). We also obtained the number of electrons involved in the reduction of one mole of depolarizer (n).

The polarograms recorded during the constant potential reduction of **I** and **II** and the anodic oxidation of the reduced product of **II** at $E = +0.08$ V are shown in Figs 6 and 7.

Polarograms obtained during the CP electrolysis of **III** are very similar to those of **II**.

It can be seen from Fig. 7 that concurrently with the lowering of the limiting curve of the reduction step of **II**, an anodic wave appears ($E^0_{1/2} = +0.04$ V) occurring just prior to the rise of the anodic background current. In the case of **I**, this anodic wave coalesces with this mercury dissolution curve, although it can be observed clearly on a graphite or carbon paste electrode (Fig. 1). It can also be seen that after anodic re-oxidation of the solution of reduced **II** (or **III**), a new compound is formed which is reduced at the DME in two steps of identical height. ($E^1_{1/2} = -0.15$ V, $E^2_{1/2} = -0.53$ V.)

The number of electrons involved in the successive steps determined coulometrically are shown in Table II. This table also gives the ratio of the diminishing of the cathodic wave ($\Delta i_{red} = i_0 - i_{red}$) to the growth of the anodic wave (i_{ox}) in the period in question, as calculated from the beginning of the electrolysis $\left(\frac{\Delta i_{red}}{i_{ox}}\right)$.

From this table the following conclusions can be drawn:

1. The number of electrons involved as obtained from coulometric measurements — excepting the series of **II** at pH = 6.2 — are much larger than the theoretically expected highest value ($n = 4$).

2. The ratio $\frac{\Delta i_{red}}{i_{ox}}$ has a value of approximately 2.

We then determined the number of electrons involved in the oxidation step using the method outlined above. This was accomplished after complete

Table II

Macro scale electrolysis and coulometry of some azo-compounds

Compound	4-aminoazobenzene (I)		2,4-diaminoazobenzene (II)		4′-ethoxy-2,4-diaminoazobenzene (III)		2,4-diaminoazobenzene (II)	
pH	3.80		3.80		3.80		6.05	
	n	$\frac{\Delta i_{red}}{i_{ox}}$	n	$\frac{\Delta i_{red}}{i_{ox}}$	n	$\frac{\Delta i_{red}}{i_{ox}}$	n	$\frac{\Delta i_{red}}{i_{ox}}$
Period 1	uncertain	—	4.5	uncertain	9.6	1.62	4.7	1.74
Period 2	14.0	—	5.8	2.05	9.2	1.63	4.7	1.80
Period 3	9.8	—	6.4	2.04	8.7	1.81	4.7	1.83
Period 4	8.2	—	7.3	2.01	8.7	1.80	4.7	1.81
Period 5	8.0	—	—	1.69*	8.5	1.73	—	—

* Value determined after the complete reduction of the depolarizer.

reduction of **II** or **III** at $E = +0.08$ V. The following values were obtained:

II.	(pH = 3.8)	1.6
II.	(pH = 6.05)	1.8
III.	(pH = 3.8)	1.7

Logarithmic analysis of the anodic wave of **II** at pH = 3.8, gave a slope of 0.035 V/log unit corresponding to $n = 2$.

4. Spectroscopic investigation of the electrolysis products

After completion of constant potential electrolytic reduction, the UV-visible spectra of the solutions were recorded. These spectra were compared with those of 1,2,4-triaminobenzene* (**IV**) and aniline (**V**) solutions prepared under identical conditions ($c = 1.00 \times 10^{-3}$ *M*, pH = 3.80, $c_{\text{alcohol}} = 20\%$ *v/v*).

Comparison of the spectra showed that:

1. the spectra of the reduced solution of **II** were identical with those obtained by the superposition of the spectra of **IV** and **V**;

2. the spectra of the solutions obtained after constant potential oxidation of the reduced solution of **II**, **III** and **IV** are very similar. The absorption band appearing at 18,800 cm^{-1} is especially characteristic.

In the case of **I** the anodic wave cannot be observed polarographically, as mercury is oxidized before this wave appears. Therefore we identified the redox system appearing on the cyclic voltammograms by the following experiment.

In addition to the experiments mentioned above, the cyclic voltammogram of **I**, **V** and *p*-phenylenediamine (**VI**) were recorded under identical conditions ($c = 5 \times 10^{-4}$ *M*, pH = 5.85, $c_{\text{alcohol}} = 10\%$ *v/v*, indicator electrode: carbon paste, Fig. 8).

From the comparison of the voltammograms the following can be concluded:

The new redox system (waves *B*, *C*) appearing after the reduction of **I** is due to the formation of **VI** and its oxidized form (1,4-benzoquinone diimine, **VII**) [10, 11].

2. **V** is only oxidized at much more positive potentials than **I**, and the redox system (waves *E*, *F*) appearing is not identical with the system mentioned above.

* Solutions of 1,2,4-triaminobenzene (**IV**) were obtained by the constant potential reduction of 1,2-diamino-4-nitrobenzene (pH = 3.80, $c_{\text{alcohol}} = 20.0$ *v/v*%, $c = 1.00 \times 10^{-3}$ *M*). The nitro-compound is reduced at the DME in a single 6-electron step [9]. During this reduction we also observed an anodic step identical in all respects with that observed during the reduction of **II** and **III** ($E_{1/2} = 0.04$ V). Constant potential oxidation of the reduced solution at $E = 0.08$ V gave an n value of 2.1.

3. The new redox system formed in the reduction of II and III is identical with that of 1,2,4-triaminobenzene and its oxidized form (*cf.* footnote, page 53).

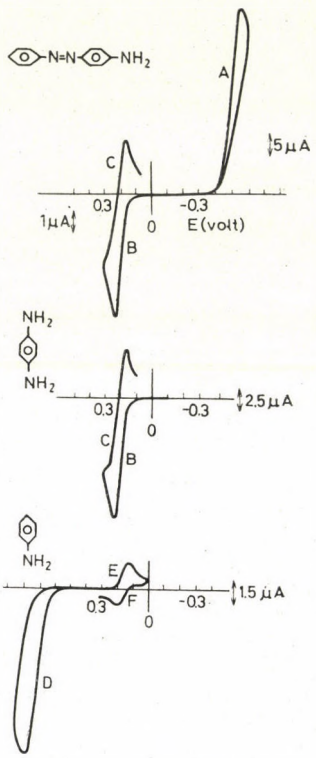

Fig.8. Cyclic voltammetry of **I**, **V** and **VI** on carbon paste electrodes

Discussion

The published data on the electrochemical reduction of aromatic azo-compounds can be summarized as follows.

Azobenzene is reduced in a two-electron step to hydrazobenzene. Hydrazobenzene in turn is oxidized in a similar process to azobenzene. If an aromatic azo-compound has nucleophilic substituents in the *ortho* or *para* positions, four-electron overall reduction processes are often encountered [12—14]. FLORENCE [15] suggests that the primary product in this case is also the hydrazobenzene derivative. The disproportionation of this yields 50% of the starting azo-compound and 50% of the product of a four-electron reduction (*ortho* or *para* substituted derivative of aniline). If this process is repeated several times at the electrode during the life-time of one drop, the limiting

current of the reduction wave approaches the n-value of 4. If the process is so slow that no disproportionation occurs during the life of the drop, the number of electrons involved is the lower limit of $n = 2$, *i.e.* the observed number of electrons can be any value between 2 and 4. This suggestion is in accord with the experimental results in the paper mentioned.

In aprotic solvents (acetnitrile, dimethylformamide) azo-compounds are reduced in two successive one-electron steps, the intermediate being a stable radical [16, 17]. HILLSON and BIRNBAUM [18] attempted to interpret the $E_{1/2}$ vs. pH function of *cis*- and *trans*-azobenzene by assuming that the reduction proceeds in two successive steps even in aqueous solutions, although the polarogram only shows one two-electron reduction wave. NYGÄRD [19, 20] investigated the adsorption of the azo–hydrazo system and came to the same conclusion.

In our case the similarity of the cyclic voltammograms seems to suggest an identical reaction mechanism for all three compounds.

Our results show conclusively that the number of electrons involved in the overall reduction step is 4, and that the new redox systems are the compounds suggested.

On the other hand, the pH dependence of the E_p values of **II** and **III** points to a two-electron process [21] (*cf.* the reduction of methylene blue). The explanation of this is that the disproportionation of hydrazo-compounds can lead to a four-electron step. As this process is a subsequent chemical reaction, it does not influence the slope of the wave, but only shifts it to more positive values [22].

Let us now examine the azo–hydrazo transformation in our case. If we assume a fast charge-transfer (charge-transfer rate constant $k > 0.2\ v^{1/2}$ cm sec^{-1}) [23], the equation

$$E_{p/2} - E_p = \frac{0.057}{n} V \tag{1}$$

can be considered valid, although it has been derived for the 'reversible' case. Thus, assuming the validity of (1), the azo–hydrazo transformation would involve only one electron which is impossible. Therefore, the overall two-electron process has to occur in two steps. This can be either an ECE mechanism or a disproportionation [24]. Assuming that the chemical reactions are not rate-determining, a possible mechanism in the case of **II** would be (see Scheme on p. 56). As E_1^0 is more negative than E_2^0, only one wave can be observed in the case of ECE mechanism. The assumption that the chemical reaction is not rate-determining is substantiated by the fact that the waves are diffusion-controlled.

Naturally this is only one of the possible mechanisms. Nevertheless, it is necessary in all mechanisms that the single-electron reduction product

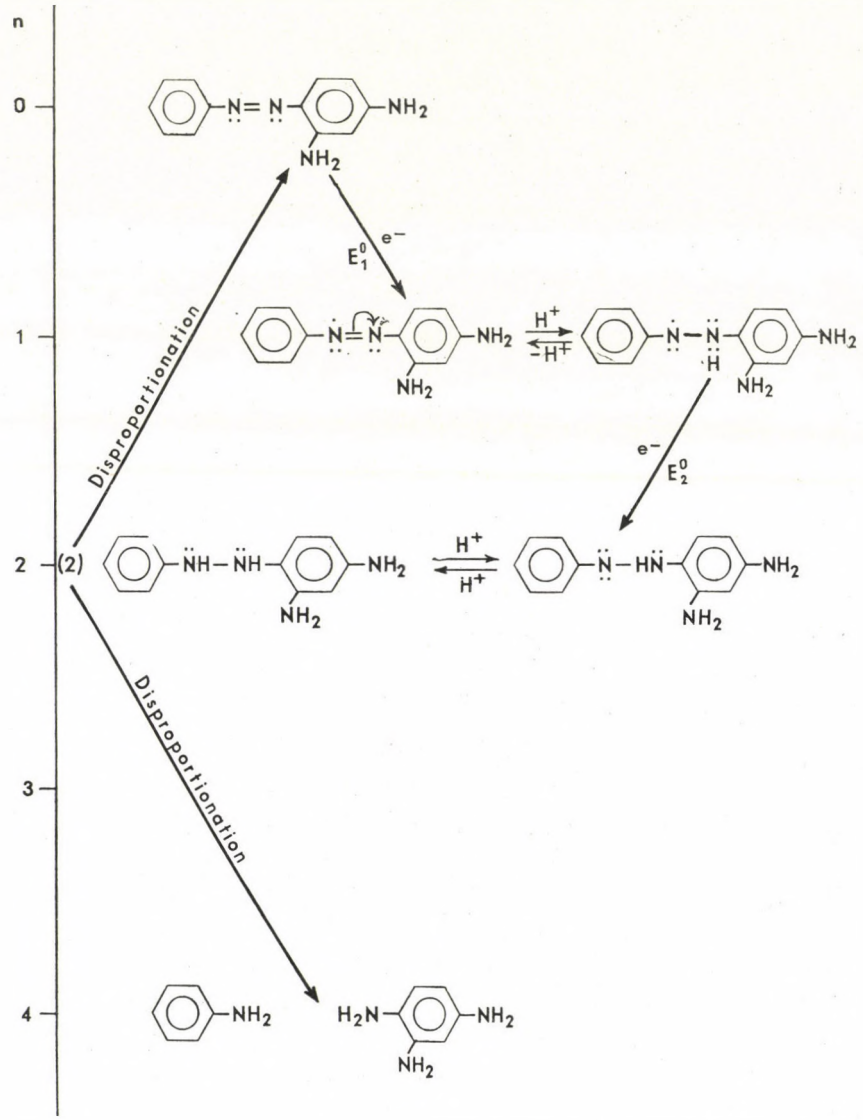

should be formed as shown by the $E_{p/2}$—E_p value of about 0.057 V. The E_p—pH diagrams constructed from our voltammograms, taking low polarization rates (0.1—0.8 V min^{-1}) can, of course, only show the overall reaction.

Results obtained from the logarithmic analysis of waves recorded at the DME (Table I) are in harmony with the results mentioned above. We obtained $E = f\left(\log \frac{i_d - i}{i}\right)$ functions with slopes of 0.06 V, *i.e.* the slope of a formally one-electron step [25].

The product on the other hand is formed in a 4-electron reduction and the formation of a hydrazo-compound as an intermediate must occur. Its formation is substantiated by the E_p—pH function of **II** and **III**. Therefore, we must conclude that the one-electron reduction is only a formally one-electron process.

In the case of *I* the E_p *vs.* pH diagram was constructed using data obtained with an impregnated graphite electrode, as the data obtained on carbon-paste were not sufficiently reproducible. As Fig. 2 shows, the measured values are on a straight line, showing no breaks. This suggests that if $pH > pK_a$ ($pK_a = 2.8$) [26], a chemical reaction precedes electron-transfer causing the deprotonation of the ammonium group before reduction.

As Table II shows, the determination of n at pH = 3.8 by coulometry, gives values significantly higher than 4. This can only be interpreted by assuming that intermediates formed during constant potential electrolysis on a macro-scale, are partially re-oxidized in chemical reactions before the final product is formed. (The reoxidation of the end-product does not occur according to our experience.) Literature data [27] prompt us to suggest the spontaneous decomposition of the protonated radical (AH.)

$$AH^{\cdot} \rightarrow A + 1/2\ H_2$$

or the reaction of the non-protonated form with water

$$A^- + H_2O \rightarrow A + 1/2\ H_2 + OH^-$$

The n-values of about 4.7 obtained from the reduction of **II** at pH = 6.05, are only slightly larger than the expected value which seems to be in accord with the above assumption. Higher pH-values obviously do not favour the decomposition process.

The ratio $\Delta i_{red}/i_{ox}$ which is about 2 (Table II) also points to an overall four-electron reduction at the mercury pool. The oxidation on the limiting current section of the anodic step is a two-electron overall process and if we assume similar diffusion constants, the $\Delta i_{red}/i_{ox}$ ratio should be exactly 2, *i.e.* the anodic wave obtained at the end of the reduction, should be exactly half of the height of the cathodic one before the constant potential reduction.

In case of **II** the E_p^B *vs.* pH diagram of the anodic wave (wave *B* in Fig. 1) consists of two straight sections with slopes of 0.065 and 0.036 V/pH, intersecting at pH 5.9. As we saw in Section 4, this wave is due to the oxidation of 1,2,4-triaminobenzene and corresponds to an overall two-electron process. The break at pH = 5.9 is in good agreement with the pK_3 value of 6.1 [28] of 1,2,4-triaminobenzene. The oxidation mechanism of 1,2,4-triaminobenzene can, therefore, be written as under pH = 5.9 (in the interval studied).

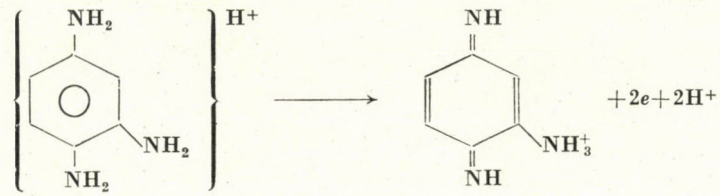

while above pH = 5.9

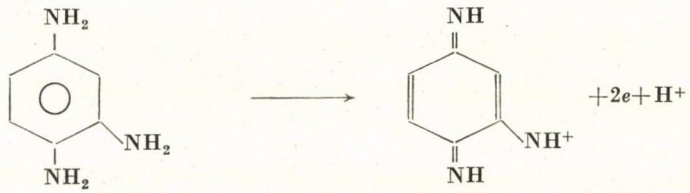

There is no evidence whether the *ortho*- or the *para*-quinoidal compound is formed as we could not isolate the end-product to date, but we think that the *para*-form is more probable. The following also seems to substantiate the mechanism mentioned above.

a) The oxidized product of 1,2,4-triaminobenzene has acid-base indicator properties (the acid form is red, the alkaline form yellow).

b) On the DME, the oxidized form is reduced in two waves of identical height. If we assume that diffusion constants of the oxidized and reduced forms are identical, both waves correspond roughly to one-electron reduction steps, according to their respective heights. The same conclusion is obtained from the difference of the peak potentials of the waves *B* and *C* on the cyclic voltammograms which is generally 0.06—0.07, *i.e.* similar to the value expected for a one-electron wave. The *C* wave is due to the first step of the two one-electron oxidation. The second step usually coalesces with wave *A* of the repeated cathodic cycle, but at some pH-values it can be recognized separately, too.

Further attemps to isolate and identify the oxidized form are in progress.

*

We are indebted to Drs. F. RUFF and GY. FARSANG for valuable discussions during the course of this work.

REFERENCES

1. CHUANG, L., FRIED, I., ELVING, P. J.: Anal. Chem. **37,** 1528 (1965)
2. SCHWARZ, W. M., SHAIN, I.: Phys. Chem. **69,** 30 (1965)
3. WOPSCHALL, R. H., SHAIN, I.: Anal. Chem. **39,** 1535 (1967)
4. GAYLOR, V. F., CONRAD, A. L., LANDERL, J. H.: Anal. Chem. **29,** 224 (1957)
5. ADAMS, R. N.: Anal. Chem. **30,** 1576 (1958)
6. DELAHAY, P.: New Instrumental Methods in Electrochemistry. Interscience, N. Y. 1954
7. MURAMATSU, M.: Bull. Soc. Chem. Japan, **31,** 864 (1958)
8. PAGE, J. A., LINGANE, J. J.: Anal. Chim. Acta **16,** 175 (1957)
9. TALLEC, A.: Ann. Chim. **4,** 67 (1969)

10. BACON, J., ADAMS, R. N.: J. Am. Chem. Soc. **90,** 6596 (1958)
11. LEE, H. Y., ADAMS, R. N.: Anal. Chem. **34,** 1587 (1962)
12. PUXEDDU, E.: Gazz. Chim. Ital. **48,** 25 (1919)
13. PUXEDDU, E.: Gazz. Chim. Ital. **50,** 149 (1920)
14. NORRIS, J., CUMMINGS, F.: Ind. Eng. Chem. **17,** 305 (1925)
15. FLORENCE, T. M.: Austr. J. Chem. **18,** 609 (1965)
16. CAUQUIS, G., FAUVELOT, G.: Polarography, p. 847. Mac Millan, London 1964
17. SADLER, J. L., BARD, A. J.: J. Am. Chem. Soc. **90,** 1979 (1968)
18. HILLSON, P. J., BIRNBAUM, P. P.: Trans. Faraday Soc. **48,** 478 (1952)
19. NYGÄRD, B.: Arkiv för Kemi **20,** 163 (1962)
20. NYGÄRD, B.: Arkiv för Kemi **26,** 167 (1966)
21. CLARK, W. M.: Oxidation–Reduction potentials of Organic Systems. Academic Press, N. Y. 1963
22. KOUTECKY, J.: Coll. Czech. Chem. Comm. **20,** 116 (1955)
23. SAVÉANT, J. M.: Rev. Chim. Min. **5,** 477 (1968)
24. MASTRAGOSTINO, M., NADJO, L., SAVÉANT, J. M.: Electrochim. Acta, **13,** 721 (1968)
25. HEYROVSKY, J., KUTA, J.: Principles of Polarography. Academic Press, N. Y. London, 1966
26. BASCOMBE, K. N., BELL, R. P.: J. Chem. Soc. **1959,** 1096
27. CAUQUIS, G., GENIÉS, M.: Bull. Soc. Chim. **1967,** 3220
28. KHARKHOROVA, G. M.: Zhurn. Obsch. Him. **26,** 1713 (1956)
29. NICHOLSON, R. S., SHAIN, I.: Anal. Chem. **36,** 706 (1964)

László LADÁNYI
Miklós VAJDA
György VÁMOS

Budapest VIII., Múzeum krt. 4/b.

Acta Chimica Academiae Scientiarum Hungaricae, Tomus 68 (1—2), pp. 61—64 (1971)

ELIMINATION OF RESISTANCE POLARIZATION IN POTENTIOSTATIC INVESTIGATIONS, II

B. LENGYEL, Jr. and J. DÉVAY

(Research Group for Electrochemistry, Hungarian Academy of Sciences, and Department of Physical Chemistry, University of Veszprém)

Received November 28, 1969

A potentiostatic method is described that renders possible the continuous measurement and automatic compensation of the resistance polarization during potentiostatic measurements. The method was employed for the study of the anodic polarization of silver in sulphate-containing solutions. The character of the anodic polarization curve was changed when the potential drop on the ohmic resistance of the solution was automatically compensated. When the automatic compensation technique was employed, the reference electrode did not need to be placed near the working electrode and thus the shielding effect of the former could be avoided.

In an earlier communication [1] we reported on a method for the continuous determination and automatic compensation of ohmic polarization in potentiostatic measurement. Essentially, this method is based on the following principle: an a.c. current proportional to the d.c. current flowing through the cell is superimposed on the d.c. current. The a.c. voltage measured between the reference electrode and the working electrode is proportional to the d.c. voltage arising across the resistance of the solution between these two electrodes. The a.c. voltage measured on this resistance is added after amplification and rectification to the d.c. voltage controlling the potentiostat. This method permits to impose on the electrode under investigation the voltage adjusted on the potentiostat regardless of the ohmic resistance.

This method was applied for the investigation of the anodic polarization of silver under potentiostatic conditions in solutions containing sulphate, because in these solutions, in addition to the resistance of the solution, a layer of relatively high resistance is also formed on the surface of the electrode.

The schematic diagram of the measuring system is shown in Fig. 1. The cylindrical silver electrode (V) in cell (1) having a surface area of 4 cm^2, was rounded off at one side, and sealed into a glass tube with Epokitt resin. This electrode (V) was concentrically surrounded by a platinum net electrode (E). The reference electrode was mercury/mercurous sulphate (R) immersed into 0.1 *n* H_2SO_4. The d. c. current flowing through cell (1) was fed into the unit consisting of the modulator (5) and of the a.c. amplifier (6), which generated an a.c. current proportional to the d.c. current. This a.c. current was supplied to cell (1) through resistance (7) and capacitor (8). Capacitor (8) served for the separation of the d.c. and a.c. circuits, while resistance (7) ensured that amplifier (6) functioned as a current generator, *i.e.* of the a.c. current flowing through the cell was independent from the cell resistance.

Reference electrode (R) was connected to the input of the differential amplifier (2) through filters (11, 12) and to the alternating voltage amplifier (9) and demodulator (10). The output voltage of demodulator (10), equal to the voltage across the ohmic resistance,

was added to the polarization voltage adjusted on the potentiometer, and fed into the other input of the differential amplifier (2). Filtering circuits (11, 12) prevented the a.c. voltage between the reference and the measuring electrodes from reaching the input of the differential amplifier (2). Inductivity (4) served to prevent a.c. shunting of the cell by the output impedance of the potentiostat.

During the measurements, the potential controlled by the potentiostat was varied continuously at a rate of 60 mV/min by means of potentiometer (13). The sliding contact of the potentiometer was moved by a motor having a constant speed of rotation, thus ensuring a linear variation of the potential with time.

For the determination of the optimum value of the frequency of the a.c. current the frequency dependence of the cell impedance was measured in an a.c. bridge circuit employing a freshly prepared and a surface coated electrode respectively in both cases. The cell impedance was found to be independent of frequency in the frequency range from 2 to 5 kHz. Therefore, an a.c. current of 3 kHz frequency was used in our investigations.

Before the measurements, the electrodes were cleaned with emery paper, etched in 10 per cent nitric acid for 5 minutes, and washed with distilled water. Each measurement was performed with a freshly treated electrode and fresh 0.1 *n* H_2SO_4 solution.

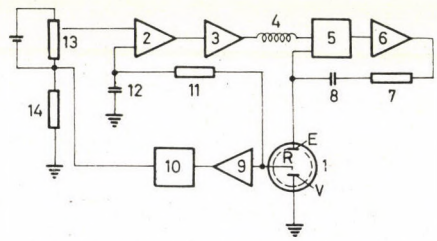

Fig. 1. Schematic diagram of the circuit used for the automatic compensation of ohmic polarization under potentiostatic conditions

The results of the measurements are shown in Fig. 2. On each of the diagrams the intensity of the d.c. current flowing through the cell was plotted on the ordinate axis. Values plotted on the abscissa were the following:

In case *a)* the polarization voltage adjusted on the potentiostat, under conditions, when the connection between (10) and (14) (*cf.* circuit diagram in Fig. 1) has been interrupted, *i.e.* the voltage across the resistance of the solution and the surface layer was not automatically compensated.

In case *b)* the electrode potential, evaluated from the applied voltage taking into account the voltage across the ohmic resistance. This value was calculated by interrupting the connection between (10) and (14), and continuously measuring and recording the d.c. output voltage of demodulator (10) with a vacuum-tube voltmeter. This voltage, which was equal to the voltage across the ohmic resistance, was subtracted in each case from the voltage polarizing the electrode.

In case *c)* the polarizing voltage adjusted on the potentiostat, the voltage across the ohmic resistance being automatically compensated (see circuit in Fig. 1).

The zero potential values on the diagrams corresponded in each case to the reversible potential of the electrode, against the mercury/mercurous sulphate electrode.

It is apparent in Fig. 2 that in case *b)*, though the potential of the potentiostat was controlled by a linear program the electrode potential did not follow linearly the polarization voltage of the potentiostat. This was caused by the change with time of the resistance of the solution and of the layer

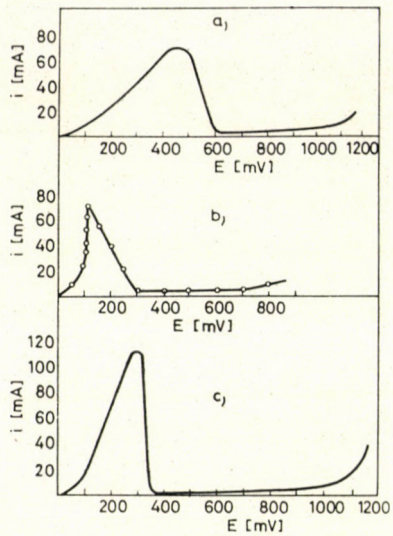

Fig. 2. Anodic polarization curve of silver in 0.1 *n* H_2SO_4 solution, a) not taking into consideration the voltage across the ohmic resistance, b) curve a) corrected for the voltage across the ohmic resistance, c) with automatic compensation of the voltage across the ohmic resistance

formed on the surface of the electrode. Owing to this fact the polarizing voltage dropped in this ohmic resistance [2.] In case *c)*, when the voltage across the ohmic resistance was continuously and automatically compensated, the electrode potential continuously followed the polarizing voltage, and the actual voltage adjusted on the potentiostat was always imposed on the electrode. This fact is also reflected by the change in the character of the polarization curves (cases *a)* and *c)*). Thus, for example, the section indicating an apparent oversaturation between 500 and 600 mV on curve *a)* disappeared on curve *c)*, and the potential range corresponding to the anodic dissolution of the metal was also diminished.

In subsequent measurements, the reference electrode (R) was placed at a distance of 5, 10 and 15 mm, respectively, from the silver electrode (V) in a 0.1 *n* H_2SO_4 solution, and in each case, the voltage across the ohmic resistance was automatically compensated. The results are shown in Fig. 3. The polarizing d.c. voltage is plotted on the abscissa of the diagram, while on the ordinate the intensity of the d.c. current flowing through the cell.

The diagram shows that, regardless of the distance from the reference electrode, the polarization curves were identical within the limits of the

experimental error. Thus, by employing automatic compensation, it is possible to place the reference electrode relatively far from the electrode to be studied and to eliminate errors arising from the approach of the reference electrode capillary to the working electrode. The screening effect of the capil-

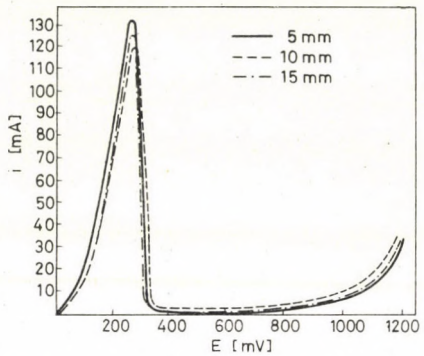

Fig. 3. The effect of increasing distance between the reference electrode and the silver electrode in 0.1 *n* H_2SO_4 solution, with automatic compensation of the voltage across the ohmic resistance

lary can change the distribution of the current density on the electrode surface. Moreover a capillary placed close to the surface of the electrode measures the potential of a small part of the electrode only, and this may considerably differ from the average electrode potential.

REFERENCES

1. DÉVAY, J., LENGYEL, B. Jr., MÉSZÁROS, L.: Magy. Kém. Foly. (In press) Acta Chim. Acad Sci. Hung. (In press)
2. DÉVAY, J., LENGYEL, B. Jr., MÉSZÁROS, L.: Magy. Kém. Foly. (In press) Acta Chim. Acad. Sci. Hung. (In press)

Béla LENGYEL Jr.
József DÉVAY
} Veszprém, Schönherz Z.-u 12. Hungary.

Acta Chimica Academiae Scientiarum Hungaricae, Tomus 68 (1—2), pp. 65—73 (1971)

COMPUTER SIMULATION OF ROVIBRATIONAL SPECTRA OF SLIGHTLY ASYMMETRIC PROLATE TOP MOLECULES

EXTENSION TO ASYMMETRIC TOP TRANSITIONS

G. JALSOVSZKY and L. NEMES

(Central Research Institute for Chemistry, Hungarian Academy of Sciences, Budapest)

Received December 15, 1969

A computer program is described for simulating the rotational structure of perpendicular vibrational transitions of slightly asymmetric prolate top molecules. In addition to R^z-type Coriolis interactions the asymmetric top transitions are taken into account exactly up to $K = 4$. A sample calculation is given for ν_7 of ethylene.

Introduction

A previous publication [1] dealt with the simulation of rovibrational bands of symmetric and slightly asymmetric prolate top molecules. In the calculations R^z-type Coriolis interaction was taken into account and by fitting the computed spectrum to the experimental one the determination of Coriolis ζ^z constants was attempted. The symmetric top approximation used in this program, however, led to serious discrepancies between the experimental and computed spectra in the region close to the centre of the perpendicular bands of asymmetric tops. If the Coriolis interacting bands are lying near to one another and so their rotational structure is strongly blended, the symmetric top approximation gives insufficient or incorrect information on the parameters to be determined.

In order to obtain the correct band structure, the computer program had to be extended to take into account asymmetry effects. Since in the case of slightly asymmetric rotors ($\varkappa \cong -1$), asymmetry splitting and level shifts play a significant role only up to $K_{-1} = 3$* (or, in more asymmetric cases $K = 4$), above this value the symmetric top approximation can be used.

The present work reports the extension of the simulation program to the calculation of asymmetric top energy levels, transitions and intensities.

The theory of asymmetric rotors has been developed by KING, HAINER and CROSS [2]. For a better understanding of the computer program, a brief account of the theory is given here.

* In the following, whenever K is used, K_{-1} is meant.

Energy levels and transition frequencies of asymmetric rotors

The energy of a rigid asymmetric rotor can be expressed as:

$$E(A,B,C) = \frac{1}{\hbar^2}\,[AP_a^2 + BP_b^2 + CP_c^2] \tag{1}$$

where P_a, P_b and P_c are the components of the angular momentum along the principal axes of the rotor, $A \geqq B \geqq C$ are the corresponding rotational constants.

Considering the commutation rules of the angular momentum components and using as basis the symmetric rotor wave functions chosen by WANG [3], MULLIKEN and VAN VLECK [4], the following matrix elements are obtained:

$$\begin{aligned}
&\langle J,\ K,\ M\,|P_y^2|\ J,\ K,\ M\rangle = \langle J,K,M\,|P_x^2|\,J,K,M\rangle = \frac{\hbar^2}{2}\,[J(J+1)-K^2] \\
&\langle J,K\pm 2,M|P_y^2|\,J,K,M\rangle = \frac{\hbar^2}{4}\,[(J\mp K)(J\pm K+1)(J\mp K-1)(J\pm K+2)]^{1/2} \\
&\langle J,K,M|P_z^2|\,J,K,M\rangle = \hbar^2 K^2
\end{aligned} \tag{2}$$

The Cartesian axes x, y, z and the principal internal axes a, b, c can be identified in 3 ! different ways, yielding six representations labelled by I^r, II^r, III^r, I^l, II^l and III^l. In the case of nearly prolate symmetric rotors, representation I^r is the most convenient one, where $x \to b$, $y \to c$ and $z \to a$.

By introducing the Ray asymmetry parameter: $\varkappa = (2B-A-C)/(A-C)$, simpler and generally usable expressions are obtained for the energy matrix elements. The correlation between the reduced and effective energy is:

$$E(1,\varkappa,-1) = E(\varkappa) = \frac{2}{A-C}\,E(A,B,C) - \frac{A+C}{A-C}\,J(J+1) \tag{3}$$

Substituting the angular momentum matrix elements into Eq. (1), and performing the transformation given by Eq. (3), the following non-vanishing elements of the $E(\varkappa)$ matrix are obtained:

$$\begin{aligned}
&\langle\, J,\ K,\ M\ |\ E(\varkappa)\ |\ J,\ K,\ M\,\rangle = FJ(J+1) + (G-F)\,K^2 \\
&\langle J,\ K,\ M\ |\ E(\varkappa)\ |\ J,\ K+2,\ M\,\rangle = \frac{H}{2}\,[J(J+1) - (K+1)\,(K+2)]^{1/2}\cdot \\
&\qquad\qquad [J(J+1) - K(K+1)]^{1/2}
\end{aligned} \tag{4}$$

where constants F, G and H depend on the representation used. For representation I^r:

$$F = \frac{1}{2}(\varkappa - 1), \qquad G = 1 \qquad \text{and} \quad H = -\frac{1}{2}(\varkappa + 1) \tag{5}$$

For the limiting prolate top, where $\varkappa = -1$, the above matrix elements yield the well-known formulas of symmetric top energy levels:

$$\langle J, K, M \mid E(\varkappa) \mid J, K, M \rangle = -J(J+1) + 2K^2 \tag{6}$$

$$\langle J, K, M \mid E(\varkappa) \mid J, K \pm 2, M \rangle = 0$$

It is seen that for the symmetric top the energy matrix becomes diagonal also in K.

Since $-J \leq K \leq J$, the energy matrices are of the order $(2J+1)$, by a suitable transformation, however, they can be transformed into smaller submatrices. The symmetric rotor wave functions, used as basis functions for the calculation of energy matrix elements, can be transformed to new basis functions, to the so called WANG functions [3]. The transformation to a representation based on these functions factors the energy matrix into four submatrices:

$$X'E\,X = E^+ \dotplus E^- \dotplus O^+ \dotplus O^- \tag{7}$$

The elements of the submatrices can be easily calculated from the matrix elements given in Eq. (5). By finding the eigenvalues of the above matrices, asymmetric top energy levels are obtained. Several methods are recommended for this procedure [2, 5], in programs, however, written for high-speed computers the diagonalization by Jacobi's method appears to be the most suitable.

The selection rules governing the transitions between the energy levels of an asymmetric top are: $\Delta J = 0 \pm 1$ and for the perpendicular bands of nearly symmetric rotors $\Delta K = \pm 1$. The above indicated changes in J give rise to the P, Q and R branches which are divided into two sub-branches according to the value of ΔK. Since among the submatrices obtained by the WANG transformation E^+ and E^- contain only elements corresponding to even K values, while O^+ and O^- matrices involve only odd K levels, transitions are allowed only between energy levels of different submatrices. Line frequencies are calculated by forming the proper energy differences between the levels, taking into account selection rules, and by combining these differences with the corresponding Coriolis-perturbed band origin.

Intensities of transitions

Rovibrational intensities are proportional to the square of the rovibrational transition moment:

$$I_{rv} \sim \sum_F |\langle v, R| \mu_F |v, R\rangle|^2 \tag{8}$$

where μ is the molecular dipole vector, v and R stand for the vibrational and rotational quantum numbers, respectively, while F represents the axes of space-fixed Cartesian system. Assuming that rotational and vibrational wave functions can be separated, the above expression can be written as the product of the vibrational transition moment and of the matrix elements of Φ_{Fg} direction cosines, so Eq. (8) is written as:

$$\sum_F |\langle v, R| \mu_F |v, R\rangle|^2 = \sum_F \sum_{g,M'M''} \left| \langle J, K, M |\Phi_{Fg}| J, K, M\rangle \langle v|\mu_g|v\rangle \right|^2 \tag{9}$$

where g represents the molecule-fixed axis system. Each direction cosine matrix element is split into three factors:

$$\langle J, K, M |\Phi_{Fg}| J, K, M\rangle = \langle J|\Phi_{Fg}| J\rangle \langle J, M|\Phi_{Fg}| J, M\rangle \langle J, K |\Phi_{Fg}| J, K\rangle \tag{10}$$

Analytical expressions calculated for these matrix elements in the symmetric rotor representation are listed in Table I [2]. For the calculation of asymmetric rotor line strengths, direction cosine matrix elements are transformed to the basis of WANG functions, by the same transformation that factors the energy matrix into submatrices:

$$\Phi^s_{Fg} = X' \Phi_{Fg} X \tag{11}$$

Thereafter a further transformation is required to the asymmetric rotor basis. This is carried out using the matrix that diagonalizes the submatrices of E:

$$\Phi^A_{Fg} = T'_2 X' \Phi_{Fg} X T_1 \tag{12}$$

where T_1 and T_2 are the eigenvector matrices of the energy blocks corresponding to the ground and excited states, respectively. Since both transformations, represented by X and T are diagonal in J and M, only the last factor of Eq. (10) should be transformed. These transformed matrix elements have been evaluated and published by SCHWENDEMAN [6]. The structure of the matrix which contains several blocks corresponding to transitions between the energy levels of different energy submatrices, is shown on Fig. 1. Each block contains nonzero elements for only one g axis, letters a, b and c refer to this axis, blocks

Table I

Direction cosine matrix elements in the symmetric top representation

Value of J'	$J+1$	J	$J-1$
$\langle J\|\Phi_{Fg}\|J'\rangle$	$\{4(J+1)[(2J+1)\cdot(2J+3)]^{1/2}\}^{-1}$	$[4J(J+1)]^{-1}$	$[4J(4J^2-1)^{1/2}]^{-1}$
$\langle J,K\|\Phi_{Fz}\|J'K\rangle$	$2[(J+1)^2-K^2]^{1/2}$	$2K$	$-2(J^2-K^2)^{1/2}$
$\langle J,K\|\Phi_{Fy}\|J'K\pm1\rangle = \mp i\langle J,K\|\Phi_{Fx}\|J'K\pm1\rangle$	$\mp[(J\pm K+1)\cdot(J\pm K+2)]^{1/2}$	$[(J\mp K)\cdot(J\pm K+1)]^{1/2}$	$\mp[(J\mp K)\cdot(J\mp K-1)]^{1/2}$
$\langle J,M\|\Phi_{Zg}\|J'M\rangle$	$2[(J+1)^2-M^2]^{1/2}$	$2M$	$-2(J^2-M^2)^{1/2}$
$\langle J,M\|\Phi_{Yg}\|J'M\pm1\rangle = \pm i\langle J,M\|\Phi_{Xg}\|J'M\pm1\rangle$	$\mp[(J\pm M+1)\cdot(J\pm M+2)]^{1/2}$	$[(J\mp M)\cdot(J\pm M+1)]^{1/2}$	$\mp[(J\mp M)\cdot(J\mp M-1)]^{1/2}$

labelled by zero correspond to forbidden transitions. The actual matrix elements are also given in [6], for saving place they are not presented here.

The remaining matrix elements in Eq. (10) need not be transformed, they can be directly calculated for each transition using proper J, ΔJ, K and ΔK values. In the absence of external field, the summation in Eq. (9) over F can be replaced by a multiplication by 3; summation over M' and M'' can be carried out algebraically; *i.e.* instead of the matrix elements given in Table I, only three quantities should be calculated depending on the value of ΔJ:

$$\sum_{F,M'',M'} |\langle J|\,\Phi_{Fg}\,|J\rangle\,\langle J,M|\,\Phi_{Fg}\,|J,M\rangle|^2 = \begin{cases}[J(2J+1)]^{-1} \text{ for } \Delta J=-1\\ [J(J+1)]^{-1} \text{ for } \Delta J=0\\ [(J+1)(2J+1)]^{-1} \text{ for } \Delta J=1\end{cases} \qquad (13)$$

Ground	Excited	J				$J+1$			
		E^+	E^-	O^+	O^-	E^+	E^-	O^+	O^-
	E^+	0	a	c	b	a	0	b	c
	E^-	a	0	b	c	0	a	c	b
J	O^+	c	b	0	a	b	c	a	0
	O^-	b	c	a	0	c	b	0	a
	E^+	a	0	b	c				
	E^-	0	a	c	b	see $J-J$			
$J+1$	O^+	b	c	a	0	block			
	O^-	c	b	0	a				

Fig 1. The block structure of the transformed direction cosine matrix

The square of the transformed direction cosine matrix element is then multiplied by the corresponding expression of Eq. (13) giving the intensity factor that depends only on the rotational states. It has been checked that for symmetric top molecules (where E is diagonal and therefore T_1 and T_2 are unit matrices) these expressions yield the Hönl-London coefficients. Therefore we have labelled the above intensity factor also for the asymmetric top transitions by A_{KJ}.

Rovibrational line intensities can be then calculated from the following expression:

$$I_{rv} = PI \cdot (2J + 1) \cdot g \cdot A_{KJ} \cdot \nu \cdot B \tag{14}$$

where PI is the perturbed vibrational intensity, g is the statistical weight for the ground state arising from nuclear spin statistics, ν denotes the computed transition frequency, and B stands for the Boltzmann factor of the rotational ground state.

Simulated and observed spectra

The correctness and performance of the program have been checked using the ν_7 C-type band of ethylene. The input data used by the simulation program are listed in Table II. Experimental spectra have been recorded on a Perkin-Elmer Model 225 spectrometer. Experimental conditions for recording are listed in Table III. On comparing the simulated spectrum to the experimental one (Fig. 2), a reasonably good fit can be observed. The remaining discrepancies are due to the neglection of centrifugal distortion effects and to the lack of simulating 'hot-bands' which arise with slightly different rotational constants. The rotational structure is analysed by SMITH and MILLS [9] who give explanation for the regular features appearing in the band.

Table II

Input data for the simulation program: molecular constants and parameters of the C-type perpendicular ν_7 band of ethylene

$T = 300°K$ $J_{max} = 50$ $K_{max} = 10$, asym. calc. up to $K = 3$

	Ground state	Excited state
A	4.861 cm^{-1}	4.861 cm^{-1}
B	1.0005 cm^{-1}	0.9953 cm^{-1}
C	0.8288 cm^{-1}	0.8236 cm^{-1}
Band origin	949.3 cm^{-1}	
Coriolis $\zeta^z_{1,10}$	0.44	

Table III

Experimental conditions for spectral recording

Pressure	10 mmHg
Cell thickness	10 cm
Spectral resolution	0.4 cm^{-1}
Wn. range:	880—1000 cm^{-1}

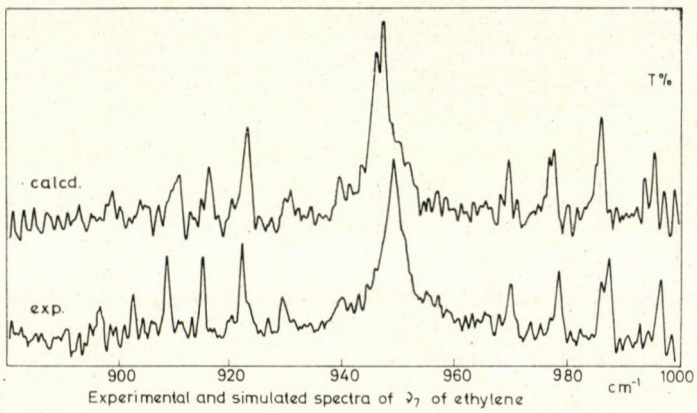

Experimental and simulated spectra of ν_7 of ethylene

Fig. 2

Description of the computer program

The program was written in Algol for an ICT 1905 computer. Segments calculating the rotation-vibration interaction, symmetric top transitions and intensities have been published in [1], so they are not dealt with here.

The first part of the program contains the necessary input instructions, where in addition to the parameters (*i.e.* rotational constants, centrifugal distortion constants*, unperturbed vibrational origins and intensities, the range and the 'resolution' of the simulated spectrum, etc.) information bits are read in giving whether symmetric or asymmetric approximation is requested; moreover the terminal values of J and K are specified. Asymmetric top transitions can be taken into account up to $K = 3$ or 4, above this limit symmetric top approximation is used.

The rovibrational Hamiltonian matrix is set up and diagonalized in the same manner as described in [1], except for the fact that perturbed band origins and intensities are calculated and stored in advance for each K value involved in the asymmetric calculation. This is due to the fact that the energy is not diagonal in K and so for each J an energy matrix should be constructed, diagonalized and its eigenvalues are assigned to the different K's.

* In the recent version of the program centrifugal distortion is taken into account only in the symmetric top transitions.

It should be noted here that even in the WANG representation the matrices to be diagonalized are roughly of order $J/2$. We have found, on the basis of PARKIN's idea [7] that since only the lowest eigenvalues are required for the present approximation, and the matrix elements belonging to higher K values hardly influence these eigenvalues, matrices of large dimension may be truncated.

It has been found that the dimension of energy submatrices need not be greater than 8. In such a way independently of the size of the computer memory it is only computer time economy that limits the maximal value of J.

Having diagonalized the energy matrices, their lowest eigenvalues are assigned to the corresponding K values and stored. As a matter of fact, energy and eigenvector values corresponding to two consecutive J values are stored at the same time. In P-type transitions level '$J + 1$' is combined with the vibrational ground state, level 'J' with the excited state, in R-type transitions the situation is reversed, while in the case of Q-type transitions level 'J' is combined with both states. When all 84 transitions corresponding to a given J level-pair have been calculated (transitions are specified in Table IV) the value of J is increased by one, the previous '$J + 1$' level is assigned to the new 'J' level, a new '$J + 1$' level is calculated and the whole procedure is reiterated.

Actual transitions are calculated by means of a subroutine which carries out the following steps.

Table IV

Transitions taken into account in the simulation program

Branch	Energy submatrices	Type	Changes in K_{-1}
Q	$E^+ \leftrightarrow O^-$	b	$0 \leftrightarrow 1,\ 2 \leftrightarrow 1,\ 2 \leftrightarrow 3,\ 4 \leftrightarrow 3$
	$E^- \leftrightarrow O^+$	b	$2 \leftrightarrow 1,\ 2 \leftrightarrow 3,\ 4 \leftrightarrow 3,$
	$E^+ \leftrightarrow O^+$	c	$0 \leftrightarrow 1,\ 2 \leftrightarrow 1,\ 2 \leftrightarrow 3,\ 4 \leftrightarrow 3$
	$E^- \leftrightarrow O^-$	c	$2 \leftrightarrow 1,\ 2 \leftrightarrow 3,\ 4 \leftrightarrow 3$
P^* and R	$E^+ \rightarrow O^+$	b	$0 \rightarrow 1,\ 2 \rightarrow 1,\ 2 \rightarrow 3,\ 4 \rightarrow 3$
	$E^- \rightarrow O^-$	b	$2 \rightarrow 1,\ 2 \rightarrow 3,\ 4 \rightarrow 3$
	$O^+ \rightarrow E^+$	b	$1 \rightarrow 0,\ 1 \rightarrow 2,\ 3 \rightarrow 2,\ 3 \rightarrow 4$
	$O^- \rightarrow E^-$	b	$1 \rightarrow 2,\ 3 \rightarrow 2,\ 3 \rightarrow 4$
	$E^+ \rightarrow O^-$	c	$0 \rightarrow 1,\ 2 \rightarrow 1,\ 2 \rightarrow 3,\ 4 \rightarrow 3$
	$E^- \rightarrow O^+$	c	$2 \rightarrow 1,\ 2 \rightarrow 3,\ 4 \rightarrow 3$
	$O^- \rightarrow E^+$	c	$1 \rightarrow 0,\ 1 \rightarrow 2,\ 3 \rightarrow 2,\ 3 \rightarrow 4$
	$O^+ \rightarrow E^-$	c	$1 \rightarrow 2,\ 3 \rightarrow 2,\ 3 \rightarrow 4$

* These transitions are calculated twice in each J cycle; at first "$J + 1$" → "J" then "J" → "$J + 1$" transitions are calculated between the indicated energy submatrices.

Energies are transformed into $E(A, B, C)$ using the appropriate (ground or excited state) rotational constants. Term difference is formed and combined with the perturbed band origin whose polarization corresponds to the polarization of the actual rotational transition. Appropriate direction cosine matrices are built up and transformed by means of the eigenvector matrices corresponding to the ground and excited states. The element defined by K' and K'' is selected, squared and multiplied by the corresponding expression of Eq. (13). Complete rovibrational strength values are then calculated on the basis of Eq. (14).

The accumulation of the computed spectrum, the slit function simulation and the conversion procedure to transmittance have been described in [1]. The total spectrum can be printed out on a line printer or punched on paper tape. In the latter case the conversion to transmittance is carried out by another program which thereafter plots the spectrum in a form directly comparable to the experimental one.

REFERENCES

1. Nemes, L.: Acta Chim. Acad. Sci. Hung. **64,** 59—65 (1970)
2. King, G. W., Hainer, R. M., Cross, P. C.: J. Chem. Phys. **11,** 27 (1943)
Cross, P. C., Hainer, R. M., King, G. W.: J. Chem. Phys. **12,** 210 (1944)
3. Wang, S. C.: Phys. Rev. **34,** 243 (1929)
4. Mulliken, R. S.: Phys. Rev. **59,** 873 (1941)
Van Vleck, J. H.: Phys. Rev. **33,** 467 (1929)
5. Gora, E. K.: J. Mol. Spectry. **2,** 259 (1958)
Bennett, J. M., Ross, I. G., Wells, E. J.: J. Mol. Spectry. **4,** 342 (1960)
6. Schwendeman, R. H.: J. Mol. Spectry. **7,** 280 (1961)
7. Parkin, J. E.: J. Mol. Spectry, **15,** 483 (1965)
8. Dowling, J. M., Stoicheff, B. P.: Can. J. Phys. **37,** 703 (1959)
9. Smith, W. L., Mills, I. M.: J. Chem. Phys. **40,** 2095 (1964)

György Jalsovszky
László Nemes
Budapest II., Pusztaszeri út 57—69.

Acta Chimica Academiae Scientiarum Hungaricae, Tomus 68 (1—2), pp. 75—86 (1971)

CHEMISTRY OF FREE RADICALS, VII

REACTION OF NITROSO COMPOUNDS WITH VINYL MONOMERS*

L. SÜMEGI, F. TÜDŐS and I. KENDE

(Central Research Institute for Chemistry of the Hungarian Academy of Sciences, Budapest)

Received December 29, 1969

The interaction of nitroso compounds and vinyl monomers was studied. The reaction occurring between methyl methacrylate and *p*-nitrosoaniline has been found pseudo-unimolecular for nitrosoaniline, with an activation energy of 15 kcal/mole. The reaction of styrene with nitrosobenzene appears to be pseudo-bimolecular for the latter compound with an activation energy of 7.5 kcal/mole. A number of experiments were carried out with N-substituted *p*-nitrosoanilines and nitrosobenzene derivatives substituted the aromatic nucleus, which were treated with methyl methacrylate or styrene, and the reaction rates and their Hammett dependence were determined. Spectrophotometric and ESR studies have led to the conclusion that free radicals of nitrogen oxide type are formed in these reactions.

Introduction

A wide range of studies have been made lately of the effect of nitroso compounds on the radical polymerization of vinyl monomers [1]. Aromatic nitroso compounds were found to be much more effective inhibitors than the widely applied types of quinone and hydroquinone. With nitroso compounds, however, owing to their high reactivities, reactions proceeding in two directions must be considered under the conditions of the polymerization: the first is a radical addition process of nitroso compounds [2], and the other a direct reaction with respective vinyl compounds.

Nitroso derivatives readily react with compounds containing double bonds. This has been shown by WICHTERLE [3] and KRESZE [4, 5]; the interactions taking place between substituted butadiene derivatives and different aromatic nitroso compounds were regarded as Diels-Adler reactions. The experiments carried out by HAMMER *et al.* [6] with olefins, as well as the results obtained by INGOLD and GOWENLOCK [7, 8], point to the formation of azoxy compounds through a four-membered heterocyclic ring. The reactions of substituted butenes with several derivatives of nitrosobenzene were studied by SULLIVAN [9]. All these investigations, however, were carried out under experimental conditions substantially different from those used in the experiments described below.

* Presented in a short form at the International Symposium on Macromolecular Chemistry, Budapest, 25—30 August, 1969. Kinetics and Mechanism of Polyreactions, **3**, 97—102 (1969).

2. Experimental

Kinetic measurements were made with styrene and methyl methacrylate monomers. The monomers were purified [10, 11], and stored at —70 °C. Their physical constants are given in Table I.

Nitroso compounds were prepared from the pure nitro compounds by Zn-dust reduction in neutral medium, followed by oxidation with $FeCl_3$, steam distillation, and subsequent recrystallizations. The nitroso compounds were stored in a refrigerator. The physical constants of the nitroso compounds used and references to the synthetic methods are shown in Table II.

Table I

Physical properties of the vinyl monomers used

Monomer	B.p., °C	Refractive index		Ref.
		Lit.	Observed	
Styrene	145.2 (760 torr)	$n_D^{25} = 1.5439$	$n_D^{25} = 1.5441$	[12]
Methyl methacrylate	100—100.1 (760 torr)	$n_D^{20} = 1.4140$	$n_D^{20} = 1.4138$	[13]

Table II

Physical properties of the nitroso compounds used

Q (para) substituent	M.p., °C		Ref.
	Lit.	Observed	
—H	68	68	[14]
$-CO_2C_2H_5$	83—84	83	[15]
—Cl	87—89	87.5—88	[16]
$-CH_3$	48.5	46—48	[17]
$-OCH_3$	101.5	102	[18]
$-NH_2$	173—4	173.5	[19]
$-NHCH_3$	118	117—8	[14]
$-N(CH_3)_2$	85	85	[14]
$-N(C_2H_5)_2$	84	83—4	[14]
—NHPh	143—4.6	144	[14]
$-NPh_2$	120.5	120	[30]

3. Kinetic measurements

The reactions of nitroso compounds with radicals and vinyl compounds can be studied separately under suitable experimental conditions. In systems containing no initiator, the formation of macro radicals below 70 °C is practically excluded, thus a direct study of the reactions with vinyl compounds is possible.

Since in preliminary experiments oxygen was found to disturb the reaction, the experiments outlined below were carried out in nitrogen atmosphere.

Photometric measurements were made with a Pulfrich photometer between 30 and 70 °C in a thermostated cell-compartment. The measurements required the construction of a special cell-compartment shown in Fig. 1. The use of this vessel facilitated the examination of the samples in air-free nitrogen atmosphere.

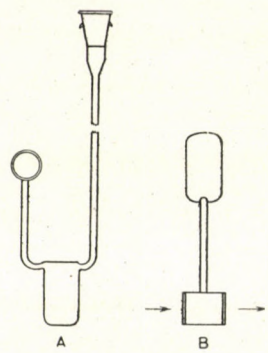

Fig. 1. Cell-compartment used in the photometric measurements

According to their behaviour, the nitroso compounds investigated may be classified as follows:

1. *p*-nitrosoaniline and its derivatives substituted in the NH_2 group;
2. other substituted derivatives of nitrosobenzene.

In support of the above grouping is the fact that marked differences could be observed between these two kinds of compounds in their reactivities towards styrene and methyl methacrylate, as well as in the reaction orders and Arrhenius parameters.

On the basis of the characteristic visible spectra of nitroso compounds, it was possible to follow the first step of the reaction by photometric measurement of the consumption of the nitroso compound. The results can most conveniently be described in the case of the *p*-nitrosoaniline derivatives, therefore these will be dealt with first.

Reaction of *p*-nitrosoaniline derivatives with methyl methacrylate

p-Nitrosoaniline derivatives actually fail to react with the slightly polar styrene, whereas the reaction with methyl methacrylate proceeds at a measurable rate. Kinetic measurements have shown that the process is of first order with respect to both reaction components. The kinetic curve of the consumption of *p*-nitrosoaniline (at a temperature of 50 °C) is shown in Fig. 2,

where E denotes the optical density which is proportional to the concentration of the nitroso compound.

This kinetic behaviour is characteristic of all N-substituted *p*-nitrosoaniline derivatives. Tables III and IV show the results of the experiments performed at 50 °C with *p*-nitroso-N-methylaniline and *p*-nitroso-N,N-diethylaniline, respectively.

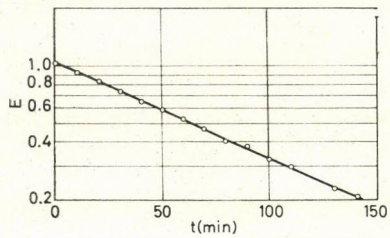

Fig. 2. Kinetic curve of the reaction in the system methyl methacrylate–*p*-nitrosoaniline at 50 °C

Table III

Kinetic data of the reaction of methyl methacrylate with p-nitroso-N-methylaniline at 50 °C $c_0 = 1.16 \cdot 10^{-2}$ mole/l

t (min)	E	t (min)	E
0	1.225	80	0.647
10	1.105	100	0.535
20	1.015	120	0.478
30	0.951	150	0.336
40	0.878	180	0.287
50	0.815	220	0.220

Table IV

Kinetic data of the reaction between methyl methacrylate and p-nitroso-N, N-diethylaniline at 50 °C $c_0 = 6.90 \cdot 10^{-3}$ mole/l

t (min)	E	t (min)	E
0	0.785	80	0.407
10	0.725	90	0.380
20	0.670	100	0.362
30	0.603	110	0.318
40	0.564	120	0.296
50	0.505	130	0.282
60	0.480	140	0.256
70	0.423	150	0.235

Table V

Bimolecular rate constants for the reaction

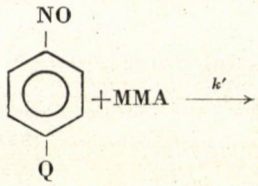

Substituent (Q)	Temperature (C°)	k' $10^3 \cdot (l \cdot mole^{-1} \cdot min^{-1})$
$-NH_2$	30	0.303
$-NH_2$	40	0.661
$-NH_2$	50	1.26
$-NH_2$	60	2.81
$-NH_2$	70	5.82
$-NHCH_3$	50	0.88
$-N(CH_3)_2$	50	1.53
$-N(C_2H_5)_2$	50	0.858
$-NHPh$	50	3.55
$-NPh_2$	50	4.38

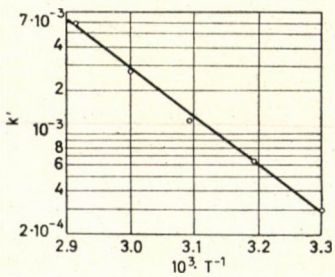

Fig. 3. Arrhenius dependence of the rate constants in reactions between methyl methacrylate and *p*-nitrosoaniline

The bimolecular rate constants of the processes have been calculated from the pseudo-unimolecular rate constants determined from the kinetic curves. These are shown in Table V.

The activation energy has been determined in the case of *p*-nitrosoaniline in the temperature range between 30 and 70 °C. The Arrhenius dependence (Fig. 3) can be described by the following equation:

$$k' = 2.3 \cdot 10^7 \cdot e^{-15000/RT}\, l \cdot mole^{-1} \cdot min^{-1} \qquad (1)$$

Reaction of other substituted derivatives of nitrosobenzene with styrene

Other substituted derivatives of nitrosobenzene react with the highly-reactive methyl methacrylate so rapidly that the reaction is almost instantaneous at the usual concentrations, therefore, it cannot be followed by photometry. On the other hand, while *p*-nitrosoaniline derivatives practically do not react with styrene, the reaction of other substituted nitrosobenzene derivatives proceeds at a measurable rate at about 50 °C.

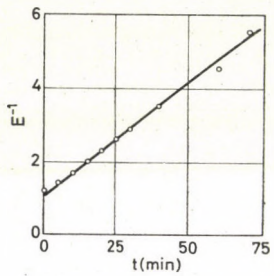

Fig. 4. Kinetic curve of the reaction in the system nitrosobenzene–styrene at 50 °C

Another significant difference was observed in the reaction order with respect to nitroso compounds. The reactions between *p*-nitrosoaniline derivatives and methyl methacrylate follow first-order kinetics with respect to the nitroso compound, while reactions of second order take place when the other nitrosobenzene derivatives and styrene are allowed to react. For example, Fig. 4 shows the kinetic curve of consumption of the nitroso compound in the reaction of nitrosobenzene and styrene, in the representation $E^{-1} = f(t)$, corresponding to second-order kinetics.

The results of experiments with *p*-nitrosoanisole and *p*-nitrosobenzoic acid ethyl ester are recorded in Tables VI and VII, respectively.

Table VI

Data of the reaction between p-nitrosoanisole and styrene at 50 °C

$c_0 = 9.07 \cdot 10^{-2}$ mole/l $\quad \varepsilon = 11.97$

t (min)	E^{-1}	t (min)	E^{-1}
0	0.922	200	1.042
5	0.926	290	1.087
10	0.930	360	1.152
20	0.926	420	1.177
60	0.944	480	1.219
110	1.000		

Table VII

Data of the reaction between p-nitrosobenzoic acid ethyl ester and styrene at 50 °C

$c_0 = 8.36 \cdot 10^{-2}$ mole/l $\varepsilon = 14.24$

t (min)	E^{-1}	t (min)	E^{-1}
0	0.840	9	2.960
1	1.154	10	3.280
2	1.346	12	4.050
3	1.538	14	4.505
4	1.776	16	5.350
5	2.028	18	6.250
6	2.193	20	6.370
7	2.479	25	9.090
8	2.702		

The rate constants (k'') derived from the kinetic curves are listed in Table VIII. With the exception of *p*-nitrosoaniline derivatives, nitroso compounds show a tendency to dimerize in apolar medium. It may thus be assumed that the nitroso compounds enter the reaction in the form of a dimer, which explains the fact: the process is of second order with respect to the nitrosomonomer. This assumption is in agreement with the other experimental facts, and will be considered in the discussion of the reaction mechanism.

The compounds in question show a behaviour different from that of the *p*-nitrosoaniline derivatives also in respect to their Arrhenius parameters. The experiments referring to this were carried out with nitrosobenzene, which may be considered the parent compound of the group, in the temperature range 30—70 °C. The Arrhenius-dependence of the constant is described by the following equation:

$$k'' = 0.78 \cdot 10^3 \cdot e^{-7500/RT} \, \mathrm{l^2 \cdot mole^{-2} \cdot min^{-1}} \tag{2}$$

A comparison of Eqs (1) and (2) shows that in the latter case both the activation energy and the preexponential factor are smaller, supporting the assumption that a nitroso dimer is involved in the reaction. In this case, the following dimerization equilibrium must be taken into account:

$$Z + Z \rightleftarrows D, \tag{3}$$

consequently,

$$K = \frac{z^2}{d}, \tag{4}$$

Table VIII

Rate constants of the reaction

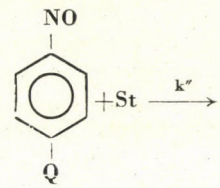

Substituent (Q)	Temperature (°C)	k'' ($l^2 \cdot mole^{-2} \cdot min^{-1}$)
H	30.3	$2.69 \cdot 10^{-2}$
H	40	$3.20 \cdot 10^{-2}$
H	45	$4.07 \cdot 10^{-2}$
H	50	$4.71 \cdot 10^{-2}$
H	50	$5.43 \cdot 10^{-2}$
H	50	$4.64 \cdot 10^{-2}$
H	60	$7.50 \cdot 10^{-2}$
H	70	$10.05 \cdot 10^{-2}$
H*	50	$4.90 \cdot 10^{-2}$
H**	50	$4.73 \cdot 10^{-2}$
$-OCH_3$	50	$8.76 \cdot 10^{-4}$
$-COOC_2H_5$	50	$3.73 \cdot 10^{-1}$
$-COOC_2H_5$	50	$3.70 \cdot 10^{-1}$
$-Cl$	50	$1.01 \cdot 10^{-1}$
$-CH_3$	50	$1.29 \cdot 10^{-2}$

* Experiment made in benzene solution: $\frac{[\text{styrene}]}{[\text{benzene}]} = 1$

** Experiment made in benzene solution: $\frac{[\text{styrene}]}{[\text{benzene}]} = \frac{1}{3}$

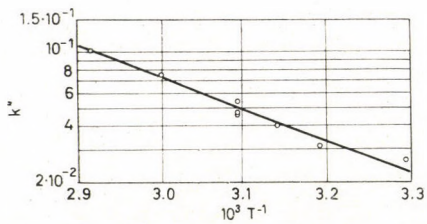

Fig. 5. Arrhenius dependence of the rate constant in reactions of nitrosobenzene with styrene

where z and d denote concentrations of the nitroso monomer and nitroso dimer, respectively. Considering Equilibrium (3), the kinetics equation for the consumption of the nitroso monomer may be given as follows:

$$-\frac{dz}{dt} = kdm = \frac{k}{K} z^2 m = k'' z^2 m , \tag{5}$$

where m is the concentration of styrene, and k the rate constant of the reaction: nitroso dimer + styrene. We must note that Eq. (5) can only be described in this simple form if the dimerization is rather slight. In order to elucidate whether this condition is satisfied or not, detailed investigations were carried out with nitrosobenzene in benzene solution over a wide concentration range. According to our measurements, the optical density of the solutions is a strictly linear function of the concentration even at room temperature; in other words, they very accurately satisfy the Beer–Lambert law, which means that the dimer concentration cannot exceed the order of magnitude of 0.1%.

On the other hand, it seems probable that in methyl methacrylate, which is considerable more polar than styrene, there is practically no dimerization, which means that the reaction can only take place with the monomeric nitroso compound. In view of these considerations, the different reaction orders are easy to explain.

It appears from expression (5) that k'' is not a real rate constant, as the denominator also comprises the equilibrium constant, which, in turn, may cause the decrease of both Arrhenius parameters. The marked difference in the reaction order indicates probably dissimilar mechanism of the two reactions, and the Arrhenius parameters may also differ owing to this reason.

The rate constants of the reaction between substituted nitrosobenzenes and styrene have been plotted as $\log k'' = f(\sigma^+)$ in Fig. 6.

From this figure, the value of ϱ is equal to + 2.3; in other words, electron-withdrawing substituents rapidly increase the reaction rate. It is remarkable that the rate constants show considerably less correlation as a function of σ. In making the choice between constants σ and σ^+, the extremely low rate constants of the p-OCH_3 derivative had to be primarily considered. These experiments lead to the conclusion that the part of the electrophilic component is played by the nitroso compound in this reaction.

In our investigations the kinetic parameters of the reactions have been determined, but the structures of the products have not been elucidated. In the course of reactions, the originally green colour gradually becomes brown and then turns bright orange-red. The colour of the product is similar to that of stable free radicals of the nitrogen oxide type.

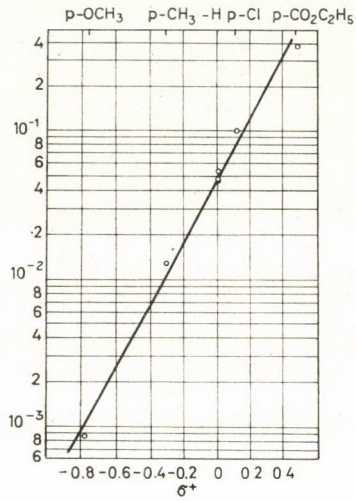

Fig. 6. Hammett-dependence of rate constants in the reaction of nitrosobenzene derivatives and styrene

4. Study of the reaction mechanism

Elucidation of the nature of the reaction products was attempted by spectrophotometric and ESR methods. In these studies we did not endeavour to obtain quantitative results (the conditions did not correspond to those of the photometric measurements), as it was not possible to carry out the measurements in nitrogen atmosphere.

Curve 1 in Fig. 7 shows the light absorption of the starting solution as a function of the wave length. Curves 2—5 show the change taking place in the course of the reaction. Observation of sections *A* and *B* of the light absorption curves reveals that light absorption decreases in section *A* and increases at *B* as

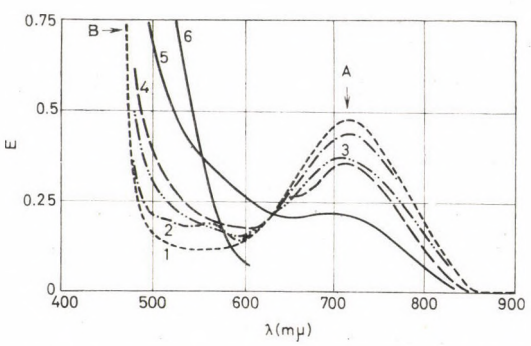

Fig. 7. Curves 1—5 show the light absorption curve of the styrene solution ($1.5 \cdot 10^{-2}$ mole/l) of nitrosobenzene, and curve 6 gives the light absorption curve of the benzene solution ($2 \cdot 10^{-2}$ mole/l) of the Banfield radical

the reaction proceeds. The latter fact suggests an increase in the concentration of the product. Curve 6 is the light absorption curve of the Banfield radical at a radical concentration corresponding to that of the starting material, nitrosobenzene. As it can be seen in the figure, the light absorptions of both the

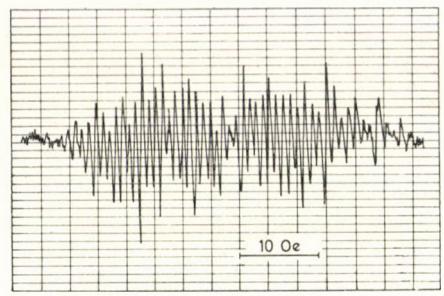

Fig. 8. ESR spectrum of radicals formed at the beginning of the reaction of nitrosobenzene with styrene

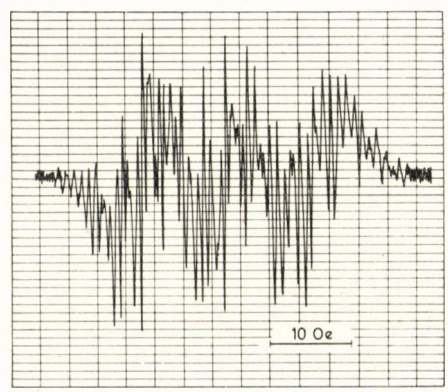

Fig. 9. ESR spectrum of radicals formed in the course of the reaction of nitrosobenzene with styrene. The period of reaction was 5 min at 100 °C

Banfield radical and the reaction product show a sudden rise below 550 μm.

These experimental results lead to the assumption that in the reaction of vinyl monomers and nitroso compounds a free radical of the nitrogen oxide type may be formed.

A study of the system nitrosobenzene–styrene at room temperature revealed an ESR signal at the initial phase of the reaction indicating the formation of free radicals in the course of the reaction.

The intesity of this absorption signal increases with time, while the spectrum also shows a structural change. The ESR spectrum of the free radical is first rather asymmetrical, then it changes gradually, as it is shown in Fig. 9.

Fig. 8 shows that the structure of the spectra of the radicals formed in the initial phase of the reaction has mainly doublet character. At the end of

the reaction, however, the structure turns out to be essentially a triplet which shows further hyperfine splitting and some signs of asymmetry (see Fig. 9).

The stable free radicals formed as the end-product of the reaction were detectable by ESR even after storage for several months at room temperature. It is thus evident that stable free radicals of the nitrogen oxide type are formed during the reaction.

ESR studies of these systems and the reaction mechanisms will be discussed in detail in a forthcoming publication.

*

We wish to express our thanks to Mr. L. JÓKAY and Mr. J. HEIDT for the preparation of several nitroso compounds, as well as to Mrs. E. ROCKENBAUER and Mrs. J. TIMÁR for their assistance in the experimental work.

REFERENCES

1. TÜDŐS, F., KENDE, I., SÜMEGI, L.: Hung. Pat. 150 550 (1961); Italian Pat. 690 950 (1963); Brit. Pat. 1 064 845 (1967)
2. KENDE, I., TÜDŐS, F., SÜMEGI, L.: Acta Chim. Acad. Sci. Hung. **54,** 315 (1967)
3. WICHTERLE, O., KOLINSZKY, M.: Coll. Czechoslov. Chem. Commun. **19,** 493 (1954)
4. KRESZE, G., FIRL, I.: Tetrahedron **19,** 1329 (1963)
5. KRESZE, G., FIRL, I., ZIMMER, H., WOLLNIK, V.: Tetrahedron **20,** 1605 (1964)
6. HAMMER, I., MACALUSO, A.: Tetrahedron Letters **6,** 381 (1963)
7. INGOLD, C. K., WEAVER, S. D.: J. Chem. Soc. **125,** 1456 (1924)
8. GOWENLOCK, B. G., LÜTTKE, W.: Quart. Revs. (London) **12,** 321 (1958)
9. SULLIVAN, A. B.: J. Org. Chem. **31,** 2811 (1966)
10. TÜDŐS, F.: Cand. chem. Thesis, Leningrad, 1956
11. FÖLDES-BEREZSNICH, T., TÜDŐS, F.: Magy. Kém. Foly. **70,** 500 (1964)
12. BOUNDI, H., BOYER, F.: Styrene, Its Polymers, Copolymers and Derivatives. Reinhold Publ. Co., New York, 1952
13. Monomers, Collection of Publication **2,** (Publisher of Foreign Literature) Moscow, 1951
14. VOGEL, A. I.: Practical Organic Chemistry, p. 939. Longhans Green and Co., London, New York, Toronto, 1948
15. HECKER, E.: Ber. **88,** 1666 (1955)
16. BAMBERGER, E.: Ber. **28,** 245 (1895)
17. BAMBERGER, E., RISING, A.: Ann. **316,** 283 (1901)
18. BAEYER, D., KNORR, E.: Ber. **35,** 3034 (1902)
19. FISCHER, O., HOPP, E.: Ber. **20,** 2475 (1887)
20. BEILSTEIN, **12,** I. 338 (1933); II. 366 (1950)

László SÜMEGI
Ferenc TÜDŐS
Imre KENDE
Budapest I, Pusztaszeri út 59—67.

Acta Chimica Academiae Scientiarum Hungaricae, Tomus 68 (1—2), pp. 87—92 (1971)

MOLECULAR FORCE FIELDS FOR SILYL ISOTHIOCYANATE AND SILYL ISOCYANATE

K. RAMASWAMY and S. RANGARAJAN

(Department of Physics, Annamalai University, Annamalainagar, India)

Received December 30, 1969

The calculation of approximate force fields for SiH_3NCS and SiH_3NCO was attempted by the methods suggested by TORKINGTON and HERRANZ and CASTANO. It is shown that TORKINGTON's method gives a better set of potential energy constants, mean amplitudes of vibration and Coriolis coupling constants which agree well with the observed experimental values.

Introduction

The exact nature of the force field of a molecule cannot be determined unambiguously from the vibrational frequencies alone. To fix the force field completely additional data like isotopic frequencies, rotation-vibration interaction constants, and mean amplitudes of vibration are often necessary. However, approximate force fields can be determined using the kinematic methods suggested by TORKINGTON [1], HERRANZ and CASTANO [2], BILLES [3] and STREY [4]. FREEMAN [5], SAWODNY [6] and PFEIFFER [7] have shown the validity of these methods in fixing the force fields for simple molecules. These kinematic methods were applied to a number of molecules of different symmetry and interesting results have been obtained [8—11].

The present paper deals with the analysis of the molecular force fields of silyl isothiocyanate and silyl isocyanate using the methods of 'characteristic set of valence co-ordinates' of HERRANZ and CASTANO and 'progressive rigidity' of TORKINGTON. The applicability of the methods for the evaluation of force constants for these molecules is also discussed on the basis of the reproducibility of other molecular constants.

Potential energy constants

Both silyl isothiocyanate and silyl isocyanate belong to the C_{3v} point group with the fundamental vibrational frequencies falling under the irreducible representations $\tau = 5a_1 \cdot 5e$. In the present calculations the vibrational assignments of EBSWORTH *et al.* [12] and the microwave data of JENKINS *et al.* [13] and GERRY *et al.* [14] were used. They are presented in Tables I and II.

Table I

Vibrational frequencies (in cm^{-1}) for SiH_3NCS and SiH_3NCO

a_1 Species		e Species	
SiH_3NCS[12]	SiH_3NCO*	SiH_3NCS	SiH_3NCO
513	577	2301	2203
1068	1455	739	716
2272	2299	989	954
2164	2198	54	35
980	961	501	621

* Private communication from Prof. EBSWORTH.

Table II

Internuclear distances (in Å) and bond angles for SiH_3NCS and SiH_3NCO

	SiH_3NCS[13]	SiH_3NCO[14]
d(Si—H)	1.489	1.506
D_1(Si—N)	1.714	1.699
D_2(N—C)	1.211	1.150
D_3(C—X)	1.560	1.179
α (H—$\widehat{\text{Si}}$—H)	111° 22′	110° 24′
β (H—$\widehat{\text{Si}}$—N)	107° 30′	108° 11′

Using the following set of symmetry coordinates for the a_1 species

$$R_1 = \Delta D_1$$

$$R_2 = \frac{1}{\sqrt{2}}(\Delta D_2 + \Delta D_3)$$

$$R_3 = \frac{1}{\sqrt{2}}(\Delta D_2 - \Delta D_3) \qquad (1)$$

$$R_4 = \frac{1}{\sqrt{3}}(\Delta d_1 + \Delta d_2 + \Delta d_3)$$

$$R_5 = \frac{1}{\sqrt{3+3v^2}}[\Delta\alpha_{12} + \Delta\alpha_{23} + \Delta\alpha_{31} + v(\Delta\beta_1 + \Delta\beta_2 + \Delta\beta_3)]$$

where

$$D_1 = \text{Si—N};\ D_2 = \text{N—C};\ D_3 = \text{C—S(O)}$$

$$d = \text{Si—H};\ \alpha = \text{H—}\widehat{\text{Si}}\text{—H}$$

$$\beta = \text{H—}\widehat{\text{Si}}\text{—N} \text{ and } r = \frac{\sqrt{3}\cos\beta}{\cos\alpha/2}$$

and with the set of coordinates given by SATHIANANDAN and MARGRAVE [15] for the e species, the G matrix elements were constructed in the usual way and the F matrix elements were obtained both by TORKINGTON's method and by HERRANZ' method.

In the method of TORKINGTON the eigenvector L of the product of the G and F matrices is triangular, the elements of which are obtained using the relation

$$G_{rs} = \sum_{\alpha}^{r} L_{r\alpha} L_{s\alpha} \; (r \leq s) \tag{2}$$

In the method of HERRANZ and CASTANO

$$L = BM^{1/2}B^{*} \tag{3}$$

where B is an orthogonal matrix which diagonalizes G. M is a diagonal matrix whose elements are the reciprocals of the eigenvalues of G. The asterisk refers to the transpose.

The symmetry force constant matrix is given by

$$F = L^{-1*}\Lambda L^{-1} \tag{4}$$

where Λ is a diagonal matrix with $\Lambda_k = 4\pi^2 C^2 \nu_k^2$. ν_k is the k-th vibrational wavenumber and C is the velocity of light in cm/sec. Using the above expressions, the F matrix elements and hence the valence force constants were obtained. The important valence force constants are presented in Table III.

Table III

Important valence force constants in mdynes/Å for SiH_3NCS and SiH_3NCO

	SiH_3NCS		SiH_3NCO	
	TORKINGTON method	HERRANZ method	TORKINGTON method	HERRANZ method
f_d	3.0271*	3.0238	2.7795	2.7902
f_{D1}	3.1401	5.6053	3.5131	6.8028
f_{D2}	13.7373	18.7027	17.1994	25.6781
f_{D3}	15.3944	18.4696	16.8575	19.5750
f_{D1D2}	2.3828	8.3725	2.3419	10.6066
f_{D1D3}	1.7335	3.8503	0.9459	4.2802
f_{D1d}	0.0306	0.1464	0.0368	0.1569
$f_\alpha - f_{\alpha\alpha}$	0.2232	0.2290	0.2113	0.2169
$f_\beta - f_{\beta\beta}$	0.2584	0.2790	0.2474	0.2671
f_θ	0.3384	0.7917	0.4944	0.9542
f_φ	0.0135	0.2653	0.0045	0.2289

* This number of significant figures is retained for internal consistency in the calculations

The vibrational mean amplitudes of different bonds were calculated by the method of CYVIN [16] and the nonbonded ones by the method of RAMASWAMY *et al.* [17]. The important mean amplitudes are given in Table IV.

The Coriolis coupling constants were calculated using the relation given by MEAL and POLO [18]. The principal axis was taken to be the z-axis in both molecules. The Coriolis coupling constants along with the available experimental values are given in Table V.

Table IV

Important vibrational mean amplitudes (in Å) at 298.16°K for SiH_3NCS and SiH_3NCO

Atom pair	SiH_3NCS		SiH_3NCO	
	TORKINGTON method	HERRANZ method	TORKINGTON method	HERRANZ method
Si—H	0.0870*	0.0893	0.0887	0.0939
Si—N	0.0524	0.0614	0.0491	0.0567
N = C	0.0375	0.0426	0.0357	0.0397
C = S	0.0331	0.0323	—	—
C = O	—	—	0.0348	0.0347
H . . . H	0.1307	0.1302	0.1495	0.1492
H . . . N	0.1165	0.1510	0.1270	0.1808

* As under Table III.

Table V

CORIOLIS *coupling constants for SiH_3NCS and SiH_3NCO*

	SiH_3NCS			SiH_3NCO	
	TORKINGTON method	HERRANZ method	Experimental [12]	TORKINGTON method	HERRANZ method
ζ_6	+0.0467*	−0.0032	+0.034	+0.0463	+0.0005
ζ_7	+0.2434	+0.1626	—	+0.2566	+0.1719
ζ_8	−0.1989	−0.1111	−0.15	−0.2094	−0.1230
ζ_9	+0.9294	+0.9638	—	+0.9310	+0,9674
ζ_{10}	+0.9885	+0.9976	—	+0.9909	+0.9986
$\sum_i \zeta i$	2.0091	2.0091	—	2.0154	2.0154
$2+\frac{B}{2A}$	2.0091			2.0154	

* As under Table III.

Results and discussion

The values of the SiH_3 group force constants in SiH_3NCS ($f_{Si-H} = 3.027$ mdynes/Å and $f_\alpha - f_{\alpha\alpha} = 0.223$ mdynes/Å) and SiH_3NCO ($f_{Si-H} = 2.780$ mdynes/Å and $f_\alpha - f_{\alpha\alpha} = 0.211$ mdynes/Å) obtained by the method of TORKINGTON compare favourably well with the values ($f_{Si-H} = 3.021$ mdynes/Å and $f_\alpha - f_{\alpha\alpha} = 0.182$ mdynes/Å) reported by SATHIANANDAN [15] and with those reported by DUNCAN [19]. Similarly the SiH_3 group force constants obtained by the method of HERRANZ agree well with the values reported by earlier workers [15, 16]. This shows that the methods of TORKINGTON and HERRANZ are applicable to groups containing hydrogen atoms. This result is in agreement with the observations made by FREEMAN [5] and PFEIFFER [7].

The values of the force constants obtained for the linear chain N—C—X (X is S or O) were found to be very high in the HERRANZ method if individual bonds were treated as internal coordinates. The potential energy distribution also indicated high mixing between the modes. Hence a linear combination of the internal coordinates was made. Even then the values of the major force constants are found to have high values ($f_{D_2} = 18.703$ mdynes/Å and $f_{D_3} =$ $= 18.470$ mdynes/Å in SiH_3NCS) as compared to the values of 12.423 mdynes/Å and 6.650 mdynes/Å, respectively, obtained using BADGER's rule [20]. The same is true in the case of SiH_3NCO. This indicates that the matrix of transformation obtained by the HERRANZ method does not truly represent the normal modes. However the values obtained by TORKINGTON's method are comparable with the ones obtained by earlier workers [15].

The large difference in the $f_{C=N}$ values in SiH_3NCS and SiH_3NCO may be traced to the large difference (0.061 Å) in the bond lengths which is again indicative of the highly polar nature of the oxygen atom. This is also reflected in the relatively smaller values of the force constants pertaining to the linear chain in SiH_3NCS. The C=N bond length is very short, approaching the value of the C≡N bond distance. The high values of the force constants show the probable likelihood of the following resonant structures

$$Si—N=C=X \leftrightarrow Si—N^+\equiv C—X^-$$

This structure is more prominent in SiH_3NCS than in SiH_3NCO. This is well reflected in the values of the force constants.

The mean amplitudes of vibration for Si—H and N=C compare very well with the values of 0.0888 Å in SiH_4 and 0.038 Å in HNCO and HNCS [21]. The vibrational mean amplitude 0.033 Å for C=S is very low when compared to the value of 0.040 Å in HNCS [21]. The nonbonded H . . . H mean amplitudes conform well with the value of 0.150 Å reported by CYVIN [21].

As seen from Table V the ζ_6 and ζ_7 values of 0.047 and —0.199 for SiH_3NCS obtained by TORKINGTON's method are close within experimental

errors to the values of 0.034 and —0.15 respectively reported by EBSWORTH *et al.* [12] while the HERRANZ method gives low values. The ζ sum rule is verified.

This shows that the HERRANZ method is a poor approximation for the determination of the molecular force fields for SiH_3NCS and SiH_3NCO. Since the TORKINGTON method gives a reasonably close set of force constants which reproduce (indirectly) the matrix of transformation between normal and symmetry coordinates, the Coriolis coupling constants and vibrational mean amplitudes, it is concluded that TORKINGTON's method gives a closer force field for SiH_3NCS and SiH_3NCO.

*

The authors are thankful to Prof. EBSWORTH (University of Edinburgh, Scotland) for his kind permission to use his unpublished data. One of the authors (S. R.) is grateful to the Council of Scientific and Industrial Research, New Delhi, for financial assistance through the award of a Junior Research Fellowship.

REFERENCES

1. TORKINGTON, P.: J. Chem. Phys. **17,** 1026 (1949)
2. HERRANZ, J., CASTANO, F.: Spectrochim. Acta, **22,** 1965 (1966)
3. BILLES, F.: Acta Chim. Acad. Sci. Hung., **47,** 53 (1966)
4. STREY, G.: J. Mol. Spectry, **24,** 87 (1967)
5. FREEMAN, D. E.: J. Mol. Spectry, **27,** 27 (1968)
6. SAWODNY, W.: J. Mol. Spectry, **30,** 56 (1969)
7. PFEIFFER, M.: J. Mol. Spectry, **31,** 181 (1969)
8. RAMASWAMY, K., KRISHNA RAO, B.: Z. phys. Chemie, **240,** 127 (1969)
9. RAMASWAMY, K., SRINIVASAN, K.: Austral J. Chem., **21,** 575 (1967)
10. RAMASWAMY, K., SRINIVASAN, K.: Austral J. Chem. **22,** 1123 (1969)
11. RAMASWAMY, K., MOHAN, N.: Indian J. Pure appl. Phys. **7,** 459 (1969)
12. EBSWORTH, F. A. V., MOULD, R., TAYLOR, R., WILKINSON, G. R., WOODWARD, L. A.: Trans. Faraday Soc., **58,** 1069 (1962)
13. JENKINS, D. R., KEWLEY, R., SUGDEN, T. M.: Trans. Faraday Soc. **58,** 1284 (1962)
14. GERRY, M. C. L., THOMPSON, J. C., SUGDEN, T. M.: Nature, **211,** 846 (1966)
15. SATHIANANDAN, K., MARGRAVE, J. L.: J. Mol. Spectry, **10,** 442 (1963)
16. CYVIN. S. J.: Spectrochim Acta, **15,** 828 (1959)
17. RAMASWAMY, K., SATHIANANDAN, K., CLEVELAND, F. F.: J. Mol. Spectry **9,** 107 (1962)
18. MEAL, J. H., POLO, S. R.: J. Chem. Phys., **24,** 1119 (1956)
19. DUNCAN, J. L.: Spectrochim. Acta, **20,** 1807 (1964)
20. BADGER, R. M.: J. Chem. Phys., **2,** 128 (1934)
21. CYVIN, S. J.: Molecular Vibrations and Mean Square Amplitudes. Universitetsforlaget Oslo, and Elsevier, Amsterdam 1968

K. RAMASWAMY
S. RANGARAJAN
Annamalai University, Annamalainagar, India.

Acta Chimica Academiae Scientiarum Hungaricae, Tomus 68 (1—2), pp. 93—132 (1971)

THIOKARBAMIDDERIVATE MIT TUBERKULOSTATISCHER WIRKUNG,* I

VERBINDUNGEN MIT HETEROCYKLISCHEM THIOKARBAMIDSKELETT

S. SÓLYOM, I. KOCZKA, G. TÓTH und L. TOLDY

(Institut für Arzneimittelforschung, Budapest)

Eingegangen am 3. November 1969

Die bei tuberkulostatisch wirksamen Thiocarbamidderivaten hinsichtlich der Wirkung vorteilhafte 1-(4-Isoamyloxyphenyl)-thiocarbamylgruppe sowie analoge, jedoch anders substituierte Thiocarbamylgruppen wurden mit Aminosäuren als biologisch bedeutenden Trägermolekülen kombiniert.

Über die aus α-, β- und γ-Aminosäuren und den entsprechenden Isothiocyanaten hergestellten Thiocarbamylaminosäuren wurden cyclische Verbindungen und zwar 2-Thiohidantoine, 2-Thiohydrouracyle und 2-Thio-4-oxo-perhydro-1,3-diazepine synthetisiert. Außerdem wurden Verbindungen hergestellt, die das Thiocarbamidskelett im Ring enthalten: 2-Thio-4-phenyl-1,2-dihydrochinazolin und 2-Arylimino-4-oxo-5-methyl-perhydro-1,3-thiazine. Die Struktur der Verbindungen wurde mit chemischen und spektroskopischen Methoden bestätigt.

Die 2-Thiohydantoine besitzen in vitro eine hohe tuberkulostatische Wirkung, sind jedoch stark toxisch. Die Perhydro-1,3-diazepine zeigten dagegen eine tranquillierende Wirkung.

Die in vitro bedeutende tuberkulostatische Wirkung einiger Thiocarbamidderivate ist bereits seit etwa 20 Jahren bekannt. Einzelne Derivate aus der großen Zahl der untersuchten Verbindungen wurden auch in die Therapie eingeführt. Ihre klinische Wirkung ist jedoch keineswegs eindeutig überzeugend, nicht einmal bei dem am meisten geprüften ISOXYL (4,4-Diisoamyloxythiocarbanilid). Diese Tatsache kann u. a. auf die unsicheren Resorptionsverhältnisse oder vielleicht auf den zu inaktiven Metaboliten führenden schnellen Abbau zurückgeführt werden [1].

Aus diesem Grund beschlossen wir, weitere Vertreter der potentiell antituberkulotischen Thiocarbamidderivate zu untersuchen.

In den synthetisierten neuen Verbindungen hielten wir meistens die bei den Thiocarbamiden bereits als vorteilhaft festgestellte 4-Alkoxyphenyl, bzw. im besonderen die 4-Isoamyloxyphenyl-Gruppe [2—5].

Daneben wünschten wir das Thiocarbamidskelett mit irgendeinem biologisch bedeutenden Träger zu verbinden. Für diesen Zweck wählten wir die Aminosäuren.

Aus α-Aminosäuren und 4-Alkoxyphenylisothiocyanaten ausgehend stellten wir nach einem modifizierten Verfahren von EDMAN [6] 3-(4-Alkoxyphe-

* Die vorliegende Arbeit ist ein Teil der Dissertation von S. SÓLYOM, Eötvös Loránd Universität, Budapest 1969.

nyl)-2-thiohydantoine her. Dieser Weg schien uns auch deshalb erfolgversprechend, weil die tuberkulostatische Wirkung einzelner 2-Thiohydantoine, so z. B. des 5-*n*-Heptyl-2-thiohydantoins [7] und des 3-(p-Sulfonamidophenyl)-2-thiohydantoins [8] bereits bekannt war, sodaß bei den durch uns hergestellten neuen Substitutionen eine Steigerung dieser Wirkung erwartet werden konnte. Die synthetisierten 3-(4-Alkoxyphenyl)-2-thiohydantoine sind in Tab. I angeführt.

Einige dieser Verbindungen wurden aus L-Aminosäuren hergestellt. Bekanntlich werden 2-Thio-hydantoine leicht racemisiert [9]. Diese Tatsache wurde auch durch unsere eigenen Beobachtungen unterstützt. Das optische Drehungsvermögen sämtlicher Verbindungen — mit Ausnahme des aus L-nor-Leucin hergestellten 2-Thiohydantoin-Derivats **VI** — nahm in alkoholischer Lösung schnell ab, während in Chloroform selbst nach längerem Stehen keine Änderung zu beobachten war. Diese Erscheinung dürfte damit zu erklären sein, daß der Protonenaustausch am asymmetrischen Kohlenstoffatom des Thiohydantoin-Ringes durch Alkohol gefördert wird.

Aufgrund einer Literaturanalogie [10] wurde aus dem aus L-Glutaminsäure hergestellten Thiohydantoin **VIII** durch Wasserentzug mit Essigsäureanhydrid das Lactam **XV** hergestellt.

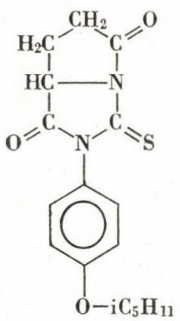

XV

Mit diesem Lactam wurden primäre und sekundäre Amine acyliert, wobei einige β-[3-(4-Isoamyloxyphenyl)-2-thiohydantoin-5]-propionsäureamide gewonnen wurden. Letztere sind in Tab. II angeführt.

Neben ihrer in vitro bedeutenden tuberkulostatischen Wirkung (0,1—0,8 μg/ml auf Dubos Nährboden) sind die in Tab. I und II angeführten Thiohydantoine in vivo an Mäusen stark toxisch. Die letztere Eigenschaft wird durch die Substitution am C-5 Kohlenstoffatom nur unwesentlich beeinflußt. Um also weniger toxische Repräsentanten dieser Verbindungsgruppe herzustellen, änderten wir die 3-Phenylsubstitution.

Zu diesem Zweck wurden Verbindungen untersucht, welche durch die Reaktion von 2,6-disubstituierten Phenylisothiocyanaten und α-Aminosäuren hergestellt wurden (Tab. IIIa und IIIb). Unter den als Primärprodukt entstehenden N-Thiocarbamylaminosäuren erfolgte jedoch ein spontaner oder durch gelinde Erwärmung hervorgerufener Ringschluß zu 2-Thiohydantoinen allein bei den aus α-Aminodicarbonsäuren hergestellten Derivaten. Bei dem Glycinderivat **XXXIII** erfolgte der Ringschluß durch saueres Kochen, während die aus sonstigen Aminosäuren hergestellten N-Thiocarbamylverbindungen **XXXIV—XL** selbst bei Säureeinwirkung keine Thiohydantoine lieferten.

Die antituberkulotische Aktivität der in Tab. IIIa und IIIb angeführten Verbindungen war in vitro geringer als die Wirkung der Verbindungen in Tab. I und II (50—100 μg/ml, Dubos), während ihre Toxizität unverändert blieb.

Die angeführten Ergebnisse zeigten also, daß die 4-Alkoxyphenylgruppe zwar hinsichtlich der tuberkulostatischen Wirkung auch bei Thiohydantoinen günstig ist, die Toxizitätsverhältnisse bei dieser Verbindungsgruppe jedoch ungünstig liegen.

Eine weitere Möglichkeit zur Eliminierung der toxischen Nebenwirkung der Thiohydantoine ergab sich aus der Steigerung der Ringgliederzahl. Die den 3-(4-Alkoxyphenyl)-2-thiohydantoinen analogen 3-(4-Alkoxyphenyl)-2-thiohydrouracyle waren bereits bekannt [11]. (Diese Verbindungen weisen in vitro auf Dubos-Nährboden in Konzentrationen von 10—20 μg/ml eine tuberkulostatische Wirkung auf.) Wir stellten das 3-(2,6-Dimethylphenyl)-2-thiohydrouracyl ebenfalls her (**XLI**), dessen antituberkulotische Wirkung in vitro — ähnlich den Thiohydanotinen mit verwandter Struktur — nur 50 μg/ml beträgt.

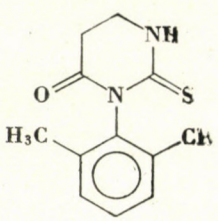

XLI

Auch bei der Hydrolyse mit $KHCO_3$ des in der Reaktion von *o*-Aminobenzophenon und Benzoylisothiocyanat erhaltenen N-Benzoylthiocarbamids wurde eine Verbindung erhalten, welche das Thiocarbamidskelett in einem sechsgliedrigen Ring enthält. Bei der Hydrolyse entsteht anstelle des zu erwartenden monosubstituierten Thiocarbamids das 2-Thio-4-phenyl-1,2-dihydrochinazolin **XLII**.

Tabelle I

5-R-3-(4-*Alkoxyphenyl*)-2-*thyohydantoine*

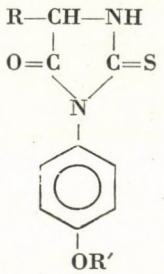

Nummer	Bezeichnung**	R	R′	Schmelzpunkt	Bruttoformel
I	T578	H	i C_5H_{11}—	226—227 °C	$C_{14}H_{18}N_2O_2S$
II*	T602	—CH_3	i C_5H_{11}—	179 °C	$C_{15}H_{20}N_2O_2S$
III	20083	—CH(CH$_3$)(CH$_3$)	i C_5H_{11}—	197—198 °C	$C_{17}H_{24}N_2O_2S$
IV*	T546	—CH_2—CH(CH$_3$)(CH$_3$)	i C_5H_{11}—	149—150 °C	$C_{18}H_{26}N_2O_2S$
V	T605	—CH(CH$_3$)(CH_2CH_3)	i C_5H_{11}—	152—153 °C	$C_{18}H_{26}N_2O_2S$
VI*	20182	—$CH_2CH_2CH_2CH_3$	i C_5H_{11}—	124 °C	$C_{18}H_{26}N_2O_2S$
VII	T606	—CH_2—C$_6$H$_5$	i C_5H_{11}—	181 °C	$C_{21}H_{24}N_2O_2S$
VIII*	T621	—CH_2CH_2—COOH	i C_5H_{11}—	142 °C Benzol	$C_{17}H_{22}N_2O_4S$
IX	20079	—CH_2—COOH	i C_5H_{11}—	219 °C Zers.	$C_{16}H_{20}N_2O_4S$
X	20055	—CH_2OH	i C_5H_{11}—	161—162 °C	$C_{15}H_{20}N_2O_3S$
XI	20054	—CH_2CH_2—S—CH_3	i C_5H_{11}—	140 °C	$C_{17}H_{24}N_2O_2S_2$

Molekulargewicht	Analyse								Verfahren Bemerkung
	Berechnet				Gefunden				
	C	H	N	S	C	H	N	S	
278,36	60,40	6,51	10,06	11,51	60,80	6,90	10,12	11,39	*A* Literatur des verwendeten 4-Isoamyloxy-phenyliso--thiocyanats [41]
292,39	61,61	6,89	9,58	10,96	61,80	7,10	9,70	10,98	*A*
320,44	63,71	7,54	8,74	10,00	63,68	7,52	8,70	10,20	*A*
334,49	64,63	7,83	8,38	9,58	64,50	7,69	8,56	9,79	*A*
334,49	64,62	7,83	8,37	9,58	64,62	8,05	8,38	9,78	*A*
334,49	64,62	7,83	8,37	9,58	64,75	7,92	8,43	9,74	*A*
368,48	68,44	6,56	7,60	8,70	68,30	6,88	7,61	8,91	*A*
350,42	58,26	6,32	7,99	9,14	58,27	6,52	7,94	9,34	*A*
336,40	57,12	5,99	8,33	9,53	57,05	6,14	8,40	9,70	*A*
308,39	58,42	6,53	9,08	10,39	58,37	6,70	9,15	10,52	*A*
352,50	57,92	6,86	7,94	18,19	57,82	6,99	8,01	18,02	*A*

Tabelle I (Forts.)

Nummer	Bezeichnung**	R	R′	Schmelzpunkt	Bruttoformel
XII*	20230	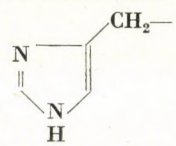	i C_5H_{11}—	169—170 °C Zers	$C_{18}H_{22}N_4O_2S$
XIII*	20129	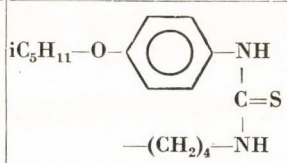	i C_5H_{11}—	153 °C	$C_{30}H_{42}N_4O_3S_2$
XIV	T607	H	C_2H_5—	196 °C Zers	$C_{11}H_{12}N_2O_2S$

* Aus L-Aminosäure hergestellt.
** Im Institut für Arzneimittelforschung, Budapest übliche Bezeichnungen.

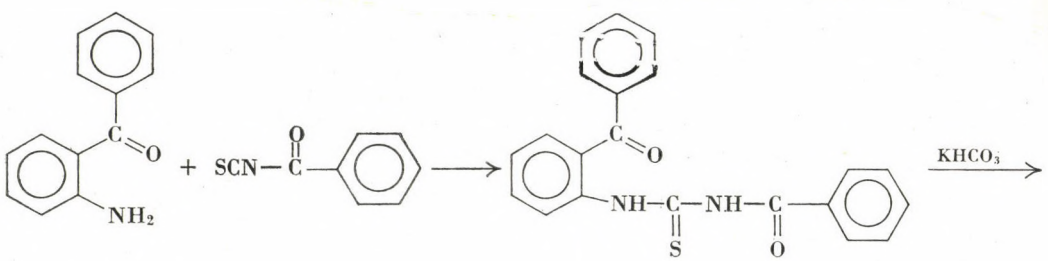

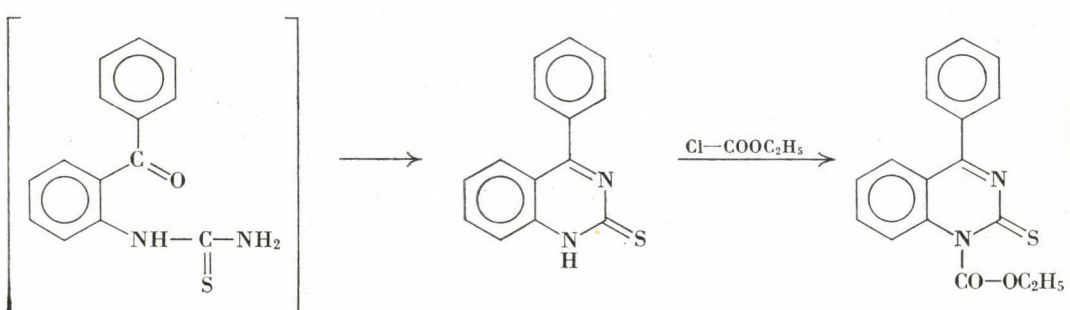

XLII XLIII

Molekulargewicht	Analyse								Verfahren Bemerkung
	Berechnet				Gefunden				
	C	H	N	S	C	H	N	S	
358,45	60,31	6,18	15,63	8,94	60,24	6,22	15,43	8,79	*A*
570,79	63,12	7,41	9,81	11,23	63,24	7,59	9,72	11,20	*A*
236,28	55,91	5,11	11,85	13,56	56,06	5,30	11,86	13,85	*A* Literatur des verwendeten 4-Äthoxyphenylisothiocyanats [31]

Im IR-Spektrum in Chloroform der Verbindung **XLII** befinden sich nähmlich weder die für Carbonyl, noch die für monosubstituierte Thiocarbamide charakteristischen Banden, während die Gegenwart der Banden bei 3380 cm^{-1} für νNH und bei 1625 cm^{-1} für νC=N sowie die Elementaranalyse die Struktur **XLII** bestätigen. Im Spektrum des Carbäthoxyderivats **XLIII** ist die Bande νNH nicht vorhanden, während die Bande νC=O bei 1730 cm^{-1} zugegen ist. Da in den UV-Spektren kein Anstieg der Konjugation bei **XLIII** im Vergleich zu **XLII** zu beobachten ist, ist die Acylgruppe offensichtlich an das Stickstoffatom gebunden.

In vitro zeigten die Verbindungen **XLII** und **XLIII** keine wesentliche tuberkulostatische Wirkung.

Wir stellten auch sechsgliedrige Heterocyclen her, in denen das Schwefelatom des Thiocarbamidskeletts im Ring enthalten ist.

Bekanntlich werden Thiocarbamid bzw. seine N,N′-disubstituierten Derivate in saurer Lösung an α,β-ungesättigte Carbonylverbindungen additioniert [12, 13] und aus dem entstandenen Isothiocarbamid wird in bestimmten Fällen durch Ringschluß 4-Oxo-1,3-thiazin gebildet. Diese Reaktion war bei symmetrisch disubstituierten Thiocarbamiden mit α,β-ungesättigten Säurechloriden bekannt und führt eindeutig zu der Struktur *B*/1, während bei monosubstituierten Thiocarbamiden drei Isomere *A*, *B* und *C* entstehen können.

Tabelle II

β-[3-(4-*Isoamyloxyphenyl*)-2-*thiohydantoin*-5]-*propionsäureamide*

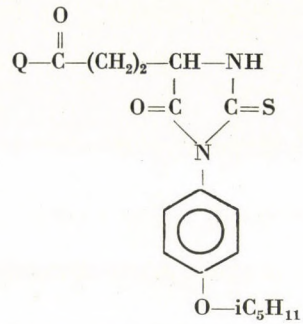

Nummer	Bezeichnung	Q	Schmelzpunkt	Bruttoformel
XVI	20133	NH_2—	174—175 °C	$C_{17}H_{23}N_3O_3S$
XVII	20134	CH_2=CH—CH_2—	167 °C	$C_{20}H_{27}N_3O_3S$
XVIII	20132	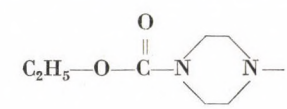	167—168 °C	$C_{24}H_{34}N_4O_5S$
XIX	20168	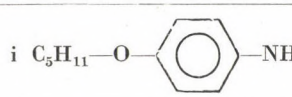	204—205°C	$C_{28}H_{37}N_3O_4S$
XX	20169	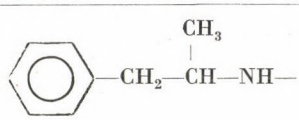	162 °C	$C_{26}H_{33}N_3O_3S$
XXI	20170	*n*-$C_{12}H_{15}$—NH—	142 °C	$C_{29}H_{47}N_3O_3S$
XXII	20184	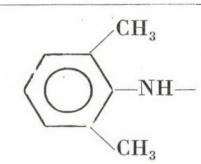	220—224 °C *b)* nach mehrfachem Kochen mit Alkohol	$C_{25}H_{31}N_3O_3S$
XXIII	20185	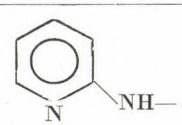	191—192 °C *n*-Propanol	$C_{22}H_{26}N_4O_3S$

Molekulargewicht	Analyse								Verfahren Bemerkung
	Berechnet				Gefunden				
	C	H	N	S	C	H	N	S	
349,44	58,42	6,63	12,02	9,17	58,43	6,67	12,11	9,19	*C*
389,52	61,66	6,98	10,79	8,23	61,55	7,17	10,75	8,19	*C*
490,61	58,75	6,98	11,42	6,53	58,90	6,94	11,34	6,46	*C*, Schmelzen, Literatur des verwendeten 1-Carbäthoxypiperazins [42]
511,66	65,72	7,29	8,21	6,26	65,90	7,40	8,25	6,41	*C*
467,61	66,77	7,11	8,98	6,85	66,96	7,12	8,95	7,01	*C*
517,75	67,26	9,15	8,11	6,19	67,34	9,30	8,13	6,39	*C*
453,59	66,19	6,89	9,26	7,07	66,5	7,03	9,25	7,23	*C* Schmelzen
426,53	61,94	6,14	13,14	7,51	62,10	6,29	12,99	7,42	*C* Schmelzen

Tabelle II (Forts.)

Nummer	Bezeichnung	Q	Schmelzpunkt	Bruttoformel
XXIV	20228		188 °C	$C_{24}H_{29}N_3O_3S$
XXV	20229		186—187 °C	$C_{20}H_{27}N_3O_3S$
XXVI	20241	$HO-(CH_2)_2-NH-$	167 °C	$C_{19}H_{27}N_3O_4S$
XXVII	20206		178—179 °C	$C_{23}H_{28}N_4O_3S$
XXVIII	20213	H_2N-NH-	174—175 °C	$C_{17}H_{24}N\,O_3S$

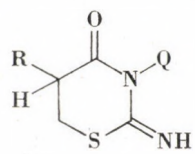

A

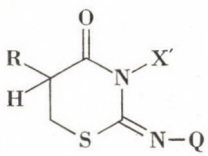

B X′=H

B/1 X′=Q

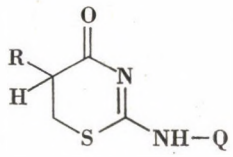

C

In unseren eigenen Untersuchungen verwendeten wir als α,β-ungesättigte Carbonylverbindung Methacrylsäure, wobei mit monosubstituierten Thiocarbamiden — ähnlich der bekannten Reaktion, das Isomere *B* (R = = —CH_3) entstand. Der Strukturbeweis ergab sich folgenderart:

a) Die Carbonylbande erschien im IR-Spektrum sämtlicher Verbindungen bei 1710—1715 cm^{-1}. Die Carbonylfrequenz weist bei dem aus 1,3-Diphenylthiocarbamid gewonnenen analogen Ketothiazin (Typ *B*/1) einen ähnlichen Wert (1700 cm^{-1}) auf [13], während die Carbonylbande im Fall einer Struktur *C* infolge der auftretenden Konjugation bei niedrigeren Wellenzahlen liegen sollte.

b) Aufgrund der in den IR-Spektren erscheinenden intensiven und ziemlich diffusen νNH-Banden kann auf eine dimere Assoziation gefolgert werden. In den in Lösung aufgenommenen IR-Spektren ändert sich die Carbonylfrequenz gegenüber den in fester Phase aufgenommenen Spektren nicht (1710 cm^{-1}) und die νNH-Bande des Monomeren tritt um 3360 cm^{-1} auf.

Diese Befunde weisen darauf hin, daß bei der in fester Phase auftretenden Bildung von Wasserstoffbrücken nicht die Carbonylgruppe, sondern das Iminostickstoffatom der Elektrondonor-Partner ist. Bei der Struktur *C* kann die Bildung von ähnlich starken Wasserstoffbrücken kaum erwartet werden,

Molekulargewicht	Analyse								Verfahren Bemerkung
	Berechnet				Gefunden				
	C	H	N	S	C	H	N	S	
439,66	65,56	6,67	9,56	7,29	65,59	6,71	9.54	7,17	*C*
389,50	61,67	6,98	10,79	8,23	61,64	7,09	10,68	8,29	*C*
393,49	57,99	6,91	10,68	8,14	57,85	7,14	10,80	8,06	*C*
440,55	62,70	6,40	12,72	7,27	62,58	6,49	12,80	7,41	*C*
364,46	56,02	6,63	15,37	8,79	55,98	6,57	15,40	8,77	*C*

während bei der Struktur *A* die Möglichkeit ihrer Bildung überhaupt nicht besteht.

c) Die Verbindungen konnten mit Hilfe der gebräuchlichen Acylierungsverfahren nicht acyliert werden.

Die synthetisierten Verbindungen mit der Struktur *B* sind in Tab. IV zusammengefaßt.

Bei dem aus Acrylsäureäthylester und 1-(4-Isoamyloxyphenyl)-thiocarbamid auf analoge Weise hergestellten Produkt erfolgt jedoch keine Ringschlußreaktion und das erhaltene Produkt **XLIX** hat eine Zwitterionenstruktur. Demgemäß erscheinen im IR-Spektrum der Verbindung die der protonierten Isothiocarbamidgruppe entsprechenden Banden für νNH (2800 cm^{-1}) und νC=N (1650 cm^{-1}).

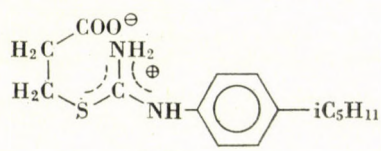

XLIX

Die in Tab. IV zusammengefaßten Perhydro-1,3-thiazine besitzen in vitro keine wesentliche tuberkulostatische Wirkung (50—100 μg/ml, Dubos), wogegen die Verbindung **XLIX** einen Titer von 1,6 μg/ml aufwies. Aufgrund dieses Befundes stellten wir einige N-(4-Isoamyloxyphenyl)-S-alkylisothiocarbamidsalze (Tab. V) her, welche in Konzentrationen von 1—8μg/ml aktiv waren. In vivo erwiesen sich diese Verbindungen jedoch als inaktiv.

Zur Herstellung von siebengliedrigen Ringen, die das Thiocarbamidskelett enthalten, wurde γ-Aminobuttersäure mit verschiedenen Isothiocyanaten

Tabelle IIIa

5-R-3-(2,6-Di-R'-phenyl)-2-thiohydantoine

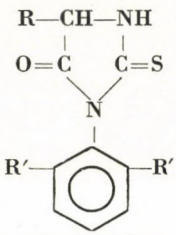

Nummer	Bezeichnung	R	R'	Schmelzpunkt	Bruttoformel
XXIX	20081	H	CH_3—	228 °C Zers. Alkohol	$C_{11}H_{12}N_2OS$
XXX	20095	HOOC—CH_2—	CH_3—	258—260 °C Zers. Alkohol	$C_{13}H_{14}N_2O_3S$
XXXI	20080	HOOC—CH_2—CH_2—	CH_3—	205 °C aus Wasser und danach aus Alkohol	$C_{14}H_{16}N_2O_3S$
XXXII	20145	HOOC—CH_2—CH_2—	Cl—	217—218 °C Alkohol–Petroläther	$C_{12}H_{10}Cl_2N_2O_3S$

in Reaktion gebracht und die so erhaltenen γ-(N-Thiocarbamyl)-aminobuttersäuren mit Polyphosphorsäure, bzw. mit Polyphosphorsäureäthylester behandelt, wobei durch Ringschluß die Möglichkeit der Bildung von drei Produkten, (*D*, *E*, *F*) besteht:

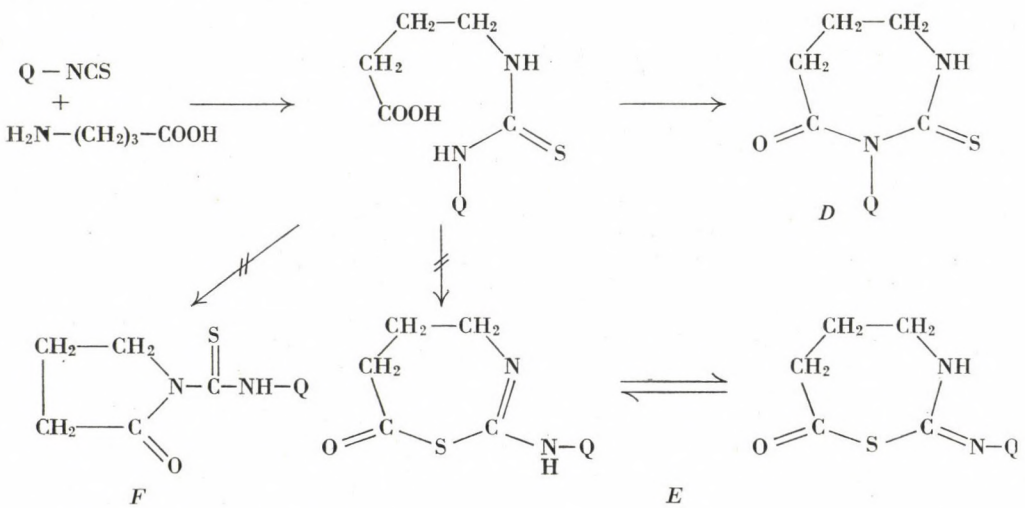

Molekulargewicht	Analyse								Verfahren Bemerkung
	Berechnet				Gefunden				
	C	H	N	S	C	H	N	S	
220,28	59,97	5,48	12,72	14,55	60,12	5,45	12,93	14,63	*B*
278,32	56,09	5,06	10,06	11,51	55,95	5,17	10,16	11,51	*B*
292,35	57,51	5,51	9,58	10,96	57,51	5,64	9,49	11,17	*B*
333,18	43,25	3,02	8,41	9,62 Cl: 21,27	43,33	3,28	8,32	9,57 Cl: 21,09	*B*

Aufgrund der hohen Stabilität der hergestellten Verbindungen kann das Perhydro-1,3-thiazepin *E*, bzw. sein Tautomer von vornherein ausgeschlossen werden.*

Die IR-Spektren der erhaltenen Verbindungen sind einander sehr ähnlich, folglich kommt für ihre Struktur einheitlich entweder Formel *D* oder Formel *F* in Frage.

Da die Elektronendonor- bzw. Elektronenakzeptoreigenschaft der Gruppe Q kaum einen Einfluß auf den Wert der $\nu C{=}O$ Frequenz ausübte, konnte zwischen den Formeln *D* und *F* nur mit Hilfe von Modellverbindungen bekannter Struktur entschieden werden. Zu diesem Zweck wurden die N-Methylderivate von *D* und *F* hergestellt (**LIII**), bzw. (**LIV**) und zwar nach folgendem Schema:

* Dies ist eine S-Acylisothiocarbamidstruktur, welche bekanntlich nur in Form von Salzen stabil ist und sonst durch Acylwanderung zu N-Acylthiocarbamid umgesetzt wird [33, 34, 35]. Auch das durch EDMAN hergestellte, der Struktur *E* analoge fünfgliedrige 2-Anilino-4-isobutyl-Δ^2-thiazolin-5-on bzw. dessen Salz ist äußerst zersetzlich [36].

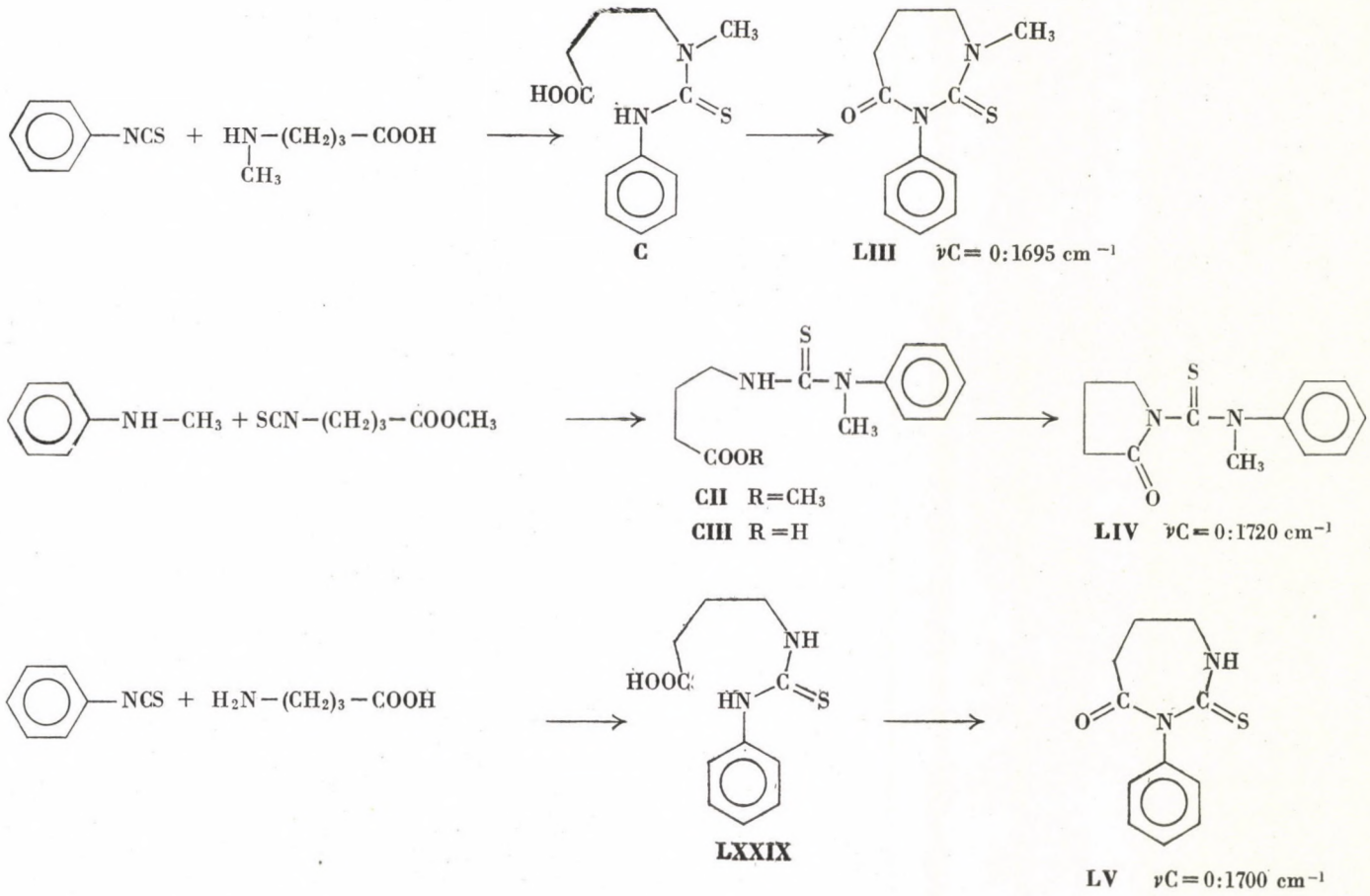
—NCS + HN—(CH2)3—COOH
CH3
HOOC
HN
N
CH3
C
S
O
LIII νC=O: 1695 cm−1
—NH—CH3 + SCN—(CH2)3—COOCH3
NH—C—N
CH3
COOR
CII R=CH3
CIII R=H
LIV νC=O: 1720 cm−1
—NCS + H2N—(CH2)3—COOH
NH
LXXIX
LV νC=O: 1700 cm−1

Es soll bemerkt werden, daß der Ringschluß bei **LIII** und **LIV** nur mit Trifluoressigsäureanhydrid durchgeführt werden konnte [43].*

Erwartungsgemäß ist die Frequenz $\nu C{=}O$ im Spektrum von **LIV** wegen der Ringspannung um 25 cm^{-1} höher, als bei **LIII**, während der Wert für diese letztere Verbindung kaum von der Frequenz $\nu C{=}O$ bei **LV** abweicht. Da auch in den IR-Spektren der durch uns hergestellten übrigen Verbindungen keine $C{=}O$ Frequenzen höher als 1710 cm^{-1} gefunden wurden, besitzen die durch Ringschluß der γ-(N-Q-Thiocarbamyl)-aminobuttersäuren hergestellten Produkte (deren Spektren analog den Spektren von **LIII** und **LV** sind) die Struktur *D*. Es handelt sich also um 2-Thio-3-Q-4-oxo-perhydro-1,3-diazepine.

Die Abweichung von der Struktur *F* wird auch durch die UV-Spektren unterstützt. Bei **LIII** und **LV**, die der Struktur *D* entsprechen, liegen zwei λ_{max} vor, bei 243 und 285 nm bzw. bei 259 und 295 nm. Bei **LIV** (Struktur *F*) tritt dagegen nur ein λ_{max} bei 296 nm auf.

Die hergestellten 2-Thio-3-Q-4-oxo-perhydro-1,3-diazepine sind in Tab. VI, die bei der Herstellung dieser Verbindungen als Intermediäre erhaltenen γ-(N-Q-Thiocarbamyl)-aminobuttersäuren in Tab. VII angeführt.

Die antituberkulotische Wirkung der in Tab. VI enthaltenen neuen Diazepine ist gering. Einige Vertreter (z. B. **LVII** und **LVIII**) besitzen dagegen eine tranquillierende Wirkung.**

Experimenteller Teil***

Verfahren A

5-R-3-(4-Alkoxyphenyl)-2-thiohydantoine I—XIV (Tab. I), **N-(2,6-Di-R′-phenylthiocarbamyl)-aminosäuren XXXIII—XL** (Tab. III/b), **α-(N-Q-Thiocarbamyl)-amino- bzw. -methylaminobuttersäuren LXXIX—CI** (Tab. VII),

0,05 *M* Aminosäure werden in ca. 2/3 einer 10%igen Alkalilösung, welche eine äquivalente Menge NaOH enthält, gelöst und mit 40 ml Alkohol verdünnt. Das Gemisch wird auf 40—50 °C erwärmt und eine alkoholische Lösung von 0,05 *M* des entsprechenden Isothiocyanats wird unter Rühren im Laufe einer halben Stunde tropfenweise zugefügt. Das Gemisch wird weitere 2 bis 3 Stunden lang bei 40—50 °C gerührt. Der pH des Reaktionsgemisches wird sowohl während dem Zutropfen, als auch während dem nachfolgenden Rühren kontrolliert und — falls nötig — mit dem Rest der Alkalilösung auf 9—9,5 eingestellt.

Danach wird die Lösung eingedampft und 10%ige Salzsäure zum viskosen Rückstand zugegeben. Bei den Verbindungen **I—XIV** erhielten wir nach dem Ansäuern in einigen Fällen Syrupe, welche jedoch beim Stehen bzw. bei Reiben mit einem Glasstab ebenfalls kristallisierten. Die Produkte können im allgemeinen aus Äthanol, die Verbindungen **LXXIX—CI** (γ-(N-Q-Thiocarbamyl)-aminobuttersäuren) aus einem Gemisch von Äthanol und Petroläther umkristallisiert werden. Die Anwendung eines davon abweichenden Lösungsmittels ist in den Tabellen angegeben.

* Auf ähnliche Art wurde die Analogverbindung zu **LIII**, das 1-Methyl-2-thio-3-(2,6-dimethylphenyl)-4-oxo-perhydro-1,3-diazepin **LXXVIII** hergestellt (Tab. VI/b).

** Die Wirkung dieser Verbindungen ist schwächer als die Wirkung der in der Therapie angewendeten Benzodiazepinskelett-Verbindungen [44].

*** Unkorrigierte Schmelzpunkte.

Tabelle IIIb

N-(2,6-Di-R'-phenyl)-thiocarbamylaminosäuren

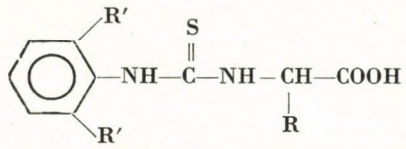

Nummer	Bezeichnung	Aminosäure	R'	Schmelzpunkt	Bruttoformel
XXXIII	20164	Gly	CH_3	175 °C Zers. Methanol	$C_{11}H_{14}N_2O_2S$
XXXIV	20082	D,L-Val	CH_3	165—166° C Zers.	$C_{14}H_{20}N_2O_2S$
XXXV	20094	L-Leu	CH_3	134 °C Benzol–Petroläther	$C_{15}H_{22}N_2O_2S$
XXXVI	20090	D,L-Phe	CH_3	156 °C Alkohol–Petroläther	$C_{18}H_{20}N_2O_2S$
XXXVII	20091	D,L-Met	CH_3	158 °C Zers.	$C_{14}H_{20}N_2O_2S_2$
XXXVIII	20084	D,L-Ala	CH_3	171 °C	$C_{12}H_{16}N_2O_2S$
XXXIX	20092	β-Ala	CH_3	165—166 °C	$C_{12}H_{16}N_2O_2S$
XL	20144	Gly	Cl	147—148 °C Zers. Aceton–Petroläther	$C_9H_8Cl_2N_2O_2S$

Verfahren B

3-(2,6-Dimethylphenyl)-2-thiohydantoin XXIX; Reaktion von 1-Aminodicarbonsäuren un 2,6-Di-R'-phenylisothiocyanaten, XXIX—XXXII (Tab. III/a)

Das Verfahren ist mit Verfahren *A* identisch, jedoch erfolgt eine Ringschlußreaktion der beim Ansäuern des Reaktionsgemisches erhaltenen N-Thiocarbamylaminosäuren entweder im Laufe des Umkristallisierens oder — bei **XXIX** — im Laufe eines einstündigen Erwärmens des angesäuerten Reaktionsgemisches auf dem Wasserbad.

β-[3-(4-Isoamyloxyphenyl)-2-thiohydantoin-5]-propionsäurelactam XV

21 g Carbonsäure **VIII** (Tab. I) wird mit 80 ml Essigsäureanhydrid 2 Stunden lang auf dem Wasserbad erwärmt, die Lösung anschließend eingedampft, der Trockenrückstand in 50 ml Äthylacetat gelöst und erneut eingedampft. Diese Operation wird einige Male wiederholt, bis ein kristallines Produkt erhalten wird, welches in Petroläther suspendiert und abgenutscht wird. Das derart erhaltene Rohprodukt (15,5 g) wird aus 35 ml Benzol — unter Entfärbung mit Knochenkohle — umkristallisiert. Ausbeute: 13,7 g reines **XV**. Schmelzpunkt 178 °C.

Analyse: $C_{17}H_{20}N_2O_3S$ (332,41).
Berechnet: C 61,42, H 6,06, N 8,43, S 9,64.
Gefunden: C 61,50, H 6,17, N 8,39, S 9,60.

Molekulargewicht	Analyse: Berechnet C	H	N	S	Gefunden C	H	N	S	Verfahren Bemerkung
238,30	55,43	5,92	11,75	13,45	55,33	6,11	12,00	13,75	*A*
280,38	59,96	7,19	9,99	11,43	60,09	7,29	10,17	11,61	*A*
294,40	61,19	7,53	9,51	10,88	61,32	7,44	9,50	10,88	*A*
328,42	65,82	6,14	8,53	9,76	65,87	5,98	8,66	9,90	*A*
312,44	53,81	6,45	8,96	20,52	54,05	6,52	8,97	20,72	*A*
252,33	57,11	6,39	11,10	12,70	57,28	6,41	11,30	12,61	*A*
252,33	57,11	6,39	11,10	12,70	57,27	6,34	10,97	12,78	*A*
279,13	38,72	2,88	10,03	11,48 Cl: 25,40	38,78	3,02	10,05	11,46 Cl: 25,63	*A*

Verfahren C

β-[3-(4-Isoamyloxyphenyl)-2-thiohydantoin-5]-propionsäureamide XVI—XXVIII (Tab. II)

3,32 g (0,01 *M*) Lactam **XV** werden mit 0,012—0,015 *M* des entsprechenden Amins (im Fall von **XVI** mit 0,07 *M* Ammoniumhydroxydlösung) im zehnfachen Volumen Benzol oder Alkohol 1/2—1 Stunde lang im Sieden gehalten. Beim Piperazinderivat **XVIII**, dem 2,6-Dimethylanilinderivat **XXII** und dem α-Aminopyridinderivat **XXIII** wurde kein Lösungsmittel angewendet, sondern das Gemisch der Reaktionspartner wurde bei 120—150 °C geschmolzen und 10—15 Minuten lang bei dieser Temperatur gehalten, wobei eine klare Schmelze erhalten wurde. Sowohl die Schmelzen als die aus der Reaktion in Lösung durch Eindampfen erhaltenen Rohprodukte kristallisieren beim Verreiben mit 5%iger Salzsäure. Die Produkte wurden filtriert, mit Wasser gewaschen und nach dem Trocknen aus Alkohol — unter Entfärbung mit Knochenkohle — umkristallisiert.

Tabelle IV

2-Arylimino-4-oxo-5-methylperhydro-1,3-thiazine

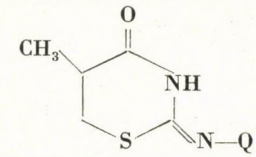

Nummer	Bezeichnung	Q	Schmelzpunkt	Bruttoformel	Molekulargewicht
XLIV	20325	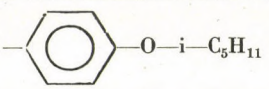	115 °C	$C_{16}H_{22}N_2O_2S$	306,41
XLV	20326	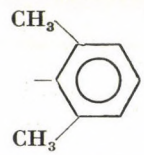	165 °C	$C_{18}H_{16}N_2OS$	248,34
XLVI	20407	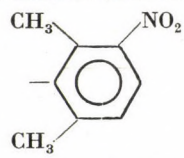	148—149 °C	$C_{13}H_{15}N_3O_3S$	293,34
XLVII	20334	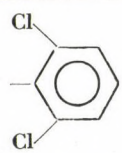	182—183 °C	$C_{11}H_{10}Cl_2N_2OS$	289,17
XLVIII	20388	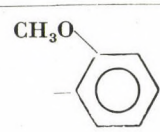	165 °C	$C_{12}H_{14}N_2O_2S$	250,31

Verfahren D

3-(2,6-Dimethylphenyl)-2-thiohydrouracyl XLI und 2-Thio-3-Q-4-oxo-perhydro-1,3-diazepine LV—LXXIV (Tab. VI/a)

Aus dem entsprechenden Isothiocyanat und bei **XLI** aus β-Alanin, bei den Diazepinen aus γ-Aminobuttersäure, werden zuerst nach Verfahren *A* die N-Q-Thiocarbamylaminosäuren **XXXIX** (Tab. III/b) bzw. **LXXIX—XCIX** (Tab. VII/a) hergestellt.

5 g N-Q-Thiocarbamylaminosäure werden bei 110—140 °C zu ungefähr 2 ml Polyphosphorsäure [14] zugegeben und das Gemisch wird 15—20 Minuten lang bei dieser Temperatur gerührt. Nach dem Abkühlen werden 60 ml Wasser zugefügt, das ausgeschiedene kristalline Produkt wird abgenutscht, mit Wasser neutral gewaschen und nach dem Trocknen aus Alkohol umkristallisiert.

Analyse								Verfahren Bemerkung
Berechnet				Gefunden				
C	H	N	S	C	H	N	S	
62,71	7,23	9,14	10,46	63,06	7,27	9,23	10,48	*F* Literatur der verwendeten Thiocarbamid-Verbindung [29]
62,87	6,49	11,28	12,91	62,84	6,44	11,34	12,92	*F* Literatur der verwendeten Thiocarbamid–Verbindung [40]
53,22	5,15	14,33	10,93	53,43	5,24	14,46	11,14	*F* Literatur der verwendeten Thiocarbamid–Verbindung [30]
45,68	3,48	9,69	11,08 Cl: 24,32	45,74	3,79	9,74	11,10 Cl: 24,31	*F* Literatur der verwendeten Thiocarbamid–Verbindung [30]
57,57	5,63	11,19	12,81	57,76	5,85	11,35	12,74	*F* Literatur der verwendeten Thiocarbamid–Verbindung [40]

Verfahren E

2-Thio-3-Q-4-oxo-perhydro-1,3-diazepine LXIX und LXXV—LXXVII (Tab. VI/a)

Diese Verbindungen wurden nach dem Verfahren *D* hergestellt, mit der Abweichung, daß die Ringschlußreaktion mit Polyphosphorsäureäthylester [15] durchgeführt wurde.

5 g γ-(N-Q-Thiocarbamyl)-aminobuttersäure werden mit 10 ml Polyphosphorsäureäthylester vermischt und 2—3 Tage lang bei Raumtemperatur stehen gelassen. Danach wird das Reaktionsgemisch mit der zehnfachen Wassermenge verrieben und mit Kaliumcarbonat neutralisiert. Ein festes Rohprodukt wurde allein bei **LXXV** erhalten, während die übrigen Verbindungen in Syrupform ausgeschieden wurden. Die letzteren wurden mit Äthylacetat aufgenommen, die Lösung mit Wasser gewaschen, über Natriumsulfat getrocknet und von dem nach dem Eindampfen als Rückstand erhaltenen Öl wurde wenig absoluter Alkohol abdestilliert. Der Rückstand kristallisiert beim Stehen bzw. beim Reiben.

Die Rohprodukte wurden aus absolutem Alkohol umkristallisiert.

Tabelle V

N-(4-Isoamyloxyphenyl)-S-alkyl-isothiocarbamide

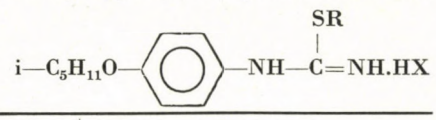

Nummer	Bezeichnung	R	Schmelzpunkt	Bruttoformel	Molekulargewicht
L	20171	C_2H_5—	96—97 °C	$C_{14}H_{23}JN_2OS$	394,32
LI	20172	i—C_5H_{11}—	135 °C	$C_{17}H_{29}BrN_2OS$	389,49
LII	20173	i—C_4H_9—	95 °C	$C_{16}H_{27}BrN_2OS$	375,36

2-Thio-4-phenyl-1,2-dihydrochinazolin XLII

5,82 g (0,06 *M*) gepulvertes Kaliumrhodanid wurden in 30 ml absolutem Aceton gelöst. Im Laufe von ca. 10 Minuten werden unter Rühren 8,4 g (0,06 *M*) Benzoylchlorid tropfenweise zugefügt. Anschließend wird das Gemisch 1/2 Stunde lang auf dem siedenden Wasserbad gerührt. Nach dem Abkühlen wird eine Lösung von 11,8 g (0,06 *M*) 2-Aminobenzophenon in 70 ml Aceton tropfenweise zugegeben und 1/2 Stunde lang im Sieden gehalten. Anschließend wird erneut abgekühlt und das ausgeschiedene Produkt abfiltriert. Die acetonische Mutterlauge wird auf das halbe Volumen eingedampft und eine fünffache Wassermenge zugegeben. Der dabei ausgeschiedene Niederschlag wird mit dem früher ausgeschiedenen Produkt vereinigt und mit Wasser gewaschen. Die nutschfeuchte Substanz wird in einem Gemisch aus 50 ml Wasser und 250 ml Alkohol suspendiert, 12 g (0,12 *M*) $KHCO_3$ werden zugegeben und 1 Stunde lang — von der völligen Auflösung gerechnet — wird zum Sieden erhitzt. Danach wird die Lösung ungefähr auf ein Viertel ihres Volumens eingedampft und mit 10%iger Salzsäure wird der pH auf 7 eingestellt, wobei ein Niederschlag ausgeschieden wird. Das ausgeschiedene Produkt wird mit Wasser gewaschen, getrocknet und aus der 100fachen Alkoholmenge umkristallisiert. Ausbeute: 9,0 g (63%). Schmelzpunkt: 226 °C (unter Zersetzung).

Analyse: $C_{14}H_{10}N_2S$ (238,30).
Berechnet: C 70,55, H 4,23, N 11,76, S 13,45%.
Gefunden: C 70,61, H 4,39, N 11,77, S 13,42%.

1-Carbäthoxy-2-thio-4-phenyl-1,2-dihydrochinazolin XLIII

2,38 g (0,01 *M*) **XLII** werden im Gemisch von 50 ml absolutem Aceton und 1,40 ml Triäthylamin suspendiert. Unter Kühlen mit kaltem Wasser werden 1,08 g (0,01 *M*) Chlorkohlensäureäthylester tropfenweise zugegeben. Das Gemisch wird 5 Stunden lang bei Raumtemperatur gerührt, über Nacht stehen gelassen, das ausgeschiedene Triäthylaminchlorhydrat filtriert und mit zweimal 10 ml absolutem Aceton gewaschen. Nach dem Eindampfen der acetonischen Lösung werden 2,20 g des gelben kristallinen Rohprodukts erhalten. Durch Umkristallisieren aus 28 ml Methanol wurden 1,70 g des reinen Produktes erhalten. Schmelzpunkt: 103—104 °C.

Analyse: $C_{17}H_{24}N_2O_2S$ (310,36).
Berechnet: C 65,78, H 4,54, N 9,03, S 10,33%.
Gefunden: C 65,79, H 4,68, N 8,92, S 10,25%.

Analyse										Verfahren Bemerkung
Berechnet					Gefunden					
C	H	N	S	X	C	H	N	S	X	
42,64	5,88	7,10	8,13	J: 32,18	42,87	5,98	7,23	8,21	J: 32,33	*G* Umkristallisieren aus Wasser
52,42	7,53	7,19	8,23	Br: 20,52	52,54	7,59	7,20	7,95	Br: 20,22	*G* Reinigung durch Fällen mit Äther aus Alkohol
51,19	7,25	7,46	8,54	Br: 21,29	51,30	7,22	7,36	8,62	Br: 20,92	*G* Reinigung durch Kochen in Petroläther

Verfahren F

2-Arylimino-4-oxo-5-methyl-perhydro-1,3-thiazine XLIX—XLVIII (Tab. IV)

0,1 *M* monosubstituiertes Thiocarbamid wird in der zehnfachen Menge *n*-Butanol suspendiert und unter Rühren mit gasförmiger Salzsäure gesättigt, wobei das Thiocarbamid gelöst wird. Es werden 17,2 g (0,2 *M*) Methacrylsäure zugegeben und das Gemisch 12—14 Stunden lang im Sieden gehalten. Nach dem Eindampfen wird das zurückbleibende Öl in 300 ml Wasser gelöst und mit $NaHCO_3$ wird neutralisiert. Die erhaltene Emulsion wird mit 3×100 ml Äthylacetat ausgeschüttelt, die vereinigten Äthylacetatphasen werden mit 10%iger $NaHCO_3$-Lösung und anschließend mit Wasser gewaschen und über Natriumsulfat getrocknet. Von dem nach dem Eindampfen zurückbleibenden Öl wird wenig absoluter Alkohol abdestilliert. Der Rückstand kristallisiert beim Verreiben mit Petroläther bzw. beim Stehen.

Das Produkt wurde aus Alkohol umkristallisiert.

N-(4-Isoamyloxyphenyl)-S-β-carboxyäthylisothiocarbamid XLIX

Diese Verbindung wird aus 1-(4-Isoamyloxyphenyl)-thiocarbamid [16] und Acrylsäureäthylester im wesentlichen nach Verfahren *F* hergestellt. Die Reaktion wurde jedoch in Äthanol durchgeführt und die Reaktionspartner wurden in äquivalenten Mengen verwendet. Nach 5stündigem Kochen wurde das Reaktionsgemisch eingedampft und anschließend 2 Stunden lang mit 10%iger wäßrigen Salzsäurelösung gekocht.

Der beim Neutralisieren des Gemisches abgeschiedene Niederschlag wird durch mehrfaches Auskochen mit Alkohol gereinigt. Schmelzpunkt: 156 °C (unter Zersetzung).

Das Produkt kann aus Alkohol mit 10% Dimethylformamidgehalt umkristallisiert werden. Schmelzpunkt: 159—160 °C (unter Zersetzung).

Analyse: $C_{15}H_{22}N_2O_3S$ (310,40).

Berechnet: C 58,04, H 7,14, N 9,02, S 10,33%.

Gefunden: C 57,92, H 7,26, N 9,18, S 10,36%.

Tabelle VI/a

2-Thio-3-Q-4-oxo-perhydro-1,3-diazepine

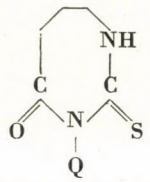

Nummer	Bezeichnung	Q	Schmelzpunkt	Bruttoformel	Molekulargewicht
LV	20690		100 °C	$C_{11}H_{12}N_2OS$	220,28
LVI	20212	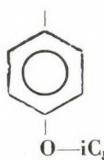	83 °C	$C_{16}H_{22}N_2O_2S$	306,41
LVII	20215	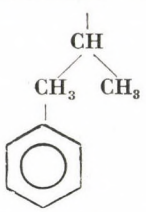	72 °C	$C_{14}H_{18}N_2OS$	262,36
LVIII	20217	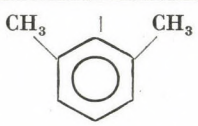	128 °C	$C_{13}H_{16}N_2OS$	248,34
LIX	20639	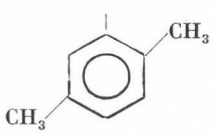	112 °C	$C_{13}H_{16}N_2OS$	248,34
LX	20242	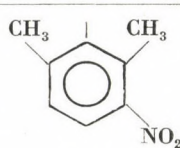	134—135 °C	$C_{13}H_{15}N_3O_3S$	293,34

Analyse								Verfahren Bemerkung
Berechnet				Gefunden				
C	H	N	S	C	H	N	S	
59,97	5,49	12,72	14,55	59,75	5,61	12,68	14,69	*D*
62,71	7,23	9,14	10,46	62,70	7,32	9,20	10,45	*D*
64,08	6,91	10,68	12,22	64,17	6,91	10,63	12,25	*D*
62,87	6,49	11,28	12,91	63,00	6,67	11,26	13,08	*D*
62,87	6,49	11,28	12,91	62,90	6,58	11,28	12,62	*D*
53,22	5,15	14,33	10,93	53,33	5,23	14,39	11,08	*D*

Tabelle VI/a (Forts.)

Nummer	Bezeichnung	Q	Schmelzpunkt	Bruttoformel	Molekulargewicht
LXI	20248	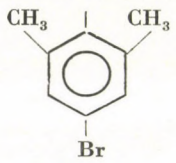	141—142 °C	$C_{13}H_{15}BrN_2OS$	327,24
LXII	20286	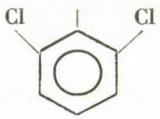	191—192 °C	$C_{11}H_{10}Cl_2N_2OS$	289,17
LXIII	20285	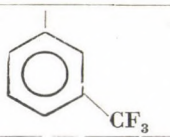	76 °C	$C_{12}H_{11}F_3N_2OS$	288,29
LXIV	20634	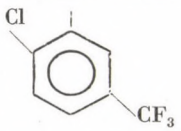	95 °C	$C_{12}H_{10}ClF_3N_2OS$	322,73
LXV	20478	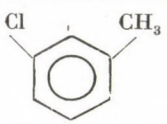	161—162 °C	$C_{12}H_{13}ClN_2OS$	268,75
LXVI	20479	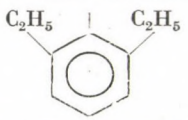	89— 90 °C	$C_{16}H_{12}N_2OS$	280,33
LXVII	20480	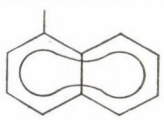	154 °C	$C_{15}H_{14}N_2OS$	270,34
LXVIII	20568	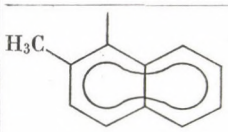	184—185 °C	$C_{16}H_{16}N_2OS$	284,37
LXIX	20524	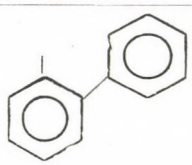	86 °C	$C_{17}H_{16}N_2OS$	296,38

Analyse								Verfahren Bemerkung
Berechnet				Gefunden				
C	H	N	S	C	H	N	S	
47,71	4,62	8,56	9,79 Br: 24,42	47,70	4,65	8,71	9,72 Br: 24,67	*D*
45,68	3,48	9,69	11,08 Cl: 24,52	45,82	3,60	9,73	10,94 Cl: 24,43	*D*
49,99	3,84	9,72	11,12	49,86	4,12	9,75	10,97	*D*
44,65	3,12	8,68	9,93	44,80	3,23	8,74	10,04	*D*
53,62	4,87	10,42	11,93 Cl: 13,19	53,57	4,95	10,49	11,97 Cl: 13,25	*D*
68,54	4,31	9,99	11,43	67,98	4,63	10,00	11,46	*D*
66,64	5,22	10,36	11,86	66,57	5,33	10,44	11,78	*D*
67,58	5,67	9,85	11,27	67,58	5,78	9,92	11,34	*D*
68,88	5,44	9,45	10,81	68,76	5,61	9,40	10,83	*E*

Tabelle VI/a (Forts.)

Nummer	Bezeichnung	Q	Schmelzpunkt	Bruttoformel	Molekulargewicht
LXX	20362	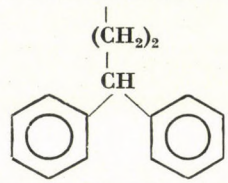	116—117 °C	$C_{20}H_{22}N_2OS$	338,45
LXXI	20569	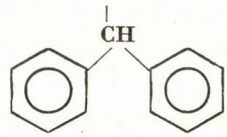	133 °C	$C_{18}H_{19}N_2OS$	311,41
LXXII	20389	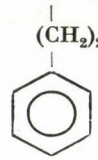	108—109 °C	$C_{13}H_{16}N_2OS$	248,34
LXXIII	20390	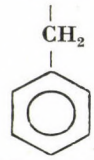	92 °C	$C_{12}H_{14}N_2OS$	234,31
LXXIV	20391	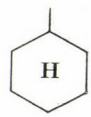	82 °C	$C_{11}H_{18}N_2OS$	226,33
LXXV	20515	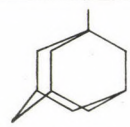	143—144 °C	$C_{15}H_{22}N_2OS$	278,40
LXXVI	20525	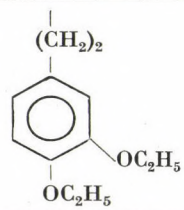	84 °C	$C_{17}H_{24}N_2O_3S$	336,44
LXXVII	20528	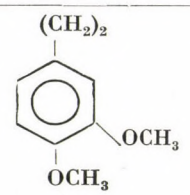	64—65 °C	$C_{15}H_{20}N_2O_3S$	308,39

Analyse								Verfahren Bemerkung
Berechnet				Gefunden				
C	H	N	S	C	H	N	S	
70,97	6,55	8,28	9,47	70,90	6,61	8,40	9,27	*D*
69,42	6,15	8,99	10,29	69,46	6,02	8,89	10,28	*D*
62,87	6,49	11,28	12,91	62,90	6,57	11,27	12,97	*D*
61,51	6,02	11,96	13,68	61,46	6,07	12,01	14,03	*D*
58,37	8,01	12,38	14,16	58,31	8,12	12,42	14,33	*D*
64,71	7,96	10,06	11,51	64,63	7,97	10,06	11,50	*E*
60,68	7,19	8,33	9,53	60,63	7,29	8,25	9,45	*E* Die im Laufe der Synthese gewonnenen N-Thiocarbamylsäuren konnten nicht in kristalliner Form isoliert werden, deshalb wurde das ölige Rohprodukt, welches aus ihrem Extrakt mit Äthylacetat durch Eindampfen erhalten wurde, unmittelbar mit Polyphosphorsäureäthylester behandelt.
58,41	6,53	9,08	10,39	58,37	6,63	9,10	10,36	

Tabelle VI/b

1-Methyl-2-thio-3-Q-4-oxo-perhydro-1,3-diazepine

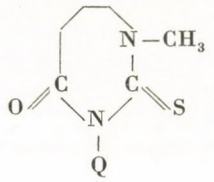

Nummer	Bezeichnung	Q	Schmelzpunkt	Bruttoformel	Molekulargewicht
LIII	20700		96 °C	$C_{12}H_{14}N_2OS$	234,31
LXXVIII	20641	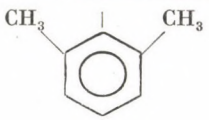	126—127 °C	$C_{14}H_{18}N_2OS$	262,36

Verfahren G

N-(4-Isoamyloxyphenyl)-S-alkyl-isothiocarbamidsalze L—LII (Tab. V)

Diese Verbindungen wurden aus 1-(4-Isoamyloxyphenyl)-thiocarbamid auf bekannte Weise [17] hergestellt.

γ-(N-Methyl-N-phenylthiocarbamyl)-aminobuttersäuremethylester CII

8 g (0,05 *M*) γ-Isothiocyanatobuttersäuremethylester [18] wurden mit 5,35 g (0,05 *M*) N-Methylanilin vermischt und am Wasserbad 1 Stunde lang erwärmt. Dann wird abgekühlt, das kristallisierte Produkt filtriert und mit Petroläther gewaschen. Das Produkt wird aus einem Gemisch von 17 ml Alkohol und 100 ml Petroläther umkristallisiert.

Ausbeute: 8,1 g. Schmelzpunkt: 54—55 °C.

Analyse: $C_{13}H_{18}N_2O_2S$ (266,35).

Berechnet: C 58,62, H 6,81, N 10,52, S 12,03%.

Gefunden: C 58,76, H 6,85, N 10,41, S 12,14%.

γ-(N-Methyl-N-phenylthiocarbamyl)-aminobuttersäure CIII

19,3 g γ-(N-Methyl-N-phenylthiocarbamyl)-aminobuttersäuremethylester werden mit 190 ml Aceton und 15 ml cc. Salzsäure vermischt und 2,5 Stunden lang zum Sieden erhitzt. Anschließend wird das Lösungmittel abgetrieben und der Rückstand mit 10%iger $NaHCO_3$-Lösung auf pH 8 eingestellt. Die abgeschiedene ölige Substanz wird mit 200 ml Äthylacetat aufgenommen und diese Lösung mit 3×80 ml 10%iger $NaHCO_3$-Lösung extrahiert. (Aus der Äthylacetatphase kann, nach Waschen mit Wasser und Trocknen, 7 g Substanz durch Ein-

Analyse								Verfahren Bemerkung
Berechnet				Gefunden				
C	H	N	S	C	H	N	S	
61,51	6,02	11,96	13,68	61,55	6,12	11,85	13,66	*H* Die Substanz wurde nach einigen Wochen ölig.
64,08	6,91	10,68	12,22	63,91	6,95	10,69	12,23	*H*

dampfen erhalten werden. Diese enthält — gemäß einem dünnschichtchromatographischen Vergleich — hauptsächlich den Ausgangsester und kann erneut der Hydrolyse unterworfen werden.)

Die ursprüngliche Lösung sowie die zur Extraktion verwendeten $NaHCO_3$-Lösungen werden vereinigt, mit Salzsäure angesäuert und das ausgeschiedene Öl wird mit 3×80 ml Äthylacetat extrahiert. Diese Lösung gibt, nach Trocknen und Eindampfen, 6 g kristallines Produkt (Schmelzpunkt 92 °C).

Die Säure kann aus einem Gemisch von Aceton und Petroläther 1 : 4 umkristallisiert werden. Nach mehrfachem Reinigen zeigte sie den Schmelzpunkt von 95°.

Analyse: $C_{12}H_{16}N_2O_2S$ (252,33).
Berechnet: C 57,11, H 6,39, N 11,10, S 12,70%.
Gefunden: C 57,27, H 6,50, N 11,13, S 12,83%.

1-(N-Methyl-N-phenylthiocarbamyl)-pyrrolidon-2 LIV

2,3 g (0,0091 *M*) γ-(N-Methyl-N-phenylthiocarbamyl)-aminobuttersäure werden in 15 ml Chloroform gelöst und eine Lösung von 6,3 g (0,03 *M*) Trifluoressigsäureanhydrid in 10 ml Chloroform wird bei —10 °C im Laufe einer halben Stunde tropfenweise zugegeben. Dann wird 24 Stunden lang bei Raumtemperatur und anschließend 4 Stunden lang bei 60 °C gerührt, bei derselben Temperatur eingedampft, der Rückstand in 60 ml Äthylacetat aufgenommen und mit 10%iger $NaHCO_3$-Lösung und danach mit Wasser neutral gewaschen. Nach dem Trocknen und Eindampfen wird wenig absoluter Alkohol vom Rückstand abdestilliert. Das erhaltene Öl kristallisiert beim Stehen. Ausbeute: 1,40 g.

Aus Aceton mehrmals umkristallisiert, ergibt sich ein Schmelzpunkt von 117—118 °C.
Analyse: $C_{12}H_{14}N_2OS$ (234,31).
Berechnet: C 61,51, H 6,02, N 11,96, S 13,68%.
Gefunden: C 61,46, H 6,18, N 12,00, S 13,73%.

Tabelle VII/a

γ-(N-Q-*Thiocarbamyl*)-*aminobuttersäuren*

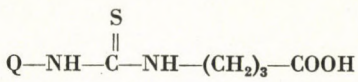

Nummer	Q	Schmelzpunkt	Bruttoformel	Molekulargewicht
LXXIX	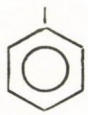	136—137 °C	$C_{11}H_{14}N_2O_2S$	283,30
LXXX	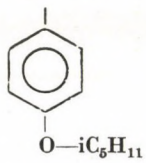	138 °C	$C_{16}H_{24}N_2O_3S$	324,43
LXXXI	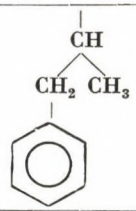	114 °C	$C_{14}H_{20}N_2O_2S$	280,38
LXXXII	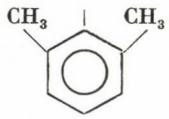	145°C	$C_{13}H_{18}N_2O_2S$	266,35
LXXXIII	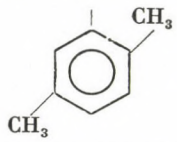	120°C	$C_{13}H_{18}N_2O_2S$	266,35
LXXXIV	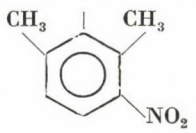	152°C	$C_{13}H_{17}N_3O_4S$	311,35
LXXXV	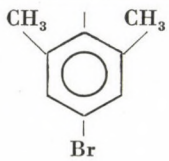	176°C	$C_{13}H_{17}BrN_2O_2S$	345,25

Analyse								Verfahren Bemerkung
Berechnet				Gefunden				
C	H	N	S	C	H	N	S	
55,44	5,92	11,76	13,45	55,40	6,05	11,82	13,50	*A*
59,23	7,45	8,63	9,88	59,38	7,59	8,68	10,02	*A* Literatur des verwendeten Isothiocyanats [41]
59,97	7,19	9,99	11,43	60,01	7,26	10,10	11,47	*A*
58,62	6,81	10,52	12,03	58,68	6,96	10,64	12,00	*A* Literatur des verwendeten Isothiocyanats [40]; hergestellt nach [20].
58,62	6,81	10,52	12,03	58,55	6,95	10,56	12,10	*A* Literatur des verwendeten Isothiocyanats [39]; hergestellt nach [20].
50,14	5,50	13,50	10,29	50,24	5,64	13,58	10,23	*A*
45,22	4,96	8,11	9,28 Br: 23,14	45,37	5,07	8,20	9,29 Br: 23,10	*A*

Tabelle VII/a (Forts.)

Nummer	Q	Schmelzpunkt	Bruttoformel	Molekulargewicht
LXXXVI	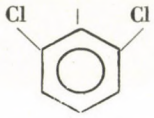	122—123 °C	$C_{11}H_{12}Cl_2N_2O_2S$	307,18
LXXXVII	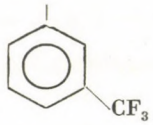	139 °C	$C_{12}H_{13}F_3N_2O_2S$	306,30
LXXXVIII	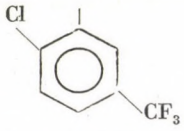	171 °C Zers.	$C_{12}H_{12}ClF_3N_2O_2S$	340,74
LXXXIX	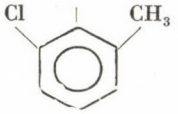	142—143 °C	$C_{12}H_{15}ClN_2O_2S$	286,76
XC	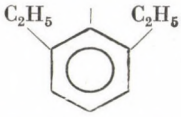	112—113 °C	$C_{15}H_{22}N_2O_2S$	294,40
XCI	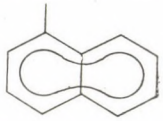	165 °C Zers.	$C_{15}H_{16}N_2O_2S$	288,36
XCII	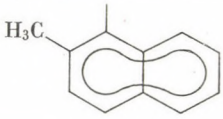	185 °C Zers.	$C_{16}H_{18}N_2O_2S$	302,38
XCIII	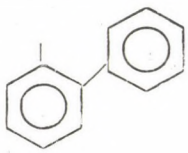	137—138 °C	$C_{17}H_{18}N_2O_2S$	314,39

Analyse								Verfahren Bemerkung
Berechnet				Gefunden				
C	H	N	S	C	H	N	S	
43,00	3,93	9,12	10,43 Cl: 23,08	43,00	3,98	9,23	10,53 Cl: 23,21	*A* Literatur des verwendeten Isothiocyanats [23].
47,05	4,27	9,15	10,46	47,28	4,35	9,25	10,58	*A* Literatur das verwendeten Isothiocyanats [22].
42,29	3,55	8,22	9,41 Cl: 10,40	42,35	3,65	8,26	9,48 Cl: 10,45	*A* Literatur des verwendeten Isothiocyanats [37]; hergestellt nach [20].
50,26	5,27	9,77	11,18 Cl: 12,36	50,35	5,40	9,85	11,20 Cl: 12,27	*A*
61,19	7,53	9,51	10,89	61,21	7,68	9,50	11,00	*A*
62,47	5,59	9,71	11,12	62,46	5,70	9,70	11,10	*A* Literatur des verwendeten Isothiocyanats [26].
63,55	6,00	9,26	10,60	63,60	6,12	9,35	10,69	*A*
64,94	5,77	8,91	10,19	64,90	5,91	9,02	10,22	*A* Literatur des verwendeten Isothiocyanats [28], hergestellt nach [20].

Tabelle VII/a (Forts.)

Nummer	Q	Schmelzpunkt	Bruttoformel	Molekulargewicht
XCIV	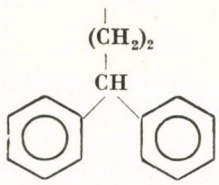	116 °C	$C_{20}H_{24}N_2O_2S$	356,47
XCV	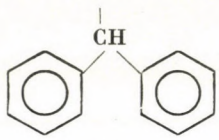	158 °C	$C_{18}H_{21}N_2O_2S$	329,43
XCVI	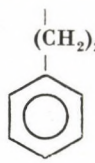	133—134 °C	$C_{13}H_{18}N_2O_2S$	266,35
XCVII	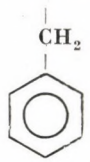	138 °C	$C_{12}H_{16}N_2O_2S$	252,33
XCVIII	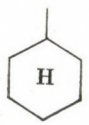	117 °C	$C_{11}H_{20}N_2O_2S$	244,35
XCIX	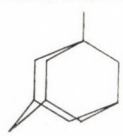	160—162 °C	$C_{15}H_{24}N_2O_2S$	296,42

Analyse								Verfahren Bemerkung
Berechnet				Gefunden				
C	H	N	S	C	H	N	S	
67,38	6,78	7,86	8,99	67,32	6,86	7,85	9,07	*A*
65,62	6,42	8,50	9,73	65,66	6,56	8,45	9,80	*A* Literatur des verwendeten Isothiocyanats [38].
58,62	6,81	10,52	12,03	58,53	6,85	10,49	11,98	*A* Literatur des verwendeten Isothiocyanats [24], hergestellt nach [21].
57,11	6,39	11,10	12,70	57,14	6,40	11,17	12,76	*A* Literatur des verwendeten Isothiocyanats [24], hergestellt nach [21].
54,06	8,25	11,46	13,12	54,02	8,26	11,50	13,12	*A* Literatur des verwendeten Isothiocyanats [25], hergestellt nach [21].
60,77	8,16	9,45	10,81	60,85	8,28	9,43	10,75	*A* Literatur des verwendeten Isothiocyanats [27].

Tabelle VIIb

γ-(N-Q-*Thiocarbamyl*)-*methylaminobuttersäuren*

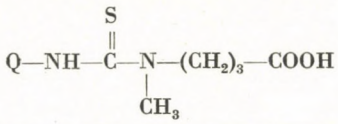

Nummer	Q	Schmelzpunkt	Bruttoformel	Molekulargewicht
C		103 °C	$C_{12}H_{16}N_2O_2S$	252,33
CI	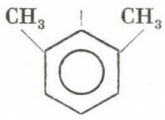	121 °C	$C_{14}H_{20}N_2O_2S$	280,38

Verfahren H

1-Methyl-2-thio-3-Q-4-oxo-perhydro-1,3-diazepine LIII und LXXVIII (Tab. VI/b)

Aus *γ*-Methylaminobuttersäure [19] und aus dem entsprechenden Isothiocyanat werden nach Verfahren *A* die *γ*-(N-Phenylthiocarbamyl)-methylaminobuttersäuren **C** und **CI** (Tab. VII/b) hergestellt. Diese werden unter Kühlen mit Eiswasser in der 2—3fachen Menge von Trifluoressigsäureanhydrid gelöst und die Lösung wird 2—3 Tage lang stehen gelassen. Dann wird das Reaktionsgemisch mit der zehnfachen Wassermenge versetzt und durch Zugabe von $NaHCO_3$ neutralisiert.

Analyse								Verfahren
Berechnet				Gefunden				
C	H	N	S	C	H	N	S	
57,11	6,39	11,10	12,70	57,10	6,48	11,03	12,71	*A*
59,97	7,19	9,99	11,43	59,92	7,28	10,03	11,48	*A*

Das rohe **LXXVIII** wird in Form eines festen Niederschlages abgeschieden; das in öliger Form abgeschiedene **LIII** wird mit Äthylacetat aufgenommen. Die letztere Lösung wird mit 10%iger $NaHCO_3$-Lösung und danach mit Wasser gewaschen und über Natriumsulfat getrocknet. Nach dem Eindampfen bleibt ein Öl zurück, welches durch Reiben zum Kristallisieren gebracht werden kann. Die Rohprodukte werden aus Äthanol umkristallisiert.

Die bei den Synthesen nach Verfahren *A*, *B*, *C*, *D*, *E* und *H* verwendeten, in der Literatur bisher nicht geschriebenen Isothiocyanate sind in Tab. VIII angeführt. Sie wurden nach bekannten Verfahren [20, 21] hergestellt.

Die Infrarotspektren wurden auf dem Zeiss Spektrophotometer IR-10 aufgenommen.

*

Für die Hilfe in der Auswertung der Spektren sei Herrn Dr. P. Sohár, für die Ausführung der Mikroanalysen Frau Dr. L. Szabó an dieser Stelle gedankt.

Tabelle VIII

Isothiocyanate

Q—N=C=S

Q	Siedepunkt	Bruttoformel	Molekulargewicht
β-Phenyl-isopropyl-	105—110 °C/0,7 mm	$C_{10}H_{11}NS$	177,26
γ, γ-Diphenylpropyl-	190—195 °C/0,4 mm	$C_{16}H_{15}NS$	253,35
β-(3,4-Dimethoxyphenyl)-äthyl-	160—163 °C/0,6 mm	$C_{11}H_{13}NO_2S$	223,28
β-(3,4-Diäthoxyphenyl)-äthyl-	160—168 °C/0,1—0,2 mm	$C_{13}H_{17}NO_2S$	251,33
2-Methyl-6-chlorphenyl-	106—108 °C/0,7—0,8 mm	C_8H_6ClNS	183,65
2,6-Dimethyl-4-bromphenyl-	—	C_9H_8BrNS	242,13
2,6-Dimethyl-3-nitrophenyl-	140—144 °C/0,2 mm	$C_9H_8N_2O_2S$	208,23
2,6-Diäthylphenyl-	106—108 °C/0,3 mm	$C_{11}H_{13}NS$	191,28
2-Methylnaphtyl-1-	146—148 °C/0,1 mm	$C_{12}H_8NS$	198,25

* Die monosubstituierten Thiocarbamide wurden nach [32] hergestellt.

Analyse				Verfahren, Bemerkung
Berechnet		Gefunden		
N	S	N	S	
7,90	18,08	7,87	17,94	nach [21]
5,53	12,65	5,45	12,50	nach [21] Nach Fraktionierung fest. Schmelzpunkt 60 °C
6,27	14,36	6,22	14,22	nach [21]
5,57	12,75	5,65	12,60	nach [21]
7,63	17,45 Cl: 19,30	7,55	17,33 Cl: 19,15	nach [20]; 16stündiges Kochen mit Chlorbenzol. Das verwendete 1-(2-Methyl-6-chlorphenyl)-thiocarbamid war unbekannt.* Schmelzpunkt 166—168 °C.
5,78	13,24 Br: 33,00	5,72	13,15 Br: 32,82	nach [20]; 8stündiges Kochen mit Chlorbenzol. Reinigung durch Extraktion mit Petroläther. 1-(2,6-Dimethyl-4-bromphenyl)-thiocarbamid [30].
13,45	15,39	13,34	15,30	nach [20]; 1-(2,6-Dimethyl-3-nitrophenyl)-thiocarbamid [30]
7,32	16,76	7,46	16,49	nach [20]; 16stündiges Kochen mit Chlorbenzol. Das 1-(2,6-Diäthylphenyl)-thiocarbamid war unbekannt.* Schmelzpunkt 196 °C. Zers.
7,06	16,17	7,15	16,22	nach [20]; 18stündiges Kochen mit Chlorbenzol. Das 1-(2-Methylnaphtyl-1)-thiocarbamid* war unbekannt. Schmelzpunkt 165 °C.

LITERATUR

1. WALTER, A. M., HEILMEYER, L.: Antibiotika Fibel, S. 419. G. Thieme Verlag, Stuttgart, 1965
2. BUU-HOI, N. P., XUONG, N. D., NAM, N. H.: C. R. Acad. Sci. (Paris) **236,** 635 (1953)
3. BUU-HOI, N. P.: Acta Tuberc. Belg. **54,** 8 (1963)
4. HUEBNER, C. F., MARSH, J. L. et al.: J. Am. Chem. Soc. **75,** 2274 (1953)
5. BUU-HOI, N. P., XUONG, N. D.: C. R. Acad. Sci. (Paris) **237,** 498 (1953)
6. EDMAN, P.: Acta Chem. Scand. **4,** 277 (1950)
7. FROELICH, E. et al.: J. Am. Chem. Soc. **76,** 3099 (1954)
8. MARTIN, D., RIECHE, A., IYER, R. N.: Arch. Pharm. **296,** 641 (1963)
9. BEHRINGER, H., SCHUNCK, R.: Chem. Ber. **100,** 564 (1967)
10. BEHRINGER, H., SCHUNCK, R.: Chem. Ber. **100,** 578 (1967)
11. GLASSER, A. C., DOUGHTY, R. M.: J. Med. Chem. **9,** 351 (1966)
12. BEHRINGER, H., ZILLIKENS, P.: Ann. Chem. Liebigs **574,** 140 (1951)
13. OVERBERGER, C. G., FRIEDMAN, H. E.: J. Org. Chem. **29,** 1720 (1964)
14. PROTIVA, M. et al.: Collection Czech. Chem. Commun. **29,** 2176 (1964)
15. POLLMANN, W., SCHRAMM, G.: Biochim. Biophys. Acta **80,** 1 (1964)
16. SPIEGEL, L., SABBATH, S.: Ber. **34,** 1943 (1901)
17. HOUBEN, J., WEYL, TH.: Meth. der Org. Chem. IX. S. 900. G. Thieme Verlag, Stuttgart, 1955
18. GARMAISE, D. L., SCHWARTZ, R., MCKAY, A. F.: J. Am. Chem. Soc. **80,** 3332 (1958)
19. MCELVAIN, S. M., VOZZA, J. F.: J. Am. Chem. Soc. **71,** 896 (1949)
20. BOXTER, J. N., CYMERMANN-CRAIG, J., MOYLE, M., WHITE, R. A.: Chem. Ind. London **27,** 785 (1954) und J. Chem. Soc. 659 **1956**
21. Org. Synth. Coll. Vol. III. 599
22. KURZER, F., CANELLE, J.: Tetrahedron **19,** 1603 (1963)
23. TOLDY, L., RADOS, M.: Ungarisches Patent 155 329 (1957)
24. DYSON, G. M., GEORGE, H. J.: J. Chem. Soc. **1924** 1705
25. SKITA, A., ROLFES, H.: Ber. **53,** 1242 (1920)
26. JOCHIMS, J. CH.: Chem. Ber. **101,** 1746 (1968)
27. STETTER, H., WULFF, C.: Chem. Ber. **95,** 2302 (1962)
28. MCMILLAN, F. H., KING, J. A.: J. Am. Chem. Soc. **72,** 4323 (1950)
29. SPIEGEL, L., SABBATH, S.: Ber. **34,** 1943 (1901)
30. TOLDY, L., FARAGÓ, K.: im Druck
31. GALSTUCHOWA, N. B., SCHTSCHUKINA, M. N.: Zhur. Obshchei Khim. **31,** 1090 (1961)
32. DOUGLAS, J. B., DAINS, F. B.: J. Am. Chem. Soc. **56,** 1408 (1934)
33. DIXON, A. E., HAWTHORNE, J.: J. Chem. Soc. **91,** 122 (1907)
34. DIXON, A. E., TAYLOR, J.: J. Chem. Soc. **91,** 912 (1907)
35. GOERDELER, J., HORSMANN, H.: Chem. Ber. **93,** 663 (1960)
36. EDMAN, P.: Acta Chem. Scand. **10,** 761 (1956)
37. KUEHLE, E., SASSE, K.: Deutsches Pat. 1 174 772 (1962)
38. KAYE, J. A., KOGON, J. C., PARRIS, C. L.: J. Am. Chem. Soc. **74** 403 (1952)
39. BUU-HOI, N. P., XUONG, N. D., NAM, N. H.: J. Chem. Soc. **1955** 1573
40. DYSON, G. M., GEORGE, H. J., HUNTER, R. F.: J. Chem. Soc. **1927** 436
41. DOUB, L. et al.: J. Am. Chem. Soc. **80,** 2205 (1958)
42. STEWART, N. W. et al.: J. Org. Chem. **13,** 134 (1948)
43. DIAZ DE TORANZO, E. G., BRIEUX, J. A.: J. Med. Chem. **10,** 982 (1967)
44. MESNARD, P., DEVAUX, G.: Prod. et Prob. Pharm. **22,** 89 (1967)

Sándor SÓLYOM
István KOCZKA
Gábor TÓTH
Lajos TOLDY

Budapest IV.,
Szabadságharcosok útja 47—49.

Acta Chimica Academiae Scientiarum Hungaricae, Tomus 68 (1—2), pp. 133—148 (1971)

NÄHERE UNTERSUCHUNG DES VERLAUFS DER MILLONSCHEN REAKTION*

J. LÁZÁR, L. MÓD und E. VINKLER

(Pharmazeutisch-chemisches Institut der Medizinischen Universität, Szeged)

Eingegangen am 15. November 1969

Die Millonsche Reaktion der substituierten Phenole wurde an den Modellverbindungen 4-Hydroxybenzoesäure **(Ib)**, 4-Hydroxybenzoesäuremethylester **(Ib)** und Tyrosin **(Ib)** untersucht.

Nach einer ausführlichen Literaturübersicht wird die Synthese der in der Millonschen Farbreaktion eine Rolle spielenden Verbindungen beschrieben. Durch Umsetzung dieser Verbindungen ineinander konnte der Verlauf der Millonschen Reaktion geklärt werden.

Verfasser stellten fest, daß die gefärbten Verbindungen die Quecksilber(II)-Komplexe der *o*-Nitrosophenole sind, u. zw. Bis-*o*-nitrosophenolmerkurat(II) **(IV)** und *o*-Nitrosophenolmerkurat(II)nitrat **(V)**. Als erste Stufe verläuft durch Einwirkung von Wärme oder bei Zimmertemperatur nach längerem Stehen eine Merkurierung. In der zweiten Stufe reagiert das entstandene Produkt **(II)** mit salpetriger Säure und es werden das *o*-Nitrosophenolderivat **(III)** bzw. dessen erwähnte gefärbte Quecksilberkomplexe **(IV** und **V)** gebildet.

Ferner wurde festgestellt, daß die Komponente des Millonschen Reagens, welche die Farbreaktion hervorruft, das Quecksilber(II)nitrit ist.

MILLON teilte im Jahre 1849 mit, daß bestimmte Proteine beim Erwärmen mit einer salpetersauren Lösung von Quecksilber eine rote Farbreaktion liefern [1, 2].

Später wurden in zahlreichen Arbeiten [3—23] Reagenzien ähnlicher Zusammensetzung — teilweise unabhängig von MILLON, teilweise mit seiner Arbeit im Zusammenhang — zum Nachweis von Proteinen bzw. Tyrosin und später von verschiedenen Phenolen empfohlen.

Seit den 1910-er Jahren bis in unsere Tage wurden durch zahlreiche Verfasser Verfahren zum Nachweis bzw. zur photometrischen Bestimmung von Phenolen, Kresolen, Vanillin [24—31], Tyrosin, Thyroxin [32—77] auf dem Gebiet der Biochemie [32—63], der Histochemie und Cytochemie [64—77], von verschiedenen, phenolische Hydroxylgruppen enthaltenden Arzneimitteln (Tubocurarin [78—80], Oestradiol [81], »Oxyphedrin« [82], »Phenylephrin« [83, 84]), von verschiedenen Estern der *p*-Oxybenzoesäure [85—96], von Protein- bzw. Aminosäurezersetzungsprodukten im Harn [97, 98] und von

* Zum Teil vorgetragen durch E. VINKLER auf der Sitzung des Komitees für organische Chemie der Ungarischen Akademie der Wissenschaften am 28. März 1967. Erschienen in Kémiai Közlemények 29, 257 (1968).

4-Oxyphenylbrenztraubensäure [99—102] mit dem Millonschen Reagens entwickelt.

Schon von der Jahrhundertwende angefangen waren Forscher damit beschäftigt, den Verlauf der Millonschen Reaktion zu klären. Im Buch von NICKEL aus dem Jahre 1890 [16] werden Nitrosophenole für das Zustandekommen der roten Farbreaktion verantwortlich gemacht. Im Zusammenhang mit der Millonschen Reaktion der Salicylsäure schrieb LINTNER 1900 [21], daß die Komponenten, welche die Farbreaktion hervorrufen, die merkurierte Salicylsäure und die salpetrige Säure sind. Beim Prüfen auf Salicylsäure soll demgemäß das Reaktionsgemisch zuerst mit Quecksilber(II)nitrat erwärmt werden; nach dem Ansäuern und Versetzen mit Natriumnitrit-Lösung entstehen dann — gemäß seiner Mitteilung — die für die Farbreaktion verantwortlichen Nitrosoverbindungen. In demselben Jahr erschien die Arbeit von VAUBEL [22], der einen zweistufigen Verlauf der Reaktion annahm: in der ersten Stufe verläuft die Nitrosierung, in der zweiten entsteht der Quecksilberkomplex.

Der Verlauf der Millonschen Reaktion wurde von GIBBS [103, 104], MCFARLANE und FULNER [37], NILSSEN [105], und später von SCHREIBER [106], KATSUMATA [107, 108], SAKAKIBARA und Mitarbeiter [109, 110] sowie NEUZIL [30] untersucht. All diese Verfasser sind einstimmig der Ansicht, daß es die Quecksilberkomplexe der im Laufe der Reaktion gebildeten Orthonitrosophenole sind, die die Farbreaktion hervorrufen. Ihre Folgerungen sind jedoch — ähnlich ihren Vorgängern vom Beginn des Jahrhunderts — durch experimentelle und analytische Angaben ungenügend unterstützt. Ihre Annahmen stützen sich auf UV-Absorptionsmaxima, papierchromatographische Konstanten, theoretische Überlegungen und Analogien.

Unser Ziel war die Isolierung und Charakterisierung der im Laufe der Millonschen Reaktion entstehenden Verbindungen, um daraus mit Hilfe der heutigen organisch-chemischen und komplex-chemischen Kenntnisse auf den Verlauf der Reaktion schließen zu können.

Die Mitteilungen von BAUDISCH [111—114] und CRONHEIM [115—117] erwiesen sich als wertvolle Hilfe in der Untersuchung der Farbreaktion, insofern als sie Angaben über die Herstellung, Eigenschaften und Komplexbildung der *o*-Nitrosophenole enthalten, ohne jedoch auf die Millonsche Reaktion hinzuweisen.

Als Modellverbindung wurde für unsere Versuche einerseits die *p*-Hydroxybenzoesäure (**Ia**) und deren Methylester (**Ib**), anderseits das in biochemischer Hinsicht interessante Tyrosin (**Ic**) gewählt. Die Verbindungen **Ia** und **Ib** erwiesen sich als besonders geeignet, da die Reaktionen von keinen störenden Nebenreaktionen begleitet werden.

Zum Hervorrufen der Millonschen Farbreaktion wurden durch die einzelnen Verfasser verschiedene Reagenzien verwendet, welche jedoch darin

übereinstimmen, daß sie alle Quecksilber(II)- und Nitritionen enthalten. So wurden z. B. salpetersaure Lösungen von metallischem Quecksilber bzw. Quecksilber(II)oxyd, sowie Gemische von Quecksilber(II)salzen z. B. Quecksilber(II)nitrat, Quecksilber(II)sulfat, Quecksilber(II)chlorid, Quecksilber(II)-acetat mit Lösungen von Kalium- bzw. Natriumnitrit verwendet.

Anfangs wurde die Reaktion gemäß der ursprünglichen Vorschrift von Millon ausgeführt; eine geringe Menge der genannten Modellverbindungen wurde mit Millonschem Reagens* erwärmt, wobei eine dunkelrote Farbreaktion auftrat. Eine ähnliche Reaktion — wie bereits seit langem bekannt ist — wurde mit tyrosinhaltigen Proteinen (z. B. mit Eiklarlösungen) und mit in verschiedenen Stellungen substituierten Phenolen erhalten [1—23].

Bei der Untersuchung der Zusammensetzung unseres Millonschen Reagens fanden wir — im Gegensatz zu der Mitteilung von DENIGES [119], daß Quecksilber(II)- und Quecksilber(I)-Ionen ungefähr im Verhältnis 3 : 2 vorliegen — daß das Reagens überwiegend Quecksilber(II)nitrat und -nitrit enthält, wobei die letztere Verbindung aus der bei der Auflösung des metallischen Quecksilbers in großen Mengen entstehenden salpetrigen Säure gebildet wird. Die Rolle der im Reagens in geringen Mengen zurückbleibenden Salpetersäure besteht darin, daß sie die Hydrolyse der entstehenden Quecksilbersalze und die Bildung von Quecksilber(I)-Ionen zurückdrängt. Dafür wird eine optimale Menge an Salpeterräure benötigt; ein Überschuß würde nämlich das wirksame Agens Quecksilbes(II)nitrit zerstören. Die im Reagens entstehende geringe Menge von Quecksilber(I)-Ionen kristallisiert als schwerlösliches Quecksilber(I)nitrit in Form eines gelben Niederschlages allmählich aus dem Reagens aus.

Mit Modellversuchen wurde festgestellt, daß unter den Komponenten des Reagens eigentlich nur das Quecksilber(II)nitrit die Farbreaktion hervorruft. Das im Reagens vorhandene Quecksilber(II)nitrit kann einerseits in dem einleitenden Schritt der Farbreaktion, der Merkurierung und anderseits in der Komplexbildung teilnehmen und trägt durch die Steigerung der Quecksilber(II)-Ionenkonzentration zu der Bildung der in Wasser leicht löslichen Komplexverbindung (V) bei, die im weiterem diskutiert wird.

Das Reaktionsgemisch aus Millonschem Reagens und *p*-Hydroxybenzoesäure bzw. deren Methylester sowie aus Tyrosin sollte nun in präparativem Maßstab hergestellt und die gebildeten Produkte sollten isoliert und identifiziert werden. Es zeigte sich, daß die Anwendung einer wäßrigen Lösung aus 1 Mol Quecksilber(II)nitrat und 2 Mol Kaliumnitrit anstelle des Millonschen Reagens, dessen Zusammensetzung sich geringfügig ändert, Vorteile hat. Es wurde

* 10 g Quecksilber werden entweder unter Kühlung in 10 g kalter rauchender Salpetersäure oder unter gelindem Erwärmen in 10 g Salpetersäure ($d = 1{,}4$) gelöst und die entstehende Lösung mit 20 ml dest. Wasser verdünnt. Nach dem Absetzen der ausgeschiedenen Kristalle wird der Reagens dekantiert [118].

festgestellt, daß in der ersten Reaktionsstufe die *p*-Hydroxybenzoesäure, ihr Methylester bzw. das Tyrosin beim Erwärmen unter der Einwirkung des Quecksilber(II)nitrits bzw. -nitrats merkuriert wird. Die entstehende Verbindung kann durch Unterbrechen der Reaktion im entsprechenden Zeitpunkt isoliert werden, jedoch hydrolisiert sie unter den Umständen der Verarbeitung zur Quecksilber(II)-hydroxyverbindung (II).

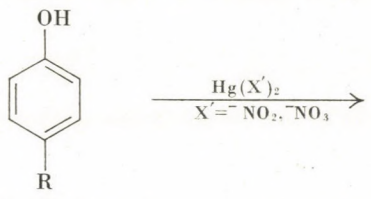

I(a, b, c) **II**

Ia: R=−COOH
Ib: R=−$COOCH_3$
Ic: R=−CH_2−CH(NH$_2$)−COOH

X″= $^-NO_2$, $-NO_3$ ill. ^-OH

Im Fall von *p*-Hydroxybenzoesäuremethylester erwies sich die Verbindung **IIc** als identisch mit dem auf andere Art [120—122] hergestellten 3-Quecksilber(II)-hydroxy-4-hydroxybenzoesäuremethylester. In dem entstehenden merkurierten Derivat **II** wird die quecksilberhaltige Gruppe durch die Wirkung der entweder ursprünglich im Reagens enthaltenen oder im Laufe der vorangehenden Merkurierungsreaktion entstandenen salpetrigen Säure mit der Nitrosogruppe ausgetauscht [123—125].

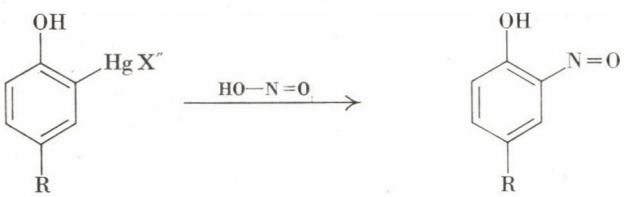

II (a, b. c) **III (a. b. c)**

Im Zusammenhang mit dieser Reaktion soll bemerkt werden, daß DIMROTH [123] bei der Reaktion von salpetriger Säure mit dem durch Merkurierung von Phenol erhaltenen 2-Quecksilber(II)-hydroxyphenol eine dunkelrote Farbreaktion beobachtete. In seiner Mitteilung bemerkt er, daß das Wesen dieser Reaktion ungeklärt sei, daß sie jedoch an die Millonsche Reaktion erinnere und nimmt an, daß letztere in jedem Falle mit der Bildung von organischen Quecksilberverbindungen in Zusammenhang stehe.

Das auf diese Weise entstehende, in statu nascendi nicht isolierbare *o*-Nitrosophenolderivat **III** bildet mit den im Reaktionsgemisch vorhandenen

Quecksilbersalzen, in Abhängigkeit von den Molverhältnissen bzw. Konzentrationsverhältnissen zweierlei Komplexverbindungen, **IV** und **V** [115, 116].

Das *o*-Nitrosophenolderivat kann aus dem Komplex freigesetzt werden und kann sogar im Fall von *p*-Hydroxybenzoesäuremethylester aus dem schwach sauren Millonschen Reaktionsgemisch, infolge der Zersetzung der Komplexe, mit Petroläther ausgeschüttelt werden.

Die Komplexbildung kann auch mit dem isolierten *o*-Nitrosophenolderivat durchgeführt werden und ebenso auch mit dem isolierten merkurierten Produkt durch Reaktion mit salpetriger Säure [21], [123]. In Abhängigkeit von der Konzentration der Quecksilbersalze entstehen zweierlei Typen von Komplexverbindungen und zwar das Bis-*o*-nitrosophenolmerkurat(II) **IV** bzw. das *o*-Nitrosophenolmerkurat(II)nitrat **V**.*

Bei *p*-Hydroxybenzoesäuremethylester kann das in Wasser unlösliche Bis-*o*-nitrosophenolmerkurat(II) **IV** leicht isoliert und unter Einhalten der entsprechenden Molverhältnisse auch hergestellt werden.

Das *o*-Nitrosophenolmerkurat(II)nitrat **V** ist nur bei entsprechend hohen Quecksilber(II)salzkonzentrationen existenzfähig, da unter abweichenden Molverhältnissen der Komplex **IV**, d. h. Bis-*o*-nitrosophenolmerkurat(II), ent-

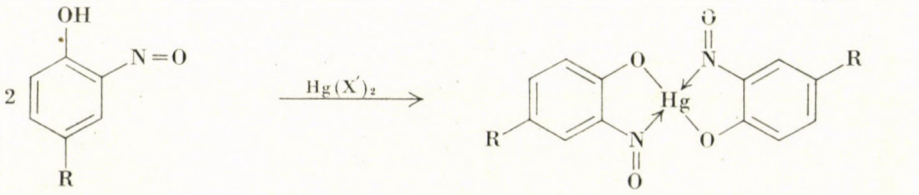

III (a, b, c) **IV (a, b, c)**

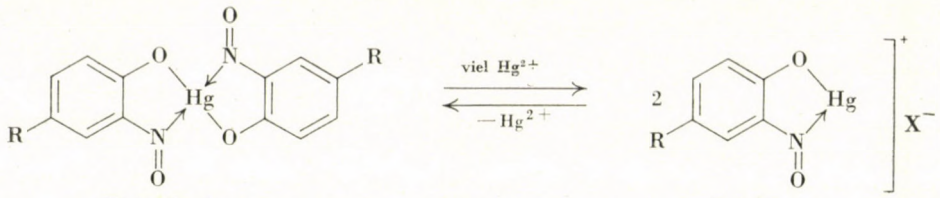

IV (a, b, c) **V (a, b, c)**

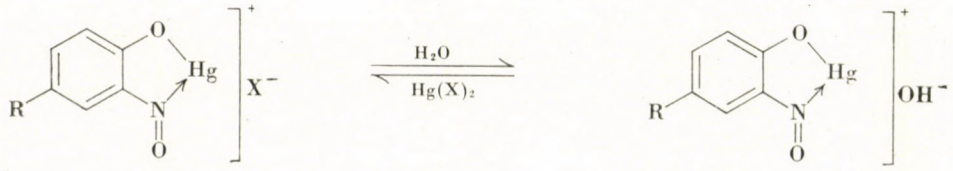

V (a, b, c) **VI (a, b, c)**

* Infolge der Tautomerie der *o*-Nitrosophenole können diese Komplexverbindungen sowohl als sechsgliedrige, als auch als fünfgliedrige Chelatringe geschrieben werden [126].

steht bzw. das entstandene *o*-Nitrosophenolmerkurat(II)nitrat **V** zu *o*-Nitrosophenolmerkurat(II)hydroxyd hydrolisiert **VI**.

Die Löslichkeitsverhältnisse und Farben der Komplexe sind verschiedenartig. Die in Wasser unlöslichen Komplexe **IV** (violett) und **VI** (kirschrot) werden unter der Wirkung von Quecksilber(II)nitratlösung zum wasserlöslichen kirschroten Komplex **V** umgesetzt.

Bei dieser Farbreaktion verschiebt sich das Gleichgewicht infolge der hohen Quecksilberionkonzentration in Richtung der Bildung der Komplexe **V**; unter Einhaltung der entsprechenden Molverhältnisse entsteht praktisch nur der lösliche, kirschrote Komplex **V**.

Wir halten es für wahrscheinlich, daß KATSUMATA und SAKAKIBARA [107, 109] diese bei der Komplexumsetzung erfolgende Farbänderung falsch deuteten und die Erscheinung durch eine wiederholte Nitrosierung der Metallkomplexe der *o*-Nitrosophenole mit der Einwirkung von salpetriger Säure erklärten (**VII**):

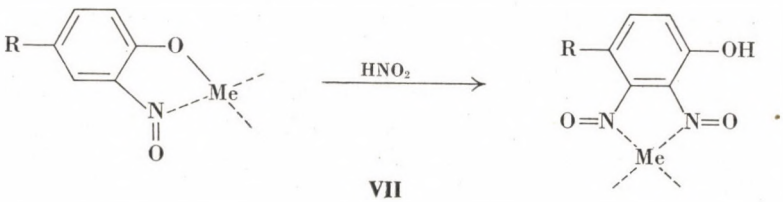

VII

Aus der dargestellten Umsetzung der Komplexe geht hervor, wie wichtig der hohe Überschuß des »Millonschen Reagens« gegenüber einer sehr geringen Menge der zu bestimmenden Verbindung bei der photometrischen Anwendung der Reaktion ist, um gut reproduzierbare Meßergebnisse zu erhalten.

Der kirschrote Komplex **V** kann mit Äther und Äthylacetat aus der wäßrigen Lösung ausgeschüttelt werden. Versucht man jedoch, das Lösungsmittel neutral zu waschen, so hydrolysiert die Verbindung und das *o*-Nitrosophenol-Quecksilber(II)hydroxyd wird in Form eines roten unlöslichen Niederschlages ausgeschieden.

Bei *p*-Hydroxybenzoesäuremethylester kristallisiert der Komplex **V** aus seiner heiß gesättigten, Quecksilber(II)nitrat enthaltenden Lösung beim Abkühlen und kann filtriert werden. Nach dem Trocknen zersetzt sich der Komplex jedoch in kurzer Zeit unter Entwicklung von nitrosen Gasen, während die Nitrosoverbindung zur Nitroverbindung oxydiert wird.

Bei *p*-Hydroxybenzoesäure erwies sich der Komplex **V** als viel stabiler und kann ohne besondere Schwierigkeiten aufbewahrt werden.

Wird die Reaktion mit dem ursprünglichen Millonschen Reagens ausgeführt, so wird ein geringer Teil der Nitrosoverbindung in der schwach sal-

petersauren Lösung — nach unseren Untersuchungen mit Frau G. SIMON — zu der Nitroverbindung **VIII** oxydiert. Dieser Vorgang kann nach BLACKALL und Mitarbeiter [127] gedeutet werden. Die isolierten trocknen Metallkomplexe werden durch Luftsauerstoff bei längerem Stehen ebenfalls oxydiert; dieser Vorgang wird durch das Erscheinen der gelben Farbe des Quecksilberoxyds und der betreffenden Nitroverbindungen angezeigt.

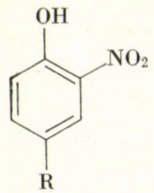

VIII (a, b, c)

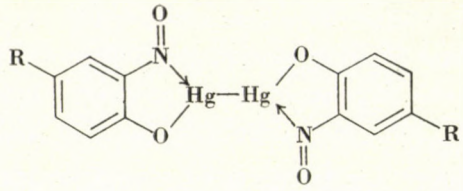

IX

Bei der Farbreaktion entstehen vermutlich außer den bereits behandelten Verbindungen in äußerst geringen Mengen Quecksilber(I)-Komplexe, infolge der eventuellen Gegenwart von geringen Mengen an Quecksilber(I)-Ionen im Reagens. Diese Annahme wird durch unsere Beobachtung unterstützt, daß das Nitrosoderivat **III**, mit Quecksilber(I)nitrat in Reaktion gebracht, zu Bis-*o*-nitrosophenolmerkurat(I) umgesetzt wird (**IX**). Diese Verbindung konnte jedoch nicht aus dem Farbreaktionsgemisch isoliert werden.

Die Gewinnung des Nitrosoderivats von Tyrosin* stieß auf Schwierigkeiten. Es gelang uns aber, die in reinem Zustand herstellbaren Silberkomplexe sowohl des Tyrosins als auch des *p*-Hydroxybenzoesäuremethylesters (**X, XI**) herzustellen.

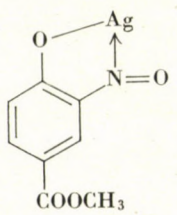

X

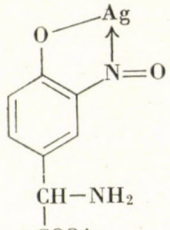

XI

Die analytischen Angaben dieser Verbindungen bestätigen die Zusammensetzung der analogen Quecksilberkomplexe in vollem Maße.

* Bei Tyrosin wurde ein fast neutrales Reagens mit Pufferwirkung verwendet (hergestellt durch Mischen von Quecksilber(II)nitrat und Kaliumnitritlösungen), womit es uns gelang, die Umsetzung der Aminogruppe zu vermeiden.

Die Lichtabsorption des Farbreaktionsgemisches stimmt mit der Lichtabsorption der Lösung des auf präparativem Wege hergestellten Komplexes **V** überein, womit die Richtigkeit unserer mittels chemischer Methoden festgestellten Schlüsse sowie die Folgerung, daß die Farbreaktion durch die kirsch-

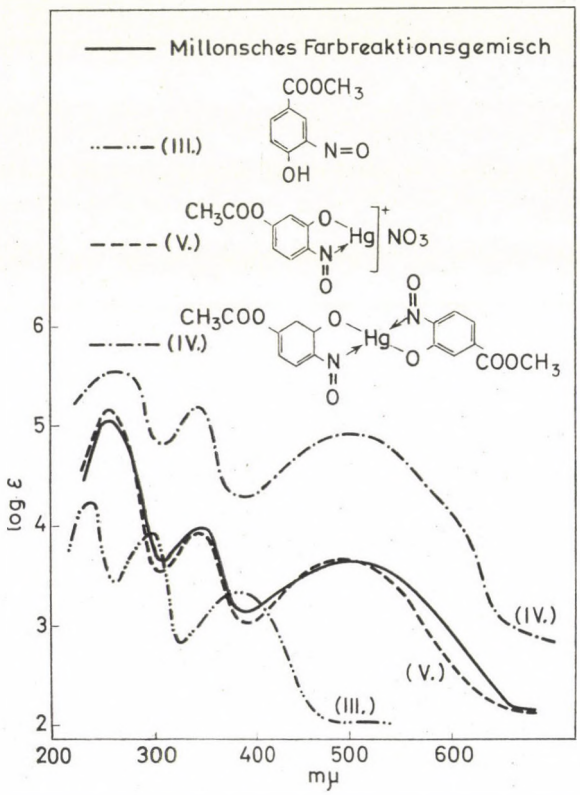

Abb. 1. Absorptionsspektrum des Millonschen Farbreaktionsgemisches und der Verbindungen **IIIb**, **IVb** und **Vb**

rote lösliche Komplexverbindung **V** hervorgerufen wird, eindeutig bewiesen werden konnte (Abb. 1).

Auf Grund unserer Versuchsergebnisse halten wir es für wahrscheinlich, daß die Millonsche Reaktion der Proteine auch im Fall des im Proteinmolekül eingebauten Tyrosins auf dem Wege der erläuterten Reaktionen zustande kommt.

Herrn Prof. Mihály Beck sei für die wertvollen Diskussionen komplexchemischer Probleme bei unserer Arbeit gedankt. Frau G. Simon danken wir für ihre Arbeit bei den Vorversuchen, Frau E. Csapó, und Frau I. Dózsai für die Analysen.

Experimenteller Teil

(Unkorrigierte Schmelzpunkte)

A) Untersuchung des Millonschen Farbreaktionsgemisches

Zu 0,15 g (0,001 *M*) 4-Hydroxybenzoesäuremethylester wurden 2—3 ml Millonsches Reagens [118] zugegeben. Nach einigen Minuten Erwärmen färbte sich das Reaktionsgemisch dunkelrot.

UV-Absorptionsmaxima:
λ_{max}: 490, 340, 256 nm.

1) 3-Nitroso-4-hydroxybenzoesäuremethylester (IIIb)

Aus dem obigen Farbreaktionsgemisch wurde nach Verreiben mit 5 g Natriumchlorid eine smaragdgrüne Verbindung mit Petroläther extrahiert. Aus dem Extrakt wurde durch Schütteln mit wäßrigen Lösungen verschiedener Schwermetallsalze (Silber, Kupfer, Quecksilber(I), Quecksilber(II) usw.) ein roter Niederschlag abgeschieden.

2) 3-Nitroso-4-hydroxybenzoesäure (IIIa), 3-Nitro-4-hydroxybenzoesäuremethylester (VIIIb), 3-Nitro-4-hydroxybenzoesäure (VIIIa)

Das nach 1) mit Petroläther bereits extrahierte wäßrige Reaktionsgemisch wurde mit Äther weiter extrahiert, wobei die 3-Nitroso-4-hydroxybenzoesäure sowie das Gemisch des 3-Nitro-4-hydroxybenzoesäuremethylesters und der 3-Nitro-hydroxybenzoesäure extrahiert wurden. Die ätherische Lösung wurde mit der wäßrigen Lösung eines Schwermetallsalzes — zweckmäßig Silbernitrat oder Kupfersulfat — geschüttelt, wobei die 3-Nitroso-4-hydroxybenzoesäure als unlösliche Komplexverbindung des Silbers bzw. Kupfers entfernt wurde, während das Gemisch der Nitroverbindungen in der ätherischen Lösung blieb. Die Trennung bzw. Identifizierung letzterer wurde mittels Dünnschichtchromatographie durchgeführt. Als Adsorbens wurde Silikagel G verwendet, als Laufmittel diente ein Gemisch von Benzol und Äther im Verhältnis 8 : 2.

3-Nitro-4-hydroxybenzoesäuremethylester (VIIIb) $R_f = 0{,}56$.
3-Nitro-4-hydroxybenzoesäure (VIIIa) $R_f = 0{,}16$.

Die im Farbreaktionsgemisch vorkommenden Verbindungen wurden durch Vergleich der aus dem in präparativen Maßstab hergestellten Gemisch nach B) isolierten Verbindungen mit authentischen Verbindungen charakterisiert, wobei die Schmelzpunkte, Mischschmelzpunkte, UV-Lichtabsorption bestimmt und Elementaranalysen durchgeführt wurden.

B) Synthese und Charakterisierung der in der Millonschen Farbreaktion eine Rolle spielenden Verbindungen

1) 3-Quecksilber(II)hydroxy-4-hydroxybenzoesäuremethylester (IIb)

a) 1,52 g (0,01 *M*) 4-Hydroxybenzoesäuremethylester (**Ib**) wurden in 10 ml Äthylalkohol gelöst und mit einer Lösung von 3,2 g (0,01 *M*) Quecksilber(II)acetat in 1 ml Eisessig und 25 ml Wasser versetzt. Das Reaktionsgemisch wurde 30 Minuten lang am Dampfbad erwärmt. Das ausgeschiedene Reaktionsprodukt wurde abfiltriert und der teilweise hydrolysierte Ester durch Waschen mit verdünntem Ammoniak entfernt, wobei das merkurierte Produkt zurückblieb.

Ausbeute: fast quantitativ.

b) Das Derivat **IIb** kann auch aus dem Millonschen Farbreaktionsgemisch isoliert werden, sofern das Gemisch im richtigen Zeitpunkt — wenn sich das Gemisch eben blaßrosa färbt — abgekühlt und das merkurierte Produkt abfiltriert wird. Das Produkt besitzt keinen reproduzierbaren Schmelz- bzw. Zersetzungspunkt.

$C_8H_8O_4Hg$ (368,753).
Berechnet: Hg 54,4%.
Gefunden: Hg 54,2%.

2) 2-Nitroso-4-hydroxybenzoesäuremethylester (IIIb)

1,52 g (0,01 *M*) 4-Hydroxybenzoesäuremethylester wurden in 7 ml Äthylalkohol gelöst und mit einer Lösung von 1,78 g (0,0055 *M*) Quecksilber(II)nitrat und 0,93 g (0,011 *M*) Kaliumnitrit in 15 ml Wasser versetzt. Das Gemisch wurde 30 Minuten lang vorsichtig auf dem Dampfbad erwärmt, wobei ein roter Niederschlag ausgeschieden wurde. Der Niederschlag wurde abfiltriert, 20%ige Salzsäure portionsweise zugegeben und die Lösung mit mehreren Portionen Petroläther extrahiert. Das Zufügen von Salzsäure und die Extraktion mit Petroläther wurde solange fortgesetzt, bis sich der Extrakt kaum mehr färbte. Die grünen Petroläther-Extrakte wurden vereinigt, mit gesättigter wäßriger Natriumchlorid-Lösung gewaschen und anschliessend mit 70 ml 5%igen Ammoniaklösung ausgeschüttelt. Die dunkelorangerote wäßrige Lösung wurde filtriert, mit Schwefelsäure angesauert und mit Petroläther extrahiert. Das Extrakt wurde mit gesättigter wäßriger Natriumchlorid-Lösung gewaschen, über geglühtem Natriumsulfat getrocknet und in Stickstoffatmosphäre auf ein Volumen von 5 ml eingedampft. Die Lösung wurde bei Zimmertemperatur und danach im Kühlschrank stehen gelassen, wobei die Kristallisation erfolgte. Anfangs wurden Verunreinigungen in Form eines gelbbraunen Öles an der Kolbenwand abgeschieden. Die Mutterlauge wurde von diesen Verunreinigungen abgegossen, das in grünen Nadeln kristallisierende Produkt wurde filtriert und in Stickstoffatmosphäre getrocknet. Im Kühlschrank, vor Sauerstoff und Licht beschützt, bleibt es längere Zeit stabil.

0,96 g, Schmelzpunkt 54—55 °C, Ausbeute 53%.
$C_8H_7NO_4$ (181,144).
Berechnet: C 53,04, H 3,89, N 7,73%,
Gefunden: C 52,84, H 3,69, N 7,85%.
UV-Absorptionsmaxima (in *n*-Hexan):
λ_{max} 385, 296, 240 nm.
log ε: 3,35, 3,96, 4,28.

3) Silber(I)-Komplex von 3-Nitroso-4-hydroxybenzoesäuremethylester (X)

Die Lösung von 3-Nitroso-4-hydroxybenzoesäuremethylester in Petroläther wurde mit 10%iger Silbernitrat-Lösung geschüttelt, wobei sich ein violettroter kristalliner Niederschlag ausschied. Der Niederschlag wurde filtriert, mit Wasser und anschließend mit Äthylalkohol gewaschen und getrocknet. Das Produkt zersetzte sich unter der Einwirkung von Licht.

Ausbeute: fast quantitativ.
Schmelzpunkt 210 °C (unter Zersetzung).
$C_8H_6NO_4Ag$ (288,016).
Berechnet: C 33,36, H 2,10, Ag 37,46%.
Gefunden: C 33,24, H 2,05, Ag 37,24%.

4) Bis-3-nitroso-4-hydroxybenzoesäuremethylestermerkurat(II) (IVb)

a) Die Lösung von 3-Nitroso-4-hydroxybenzoesäuremethylester (**IIIb**) in Petroläther wurde mit einer wäßrigen Lösung von Quecksilber(II)nitrat oder Quecksilber(II)acetat geschüttelt (Molverhältnis 2 : 1). Ein bronzeroter, in Wasser unlöslicher Niederschlag wurde abgeschieden, der in Alkohol, quecksilber(II)nitrathaltigem Wasser und in konz. Schwefelsäure löslich war.

Ausbeute: fast quantitativ.
Schmelzpunkt 173 °C.
$C_{16}H_{12}N_2O_8Hg$ (560,886).
Berechnet: Hg 35,76%.*
Gefunden: Hg 36,05%.
UV-Absorptionsmaxima (in Äthylalkohol):
λ_{max}: 496, 339, 256 nm.
log ε: 3,69, 3,97, 5,20.

b) Die Lösung von 3-Nitroso-4-hydroxybenzoesäuremethylester (**IIIb**) in Petroläther wurde im Molverhältnis 1 : 1 mit einer wäßrigen Lösung von Quecksilber(II)nitrat geschüttelt, wobei Bis-3-nitroso-4-hydroxybenzoesäuremethylestermerkurat(II) (**IVb**) ausfiel.

* Der Quecksilbergehalt wurde nach Zerstören mit konz. Schwefelsäure und Wasserstoffperoxyd durch Titrieren mit 0,1 *n* Kaliumrhodanid bestimmt.

5) 3-Nitroso-4-hydroxybenzoesäuremethylestermerkurat(II)nitrat (Vb)

a) Die Lösung von 3-Nitroso-4-hydroxybenzoesäuremethylester (**IIIb**) in Petroläther wurde mit einem großen Überschuß von 20%iger wäßriger Quecksilber(II)nitratlösung versetzt. Der kirschrote Niederschlag war 3-Nitroso-4-hydroxybenzoesäuremethylestermerkurat(II)nitrat (**Vb**). Der zersetzliche Niederschlag wurde filtriert, mit wenig verdünnter Salpetersäure gewaschen und in Stickstoffatmosphäre sofort getrocknet. Der Überschuß des Reagens kann nicht völlig aus dem Reaktionsprodukt entfernt werden, da das Produkt schnell hydrolysiert. Es zersetzt sich bereits bei Zimmertemperatur unter Entwicklung von nitrosen Gasen und besitzt keinen reproduzierbaren Schmelz- bzw. Zersetzungspunkt.

$C_8H_6N_2O_7Hg$ (442,762).
Berechnet: Hg 46,66%.
Gefunden: Hg 47,72%.
UV-Absorptionsmaxima (in Äther):
λ_{max}: 500, 340, 246 nm.

b) Die Verbindung **Vb** wird auch erhalten, wenn Bis-3-nitroso-4-hydroxybenzoesäuremethylestermerkurat(II) (**IVb**) unter Erwärmen mit 30%iger Quecksilber(II)nitratlösung aufgelöst wird. Das beim Abkühlen auskristallisierende Reaktionsprodukt (**Vb**) ist jedoch beim Erwärmen entstehenden Zersetzungsprodukten verunreinigt.

6) 3-Nitroso-4-hydroxybenzoesäuremethylestermerkurat(II)-hydroxyd (VIb)

In Wasser verteilt, hydrolysiert das 3-Nitroso-4-hydroxybenzoesäuremethylestermerkurat(II)nitrat bei Raumtemperatur langsam, bei 40—50 °C schnell. Der ausgeschiedene pulverartige, schwere, bronzefarbige Niederschlag ist in Wasser und organischen Lösungsmitteln unlöslich und löst sich in konz. Schwefelsäure unter Violettrotfärbung.

Ausbeute: fast quantitativ. Das Produkt besitzt keinen reproduzierbaren Schmelz- bzw. Zersetzungspunkt.

$C_8H_7NO_5Hg$ (397,739).
Berechnet: Hg 50,43%.
Gefunden: Hg 50,13%.

7) Bis-3-nitroso-4-hydroxybenzoesäuremethylestermerkurat(I) (IX)

Die Lösung von 3-Nitroso-4-hydroxybenzoesäuremethylester (**IIIb**) in Petroläther wurde im Molverhältnis 2 : 1 mit einer wäßrigen Quecksilber(II)nitratlösung geschüttelt. Es entstand ein in organischen Lösungsmitteln unlöslicher violettroter Niederschlag.

Ausbeute: fast quantitativ.
Schmelzpunkt: 140 °C.
$C_{16}H_{12}N_2O_8Hg_2$ (761,496).
Berechnet: Hg 52,69%.
Gefunden: Hg 52,65%.

8) 3-Nitro-4-hydroxybenzoesäuremethylester (VIIIb)

a) 3-Nitroso-4-hydroxybenzoesäuremethylester (**IIIb**) wurde längere Zeit an der Luft stehen gelassen oder es wurde Sauerstoff bzw. Luft durch seine alkoholische Lösung geleitet. Aus 50%igem Alkohol umkristallisiert wurden gelbe nadelförmige Kristalle erhalten. Schmelzpunkt 71 °C. Das Produkt **VIIIb** war mit der auf anderem Wege [128] hergestellten Verbindung identisch (Schmelzpunkt, Mischschmelzpunkt).

UV-Absorptionsmaxima (in Methanol):
λ_{max} 287, 340, 395 nm.

b) Nach der durch längerem Stehen an der Luft bewirkten Zersetzung der Metallkomplexe **Vb**, **VIb**, **IX**, **X** wurde durch ihre Extraktion mit Äther ein gelbes öliges Produkt isoliert. Aus 50%igem Alkohol umkristallisiert, erhielten wir die Verbindung **VIIIb**.

c) Das produkt **VIIIb** kann in geringen Mengen auch aus dem mit salpetersäurehaltigem Millonschen Reagens hergestellten Farbreaktionsgemisch nach A/2 isoliert werden.

9) 3-Quecksilber(II)hydroxy-4-hydroxybenzoesäure (IIa)

Die Merkurierung von 4-Hydroxybenzoesäure **Ia** erfolgte nach B/1. Das Produkt war in Natriumhydroxyd und Ammoniak leicht, in Äthylacetat wenig löslich.

Ausbeute: fast quantitativ. Das Produkt besitzt keinen reproduzierbaren Schmelz- bzw. Zersetzungspunkt.

$C_7H_6O_4Hg$ (354,716).
Berechnet: Hg 56,55%.
Gefunden: Hg 56,84%.

10) 3-Nitroso-4-hydroxybenzoesäure (IIIa)

1,38 g (0,01 *M*) 4-Hydroxybenzoesäure **Ia** wurden in 10 ml Äthylalkohol gelöst und mit einer Lösung von 1,78 g (0,0055 *M*) Quecksilber(II)nitrat und 0,93 g (0,011 *M*) Kaliumnitrit in 15 ml Wasser versetzt; nach 30 Minuten dauerndem vorsichtigem Erwärmen auf dem Dampfbad wurde ein roter kristalliner Niederschlag abgeschieden, der nach dem Abfiltrieren mit Salzsäure zersetzt und mit Äther extrahiert wurde. Der Extrakt wurde mit 5%iger Natriumhydroxydlösung geschüttelt, die wäßrige Phase filtriert, mit verdünnter Schwefelsäure angesäuert und mit Äther extrahiert. Aus dem Extrakt wurde der Kupfer(II)-Komplex des Nitrosophenols durch Schütteln mit 5%iger wäßriger Kupfer(II)sulfatlösung abgeschieden. Der Kupferkomplex wurde mit Salzsäure zersetzt, mit Alkali in die wäßrige Phase übergeführt, angesäuert und erneut mit Äther extrahiert, wobei eine dunkelgrüne Lösung erhalten wurde. Aus dieser Lösung konnte durch Eindampfen auf ein geringes Volumen oder durch Fällen mit Petroläther das grüne kristalline Produkt gewonnen werden.

0,96 g; Schmelzpunkt 153 °C; Ausbeute: 56,29%.
$C_7H_5NO_4$ (167,123).
Berechnet: C 50,31, H 3,02, N 8,38%.
Gefunden: C 50,12, H 3,17, N 8,51%.

11) 3-Nitro-4-hydroxybenzoesäure (VIIIa)

Die 3-Nitroso-4-hydroxybenzoesäure **IIIb** wurde längere Zeit an der Luft stehen gelassen. Das gelbbraune Rohprodukt lieferte nach Umkristallisieren aus 50%igem Alkohol gelbe Kristalle.

Schmelzpunkt 185 °C.

Das Produkt war mit der auf anderem Wege [129] hergestellten Verbindung identisch (Schmelzpunkt, Mischschmelzpunkt).

12) Bis-3-nitroso-4-hydroxybenzoesäuremerkurat(II) (IVa)

1,67 g (0,01 *M*) 3-Nitroso-4-hydroxybenzoesäure **IIIa** wurden in 80 ml Äther gelöst und mit der Lösung von 1,62 g (0,005 *M*) Quecksilber(II)nitrat in 15 ml Wasser geschüttelt. Die Ätherphase färbte sich braunlichrot und ein violettroter Niederschlag wurde abgeschieden. Nach Abkühlen zu 0 °C wurde filtriert und mit Wasser gewaschen. Das Produkt war in Wasser, Äther, Alkohol unter Rotfärbung geringfügig löslich. Es besaß keinen reproduzierbaren Schmelz- bzw. Zersetzungspunkt.

$C_{14}H_8N_2O_8$ (532,813).
Berechnet: Hg 37,7%.
Gefunden: Hg 37,5%.

13) 3-Nitroso-4-hydroxybenzoesäuremerkurat(II)nitrat (Va)

1,67 g (0,01 *M*) 3-Nitroso-4-hydroxybenzoesäure **IIIa** wurden in 60 ml Äther gelöst und mit 30 ml einer 30%igen Quecksilber(II)nitratlösung 15—20 Minuten lang geschüttelt. Ein kirschroter Niederschlag wurde abgeschieden, welcher filtriert, mit verdünnter Salpetersäure und anschließend mit wenig Alkohol gewaschen wurde.

Das Produkt war in Wasser und Alkohol unter Rotfärbung geringfügig löslich.

In Wasser von 40—50 °C suspendiert, hydrolysiert das Produkt langsam zu 3-Nitroso-4-hydroxybenzoesäuremerkurat(II)hydroxyd.

Schmelzpunkt 142 °C (verknallt).
$C_7H_4N_2O_7Hg$ (428,706).
Berechnet: Hg 46,44%.
Gefunden: Hg 47,86%.

14) 3-Nitrosotyrosinsilber(I) (XI)

1,82 g (0,01 *M*) Tyrosin wurden in 10 ml Wasser suspendiert und mit der Lösung von 4,87 g (0,015 *M*) Quecksilber(II)nitrat und 0,85 g (0,01 *M*) Kaliumnitrit in 15 ml Wasser versetzt. Das Gemisch wurde 30 Minuten lang im Wasserbad bei 80 °C gehalten. Ein violettrotes Produkt (4,0 g) wurde abgeschieden. Dieses wurde in 10%igem Ammoniak suspendiert, 1—2 Minuten lang geschüttelt und zentrifugiert. Die vom Niederschlag abgeschüttete Lösung wurden mit Salpetersäure neutralisiert und mit Essigsäure schwach angesäuert. Mit 10%iger Silbernitratlösung im Überschuß entstand ein schwer filtrierbarer, rotbrauner Niederschlag, der mit heißem Wasser silberionenfrei gewaschen wurde.

Schmelzpunkt 166—167 °C (unter Zersetzung).
$C_9H_8N_2O_4Ag_2$ (423,93).
Berechnet: C 25,52, H 1,90, Ag 50,94%.
Gefunden: C 25,13, H 1,95, Ag 51,33%.

15) 3-Nitrosotyrosinmerkurat(II)nitrat (Vc)

Die nach 14) hergestellte und angesäuerte Lösung des 3-Nitrosotyrosins wurde anstelle von Silbernitratlösung mit einem Überschuß von 20%iger Quecksilber(II)nitrat lösung geschüttelt. Ein violettroter kristalliner Niederschlag wurde erhalten. Das Produkt besaß keinen reproduzierbaren Schmelz- bzw. Zersetzungspunkt.

$C_9H_8N_3O_7Hg_2$ (671,36).
Berechnet: Hg 52,7%.
Gefunden: Hg 52,4%.

16) 3-Nitrotyrosin (VIIIc)

Bei der Herstellung des Silber- bzw. Quecksilberkomplexes des 3-Nitrosotyrosins gemäß 14) wurde aus der Mutterlauge, die nach dem Filtrieren des Millon-Reaktionsproduktes des Tyrosins zurückbleibt, beim Stehen ein gelbes kristallines Produkt ausgeschieden, welches nach dem Filtrieren in Ammoniak gelöst wurde. Mit Essigsäure angesäuert, wurden gelbe nadelförmige Kristalle abgeschieden (0,15 g). Das Produkt war identisch mit auf anderem Wege [122] hergestelltem Nitrotyrosin (Schmelzpunkt, Mischschmelzpunkt).

17) 3-Quecksilber(II)hydroxytyrosin (IIc) (aus dem Farbreaktionsgemisch)

Die Millonsche Farbreaktion des Tyrosins wurde im entsprechenden Zeitpunkt — als sich die Farbe des Gemisches eben nach blaßrosa veränderte — durch Abkühlen unterbrochen, wobei das merkurierte Derivat des Tyrosins erhalten wurde. Das Produkt erwies sich aufgrund analytischer Daten und chemischer Eigenschaften als identisch mit dem auf anderem Wege [120, 121, 122] hergestellten 3-Quecksilber(II)hydroxytyrosin. Es besaß keinen reproduzierbaren Schmelz- bzw. Zersetzungspunkt.

Die wäßrige Suspension des merkurierten Produktes gab mit Kalium- bzw. Quecksilbernitrit bereits bei Zimmertemperatur die für die Millonsche Reaktion charakteristische Färbung.

$C_9H_{11}O_4NHg$ (397,70).
Berechnet: Hg 50,44%.
Gefunden: Hg 51,20%.

LITERATUR

1. Millon, M. E.: C. r. Hebd. Séances Acad. Sci. **28,** 40 (1949); Annalen d. Chem. u. Pharm. **72,** 349 (1849)
2. Millon, M. E.: Annalen Chim. et phys. **29,** 507 (1850)
3. Hoffmann, R.: Annalen d. Chem. u. Pharm. **87,** 123 (1853)
4. Städeler, G.: Annalen d. Chem. u. Pharm. **116,** 37 (1860 oder 1861) C. **6,** 49 (1861)
5. Meyer, L.: Annalen d. Chem. u. Pharm. **132,** 156 (1864)
6. Kühne, W., Rudneff, A.: Archiv f. pathol. Anat. **33,** 66 (1875)
7. v. Vintschgau, M.: Sitzungsber. d. k. Akad. Wiss. 2 Wien **60,** 276/1869 (1870)
8. Plugge, P. C.: Z. anal. Chem. **11,** 173 (1872)
9. Plugge, P. C.: Pflügers Archiv f. Physiol. **5,** 538 (1872)

9. a. Plugge, P. C. Arch. Pharm. **210,** 9 (1890)

10. ALMEN, A.: Arch. Pharm. **210,** (Reihe 3, **10,**) 44 (1877)
NEUBAURER, C.: Z. anal. Chem. **17,** 103 (1878)
11. BAUMANN, E.: Ber. **12,** 1452 (1879)
12. NASSE, O.: Ber. Naturforsch. Ges. Halle **1879,** 23, C. **1879,** 487
13. HIRSCHSOHN, E.: Pharm. J. **12,** 21 (1881)
14. KRASSER, F.: Sitzungsber. Akad. Wiss. Wien. **93,** 127 (1886)
15. PHARMAZ. Zhall. Deutschland **29,** 286 (1888)
16. NICKEL, E.: Die Farbreaktionen der Kohlenstoffverbindungen. Berlin 1890
17. BRAND, J.: Z. ges. Brauw. **15,** 303 (1893) C. **1893** II 698
18. BRAND, J.: Z. ges. Brauw. **16,** 131 (1894)
19. BRAND, J.: Ber. **27,** 806 (1894)
20. BLUM, F., VAUBEL, W.: J. prakt. Chem. **165, (57)** 387 (1898)
21. LINTNER, C. J.: Z. angew. Chem. **1900,** 707 C. **1900** II 498
22. VAUBEL, W.: Z. angew. Chem. **1900,** 1125
23. NASSE, O.: Arch. ges. Physiol. **83,** 361 (1901)
24. BACH, H.: Z. anal. Chem. **50,** 736 (1911)
25. ELVOVE, E.: Bull. Hyg. lab. U.S.P.H. **110,** 25. (1917)
26. CHAPIN, R. M.: J. Ind. Eng. Chem. **12,** 711 (1920)
27. THORPE, W. V., WILLIAMS, R. T.: J. Chem Soc. **1937** 494
28. NEUZIL, E., CÉSAIRE, G. O., JOSSELIN, J.: P.harmacia milliterranea. **3,** 252 (1960)
29. JOSSELIN, J.: Thèse doct. Pharm. Bordeaux, 1961 (E. Drovillard, Bordeaux, 1963)
30. NEUZIL, E., JENSEN, (M^{me} H.) JOSSELIN, J.: Ann. pharm. franc. **25,** 127 (1967)
31. NEUZIL, E., JOSSELIN, J., JENSEN (M^{me} H.), CESAIRE, G. O.: Ann. pharm. franc. **25,** 215 (1967)
32. WEISS, M.: Biochem. Z. **97,** 170 (1919)
33. FÜRTH, O., FISCHER, A.: Biochem. Z. **154,** 1 (1924)
34. ZUWERKALOW, D.: Hoppe-Seyler' s Z. Physiol. Chem. **163,** 185 (1927)
35. FOLLIN, O., CIOCOLTEAU, V.: J. Biol. Chem. **73,** 627 (1927)
36. FOLLIN, O., MARENZI, A. D.: J. Biol. Chem. **83,** 89 (1929)
37. MC. FARLANE, W. O., FULNER, H. L.: Biochem. J. **24,** 160 (1930)
38. MÉDÈS, G.: Biochem J. **26,** 917 (1932)
39. LEIPERT, T., ALCOCH, R.: Biochem. Z. **270,** 99 (1934)
40. VON DESEŐ, D.: Biochem. Z. **271,** 142 (1934)
41. CAVETT, J. W.: J. Biol. Chem. **114,** 65 (1936)
42. ANSON, M. L.: J. gen. Physiol. **20,** 565 (1936)
43. KUHN, R., DESNUELLEN, P.: Ber. **70,** 1907 (1937)
44. ARNOV, L. E.: J. Biol. Chemistry **118,** 531 (1937)
45. LUGG, J. W. H.: Biochem. J., **31,** 1422 (1937)
46. LUGG, J. W. H.: Biochem. J., **32,** 775 (1938)
47. BERNHART, F. W.: J. Biol. Chem. **123,** X (1938)
48. BÁLINT, P.: Biochem. Z. **299,** 133 (1938)
49. BLOCH, R. J.: The Determination of Amino Acids. Burgess Publishing Co. Minneapolis, Minn. 1938
50. ANSON, M. L.: J. gen. Physiol. **22,** 79 (1939)
51. BRAND, E., KASSEL, B.: J. Biol. Chem. **131,** 489 (1939)
52. TRIMM, A. R.: Biochem. J. **35,** 1088 (1941)
53. SCHÄFFNER A., TRUELLE, M.: Biochem. Z. **315,** 391 (1943)
54. ROCHE, J., MICHEL, R.: Biochim. Biophys. Acta (Amsterdam) **1,** 335 (1947)
55. PAINTER, H. A., ZILVA, S. S.: Biochem. J. **41,** 511 (1947)
56. CONSDEN, R., GLYNN, L. E., STAINER, W. M.: Biochem. J. **55,** 248 (1953)
57. HACKMAN, R. H.: Biochem. J. **54,** 367 (1953)
58. CORFIELD, M. C., ROBSON, A.: Biochem. J. **59,** 62 (1955)
59. FRITZE, E. R., ZAHN, H.: Melliand. Textilber. **36,** 1136 (1955)
60. FORSCHER, B. K., CECIL, H. C.: Arch. Biochem. Biophysics **70,** 367 (1957)
61. SUNDARARAJAN, T. A., SARMA, P. S.: Biochem. J. **65,** 261 (1957)
62. ASHBOLT, R. F., PYDON, H. N.: Biochem. J. **66,** 237 (1957)
63. DUVAL, M., DELGA, J.: Ann. pharmac. franc. **19,** 94 (1961)
64. BENSLEY, R. R., GERSH, I.: Anat. Rec. **57,** 217 (1933)
65. SERRA, J. A.: Stain Technol. **21,** 5 (1946)
66. MIRSKY, A. E., POLLISTER, A. W.: J. Gen. Physiol. **30,** 117 (1946)
67. POLLISTER, A. W., MIRSKY, A. E.: Anat. Rec. **94,** 346 (1946)
68. POLLISTER, A. W., RIS, H.: Cold. Spr. Harb. Symp. Quant. Biol. **12,** 147 (1947)
69. POLLISTER, A. W., LEUCHTENBERGER, C.: Proc. Nat. Acad, Sci. **35,** 66 (1949)

70. LEUCHTENBERGER, C.: Chromosoma. **3,** 449 (1950)
71. ALFRET, M., BERN, H. A.: Proc. Nat. Acad. Sci. **37,** 202 (1951)
72. BRYAN, J. H. D.: Chromosoma. **4,** 369 (1951)
73. LILLIE, R. D.: Histopathologie Technic and Practical Histochemistry. Blakiston, New York, 1954
74. ALFRET, M., BERN, H. A., KAHN, R. H.: Acta Anat. **23,** 185 (1956)
75. BAKER, J. R.: Quart. J. Micr. Sci. **97,** 191 (1956)
76. WOODARD, J. W.: J. Biophys. Biochem. Cytol. **4,** 383 (1958)
77. RASCH, E., SWIFT, H.: J. Histochem. Cytochem. **8,** (1) 4 (1960); C. A. **60,** 7131 (1964)
78. FOSTER, G. E.: Analyst. **72,** 62 (1947)
79. FOSTER, G. E., TURNER, J. V.: Quart, J. Pharmac. Pharmacol. **20,** 228 (1947)
80. PRYDE, A. M., SMITH, F. R.: J. Pharmacy, Pharmacol. **1,** 192 (1949)
81. ROY, A. C.: Indien J. Pharmac. **20,** 321 (1958)
82. VOLDAN, M.: Ceskoslov. Farmac. **5,** 164 (1956)
83. ELLIN, R. I., KONDRITZER, A. A.: J. Amer. pharmac. Assoc. sci. Adit. **41,** 71 (1952)
84. FAGARD, J.: J. Pharmac. Belgique. **16,** 128 (1961)
85. KREIS, H., STUDINGER, J.: Mitt. Lebensmittelunters. Hyg. **18,** 333 (1927)
86. WEISS, F.: Z. Unters. Lebensmittel **55,** 24 (1928); C. A. **22,** 2013 (1928)
87. WEISS, F.: Z. Unters. Lebensmittel **59,** 472 (1930); C. A. **24,** 5886 (1930)
88. FELLENBERG, T., KRAUZE, S.: Mitt. Lebensmittelunters. Hyg. **23,** 111 (1932)
89. SABALITSCHKA, T.: Microchim. Acta (Ö) **2,** 111 (1937)
90. ARNOV, L. E.: J. Biol. Chem. **118,** 531 (1937)
91. ADWARDS, F. W., NAUJI, H. R., HASSEN, M. K.: Analyst. **62,** 178 (1937)
92. DEIMAIR, W., RIFFART, H., SCHMELK, E.: Mikrochemie **25** 247 (1938); C. A. **33,** 1822 (1939)
93. FRIEND, J. A.: J. Roy. Soc. New-South Wales, **80,** 244 (1942); Quart. J. Pharmac. Pharmacol. **20,** 553 (1947)
94. JOHNSON, H. W.: Analyst. **71,** (1946)
95. NEWBURGER, S. H.: J. Assoc. Offic. Agr. Chemists. **30,** 683 (1947); C. A. **42,** 1020 (1948)
96. COPPINI, C., MANZANI, A.: Ind. Conserve (Parma) **33** 117 (1958); C. A. **52,** 19715 (1958)
97. GLAUNER, W.: Münch. med. Wochenschr. **94,** 199 (1952); C. A. **47,** 1824 (1953)
98. SANO, J., MIYANOKI, T.: Seikagaku **27,** 153 (1955); C. A. **54,** 25149 (1960)
99. EMRICH, R.: Z. ges. exptl. Med. **109,** 604 (1941)
100. FELIX, K., TESKE, R.: Hoppe-Seyler's Z. physiol. Chem. **267,** 173 (1941)
101. FELIX, K.: Hoppe-Seyler's Z. physiol. Chem. **281,** 36 (1944)
102. STUBENRAUCH, W., HUBER, L.: Dtsch. med. Wschr. **74,** 404 (1949)
103. GIBBS, H. D.: Chem. Rev. **3,** 291 (1926)
104. GIBBS, H. D.: J. Biol. Chem. **71,** 445 (1926)
105. NILSSEN, B.: Tids. Textiltek. **5,** 101 (1947); C. A. **42,** 2436 (1948)
106. SCHREIBER, H.: Arch. Toxicol, **16,** 196 (1956); C. A. **53,** 22180 (1958); C. **129,** 1822 (1958)
107. KATSUMATA, M.: J. Jap. Biochem. Soc. **27,** 565, (1955); C. A. **55,** 1742 (1961); C. **128,** 11972 (1957)
108. KATSUMATA, M.: J. Jap. Biochem. Soc. **27,** 568 (1955); C. A. **55,** 1742 (1961); C. **128,** 13517 (1957)
109. SAKAKIBARA, E., KATSUMATA, M.: Kagaku no Ryoki **11,** 786 (1957); C. A. **51,** 1807 (1957)
110. SAKAKIBARA, E., KATSUMATA, M., INOUE, H., HAGIWARA, K., IGUCHI, M., KOWAGISHI, S.: Seikagaku (Biochemistry) **30,** 268 (1958); C. A. **55,** 22003 (1961); C. **130,** 11833 (1959)
111. BAUDISCH, O.: Naturwiss, **27,** 768 (1939)
112. BAUDISCH, O., SMITH, S. H.: Naturwiss, **27,** 769 (1939)
113. BAUDISCH, O.: Science **92,** 336 (1940)
114. BAUDISCH, O.: J. Am. Chem. Soc. **63,** 622 (1941)
115. CRONHEIM, G.: J. org. Chem. **12,** 1 (1946)
116. CRONHEIM, G.: J. org. Chem. **12,** 7 (1946)
117. CRONHEIM, G.: J. org. Chem. **12,** 20 (1946)
118. Die organische Analyse. Unter besonderer Berücksichtigung der Arzneistoffe. K. H. Bauer, H. Moll. R. Pohludek-Fabini, Th. Beyrich. Akademische Verlagsgesellschaft, Geest & Portig K.—G. Leipzig 1967. S. 129
119. DENIGES, G.: Bull. Trav. Soc. Pharm. Bordeaux **64,** 3 (1926)
120. MASCHMANN, H.: Annalen. **450,** 85 (1926)
121. MASCHMANN, H.: Annalen. **450,** 98 (1926)
122. BAUER, H., STRAUSS, E.: Ber. **68,** 1108 (1935)
123. DIMROTH, O.: Ber. **35,** 2856 (1902)
124. IRVIN, L., TAYLOR, F. L.: J. Am. Chem. Soc. **57,** 2460 (1935)

125. TITOV, A. I., LAPTEV, N. G.: Zhur. Obshchei. Khim. (J. Gen. Chem.) **19,** 267 (1949); C. A. **43,** 6586 (1949)
126. DYRSSEN, D., DYRSSEN, M., JOHANSSON, E.: Acta Chem. Scand. **10,** 106 (1956)
127. BLACKALL, E. L., HUGHES, E. D., INGOLD, C. K.: J. Chem. Soc. **1952,** 28
128. AUWERS, K., RÜHRIG, H.: Ber. **30,** 991 (1897). Siehe auch: Beil. **10,** 182
129. DIEPOLDER, E.: Ber. **29,** 1756 (1896). Siehe auch: Beil. **10,** 181

János LÁZÁR
László MÓD
Elemér VINKLER
Szeged, Eötvös u. 2. Ungarn.

Acta Chimica Academiae Scientiarum Hungaricae, Tomus 68 (1—2), pp. 149—154 (1971)

THE DARZENS CONDENSATION, II*

EFFECT OF SUBSTITUENTS ON THE BASE-CATALYZED DARZENS CONDENSATION

GY. SIPOS, GY. SCHÖBEL and L. BALÁSPIRI

(Institute of Applied Chemistry, A. József University, Szeged)

Received December 18, 1969

Darzens condensations of several *p*-substituted phenacyl halides and benzaldehydes have been achieved in dioxan using sodium methoxide as the catalyst. Based on the yields of the epoxy ketones, qualitative conclusions have been drawn regarding the influence of the substituents on the condensation. It has been found that the effect of the substituents is the same in the acid-catalyzed and the base-catalyzed Darzens condensation. However, the effect of the substituents in the phenacyl halides on the Darzens condensation is the opposite to that observed in the base-catalyzed aldol condensation.

The effect of substituents on the base-catalyzed Darzens condensation has hardly been studied. In the reactions of phenacyl bromide with different substituted benzaldehydes BODFORSS demonstrated that the presence of electron-withdrawing substituents ('negative groups') in the benzaldehyde component favour the condensation [1]. This statement has been confirmed by other authors [2, 3].

In JÖRLANDER's experiments, the condensation of 4-acetamino-5-nitrophenacyl chloride with *m*-nitrobenzaldehyde failed to take place; from this result it was concluded that the presence of a nitro group in the phenacyl halide component hinders the condensation [4].

The reaction components used in our experiments are shown in Table I.

Table I

Reaction components of the base-catalyzed Darzens condensation

Phenacyl halide	Benzaldehyde
1. Phenacyl chloride and bromide	1. Benzaldehyde
2. 4-Methoxyphenacyl chloride and bromide	2. 4-Methoxybenzaldehyde
3. 4-Methylphenacyl chloride and bromide	3. 4-Methylbenzaldehyde
4. 4-Chlorophenacyl chloride and bromide	4. 4-Chlorobenzaldehyde
5. 4-Bromophenacyl chloride and bromide	5. 4-Nitrobenzaldehyde
6. 4-Nitrophenacyl chloride and bromide	

* Part I: GY. SIPOS, GY. SCHÖBEL and L. BALÁSPIRI: J. Chem. Soc. 1970, 1154.

Table II

Epoxyketones from the Darzens condensation

No.	Ethylene oxide	Formula	Mol. wt.	Carbon		Hydrogen		Nitrogen		M.p., °C	
				Calcd.	Found	Calcd.	Found	Calcd.	Found	Found	Lit.
1.	1-Benzoyl-2-phenyl	$C_{15}H_{12}O_2$	225.1	80.3	80.4	5.4	5.5	—	—	88	90 [3,24]
2.	1-Benzoyl-2-*p*-chlorophyl	$C_{15}H_{11}ClO_2$	258.6	69.6	69.7	4.3	4.3	—	—	76	80 [3,25]
3.	1-Benzoyl-2-*p*-nitrophenyl	$C_{15}H_{11}NO_4$	269.2	66.9	67.0	4.1	4.2	5.2	5.3	150	148 [3,25]
4.	1-*p*-Methoxybenzoyl--2-phenyl	$C_{16}H_{14}O_3$	254.2	75.5	75.7	5.5	5.6	—	—	80	82 [26]
5.	1-*p*-Methoxybenzoyl--2-*p*-chlorophenyl	$C_{16}H_{13}ClO_3$	288.7	66.5	66.5	4.5	4.6	—	—	119	117 [5]
6.	1-*p*-Methoxybenzoyl--2-*p*-nitrophenyl	$C_{16}H_{13}NO_5$	299.2	64.2	64.3	4.3	4.4	4.7	4.8	146	168+ [27]
7.*	1-*p*-Methoxybenzoyl--2-*p*-methylphenyl	$C_{17}H_{16}O_3$	268.1	76.1	76.3	6.0	6.1	—	—	81	—
8.	1-*p*-Methylbenzoyl--2-phenyl	$C_{16}H_{14}O_2$	238.2	80.6	80.8	5.9	5.8	—	—	85	85 [28]
9.	1-*p*-Methylbenzoyl--2-*p*-chlorophenyl	$C_{16}H_{13}ClO_2$	272.7	70.4	70.4	4.8	4.7	—	—	106	105 [5]
10.	1-*p*-Methylbenzoyl--2-*p*-nitrophenyl	$C_{16}H_{13}NO_4$	283.2	67.8	67.6	4.6	4.5	4.9	5.0	152	150 [5]
11.*	1-*p*-Methylbenzoyl--2-*p*-methylphenyl	$C_{17}H_{16}O_2$	252.1	80.9	80.6	6.3	6.4	—	—	101	—
12.	1-*p*-Chlorobenzoyl--2-phenyl	$C_{15}H_{11}ClO_2$	258.6	69.6	69.7	4.3	4.3	—	—	123	123 [29]
13.	1-*p*-Chlorobenzoyl--2-*p*-chlorophenyl	$C_{15}H_{10}Cl_2O_2$	293.1	61.4	61.3	3.4	3.5	—	—	119	121 [30]
14.	1-*p*-Chlorobenzoyl--2-*p*-nitrophenyl	$C_{15}H_{10}ClNO_4$	303.6	59.3	59.2	3.3	3.3	4.6	4.7	162	160 [5]
15.	1-*p*-Bromobenzoyl--2-phenyl	$C_{15}H_{11}BrO_2$	303.1	59.4	59.2	3.6	3.7	—	—	123	125 [5]
16.	1-*p*-Bromobenzoyl--2-*p*-chlorophenyl	$C_{15}H_{10}BrClO_2$	337.6	53.3	53.3	2.9	3.0	—	—	130	131 [5]
17.	1-*p*-Bromobenzoyl--2-*p*-nitrophenyl	$C_{15}H_{10}BrNO_4$	348.1	51.7	51.5	2.9	2.8	3.9	4.0	165	165 [5]
18.	1-*p*-Nitrobenzoyl--2-*p*-nitrophenyl	$C_{15}H_{10}N_2O_6$	314.2	57.3	57.4	3.2	3.1	8.9	9.0	184	184 [5]

* New compounds
+ Probably misprint

These reactants are the same as those used in the acid-catalyzed Darzens condensation [5].

Except for two compounds, also the epoxy ketones obtained in the present experiments are the same (Table II).

The base-catalyzed reactions were carried out by allowing the reactants to stand at 10 °C for ten minutes in dioxan solution in the presence of sodium methoxide catalyst. In the condensations a 10% excess of the benzaldehyde component was used in order to avoid self-condensation [6—8]. Table III lists the yields of the epoxy ketones.

It is seen that highest yields were obtained with *p*-nitrobenzaldehyde. The yields are lower with *p*-chlorobenzaldehyde and the lowest with benzaldehyde: however, in two cases (with phenacyl chloride and bromide) the yields are the same, and in one case (with *p*-chlorophenacyl chloride) benzaldehyde gave a higher yield. *p*-Methylbenzaldehyde reacted only with *p*-methoxy- and *p*-methylphenacyl chloride and bromide.

On the basis of the results it can be concluded that the substituents attached to the benzaldehyde promote the condensation in the following order:

$$4\text{-}NO_2 > 4\text{-}Cl > H > 4\text{-}CH_3 \text{ and } 4\text{-}OCH_3$$

Table III

Yields (%) of the epoxiketones at 10 °C

Phenacyl chloride, *p*-substituent

Benzaldehyde, *p*-substituent	H	MeO	Me	Cl	Br	NO_2
OMe	—	—	—	—	—	—
Me	—	9	34	—	—	—
H	9	41	27	16	11	—
Cl	9	57	30	9	24	—
NO_2	40	66	50	21	29	

Phenacyl bromide, *p*-substituent

Benzaldehyde, *p*-substituent	H	MeO	Me	Cl	Br	NO_2
OMe	—	—	—	—	—	—
Me	—	12	32	—	—	—
H	28	49	30	30	28	—
Cl	28	55	63	35	32	—
NO_2	54	63	82	54	52	18

The above order means that the presence of electron-withdrawing substituents in the benzaldehyde component is favourable, while electron-releasing substituents are unfavourable in the base-catalyzed Darzens condensation of substituted benzaldehydes with phenacyl halides. This effect of the substituents is the same as in the acid-catalyzed Darzens [5] and the base-catalyzed aldol condensations [9—18]. Owing to the similarity of the base-catalyzed Darzens [20—22] and base-catalyzed aldol condensations [9—23], this result is to be expected.

It is well known that electron-withdrawing substituents of benzaldehyde increase the pK_{BH+} values, thereby increasing the electrophilic character of the carbon atom in the carbonyl group (supposing that pK_{BH+} is directly related to electrophilicity). In consequence of this, the rate of the condensation is accelerated in the aldolization step by electron-withdrawing, and retarded by electron-releasing, substituents. These considerations are in agreement with the experimental results.

On the basis of the yields in Table III conclusions could also be drawn concerning the influence of the substituents of the acetophenone component on the condensation. *p*-Methoxyphenacyl- and *p*-methylphenacyl chloride and bromide gave the best yields with each aldehyde. They could be brought into reaction also with *p*-methyl- and *p*-methoxy-benzaldehyde which did not react in the acid-catalyzed Darzens condensation [5]. *p*-Nitrophenacyl chloride did not give an epoxy ketone with any one of the aldehydes used. *p*-Nitrophenacyl bromide reacted only with *p*-nitrobenzaldehyde, — like in the acid-catalyzed Darzens condensation [5]. These results prove that the *p*-methoxyl and *p*-methyl groups as substituents of the phenacyl halide have favourable effect, while the *p*-nitro group has a retarding influence on the condensation [4]. The yields obtained from the other phenacyl halides are lower than in the reactions of *p*-methoxyphenacyl and *p*-methylphenacyl halides, but they are much higher yields than in the case of *p*-nitrophenacyl bromide. Thus the following order seems to be correct concerning the favourable effect of substituents of the acetophenone component:

$$4\text{-}OCH_3 \text{ and } 4\text{-}CH_3 > 4\text{-Cl, 4-Br and H} > 4\text{-}NO_2$$

According to the above order, the electron-releasing *p*-methoxyl and *p*-methyl groups are advantageous, while the electron-withdrawing *p*-nitro substituent is disadvantageous on the condensation. This effect of the substituents is the same as in the acid-catalyzed Darzens condensation [5] and it is just opposite to the effect observed in the base-catalyzed aldol condensation [9—18]. A probable explanation of this fact is the following:

On the basis of the reaction mechanism of the two base-catalyzed reactions, it is expected that the influence of the substituents on the first two

steps (enolization and aldolization) must be the same both in the Darzens and aldol condensations.

In the final step of the Darzens condensation a chloride ion is eliminated from the neighbouring carbon atom of the carbonyl group of the chlorohydrin molecule. In the aldol condensation a proton must leave the ketol molecule from the same carbon atom. As in the first case it is a chloride ion and in the second a proton which is eliminated from the same carbon atom, it seems reasonable that the effects of substituents in the ketonic component should be opposite in the Darzens and aldol condensations. Thus it is expected that electron-releasing substituents present in the ketone are favourable for the elimination of the chloride ion in the Darzens condensation, whereas electron-withdrawing substituents are advantageous for the removal of the proton in the aldol condensation.

Darzens [20–22]

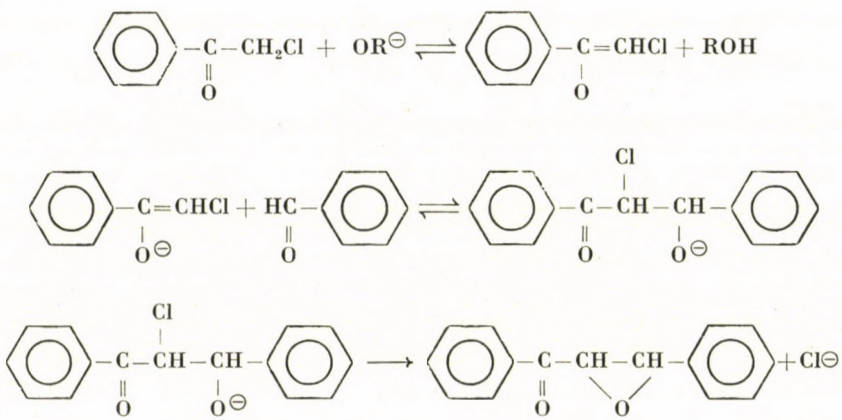

Aldol [9–23]

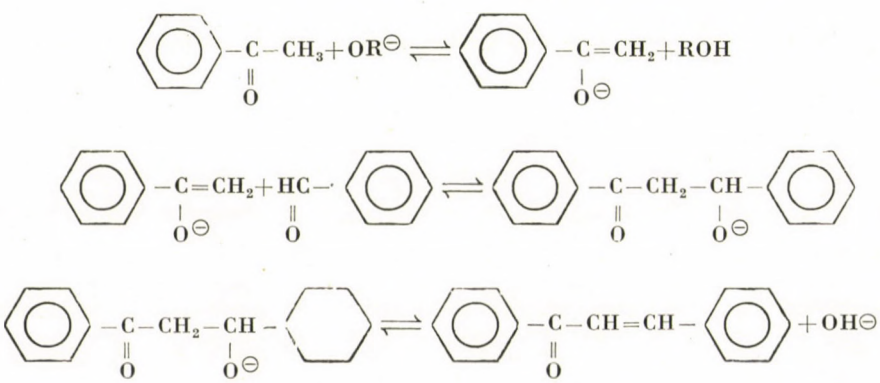

Experimental

1 mmole of the phenacyl halide (chloride or bromide) and 1.1 mmole of the benzaldehyde were dissolved in 10 ml of dioxan at 10 °C. A solution containing 2 mmoles of sodium methoxide in methanol was added, and the reaction mixture was allowed to stand at 10 °C for 10 min. The reaction was stopped by diluting the mixture with water to 40—50 ml, and neutralization to pH 7 with aqueous hydrochloric acid. After allowing the mixture to stand several days at room temperature, the precipitate was filtered off and recrystallized from 95% ethanol or acetone.

REFERENCES

1. Bodforss, S.: Ber. **51,** 192 (1918)
2. Ballester, M.: Anales real. soc. espan. fis. y quim. **50B,** 759 (1954); C. A. **49,** 8177 (1955)
3. Roth, H. J., Schwartz, M.: Arch. Pharm. **294,** 478 (1961)
4. Jörlander, H.: Ber. **50,** 1457 (1917)
5. Sipos, Gy., Schőbel, Gy., Baláspiri, L.: J. Chem. Soc. **1970,** 1154
6. Fritz, Z.: Ber. **28,** 3028 (1895)
7. Paal, C., Stern, H.: Ber. **32,** 530 (1899)
8. Paal, C., Schulze, H.: Ber. **36,** 2405 (1903)
9. Coombs, E., Evans, P. D.: J. Chem. Soc. **1940,** 1295
10. Schraufstätter, E., Deutsch, S.: Ber. **81,** 489 (1948)
11. Walker, E. A., Young, J. R.: J. Chem. Soc. **1957,** 2041
12. Széll, T.: Ber. **91,** 2609 (1958)
13. Sipos, Gy., Széll, T.: Acta Phys. et Chem. Szeged, **6,** 109 (1960)
14. Dhar, D. N.: J. Indian Chem. Soc. **37,** 799 (1960)
15. Sipos, Gy., Furka, A., Széll, T.: Monatsch. **91,** 643 (1960)
16. Széll, T., Eastham, A. M., Sipos, Gy.: Can. J. Chem. **42,** 2417 (1964)
17. Sipos, Gy., Széll, T.: Acta Phys. et Chem. Szeged. **11,** 43 (1965)
18. Széll, T., Sohár, I.: Acta Chim. Acad. Sci. Hung. **62,** 429 (1969)
19. Sipos, Gy., Cseh, I., Kalmár, A.: Acta Phys. et Chem. Szeged, **16,** 45 (1970)
20. Ballester, M., Bartlett, P. D.: J. Am. Chem. Soc. **75,** 2042 (1953)
21. Ballester, M.: Chem. Rev. **55,** 283 (1955)
22. Ballester, M., Perez-Blanco, D.: J. Org. Chem. **23,** 652 (1958)
23. Noyce, D. S., Pryor, W. A., Bottini, A. H.: J. Am. Chem. Soc. **77,** 1402 (1955)
24. Widman, O.: Ber. **49,** 477 (1916)
25. Bodforss, S.: Ber. **49,** 2795 (1956)
26. Jörlander, H.: Ber. **49,** 278s (1916)
27. Ballester, M.: Anales real. sec. espan. fis. y quim. **50B,** 475 (1954); C. A. **49,** 8901 (1955)
28. House, H. O., Ryerson, D. G.: J. Am. Chem. Soc. **83,** 979 (1961)
29. Jörlander, H.: Ber. **50,** 406 (1917)
30. House, H. O.: J. Am. Chem. Soc. **78,** 2298 (1956)

György Sipos
György Schöbel
Lajos Baláspiri
Szeged, Béke-épület, Rerrich tér, Hungary.

Acta Chimica Academiae Scientiarum Hungaricae, Tomus 68 (1—2), pp. 155—159 (1971)

STRUCTURE ELUCIDATION OF TWO TETRABROMO-TETRADEOXYHEXITOL ISOMERS BY MASS SPECTROMETRY

(SHORT COMMUNICATION)

GY. HORVÁTH and J. KUSZMANN

(Research Institute for Pharmaceutical Chemistry, Budapest)

Received May 20, 1970

The structure of two tetrabromohexitols obtained *via* the reaction of 1,6-dibromo-1,6-dideoxy-2,3:4,5-dianhydrogalactitol with hydrogen bromide was elucidated by mass spectrometry, as being 1,3,4,6-tetrabromo-1,3,4,6-tetradeoxyallitol and 1,2,4,6-tetrabromo-1,2,4,6-tetradeoxy-D,L-mannitol, respectively.

Cleavage of the epoxy rings in 1,6-dibromo-1,6-dideoxy-2,3 : 4,5-dianhydrogalactitol (**I**) by hydrogen bromide yielded two compounds *A* and *B*, both being tetrabromo-tetradeoxyhexitols as shown by their analytical data [1]. According to the attack of the bromide ions on the different bridge atoms, four isomers **II**, **IIIa**, **IIIb** and **IV** may be formed theoretically. As the possibility of an epoxy migration [2] cannot be excluded, the appearance of further four compounds **Va**, **Vb**, **VIa** and **VIb** has to be taken into consideration. The mannitol derivatives **IIIa** + **IIIb** and the two pairs of the tallitol derivatives **Va** + **Vb** and **VIa** + **VIb**, respectively, being antipodes, will form the corresponding racemates **III**, **V** and **VI**.

For elucidating the structure of the separated compounds *A* and *B* mentioned above, their mass spectra were taken. As compounds differing only in their configuration give identical mass spectra [3], the tetrabromohexitols **II**—**VI** are all included in the four structure isomers **VII**—**X**, which are expected to give different fragmentation patterns.

The fission of bonds being in α-position to the hydroxyl groups will strongly influence the mass spectrometric behaviour of alcohol derivatives [4]. Accordingly it can be predicted, which fragment ions must be among others of considerable abundance in the spectra of the isomeric structures **VII**—**X**.

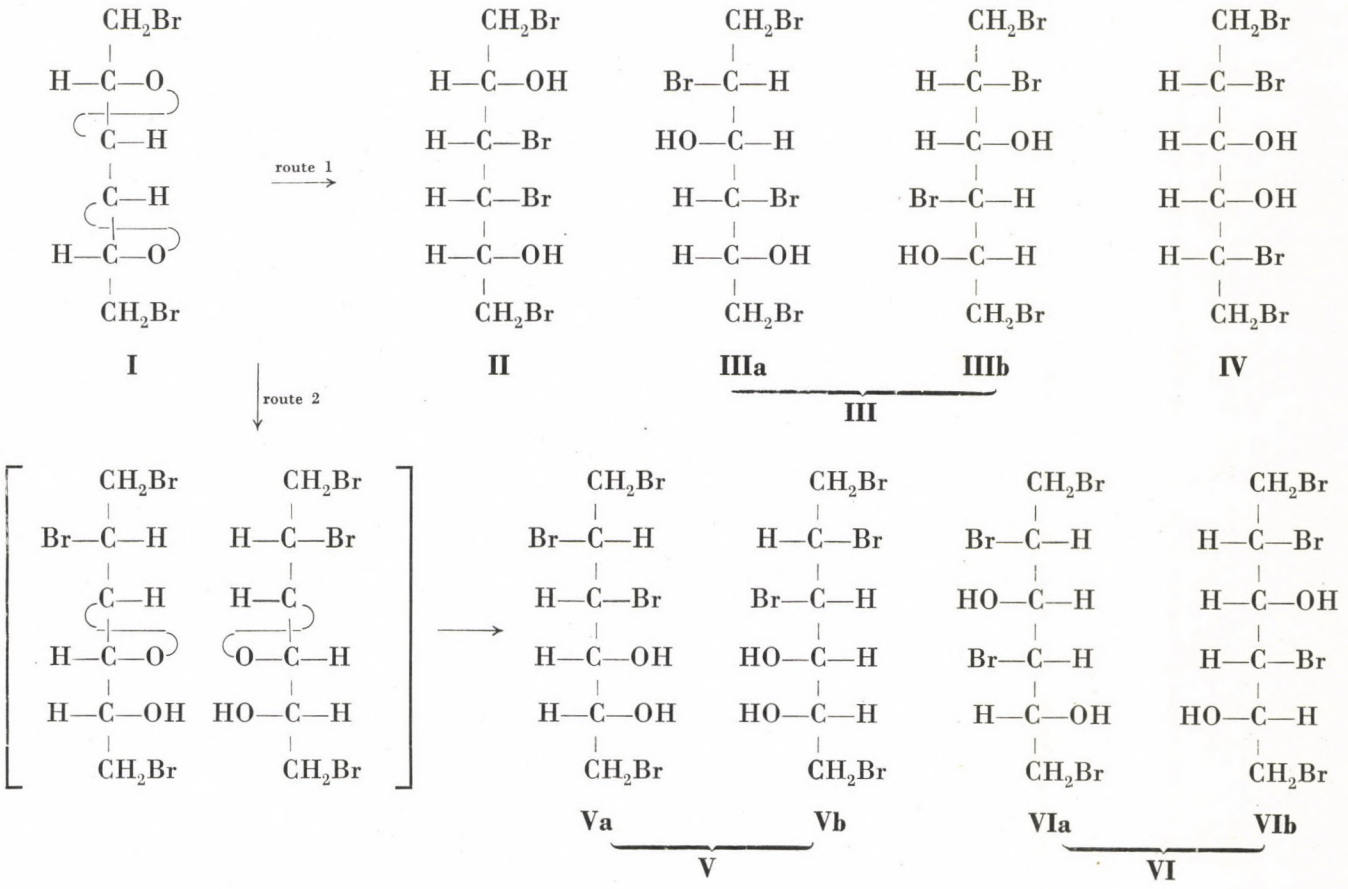
route 1
route 2
I
II
IIIa
IIIb
III
IV
Va
Vb
V
VIa
VIb
VI

In the spectrum of structure **VII**:

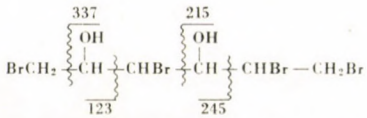

VII

the ions $m/e = 337$; 245; 215 and 123.*

In the spectrum of structure **VIII**:

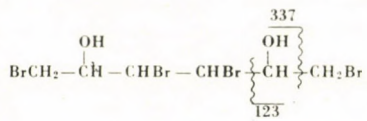

VIII

the ions $m/e = 337$ and 123.*

In the spectrum of structure **IX**:

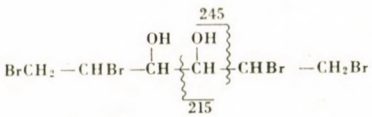

IX

the ions $m/e = 245$ and 215,* the latter with high abundance [5].

In the spectrum of structure **X**:

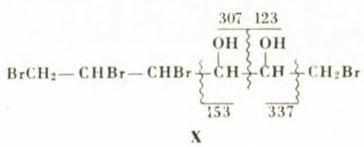

X

the ions $m/e = 337$; 307; 153 and 123.*

Comparing these considerations with the two spectra obtained, it can be seen that the spectrum of compound *A* (Fig. 1) belongs to structure **VIII** and that of compound *B* (Fig. 2) to structure **VII**. The latter corresponds to the isomers **III** and **VI**, but structure **VIII** is due to compound **II** only. The isomers **II** and **III** are formed *via* the same route (*1*) while route *2* ought to give, besides isomer **VI**, at least some of isomer **V**, which was not detectable. Accordingly, route *2* can be ruled out, and so the structure of compound *A* corresponds to 1,3,4,6-tetrabromo-1,3,4,6-tetradeoxyallitol (**II**) and that of compound *B* to 1,2,4,6-tetrabromo-1,2,4,6-tetradeoxy-D,L-mannitol (**III**). The absence of the

* Each with the corresponding bromine isotope-peak distribution.

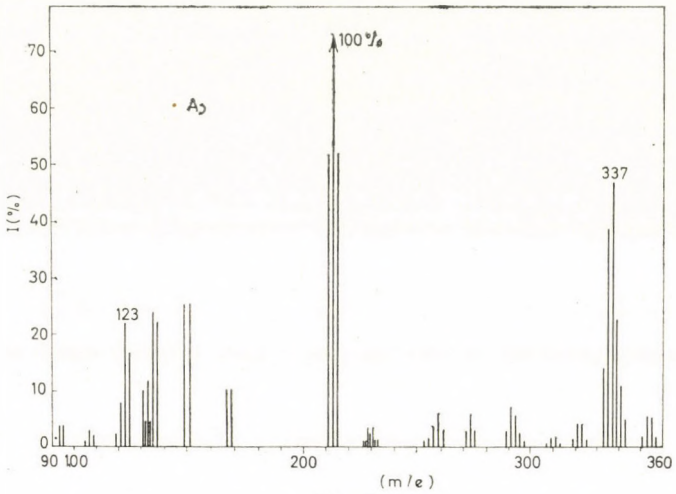

Fig. 1

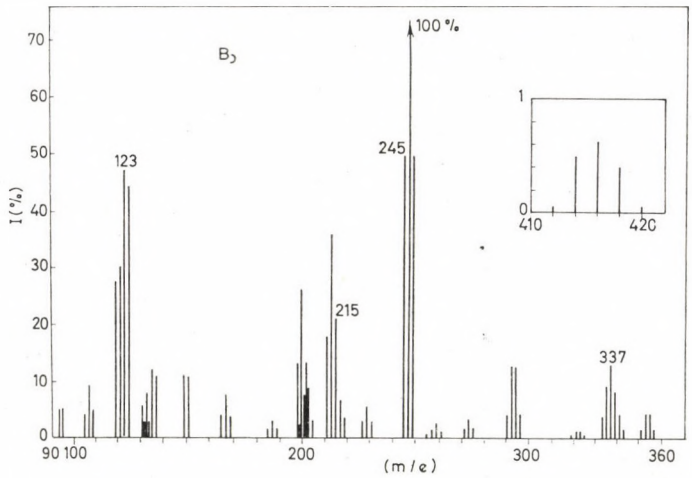

Fig. 2

allitol derivative **IV**, which also should be formed by the same route (*1*), can be explained by conformational considerations [1].

The rearrangements leading to the loss of water and the fragmentations connected with them will be discussed in detail later.

Experimental

Mass spectra were recorded on a MAT-CH-4 instrument with TO-4 inlet system at an evaporation temperature of 70 °C.

*

Compounds *A* and *B* were obtained according to the literature [1] by treating compound **I** with hydrobromic acid. The crude mixture of the tetrabromo derivatives (*A* + *B*) was separated by column chromatography on silicic acid, using chloroform–ethyl acetate

(3 : 1) as solvent. The fractions containing the separated components were evaporated and the residues recrystallized from ethyl acetate–ether to give pure compound *A* (**II**), m. p. 127—128 °C, (found: C 16.98; H 2.37; Br 73.58%) and *B* (**III**), m. p. 125—126 °C, (found: C 16.72; H 2.39; Br 73.42%; calcd. for $C_6H_{10}O_2Br_4$: C 16.61; H 2.32; Br 73.68%). Both compounds gave single spots on thin-layer chromatograms (Kieselgel G, chloroform–ethyl acetate 3 : 1) $A = R_f$ 0.45 and $B = R_f$ 0.35. They were optically inactive (acetone) and consumed no periodate.

*

Our thanks are due to Prof. G. SNATZKE (Bonn) for providing us with the mass spectra.

REFERENCES

1. KUSZMANN, J., VARGHA, L.: Carbohyd. Res. **16**, 261 (1971)
2. (*a*) JARMAN, M., ROSS, W. C. J.: Carbohyd. Res. **9**, 139 (1969)
   (*b*) BUCHANAN, J. G., EDGAR, A. R.: Carbohyd. Res. **10**, 295 (1969)
3. SPITELLER, G.: Massenspektrometrische Strukturanalyse organischer Verbindungen, p. 199. Verlag Chemie, Weinheim, 1966
4. BUDZIKIEWICZ, H., DJERASSI, C., WILLIAMS, D. H.: Mass Spectrometry of Organic Compounds, p. 94. Holden—Day, San Francisco 1967
5. (*a*) WULFSON, N. S., GOLOVKINA, L. S., VAVER, V. A., PROKAZOVA, N. V., BERGELSON, L. D.: Izv. Akad. Nauk S. S. S. R. Ser. Chim, **1967**, 2415
   (*b*) Ref. 4. p. 104

Gyula HORVÁTH
János KUSZMANN
Budapest IV., Szabadságharcosok u. 47.

Acta Chimica Academiae Scientiarum Hungaricae, Tomus 68 (1—2), pp. 161—167 (1971)

POLYMERISATION DES METHYLMETHACRYLATS BEI HOHEN UMSÄTZEN, V

UNTERSUCHUNG DER VERZÖGERUNGSWIRKUNG VON DINITROBENZOLEN

I. MONDVAI, L. HALÁSZ und A. KESCHITZ

(Lehrstuhl für die Plast- und Gummiindustrie der Technischen Universität, Budapest)

Eingegangen am 3. Oktober 1969

Die Blockpolymerisation von Methylmethacrylat wurde bei unterschiedlichen Temperaturen in Gegenwart von *o*-, *m*- und *p*-Dinitrobenzol untersucht. Es wurden die relativen Geschwindigkeitskonstanten k_5/k_2 und die für das Absinken der Polymerisationsgeschwindigkeit bei hohen Umsätzen charakteristischen $K_{1,rel}$-Werte bestimmt. Beim Vergleich fällt auf, daß von der untersuchten Verzögerern das *o*-Dinitrobenzol der wirksamste ist. Die Verzögererwirkung aller drei Isomere ist dem Effekt der Mononitrophenole ähnlich.

Die Polymerisation von mit Azo-diisobuttersäurenitril initiiertem Methylmethacrylat in Gegenwart von *p*-Dinitrobenzol ist durch KICE [1] untersucht worden. Bei der Polymerisation von Methylacrylat wurde neben dem erwähnten Dinitrobenzol [2, 3, 4] auch die verzögernde Wirkung des *o*-Dinitrobenzols [3] studiert. In Gegenwart aller drei Dinitrobenzol-Isomere untersuchten die Styrolpolymerisation TÜDŐS und Mitarbeiter [5], während die Vinylacetatpolymerisation von mehreren Autoren [4, 6, 7, 8] bearbeitet wurde. Im Falle des letztgenannten Monomers sind die Werte von k_5/k_2 so groß, daß man anstelle von Verzögerung besser von Inhibierung sprechen sollte.

Experimenteller Teil

Über die Versuchsmethodik sowie die Monomer- und Initiatorreinigung wurde bereits in der vorangegangenen Arbeit [9] berichtet.

Alle drei verwendeten Dinitrobenzole waren von handelsüblicher analytisch reiner Qualität und besaßen folgende, nach der Mikromethode von Kofler bestimmte Schmelzpunkte:

o-Dinitrobenzol: 117 °C,
m-Dinitrobenzol: 90 °C,
p-Dinitrobenzol: 172 °C.

Ergebnisse

Unsere Versuche wurden neben gleicher Initiator-Konzentration ($7{,}48 \cdot 10^{-2}$ Mol l^{-1} bei 50 °C, $3{,}31 \cdot 10^{-2}$ Mol l^{-1} bei 60 °C und $6{,}61 \cdot 10^{-3}$ Mol l^{-1} bei 70 °C), aber verschiedenen Verzögerermengen durchgeführt. Unter den Zeit-Umsatz-Kurven stellen wir die in Gegenwart von *p*-Dinitrobenzol erhaltenen Kurven in Abb. 1 vor. Die mit den anderen zwei Dinitro-

benzolen erhaltenen Kurven haben einen ähnlichen Verlauf. Zur Bestimmung der Anfangsgeschwindigkeit der Polymerisation wurden die Werte von $\lg \frac{1}{1-x}$ als Funktion der Zeit dargestellt. Die erhaltenen Geraden, aus deren Anstieg die Anfangsgeschwindigkeit der Polymerisation berechnet wurde, sind aus Abb. 2 ersichtlich. Die Zahlenwerte für die Anfangsgeschwindigkeit der Polymerisation enthalten die Tabellen I, II und III.

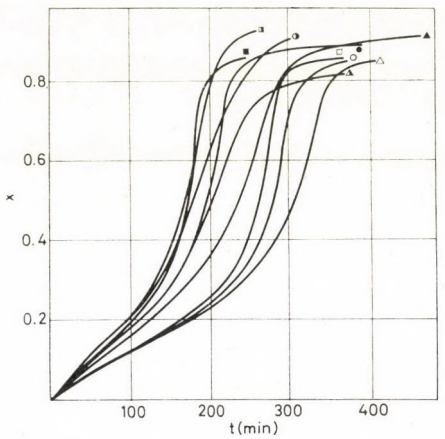

Abb. 1. Zeit-Umsatz-Kurven in Gegenwart von verschiedenen Mengen *p*-Dinitrobenzol

Temperatur 50 °C
Benzoylperoxydkonzentration: $7{,}48 \cdot 10^{-2}$ Mol l^{-1}

Temperatur 60 °C
Benzoylperoxydkonzentration: $3{,}31 \cdot 10^{-2}$ Mol l^{-1}

Temperatur 70 °C
Benzoylperoxydkonzentration: $6{,}61 \cdot 10^{-2}$ Mol l^{-1}

Verzögererkonzentrationen:

□ $2{,}66 \cdot 10^{-2}$ Mol l^{-1}
○ $3{,}99 \cdot 10^{-2}$ Mol l^{-1}
△ $5{,}33 \cdot 10^{-2}$ Mol l^{-1}

■ $3{,}02 \cdot 10^{-2}$ Mol l^{-1}
● $5{,}59 \cdot 10^{-2}$ Mol l^{-1}
▲ 0,112 Mol l^{-1}

◨ $2{,}79 \cdot 10^{-2}$ Mol l^{-1}
◑ $4{,}36 \cdot 10^{-2}$ Mol l^{-1}
◭ $5{,}92 \cdot 10^{-2}$ Mol l^{-1}

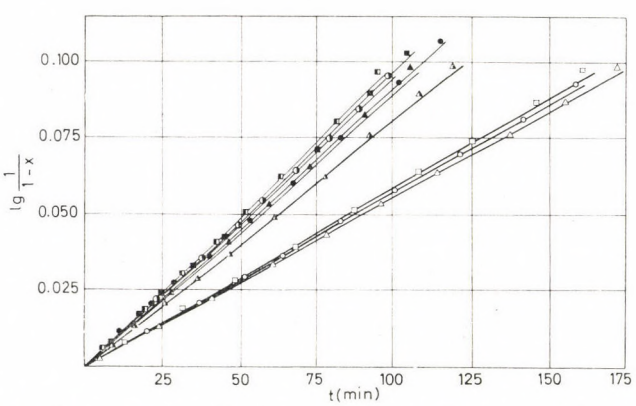

Abb. 2. Einfluß der Änderung der Konzentration des *p*-Dinitrobenzols auf die Anfangsgeschwindigkeit der Polymerisation

Tabelle I

Charakteristische Daten der Polymerisation in Gegenwart von o-Dinitrobenzol
Benzoylperoxydkonzentrationen: $7{,}48 \cdot 10^{-2}$ Mol l^{-1} bei 50 °C, $3{,}31 \cdot 10^{-2}$ Mol l^{-1}bei 60 °C, $6{,}61 \cdot 10^{-3}$ Mol l^{-1} bei 70 °C

Temperatur	z Mol l^{-1}	W_{st} Mol l^{-1} sec^{-1}	K_1	x_1	x_2
50 °C	$9{,}45 \cdot 10^{-3}$	$2{,}000 \cdot 10^{-4}$	0,061	0,28	0,90
50 °C	$1{,}42 \cdot 10^{-2}$	$1{,}898 \cdot 10^{-4}$	0,046	0,24	0,86
50 °C	$1{,}89 \cdot 10^{-2}$	$1{,}803 \cdot 10^{-4}$	0,033	0,20	0,82
60 °C	$7{,}45 \cdot 10^{-3}$	$3{,}481 \cdot 10^{-4}$	0,113	0,30	0,85
60 °C	$1{,}49 \cdot 10^{-2}$	$3{,}339 \cdot 10^{-4}$	0,054	0,22	0,87
60 °C	$2{,}97 \cdot 10^{-2}$	$3{,}245 \cdot 10^{-4}$	0,022	0,13	0,91
70 °C	$1{,}19 \cdot 10^{-2}$	$3{,}056 \cdot 10^{-4}$	*	*	*
70 °C	$1{,}79 \cdot 10^{-2}$	$2{,}638 \cdot 10^{-4}$	*	*	*
70 °C	$2{,}38 \cdot 10^{-2}$	$2{,}284 \cdot 10^{-4}$	*	*	*

* Bei hohen Umsätzen sank die Polymerisationsgeschwindigkeit so weit ab, daß keine Daten mehr bestimmt werden konnten.

Tabelle II

Charakteristische Daten der Polymerisation in Gegenwart von m-Dinitrobenzol
Benzoylperoxydkonzentrationen: $7{,}48 \cdot 10^{-2}$ Mol l^{-1} bei 50 °C, $3{,}31 \cdot 10^{-2}$ Mol l^{-1} bei 60 °C, $6{,}61 \cdot 10^{-2}$ Mol l^{-1} bei 70 °C

Temperatur	z Mol l^{-1}	W_{st} Mol l^{-1} sec^{-1}	K_1	x_1	x_2
50 °C	$5{,}64 \cdot 10^{-2}$	$2{,}142 \cdot 10^{-4}$	0,095	0,28	0,85
50 °C	$8{,}46 \cdot 10^{-2}$	$2{,}111 \cdot 10^{-4}$	0,071	0,26	0,84
50 °C	0,113	$2{,}079 \cdot 10^{-4}$	0,054	0,25	0,84
60 °C	$4{,}13 \cdot 10^{-2}$	$3{,}323 \cdot 10^{-4}$	0,127	0,30	0,86
60 °C	$8{,}25 \cdot 10^{-2}$	$3{,}197 \cdot 10^{-4}$	0,060	0,22	0,89
60 °C	0,165	$2{,}945 \cdot 10^{-4}$	0,026	0,13	0,88
70 °C	$3{,}55 \cdot 10^{-2}$	$3{,}733 \cdot 10^{-4}$	0,039	0,23	0,92
70 °C	$5{,}33 \cdot 10^{-2}$	$3{,}701 \cdot 10^{-4}$	0,035	0,18	0,90
70 °C	$7{,}10 \cdot 10^{-2}$	$3{,}670 \cdot 10^{-4}$	0,029	0,13	0,88

Aus den Anfangsgeschwindigkeiten berechneten wir die von BAGDASARJAN [10] eingeführten Verzögerungsparameter. Unter diesen haben wir die aus den in Gegenwart von *p*-Dinitrobenzol vorgenommenen Messungen berechneten Werte auf Abb. 3 aufgeführt. Aus den Verzögerungsparametern lassen sich die Werte von k_5/k_2 mit Hilfe der folgenden Gleichung berechnen [10]

$$\frac{FW_0}{z} = \frac{k_5}{k_2} \frac{k_2^2}{k_4} m a, \tag{1}$$

Tabelle III

Charakteristische Daten der Polymerisation in Gegenwart von p-Dinitrobenzol
Benzoylperoxydkonzentrationen: $7{,}48 \cdot 10^{-2}$ Mol l^{-1} bei 50 °C, $3{,}31 \cdot 10^{-2}$ Mol l^{-1} bei 60 °C, $6{,}61 \cdot 10^{-2}$ Mol l^{-1} bei 70 °C

Temperatur	z Mol l^{-1}	W_{st} Mol $l^{-1}sec^{-1}$	K_1	x_1	x_2
50 °C	$2{,}66 \cdot 10^{-2}$	$2{,}095 \cdot 10^{-4}$	0,176	0,33	0,86
50 °C	$3{,}99 \cdot 10^{-2}$	$2{,}048 \cdot 10^{-4}$	0,127	0,32	0,86
50 °C	$5{,}33 \cdot 10^{-2}$	$2{,}000 \cdot 10^{-4}$	0,100	0,31	0,86
60 °C	$3{,}02 \cdot 10^{-2}$	$3{,}449 \cdot 10^{-4}$	0,210	0,33	0,86
60 °C	$5{,}59 \cdot 10^{-2}$	$3{,}260 \cdot 10^{-4}$	0,105	0,28	0,90
60 °C	0,112	$2{,}898 \cdot 10^{-4}$	0,047	0,23	0,92
70 °C	$2{,}79 \cdot 10^{-2}$	$3{,}504 \cdot 10^{-4}$	0,068	0,23	0,95
70 °C	$4{,}36 \cdot 10^{-2}$	$3{,}347 \cdot 10^{-4}$	0,059	0,20	0,89
70 °C	$5{,}92 \cdot 10^{-2}$	$3{,}197 \cdot 10^{-4}$	0,049	0,18	0,83

wobei F der Verzögerungsparameter, W_0 die Anfangsgeschwindigkeit der Polymerisation in Abwesenheit des Verzögerers, z die Verzögererkonzentration, k_2, k_4 und k_5 die Geschwindigkeitskonstanten der Wachstums-, Abbruchs- und Verzögerungsreaktion und m die Monomerkonzentration ist. Die Werte von a gibt der folgende Ausdruck an:

$$a = (1-q)\ (1 + \lambda). \tag{2}$$

Hier bedeutet q die Wahrscheinlichkeit der Kettenregenerierungsreaktion,

$$\lambda = \frac{k_5\, r\, z}{k_5\, r\, z + k_6\, z^2}, \tag{3}$$

wobei r die Radikalkonzentration und k_6 die Geschwindigkeitskonstante der bimolekularen Abbruchsreaktion der aus den Verzögerermolekülen gebildeten intermedieren Radikale ist.

Die Geschwindigkeit der letztgenannten Reaktion ist — allgemein aus chemischen Gründen — gewöhnlich viel kleiner als die der Reaktion zwischen den intermediären Radikalen und den Polymerradikalen (gemischte Rekombination) und ist deshalb nicht konkurrenzfähig. Dem ist es zuzuschreiben, daß sie meist unberücksichtigt bleibt, in welchem Falle der Wert von λ definitionsgemäß $\lambda = 1$ ist. Wenn F dem Bruch z/W_0 proportional ist, gibt es keine Regenerierung der Ketten ($q = 0$ und $a = 2$).

Auch in Gegenwart der anderen beiden Dinitrobenzole erhielten wir ähnliche Ergebnisse wie der auf Abb. 3 gezeigte Zusammenhang. Die Anstiege

der erhaltenen Geraden und die berechneten Werte von k_5/k_2 enthält Tabelle IV. Zur Berechnung der Verzögerungsparameter wurden die zu den bei verschiedenen Temperaturen benutzten Benzoylperoxydkonzentrationen gehörenden Werte der Anfangspolymerisationsgeschwindigkeit aus Zitat [9] übernommen. Auf Grund der Arbeiten [11, 12] berechneten wir die Werte für k_2^2/k_4, die bei 50 °C $5{,}40 \cdot 10^{-3}$, bei 60 °C $1{,}04 \cdot 10^{-2}$ und bei 70 °C $1{,}80 \cdot 10^{-2}$ $Mol^{-1}\,l\,sec^{-1}$ betragen. Es sei bemerkt, daß bei einer Temperatur von 60 °C die

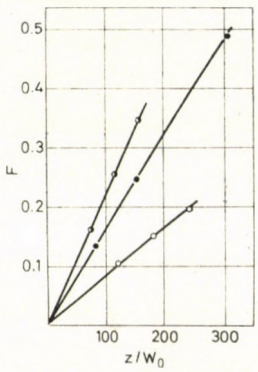

Abb. 3. Abhängigkeit der Verzögerungsparameter von den z/W_0-Werten, in Gegenwart von *p*-Dinitrobenzol ○: Temperatur 50 °C, ●: Temperatur 60 °C, ◑: Temperatur 70 °C

Konzentrationserhöhung von *o*- und *m*-Dinitrobenzol eine Abweichung von der Geraden bewirkt. Wenn $\lambda = 1$ angenommen wird, so ist in Gegenwart des *o*-Dinitrobenzols bei einer Verzögererkonzentration von $1{,}49 \cdot 10^{-2}$ Mol l^{-1} $q = 0{,}14$ aus der Abweichung berechnet, während für eine Verzögererkonzen-

Tabelle IV

Verzögerungswirkung von Dinitrobenzolen im Anfangsabschnitt der Polymerisation

	Temperatur	$\frac{F\,W_0}{z}$ 10^3	$\frac{k_5}{k_2}$ 10^2
	50 °C	4,60	4,51
o-Dinitrobenzol	60 °C	5,72	2,90
	70 °C	15,8	4,65
	50 °C	0,23	0,225
m-Dinitrobenzol	60 °C	1,85	0,939
	70 °C	0,36	0,106
	50 °C	0,84	0,824
p-Dinitrobenzol	60 °C	1,61	0,817
	70 °C	2,20	0,647

tration von $2{,}97 \cdot 10^{-2}$ Mol l^{-1} $q = 0{,}44$ ist. Ähnlich ist in Gegenwart des *m*-Dinitrobenzols bei einer Verzögererkonzentration von $8{,}25 \cdot 10^{-2}$ Mol l^{-1} $q = 0{,}33$, während für eine Verzögererkonzentration von 0,165 Mol l^{-1} $q = 0{,}69$ ist.

Ähnlich wie bei den in früheren Arbeiten untersuchten Verzögerern [13, 14] werteten wir den Polymerisationsabschnitt nach Auftreten des Geleffekts mit Hilfe der Gleichung von SAWADA [15] aus. Wenn wir gemäß der Gleichung die Werte von $\frac{1}{x_2 - x_1} \ln \frac{x - x_1}{x_2 - x}$ als Funktion der Zeit darstellen,

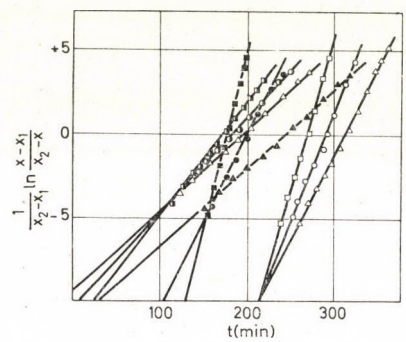

Abb. 4. Einfluß der Änderung der Konzentration von *p*-Dinitrobenzol auf die Polymerisation bei hohen Umsätzen

so erhalten wir Geraden, die auf Abb. 4 gezeigt sind. Die Steilheit der Geraden liefert die für die durch den Geleffekt verursachte Geschwindigkeitserhöhung charakteristischen K_1 Werte, die zusammen mit den Werten x_1 und x_2 in den Tabellen I, II und III zusammengefaßt sind. Wie aus den Tabellen hervorgeht, wird mit der Zunahme der Verzögererkonzentration der Umsatz x_1, bei dem der Geleffekt auftritt, kleiner. Der Grenzumsatz (x_2) stellt keine eindeutige Funktion der Verzögererkonzentration dar, in den meisten Fällen erreicht er innerhalb eines gegebenen Bereiches der Verzögererkonzentration ein Maximum, dessen Wert gleich oder größer ist als der in Anwesenheit der gleichen Initiatormenge, jedoch ohne Verzögerer gemessene Wert. Die Temperaturabhängigkeit des Grenzumsatzes besitzt auch hier den gleichen Charakter wie bei den früher untersuchten Verzögerern [13, 14]. Es sei erwähnt, daß in Gegenwart von *o*-Dinitrobenzol bei 70 °C der Grenzumsatz überraschend klein ist. Der durch Extrapolation der Zeit-Umsatz-Kurven erhaltene Wert beträgt bei einer Konzentration von $2{,}38 \cdot 10^{-2}$ Mol l^{-1} 0,12 und auch im Falle einer Verzögererkonzentration von $1{,}19 \cdot 10^{-2}$ Mol l^{-1} nur 0,5.

Zur Charakterisierung der Wirksamkeit der untersuchten Verzögerer bei hohen Umsätzen wurden auch hier die $K_{1,\,rel}$-Werte (der Quotient der in Gegenwart bzw. in Abwesenheit des Verzögerers gemessenen K_1-Werte) verwendet, die auf Abb. 5 in Abhängigkeit von der Verzögererkonzentration dargestellt

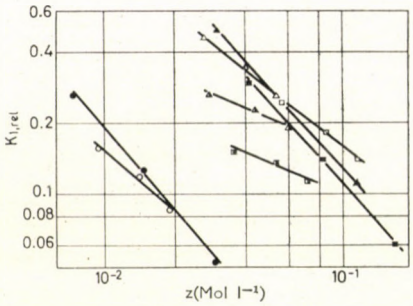

Abb. 5. Einfluß der Konzentrationsänderung des Verzögerers auf die $K_{1,rel}$-Werte

○: *o*-Dinitrobenzol bei 50°C ●: bei 60 °C
□: *m*-Dinitrobenzol bei 50 °C ■: bei 60 °C ◨: bei 70 °C
△: *p*-Dinitrobenzol bei 50 °C ▲: bei 60 °C ◭: bei 70 °C

sind. Übereinstimmend mit unseren früheren Untersuchungen fallen die $K_{1,rel}$-Werte beim Anstieg der Verzögererkonzentration stark ab [13, 14]. Ebenso ist das Absinken der Polymerisationsgeschwindigkeit im Anfangsabschnitt der Reaktion bedeutend geringer als bei hohen Umsätzen.

Ein Vergleich der Wirksamkeit der untersuchten Verzögerer sowohl im Anfangsabschnitt der Polymerisation als auch bei hohen Umsätzen zeigt, daß das *o*-Dinitrobenzol am aktivsten ist. Zwischen der Wirksamkeit der anderen beiden Dinitrobenzole gibt es keinen wesentlichen Unterschied. Beim Vergleich des mit *m*-Dinitrobenzol erhaltenen k_5/k_2-Wertes mit dem von KICE [1] bei 44,1 °C gemessenen Wert von $4{,}8 \cdot 10^{-3}$ wurde gute Übereinstimmung erhalten.

LITERATUR

1. KICE, J. L.: J. Am. Chem. Soc. **76,** 6274 (1954)
2. KICE, J. L.: J. Polymer Sci. **19,** 123 (1956)
3. SINICINA, Z. A., BAGDASARJAN, H. S.: Zr. Fiz. Him. **32,** 2663 (1958)
4. BAGDASARJAN, H. S., SINICINA, Z. A.: J. Polymer Sci. **52,** 31 (1961)
5. TÜDŐS F., KENDE J., AZORI M.: Vyshok. Soiedy. **4,** 1962 (1962)
6. BARTLETT, P. D., KWART, H.: J. Am. Chem. Soc. **72,** 1051 (1950)
7. BARTLETT, P. D., KWART, H.: J. Am. Chem. Soc. **74,** 3969 (1952)
8. SINICINA, Z. A., BAGDASARJAN, H. S.: Zr. Fiz. Him. **34,** 1110 (1960)
9. MONDVAI I.: Acta Chim. Acad. Sci. Hung. **47,** 281 (1966); Magy. Kém. Foly. **72,** 163 (1966)
10. BAGDASARJAN, H. S.: Zr. Fiz. Him. **32,** 2614 (1958)
11. O'BRIEN, J. L., GORMICK, F.: J. Am. Chem. Soc. **77,** 4757 (1955)
12. BENGOUGH, W. J., MELVILLE, H. W.: Proc. Roy. Soc. **A 249,** 455 (1959)
13. MONDVAI I., GÁL J.: Acta Chim. Acad. Sci. Hung. **51,** 423 (1967); Magy. Kém. Foly. **72,** 473 (1966)
14. MONDVAI I., IGLÓY M.: Acta Chim. Acad. Sci. Hung. **55,** 117 (1968); Magy. Kém. Foly. **73,** 350 (1967)
15. SAWADA, H.: J. Polymer Sci. **B 1,** 305 (1963)

Imre MONDVAI
László HALÁSZ
Antal KESCHITZ
Budapest XI., Műegyetem-rkpt. 3.

Acta Chimica Academiae Scientiarum Hungaricae, Tomus 68 (1–2), pp. 169–175 (1971)

POLYMERISATION DES METHYLMETHACRYLATS BEI HOHEN UMSÄTZEN, VI

ZUSAMMENFASSENDE WERTUNG DER ERGEBNISSE

I. MONDVAI und L. HALÁSZ

(Lehrstuhl für die Plast- und Gummiindustrie der Technischen Universität, Budapest)

Eingegangen am 3. Oktober 1969

Bei der Untersuchung der Blockpolymerisation von Methylmethacrylat wurden Zusammenhänge festgestellt zwischen den für die Polymerisation bei hohen Umsätzen charakteristischen Werten und der Anfangsgeschwindigkeit der Polymerisation. Es wurden die in den Gleichungen angeführten Koeffizienten und Potenzen in Gegenwart der untersuchten Initiatoren und Verzögerer bestimmt. Zwischen der chemischen Struktur und der Reaktionsfähigkeit der untersuchten Verzögerer wurden Zusammenhänge gefunden.

Bei der Polymerisation verschiedener Monomere (Styrol, Methylmethacrylat, Vinylchlorid) wurde festgestellt, daß die momentane Geschwindigkeit des Vorganges in einem ziemlich breiten Umsatzgebiet der im System befindlichen Polymermenge proportional ist. Im Falle von Styrol läßt sich der Geleffekt nur durch den Umstand bemerken, daß die anfängliche stationäre Geschwindigkeit der Polymerisation nicht dergestalt abnimmt, als auf Grund der Verminderung der Monomerkonzentration zu erwarten wäre. Bei der Polymerisation des Methylmethacrylats nimmt die momentane Geschwindigkeit der Reaktion nach Erreichen eines gegebenen Umsatzes ständig zu. Die Differenz zwischen der maximalen Geschwindigkeit und der anfänglichen Geschwindigkeit kann auch eine Größenordnung betragen. Die Polymerisation von Vinylchlorid verläuft in heterogener Phase vom Anfang an mit ständig zunehmender Geschwindigkeit.

Bei allen drei Monomeren besteht jedoch der erwähnte lineare Zusammenhang zwischen Polymerisationsgeschwindigkeit und Umsatz. Dieser Befund diente BURNETT und DUNCAN [1] sowie SAWADA [2] als Grundlage zur Aufstellung ihrer Gleichungen für die Polymerisation von Methylmethacrylat bei hohen Umsätzen.

Zur Illustration der Zusammenhänge Polymerisationsgeschwindigkeit-Umsatz beim Methylmethacrylat diente die Darstellung der mit verschiedenen Mengen Benzoylperoxyd bei 50 °C erhaltenen Ergebnisse in Abb. 1. Die aus den geraden Strecken gerechneten $\Delta W/\Delta x$ Werte sind charakteristisch für die bei hohen Umsätzen erfolgende Polymerisation. Stellt man die Werte $\Delta W/\Delta x$ als Funktion der anfänglichen stationären Geschwindigkeit der Polymerisation dar, so erhält man die in Abb. 2 gezeigten Geraden. Ebensolche

Geraden erhält man, wenn statt der Werte von $\Delta W/\Delta x$ die aus der Gleichung von SAWADA errechneten K_1-Werte dargestellt werden, nur ist die Streuung der Versuchspunkte etwas größer.

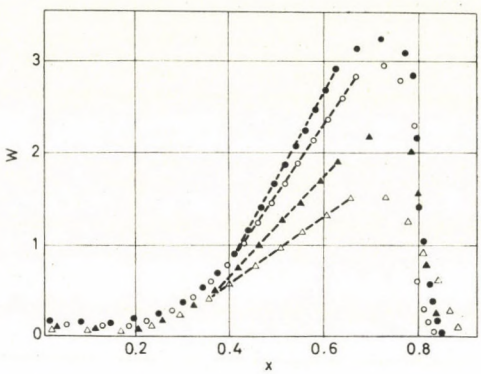

Abb. 1. Polymerisationsgeschwindigkeit-Umsatzgrad-Zusammenhänge bei 50 °C, in Gegenwart verschiedener Mengen von Benzoylperoxyd. Initiatorkonzentrationen: ● 11,24 · 10^{-2} Mol l^{-1}; ○ 7,48 · 10^{-2} Mol l^{-1}; ▲ 4,13 · 10^{-2} Mol l^{-1}; △ 2,30 · 10^{-2} Mol l^{-1}

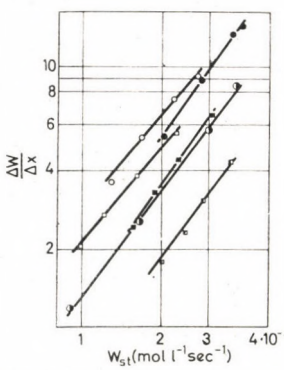

Abb. 2. Die Werte von $\Delta W/\Delta x$ als Funktionen der Anfangsgeschwindigkeit der Polymerisation. Benzoylperoxyd bei 50 °C (○), bei 60 °C (●), bei 70 °C (◑); Lauroylperoxyd bei 50 °C (□), bei 60 °C (■), bei 70 °C (◨)

Demgemäß lassen sich folgende Gleichungen zwischen der anfänglichen Geschwindigkeit der Polymerisation und den Werten $\Delta W/\Delta x$ bzw. K_1 aufschreiben:

$$\Delta W/\Delta x = a\, W_{st}^n \tag{1}$$

$$K_1 = b\, W_{st}^n \cdot \tag{2}$$

Die numerischen Werte der Koeffizienten und der Potenzexponenten wurden in Gegenwart von Benzoylperoxyd und Lauroylperoxyd als Initiatoren bei verschiedenen Temperaturen errechnet (Tab. I und Tab. II). Die hierzu benützten Versuchsdaten sind in Veröffentlichungen [3] und [4] zu finden.

Tabelle I

Werte der Koeffizienten und Potenzexponenten der Gleichung (1)

Initiator	Temperatur °C	$a \cdot 10^{-3}$	n
Benzoylperoxyd	50	214	1,22
	60	1260	1,45
	70	397	1,37
Lauroylperoxyd	50	158	1,22
	60	820	1,45
	70	220	1,37

Tabelle II

Werte der Koeffizienten und Potenzexponenten der Gleichung (2)

Initiator	Temperatur °C	$b \cdot 10^{-3}$	n
Benzoylperoxyd	50	11,2	1,22
	60	44,0	1,45
	70	12,5	1,37
Lauroylperoxyd	50	10,9	1,22
	60	59,6	1,45
	70	14,8	1,37

Aus Tab. I und Tab. II ist zu sehen, daß die Werte der Potenzexponenten n nur von der Temperatur beeinflußt werden. Die numerischen Werte der Potenzexponenten und auch der Koeffizienten a und b sind bei 60 °C am größten.

Mit steigender Temperatur nimmt auch die anfängliche Polymerisationsgeschwindigkeit zu, ebenso die Diffusionsgeschwindigkeit des Monomers im monomeren-polymeren Gel. Unter solchen Umständen nimmt die Möglichkeit der Radikale zur Ansammlung ab, folglich auch die der spontanen Erhöhung der Polymerisationsgeschwindigkeit bei hohen Umsätzen. Unter den angewandten Reaktionsverhältnissen, d. h. wenn der isothermische Verlauf der Polymerisation durch gegebene Versuchsbedingungen gesichert werden konnte, wächst bei 60 °C der für die Polymerisation bei hohen Umsätzen charakteristische Wert $\Delta W/\Delta x$ bzw. K_1 als Funktion der anfänglichen Geschwindigkeit der Reaktion am stärksten. Durch die doppelte Wirkung der Temperaturerhöhung läßt sich auch der Befund erklären, daß der Höchstwert der zur gleichen Anfangsgeschwindigkeit gehörenden Werte $\Delta W/\Delta x$ bzw. K_1 bei 50 °C liegt.

In Gegenwart von Verzögerern nimmt die Polymerisationsgeschwindigkeit ab. Aus den im Anfangsstadium der Polymerisation gemessenen Reaktionsgeschwindigkeitswerten [5—7] wurden, in Kenntnis der für die Verzögerungsreaktion charakteristischen Werte k_5/k_2 bzw. k_2 [8, 9], die Werte k_5 errechnet (Tab. III). Bei schwächeren Verzögerern, wie *m*-Nitrophenol bei 60 °C und *m*-Dinitrobenzol bei 70 °C, hat man unwahrscheinlich kleine k_5 Werte erhalten. Hier mußte nämlich eine hohe Verzögererkonzentration angewandt werden, um eine entsprechende Verminderung für die K_1-Werte zu erhalten, wodurch wahrscheinlich eine Kettenregeneration auftrat. Dadurch aber erhielt man niedrigere k_5-Werte als die tatsächlichen.

Hinsichtlich der Wirksamkeit der untersuchten Verbindungen ergab sich bei beiden Temperaturen eine Größenordnungsdifferenz in folgender Reihenfolge: Dinitrophenole ≫ *o*-Nitrophenol ≫ Dinitrobenzole und die beiden anderen Mononitrophenole. Lage und Zahl der Nitrogruppen beeinflussen

Tabelle III

Geschwindigkeitskonstanten von Verzögerungsreaktionen

Verzögerer	Temperatur °C	$\frac{FW_0}{z}$ 10^2	$\frac{k_5}{k_2}$ 10^2	k_5 $1\ \mathrm{Mol^{-1}sec^{-1}}$
o-Nitrophenol	50	0,30	2,94	9,41
	60	2,85	14,5	84,1
m-Nitrophenol	50	0,19	1,86	5,95
	60	0,08	0,406	2,35
p-Nitrophenol	50	0,10	0,980	3,14
	60	0,12	0,619	3,53
2,4-Dinitrophenol	50	4,10	40,2	129
	60	9,80	49,7	288
2,5-Dinitrophenol	50	12,4	122	390
	60	14,7	74,6	433
2,6-Dinitrophenol	50	5,14	50,4	161
	60	11,0	55,8	324
	50	0,460	4,51	14,4
o-Dinitrobenzol	60	0,572	2,90	16,8
	70	1,58	4,65	44,6
	50	0,023	0,255	0,72
m-Dinitrobenzol	60	0,185	0,939	5,45
	70	0,036	0,106	1,02
	50	0,084	0,824	2,64
p-Dinitrobenzol	60	0,161	0,817	4,74
	70	0,220	0,647	6,21

folglich die Reaktionsfähigkeit der Verbindungen. Die größte Rolle spielt die zwischen den benachbarten Nitro- und phenolischen Hydroxylgruppen zustandekommende Wasserstoffbrücke. Das eine Sauerstoffatom der Nitrogruppe sitzt in diesem Falle locker, weshalb die Fähigkeit der Verbindungen, Radikale zu akzeptieren, viel kräftiger wird. Die Einführung einer zweiten Nitrogruppe bringt nur dann eine bedeutend höhere Reaktionsfähigkeit

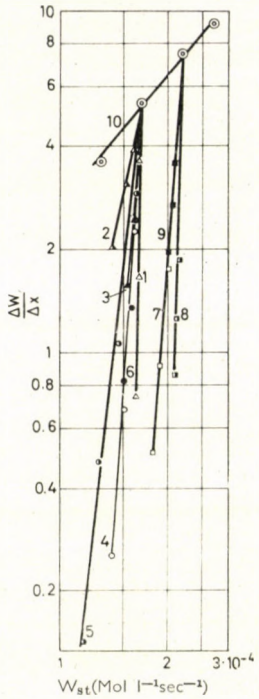

Abb. 3. Die Werte von $\Delta W/\Delta x$ als Funktionen der Anfangsgeschwindigkeit der Polymerisation bei 50 °C 1. (△) *o*-Nitrophenol, 2. (▲) *m*-Nitrophenol, 3. (▲) *p*-Nitrophenol, 4. (○) 2,4-Dinitrophenol, 5. (◑) 2,5-Dinitrophenol, 6. (●) 2,6-Dinitrophenol, 7. (□) *o*-Dinitrobenzol, 8. (◧) *m*-Dinitrobenzol, 9. (■) *p*-Dinitrobenzol, 10. (⊙ ohne Verzögerer

mit sich, wenn Möglichkeit zur Bildung der Wasserstoffbrücke besteht. Innerhalb der einzelnen Gruppen verursachen strukturale Verschiedenheiten keine bedeutenden Differenzen in der Reaktionsbereitschaft, auch die Wirksamkeits-Reihenfolge ist bis zu einem gewissen Grad eine Funktion der Temperatur.

Bei hohen Umsätzen läßt sich die Wirksamkeit der angewandten Verzögerer gut vergleichen, sofern die Werte $\Delta W/\Delta x$ und K_1 als Funktion der Anfangsgeschwindigkeit der Polymerisation dargestellt werden. In Abb. 3 ist als Beispiel die Abhängigkeit der berechneten Werte $\Delta W/\Delta x$ als Funktion der Anfangsgeschwindigkeit der Polymerisation bei 50 °C zu sehen. Die aus Versuchen mit verschiedenen Verzögerermengen berechneten Daten liegen entlang einer Geraden und treffen sich im entsprechenden Punkt der Geraden,

die erhalten wurde im Versuch mit gleicher Initiatorkonzentration jedoch ohne Verzögerer. Ähnliche Zusammenhänge erhält man bei der Darstellung der bei 60 °C gewonnenen Werte $\Delta W/\Delta x$ bzw. K_1. Auch aus Abb. 3 geht hervor, daß sich die bei hohen Umsätzen gemessene Reaktionsgeschwindigkeit bei gleicher anfänglicher Polymerisationsgeschwindigkeit durch Anwendung von Verzögerern in erheblicherem Maße vermindern läßt als durch Verminderung der Initiatorkonzentration.

Zwischen der anfänglichen Geschwindigkeit der Polymerisation und den Werten $\Delta W/\Delta x$ bzw. K_1 bestehen die folgenden Beziehungen:

$$\frac{1}{(\Delta W/\Delta x)_{rel}} = \left(\frac{1}{W_{rel}}\right)^m, \tag{3}$$

$$\frac{1}{K_{1,rel}} = \left(\frac{1}{W_{rel}}\right)^k, \tag{4}$$

wo W_{rel} die relative Polymerisationsgeschwindigkeit (d. h. Quotient der in Gegenwart und in Abwesenheit von Verzögerern gemessenen Polymerisationsgeschwindigkeit) ist, während $(\Delta W/\Delta x)_{rel}$ und $K_{1,\,rel}$ die entsprechenden relativen Werte sind. Die numerischen Werte der Potenzexponenten sind in Tab. IV und Tab. V enthalten. Wie ersichtlich, stehen die Werte von m und k, von einigen Ausnahmen abgesehen, nahe zueinander, in der Wirksamkeit der untersuchten Verzögerer besteht also in der anfänglichen Strecke der Polymerisation und bei hohen Umsätzen eine Ähnlichkeit.

Tabelle IV

Werte der Potenzexponenten der Gleichung (3)

Verzögerer	m	
	bei 50 °C	bei 60 °C
o-Nitrophenol	47	12
m-Nitrophenol	5	15
p-Nitrophenol	18	19
2,4-Dinitrophenol	20	18
2,5-Dinitrophenol	10	17
2,6-Dinitrophenol	20	19
o-Dinitrobenzol	15	39
m-Dinitrobenzol	42	14
p-Dinitrobenzol	15	12

Tabelle V

Werte der Potenzexponenten der Gleichung (4)

Verzögerer	k	
	bei 50 °C	bei 60 °C
o-Nitrophenol	44	9
m-Nitrophenol	6	8
p-Nitrophenol	17	13
2,4-Dinitrophenol	29	17
2,5-Dinitrophenol	10	15
2,6-Dinitrophenol	25	17
o-Dinitrobenzol	16	11
m-Dinitrobenzol	44	13
p-Dinitrobenzol	15	11

LITERATUR

1. Burnett, G. M., Duncan, G. L.: Makromol. Chem. **51,** 154 (1962)
2. Sawada, H.: J. Polymer Sci. **B 1,** 305 (1963)
3. Mondvai, I.: Acta Chim. Acad. Sci. Hung. **47,** 281 (1966) Magy. Kém. Foly. **72,** 163 (1966)
4. Mondvai, I., Nagy, J.: Acta Chim. Acad. Sci. Hung. **51,** 417 (1967) Magy. Kém. Foly. **72,** 471 (1966)
5. Mondvai, I., Gál, J.: Acta Chim. Acad. Sci. Hung. **51,** 423 (1967) Magy. Kém. Foly. **72,** 473 (1966)
6. Mondvai, I., Iglóy, M.: Acta Chim. Acad. Sci. Hung. **55,** 117 (1968) Magy. Kém. Foly. **73,** 350 (1967)
7. Mondvai, I., Halász, L., Keschitz, A.: Acta Chim. Acad. Sci. Hung. **68,** 119 (1971) Magy. Kém. Foly. **75,** 353 (1969)
8. O'Brien, J. L., Gormick, F.: J. Am. Chem. Soc. **77,** 4757 (1955)
9. Bengough, W. J., Melville, H. W.: Proc. Roy. Soc. **A 249,** 455 (1959)

Imre Mondvai
László Halász
Budapest XI., Müegyetem-rkpt. 3—9.

INDEX

CHEMICAL TECHNOLOGY – CHEMISCHE TECHNOLOGIE – ХИМИЧЕСКАЯ ТЕХНОЛОГИЯ

ACTA CHIMICA

ТОМ 68—ВЫП. 1—2

РЕЗЮМЕ

Определение следов европия

М. ФАБИАН-МОХАИ, Э. УПОР и Дь. НАДЬ

Был разработан метод определения небольших количеств европия. Две из трех разновидностей берут за основу люминесценцию, описанную Полуэктовым; селективное отделение европия с помощью амальгамированного натрия позволило, однако, использовать арсеназу III для определения содержания европия в обогащенных образцах редкоземельных металлов.

Отделение от примесей редкоземельных металлов, являющихся помехой, было осуществлено с помощью оксалатного высаждения, экстракцией дибутилфосфорной кислотой и антагонистической реэкстракцией.

Чувствительность метода составляет $1 \cdot 10^{-5}\%$ (сплавление-люминесценция), $2 \cdot 10^{-4}\%$ (о-фенантролин + новатофан) и $1 \cdot 10^{-3}\%$ (арсеназа III).

После описанного разделения все три метода могут быть применимы для одного и того же раствора. Описанные методы могут быть применимы для одного и того же раствора. Описанные методы могут быть использованы для определения европия в монацитах, апатитах, минеральных породах и соединениях редкоземельных металлов.

Получение и исследование $CaSO_4$ Mn, пригодного для дозиметрических целей

И. КАША, И. ПОРУБСКИЙ и Л. КИШ

Изучались условия получения препарата сульфата кальция—фосфора, активированного марганцем, пригодного дгя дозиметрических целей, и их влияние на термолюминесцентные свойства препаратов. Был разработан оптимаяьный способ введения активатора. Наилучшими свойствами обладают те фосфоры, при получении которых введение активатора проводится перед осаждением сульфата кальция, в кислых средах. Изучая влияние атмосферы термообработки на чувствительность, было установлено, что ответственными за меньшую чувствительность образцов, прокаленных на воздухе, являются ионы марганца, окислившиеся до валентностей, превышающих 2, поскольку, либо последующим восстановлением их до двухвалентного марганца, либо удалением, удалось достигнуть, что светоинтенсивность или чувствительность таких образцов, приготовленных на воздухе, приближается к значениям, полученным при приготовлении образцов в восстанавливающей атмосфере. Все образцы, в изученном интервале ($10^{-2} \div 10^{2}$ R), дают линейную зависимость от дозы гамма-облучения.

О термодинамике реакции, протекающей между трихлорсиланом и хлористым винилом при высоких температурах в газовой фазе

Д. КНАУС

На основе константы равновесия реакции, протекающей между трихлорсиланом и хлористым винилом, была рассчитана теплота образования этого соединения и было установлено, что данное значение согласуется с литературными данными для теплот образования родственных соединений. Были рассчитаны величины константы равновесия реакции при различных температурах, и на основе их были получены значения средней теплоты реакции и среднего изменения энтеропии реакции в интервале температур 600—821°K.

Изучение адсорбционных явлений на платиновой электроде с помощью техники радиоактивной индикации, V

О зависимости адсорбции хлористых ионов от потенциала

ДЬ. ХОРАНИ, Я. ШОЛТ и Ф. НАДЬ

1. Адсорбция ионов Cl^- изучалась в IN растворе $HClO_4$ на платиновом электроде с помощью техники радиоактивной индикации.

2. Зависимость адсорбции ионов Cl^- от потенциала изменяется с изменением состояния электрода; на свежеприготовленных и регенерированных электродах наблюдаются две дискретные ступени, которые смываются со «старением» электрода.

Изучение адсорбционных явлений на платиновой электроде с помощью техники радиоактивной индикации, VI

Роль адсорбционного равновесия в гетерогенном каталитическом гидрировании в водных средах

ДЬ. ХОРАНИ, Я. ШОЛТ и Ф. НАДЬ

На основе конкретных примеров было показано, что при каталитическом гидрировании и электрогидрировании в водных средах — в противоположность более ранним взглядам — нельзя полагать о наличии адсорбционного равновесия субстрата.

На основе этого необходимо внести изменения и в кинетическую картину реакций. Согласно этому, приводятся некоторые общие положения.

Изучение электрохимических свойств аминоазобензола, I

Механизм электрохимического восстановления 4-аминоазобензола, 2,4-диаминоазобензола и 4'-этокси-2,4-диаминоазобензола

Л. ЛАДАНЬИ, М. ВАЙДА и ДЬ. ВАМОШ

Механизм электрохимического восстановления некоторых производных аминоазобензола (4-аминоазобензол, 2,4-диаминоазобензол, 4'-этокси-2,4-диаминоазобензол) изучался с помощью вольтаметрического, потенциостатического и спектрофотометрического методов. Было установлено, что брутто двухэлектронное восстановление азо-группы представляет собой двухступенчатый процесс, который протекает по ECE-механизму через образование промежуточного соединения, являющегося продуктом присоединения одного электрона к азо-группе, и через диспропорционирование. Дальнейшее диспропорционирование гидразо-формы приводит в брутто к 4-ех электронному восстановлению. Изучение электрохимических свойств ароматических аминов, образующихся в последнем процессе, (1,2,4-триаминобензол, 1,4-фенилендиамин) позволило определить подробный механизм восстановления.

Устранение поляризации сопротивления в потенциостатических исследованиях, II

Б. ЛЕНДЬЕЛ, МЛ. и Й. ДЕВАИ

Был разработан метод непрерывного измерения и компенсирования поляризации сопротивления во время измерения в условиях потенциостатических исследований. Для проверки метода исследовалась анодная поляризация серебра в сульфатных растворах. Было установлено, что в случае автоматического компенсирования напряжения на омическом

сопротивлении изменяется характер кривой анодной поляризации. Помимо этого, было установлено, что в случае автоматического компенсирования нет необходимости в помещении электрода референции вблизи измеряемого электрода, а тем самым можно избежать погрешности, возникающей за счет экранирующего влияния электрода референции.

Симуляция вращательно-колебательных спектров молекул типа слегка асимметрического удлиненного волчка с помощью ЭВМ

Распространение к переходам в асимметричном ротаторе

ДЬ. ЯЛШОВСКИЙ и Л. НЕМЕШ

Описывается программа для симулирования на ЭВМ вращательной структуры перпендикулярных колебательных переходов в молекулах типа слегка асимметричного удлиненного волчка. В дополнение к кориолисовым взаимодействиям типа R^z принимаются во внимание переходы в асимметричном ротаторе с точностью вплоть до $K = 4$. Расчет иллюстрируется на примере ν_7 этилена.

Химия свободных радикалов, VII

Реакция взаимодействия нитрозосоединений с виниловыми мономерами

Л. ШЮМЕГИ, Ф. ТЮДЁШ и И. КЕНДЕ

Изучалась реакция взаимодействия нитрозосоединений с виниловыми мономерами. Реакция метилметакрилата с п-нитрозоанилином является псевдо-унимолекулярной по интрозоанилину, и величина энергии активации равна 15 ккал/моль. Реакция же стирола с нитрозобензолом является псевдо-бимолекулярной по нитрозобензолу, и величина энергии активации равна 7,5 ккал/моль. Помимо реакций вышеупомянутых соединений, изучались реакции взаимодействия некоторых N-замещенных п-нитрозоанилина и многих производных нитрозобензола, замещенных в кольце, с метилметакрилатом и стиролом; определялись константы скоростей этих реакций и их зависимости типа Гамметта. На основе спектрофотометрических исследований и спектров ЭПР можно было заключить, что в течение реакции образуются свободные радикалы типа окиси азота.

Молекулярное силовое поле для силильных изотиоцианатов и силильных изоцианатов

К. РАМАСВАМИ и С. РАНГАРАДЖАН

Расчет приближенного силового поля SiH_3NCS и SiH_3NCO производился методом, предложенным Торкингтомом, Херанзем и Кастано, соответственно. Было показано, что метод Торкингтона дает лучшую серию величин констант потенциальной энергии, средних амплитуд колебаний и кориолисовых постоянных, которые хорошо согласуются с наблюдаемыми экспериментальными величинами.

О более детальном изучении протекания реакции Миллона

Я. ЛАЗАР, Л. МОД и Э. ВИНКЛЕР

Реакция Миллона для замещенных фенолов изучалась на следующих модельных соединениях: 4-гидроксибензойная кислота (**Ia**), метиловый эфир 4-гидроксибензойной кислоты (**Ib**) и тирозин (**Ic**).

После исчерпывающего обзора литературных данных, относящихся к данной теме, синтезировались соединения, играющие роль в возникновении цветной реакции Миллона, и превращением последних друг в друга доказывалось протекание реакции Миллона.

Было установлено, что окрашенными соединениями являются комплексы ртути(II) с о-нитрозофенолами: бис-о-нитрозофенол-меркурат(II) (**IV**) и о-нитрозофенол-меркурат (II)-нитрат (**V**). Вначале, под влиянием нагрева или при продолжительном стоянии при комнатной температуре, происходит меркурирование, вслед за чем образующийся продукт (**II**), реагируя с азотной кислотой, превращается в производную о-нитрозофенола (**III**) и затем в вышеупомянутые окрашенные комплексы ртути (**IV**, **V**).

Было установлено также, что компонентом *реагента Миллона* вызывающим цветную реакцию, является нитрит трути(II).

Производные тиокарбамида с туберкулостатической активностью, I

Ш. ШОЛЬОМ, Й. КОЦКА, Г. ТОТ и Л. ТОЛДИ

В тиокарбамидных производных с туберкулостатической активностью комбинировались 1-(4-изоамил-оксифенил)-тиокарбамильные группы, являющиеся наиболее подходящими с точки зрения оказываемого влияния, а также аналогичные, но иначе замещенные тиокарбамильные группы с аминокислотами, как биологически важными молекулами носителя.

Из α-, β- и γ-аминокислот и соответствующих изотиоцианатов через киокарбамиламинокислоты были получены следующие циклические соединения: 2-тиохидантоины, 2-тио-гидроурацилы, а также 2-тио-4-окси-пергидро-1,3-диазепины. Помимо последних, были синтезированы другие шестичленные гетероциклические соединения, содержащие тиокарбамидный скелет в кольце, такие как, 2-тио-4-фенил-1,2-дигидрохиназолин и 2-арилимино-4-оксо-5-метил-пергидро-1,3-тиазины. Строение соединений доказывалось на основе химических и спектроскопических исследований.

2-Тиохидантоины обладают значительной туберкулостатической активностью in vitro, но сильно токсичны, в то время как пергидро-1,3-диазепины оказались успокаивающими средствами.

Конденсация Дарзенса, II

Влияние заместителей на конденсацию Дарзенса, катализированную основаниями

ДЬ. ШИПОШ, ДЬ. ШЁБЕЛ и Л. БАЛАШПИРИ

Проводилась реакция конденсации Дарзенса между галогенидами *n*-замещенных фенацилов и *n*-замещенными бензальдегидами в диоксане, в присутствии метилата натрия в качестве катализатора. На основе данных выхода этоксикетонов делались качественные заключения относительно влияния заместителей на реакцию конденсации. Было установлено, что влияние заместителей на реакцию конденсации Дарзенса является одинаковым как в случае кислот, так и в случае оснований, использованных в качестве катализаторов. Однако, влияние заместителей в галогенидах фенацила на конденсацию Дарзенса является противоположным по сравнению с их влиянием на альдольную конденсацию, катализированную основаниями.

Определение структуры двух изомеров тетрабромо-тетрадеокси-гекситола с помощью масс-спектрометрии

ДЬ. ХОРВАТ и Й. КУСМАНН

Структура двух тетрабромо-гекситолов, полученных при взаимодействии 1,6-дибромо-1,6-дидеокси-2,3 : 4,5-диангидро-галактитола с бромистым водородом, определялась с помощью масс-спектрометрии. Было установлено, что они представляют 1,3,4,6-тетрабромо-1,3,4,6-тетрадеокси-аллитол и 1,2,4,6-тетрабромо-1,2,4,6-тетрадеокси-0,L-маннитол, соответственно.

Полимеризация метилметакрилата при высоких степенях конверсии, V

Изучение замедляющего эффекта динитробензолов

И. МОНДВАИ, Л. ХАЛАС и А. КЕШИЦ

Изучалась блочная полимеризация метилметакрилата при различных температурах в присутствии 1,2-, 1,3- и 1,4-динитробензолов. Определялись отношения констант скоростей k_s/k_2 и величин $K_{1,\ отн.}$, характеризующие уменьшение скорости полимеризации при высоких степенях превращения. При сравнении их можно заключить, что наиболее сильным замедлителем является 1,2-динитробензол. Замедляющая способность всех трех изомеров подобна замедляющей способности мононитрофенолов.

Полимеризация метилметакрилата при высоких степенях превращения, VI

Общее обсуждение полученных результатов

И. МОНДВАИ и Л. ХАЛАС

При исследовании блочной полимеризации метилметакрилата были установлены зависимости между параметрами, характеризующими полимеризацию при высоких степенях превращения и начальной скоростью полимеризации. В присутствии различных инициаторов и замедлителей определялись параметры этих зависимостей (коэффициенты и показатели степеней). Была найдена зависимость между реакционной способностью замедлителей и их химическим строением.

Printed in Hungary

A kiadásért felel az Akadémiai Kiadó igazgatója — Műszaki szerkesztő: Várhelyi Tamás

A kézirat nyomdába érkezett: 1970. XII. 10. — Terjedelem: 15,75 (A/5) ív, 66 ábra

71.70859 Akadémiai Nyomda Budapest — Felelős vezető: Bernát György

The Acta Chimica publish papers on chemistry, in English, German, French and Russian.

The Acta Chimica appear in volumes consisting of four parts of varying size, 4 volumes being published a year.

Manuscripts should be addressed to

Acta Chimica
Budapest 112/91 Műegyetem

Correspondence with the editors should be sent to the same address.

The rate of subscription is $ 16.00 a volume.

Orders may be placed with "*Kultúra*" Foreign Trade Company for Books and Newspapers (Budapest I., Fő utca 32. Account No. 43-790-057-181) or with representatives abroad.

Les Acta Chimica paraissent en français, allemand, anglais et russe et publient des mémoires du domaine des sciences chimiques.

Les Acta Chimica sont publiés sous forme de fascicules. Quatre fascicules seront réunis en un volume (4 volumes par an).

On est prié d'envoyer les manuscrits destinés à la rédaction à l'adresse suivante:

Acta Chimica
Budapest 112/91 Műegyetem

Toute correspondance doit être envoyée à cette même adresse.

Le prix de l'abonnement est de $ 16.00 par volume.

On peut s'abonner à l'Entreprise pour le Commerce Extérieur de Livres et Journaux «*Kultúra*» (Budapest I., Fő utca 32. Compte-courant No. 43-790-057-181) ou à l'étranger chez tous les représentants ou dépositaires.

«*Acta Chimica*» издают трактаты из области химической науки на русском, французском, английском и немецком языках.

«*Acta Chimica*» выходят отдельными выпусками разного объема. 4 выпуска составляют один том. 4 тома публикуются в год.

Предназначенные для публикации рукописи следует направлять по адресу:

Acta Chimica
Budapest 112/91 Műegyetem

По этому же адресу направлять всякую корреспонденцию для редакции.

Подписная цена — $ 16.00 за том.

Заказы принимает предприятие по внешней торговле книг и газет «*Kultúra*» (Budapest I., Fő utca 32. Текущий счет № 43-790-057-181) или его заграничные представительства и уполномоченные.

Reviews of the Hungarian Academy of Sciences are obtainable at the following addresses:

ALBANIA

Drejtorija Qändrone e Pärhapjes dhe Propagandimit tä Librit
Kruga Konferenca e Päzes
Tirana

AUSTRALIA

A. Keesing
Box 4886, GPO
Sydney

AUSTRIA

GLOBUS
Höchstädtplatz 3
A-1200 Wien XX

BELGIUM

Office International de Librairie
30, Avenue Marnix
Bruxelles 5
Du Monde Entier
5, Place St. Jean
Bruxelles

BULGARIA

HEMUS
11 pl Slaveikov
Sofia

CANADA

Pannonia Books
2, Spadina Road
Toronto 4, Ont.

CHINA

Waiwen Shudian
Peking
P. O. B. 88

CZECHOSLOVAKIA

Artia
Ve Směčkách 30
Praha 2
Poštovní Novinová Služba
Dovoz tisku
Vinohradská 46
Praha 2
Mad'arská Kultura
Václavské nám. 2
Praha 1
SLOVART A. G.
Gorkého
Bratislava

DENMARK

Ejnar Munksgaard
Nörregade 6
Copenhagen

FINLAND

Akateeminen Kirjakauppa
Keskuskatu 2
Helsinki

FRANCE

Office International de Documentation et Librairie
48, rue Gay Lussac
Paris 5

GERMAN DEMOCRATIC REPUBLIC

Deutscher Buch-Export und Import
Leninstraße 16
Leipzig 701
Zeitungsvertriebsamt
Fruchtstraße 3—4
1004 Berlin

GERMAN FEDERAL REPUBLIC

Kunst und Wissen
Erich Bieber
Postfach 46
7 Stuttgart S.

GREAT BRITAIN

Blackwell's Periodicals
Oxenford House
Magdalen Street
Oxford
Collet's Subscription Import Department
Denington Estate
Wellingsborough. Northants.
Robert Maxwell and Co. Ltd.
4—5 Fitzroy Square
London W. 1

HOLLAND

Swetz and Zeitlinger
Keizersgracht 471—487
Amsterdam C.
Martinus Nijhof
Lange Voorhout 9
The Hague

INDIA

Hind Book House
66 Babar Road
New Delhi 1

ITALY

Santo Vanasia
Via M. Macchi 71
Milano
Libreria Commissionaria Sansoni
Via La Marmora 45
Firenze

JAPAN

Kinokuniya Book-Store Co. Ltd.
826 Tsunohazu 1-chome
Shinjuku-ku
Tokyo
Maruzen and Co. Ltd.
P.O. Box 605
Tokyo-Central

KOREA

Chulpanmul
Phenjan

NORWAY

Tanum-Cammermeyer
Karl Johansgt 41—43
Oslo 1

POLAND

RUCH
ul. Wronia 23
Warszawa

ROUMANIA

Cartimex
Str. Aristide Briand 14—18
Bucureşti

SOVIET UNION

Mezhdunarodnaya Kniga
Moscow G—200

SWEDEN

Almquist and Wiksell
Gamla Brogatan 26
S—101 20 Stockholm

USA

F. W. Faxon Co. Inc.
15 Southwest Park
Westwood Mass. 02090
Stechert Hafner Inc.
31. East 10th Street
New York, N. Y. 10003

VIETNAM

Xunhasaba
19, Tran Quoc Toan
Hanoi

YUGOSLAVIA

Forum
Vojvode Mišića broj 1
Novi Sad
Jugoslovenska Knjiga
Terazije 27
Beograd

19. V. 1971

Index: 26.007

ACTA CHIMICA

ACADEMIAE SCIENTIARUM HUNGARICAE

TOMUS 68 FASCICULUS 3

AKADÉMIAI KIADÓ, BUDAPEST

1971

ACTA CHIM. ACAD. SCI. HUNG.

ACTA CHIMICA

A MAGYAR TUDOMÁNYOS AKADÉMIA KÉMIAI TUDOMÁNYOK OSZTÁLYÁNAK IDEGEN NYELVŰ KÖZLEMÉNYEI

Az Acta Chimica német, angol, francia és orosz nyelven közöl értekezéseket a kémiai tudományok köréből.

Az Acta Chimica változó terjedelmű füzetekben jelenik meg, egy-egy kötet négy füzetből áll. Évente átlag négy kötet jelenik meg.

A közlésre szánt kéziratok a szerkesztőség címére (Budapest 112/91 Műegyetem) küldendők.

Ugyanerre a címre küldendő minden szerkesztőségi levelezés. A szerkesztőség kéziratokat nem ad vissza.

Megrendelhető a belföld számára az „Akadémiai Kiadó"-nál (Budapest V., Alkotmány utca 21. Bankszámla 05-915-111-46), a külföld számára pedig a „Kultúra" Könyv- és Hírlap Külkereskedelmi Vállalatnál (Budapest I., Fő utca 32. Bankszámla: 43-790-057-181) vagy annak külföldi képviseleteinél és bizományosainál.

Die Acta Chimica veröffentlichen Abhandlungen aus dem Bereiche der chemischen Wissenschaften in deutscher, englischer, französischer und russischer Sprache.

Die Acta Chimica erscheinen in Heften wechselnden Umfanges. Vier Hefte bilden einen Band. Jährlich erscheinen 4 Bände.

Die zur Veröffentlichung bestimmten Manuskripte sind an folgende Adresse zu senden:

Acta Chimica
Budapest 112/91 Műegyetem

An die gleiche Anschrift ist auch jede für die Redaktion bestimmte Korrespondenz zu richten. Abonnementspreis pro Band: $ 16.00.

Bestellbar bei dem Buch- und Zeitungs-Außenhandels-Unternehmen »*Kultúra*« (Budapest I., Fő utca 32. Bankkonto No. 43-790-057-181) oder bei seinen Auslandsvertretungen und Kommissionären.

Acta Chimica Academiae Scientiarum Hungaricae, Tomus 68 (3), pp. 177—182 (1971)

THE SELECTIVITY OF ION-SPECIFIC ELECTRODES, I

SILVER IODIDE MEMBRANE ELECTRODE

Z. PUCHONY, K. TÓTH and E. PUNGOR

(Department of Analytical Chemistry, University of Chemical Industries, Veszprém)

Received December 15, 1969

The selectivity of iodide membrane electrodes was studied in the presence of various precipitate-forming anions, complexing agents and metal ions forming complexes with iodide ions. The results prove the theoretical conception of the selectivity constant.

It has been found that metal iodo-complexes show the same behaviour to an iodide electrode as cyanide complexes to a cyanide electrode. Further research in this field is in progress.

Introduction

The advent of precipitate membrane electrodes has opened new possibilities in the field of potentiometry. They made possible the direct (pX determination) and indirect (titrimetric) determination of various anions and cations.

The selectivity of an ion-specific electrode is one of its characteristic parameters. The selectivity of an electrode to anions forming precipitates with the cation of the precipitate incorporated in the membrane has been studied theoretically [1]. Furthermore, the membrane potential equation has been interpreted for reactions other than the precipitate exchange reaction (*e.g.* complex formation [2]).

Both homogeneous and heterogeneous membrane electrodes behave electrochemically in the same way. A difference is only found between the structures of the membranes. The membrane potential equation for 1 : 1 electrolytes is as follows:

$$E = E_0 + \frac{RT}{F} \ln \left(a_i + a_i^* + K_{i,x} \cdot a_x^n + \sum_j K_{i,j} \cdot a_j\right)$$

where E_0 = standard electrode potential,
i = the ion to which the electrode is reversible,
a_i = activity of ion i in the solution,
a_i^* = activity of ion i released by the complexing agent in the boundary membrane layer, being equal to a_x/n,
a_x = activity of the complexing agent in the solution,
a_j = activity of ion j in the solution,

$K_{i,x}$ = selectivity of the electrode to the complexing agent; this value becomes equal to unity if the complexing agent dissolves the precipitate in the membrane completely,

$K_{i,j}$ = selectivity of the electrode to ion j, which gives only a precipitate exchange reaction,

n = number of ligands in the complex formed,

J = number of the ions taking part in the precipitate exchange reaction.

Many papers have dealt with the determination of the selectivity constant of ion-specific electrodes [1, 3, 4]. The selectivity constant is defined as a ratio which unambiguously shows the lowest concentration at which an ion can be measured in the presence of another ion. The value of the selectivity constant can be determined by a direct or indirect potentiometric method in solutions containing both the ion measured and the interfering ion.

RECHNITZ [3] determined the selectivity constant of ion-selective electrodes in an analogous way to that used for glass electrodes. The selectivity constant obtained in this way is called the apparent selectivity constant, and cannot be used for theoretical conclusions.

The aim of this paper is to study the selectivity of iodide membrane electrodes to various anions and cations. The selectivity constants of the electrodes indicate the possible applications.

Experimental

The following ions were studied:

Anions: Br^-, Cl^-, CN^-, SCN^-, OH^-, $S_2O_3^{2-}$, SO_3^{2-}, CrO_4^{2-}, AsO_4^{3-}, PO_4^{3-}, $Fe(CN)_6^{4-}$.

Cations: Ag^+, Cd^{2+}, Hg^{2+}, Pb^{2+}.

Apparatus: a RADELKIS (Budapest, Hungary) Blood pH-Meter (Type OP-203) and a RADIOMETER (Copenhagen, Denmark) Automatic Titrimeter (Type TTT 1) were used for the measurements. The indicator electrode was a RADELKIS OP-I-711 electrode and the reference electrode was a Ag/AgCl electrode with a KNO_3 agar-agar bridge.

Reagents: $AgNO_3$, KBr, KCl, KCN, KSCN, NaOH, $Na_2S_2O_3$, Na_2SO_3, K_2CrO_4, Na_3AsO_4, Na_2HPO_4, K_4 $Fe(CN)_6$, $CdSO_4$, $Hg(NO_3)_2$, $Pb(NO_3)_2$, of analytical grade were used for the solutions and were standardized by classical analytical methods. The ionic strengths of the solutions were kept constant by the addition of potassium nitrate.

Determination and the theoretical calculation of the selectivity constants

In practice the determination of the selectivity constants can be carried out in two different ways. If the values of the selectivity constants are low, the measurements can be done in solutions containing a constant concentration of iodide and various concentrations of the other ion studied. From the e.m.f. values measured, the concentration of the other ion which begins to influence

the behaviour of an iodide membrane electrode is determined. This concentration is given by the break point of the e.m.f. *vs.* log a_x curve (a_x is the activity of the other ion). The break point can be determined by the intersection of the tangents to the curve.

In the other method, a solution containing iodide and another anion is titrated with silver nitrate. Knowing the initial iodide concentration and the potential jump, the iodide concentration at which co-precipitation of the other ion starts can be determined. The selectivity constant is given by the ratio of this iodide activity and the activity of the interfering anion:

$$K_{ik} = \frac{(I_i)^{b/a}}{(I_k)^{m/n}}$$

where I_i and I_k are the activities of ions i and k in the solution at co-precipitation,

a, b, m, n will be discussed later.

The theoretical calculation of the selectivity constant was carried out using the following equation:

$$K_{ik} = \frac{S_{ji}^{1/a}}{S_{jk}^{1/n}}$$

where S_{ji} is the solubility product of the precipitate incorporated in the membrane $(I_j)_a(I_i)_b$,

S_{jk} is the solubility product of the precicipitate formed during the exchange reaction $(I_j)_n(I_k)_m$,

a, b, n, m are the stoichiometric constants of the precipitates.

Results and discussion

The experimental results are summarized as follows:

1. *Examination of ions forming precipitates with silver ions, by means of the titration method.* The titration curves are shown in Fig. 1. The selectivity constants calculated from these curves are compared with the theoretical values in Table I.

2. *Study on anions forming complexes with silver, by means of the direct method.* The results are given in Fig. 2 and Table II.

3. *Examination of metal ions forming complexes or precipitates with iodide ions.* The results obtained are given in actual iodide concentration *vs.* iodide mole fraction. The actual iodide concentration was calculated from the potentials measured with the help of the electrode calibration curve. Figs 3 and 4 show the results obtained in the presence of Hg^{2+} and Ag^{+}.

The experimental results prove the theoretical conception of the selectivity constant. On the basis of the experimental results it can be said that the theory is valid for more complicated precipitates of anions with a valency higher than one. The calculation of the selectivity constant for relatively

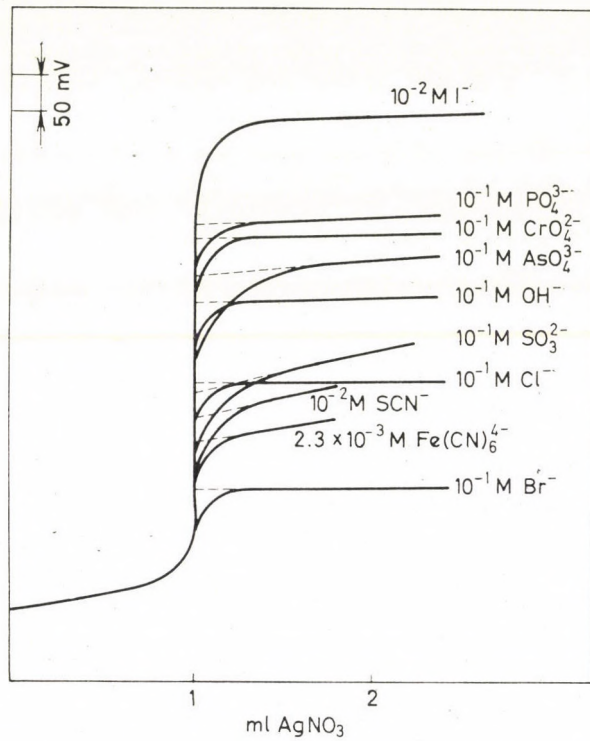

Fig. 1. Potentiometric tiration of solutions containing 10^{-2} *M* KI and *X M* of an interfering ion, with 10^{-1} *M* $AgNO_3$

Table I

Measured and calculated selectivity constants

Anion	K_{ik} (measured)	K_{ik} (calculated)
Cl^-	9.6×10^{-7}	3.7×10^{-7}
Br^-	1.9×10^{-4}	1.8×10^{-4}
SCN^-	3.0×10^{-5}	3.0×10^{-4}
OH^-	9.1×10^{-9}	1.0×10^{-8}
CrO_4^{2-}	6.6×10^{-11}	5.0×10^{-11}
AsO_4^{3-}	2.7×10^{-10}	3.2×10^{-10}
PO_4^{3-}	0.2×10^{-10}	1.2×10^{-10}
$Fe(CN)_6^{4-}$	3.5×10^{-6}	2.4×10^{-6}

simple systems was facilitated, by assuming that the solubility products were the same for the swollen boundary phases of the membrane as for the solution phase. This assumption implies that the activity coefficients are the same in the membrane swollen layer as in the solution.

In the presence of complexing agents, the selectivity constant cannot be expressed by the equation derived for precipitate-forming ions. As the experimental results show [2], the selectivity constant of the electrode for the com-

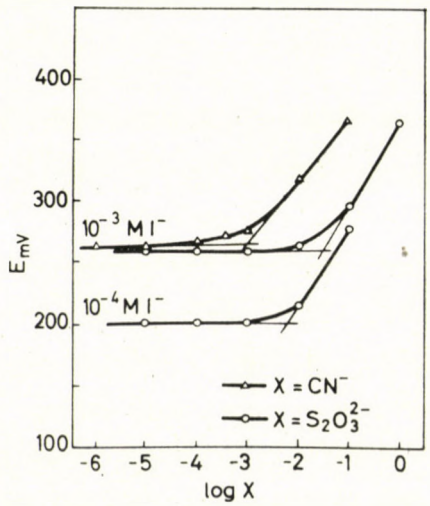

Fig. 2. Behaviour of an iodide-selective membrane electrode in a solution containing I^- and $S_2O_3^{2-}$, and I^- and CN^- ions, respectively

plex-forming ion is always equal to unity when the complex-forming ion dissolved the precipitate to an appreciable extent. The results obtained so far have not indicated how it is possible to calculate theoretically these selectivity constants to ions forming complexes. Experiments in this direction are in progress.

A theoretically interesting problem is presented by the metal ions which give complexes or precipitates with iodide ions. In the presence of precipitate-

Table II

Selectivity constants of an iodide membrane electrode to some complexing agents

Anion	K_{ik} (measured)
CN^-	1
$S_2O_3^{2-}$	4.2×10^{-2}
SO_3^{2-}	5.5×10^{-7}

forming ions there is no real problem; the electrode measures only the free iodide in the solution as shown in Figs 3 and 4. Experiments carried out with iodide complexes indicated that these complexes give a direct exchange reaction with the precipitate in the boundary layer of the membrane. This result is of importance, since the iodide electrode is not suitable for the determination of the stability constants of these iodide complexes.

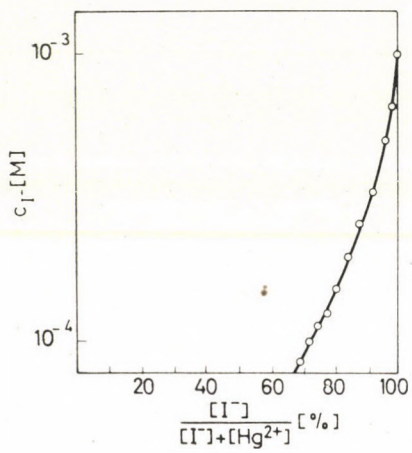

Fig. 3. Effect of Hg^{2+} on the potential value of iodide ions, measured by iodide electrode

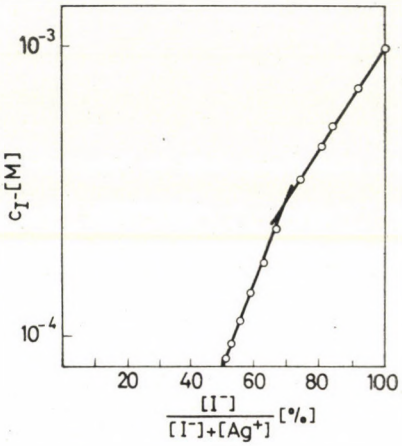

Fig. 4. Effect of Ag^+ on the potential value of iodide ions, measured by iodide electrode

In the case of cyanide electrodes it was found that a cyanide electrode can detect the cyanide released by the dissociation of cyanide complexes having a β value* greater than that of silver dicyanide. Complexes with lower β values than silver dicyanide give a direct exchange reaction with the precipitate of the electrode. Allowance must be made for a slight shielding effect of the central metal atom on the ligands.

REFERENCES

1. PUNGOR, E.: Anal. Chem. **39**, (No. 11) 28A (1967)
2. PUNGOR, E., TÓTH, K.: In preparation
3. RECHNITZ, G. A., KRESS, M. R., Zamochnick, S. B.: Anal. Chem. **38**, 973 (1966)
4. HAVAS, J., PAPP, E., PUNGOR, E.: Acta Chim. Acad. Sci. Hung. **58**, 9 (1968)
5. EISENMAN, G.: Biophys. J. **2**, 264 (1962)
6. PUNGOR, E., TÓTH, K.: Hung. Sci. Instr. **14**, 15 (1968)

Ernő PUNGOR
Klára TÓTH
Zita PUCHONY
Veszprém, Schönherz Z. u 12. Hungary.

* is the negative logarithm of the overall dissociation constant (K_d) of a complex; $\beta = -\log K_d$.

Acta Chimica Academiae Scientiarum Hungaricae, Tomus 68 (3), pp. 183—187 (1971)

A CRITICAL EXAMINATION OF THE STABILITY CONSTANTS OF SOME LANTHANIDE-α-HYDROXYCARBOXYLIC ACID COMPLEXES

A. GERGELY and I. NAGYPÁL

(Institute of Inorganic and Analytical Chemistry, L. Kossuth University, Debrecen)

Received January 16, 1970

On the basis of experimental data reported in the literature and using the curve-reduction procedure, the stability constants of the equilibrium systems Nd(III)-methylpropylglycollate, Yb(III)-isobutylmethylglycollate, -isopropylmethylglycollate, and -diethylglycollate, Er(III)-α-hydroxycyclohexanecarboxylate and Sm(III)-mandelate were critically re-examined. By means of this procedure, the regions of the formation curves suitable for the development of MA_n type complexes were selected. From these regions of the curves the exact values of the constants were calculated by the method of least squares, and compared with the literature data.

The earliest applied complexing agents for the ion-exchange separation of lanthanides were α-hydroxycarboxylic acids. Accordingly, numerous authors have studied the equilibrium relationships of these systems [1]. However, the literature of coordination chemistry up to the present time contains relatively few data for the stability constants [2]. This is explained in part by the experimental difficulties resulting from the low stabilities of the complexes. In addition to the formation of mononuclear complexes, other processes may also occur in these systems, for instance, hydrolysis of the complexes, formation of polynuclear complexes, dissociation of the alcoholic hydrogen from the bound ligand, etc. For example, according to SEYB [3], as a consequence of this last process, MA_3^- is formed too.

In the literature many contradictory data may be found for the stability constants of various metal complexes. Hence a critical re-examination of these data seems desirable. For the reasons mentioned above, a re-examination is even more justified in the case of the lanthanide-α-hydroxycarboxylic acid systems.

The purpose of the present work was such a critical re-examination of the stability constants of some lanthanide-α-hydroxycarboxylic acid systems and the calculation of the correct values on the basis of experimental data reported in the literature.

CHOPPIN *et al.* [4, 5] made ion-exchange and electrophoretic studies on lanthanide glycollate, -lactate and -α-hydroxyisobutyrate systems and found that negatively-charged MA_4^- complexes were also formed in these systems. From the experimental potentiometric data they calculated three

constants [6]; the fourth value was not evaluated, in all probability, because of the reasons mentioned above.

THUN *et al.* [7, 8, 9], dealing with the equilibrium conditions of lanthanide complexes of glycollic acid derivatives, generally calculated four constants from the experimental data. In their calculations they did not take into account that other processes may also take place besides the formation of mononuclear complexes. Therefore, although the experiments were performed under well controlled conditions, the values of the calculated constants and the ratio of the successive constants sometimes do not appear reasonable. In the case of α-hydroxyisobutyrate systems, for instance with the series Pr, Nd and Sm, they obtained for log K_2/K_3 0.55, 0.12 and 0.62 and for log K_3/K_4 0.45, 0.96 and 0.19 [8]. The reason for the abnormal variation of the ratios can only be the inaccuracy of the constants.

In an earlier publication [10] we proposed a new calculation procedure: the curve-reduction method. This method can be used to select the portion of the formation curve which is fully characterized by the BJERRUM function [11]. The simultaneously calculated constants afford a good approximation, and the method of least squares is only applied to a selected section of the curve. In the former publication [10] we determined all four stability constants of the Ce(III)-glycollate system on the basis of experimental data taken from the literature. With this we supplemented [6] and corrected [12] the data published earlier.

In the present work we employed this method for a critical examination of the Nd(III)-methylpropylglycollate, Yb(III)-isobutylmethylglycollate, -isopropylmethylglycollate, -diethylglycollate [7], Er(III)-α-hydroxycyclohexanecarboxylate [13] and Sm(III)-mandelate [14] systems. By means of the curve-reduction method we selected usable experimental data for the calculation of the constants, and then determined their precise values on the basis of least squares principle.

The formation curve reduction was performed for each of the systems listed above. In Fig. 1 can be seen the experimental formation curve and the partial formation curves of the Yb(III)-isopropylmethylglycollate system.

It can be seen that the experimental formation curve (1) approaches a value of four. From this it might be concluded that up to $\bar{n} \sim 3.8$ only the simple mononuclear complexes are important in the equilibria. We fitted the partial formation curves to the SILLEN [15] normalized group of curves (the sections of the partial formation curves deviating from the best fit are drawn with a broken line). The $\bar{n}_{(0.2)}(pA)$ partial formation curve (2) is symmetrical about the middle-point. It follows from this that in this pA range, apart from the formation of MA_n type complexes, no other process plays a significant part in the equilibrium reactions. From an analysis of the $\bar{n}_{(1.3)}(pA)$ and $\bar{n}_{(2.4)}(pA)$ curves (3 and 4), however, it is clear that these are only symmetrical

about the middle-point up to a definite pA value ($pA \sim 1.7$, $\bar{n} \sim 2.6$). Below this pA value it is necessary to consider the other processes in addition to the formation of MA_n type complexes. However, the experimental data are not sufficient for the identification of these other complex species. Hence, in our calculations we ignored those sections of the curves which no longer fitted the

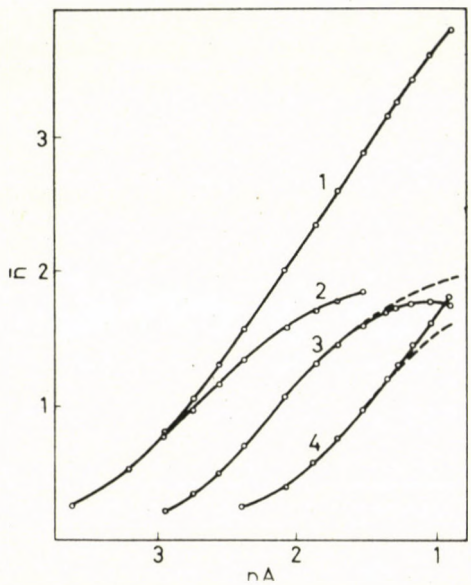

Fig. 1. Original and reduced formation curves of the Yb(III)-isopr. v methylglycollate system. (1) Experimental formation curve; (2) $\bar{n}_{(0.2)}$ (pA); (3) $\bar{n}_{(1.3)}$ (pA); (4) $\bar{n}_{(2.4)}(pA)$ partial ormation curves

BJERRUM formation curves. Accordingly, in the system under consideration the values of log K_n were calculated only from the sections of the curves extending to $pA = 1.702$.

The analysis of the formation curves and the calculations were performed for all the systems under examination. The constants we obtained together with the corresponding literature data are summarized in Table I.

The first line of the Table shows the limiting values of $\bar{n}$ up to which we and the authors cited took into account the measured points. The number of measured points used for the calculation of the constants is denoted by p, and the last line of the Table gives the values of the mean square differences in $\bar{n}$. From the results obtained for the Nd(III)-methylpropylglycollate, Yb(III)-isobutylmethylglycollate, -isopropylmethylglycollate and -diethylglycollate systems it is evident that, as expected, the values of log K_1 and log K_2 are only slightly affected by the fact that the cited authors used also the ill-defined sections of the curves in their calculations. However, for log K_3 and log K_4, the

differences compared with our accurately calculated constants become increasingly important. It follows that the other processes play a more and more important role in the sections of the curves which correspond to MA_3 and MA_4^- formation. This is also shown by the fact that the value of log K_3 is always

Table I

Stability constants of some lanthanide-α-hydroxycarboxylic acid systems as given in the literature and calculated by the present method

	Nd(III)-methyl, propylglycollate		Yb(III)-isobutyl-methylglycollate		Yb(III)-isopropyl-methylglycollate	
	[9]	x	[7]	x	[7]	x
$\bar{n}_{\text{limit}}$	3.502	3.025	3.408	2.893	3.816	2.602
p	24	20	15	13	15	9
log K_1	2.38	2.39	3.21	3.23	3.12	3.10
log K_2	1.85	1.81	2.74	2.70	2.44	2.41
log K_3	1.17	1.25	1.75	1.83	1.65	1.74
log K_4	1.06	0.97	1.40	1.27	1.39	1.23
log β_4	6.46	6.42	9.10	9.03	8.60	8.48
$[\Sigma(\Delta\bar{n})^2/p] \cdot 10^5$	12	4	26	8	18	4

	Yb(III)-diethyl-glycollate		Er(III)-hydroxy-cyclohexanecarboxy-late		Sm(III)-mandelate	
	[7]	x	[13]	x	[14]	x
$\bar{n}_{\text{limit}}$	3.514	2.878	—	1.728	1.918	1.918
p	15	12	—	13	23	23
log K^1	3.10	3.13	2.48	2.58	2.56	2.56
log K^2	2.26	2.22	2.35	1.94	2.00	2.01
log K^3	1.31	1.40	—	1.96	1.38	1.37
log K^4	1.09	0.82	—	—	—	—
log β^4	7.76	7.57	—	—	—	—
$[\Sigma(\Delta\bar{n})_2/p] \cdot 10_5$	24	5	—	13	5	5

* Data calculated by the present method.

greater and the values of log K_4 and log β_4 are smaller than the literature data. The greater accuracy of our constants is proved in that the $\bar{n}$ mean square difference shown in the last line of the Table are substantially smaller according to our calculations.

In the systems discussed so far the use of the curve-reduction method is justified by the occurrence of troublesome side reactions. For the Er(III)-α-hydroxycyclohexanecarboxylate system shown in the Table, the reported [13]

$\bar{n}$ values are only about 1.7 because MA_3 separated as a precipitate. According to the measured data, the authors determined only log K_1 and log K_2, disregarding the formation of MA_3. With the curve-reduction method it has been shown that it is necessary to take into account the presence of MA_3 even at $\bar{n} > 1$, and at $\bar{n} \sim 1.7$ the value of α_3 is as high as 0.25. Our value of log K_3 is naturally less accurate than log K_1 and log K_2, since in the range studied MA_3 is formed in comparatively small amounts. Still it must be taken into consideration if accurate values of log K_1 and log K_2 are desired. Bearing all this in mind, we calculated the constants once again, and the results differ significantly from the previously reported data.

The last column of the Table shows the Sm(III)-mandelate system which had been examined by POWELL and NEILLIE [14]. In their calculations they took into account the formation of MA_3, and thus the published data are accurate.

From an investigation by the curve-reduction method of the Nd(III)-methylpropylglycollate, Yb(III)-isobutylmethylglycollate, -isopropylmethylglycollate and -diethylglycollate complex equilibrium systems it is evident that different processes may play a part in the overall equilibria. Therefore, the exact values of the constants are only obtainable if the ill-defined sections of the curves are not considered in the calculations.

REFERENCES

1. MOELLER, T., MARTIN, D. F., THOMPSON, L. C., FERRUS, R., FEISTEL, G. R., RANDALL, W. J.: Chem. Rev. **66,** 1 (1965)
2. Stability Constants of Metal Ion Complexes. Edited by Sillén, L. G. Martell, A. (Special Publication No. 17), London, 1964
3. SEYB, K. E.: J. Inorg. Nucl. Chem. **26,** 231 (1964)
4. CHOPPIN, G. R., MOY, D., HOLM, L. W.: Radioisotopes in the physical sciences and industry, p. 284, Copenhagen, 1960
5. HOLM, L. W., CHOPPIN, G. R., MOY, D.: J. Inorg. Nucl. Chem. **19,** 251 (1958)
6. CHOPPIN, G. R., CHOPOORIAN, J. A.: J. Inorg. Nucl. Chem. **22,** 97 (1961)
7. THUN, H., VERBEEK, F.: J. Inorg. Nucl. Chem. **27,** 1831 (1965)
8. DEELSTRA, H., VERBEEK, F.: Anal. Chim. Acta **31,** 251 (1964)
9. EECKHAUT, L., VERBEEK, F., DEELSTRA, H., HOSTE, J.: Anal. Chim. Acta **30,** 369 (1964)
10. NAGYPÁL, I., GERGELY, A., JÉKEL, P.: J. Inorg. Nucl. Chem. **31,** 3447 (1969)
11. BJERRUM, J.: Metal Ammine Formation in Aqueous Solution. P. Haase and Son, Copenhagen, 1941
12. DEELSTRA, H., VANDERLEEN, W., VERBEEK, F.: Bull. Soc. Chim. Belg. **72,** 632 (1963)
13. SCHURMANS, H., THUN, H., VERBEEK, F.: J. Inorg. Nucl. Chem. **29,** 1759 (1967)
14. POWELL, J., NEILLIE, W. F. S.: J. Inorg. Nucl. Chem. **29,** 2371 (1967)
15. SILLÉN, L. G.: Acta Chem. Scand. **10,** 186 (1956)

Arthur GERGELY
István NAGYPÁL
Debrecen 10. Hungary.

Acta Chimica Academiae Scientiarum Hungaricae, Tomus 68 (3), pp. 189—203 (1971)

THEORETICAL MAGNETIC RESONANCE SPECTRA OF AA'A''... XX'X''... SYSTEMS

THE CASE OF DECEPTIVE SIMPLICITY

A. ROCKENBAUER and L. RADICS

(Central Research Institute for Chemistry, Hungarian Academy of Sciences, Budapest)

Received September 5, 1969

The theoretical magnetic resonance spectra of $AA'A''\ldots XX'X''\ldots = A_n^+X_m^+$ systems have been investigated in the limiting case where coupling between particles A is strong in comparison to that between particles A and X and coupling between particles X is negligible (limiting case of strong coupling). Our calculations can be applied for the description of both NMR and ESR spectra. We studied conditions resulting in 'deceptively simple' spectra, that is when the spectra of an $A_n^+X_m^+$ system are identical with those of an A_nX_m system consisting of magnetically equivalent particles. We found that the spectra of the $A_n^+X_m^+$ system are deceptively simple only if the symmetry point group of the A_n^+ subsystem is Abelian: in this case only the average of coupling constants J_{AX} can be obtained. However, when the symmetry point group of the A_n^+ subsystem is non-Abelian, rather complex spectra were obtained from the degenerate levels of the A_n^+ subsystem and this kind of spectra provides additional information about the coupling constants J_{AX}.

We have calculated the theoretical spectra of a few strongly coupled $A_n^+X_m^+$ systems and have reinterpreted the proton resonance spectra of a few phosphorus-nitrogen compounds. The difference between the A and X parts in the spectra of the $A_3^+X_3^+$ and $A_4^+X_4^+$ systems is also explained by the non-Abelian character of the symmetry point groups.

Introduction

Magnetically and chemically equivalent particles play an important part in the theory of magnetic resonance spectra. The characteristic feature of magnetically equivalent particles, *viz.* that coupling between themselves does not affect the resonance pattern, applies for chemically equivalent particles only in special limiting cases. This phenomenon was first studied by ABRAHAM and BERNSTEIN [1] in connection with the $AA'XX'$ spin system. These authors showed that in the particular case when $J_{AA'} \gg |J_{AX} - J_{A'X}|$ and the coupling between particles X is negligibly small, both the A and X parts of the spectrum will consist of a 1 : 2 : 1 triplet with a spacing of $1/2\,(J_{AX}+J_{A'X})$, *i.e.* the spectrum will be identical with that of the A_2X_2 system consisting of magnetically equivalent particles.

This type of limiting case of strong coupling resulting in deceptively simple spectra for the more complex $X_mAA'X'_m$ and $A_nA'_mX_p$ spin systems was investigated by HARRIS [2] and DIEHL [3]. As in the previous case, the spectra were found to consist of the same lines that are expected for the respective A_2X_{2m} and $A_{n+m}X_p$ systems; the line separations being the weighted arithmetical mean of the coupling constants J_{AX} and $J_{A'X}$.

No attempt has been made, however, to generalize these rules for systems containing more than two kinds of magnetically non-equivalent but chemically equivalent particles. By simple analogy, MUSHER and COREY [4] suggested that the above conclusions apply for the system $AX\ A'X'\ A''X'' \ldots$ as well, which, however, is not the case. In studying the electron resonance spectrum of a symmetrical nitroxide triradical, HUDSON and LUCKHURST [5] found that the theoretical hyperfine spectrum, which is the ESR equivalent of the A resonance pattern of an $AA'A''XX'X''$ nuclear spin system is more complex than could be expected by analogy with more simple systems, although the above conditions leading to deceptive simplicity were included into their calculations. As a result, the calculated spectrum contains, in addition to the lines characteristic of the A_3X_3 system, 'irregularly spaced' lines as well.

The occurrence of these lines in the spectrum seems to indicate that the conditions imposed on the ratios of coupling constants are generally insufficient for resulting in deceptively simple spectra in case of more complex systems. One may intuitively suggest that the required additional conditions are provided by the symmetry properties of the system.

In this paper we shall be concerned with the analysis of magnetic resonance spectra arising from $AA'A'' \ldots XX'X'' \ldots$ type spin systems in the limiting case of strong coupling. In a recent publication HARRIS [6] reported on the analysis of this system for a particular case in which the conditions of strong coupling were not satisfactorily fulfilled. The sub-spectral breakdown of $AA'A''XX'X''$ has also been presented [7]. Its application for the above limiting case, however, was not carried out as the degeneration of sub-spectra can be determined only tediously. As pointed out by JONES and WALKER [8], and DIEHL and TRAUTMANN [9], the analysis of more complex systems, like $AA'A''A'''\ XX'X''X'''$, cannot be performed by means of sub-spectral transformations owing to the existence of limitations in this method. In our calculations therefore, we made use of a different approach provided by the great separability of the Hamiltonian in the limiting case of strong coupling.

Description of the system

In order to emphasize the analogy between magnetic equivalence and chemical equivalence in the limiting case of strong coupling the system investigated will be designated as

$$AA'A'' \ldots XX'X'' \ldots = A_n^+ X_m^+$$

where the symbol $+$ indicates that both A^+ and X^+ particles are magnetically non-equivalent and chemical equivalence is due to the symmetry properties of the system (A^+ and X^+ particles are symmetrically equivalent). This means

that among the symmetry operations of point group R there is at least one which transforms $A^{(i)}$, arbitrarily chosen from particles $A^{(1)}, A^{(2)}, \ldots A^{(n)}$, into the likewise arbitrarily selected $A^{(j)}$. There must also be at least one such symmetry operation where $X^{(i)}$ arbitrarily chosen from $X^{(1)}, X^{(2)}, \ldots X^{(m)}$, is transformed into the arbitrary $X^{(j)}$. We do not predetermine what particular permutation of $X^{(1)}, X^{(2)}, \ldots X^{(m)}$ corresponds to a permutation of $A^{(1)}, A^{(2)}, \ldots A^{(n)}$ and thus, instead of the whole point group R, the point groups R_A and R_X of the A_A^+ and X_X^+ subsystems, resp. will be considered. The preceding symmetry requirements are fulfilled when *e.g.* we have an A_3^+ subsystem with C_{3v} symmetry, or an A_4^+ subsystem with T_d, C_{4v}, or C_{2v} symmetry.

We shall confine our discussion to systems where anisotropy effects are negligible, hence the spin Hamiltonian contains only isotropic terms:

$$\mathscr{H} = \mathscr{H}_A + \mathscr{H}_{AA} + \mathscr{H}_X + \mathscr{H}_{AX} \tag{1}$$

where

$$\mathscr{H}_A = \nu_A \sum_{i=1}^{n} I_z(A^{(i)}) = \nu_A I_z(\mathrm{A}), \tag{2a}$$

$$\mathscr{H}_{AA} = \sum_{i>j=1}^{n} J_A(i,j)\, \bar{I}(A^{(i)}) \cdot \bar{I}(A^{(j)}), \tag{2b}$$

$$\mathscr{H}_X = \nu_X \sum_{i=1}^{m} I_z(X^{(i)}) = \nu_X I_z(X), \tag{2c}$$

$$\mathscr{H}_{AX} = \sum_{i=1}^{n} \sum_{j=1}^{m} J_{AX}(i,j)\, \bar{I}(A^{(i)}) \cdot \bar{I}(X^{(j)}). \tag{2d}$$

Here ν_A and ν_X are the respective Zeeman energies, $\bar{I}(A^{(i)})$ and $\bar{I}(X^{(j)})$ denote the spin vector of $A^{(i)}$ and $X^{(j)}$ nuclei (or unpaired electrons), $J_A(i,j)$ and $J_{AX}(i,j)$ are the appropriate coupling constants. As stated previously, interactions between $X^{(i)}$ and $X^{(j)}$ are neglected.

We shall assume that ν_A and $|\nu_A - \nu_X|$ are greater than the coupling constants and all non-vanishing J_A are greater than J_{AX}. These conditions can be fulfilled not only for special nuclear spin systems, but also for systems containing unpaired electrons, if the exchange coupling of unpaired electrons is much greater than the hyperfine couplings.

The eigenvalues in the strong coupling case

Since the first three members of the Hamiltonian commute, the eigenfunctions of $\mathscr{H}_A$

$$I_z(A)|m_A\rangle = m_A|m_A\rangle \tag{3}$$

are simultaneously eigenfunctions of $\mathscr{H}_X$ and $\mathscr{H}_{AA}$. Since, furthermore, $\nu_A \gg J_{AX}$, it is sufficient to retain in $\mathscr{H}_{AX}$ only those terms that result in non-vanishing matrix elements between eigenfunctions with the same m_A. Accordingly, from all scalar products,

$$I(A^{(i)}) \cdot I(X^{(j)})$$

it is satisfactory to consider the z components only. Let the truncated $\mathscr{H}_{AX}$ be denoted by $\mathscr{H}'_{AX}$, we then have:

$$\mathscr{H}'_{AX} = \sum_{i=1}^{n} \mathscr{H}'_{AX}(i) = \sum_{i=1}^{n} I_z(A^{(i)}) \sum_{j=1}^{m} J_{AX}(i,j)\, I_z(X^{(j)})\,. \tag{4}$$

Contrary to the original $\mathscr{H}_{AX}$, $\mathscr{H}'_{AX}$ does commute with $\mathscr{H}_X$, therefore, in addition to $\mathscr{H}_A$ and $\mathscr{H}_{AA}$ (which are greater than $\mathscr{H}_{AX}$) $\mathscr{H}_X$ may also be considered as part of the unperturbed Hamiltonian, irrespective of the relative magnitude of $\mathscr{H}_{AX}$ and $\mathscr{H}_X$. Thus the unperturbed Hamiltonian may be written as

$$\mathscr{H}_0 = \mathscr{H}_A + \mathscr{H}_X + \mathscr{H}_{AA}\,, \tag{5}$$

where $\mathscr{H}_{AA}$ is the only term where the eigenvalue problem cannot be solved trivially. The eigenvalue equation for $\mathscr{H}_{AA}$ may be written in the form

$$\mathscr{H}_{AA}|m_A, u, v> = \nu_{AA}(u)|m_A, u, v> \tag{6}$$

where u counts the ν_{AA} eigenvalues of $\mathscr{H}_{AA}$, and v the degenerate eigenkets corresponding to the same u and m_A. Since $\mathscr{H}_{AA}$ commutes with

$$\bar{I}^2(A) = \left[\sum_{i=1}^{n} \bar{I}(A^{(i)})\right]^2$$

and is, on the other hand, invariant under the symmetry operations, the $\nu_{AA}(u)$ eigenvalues can be characterized by the I_A eigenvalues of the $I(A)$ operator and by irreducible representations D_u of the symmetry point group R_A. It is easy to see that the magnitude of $\nu_{AA}(u)$ pertaining to a given I_A is independent of m_A [10]. If we exclude the possibility of accidental degeneracy, then the number of functions belonging to the same $\nu_{AA}(u)$ and m_A is equal to d_u, the dimension of the appropriate D_u.

The third term of the unperturbed Hamiltonian, $\mathscr{H}_X$ has common eigenkets with $I_z(X)$:

$$I_z(X)|m_X> = m_X|m_X>. \tag{7}$$

Now the solution of the eigenvalue equation for the unperturbed $\mathscr{H}_0$ Hamiltonian can be obtained from Eqs (3), (6) and (7):

$$\mathscr{H}_0|m_A, u, v > |m_X > = [\nu_A m_A + \nu_X m_X + \nu_{AA}(u)]|m_A, u, v > |m_X > . \tag{8}$$

Treatment of perturbation $\mathscr{H}'_{AX}$ is facilitated through a special property of the matrix $J_{AX}(i, j)$. This is based on the fact that $\mathscr{H}_{AX}$ is invariant with respect to the symmetry operation of point group R. Let $R(1, i)$ be an operation which transforms $A^{(1)}$ into $A^{(i)}$, *i.e.* $I_z(A^{(1)})$ into $I_z(A^{(i)})$, and applied on $\mathscr{H}'_{AX}$ (1). Since operation $R(1, i)$ results in some non-specified permutation of particles $X^{(1)}, \ldots X^{(m)}$, we have

$$\begin{aligned} R(1,i)\,\mathscr{H}'_{AX}(1)\,R^{-1}(1,i) &= I_z(A^{(i)}) \sum_{j=1}^{m} J_{AX}(1,j)\,R(1,i)\,I_z(X^{(j)})^{-1}(1,i) = \\ &= I_z(A^{(i)}) \sum_{j=1}^{m} J_{AX}(1,j)\,I_z(X^{(k)}) = I_z(A^{(i)}) \sum_{k=1}^{m} J_{AX}(1,j)\,I_z(X^{(k)}) . \end{aligned} \tag{9}$$

It can be seen that the transform of $\mathscr{H}'_{AX}$ (1) and

$$\mathscr{H}'_{AX}(i) = I_z(A^{(i)}) \sum_{k=1}^{m} J_{AX}(i,k)\,I_z(X^{(k)}) \tag{10}$$

differ only in the respective coefficients $J_{AX}(1, j)$ and $J_{AX}(i, k)$. Owing to invariance of $\mathscr{H}_{AX}$ with respect to $R(1, i)$ these coefficients have to be identical, *i.e.* each row of the matrix $J_{AX}(i, j)$ consists of the same elements, arranged, however, differently in different rows. The transformation properties of X^+ being the same as those of particles A^+, the above applies also to the columns, *i.e.* we have the same elements in every column as well. Hence the arithmetical mean of the elements in each row and each column will be the same

$$J_0 = \frac{1}{m} \sum_{j=1}^{m} J_{AX}(i,j) = \frac{1}{n} \sum_{i=1}^{n} J_{AX}(i,j) . \tag{11}$$

Note that if some of the particles are magnetically equivalent, a corresponding number of rows and columns will have the elements in the same order.

$\mathscr{H}'_{AX}$ can be conveniently re-written by making use of the following summation rule:

$$\sum_{i=1}^{n} a_i b_i = \frac{1}{n} \sum_{i=1}^{n} a_i \sum_{i=1}^{n} b_i - \frac{1}{n} \sum_{i>k=1}^{n} (a_i - a_k)(b_i - b_k) . \tag{12}$$

Omitting temporarily the second term, for the first part of $\mathscr{H}'_{AX}$ we have

$$\mathscr{H}^{\mathrm{I}}_{AX} = \frac{1}{n} \sum_{i=1}^{n} I_z(A^{(i)}) \sum_{i=1}^{n} \sum_{j=1}^{n} J_{AX}(i,j)\, I_z(X^{(j)}) = \\ = I_z(A) \sum_{j=1}^{m} I_z(X^{(j)}) \frac{1}{n} \sum_{i=1}^{n} J_{AX}(i,j) = J_0\, I_z(A)\, I_z(X). \tag{13}$$

Since $\mathscr{H}^{\mathrm{I}}_{AX}$ obviously commutes with each operator in the remaining Hamiltonian

$$\mathscr{H}_A + \mathscr{H}_X + \mathscr{H}_{AA} + \mathscr{H}_{AX} \tag{14}$$

the corresponding eigenvalues can be readily obtained:

$$\nu_A\, m_A + \nu_X\, m_X + \nu_{AA}(u) + J_0\, m_A\, m_X. \tag{15}$$

It can be seen that the eigenvalues thus obtained are identical with those expected in the case of magnetic equivalence and the average coupling constant J_0 corresponds to J_{AX} characterizing the interaction in the A_nX_m system.

Deviations from the spectrum of the A_nX_m system may thus be due to the second term of $\mathscr{H}'_{AX}$,* in other words, we can expect deceptively simple spectra for the $A_n^+X_m^+$ system only if the matrix elements of $\mathscr{H}^{\mathrm{II}}_{AX}$ between degenerate functions of the unperturbed Hamiltonian are zero.

In order to find the conditions that cause the matrix elements to vanish, first we write

$$\mathscr{H}^{\mathrm{II}}_{AX} = \frac{1}{n} \sum_{i>k=1}^{n} \left(I_z(A^{(i)}) - I_z(A^{(k)})\right) \sum_{j=1}^{m} \left(J_{AX}(i,j) - J_{AX}(k,j)\right) I_z(X^{(j)}). \tag{16}$$

Then for the matrix elements between degenerate functions we have

$$\langle m_A, u, v' | \langle m(X^{1)}) | \ldots \langle m(X^{(m)}) | \mathscr{H}^{\mathrm{II}}_{AX} | m_A, u, v \rangle | m(X^{(1)}) \rangle \ldots | m(X^{(m)}) \rangle \\ = \frac{1}{n} \sum_{i>k=1}^{n} \langle m_A, u, v' | I_z(A^{(i)}) - I_z(A^{(k)}) | m_A, u, v \rangle = \\ = \sum_{j=1}^{n} \left(J_{AX}(i,j) - J_{AX}(k,j)\right) m(X^{(i)}) = 0 \tag{17}$$

for all u, v, v', m_A and m $(X^{(1)}), \ldots m(X^{(m)})$ values. This equality is fulfilled obviously if either

$$J_{AX}(i,j) = J_{AX}(k,j) \tag{18}$$

* Ishikawa [10] neglected this term in his calculations without offering an adequate explanation.

for each i and k, *i.e.* when the particles are magnetically equivalent in sets A and X, or

$$\langle m_A, u, v' | I_z(A^{(i)}) | m_A, u, v \rangle = \langle m_A, u, v' | I_z(A^{(k)}) | m_A, u, v \rangle \tag{19}$$

for every i, k, u, v, v' and m_A.

The latter case corresponds to what we call the criterion of deceptive simplicity. Since it depends exclusively on particles A, its validity may be iextended to more general $A_n^+ X_m^+ Y_p^+ \ldots$ systems, provided that restrictions mpo sed on particles X^+ are fulfilled also with particles Y^+.

Consider now how this criterion is affected by the degeneracy of $| m_A, u, v >$ states and the symmetry properties of sub-system A_n^+. If the state is non-degenerate, *i.e.* if $| m_A, u, v > = | m_A, u >$, criterion (19) is always satisfied. This can be shown as follows.

Among the operations of point group R_A, there is at least one, $R(i, k)$, for which we can write

$$R(i, k)\, I_z(A^{(i)})\, R^{-1}(i, k) = I_z(A^{(k)}). \tag{20}$$

Since now D_u is a one-dimensional representation, the transformational properties of $| m_A, u >$ are:

$$R\ (i, k) | m_A, u > = D_u\big(R(i, k)\big) | m_A, u > \tag{21}$$

and

$$R^{-1}(i, k) | m_A, u > = D_u^+\big(R(i, k)\big) | m_A, u > . \tag{22}$$

Substitution of Eqs (21) and (22) into (19) gives:

$$\begin{aligned} &\langle m_A, u | I_z(A^{(i)}) | m_A, u \rangle = \\ &= \langle m_A, u | R^{-1}(i, k)\, R(i, k)\, I_z(A^{(i)})\, R^{-1}(i, k)\, R(i, k) | m_A, u \rangle = \\ &= \langle m_A, u | D_u^+\big(R(i, k)\big)\, I_z(A^{(k)})\, D_u\big(R(i, k)\big) | m_A, u \rangle = \\ &= \langle m_A, u | I_z(A^{(k)}) | m_A, u \rangle . \end{aligned} \tag{23}$$

In the case of degenerate $| m_A, u, v >$ states, criterion (19) is generally not fulfilled. (States with $m_A = 0$ provide, in accordance with spin inversion, an exception from this statement.) As a result of this, the position of lines associated with degenerate states are determined by values of $m(X^{(i)})$ ($i = 1, 2, \ldots m$) as well. In complex spin systems the numbers of possible sets of $m(X^{(i)})$ may be very large, hence the same is true for the number of lines obtained from degenerate states, consequently, their intensity is generally low as compared to that of the 'main lines' arising from non-degenerate states.

As we have seen the main factor determining the structure of the spectrum in the limiting case of strong coupling is the degeneracy of eigenstates of the unperturbed Hamiltonian. Thus we can expect deceptively simple spectra in those cases where each and every state of the A_n^+ sub-system is non-degenerate. This is equivalent to the requirement that sub-group R_A permuting the particles A be Abelian.

Actually, R_A can be only Abelian when $n = 2$ and this may explain why calculations on $A_2^+X_m^+$ systems always yielded deceptively simple spectra in the limiting case of strong coupling. If, however, n is greater than 2, R_A may be either Abelian or non-Abelian. Thus, for example, if $n = 3$, R_A is of C_{3v} symmetry which is non-Abelian, whereas, if $n = 4$ the symmetry point group may be T_d, C_{4v} or C_{2v}, among which C_{2v} is Abelian.

At this point it is convenient to show what parameters, in addition to the average coupling constant, can be derived from the spectra when the conditions of deceptive simplicity are not fulfilled.

As an illustrative example, consider the $A_3^+X_3^+$ system. In this case deviation from deceptive simplicity may arise from the doubly degenerate state $u(1/2, E)$ characterized by the eigenvalue I_A and D_u symmetry species. Owing to the C_{3v} symmetry, the perturbing operator $\mathscr{H}'_{AX}$ contains only two different coupling constants, the diagonal $J_{AX}(i, i) = J$ and non-diagonal $J_{AX}(i, j) = J'$. It is convenient to introduce the average coupling constant defined as $J_0 = 1/3\,(J+2\,J')$ together with the parameter $\Delta J = =1/3\,(J - J')$ indicating the degree of deviation from magnetic equivalence.

Diagonalization of $\mathscr{H}'_{AX}$ and subsequent determination of transition probabilities result in the partial spectrum belonging to the degenerate $u(1/2, E)$ state. Fig. 1 shows the appropriate energy levels of the whole system, whereas Fig. 2 gives the X resonance pattern for different values of ΔJ. In the particular case when $\Delta J = 0$, calculations lead to a doublet with line separation J_0. [This doublet, together with the quadruplet arising from the non-degenerate $u(3/2, A_1)$ state, results in the simple 1 : 3 : 3 : 1 resonance pattern.] If, however, $\Delta J \neq 0$, each component of the doublet splits into a 1 : 4 : 6 : 4 : 1 quintuplet. The spacing between the quintuplet lines being ΔJ, if the relative signs are known, the spectrum provides both J and J'. Analysis of the A part of the spectrum gives similar results concerning the determination of the coupling constants, though the X and A parts of the spectrum have different patterns.

Similar calculations on the $A_4^+X_m^+$ system show that, depending upon whether the symmetry of the R_A point group is T_d or C_{4v}, both of the two different, or two of the three coupling constants, can be obtained from the spectrum. This leads to the expected generalization, stating that the amount of information that can be obtained on the couplings depends on the symmetry of the system.

The second important consequence of the deviation from deceptive simplicity is the different structure of the A and X parts of the spectrum. Differences expected to be in the $A_n^+ X_m^+$ systems even when $n = m$.

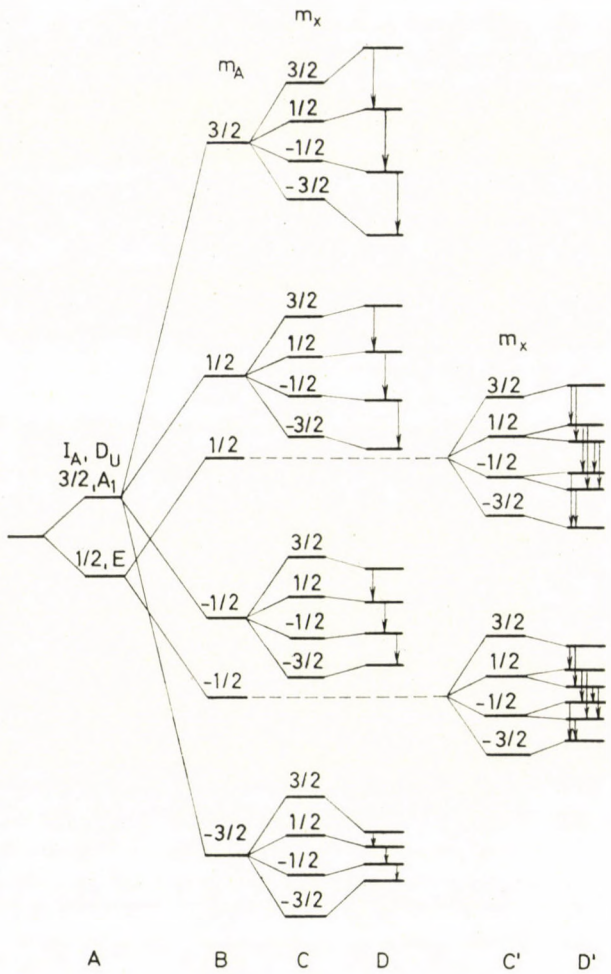

Fig. 1. Energy levels of the $A_3^+ X_3^+$ system with strong coupling and transitions of X resonance ($\Delta m_A = 0$, $\Delta m_X = +1$)
A: $\mathscr{H}_A$, B : $\mathscr{H}_{AA}$, C and C' : $\mathscr{H}_X$, D and D': $\mathscr{H}_{AX}$

Consider for this purpose the partial spectra associated with the non-degenerate $u(I_A, D_u)$ states.

According to the selection rules for the A and X parts,

$$\Delta m_A = \pm 1 \text{ and } \Delta m(X^{(i)}) = 0 \text{ for } \quad i = 1, \ldots m \tag{24}$$

and

$$\Delta m_A = 0, \ \Delta m(X^{(i)}) = \pm \delta_{ij} \quad \text{for } i, j = 1, \ldots m,^* \tag{25}$$

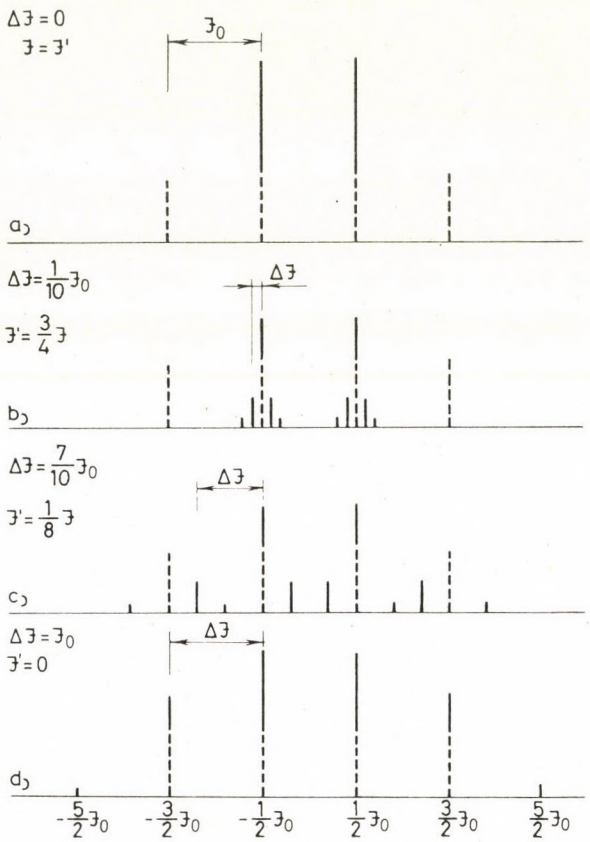

Fig. 2. X part of the spectrum of the $A_3^+X_3^+$ system with strong coupling
a) $J = J'$; b) $J' = 3/4\,J$; c) $J' = 1/8\,J$; d) $J' = 0$

respectively. Hence, the resonance frequencies are given by

$$\nu^A = \nu_A + J_0 m_X \tag{26}$$

and

$$\nu^X = \nu_X + J_0 m_A. \tag{27}$$

The relative intensities in the A part of the partial spectrum are governed by the number of possible combinations of $m(X^{(i)})$ giving the same m_X values, as for the A part of the complete A_nX_m spectrum, and hence the A part of every

* In the limiting case of strong coupling there is no combinational line.

partial spectrum associated with the non-degenerate $u(I_A, D_u)$ states is identical with the A part of the A_nX_m spectrum. On the contrary, the relative intensities in the X part are independent of m_A, hence this part of the partial spectrum will consist of $2I_A + 1$ lines of equal intensity. If each state of the system is non-degenerate, the resonance pattern obtained by superposition of these lines is identical with the X part of the A_nX_m spectrum. Consequently, the A and X parts of the spectrum of an $A_n^+X_m^+$ system (note $n = m$) are identical when the symmetry point group is Abelian.

If, however, the R_A symmetry point group is non-Abelian, the A and X parts of $A_n^+X_m^+$ spectrum will certainly differ, since superposition of the partial spectra obtained from the non-degenerate states does not result in an A_nX_n spectrum in the X part, while it does in the A part. The partial spectra corresponding to degenerate states cannot equalize this difference owing to the irregular spacing of these lines. This difference between the A and X parts will still persist if conditions for strong coupling are not valid, since a continuous change in the ratios of coupling constants $J_{AA'}$, J_{AX} and J_{XX} can result only in continuous changes in the resonance pattern.

Consider now the $A_3^+X_3^+$ system. Since the symmetry point group is C_{3v}, *i.e.* non-Abelian, the A and X parts of the spectrum will be different in agreement with the results of sub-spectral analysis [7].

The $A_4^+X_4^+$ system represents a more interesting example. As it was pointed out by JONES and WALKER [8], the subspectral analysis cannot be applied to this system, and thus it was not possible to show whether the A and X parts of the spectrum are identical or not. Now we can state that if the symmetry point group is T_d or C_{4v}, *i.e.* non-Abelian, then the A and X parts are different. If, however, the symmetry point group is C_{2v}, *i.e.* Abelian, then the A and X parts are identical in the limiting case of strong coupling. If the conditions for strong coupling are not fulfilled, then the A and X parts will again differ, since the C_{2v} symmetry can be produced by infinitesimal distortion of the C_{4v} symmetry.

Appearance of deceptively simple spectra in special systems

There is not much information in the literature about systems containing more than two chemically equivalent but magnetically non-equivalent particles with deceptively simple spectra. Let us take the cases where a well resolved pattern could be observed in the A part of the spectrum, *e.g.* symmetrical multiradicals [5, 11] and the group $Mn(II)_4$ embedded in a silicon lattice [12], where the hyperfine pattern in the ESR spectrum represents the A part of the spectra.

The iminoxy triradical studied by HUDSON and LUCKHURST [5] can be classified as of the $A_3^+X_3^+$ type since splitting is caused by one ^{14}N nucleus in

each iminoxy group. The symmetry point group of the system is C_{3v}. HUDSON and LUCKHURST have derived the theoretical spectrum in the limiting case of strong coupling, *i.e.* when the exchange coupling between the unpaired electrons is strong in comparison to the hyperfine coupling constants. They found irregularly spaced lines, too, besides the equidistant ones, which is in agreement with our criterion: when the symmetry point group is non-Abelian the spectrum is not deceptively simple. In the experimental spectrum only the equidistant lines were observed. The authors explained this fact by a special relaxation mechanism which is effective only in the degenerate states caused by the modulation of coefficients J_A.

A similar explanation can be given for the fact that ROZANTSEV *et al.* [11] have found deceptively simple spectra for different tetraradicals (systems of $A_4^+X_4^+$ type): even if the symmetry point group is non-Abelian (*e.g.* T_d or C_{4v}) the above-mentioned relaxation mechanism prevents the observation of irregularly spaced lines arising from the degenerate states.

The $Mn(II)_4$ group embedded in a silicon lattice [12] represents an interesting example of the $A_4^+X_4^+$ systems. The ESR spectrum corresponds to a typical deceptively simple spectrum. In this case, probably, the anisotropic effects prevent the observation of irregularly spaced low intensity lines.

Relatively well splitted patterns can be observed in the X part of the spectra in the proton resonance spectrum of some phosphorus compounds. The following examples can be found in the literature for $n = 3$.

a) The complex

$$cis\text{-}\ [Mo(CO)_3\ \{P(OCH_2)_3\ CR\}_3].$$

studied by STANCLIFT and HENDRICKER [13], where

$$R = CH_3,\ C_2H_5 \text{ or } C_3H_7.$$

b) The compound synthesized by HEWLETT and SHAW [14]: ethoxy-cyclotriphosphasatrien $(P_3N_3(OCH_2CH_3)_6$ (if the methyl groups are disregarded which may be attained by decoupling the methyl protons).

The first example may be classified as $A_3^+X_{18}^+ = A_3^+(X_6)_3^+$, and the second as $A_3^+X_{12}^+ = A_3^+(X_4)_3^+$ (coupling with nitrogens has been neglected due to quadrupole relaxation). The symmetry point group is C_{3v} in both cases, *i.e.* the molecules satisfy the symmetry requirements.

The authors interpreted the proton resonance spectra in terms of deceptively simple pattern with the intensity ratio 1 : 3 : 3 : 1. We expect, however, deviations from this pattern, since the criterion of deceptive simplicity is not fulfilled. In the first example the spectrum is not resolved adequately to discuss this question and therefore only the spectrum of ethoxy-cyclotriphosphasatrien will be treated. Since the four lines in the experimental spectrum have about the same line-width, the conditions for strong coupling must be satisfied.

Taking into account $\mathscr{H}'_{AX}$ as perturbation, it has only to be diagonalized between the degenerate $u(1/2, E)$ states for all possible combinations of the $m(X^{1}_{)})$, $m(X^{(2)}), \ldots$ $m(X^{(12)})$ values. The perturbation term has the form:

$$\mathscr{H}'_{AX} = \sum_{i=1}^{3} I_z(A^{(i)}) \sum_{j=1}^{12} J_{AX}(i, j)\, I_z(X^{(j)}) \tag{28}$$

where

$J_{AX}(i, j) = J$ if the j-th proton is in one of the two ethyl groups coupled with the i-th phosphorus atom, otherwise

$J_{AX}(i, j) = 0$ *i.e.* the long-range J_{PH} couplings are neglected. Then $J_0 = J/3$.

By performing the diagonalization and calculating the transitional intensities, we obtain the partial spectrum arising from the $u(1/2, E)$ degenerate state. The other partial spectrum can be calculated from the non-degenerate

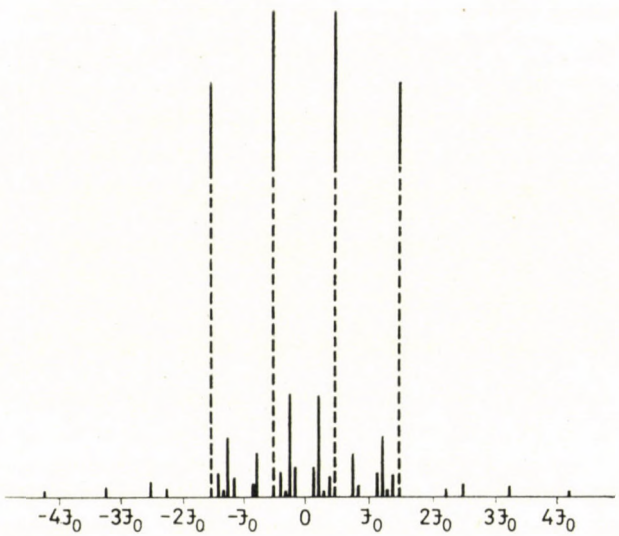

Fig. 3. X part of the system $A_3^+ (X_4)_3^+$ with strong coupling when $J_0 = 1/3\, J$, that is $J' = 0$. Lines more than 100 times smaller than the four principal lines are not indicated here

$u(3/2, A_1)$ state. As it was shown earlier, it constitutes an equidistant quadruplet, with the intensity ratio 1 : 1 : 1 : 1. The complete spectrum is shown in Fig. 3. Owing to the great number of non-equidistant lines and the large line-width, the irregularly spaced lines cannot be detected, only their indirect effect can be seen: by incorporating the unresolved lines into the four main lines, a 1 : 1.34 : 1.34 : 1 intensity ratio is obtained, which is in good agreement with the experimental spectrum given by HEWLETT and SHAW [14].

Among phosphorus—nitrogen compounds, there are some with cyclic [15] or cage structures [16—18] that can be classified as of the $A_4^+ X_m^+$ type. The spectra of these compounds contain generally a narrow doublet and a wide central line. HARRIS [6] explained this pattern by supposing that J_A and J_{AX} have about the same magnitude, *i.e.* the condition of strong coupling is not fulfilled. The only exception is the spectrum of $(SP)_4(NMe)_6$ studied by HOLMES and FORSTNER [17], where three strong lines and several weak lines can be observed. The authors interpreted the large triplet as a 1 : 2 : 1 pattern corresponding to the proton spectrum coupled with two magnetically equivalent phosphorus atoms, while the lines with small intensity were assumed to be due to the long-range coupling $^5J_{PH}$.

In our opinion it is more convenient to consider the proton resonance spectrum of $(SP)_4(NMe)_6$ as derived from an $A_4^+(X_3)_6^+$ system, rather than from an A_2X_3 system. The system in question would have the same pattern as the A_2X_3 system only if the J_P couplings were negligible in comparison to the J_{PH} couplings. For obtaining approximately the ratio of J_P and J_{PH} let us compare the spectra of the following analogous compounds: $P_2(NMe)_6$, $P_4(NMe)_6$, $(SP)_2(NMe)_6$ and $(SP)_4(NMe)_6$. In the first two cases the central line of the deceptively simple triplet is wide, showing that J_P is approximately equal to J_{PH}, while in case of $(SP)_2(NMe)_6$ it is narrow, *i.e.* the J_P/J_{PH} ratio is large. The increase in phosphorus valency corresponds to nearly the same difference of chemical shifts in case of the pairs $P_2(NMe)_6$, $(SP)_2(NMe)_6$ and $P_4(NMe)_6$, $(SP)_4(NMe)_6$ [16, 17, 18], which suggests a similar tendency for the values of J_P, too, and therefore J_P has to be large in comparison to J_{PH} in case of $(SP)_4(NMe)_6$.

Assuming thus an $A_4^+(X_3)_6^+$ system with strong coupling between particles A^+, we may easily estimate the intensity of the principal lines in the X part of the spectrum. The molecule in question has a tetrahedral symmetry, therefore diagonalization of $\mathscr{H}'_{AX}$ must be carried out in the $u(2, A_1)$, $u(1, T_2)$ and $u(0, E)$ states. Since $u(2, A)$ is non-degenerate, five equidistant lines of equal intensity may be derived; in the $u(0, E)$ and $u(1, T_2)$ states, when $m_A = 0$, all matrix elements of $\mathscr{H}'_{AX}$ are zero, as a result of which the intensity of the central line will be six times as high as that of the four outer lines. There remains still the diagonalization of the third order $\mathscr{H}'_{AX}$ matrices in the $u(1, T_2)$ state when $m_A = \pm 1$ for all different combinations of the set $m(X^{(1)})\ m(X^{(2)}), \ldots m(X^{(18)})$. Due to the great number of sets, all giving different eigenvalues, we may obtain so many lines from this state that the intensity of the particular lines will be much smaller than that of the principal lines and will thus slightly modify the spectrum. The proton resonance spectrum reported by HOLMES and FORSTNER [17] is in agreement with the picture thus obtained if we take into account that the amplitudes of the three inner lines are smaller than those corresponding to the theoretical ratio

1 : 1 : 6 : 1 : 1, since the conditions of strong coupling have not been satisfactorily fulfilled.

Let us consider how to evaluate the coupling constants $^3J_{PH}$ and $^5J_{PH}$ in the two above mentioned cases. If the main triplet is interpreted as the X part in the spectrum of the A_2X_3 system, then the separation of the triplet is equal to $J_{AX} = {}^3J_{PH}$. We have assumed, however, that this triplet constitutes the two outer and the central lines of the equidistant quintuplet and thus the separation in question is equal to $2J_0$. Since each proton is coupled with four phosphorus atoms with coupling constants $^3J_{PH}$, $^3J_{PH}$, $^5J_{PH}$ and $^5J_{PH}$, respectively, thus $2J_0 = {}^3J_{PH} + {}^5J_{PH}$, and if $^5J_{PH}$ is negligible, then two kinds of interpretation give the same value for $^3J_{PH}$.

To explain the appearance of weak lines in the spectrum, HOLMES and FORSTNER had to assume a relatively large value for $^5J_{PH}$, while in our case the weak lines can be regarded as a consequence of the non-deceptive simplicity of the spectrum.

REFERENCES

1. ABRAHAM, R. J., BERNSTEIN, H. J.: Canad. J. Chem. **39,** 216 (1961)
2. HARRIS, R. K.: Canad. J. Chem. **42,** 2275 (1964)
   HARRIS, R. K., WOODMAN, C. M.: Mol. Phys. **10,** 437 (1966)
   FINER, E. G., HARRIS, R. K.: Mol. Phys. **12,** 457 (1967)
   FINER, E. G., HARRIS, R. K.: Mol. Phys. **13,** 65 (1967)
3. DIEHL, P.: Helv. Chim. Acta **47,** 1 (1964)
4. MUSHER, J. I., COREY, E. J.: Tetrahedron **18,** 791 (1962)
5. HUDSON, A., LUCKHURST, G. R.: Mol. Phys. **13,** 409 (1967)
6. HARRIS, R. K.: Inorg. Chem. **5,** 701 (1966)
7. DIEHL, P.: Helv. Chim. Acta **48,** 567 (1965)
8. JONES, R. G., WALKER, S. M.: Mol. Phys. **10,** 363 (1966)
9. DIEHL, P., TRAUTMANN, D.: Mol. Phys. **11,** 531 (1966)
10. ISHIKAWA, Y.: J. Phys. Soc. Japan **21,** 1473 (1966)
11. NEIMAN, M. B., ROZANTSEV, E. G., GOLUBOV, V. A.: Izv. Akad. Nauk SSSR. Ser. Khim. **1965,** 548
    ROZANTSEV, E. G., GOLUBOV, V. A.: Izv. Akad. Nauk SSSR. Ser. Khim. **1965,** 718
12. LUDWIG, G. W., WOODBURY, H. H., CARLSON, R. O.: Phys. Chem. Solids **8,** 490 (1959)
13. STANCLIFT, W. E., HENDRICKER, D. G.: Inorg. Chem. **7,** 1242 (1968)
14. HEWLETT, C., SHAW, R. A.: J. Chem. Soc. **A. 1966,** 56
15. ALLEN, G., OLDFIELD, D. J., PADDOCK, N. L., RALLO, F., SERREGI, J., TODD, S. M.: Chem. Ind. **1965,** 1032
16. HOLMES, R. R.: J. Am. Chem. Soc. **83,** 1334 (1961)
17. HOLMES, R. R., FORSTNER, J. A.: Inorg. Chem. **2,** 377 (1963)
18. PAYNE, D. S., NÖTH, H., HENNIGER, G.: Chem. Commun. London, **1965,** 327

Antal ROCKENBAUER
Lajos RADICS
Budapest II., Pusztaszeri út 59/67.

Acta Chimica Academiae Scientiarum Hungaricae, Tomus 68 (3), pp. 205—216 (1971)

HYDROGENATION OF OXO COMPOUNDS, I

HYDROGENATION AND ELECTROHYDROGENATION OF ACETONE IN ACIDIC MEDIUM. EXPERIMENTAL

GY. HORÁNYI, S. SZABÓ, J. SOLT and F. NAGY

(Central Research Institute for Chemistry, Hungarian Academy of Sciences, Budapest)

Received December 6, 1969

The hydrogenation and electrohydrogenation of acetone were studied in acidic medium (1 *N* $HClO_4$) with a volumetric method on platinum powder and on a platinized platinum electrode, with galvanostatic and potentiostatic methods. It was found that under our experimental conditions the product of both hydrogenation and electrohydrogenation is propane.

An analysis was performed from a thermodynamic point of view of under what conditions isopropanol can appear among the products of electrohydrogenation of acetone.

It was shown that the current decrease accompanying the appearance of isopropanol in the potentiostatic measurements is not unconditionally to be considered an ageing process.

With the use of charging curves it was shown that acetone does not affect the adsorption of hydrogen.

Introduction

The hydrogenation and electrohydrogenation of ketones, as known from the literature [1], can give rise to various products depending on the experimental conditions. This is illustrated by the following scheme

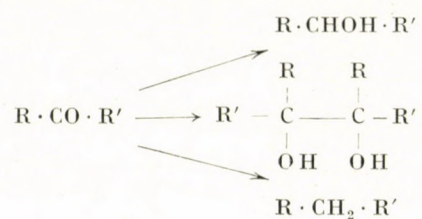

R and R′ may be alkyl or aryl groups. When hydrogenation is carried out in the aqueous phase, an alkaline medium favours (a) and (b) whereas in acidic medium the reaction proceeds for the most part in the direction of (c). That is, in the hydrogenation of ketones the effect of the medium is very pronounced and so this reaction can serve as a model illustrating medium effects in catalytic hydrogenation in the solution phase. The products of hydrogenation in acid and alkaline media differ from each other not only in the case of oxo compounds but also in the hydrogenation of unsaturated alcohols.

During the hydrogenation of allyl alcohol on platinum in alkaline medium propanol is formed, whilst in acidic medium propane, propene, and to a smaller extent methane and ethane too are evolved [2].

It must be added that propanol is not hydrogenated under the given experimental conditions. The situation is similar in the hydrogenation of ketones in acidic medium and the corresponding secondary alcohols are not hydrogenated under the given conditions; that is, the alcohol can hardly be an intermediate in the series of steps leading to the formation of the hydrocarbon. At the same time, hydrogenation in alkaline medium terminates with the formation of the secondary alcohol.

The change of the reaction path and the appearance of hydrocarbon in the product are fundamentally due to the change of pH. This permits the conclusion that the medium in a given case plays a much larger part in the hydrogenation reaction than previously thought, and the complete elucidation of the mechanism of hydrogenation is possible only with a knowledge and consideration of the medium effects.

We began our work relating to the study of the medium effect with the hydrogenation and electrohydrogenation of acetone on platinized platinum in acidic medium. In the papers of DE HEMPTINNE and SCHUNCK [3, 4] dealing with the electrohydrogenation of acetone and butanone, very fundamental conclusions can be found. In what follows, our own observations and the results of these authors will often be compared, naturally bearing in mind that the experimental conditions in the two cases differ from each other to a certain extent.

1. Experimental

Methods reported earlier [5] were used for the study of electrohydrogenation. The main electrode was separated by ground joints from the auxiliary and reference electrodes. The gas space of the cell compartment containing the principal electrode was connected to a gas burette in order to measure the volume of gases evolved during electrohydrogenation. Gal-

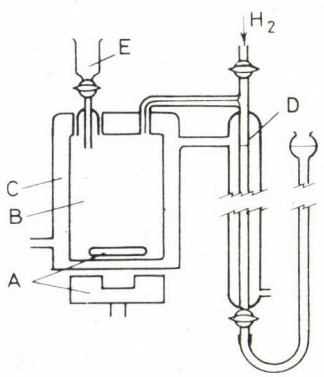

Fig. 1. A: magnetic stirrer, *B:* reaction vessel, *C:* thermostating jacket, *D:* gas burette, *E:* substrate feed

vanostatic and potentiostatic procedures were used. The geometrical surface of the disk-shaped platinum main electrode was 10 cm^2. With platinization a roughness factor of 500—1000 was attained; this was determined by means of charging curves. 1 N $HClO_4$ was used as base solution, and the electrode potential referred to a 1 atmosphere hydrogen electrode immersed into this solution. The hydrogenation studies were carried out at 25 °C with platinum powder, again in 1 N $HClO_4$ solution, in the apparatus shown in Fig. 1.

2. Direction of the hydrogenation reaction

During electrohydrogenation, at potentials more positive than the hydrogen evolution potential (in agreement with [3]), gas evolution may be observed on the electrode; gas chromatographic analysis showed this to be exclu-

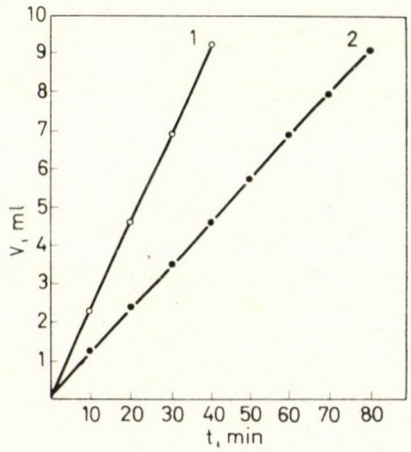

Fig. 2. Variation of the volume of gas evolved with time at constant current (30 mA) (1) in 1 N $HClO_4$ base solution, (2) in 0.3 M acetone in the base solution

sively propane. Thus the following overall reaction takes place at all events

$$CH_3.CO.CH_3 + 4\,H^+ + 4\,e^- \rightarrow CH_3.CH_2.CH_3 + H_2O \qquad (1)$$

To decide whether the already mentioned side reactions occur, the current efficiency relating to propane was determined by the volumetric measurement of the gas evolved. To avoid possible errors, a comparative measurement was applied. The volume was measured of the hydrogen evolved on the same electrode in the base solution without acetone at the same current with which the electrohydrogenation of acetone was studied.

According to the reaction

$$2\,H^+ + 2\,e^- \rightarrow H_2$$

a charge of 2 F is necessary for the evolution of 1 mole of hydrogen, and of 4 F for 1 mole of propane. Fig. 2 shows the dependence of the gas evolution on time for hydrogen (curve 1) and propane (curve 2). It can be seen that in a

given time the volume of hydrogen formed is twice that of the propane. This proves that during the hydrogenation of acetone in our case the total current is devoted to reaction (1).

From our earlier work [5] it follows unambiguously that in the hydrogenation carried out with hydrogen on platinum powder (disregarding hydrogen activation and dissociative adsorption) the same processes must occur as in electrohydrogenation. In the present case, since the formation of several products is thermodynamically reasonable and of these only one is gaseous,

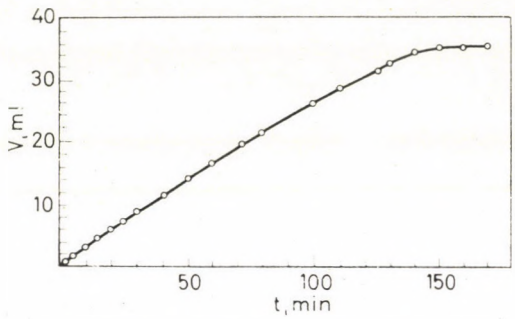

Fig. 3. Variation with time of the volume decrease occurring during the hydrogenation of 1.4×10^{-3} mole of acetone

we have the possibility of the direct proof of this too. If it is supposed that the same reactions take place during hydrogenation as during electrohydrogenation, the hydrogenation reaction will be

$$CH_3.CO.CH_3 + 2\ H_2 \rightarrow CH_3.CH_2.CH_3 + H_2O \qquad (2)$$

That is, in the gas volumetric measurement, for the conversion of 1 mole of acetone the overall gas absorption observed will be 1 mole.

During our experiments, it was made sure that the apparent gas uptake did indeed correspond to 1 mole and that propane did appear in the gas space. In Fig. 3 is given a gas uptake-time graph obtained during the hydrogenation in the presence of 1 g of platinum powder of 100 ml of a 1.4×10^{-3} *M* acetone solution.

To prove that in the present case hydrogenation occurs completely according to reaction (2), the following experiment was carried out.

The catalyst and a solution containing a large amount of acetone were placed in the hydrogenation vessel which was then filled with nitrogen. Part of the latter was replaced by a known volume of hydrogen. If Eq. (2) is true then, taking into account the solubility of propane in the solution phase, the volume decrease occurring during hydrogenation must be exactly half the volume of hydrogen introduced. Fig. 4 shows the course of hydrogenation with time.

From the graph it may be seen that the reaction stops at a certain volume V_v which is somewhat greater than half the volume of hydrogen introduced, but, if it is corrected for the amount of propane in the solution phase, V_{corr} so obtained gives the expected result exactly.

From the above, it is obvious that under our experimental conditions in a 1 N $HClO_4$ solution both hydrogenation and electrohydrogenation of acetone result in propane.

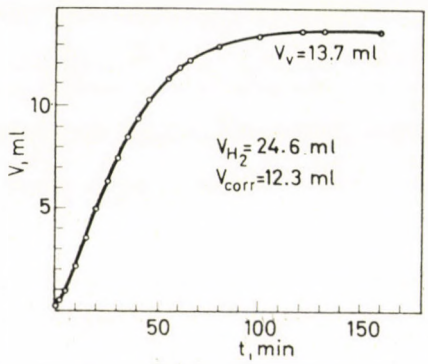

Fig. 4. Variation of volume on hydrogenation with a given volume (24.6 ml) of hydrogen

3. Thermodynamic considerations in connection with the direction of the hydrogenation reaction

Our studies in the previous part connected with the direction of the reaction were carried out with a galvanostatic method. As may be seen in the polarization curves obtained with the galvanostatic method and shown in Fig. 5, electrohydrogenation already takes place at an appreciable rate at potentials above 100 mV. According to the studies of DE HEMPTINNE and SCHUNCK [3, 4], isopropanol may also appear among the products of hydrogenation depending on the state of the electrode. However, their measurements were carried out at a negative potential for the most part. In the following, a study is made from a thermodynamic viewpoint of what product is formed during the hydrogenation of acetone depending on the potential.

In an earlier publication [6] the thermodynamic relations of hydrogenation were treated in complete generality. From those considerations, the two reactions possible in theory are considered to be reversible. That is, we have existing in parallel the two equilibria

$$\begin{aligned} CH_3.CO.CH_3 + 4\,H^+ + 4\,e^- &\rightarrow CH_3.CH_2.CH_3 + H_2O \\ CH_3.CO.CH_3. + 2\,H^+ + 2\,e^- &\rightarrow CH_3.CHOH.CH_3 \end{aligned} \qquad (3)$$

(It must be remembered that the hydrogenation of isopropanol, although thermodynamically possible, does not take place under the conditions used.)

With the calculations applied in the publication mentioned, we obtain for the standard potential of the first reaction $E_{01} = 261$ mV, and for the second $E_{02} = 34$ mV. The latter value seems a little low. Data to be found in references [7] and [8] were used for the calculation. In contrast to this, according to reference [9] $E_{02} = 132$ mV. The free enthalpy of formation of isopropanol is given as -38.83 kcal in refs. [6] and [7] but as -43.28 kcal in ref. [9], and the significant difference in E_{02} is evidently due to this. With the aim of an order of magnitude estimation, a value of about 120 mV is conditionally accepted for E_{02}. (From the point of view of the considerations which follow this is

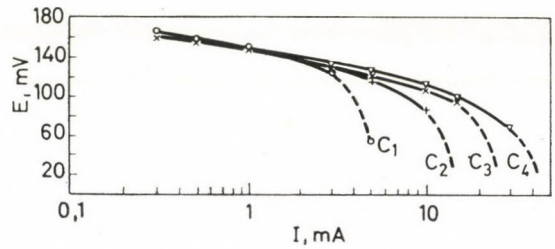

Fig. 5. Galvanostatic electrohydrogenation of acetone. $C_1 = 0.03$ *M*, $C_2 = 0.075$ *M*, $C_3 = 0.152$ *M*, $C_4 = 0.30$ *M*

the most unfavourable for us.) In possession of E_{01} and E_{02}, we can already conclude to a certain extent at what potentials propane is the exclusive product of hydrogenation. It can readily be seen that for the formation of isopropanol from acetone with a finite rate at potentials around E_{02} it is necessary that the reaction in the reverse direction also takes place at a finite rate. However, it is also an experimental fact that at such potentials isopropanol cannot oxidize to acetone. Thus, it must also be stated (if we do not wish to violate thermodynamics) that isopropanol cannot form either. The formation of isopropanol can only be expected at potentials far enough from the standard potential. This may be formulated also by stating that the electrohydrogenation of acetone to isopropanol is only attainable at a certain overvoltage. This is essentially the situation in the case of propane but E_{01} has a sufficiently high value for the reaction to take place already at 100—140 mV with a considerable rate.

In our opinion, these findings succeed in resolving those apparent inconsistencies between our own previously reported studies and the measurements of DE HEMPTINNE and SCHUNCK. Isopropanol appears only at small positive or negative potentials. DE HEMPTINNE and SCHUNCK, as has already been mentioned, carried out a good proportion of their measurements at negative potentials.

4. Study of electrohydrogenation by potentiostatic method

The current—potential curves determined with the potentiostatic method for various acetone concentrations are given in Fig. 6.

From the curves to be seen here, it appears that with the change occurring towards negative potentials the current increases only for a time, a limiting current is reached, and in the potential interval preceding evolution of hydrogen the current even decreases to a small extent. The current again increases as a consequence of the evolution of hydrogen at potentials more negative

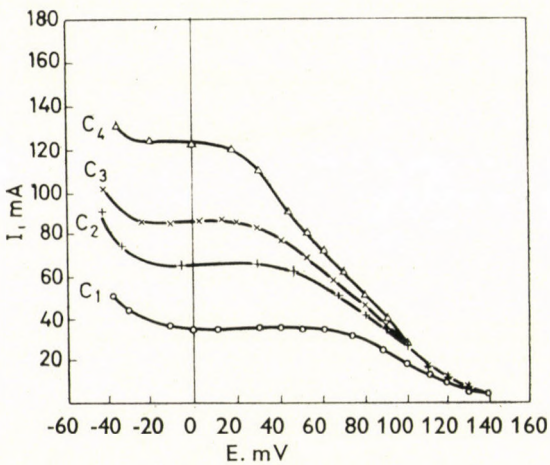

Fig. 6. $C_1 = 0.15$ *M*, $C_2 = 0.3$ *M*, $C_3 = 0.45$ *M*, $C_4 = 0.6$ *M*

than zero. With increasing concentration, the limiting current too increases. Firstly it must be recorded that the observed limiting current can in no way be a limiting diffusion current. This may be seen from a comparison with the limiting diffusion current of hydrogen which under our experimental conditions is about 8 mA. At this limiting current, the concentration of hydrogen in the solution is less than 10^{-3} *M*. Although the diffusion constant of acetone is less than that of hydrogen, a charge of 2 *F* is necessary for the discharge of 1 mole hydrogen but of 4 *F* for the reduction of 1 mole of acetone.

From this it follows that at the concentrations relating to the curves shown in Fig. 6 (0.15, 0.3, 0.45 and 0.6 *M*) the limiting diffusion currents are almost two orders of magnitude larger than the observed limiting current. However, this means that the occurrence of the limiting current must be attributed to other processes. The observed limiting current is not always constant; at times a weak minimum and maximum may be observed within the limiting current section. The maximum and minimum become observable particularly at lower concentrations, and whether they appear at all depends to a large extent on the life history of the electrode.

In Fig. 7 may be seen the polarization curve (1) obtained at a lower concentration than the previous ones, and the hydrogen evolution polarization curve (2). The latter was determined from measurements in an argon atmosphere in the pure base solution.

The difference between the two curves corresponds to the proper electrohydrogenation curve (3) if it is assumed that no change takes place in hydrogen

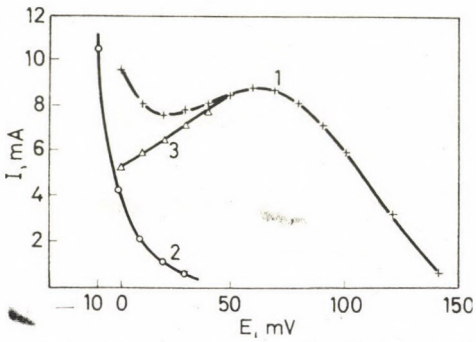

Fig. 7. Electrohydrogenation curve of 6.5×10^{-2} *M* acetone

evolution because of the presence of acetone or of the hydrogenation reaction. In the following we study how the changes taking place in the composition of the product may appear in the potentiostatic measurements.

Earlier it was stressed that the observed limiting current does not depend on the stirring, that is it is not of a diffusion nature. Without going into details connected with the mechanism of the hydrogenation reaction, it appears very probable that this limiting current occurs because of adsorption control. However, this means that all molecules adsorbed in unit time must react. Limiting currents of various magnitude may belong to one and the same limiting adsorption rate depending on how many F are necessary per mole, directly or indirectly, for the reaction to take place. As has been seen, in the hydrogenation of acetone two types of product may be formed. A charge of 4 F ($z_1 = 4$) per mole is necessary for the formation of propane, and of 2 F($z_2 = 2$) for isopropanol. If the number of moles reacting in unit time at the limiting adsorption rate is denoted by n, and it is assumed that propane and isopropanol can be formed simultaneously, then the relation

$$i_l = F(z_1 n_1 + z_2 n_2) \tag{4}$$

will be valid, for the limiting current (i_l), where n_1 and n_2 are the numbers of moles of acetone converted to propane and isopropanol, respectively, in unit time. Naturally, at the same time the equality

$$n \equiv n_1 + n_2 = \text{constant} \tag{5}$$

must hold.

From what was said earlier, however, it appears that propane and isopropanol are simultaneous products only from certain potentials. Supported by the normal electrochemical attitude and by the literature, it can be stated with certainty that the ratio of isopropanol and propane in the product of hydrogenation at a given acetone concentration is a function of the potential, $f(E)$, that is

$$\frac{n_2}{n_1} = f(E) . \tag{6}$$

From equality (4)

$$i_l = Fn_1[z_1 + z_2 f(E)] \tag{7}$$

and from Eq. (5)

$$n_1 = \frac{n}{1+f(E)} . \tag{8}$$

Therefore

$$i_l = \frac{Fn}{1+f(E)} [z_1 + z_2 f(E)] . \tag{9}$$

It follows from Eq. (9) that i_l can range between Fnz_1 and Fnz_2 depending on the magnitude of $f(E)$. The two extreme cases correspond to the formation of either propane or isopropanol. The experimental facts prove that the first case does indeed exist, and on freshly regenerated electrodes at positive potentials primarily, only propane is formed. That is, it can be conceived that the decrease of the limiting current at small positive and negative potentials is related to the presence of isopropanol in the product. Since the isopropanol amounts to only a very small fraction of the product, a relatively significant increase of its amount does not result in an important decrease of the limiting current.

On the basis of what has been said, certain phenomena, previously considered as ageing, must now be viewed in another light. In electrohydrogenation, one speaks in general of ageing (decrease of activity) if the current decreases in time at a given potential. The curves to be seen in Fig. 8 are obtained over a long period at negative potentials [3, 4]. In the Figure i_l is the total current and i_p, i_i and i_{H_2} the currents corresponding to propane, isopropanol and hydrogen evolution. According to the authors the decrease of the activity of the electrode is reflected in the decrease of i_l, while the appearance of isopropanol and the increase in its proportion are parallel with this ageing.

From the earlier arguments, however, it follows that at such a time we may talk at most of the change occurring in the selectivity, because a decreasing current must also be obtained in the case of an unchanging adsorption rate of acetone if the formation rate of isopropanol increases. To illustrate this, an idealized case is shown in Fig. 9, with the assumption that the rate of formation of isopropanol varies linearly with time. (For the meaning of the individual notations, see the text relating to Fig. 8.)

From a comparison of Figs 8 and 9, all that has previously been stated may clearly be seen. From the point of view of the reaction of acetone, the decrease of i_t by no means signifies the decreasing activity of the electrode catalyst.

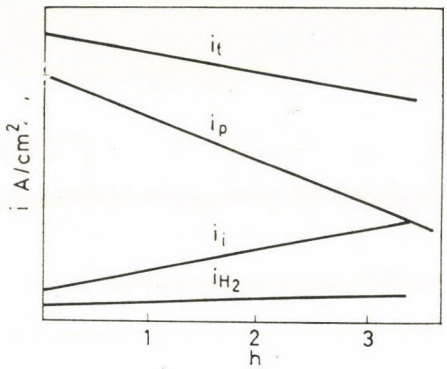

Fig. 8. Decrease of the activity of the electrode, according to Ref. [3]

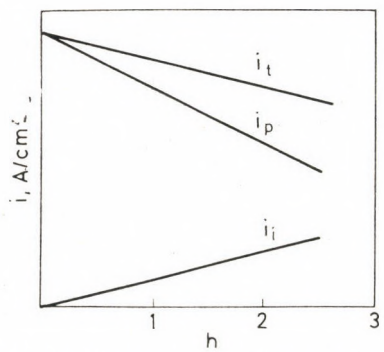

Fig. 9. Effect of the change of the electrode selectivity on the observed total current density

5. Hydrogen adsorption in the presence of acetone

From the point of view of the elucidation of the kinetics and mechanism of the hydrogenation of acetone, it is extremely important to decide in what manner hydrogen adsorption is modified by acetone. According to the evidence of the charging curves, at those potentials at which there is already no reaction, hydrogen adsorption is essentially not changed in the presence of acetone. This may be seen in Fig. 10. Curve (1) in the Figure relates to the pure base solution (1 N $HClO_4$), and curve (2) to a similar solution containing 10^{-1} M acetone. There is no significant difference between the two curves. The level part on curve (2) after the double-layer section clearly occurs as a result of the oxidation of acetone.

The most significant finding, which according to the evidence of the present experimental data may play an important part in the further work, is clearly that the adsorption of hydrogen and acetone may be regarded as independent of each other. This independence can be conceived by both being adsorbed, but at different active sites.

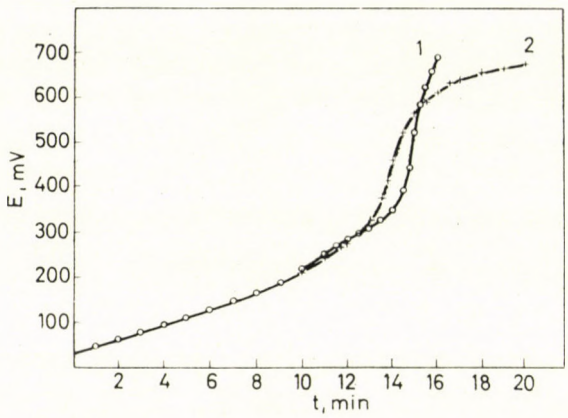

Fig. 10. Galvanostatic charging curves in (1) 1 *N* $HClO_4$ and (2) 1 *N* $HClO_4$ containing 10^{-1} *M* acetone

6. The effect of anions on electrohydrogenation

The nature of anions in the case of $HClO_4$, H_2SO_4 and H_3PO_4 apparently does not significantly affect the direction and rate of the electrohydrogenation of acetone [3]. So it seems very surprising to find in the literature [4] that in the presence of Cl^- ions the hydrogenation reaction does not occur at all. Our own experiments disprove this.

The electrohydrogenation curve obtained in a 0.15 *M* solution of acetone in 1 *N* HCl base solution is given in Fig. 11.

As may be seen from a comparison of Figs 6 and 11, there is no significant difference between the measurements in $HClO_4$ and in HCl.

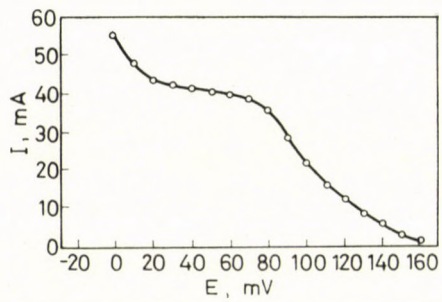

Fig. 11. The electrohydrogenation curve of acetone (0.15 *M*) in 1 *N* HCl base solution

REFERENCES

1. SOKOLSKI, D. V.: Gidrirovanie v rastvorah, Alma-Ata, 1962
2. MANZHELEY, M. E., SOLIN, A. F.: Zhur. Fiz. Khim. **XXXVII**, 1825 (1963)
3. DE HEMPTINNE, X., SCHUNCK, K.: Trans. Faraday Soc. **65**, 591 (1969)
4. DE HEMPTINNE, X., SCHUNCK, K.: Ann. Soc. Sci. Bruxelles **80**, 289 (1966)
5. NAGY, F., TELCS, I., HORÁNYI, G.: Acta Chim. Acad. Sci. Hung. **37**, 295 (1963)
   HORÁNYI, GY., NAGY, F.: Magyar Kém. Foly. **72**, 370 (1966)
6. NAGY, F., HORÁNYI, G.: Acta Chim. Acad. Sci. Hung. **49**, 243 (1966)
7. LANGE, N. A.: Handbook of Chemistry, Tenth Edition, McGraw-Hill, 1963
8. PERRY, J. H.: The Chemical Engineer's Handbook. Fourth Edition, McGraw-Hill, 1963
9. CLARK. W. M.: Oxidation-Reduction Potentials of Organic Systems, p. 505, The Williams and Wilkins Company, Baltimore, 1960

György HORÁNYI
Sándor SZABÓ
János SOLT
Ferenc NAGY

Budapest II., Pusztaszeri út 59—67.

Acta Chimica Academiae Scientiarum Hungaricae, Tomus 68 (3), pp. 217—228 (1971)

OXIDATION ON THE NICKEL HYDROXIDE ELECTRODE, III

DETERMINATION OF OXIDATION RATE BY AN ELECTROCHEMICAL METHOD

Gy. VÉRTES, Gy. HORÁNYI and F. NAGY

(Central Research Institute for Chemistry of the Hungarian Academy of Sciences, Budapest)

Received December 16, 1969

The rate of oxidation of alcohols was studied on a nickel hydroxide electrode. Considering that there is no unequivocal relation between the electrode potential and the amount of nickel(III) oxide hydroxide effective from the point of view of oxidation, an indirect method was elaborated for the determination of the rate of oxidation. The method sets out from the basic principle that the reaction rate can be determined from the complete discharge times (corresponding to the reduction of the total NiOOH available) measured for different currents, the electrode having been discharged with a given current and the substrate together.

It was found that the rate of oxidation of ethanol on a nickel hydroxide electrode is proportional at a given moment to the amount of nickel(III) oxide hydroxide present on the electrode.

In earlier communications [1, 2] we studied the possibilities of the electrochemical accomplishment of oxidation reactions with nickel(III) oxide hydroxide. We showed that using electrochemical methods with a nickel hydroxide electrode, complex heterogeneous reactions can be studied much more simply than on nickel hydroxide powder.

Clearly it is expedient in the study of the oxidation kinetics too to rely on these findings, but it must be considered that the method normally employed (polarization curves) for the determination of the rates of electrochemical reactions can be used in the present case only with certain limitations.

In oxidations on the nickel hydroxide electrode the combination of two disturbing factors prevent us from drawing quantitative conclusions from simple polarization curves. One of the problems is that the reactions only take place at electrode potentials more positive than that for the evolution of oxygen (the electrode discharge occurs between 1350 and 1250 mV [1], *i.e.* the potential of the almost completely discharged electrode too is more positive than 1230 mV). This means that in addition to the oxidation of the given compound, part of the current is used for oxygen evolution; hence it is not possible to calculate the reaction rate directly from the current intensity.

In principle the possibility exists that if two reactions take place simultaneously on an electrode, the ratio of their rates can be determined from a knowledge of the electrode potential. In the case of the nickel hydroxide electrode, however, no unequivocal relation has been found even between the potential and the degree of oxidation of the electrode [1, 3]. On this basis it

may be expected (and in a later communication we shall prove this experimentally) that the relation between the electrode potential and the oxidation rate is not unequivocal either; that is, it cannot be decided what proportions of the current are used for oxidation and for oxygen evolution.

Therefore, for the determination of the rate of a process we use the classical principle of reaction rate measurement. According to this, the concentration change of any reactant can be used to characterize the rate. The overall reaction between the charged NiOOH electrode and an alcohol is:

$$R—CH_2OH + 4\ NiOOH + OH^- \rightarrow R—COO^- + 4\ Ni(OH)_2$$

Since the reaction takes place in excess alkali, the process can be followed by measuring the hydroxide concentration only with great uncertainty, and in this case there is a need for extremely precise measurements. In principle the determination of the amount of alcohol or carboxylate ion in solution does not cause any problems. In the course of the reaction it is necessary to take samples from the solution on a number of occasions, and these must be analyzed individually. This can be solved only with difficulty even for moderately fast reactions, but for reaction times shorter than ten minutes a quite special apparatus is required. For just this reason it seemed expedient to follow the progress of the reaction through changes in the amount of nickel hydroxide.

As a result of the causes mentioned above, there is no possibility to follow continuously the amount of nickel(III) oxide hydroxide on the electrode, but the exhaustion of the total amount is signified by a sharp change of the electrode potential [1]. This method is suggestive of the potentiometric end-point indication of titration curves, and of the determination of the adsorbed quantity with the chronopotentiometric method.

In our first communication (Fig. 5) it was also seen that different alcohols discharge one and the same nickel hydroxide electrode in different times; in other words, identical amounts of nickel(III) oxide hydroxide are reduced by different alcohols in different times. It is obvious that the time necessary for the reaction of a given amount of substance depends on the rate of reaction. The average reaction rates are reflected in such a sense by Fig. 1 too, where the discharge curves of a platinum plate of 10 cm^2 surface coated with NiOOH may be seen in ethanol solutions of different concentrations.

We note here that the preparation and discharge of the electrode were done in the manner reported in our first communication (discharge in 1 *N* NaOH background solution at 25 °C). In all cases the charging of the electrode was carried out in a separate vessel in pure 1 *N* NaOH, because otherwise a considerable concentration decrease would occur for small substrate concentration and in the case of strong or concentrated reductants the complete charging of the electrode would not be ensured.

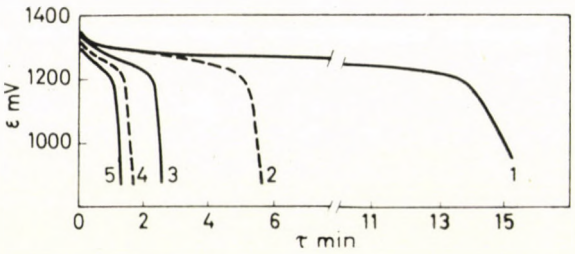

Fig. 1. Change of the average reaction rate with the concentration of ethanol. 1 *N* KOH background solution. Ethanol concentration: 1: 0.5 *M*; 2: 1 *M*; 3: 2.5 *M*; 4: 5 *M*; 5: 10 *M*

Rate-determining role of diffusion

Before a more detailed study of the rate of oxidation of alcohols it is necessary to clear up the role of transport processes, in particular of the diffusion of the alcohol. This process evidently precedes the chemical reaction proper, and it may be conceived that it is rate-determining. If this is the case, then the measured values are characteristic not of the chemical reaction proper but of the diffusion. The possibility of settling this question arises with the comparison of the oxidation rates of different substances. The diffusion coefficients of substances of nearly the same molecular weight are practically identical, and so, under otherwise identical conditions, if the reaction rates of two substances differ to a significant extent (a difference of one order of magnitude may be found between them), then the smaller rate cannot originate from diffusion control. Since the rate of diffusion is proportional to the concentration of the diffusing substance and the measurement of rates differing to a significant extent is methodically difficult, the comparison measurement may be carried out with reagents of different concentrations.

A nickel plate of 10 cm^2 surface coated with NiOOH can be discharged in 9.2 minutes in a 1 *N* NaOH background solution with a current strength of 60 μA; this means that the NiOOH on the electrode corresponds to a charge of 33 mC. If cathodic polarization is carried out in $\sim$0.1 *M* ethanol (for the necessity of combined chemical and electric discharge, see later), then the discharge lasts about half as long. To discharge the 33 mC, about 20 mC of electric charge was necessary while the remaining NiOOH reacted with the alcohol. If the 60 μA cathodic polarization is carried out in 5×10^{-4} *M* formaldehyde, then (as may be seen in Fig. 2) the discharge lasts an even shorter time. This shows that carrying out the discharge with the same cathodic polarizing current on a given electrode, the electrode discharges in a shorter time in formaldehyde than in ethanol, even when the former is the more dilute by more than two orders of magnitude. This proves that diffusion may be

disregarded in a study of the rate-determining steps in the oxidation of 0.1 *M* ethanol. The concentration of alcohol in the immediate vicinity of the surface differs by less than 1% from the concentration measurable in the bulk of the solution.

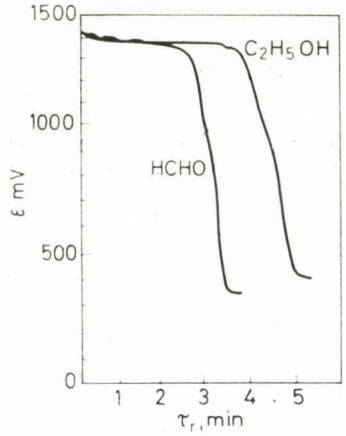

Fig. 2. Exclusion of the rate-determining role of ethanol diffusion. $Q_0 = 33$ mC. Cathodic polarizing current 60 μA. Ethanol concentration ~0.1 *M*; formaldehyde concentration 5×10^{-4} *M*

The rate equation of oxidation

Having succeeded in showing that the measured rates are not diffusion rates, in addition to a knowledge of the average reaction rate, the determination of the instantaneous values is necessary. By definition the rate of reaction is

$$w = -\frac{dQ}{d\tau} \tag{1}$$

where Q is the amount of NiOOH on the electrode at time τ (if Q is measured in mC, then the rate is obtained in mA). For the determination of the instantaneous values of the reaction rate, a knowledge of the corresponding Q, τ pairs is necessary during the whole reaction time. From the measurements merely the change of the electrode potential with time (the ε *vs.* τ relation) is known. It may be seen from the discharge curves (ref. [1], Fig. 1) determined from measurements in pure alkali solution on a NiOOH electrode that a significant change in the amount of NiOOH (or of the charge equivalent to this) involves but a small change in the electrode potential. The electrode potential is not an unequivocal function of the electrode charge. In many cases the uncertainty following from this in the potential can reach or even exceed the potential shift caused by the change in charge. In such a way the change in the charge of the electrode cannot be followed with the help of the elec-

trode potential during the whole discharge time. However, Eq. (1) can be solved (and from it the w *vs.* τ relation can be obtained) if we assume an integrable formula for the change of reaction rate with time. The correctness of the assumption can be checked with the help of the experimental data.

If we compare the discharge curves obtained from measurements in the pure background solution with current and in the substrate solution without current, we can see that their forms are similar. We can attempt, therefore, the assumption that (similarly to the discharge with electric current) the reaction rate is constant during the whole discharge time. In this case Eq. (1) can be written in the form

$$Q = Q_0 - w\tau_a \tag{2}$$

where Q_0 is the amount of charge on the electrode at the beginning of reaction (the total charge that may be taken up by the electrode, in other words, the electrochemical capacity of the electrode), and τ_a is the reaction time. Q_0 can be determined by cathodic polarization of the electrode in pure alkali in such a way that the period necessary for the reduction of NiOOH is multiplied by the current used

$$Q_0 = I\tau_0^* \tag{3}$$

where τ_0^* is the total discharge time in alkali, and I (just like Q and w in the earlier equations) is by definition a positive quantity.

If the reaction is stopped at a given time τ_a and the amount of unreacted NiOOH is determined (either the electrode is removed from the solution and after washing is polarized cathodically with constant current in pure alkali, or it is discharged in the solution with a current greater by at least an order of magnitude than the reaction rate), then w can be calculated on the basis of Eq. (2). If the w values calculated in the different measurements are identical, then the initial assumption that the reaction rate is constant during the discharge is correct.

The experimental results in connection with this are shown in Fig. 3.

If an electrode is discharged in a solution the substrate concentration of which is not too large (less than molar), then its potential changes according to curve 1. If the reaction rate were constant then at 0.75 τ_a^* it would be possible to find a charge of 0.25 Q_0 on the electrode. According to the evidence of the Figure, with cathodic polarization the potential of the electrode changes abruptly in a negative direction as the result of a substantially smaller charge than this. These experimental results force the rejection of the assumption contained in Eq. (2). After this it would seem obvious to make the assumption that the rate of reaction decreases with decreasing amount of unreacted NiOOH, and this would cause the slowing down of the discharge of the electrode to a large extent in the final stage. On the basis of the literature and our

own experience it is conceivable, however, that after the reaction of the main bulk of NiOOH, the remaining NiOOH, in individual inclusions, places accessible only with difficulty for the substrate, where an electric contact still exists with the electrode metal, is still capable of keeping the electrode potential at a value corresponding to the reaction

$$NiOOH + e^- + H_2O \rightleftharpoons Ni(OH)_2 + OH^-$$

and so the change of the electrode potential is not directly connected with the reaction rate [4]. The assumption of the existence of inclusions is also supported by the observation that after interrupting the discharge with electric current, the electrode potential is shifted to about +1200 mV from the +200 mV value reached as a result of the negative polarization during discharge, despite the fact that the demonstration of a considerable amount of NiOOH with repeated discharge was not successful.

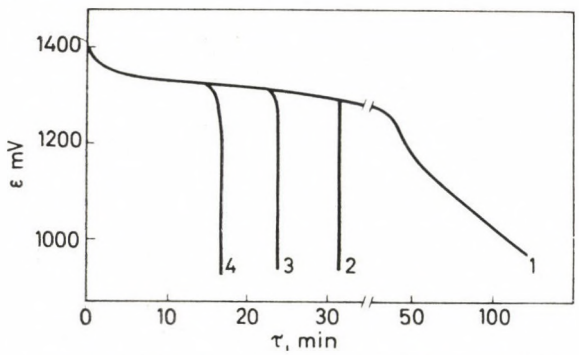

Fig. 3. The discharge of 70 mC NiOOH on a 2 cm^2 nickel plate in 0.2 *M* ethanol. 1: Without cathodic polarization; 2: dischargeable with 0.5 mC after 31 min.; 3: dischargeable with 2.5 mC after 23 min.; 4: dischargeable with 4.5 mC after 15 min.

On the basis of these results it can be said that the time of potential change signifying the end of discharge can only be brought into a real connection with the reaction rate if it is ensured that the effect of the inclusions mentioned be eliminated in some way. Therefore in the following experiments it is necessary to polarize cathodically the electrode with a given current I simultaneously with the discharge by added substrate. In the case of the joint (with current and substrate) discharge, the potential change signifying the disappearence of NiOOH does indeed mark the time of exhaustion of NiOOH; the potential change is more steep, *i.e.* it will be more accurately evaluable. This latter effect is enhanced by the fact that a second potential plateau appearing for very small rates in certain cases does not now appear. In this case Eq. (1) is modified as follows

$$-\frac{dQ}{d\tau} = w + I. \tag{4}$$

If the reaction rate is constant during the whole discharge time, then solving Eq. (4) we have

$$Q = Q_0 - (w + I)\tau_r \tag{5}$$

where τ_r is the total time elapsed from the beginning of discharge with current and substrate. If the time for complete discharge (τ_r^*) is substituted (*i.e.* when $Q = 0$) and the equation is rearranged, we obtain

$$\frac{Q_0}{\tau_r^*} = w + I \tag{6}$$

and the experimental results can be plotted on the basis of Eq. (6). Having determined the value of the complete discharge time at a given ethanol concentration with different currents, it should be possible to calculate w from the intercept of the graph of $Q_0/\tau_r^* - I$.

It may be seen from Fig. 4 that the experimental data do not lie on a straight line, consequently Eq. (6), *i.e.* the starting assumption, is incorrect.

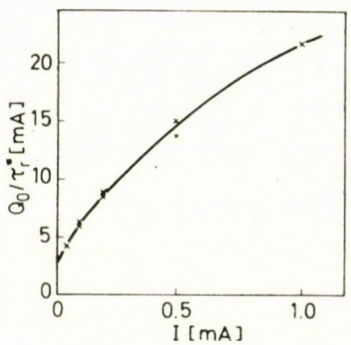

Fig. 4. Demonstration of w = constant. 1 *M* ethanol in 1 *N* NaOH on a 10 cm² nickel plate. Q_0 = 650 mC NiOOH

Having thus reassuringly succeeded in excluding the possibility that the reaction rate is constant during the oxidation, we can return to the original conception that the reaction rate decreases with the decreasing amount of unreacted NiOOH:

$$w = k \cdot Q \tag{7}$$

where k is a constant. Hence Eq. (4) is modified in the following way:

$$-\frac{dQ}{d\tau_r} = I + k \cdot Q. \tag{8}$$

Solving for Q in the form

$$Q = -\frac{I}{k} + Ke^{-k\tau_r} \tag{9}$$

the integration constant K can be determined from the boundary condition ($Q = Q_0$ at $\tau_r = 0$)

$$Q = \left(\frac{I}{k} + Q_0\right) e^{-k\tau_r} - \frac{I}{k} \tag{10}$$

At the time of complete discharge ($\tau_r = \tau_r^*$) the amount of NiOOH on the electrode is zero ($Q = 0$); that is

$$\left(\frac{I}{k} + Q_0\right) e^{-k\tau_r^*} = \frac{I}{k} . \tag{11}$$

By rearrangement we obtain the relation

$$\frac{I}{1 + k \cdot Q_0} = e^{-k\tau_r^*} . \tag{12}$$

Using Eq. (12) the proportionality factor k can be calculated from the times of the potential plateaus of the discharge curves in the case of a given ethanol concentration with different currents.

The method of constant differences may be used in the calculation. The $I - \tau_r^*$ curve is drawn through the measured points. Values τ_{r1}^* and τ_{r2}^* are selected. Their difference is

$$\Delta\tau_r^* = \tau_{r2}^* - \tau_{r1}^* \tag{13}$$

Eq. (12) is also valid for τ_{r1}^* and τ_{r2}^*. If the equations for both are written and one is divided by the other we obtain

$$\frac{\dfrac{I_1}{I_1 + kQ_0}}{\dfrac{I_2}{I_2 + kQ_0}} = \frac{e^{-k\tau_{r1}^*}}{e^{-k\tau_{r2}^*}} = e^{k\Delta\tau_r^*} . \tag{14}$$

If a series of such pairs is chosen from the τ_r^* value region that relation (13) is valid for each pair, then the right-hand side of Eq. (14) is constant

$$e^{k\Delta\tau_r^*} = A . \tag{15}$$

Rearranging Eq. (14) we obtain

$$I_1(I_2 + kQ_0) = AI_2(I_1 + kQ_0) \tag{16}$$

Dividing both sides by $I_1 I_2$ and rearranging

$$\frac{1}{I_2} = \frac{A - 1}{kQ_0} + A\frac{1}{I_1} . \tag{17}$$

At current strength I_2 the discharge time is greater by exactly $\Delta\tau_r^*$ than the discharge time observed at I_1. In the case of plotting $1/I_1$ against $1/I_2$, according to the assumption a straight line must be obtained. From the slope of this, using Eq. (15), the value of k can be calculated.

Fig. 5 serves to illustrate the calculation. On the basis of the discharge curves for 0.1 M ethanol $1/I - \tau_r^*$ relation can be plotted. If the value of

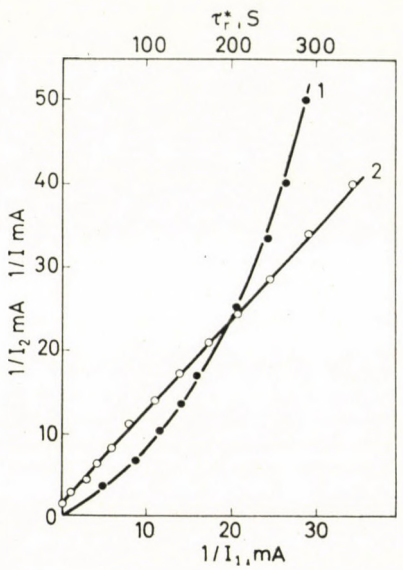

Fig. 5. Oxidation of 0.1 M ethanol on a NiOOH electrode. 1. $1/I - \tau_r^*$ relation, 2. $1/I_2 - 1/I_1$ transformation on the basis of Eq. (17). $\Delta\tau_r^* = 20$ sec.

$\Delta\tau_r^*$ is chosen as 20 sec, then the current relating to $\tau_{r2}^* = 20$ sec is I_2 whilst that relating to $\tau_{r1}^* = 0$ sec is I_1. With the following point for example the current relating to $\tau_{r2}^* = 40$ sec is I_2 and that to be found at $\tau_{r1}^* = 20$ sec is I_1, etc. The series of points so plotted forms the $1/I_2 - 1/I_1$ relation.

It may be seen in Fig. 5 that the points give a straight line to a good approximation, and from the slope of this, using Eqs (17) and (15), the value of constant k can be calculated. In this way Eq. (7) proved to be the correct initial assumption, and this also means that Eq. (7) [in the case of the application of cathodic polarization, Eq. (8)] does indeed describe the rate of oxidation of ethanol (and on the basis of other findings, of other primary alcohols) on a nickel hydroxide electrode. The relation shows that the rate of oxidation during the complete time of reaction is proportional to the amount of nickel(III) oxide hydroxide on the electrode. Thus the constant k may be considered as an apparent rate constant because it is the proportionality factor in the relationship connecting the reaction rate and the instantaneous amount of one

of the reactants. The dependence of the reaction rate on the concentration of the other reactant (alcohols) will be treated in a subsequent paper.

It is worthwhile here to deal in somewhat greater detail with this equation. As is suitable for heterogeneous reactions, not the concentration but the amount of substance in the solid phase appears in the relation. Thus the reaction rate is a derivative with respect to time of the amount of substance either reacting or forming. It follows from this that the dimension of k is sec^{-1}. Because of the electrochemical methods used, in the equation it is expedient to give the amount of material not in moles or equivalents but as the product of the latter with the Faraday number, that is in coulombs; the dimensions of the reaction rate will then be amperes.

The description of a reaction rate according to Eq. (7), where the rate is proportional to the amount of one of the substances in the solid phase, is not unknown in heterogeneous kinetics. We shall give two examples of the dependence of the reaction rate on the amount of oxidant in the solid phase. PICKERING [5] studied the reaction of an alkaline solution of hydrazine with AgO. This author has found that the reaction rate is proportional to the amount of AgO as well as to the hydrazine concentration. HARIVEL and LAURENT [6] studied the kinetics of reduction of the nickel hydroxide electrode. They determined the decrease of "active oxygen content" in KI solution of an electrode of given electrochemical capacity. They found likewise that the reaction rate is proportional to the amount of unreacted NiOOH.

Reproducibility of the measurements

The quantitative determination of the reproducibility of the measurements is absolutely necessary for the evaluation of the above results. This question consists of two parts: to what extent the amount of charge which can be brought onto the electrode varies after repeated charging and discharging (cycling), and secondly, how does the reaction rate (*i.e.* the value of k) vary as a function of time or the number of measurements.

The amount of charge which can be brought onto the electrode was determined by discharging with constant current in 1 N NaOH after electrolytic charging carried out in a pure solution of alkali. The value of Q_0 can be redetermined in the above manner after recording the discharge curves in alcohol, possibly at different concentrations and different currents. According to the findings 50—100 discharges can be performed on an electrode without a significant change in the amount of the dischargeable charge.

The reproducibility can be seen in Fig. 6 for different amounts of nickel hydroxide. The electrochemical capacity Q_0 determined with constant current is plotted on the ordinate, and the number of cycles on the abscissa. The longer blank intervals between the points on the abscissa, corresponding to 10—20

units, represent discharge cycles in alcohol. It must be mentioned that if the nickel hydroxide electrode has stood in distilled water or in dry air for several weeks, then a more significant decrease may be observed in the value of Q_0. This phenomenon appears especially with freshly prepared electrodes and may be explained by the incorporation of water layers into the nickel hydrox-

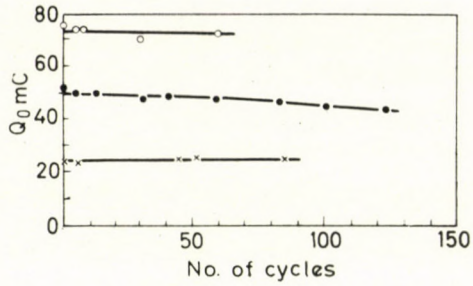

Fig. 6. Reproducibility of the amount of NiOOH which can be brought onto the electrode during cycling

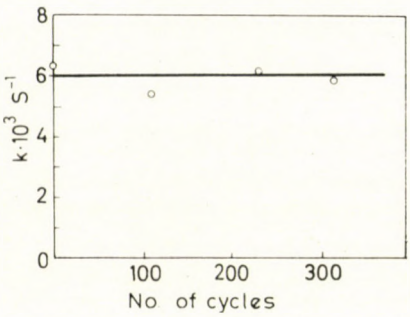

Fig. 7. Change of the rate of oxidation of 0.1 *M* ethanol on a NiOOH electrode during cycling

ide lattice during the cycles, or by the increase of the distance between the lattice planes during some other rearrangement; this can lead to the peeling off of the nickel hydroxide during the disintegration of the lattice.

The constancy of Q_0 reported here proves that the layer adheres quite strongly, and the amount of nickel hydroxide does not change even during prolonged use.

However, this by no means excludes the occurrence of possible structural changes the result of which would be the change of the apparent rate constant k characteristic of the oxidation of alcohols.

Therefore the change of the rate constant must be studied as a function of the use of the electrode. Measurements connected with this are shown in Fig. 7. The number of cycles again appears on the abscissa, while on the or-

dinate are the apparent rate constant values determined in 0.1 *M* ethanol and calculated according to Eq. (17) derived from Eq. (7). It can be seen from the Figure that during the interval studied, the ageing of the electrode need not be considered in the oxidation of alcohols on nickel hydroxide.

REFERENCES

1. VÉRTES, G., HORÁNYI, G., NAGY, F.: Acta Chim. Acad. Sci. Hung. **67,** 145 (1971)
2. HORÁNYI, G., VÉRTES, G., NAGY, F.: Acta Chim. Acad. Sci. Hung. **67,** 357 (1971)
3. BODE, H., DEHMELT, K., WITTE, J.: Z. anorg. allg. Chemie **366,** 1 (1969)
4. BRIGGS, G. W. D., WYNNE-JONNES, W. F. K.: Trans. Faraday Soc. **52,** 1272 (1956)
5. PICKERING, W. F.: Rev. Pure and Appl. Chem. **16,** 185 (1965)
6. HARIVEL, J. P. LAURENT, J. F.: Electrochim. Acta **9,** 703 (1964)

György VÉRTES
György HORÁNYI
Ferenc NAGY
Budapest II., Pusztaszeri út 59—67.

Acta Chimica Academiae Scientiarum Hungaricae, Tomus 68 (3), pp. 229—235 (1971)

INVESTIGATION OF ADSORPTION PHENOMENA ON PLATINIZED Pt ELECTRODES BY TRACER METHODS, VII

SIMULTANEOUS STUDY OF THE ADSORPTION AND ELECTROHYDROGENATION OF PHENYLACETIC ACID

Gy. HORÁNYI and F. NAGY

(Central Research Institute for Chemistry of the Hungarian Academy of Sciences, Budapest)

Received December 18, 1969

1. During the electrohydrogenation of phenylacetic acid the rate of hydrogenation and the adsorption of substrate were measured simultaneously.

2. It was found that, corresponding to expectations, linearity exists between the coverage and the rate.

In an earlier communication [1] it was shown that it would be extremely advantageous if at any moment of time in heterogeneous catalytic hydrogenation or electrohydrogenation the concentrations of the individual components on the surface of the catalyst or electrode were known. In the main only assumptions are found in the literature regarding the connection between the amount adsorbed and the reaction rate, and in general direct experimental data are not available.

We earlier reported [2] our work in connection with the adsorption of aromatic compounds, among them phenylacetic acid.

It was shown with regard to phenylacetic acid that the adsorption equilibrium is not attained during the hydrogenation reaction; moreover, compared with the usual reaction rates the desorption rate of phenylacetic acid is negligible. On the other hand, the desorption of the hydrogenated product is very fast and so under the conditions of hydrogenation it is not necessary to consider the adsorption of the product. At the same time it was also proved that a fraction of the adsorbed phenylacetic acid molecules do not take part in the reaction; this must be taken into consideration in a kinetic study of this process.

In the present communication we report on our work in connection with the detailed analysis of the relation between the rate of hydrogenation of phenylacetic acid and its adsorption.

Experimental

The apparatus and cell already described [1] were used in the study. A potentiostatic method was applied. ^{14}C-labelled phenylacetic acid of 0.1 mCi/mmole specific activity was used.

The studies consisted essentially in the simultaneous measurement of two quantities, the current and the count rate proportional to the adsorption. After adjusting the appropriate

potential the changes in both quantities were followed with time until a (quasi-) stationary state was obtained. This is shown in Fig. 1 for a concentration of 1×10^{-3} M. Curve 1 refers to the current, and curve 2 to the count rate.

As has already been mentioned, the measured overall count rate (I_E) cannot be directly connected with the adsorbed amount active with respect to the reaction. For the determination of this latter amount it is necessary to know the number of counts (I_M) originating from the permanently bound active material on the surface. Various methods can be used for the measurement of this. If the substrate concentration is small, I_M is most simply determined by ensuring with the appropriate adjustment of the potential, *i.e.* the reaction rate, that in the stationary state the mobile adsorbed amount important from the point of view of the

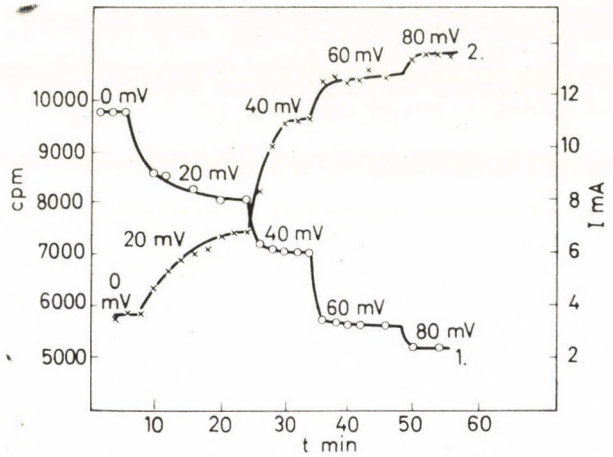

Fig. 1. Change in time of the current (1) and the count rate (2), as a function of the potential

reaction should be practically zero. The count rate measured at such time will clearly be proportional to the amount of residually adsorbed phenylacetic acid.

Another possible method for the determination of I_M is that before the end of the measurements with potentials at which the reaction proceeds with a considerable rate, inactive phenylacetic acid is added in great excess to the solution. Under such conditions the fraction remaining on the surface, which is not exchangeable, is equal to I_M.

It should be noted here that during a too long experimental time the value of I_M can change to a significant extent, and therefore we strived to carry out our measurements relatively quickly and tocheck the magnitude of I_M several times in accordance with the possibilities. Only the experimental observations provided information relating to the magnitude of I_M, and no correlation could be found between it and other parameters. The values of I_M from the individual measurements, as may be seen in Table I, were extremely variable, though the experiment was begun with a clean electrode surface pre-treated identically for all measurements.

The first step of this pre-treatment was anodic regeneration. As already shown [2], under such conditions the permanently adsorbed fraction is removed, presumably by oxidation. The anodic regeneration was continued until the count rate reached the background value. After this, cathodic regeneration was applied for 5—10 minutes. Following the cathodic regeneration the solution in the cell was exchanged for pure base solution.

The potential of the main electrode was adjusted with a potentiostat to 100—150 mV and then the labelled phenylacetic acid was added to the system. Measurements were begun after the stabilization of the count rate.

In order to study the relation between the current and the coverage, the count rate corresponding to maximum mobile adsorption (I_{max}—I_M) must also be known. This can be determined from the count rate measured at potentials at which the reaction no longer takes place or occurs only with low rates. (At the studied concentrations, even if an adsorption equilibrium existed, saturation would already be reached.)

Table I

E (mV)	i (mA)	$I_E - I_M$	Θ_s
$c = 10^{-3}$ M; $I_M = 2500$ cpm			
120	0.40	2700	1.00
100	0.72	2700	1.00
80	1.80	2700	1.00
70	2.72	2700	1.00
60	4.05	2500	0.92
50	5.15	2100	0.77
40	5.70	1800	0.66
30	5.80	1000	0.37
20	5.90	600	0.22
10	6.10	400	0.15
$c = 2\times10^{-4}$ M; $I_M = 1600$ cpm			
150	0.30	4000	1.00
100	0.75	3800	0.95
80	1.74	3700	0.92
60	2.50	2600	0.65
40	2.54	1500	0.35
20	3.10	800	0.20
0	4.50	600	0.15
$c = 5\times10^{-4}$ M; $I_M = 4000$ cpm			
100	0.54	3000	1.00
90	0.72	3000	1.00
80	1.04	3000	1.00
70	1.46	3000	1.00
60	1.94	2700	0.90
50	2.25	2000	0.66
40	2.28	1400	0.47
20	2.80	900	0.30
0	4.50	300	0.10

On the basis of what has been said, the stationary coverage relating to the mobile fraction can be calculated using the relation

$$\Theta_s = \frac{I_E - I_M}{I_{\max} - I_M} \tag{1}$$

A number of experimental data appear in Table I; the appropriate calculations were performed using Eq. (1).

Interpretation of the results

In our earlier work [3] it was supposed that a relation of the type

$$i = \Theta_s f(E) \tag{2}$$

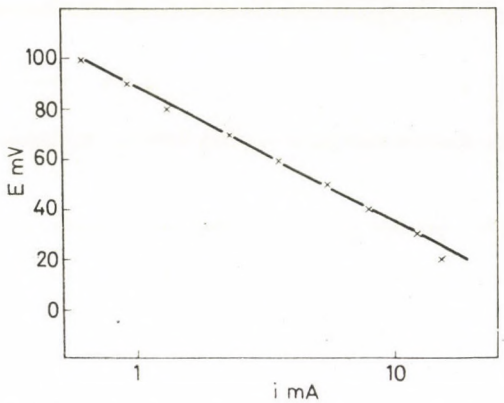

Fig. 2. Electrohydrogenation of phenylacetic acid at a concentration of 10^{-2} M

is valid for electrohydrogenation. E is the potential, and in many cases the function $f(E)$ to a good approximation can be written as

$$f(E) = k_r \cdot 10^{-bE} \tag{3}$$

where b is a constant.

As shown in Fig. 2, at sufficiently large concentrations (10^{-2} M) the relation $\log i = a + bE$ is approximately valid for phenylacetic acid too.

At such concentrations the adsorption may be considered almost constant over the whole potential interval, as may be seen in Fig. 3.

At concentrations greater than 10^{-2} M the polarization curve shown in Fig. 2 already changes only slightly, in agreement with the fact that there is no considerable possibility of variation in the adsorption.

Thus only at lower concentrations is there a question of the verification of relations (2) and (3). In these circumstances diffusion too is present among the rate-determining processes. In this case (as stated in our previous communication), under stationary conditions, if the calculation of Θ_s is performed according to Eq. (1), then the equations

$$\begin{gathered} i = k_D(c_0 - c_f) = k_A(1-\Theta_M)\, c_f(1-\Theta_s) = k'_A\, c_f(1-\Theta_s) = k_r \cdot 10^{-bE} \cdot \Theta_s \\ k_D\, c_0 \frac{k'_A(1-\Theta_s)}{k_D\, k'_A(1-\Theta_s)} = k'_r\, \Theta_s = i \end{gathered} \tag{4}$$

will be valid, where k_D is the rate constant for mass transport by diffusion, k_A is the adsorption rate constant, $k_r' = k_r \cdot 10^{-bE}$, the rate constant of the hydrogenation reaction, and Θ_s and Θ_M are the coverages relating to the mobile and permanent adsorbed fractions. $\Theta_M = I_M/I_{max}$. If $k_D \ll k_A$ then

$$i = k_D c_0 \tag{5}$$

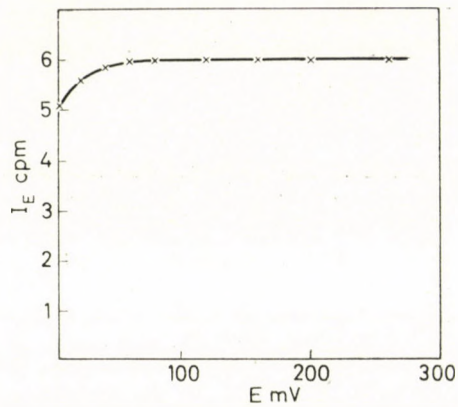

Fig. 3. Potential dependence of the adsorption at a phenylacetic acid concentration of 10^{-2} *M*

The ratio of k_D and $k_r \cdot 10^{-bE}$ depends on the potential, thus by changing the potential, the validity of Eq. (5) should be attainable. Under such conditions a limiting diffusion current may be observed.

This can be seen for example in the potential-current curve in Fig. 4 which was obtained with 10^{-4} *M* phenylacetic acid.

At potentials more negative than 30 mV the current increases because of hydrogen evolution. Taking this into consideration the dashed line was drawn, and this indeed corresponds to the limiting diffusion current.

With a knowledge of Θ_s and i, the possibility arises for the study of the validity of relations (2) and (3) by plotting $\log i/\Theta_s - E$ curves. Naturally, for the calculation of i/Θ_s only the current used for the hydrogenation reaction must be considered.

In Figs 5, 6 and 7, the values of $\log i$ (×) (1) and $\log i/\Theta_s$ (○) (2) are plotted as a function of potential at concentrations of 10^{-3} *M*, 2×10^{-4} *M* and 5×10^{-4} *M*.

It may be seen from all three graphs that $\log i/\Theta_s$ is a linear function of the potential; at high concentrations (*i.e.* at $\Theta_s \approx 1$) the slopes of the electrohydrogenation curves agree essentially with these slopes.

To summarize the experimental observations, it was found possible in the given concrete case to verify the validity of Eqs (1) and (2). The fact that

on a concrete example we were successful in verifying the applicability of our method to the study of adsorption phenomena occurring during electrode reactions must be considered as another very significant result.

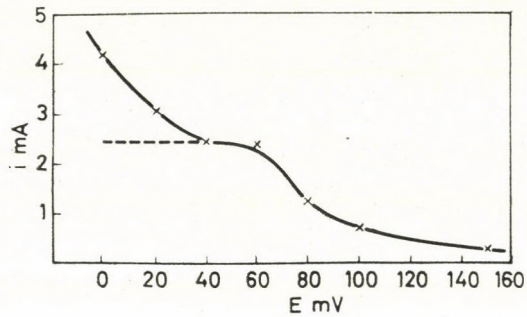

Fig. 4. Electrohydrogenation curve of phenylacetic acid at a concentration of 10^{-4} *M*

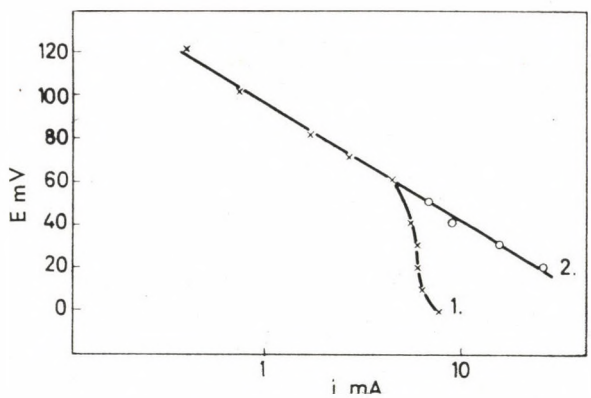

Fig. 5. Plots of log i and log i/Θ_s as functions of the potential at a concentration of 10^{-3} *M*

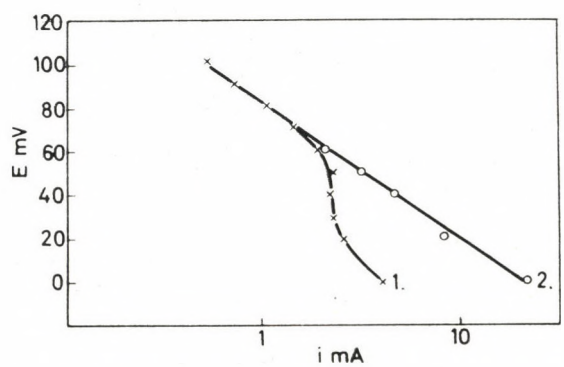

Fig. 6. Plots of log i and log i/Θ_s as functions of the potential at a concentration of 2×10^{-4} *M*

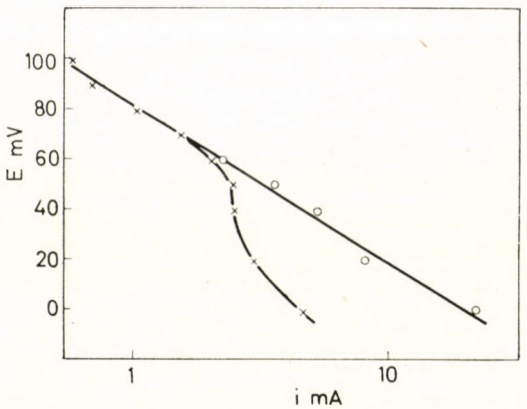

Fig. 7. Plots of log i and log i/Θ_s as a function of the potential at a concentration of 5×10^{-4} M

REFERENCES

1. Solt, J., Horányi, Gy., Nagy, F.: Magy. Kém. Foly. **73,** 414 (1967)
2. Horányi, Gy., Solt, J., Nagy, F.: Magy. Kém. Foly. (In press)
3. Nagy, F., Telcs, I., Horányi, Gy.: Acta Chim. Acad. Sci. Hung. **37,** 295 (1963). Magy. Kém. Foly. **72,** 370 (1966)

György Horányi
Ferenc Nagy
Budapest II., Pusztaszeri út 59—67.

Acta Chimica Academiae Scientiarum Hungaricae. Tomus 68 (3), pp. 237—244 (1971)

ЭЛЕКТРООСАЖДЕНИЕ ИЗОТОПОВ ИРИДИЯ И ПЛАТИНЫ, СВОБОДНЫХ ОТ НОСИТЕЛЕЙ

Й. МОЛНАР и Ирэн МОЛНАР

(Центральный институт физических исследований АН ВНР Будапешт, Венгрия)*

Поступило: 30 XII 1969 г.

Изучались электроосаждение изотопов иридия и платины без носителя, зависимость выделения от состава электролита и от других параметров.

На основе экспериментальных данных были разработаны методы, с помощью которых изготавливаются источники нейтронно-дефицитных изотопов иридия и платины для ядерно-спектроскопических измерений.

Иридий и платина — благородные металлы, и электроосаждение их изотопов без носителя на тонкую проволоку или фольгу кажется лучшим способом при изготовлении источников излучения для исследования их ядерных свойств на магнитных бета-спектрометрах. Практическое использование электролиза для этой цели вызывает трдности, которые — ввиду того, что в литературе мало данных по электроосаждению изотопов иридия и платины без носителя [1] — привели нас к решению более подробно исследовать электролитическое выделение изотопов иридия и платины.

Экспериментальная часть

а) *Электролитическая ячейка и подготовка электродов*

В экспериментах по подбору оптимальных условий электроосаждения использовалась так называемая капиллярная ячейка, описанная нами в другой работе [2]. Анодом служила платиновая проволока диаметром 0,1 мм, катодом — проволока из сплава NiCr (марка Х20Н80) диаметром 0,1 мм; аноды и катоды погружались в хромовую смесь приблизительно на 1 час, потом обмывались дистиллированной водой, а перед началом опыта катоды дополнительно промывались и хлороформом. Объем раствора в ячейке ~0,045 мл. Источником тока служила батарея; во время электролиза ток регулировался с помощью реостата.

* Работа выполнена в Объединенном институте ядерных исследований, г. Дубна.

б) *Изотопы*

В исследованиях использовались изотопы ^{189}Ir и ^{188}Pt, полученные при глубоком расщеплении ядер золота, облученного протонами с энергией 660 Мэв. Перед обработкой облученная мишень выдерживалась в течение 20 дней, затем растворялась в царской водке и после разрушения нитратов золото экстрагировалось изоамилацетатом из раствора 4 M HCl [3]. Водная фаза, содержащая изотопы иридия и платины, упаривалась почти досуха, остаток обрабатывался 0,3 M HCl и раствор пропускался через колонку, наполненную смолой Дауэкс-50 $\times$ 12. Далее иридий и платина сорбировались на смолу Дауэкс-1 $\times$ 8 в колонке, откуда иридий вымывался 9 M HCl [4]. Для элюирования платины использовалась 50% $HClO_4$. Раствор платины упаривался почти досуха с добавлением соляной кислоты. Остаток растворялся в 3 M HCl + 3% $SnCl_2$ и Pt экстрагировалась диэтиловым эфиром [5]. Тем же самым методом экстракции очищался препарат перед началом электроосаждения, чтобы удалить изотоп ^{188}Ir, образующийся из ^{188}Pt. Препараты изотопов иридия и платины, полученные таким образом, являются радиохимически чистыми и свободными от изотопных носителей.

в) *Реактивы и растворы*

Для изготовления растворов-электролитов использовались реактивы квалификации ч. д. а. Значения pH растворов устанавливались: в кислом диапазоне кислотой, отвечающей кислотному компоненту соли или уксусной кислотой; в щелочном диапазоне — аммиаком или карбонатом натрия. Растворы, содержащие изотопы иридия или платины, приготовлялись растворением сухого препарата ^{189}Ir или ^{188}Pt в электролите данного состава.

г) *Измерение*

Радиоактивность изотопов, выделенная на катоде, на аноде и оставшаяся в растворе, измерялась сцинтилляционным счетчиком NaI/Tl/ с колодцем при телесном угле $\sim 4\pi$ в одинаковых геометрических условиях. Наши данные получены из трех параллельных опытов; относительное стандартное отклонение составляет $\sim \pm 6\%$.

Результаты и обсуждение

а) *Электроосаждение изотопов иридия*

С целью получения общей картины по электроосаждению изотопов иридия без носителя исследовалось их электролитическое выделение из 0,1 M растворов разных солей, при разных значениях pH. Основные результаты

измерений приведены в таблице 1. Цифры в колонках означают осаждение изотопа ^{189}Ir без носителя в процентах; цифры в скобках означают осаждение изотопа ^{192}Ir с носителем в процентах (в последнем случае концентрация иридия в исследованных растворах ~0,001 М). По данным можно установить, что имеется большая разница в электроосаждении изотопов иридия без носителя и иридия при макроконцентрации. Выделение иридия из большинства исследованных растворов незначительно, в то время как выделение изотопов иридия без носителя достигает или превышает 50% из многих растворов. Особое внимание следует уделить при этом раствору хлористого аммо-

Таблица 1

Электроосаждение изотопов иридия без носителя из разных электролитов

Катод — из проволоки NiCr; ток — 10 мА; время электролиза — 25 мин. Цифры в колонках означают выделенное на катоде количество изотопов иридия в процентах

Основной электролит	Диапазон pH				
	1,5—3	3—5	5—7	7—9	9—11
0,1 М NaF	43 (19)	40 (9)	44 (9)	30 (7)	22 (4)
0,1 М NH_4F	58	56	59	58	29
0,1 М NaCl	76 (20)	76 (20)	61 (15)	60	55 (7)
0,1 М NH_4Cl	90 (26)	89 (51)	87 (33)	82 (65)	69(14)
0,1 М NaBr	20	35	34	31	23
0,1 М NH_4Br	66	54	50	35	31
0,1 М $NaNO_3$	52 (15)	51 (9)	63 (10)	53 (10)	45 (5)
0,1 М NH_4NO_3	48	46	47	57	49
0,1 М $NaClO_4$	52 (6)	55 (5)	34 (6)	55 (9)	62 (8)
0,1 М NH_4ClO_4	52 (8)	71 (8)	53 (8)	58 (10)	18 (20)
0,1 М Na_2SO_4	41 (6)	40 (6)	51 (7)	57 (6)	35 (8)
0,1 М $(NH_4)_2SO_4$	78 (4)	71 (8)	73 (3)	64 (6)	49 (11)
0,1 М Na_2HPO_4	22	31	32	40	47
0,1 М $(NH_4)_2HPO_4$	35	36	23	43	26
0,1 М NaSCN	12	4	6	6	3
0,1 М NH_4SCN	39	26	23	18	3
0,1 М CH_3COONa		29	26	25	46
0,1 М CH_3COONH_4		19	9	20	6
0,1 М $Na_2(COO)_2$	35 (13)	53 (21)	61	76	68 (25)
0,1 М $(NH_4)_2(COO)_2$	22	22	38	41	12
0,1 М $Na_2C_4H_4O_6$	10	6	7	10	11
0,1 М $(NH_4)_2C_4H_4O_6$	4	5	7	10	6
0,1 М $Na_3C_6H_5O_7$	5	14	13	14	13
0,1 М $(NH_4)_2HC_6H_5O_7$	4	10	12	5	5

ния. В этом случае выделение макроколичества иридия достигает 50%, а максимальный выход осаждения изотопов без носителя ≈90%.

Влияние катионного компонента солей не однозначно: в случае фторидов, хлоридов, бромидов, сульфатов, сульфоцианидов выделение больше из аммониевых солей, а в случае нитратов, ацетатов и оксалатов — выход больше из натриевых солей. Величина pH раствора мало влияет на осаждение; наблюдается однозначное уменьшение только при pH выше 9.

Исследовалась зависимость электроосаждения от концентрации тех солей, из 0,1 М растворов которых выход превышает 60%. Результаты показаны на рис. 1. Видно, что выход сильно меняется с изменением концентрации; при этом кривые переходят через максимум. Оптимальной концентрацией является 0,1 М (кроме раствора бромистого аммония).

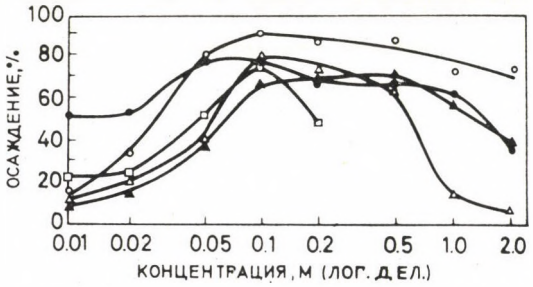

Рис. 1. Зависимость электроосаждения изотопов иридия без носителя от концентраций различных солей. Катод — из проволоки NiCr; ток — 10 мА; время электролиза — 25 мин. ○ NH_4Cl; ● NaCl; △ $(NH_4)_2SO_4$; ▲ NH_4Br; □ $Na_2(COO)_2$

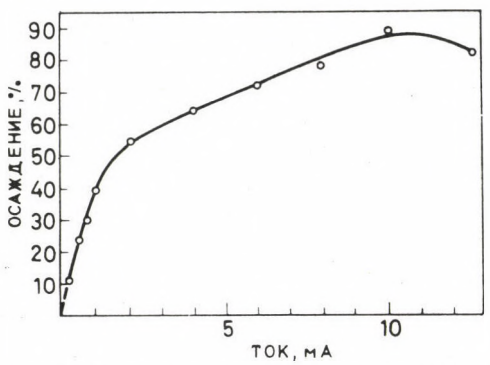

Рис. 2. Зависимость электроосаждения изотопов иридия без носителя от силы тока. Катод — из проволоки NiCr; электролит — 0,1 М NH_4Cl; время электролиза — 25 мин.

Измерялась зависимость электроосаждения от силы тока и от времени из 0,1 М раствора хлористого аммония, который, по нашим данным, является оптимальным по составу электролитом. С увеличением силы тока выход постепенно возрастает, достигает максимума около 10 мА, что отвечает плотности тока ~210 мА/см² (рис. 2). Из рис. 3 видно, что осаждение про-

текает быстро и за 15 мин. достигает 70%, в дальнейшем выход возрастает медленно.

Выделение изотопов иридия без носителя на аноде превышало 2% в случае трех солей; его максимальное значение из раствора 0,1 M NaF — 45%, из 0,1 M NH_4F — 38%, из 0,1 M CH_3COONa — 25%.

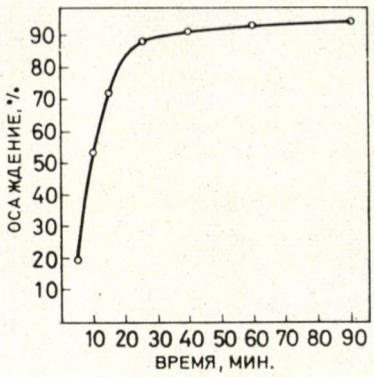

Рис. 3. Зависимость электроосаждения изотопов иридия без носителя от времени электролиза. Катод — из проволоки NiCr; электролит — 0,1 M NH_4Cl; ток — 10 мА.

б) *Электроосаждение изотопов платины*

Известно, что платина достаточно легко выделяется при электролизе на катод в виде металла; поэтому ожидается выделение на катод и изотопов платины без носителя. Но наблюдавшееся для микроколичеств платины анодное выделение заставило нас исследовать поведение платины при электролизе подробнее.

Измерялось выделение изотопов платины на катод и на анод из 0,1 M растворов разных солей. Результаты представлены в таблице 2 и 3. Как и ожидалось, выделение на катод проходило с большим выходом из многих растворов, но не из всех. Самый большой выход получается из 0,1 M раствора хлористого аммония. О влиянии pH раствора на выход интересно заметить только, что из раствора фосфата натрия большой выход получается при низком и при высоком значении pH; при средних значениях pH выход небольшой.

Особый интерес представляют собой данные таблицы 3, согласно которым выделение изотопов платины без носителя на анод может достигать значительной величины, т. е. 40—50%. При этом следует учесть небольшой размер анодов, использованных в ячейках при электролизе. Причиной выделения на анод может быть образование нерастворимых окислов на поверхности анода, а может быть и изотопный обмен между атомами платинового анода и ионами изотопов платины под влиянием процессов, протекающих во время электролиза. В пользу последней причины говорит тот факт, что удаление изотопов платины с поверхности платиновых анодов нам удалось осуществить только

Таблица 2

Электроосаждение изотопов платины без носителя из разных электролитов

Катод — из проволоки NiCr; ток — 10 мА; время электролиза — 25 мин. Цифры в колонках означают выделенное на катоде количество изотопов платины в процентах

Основной электролит	Диапазон pH				
	1,5—3	3—5	5—7	7—9	9—11
0,1 M NaF	48	18	32	21	27
0,1 M NH_4F	79	73	77	72	55
0,1 M NaCl	53	28	31	18	15
0,1 M NH_4Cl	96	87	92	96	83
0,1 M NaBr	54	44	25	19	8
0,1 M NH_4Br	88	69	84	86	78
0,1 M Na_2SO_4	37	41	44	31	10
0,1 M $(NH_4)_2SO_4$	89	68	58	56	66
0,1 M Na_2HPO_4	92*	19	25	39	77
0,1 M $(NH_4)_2HPO_4$	87	87	81	75	90
0,1 M CH_3COONa		29	10	7	4
0,1 M CH_3COONH_4		48	30	21	9

* pH = 1,5

Таблица 3

Выделение изотопов платины без носителя на платиновый анод из разных электролитов

Ток — 10 мА; время электролиза — 25 мин. Цифры в колонках означают выделенное на аноде количество изотопов платины в процентах

Основной электролит	Диапазон pH				
	1,5—3	3—5	5—7	7—9	9—11
0,1 M NaF	23	33	46	40	35
0,1 M NH_4F	10	11	13	13	1
0,1 M NaCl	25	23	29	30	41
0,1 M NH_4Cl	1	1	1	1	1
0,1 M NaBr	2	4	5	13	17
0,1 M NH_4Br	1	1	1	1	6
0,1 M Na_2SO_4	25	20	28	26	47
0,1 M $(NH_4)_2SO_4$	6	7	19	16	2
0,1 M Na_2HPO_4	1	23	1	10	40
0,1 M $(NH_4)_2HPO_4$	1	3	5	7	1
0,1 M CH_3COONa		40	51	35	32
0,1 M CH_3COONH_4		1	10	12	1

растворением поверхностного слоя в царской водке. Окончательный ответ на этот вопрос требует дальнейшего исследования.

Исследовалась зависимость выделения изотопов платины без-носителя на катод из раствора 0,1 М хлористого аммония при pH ~ 2 от силы тока и от времени электролиза. Результаты измерений показаны на рис. 4 и 5. Выход

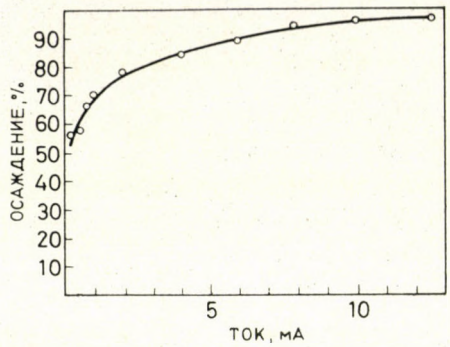

Рис. 4. Зависимость электроосаждения изотопов платины без носителя от силы тока. Катод — из проволоки NiCr; электролит — 0,1 М NH_4Cl; время электролиза — 25 мин.

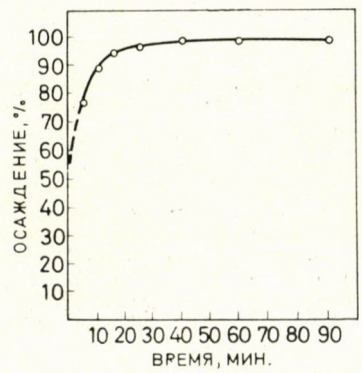

Рис. 5. Зависимость электроосаждения изотопов платины без носителя от времени электролиза. Катод — из проволоки NiCr; электролит — 0,1 М NH_4Cl; ток — 10 мА.

постоянно возрастает с увеличением силы тока до практически полного выделения при 10 мА, что отвечает ~210 мА/см². Выделение протекает быстро: за 10 мин. 90% изотопов платины осаждается на катоде.

На основе экспериментальных данных нами были разработаны методы для изготовления источников излучения нейтронно-дефицитных изотопов иридия и платины для измерения их на магнитных бета-спектрометрах и спектрографах.

При этом препараты изотопов иридия и платины получаются по методу пункта б) экспериментальной части работы с тем лишь отличием, что обработка мишени производится вскоре после конца облучения.

а) *Источники изотопов иридия*

При элюировании изотопов иридия 9 M HCl 8—12 пиковых капель собирается в посуду из тефлона и упаривается под инфракрасной лампой досуха. Остаток растворяется в 0,1 мл 0,1 M NH_4Cl и раствор переносится в ячейку электролизера, описанного Новгородовым и др. [6]. Настоящая ячейка отличается от описанной тем, что изготавливается из тефлона, а анодом служит тонкая платиновая проволока, расположенная на дне ячейки. Затем опускается катод — проволока толщиной 0,1 мм или фольга шириной 0,4—0,6 мм из сплава NiCr, закрепленная в рамке — до соприкосновения катода с поверхностью раствора, и ведется электролиз при плотности тока ~200 мА/см² в течение 20—30 минут. 70—80% изотопов иридия без носителя осаждается на катоде. Слой осажденных изотопов тонкий; об этом свидетельствует тот факт, что при измерении энергии конверсионных электронов с использованием этих источников разрешение по энергии не превышает более 20% приборного.

б) *Источники изотопов платины*

После экстракции изотопов платины диэтиловым эфиром, органическая фаза 5 раз промывается 3 M HCl, насыщенной эфиром. Затем эфир упаривается, остатки его разрушаются перекисью водорода. Изотопы платины растворяются в 0,1 мл 0,1 M NH_4Cl. Дальнейшие операции выполняются точно так же, как в случае иридия.

Summary

The dependence of the electrolytic precipitation of carrier-free iridium and platinum isotopes on the composition of the electrolyte and on other factors has been investigated.

On the basis of experimental results, methods have been developed by means of which the radiation sources of iridium and platinum isotopes with neutron deficit are prepared, for purposes of nuclear spectroscopic measurements.

ЛИТЕРАТУРА

1. Saito, K., Inone, Y., Yamazaki, T.: Nippon Kagaku Zasshi **84,** 220 (1963); NSA **17,** 27459 (1963)
2. Молнар, Й., Молнар, И.: Acta Chim. Acad. Sci. Hung. **67,** 15 (1971)
3. Goto, H., Suzuki, S., Saito, M., Kisimoto, M.: J. Chem. Soc. Japan **85,** 75 (1964)
4. Дема, Й., Зайцева, Н. Г., Ким Хон Сил, Новиков, В. П.: Тезисы докладов 15-го ежегодного совещания по ядерной спектроскопии, Минск, 1965 г., стр. 73., Из-во «Наука» М.—Л. 1965 г.
5. Gile, J. D., Harrison, W. H. Hamilton, J. G.: U. S. Atomic Energy Commission Report, UCRL—1418
6. Новгородов, А. Ф., Кочетков, В. Л., Лебедев, Н. А., Халкин, В. А.: Радиохимия **6,** 73—78 (1964)

József Molnár
Irén Molnár
Budapest XII., Konkoly Thege M. út.

Acta Chimica Academiae Scientiarum Hungaricae, Tomus 68 (3), pp. 245—251 (1971)

ЭЛЕКТРООСАЖДЕНИЕ ИЗОТОПОВ ОСМИЯ, СВОБОДНЫХ ОТ НОСИТЕЛЕЙ, И МЕТОД ИХ КОНЦЕНТРИРОВАНИЯ В МАЛОМ ОБЪЕМЕ

Й. МОЛНАР и Ирэн МОЛНАР

(Центральный институт физических исследований АН ВНР Будапешт, Венгрия)*

Поступило: 30. XII. 1969

Был разработан новый метод концентрирования изотопов осмия без носителя в малом объеме. Исследовалась зависимость электроосаждения этих изотопов от состава электролита, плотности тока и времени электролиза. На основе экспериментальных данных был разработан метод, с помощью которого изготавливаются источники нейтронно-дефицитных изотопов осмия для ядерно-, спектрометрических измерений.

Спектры бета-частиц и конверсионных электронов нейтронно-дефицитных изотопов осмия недостаточно изучены; это, по-видимому, связано с трудностями получения источников для таких измерений.

Химический процесс получения источников для бета-спектроскопических измерений включает в себя три этапа.

1. Отделение изотопов данного элемента от облученной мишени и от изотопов других элементов, образовавшихся в мишени.

2. Концентрирование отдельных радиохимически чистых изотопов в малом ($\sim$0,1 мл) объеме раствора, который не содержит химических реактивов, мешающих при самом изготовлении источника.

3. Нанесение радиоизотопов из концентрата на тонкую подложку небольшого размера ($0{,}1 \times 10$ мм^2).

Вся химическая операция должна проводиться по возможности быстро и с помощью защитных устройств.

Насколько нам известно, в литературе до настоящего момента имелось только две работы, в которых описывались методы получения источников изотопов осмия без носителя. По методу Ньютона [1] изотопы осмия, полученные при облучении вольфрама альфа-частицами, отделялись от мишени дистилляцией и поглощались раствором 0,1 M $NaHSO_4$, который вследствие этого разбавлялся до $\sim$0,03 M. Непосредственно из этого раствора проводилось выделение изотопов осмия электролизом на катоды из платины, никеля и нержавеющей стали. Диаметр проволоки — 0,01 дюйма, сила тока — 150 мА, время электролиза — 10 мин. Отмечалось, что на катоде часто появлялся черный слой, который нежелателен при измерении. Кроме того, нет данных по выходу процесса. Беляев и др. [2] коротко указывают, что изотопы осмия при

* Работа выполнена в Объединенном институте ядерных исследований, г. Дубна.

их дистилляции поглощались этиловым спиртом, насыщенным SO_2. Источники для бета-спектрометрических измерений приготовлялись упариванием этого раствора на алюминиевой фольге.

Исследование ядерных свойств нейтронно-дефицитных изотопов осмия в ОИЯИ потребовало разработки нового метода изготовления источников, ввиду того, что методы, описанные выше, в наших условиях оказались неосуществимыми.

Благодаря тому, что OsO_4 легко отгоняется из водного раствора, первый этап не встречает трудностей; 2-й и 3-й этапы требуют более подробного изучения. Результаты этих исследований представлены в настоящей работе.

А. Метод концентрирования изотопов осмия без носителя

Нейтронно-дефицитные изотопы осмия получаются в реакциях глубокого расщепления ядер золота протонами с энергией 660 Мэв. Затем золото (~2 гр) растворяется в царской водке и при нагревании изотопы осмия перегоняются вместе с парами кислого водного раствора и конденсируются. Объем составляет ~10 мл. Из этого раствора изотопы осмия должны быть сконцентрированы в объеме ~0,1 мл. Это осуществляется по методу, разработанному нами следующим образом:

При перегонке изотопов осмия из царской водки летучие компоненты поглощаются четыреххлористым углеродом, охлаждаемым водой; ~90% изотопов осмия находится в CCl_4. Затем органическая фаза отделяется от образовавшейся водной фазы и промывается раствором 1 M Na_2HPO_4 для удаления кислоты. Потери осмия при промывке ~5%. CCl_4 перегоняется, причем изотопы осмия количественно тоже переходят в дистиллят. Из последнего осмий реэкстрагируется раствором 1 M NH_4OH. После этого производится упаривание раствора при давлении ~20 мм ртутного столба в водяной бане досуха; для того, чтобы при упаривании раствор оставался щелочным, к нему предварительно добавляется ~0,1 мл 0,001 M NaOH. Сухой остаток растворяется в ~0,1 мл воды или нужного электролита. В этом препарате содержится 70—80% осмия, образовавшегося при облучении золота. Такой метод получения концентрата мы использовали во всех наших экспериментах.

Б. Электроосаждение изотопов осмия без носителя

Одним из лучших методов для изготовления бета-источников из концентрата, полученного вышеописанным образом, по-видимому является электроосаждение. Ввиду того, что в литературе мало данных по электроосаждению изотопов осмия, возникла необходимость подробного исследования для установления оптимальных, с нашей точки зрения, условий изготовления источников.

Экспериментальная часть

а) *Электролитическая ячейка и подготовка электродов*

В экспериментах использовалась капиллярная ячейка [3]. Анодом служила платиновая проволока диаметром 0,1 мм, катодом — проволока из сплава NiCr (марка X20H80) диаметром 0,1 мм; аноды и катоды погружались в хромовую смесь приблизительно на 1 час, потом обмывались дистиллированной водой. Перед началом опыта катоды промывались хлороформом. Объем раствора в ячейке ~0,045 мл. Источником тока служила батарея; во время электролиза ток регулировался с помощью реостата.

б) *Изотоп*

В исследованиях использовался изотоп ^{185}Os, полученный вышеописанным образом из мишени золота, облученной протонами с энергией 660 Мэв, которая выдерживалась в течение 30 дней перед обработкой.

в) *Реактивы и растворы*

Для изготовления растворов-электролитов использовались реактивы квалификации ч. д. а. Значение pH растворов устанавливалось в кислом диапазоне кислотой, отвечающей кислотному компоненту соли, или уксусной кислотой; в щелочном диапазоне аммиаком или карбонатом натрия. Растворы радиоосмия приготовлялись следующим образом: 1 капля раствора, содержащая изотоп ^{185}Os без носителя, упаривалась досуха при комнатной температуре и сухой остаток растворялся в заданном электролите.

г) *Измерение*

Радиоактивность изотопа, выделенного на катоде, на аноде и оставшегося в растворе измерялась отдельно сцинтилляционным счетчиком NaI(Tl) с колодцем при телесном угле ~4π в одинаковых геометрических условиях. Наши данные являются среднеарифметическими трех параллельных опытов; относительное стандартное отклонение составляет ~$\pm 5\%$.

Результаты и обсуждение

С целью получения общих сведений о поведении изотопов осмия без носителя при электролизе, исследовалось их электроосаждение из электролитов различного состава. Для приготовления 0,1 М растворов-электролитов были взяты 24 соли; в качестве катиона брался натрий или аммоний, в качестве аниона — 12 анионов органических и неорганических кислот. (Эти соли часто служат компонентами электролитов при электроосаждении металлов). При этом из каждой соли приготовлялись растворы с разным зна-

чением pH. Остальные условия электролиза — объем, электроды, плотность тока, время — были одинаковые. Результаты измерений даны в табл. 1. При этом удивляет то, что несмотря на благородный характер элемента осмия, выход электроосаждения его изотопов из большинства растворов небольшой; он достигает или немного превышает 50% только из некоторых электролитов. Из растворов лимоннокислых и виннокислых солей выделения совсем незначительны. Выделение мало зависит от исходного значения pH,* в случае некоторых электролитов наблюдается однозначное уменьшение выхода с увеличением pH.

В дальнейшем исследовалась зависимость электроосаждения от концентрации электролитов, из которых выход при концентрации 0,1 M достигает ~50%. Результаты измерений показаны на рис. 1. Как видно из рисунка, выделение зависит от концентрации, при этом кривые проходят через максимум. В случае уксуснокислого натрия максимум наблюдается при концентрации 0,05 M, а в случае фтористого аммония — при 1,5—2 M. Выход при максимумах значителен и превышает 75%.

На рис. 2 изображены три функциональных зависимости. Кривая I дает зависимость выхода электроосаждения от концентрации уксусной кислоты при постоянной концентрации уксуснокислого натрия, равной 0,05 M. Оптимальная концентрация равна 1 M. Кривая II изображает зависимость выхода от концентрации уксуснокислого натрия при постоянной концентрации уксусной кислоты, равной 1 M. Оптимальной концентрацией является также 0,05 M (неполное совпадение с соответственной кривой рис. 1 объясняется разницей концентраций уксусной кислоты). Кривая III показывает зависимость выхода от концентрации фтористоводородной кислоты при постоянной концентрации фтористого аммония, равной 1,5 M. При небольших концентрациях HF выход мало изменяется, а при концентарциях выше 0,2 M выход падает.

Измерялась и зависимость выхода осаждения от силы тока при составе электролита 0,05 M CH_3COONa + 1 M CH_3COOH; результаты показаны на рис. 3. Выход медленно возрастает с увеличением силы тока и достигает насыщения при токе около 10 мА; это отвечает плотности тока ~210 мА/см².

На рис. 4 показана зависимость электроосаждения осмия от времени из раствора 0,05 M CH_3COONa + 1 M CH_3COOH при плотности тока 210 мА/см². Как видно, процесс выделения быстрый, кривая резко поднимается; выход за 30 мин. достигает 75%, а в дальнейшем увеличение небольшое.

Следует отметить, что выделение изотопов осмия на аноде не превышало 2%.

Суммируя вышесказанные, можно отметить следующее: способность изотопов осмия без носителя к электроосаждению невелика даже при благо-

* Из-за малого объема и небольшой буферной емкости растворов pH, в большинстве случаев, меняется во время электролиза.

Таблица 1

Электроосаждение изотопов осмия без носителя из разных электролитов

Катод — из проволоки NiCr; ток — 10 мА; время электролиза — 25 мин. Цифры в колонках означают выделенное на катоде количество изотопов осмия в процентах

Основной электролит	Диапазон pH				
	1,5—3	3—5	5—7	7—9	9—11
0,1 M NaF		49	43	43	35
0,1 M NH_4F		51	36	32	31
0,1 M NaCl	51	19	43	28	21
0,1 M NH_4Cl	53	32	39	44	37
0,1 M NaBr	21	24	11	16	12
0,1 M NH_4Br	43	14	14	16	12
0,1 M $NaNO_3$	15	27	20	29	11
0,1 M NH_4NO_3	26	10	24	29	17
0,1 M $NaClO_4$	16	24	20	26	17
0,1 M NH_4ClO_4	45	37	45	46	15
0,1 M Na_2SO_4	25	34	22	29	25
0,1 M $(NH_4)_2SO_4$	40	35	47	34	32
0,1 M Na_2HPO_4	50	21	15	22	6
0,1 M $(NH_4)_2HPO_4$	32	16	15	22	33
0,1 M NaSCN	14	7	7	10	12
0,1 M NH_4SCN	27	6	6	12	5
0,1 M CH_3COONa		62	64	50	42
0,1 M CH_3COONH_4		44	17	18	7
0,1 M $Na_2(COO)_2$	23	39	33	31	32
0,1 M $(NH_4)_2(COO)_2$	54	50	47	40	26
0,1 M $Na_2C_4H_4O_6$	5	1	5	9	7
0,1 M $(NH_4)_2C_4H_4O_6$	3	3	5	1	2
0,1 M $Na_3C_6H_5O_7$	2	5	4	7	6
0,1 M $(NH_4)_2HC_6H_5O_7$	4	5	11	5	2

приятных геометрических условиях (отношение поверхности катода к объему раствора велико); условия, при которых изотопы осмия осаждаются на катоде с выходом $> 75\%$, за 30 мин. были найдены только на основе обширных исследований.

На основе наших экспериментальных данных был создан метод изготовления источников излучения нейтронно-дефицитных изотопов осмия без носителя для их измерения на магнитных бета-спектрометрах и спектрографах. Препарат изотопов осмия получается по методу пункта А с тем лишь отличием, что обработка мишени производится вскоре после конца облучения. Перед упариванием к 1 М раствору NH_4OH, содержащему изотопы осмия,

добавляется ~0,1 мл 2 М NH_4F и упаривается до объема ~0,1 мл. Этот раствор переносится в ячейку электролизера, описанного Новгородовым и др. [4]. Эта ячейка отличается от описанной тем, что изготавливается из теф-

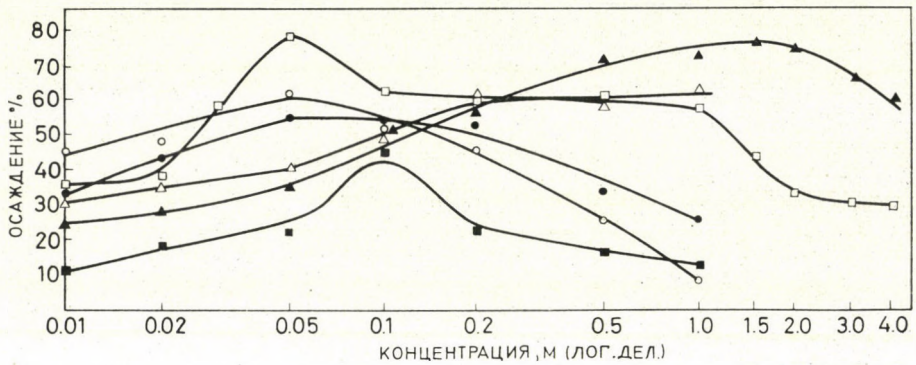

Рис. 1. Зависимость электроосаждения изотопов осмия без носителя от концентрации различных солей. Катод — из проволоки NiCr; ток — 10 мА; время электролиза — 25 мин. ○ NaCl; ● NH_4Cl; □ CH_3COONa; ■ CH_3COONH_4; △ NaF; ▲ NH_4F

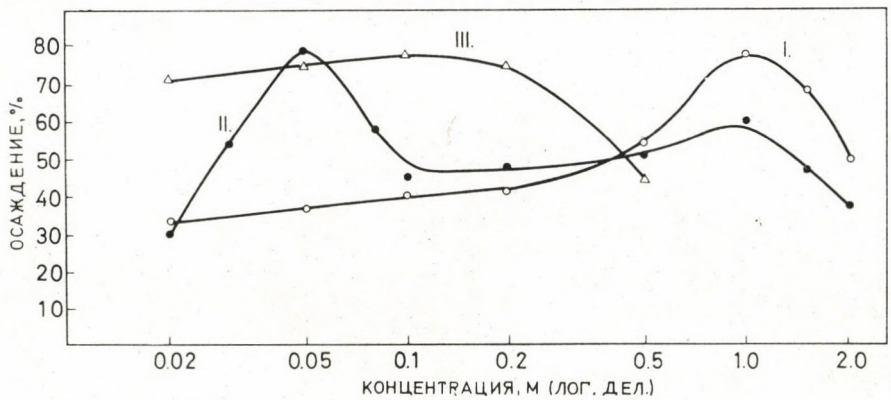

Рис. 2. Зависимость электроосаждения изотопов осмия без носителя от концентраций различных электролитов. Катод — из проволоки NiCr; ток — 10 мА; время электролиза — 25 мин.

лона, а анодом служит тонкая платиновая проволока, расположенная на дне ячейки. Затем опускается катод — проволока толщиной 0,1 мм или фольга шириной 0,4—0,6 мм из сплава NiCr, закрепленная в рамке — до соприкосновения катода с поверхностью раствора, и ведется электролиз при плотности тока ~200 мА/см² в течение 20—30 мин. 65—75% изотопов осмия без носителя осаждается на катод.

Слой осажденных изотопов тонкий; об этом свидетельствует тот факт, что при измерении энергии конверсионных электронов с использованием этих источников разрешение по энергии не превышает более 20% приборного.

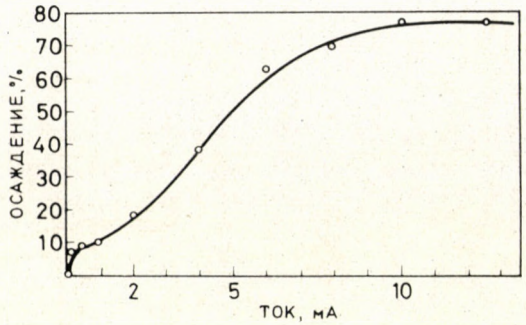

Рис. 3. Зависимость электроосаждения изотопов осмия без носителя от силы тока. Катод — из проволоки NiCr; электролит — 0,05 М CH_3COONa + 1 М CH_3COOH; время электролиза — 25 мин.

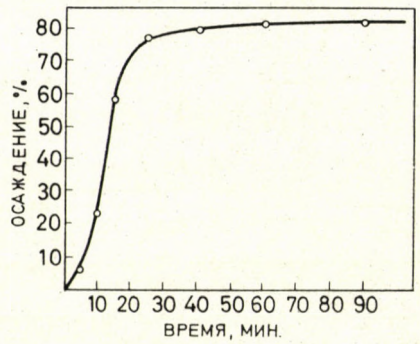

Рис. 4. Зависимость электроосаждения изотопов осмия без носителя от времени электролиза. Катод — из проволоки NiCr; ток — 10 мА; электролит — 0,05 М CH_3COONa + 1 М CH_3COOH

Summary

A new method for the concentration of carrier-free osmium isotopes to a small volume has been developed.

The dependence of the electrolytic precipitation of these isotopes on the composition of the electrolyte, on current density and on the time of electrolysis has been investigated.

On the basis of experimental results, methods have been developed, by means of which radiation sources of osmium isotopes with neutron deficit are prepared for purposes of nuclear spectroscopic measurements.

ЛИТЕРАТУРА

1. Newton, J. O.: Phys. Rev. **117**, 1510 (1960)
2. Беляев, Б. Н., Гудов, В. И., Крижанский, Л. М., Усиков, Б. С.: Ядерная физика т. 7, 4, 720 (1968)
3. Молнар, Й., Молнар Ирэн: Acta Chim. Acad. Sci. Hung. (In press)
4. Новгородов, А. Ф., Кочетков, В. Л., Лебедев, Н. А., Халкин, В. А.: Радиохимия, **6**, 73—78 (1964)

József Molnár
Irén Molnár
Budapest XII., Konkoly Thege M. út

Acta Chimica Academiae Scientiarum Hungaricae, Tomus 68 (3), pp. 253—259 (1971)

APPLICATION OF THE MODIFIED VON BRAUN DEMETHYLATION PROCEDURE, I

GRIGNARD REACTIONS OF AMINOKETONES; PREPARATION OF 3-SUBSTITUTED TROPAN-3-OLS

J. G. FISCHER and Gy. MIKITE

Research Laboratory II, United Works for Pharmaceutical and Dietetic Products, Budapest)

Received August 19, 1969

3-Substituted nortropan-3-ol derivatives have been prepared by reaction of N-ethoxycarbonylnortropinone with Grignard reagents. Such compounds are inaccessible in other ways, *e.g.* by reaction of tropinone with Grignard reagents. The carbamate moiety of the molecule remains intact during reaction with RMgX. Further evidence has been presented for the stereoselectivity of the reaction between tropinone or N-ethoxycarbonylnortropinone and RMgX to give the pure axial-OH stereoisomer.

The dealkylation reaction described by VON BRAUN [1] was modified a few years later. Accordingly, ethyl chloroformate was used instead of cyanogen bromide [2]. This variant of the procedure is considerably more suitable in synthetic work than the original one. Reaction of a tertiary amine (**I**) with ethyl chloroformate (**II**) gives a substituted urethan (**III**), which affords a secondary amine (**IV**) on hydrolysis.

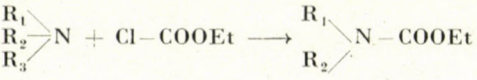

I **II** **III**

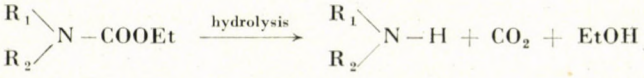

IV

The modified VON BRAUN dealkylation procedure is particularly suitable for the removal of small alkyl groups from nitrogen, *e.g.* for the demethylation of tropane derivatives. According to GADAMER and KNOCH [3] the piperidine, pyrrolidine and tetrahydroquinoline ring-systems are stable towards ethyl chloroformate.

The procedure was also employed in 1966 [4] for the large-scale production of nortropane. Reaction of tropane (**V**) and ethyl chloroformate gave N-ethoxycarbonylnortropane (**VI**) in 90% yield, which on hydrolysis with hydrochloric acid yielded nortropane (**VII**) in almost quantitative yield.

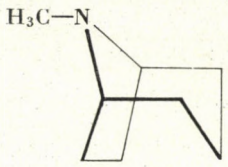

V

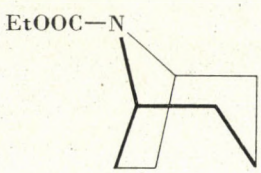

VI

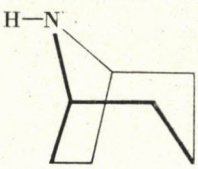

VII

In addition to the high yield (by means of the cyanogen bromide procedure yields as low as 20% could only be achieved [5]), another advantage of the method is that it gives pure product, in which even thin-layer chromatography failed to detect contaminations. Methods based on oxidation afford highly contaminated products only.

In the present work, N-ethoxycarbonylnortropinone (**IX**) was prepared from tropinone (**VIII**), in the course of an examination of the reaction between the latter and Grignard reagent.

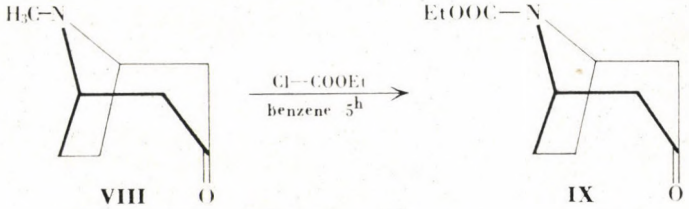

VIII IX

N-Ethoxycarbonylnortropinone reacts with Grignard-reagents and in this way the preparation of a number of 3-substituted N-ethoxycarbonylnortropan-3-ol derivatives (**X**) is possible. In these reactions it could be proved unambiguously that the carbamate moiety of the molecule remained intact, and the Grignard-reagent reacted selectively with the carbonyl group.

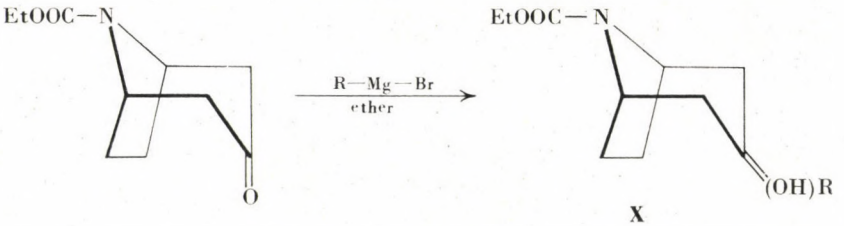

X

The reaction of tropinone with Grignard reagent was examined some twenty years ago by ADAMSON [6]. He treated tropinone with phenylmagnesium bromide to obtain 3-phenyltropan-3-ol, but the yield was poor and the steric structure of the product was not reported. The same compound was

prepared in better yield by COPE and D'ADDIECO, using phenyllithium instead of phenylmagnesium bromide. The product had a characteristic sharp melting point [7]. On the basis of infrared spectroscopic evidence, ARCHER stated in 1954 that the steric structure of the product was analogous to that of tropine [8], *i.e.* the hydroxyl group was present in α-orientation. This

Table I

3-Substituted nortropan-3-ols and tropan-3-ols **(XI)**

No.	R	R_1	M.p., °C	B.p. °C	Yield, %	Ref.
1	CH_3	phenyl	161.5—2.5	—	5—10	[6, 7]
2	CH_3	benzyl	140	—	11	—
3	COOEt	benzyl	108—110	—	50	—
4	CH_3	*p*-chlorophenyl	188—191	—	7	—
5	COOEt	CH_3	84— 88	145—8 (6 torr)	32	—
6	COOEt	ethyl	—	101—102 (0.02 torr)	33	—
7	COOEt	propyl	—	124—125 (0.05 torr)	23	—
8	CH_3	ethynyl	162	—	13	[9]
9	CH_3	ethyl	?	?	?	[9]

proved the stereoselectivity of the reaction between tropinone and Grignard reagent, which may be caused, *inter alia*, by steric hindrance.

In 1963, MIČOVIČ [9] treated tropinone with acetylene in the presence of potassium 2-methyl-2-butoxide to obtain 3-ethynyltropan-3-ol in 13% yield. The steric structure of the product was considered analogous to that of tropine, the other isomer could not be isolated. Hydrogenation afforded 3-ethyltropan-3α-ol (*cf.* Table I).

The stereoselectivity of the reaction has raised the question, whether a reduction of the space requirement of the Grignard reagent would permit the formation of the β-isomer, as well. In our experiments tropinone was reacted with methyl- and ethylmagnesium iodide in ether, tetrahydrofuran and xylene. These attempts failed, and unchanged tropinone could be isolated in all cases. Presumably the failure was caused by the formation of a highly insoluble adduct of the Grignard reagent with the tertiary amino group, which prevented the reaction even when a manifold excess of the reagent was used.

In contrast to tropinone, N-ethoxycarbonylnortropinone is not basic, it does not give an adduct with the Grignard reagent, and has proved suitable for the preparation of 3-substituted tropan-3α-ols, which are hardly accessible in other ways, if at all.

Table I shows that, as compared with 3-benzyltropan-3α-ol, 3-benzyl-N-ethoxycarbonylnortropan-3-ol can be prepared in a considerably higher yield, without any change in the carbamate moiety of the molecule. This statement has been unambiguously confirmed by the elemental analyses and the infrared spectroscopic data. 3-Methyl-N-ethoxycarbonylnortropane-3α-ol, a compound related to 3-methyltropan-3α-ol, inaccessible by Grignard reaction, was obtained in good yield.

Like the corresponding 3-substituted tropan-3α-ols, the 3-substituted N-ethoxycarbonylnortropan-3-ols showed sharp melting and boiling points and proved to be stereohomogeneous products.

As far as one accepts that the rarely successful reaction of tropinone with a Grignard reagent gives rise stereoselectively to the pure 3-substituted tropan-3α-ol isomer, one may also presume that the steric orientation of the hydroxyl group is *axial* in our new nortropine derivatives, too. In one case this assumption has been proved preparatively. Namely, the reaction of 3-benzyltropine (**XII**) with ethyl chloroformate and that of ethoxycarbonylnortropinone with benzylmagnesium chloride afforded the same product (**XIII**).

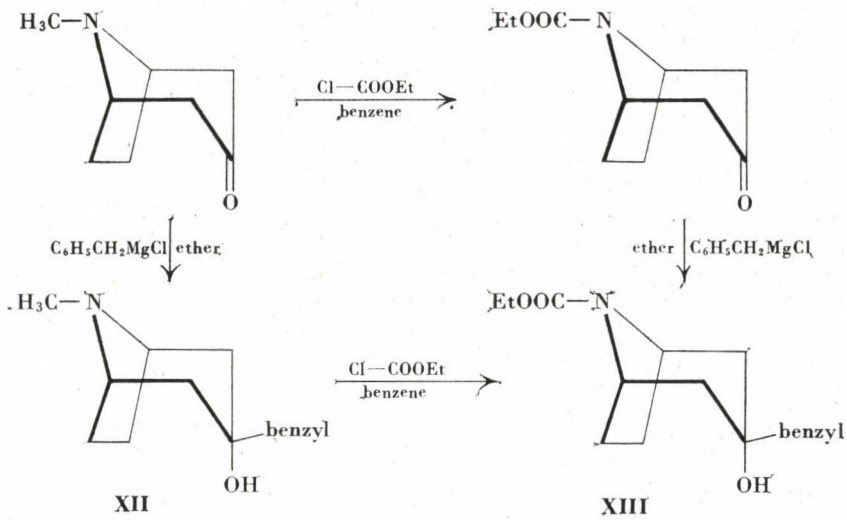

XII **XIII**

Attempt was made in every case to isolate the other stereoisomeric product containing the hydroxyl group in *equatorial* position, but it never succeeded. The amount of tropinone or N-ethoxycarbonylnortropinone recovered also suggested that this isomer did not form at all. Therefore, the reactions of tropinone and N-ethoxycarbonylnortropinone with Grignard reagents appear to be stereoselective. Thin-layer chromatographic analysis also indicated that the isolated tertiary alcohols were homogeneous products.

Experimental

N-Ethoxycarbonylnortropinone (IX)

A solution of 570 ml of ethyl chloroformate in 350 ml of benzene was added dropwise with stirring during 2 hrs. to a boiling solution of 278 g (2.0 moles) of tropinone in 350 ml of abs. benzene, and the mixture was refluxed for a further 3—4 hrs., when tropinone methochloride began to deposit (20—30 g). The solution was washed with 100 ml of 10% acetic acid and 200 ml of water, dried over anhydrous Na_2SO_4 and evaporated in vacuum. Fractional distillation of the residue (388 g) gave 320 g (82%) of **IX**, $b_{2\cdot 0}$ 118—122 °C.

$C_{10}H_{15}NO_3$ (197.24). Calcd. C 60.89; H 7.67; N 7.10. Found C 60.95; H 7.72; N 7.05%.

3-Benzyltropine (XII; *cf.* Table I, No. 2)

A solution of 90.0 g (0.65 mole) tropinone in 200 ml of abs. ether was added dropwise with stirring and cooling to a Grignard reagent prepared as usual from 19.0 g (0.78 mole) Mg turnings and 90.0 ml (0.77 mole) benzyl chloride in 280 ml of abs. ether. A voluminous precipitate deposited immediately. The mixture was refluxed for 2 hrs. with stirring, cooled and filtered. Decomposition of the organometallic halide was effected by adding a solution of 80 g Na_2CO_3 in 600 ml of water with stirring in about 1 hr. at room temperature. The obtained inorganic precipitate was removed by filtration, and the filtrate extracted with chloroform. The organic phase was dried and evaporated in vacuum and the residue fractionated to give 50.0 g of tropinone at 85 °C and 5 mm. The residue was treated with acetone to give white crystals, which were collected and washed with acetone. The crude product (16.0 g; 11%) melted at 140 °C. Recrystallization from petroleum ether did not raise the m.p. Thin-layer chromatographic analysis (adsorbent: Kieselgel GF_{254}; solvent: benzene–ethanol–25% NH_4OH (80 : 20 : 1); visualization with $KMnO_4$ in conc. H_2SO_4 or in UV light) revealed the presence of one substance only, R_f 0.09.

$C_{15}H_{21}NO$ (231.34). Calcd. C 77.88; H 9.15; N 6.06. Found C 77.35; H. 9.24; N 5.95%. The HCl salt melted at 195—196 °C (deposited in acetone); the HBr salt melted at 181—184 °C (deposited in acetone); the infrared spectrum of the HBr salt had the following characteristic absorption bands:

νC—O(H):	1047 cm^{-1}
νO—H:	3180 cm^{-1}
γC—C:	708 cm^{-1} (monosubstituted aromatic out-of-plane bending band)

The picrate was precipitated from alcohol and it melted at 159—161 °C; the methiodide (from acetone) had m.p. 222—224 °C.

The O-acetyl derivative was prepared by refluxing 3-benzyltropine hydrochloride with acetyl chloride for 5 hrs. to give 3-benzyl-3-acetoxytropane hydrochloride, from which the base was liberated as usual, m.p. 109—111 °C.

$C_{17}H_{23}NO_2$ (273.38). Calcd. C 74.69; H 8.84; N 5.12. Found C 74.65; H 8.24; N 5.35%. The infrared spectrum had the following characteristic absorption bands:

νC—O(Ac):	1045 cm^{-1}
νC=O:	1710 cm^{-1} (ketone)
γC—C:	705 cm^{-1} (*cf.* above)

The hydrochloride melted at 240 °C (from chloroform–petroleum ether); the methiodide was precipitated from acetone, m.p. 222—223 °C.

3-(p-Chlorophenyl)tropine (*cf.* Table I, No. 4)

A Grignard reagent prepared from 46.5 g (0.25 mole) of *p*-chlorobromobenzene and 6.1 g (0.25 mole) of magnesium turnings in 150 ml of abs. ether in the usual way was reacted with 10 g (0.07 mole) of tropinone just as in the case of 3-benzyltropine. The distillation residue was treated with petroleum ether to precipitate the product (1.2 g; 7%), m.p. 188—191 °C.

$C_{14}H_{18}ClNO$ (251.76). Calcd. C 66.79; H 7.21; N 5.56; Cl 14.08. Found C 66.51; H 7.08; N 5.35; Cl 13.65%.

N-Ethoxycarbonyl-3-benzylnortropine (XIII; *cf.* Table I, No. 3)

A Grignard reagent prepared from 63.5 ml of benzyl chloride and 15 g magnesium in 450 ml of abs. ether was added to a refluxing solution of 98.5 g (0.50 mole) of N-ethoxycarbonylnortropinone in 250 ml of abs. ether. The heterogeneous, white mixture was refluxed for 2 hrs. and allowed to stand overnight. The mixture was filtered, the filtrate treated with a solution of 90 g ammonium chloride in 500 ml of water, and then extracted with chloroform. The organic phase was dried, the solvent removed, and the residue heated in vacuum to distil out 9.0 g of the starting material at 110 °C and 1 mm. The residue was mixed with 30 ml of acetone to obtain 55.0 g white, crystalline product m.p. 109—110 °C. A further 12.0 g of the product with the same m.p. could be isolated from the mother liquor, corresponding to 47% overall yield. Thin-layer chromatography, under conditions identical with those described for **XII**, showed the product homogeneous, R_f 0.67.

$C_{17}H_{23}NO_3$ (289.38). Calcd. C 70.56; H 8.01; N 4.64%. Found C 70.56; H 8.31; N 4.62%. The data of elemental analysis exclude the possibility of the following two carboxamide structures:

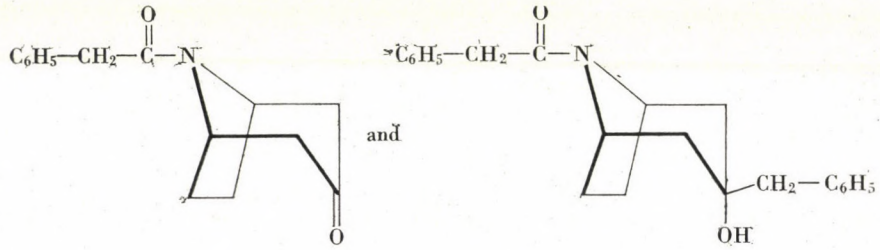

The infrared spectrum contained the following characteristic absorption bands:

νC—O(H):	1050 cm^{-1}
νC=O:	1675 cm^{-1} (urethan)
γC—C:	705 cm^{-1} (*cf.* above)

N-Ethoxycarbonyl-3-alkylnortropines

XI; where R_1 = methyl, ethyl, propyl, *cf.* Table I, Nos 5, 6, 7)

These compounds were prepared similarly to N-ethoxycarbonyl-3-benzylnortropine. Their physical constants and the yields of preparation are summarized in Table I.

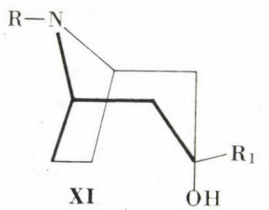

XI

The 3-ethyl and 3-propyl derivatives are pale yellow oils, while N-ethoxycarbonyl-3-methylnortropine crystallized after distillation. After crystallization from petroleum ether it had m.p. 83—87 °C.

*

The authors are indebted to the United Works for Pharmaceutical and Dietetic Products for financial support of this work, to Dr. J. RÁKÓCZI, C. Sc. for discussions, and to Dr. L. BUDA for the microanalyses and IR spectra.

REFERENCES

1. VON BRAUN, J.: Ber. **33,** 1438 (1900)
2. DRP 255, 942, Farbf. Bayer; Frdl. **11,** 115 (1911)
3. GADAMER, J., KNOCH, F.: Archiv der Pharmazie **259,** 135 (1921)
4. Neth. Application 6,510.033 (1966); Chem. Abstr. **65,** 3846 (1966)
5. VON BRAUN, J.: Ber. **44,** 1259 (1911)
6. ADAMSON, D. W.: Brit. Pat. 644,115 (1950)
7. COPE, A., D'ADDIECO, A. A.: J. Am. Chem. Soc. **73,** 3419 (1951)
8. ARCHER, S., LEWIS, T. R.: Chem. and Ind. **1954** 853
9. MIČOVIČ, V. M., MLADENOVIČ, S., STEFANOVIČ, M.: Glasnik Him. Drustva, **28,** 285 (1963)

János FISCHER
Gyula MIKITE } Budapest X., Kereszturi út 30—38.

Acta Chimica Academiae Scientiarum Hungaricae, Tomus 68 (3), pp. 261—266 (1971)

APPLICATION OF THE MODIFIED VON BRAUN DEMETHYLATION PROCEDURE, II

A NEW METHOD OF PREPARATION OF NORTROPINONE

J. G. FISCHER and Gy. MIKITE

(Research Laboratory II, United Works for Pharmaceutical and Dietetic Products, Budapest)

Received August 19, 1969

Nortropinone was prepared from tropinone in high yield by a modified von Braun demethylation procedure. In the first step tropinone was converted to its ethylene ketal, then this protected derivative reacted with ethyl chloroformate to give nortropinone ethylene ketal, and finally the protecting group was removed in almost quantitative yield by hydrolysis with 10% hydrochloric acid. The cyclic ketals of tropinone and nortropinone are stable, in contrast to the parent compounds.

Nortropinone was first synthesized by WILLSTÄTTER [1] in 1896. The procedure consisted of the following steps: oxidation of tropine (**I**) with alkaline permanganate gave nortropine in 50% yield, which was converted to nortropine carbamate (**II**) with carbon dioxide, and isolated in this form. Chromic acid oxidation of **II** afforded nortropinone (**III**), a material unstable to air; it was hygroscopic and absorbed carbon dioxide. The yield of this final step was not given.

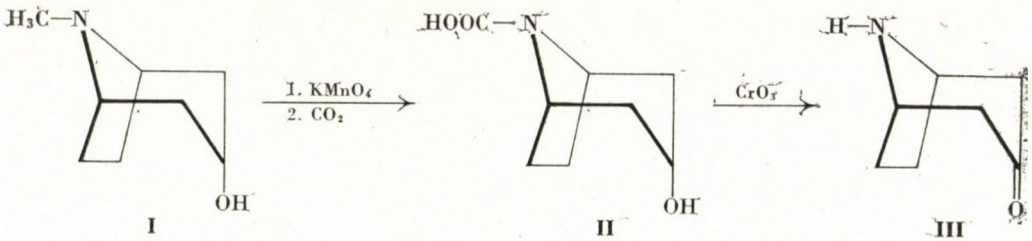

I II III

In 1927 POLONOWSKI [2] oxidized tropinone (**IV**) with 30% hydrogen peroxide to tropinone oxide (**V**), which on treatment with acetic anhydride at 0 °C afforded acetylnortropinone (**VI**) in poor yield. Acid hydrolysis of **VI** gave nortropinone hydrochloride, m.p. 201 °C, identical with that reported by WILLSTÄTTER.

A new and different approach was reported by Japanese researchers (SHIMIZU and UCHIMARU) in 1961 [3]. This procedure consisted of a Robinson—Schöpf condensation with the modification that ammonium chloride was employed instead of methylamine. The yield was 45%.

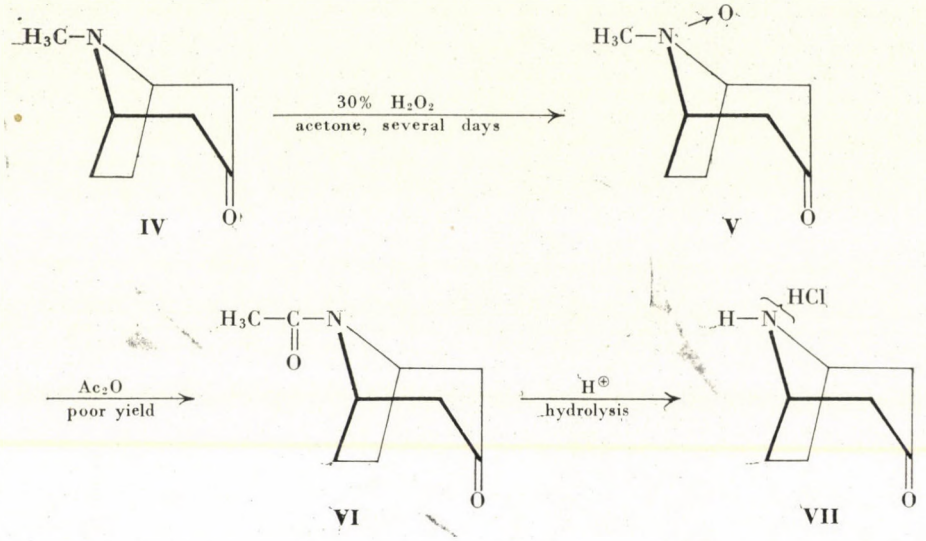

In the present work the modified von Braun demethylation procedure using ethyl chloroformate was employed, which has been found by us [4] and others [5] very suitable for the preparation of nortropane and its derivatives. In the first series of experiments the hydrolysis of N-ethoxycarbonylnortropinone (**VIII**) was attempted according to the reaction scheme:

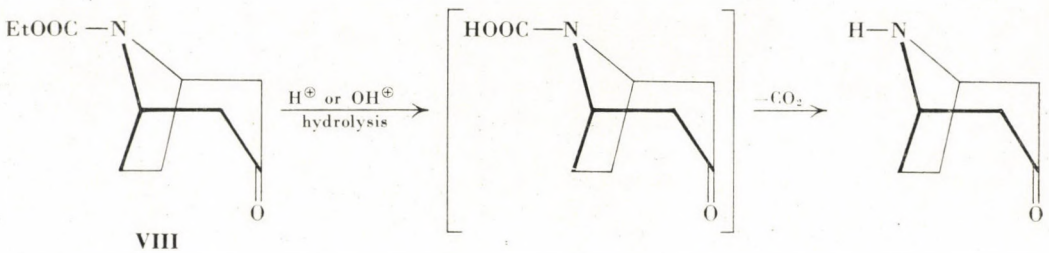

However, this approach failed to give satisfactory results, since the starting material decomposed under the conditions of both acidic and alkaline hydrolysis. Therefore, in the next series of experiments the carbonyl group was protected by means of transformation to a cyclic ketal. Such protected derivatives may easily be prepared by reaction of the corresponding oxo compound, *e.g.* tropinone, with various diols, such as ethylene glycol, glycerol, or 1,3-propanediol. The cyclic ketals prepared by us are listed in Table I. However, the cyclic ethylene ketal of N-ethoxycarbonyl-nortropinone (**XII**) could not be prepared from **VIII** (this was only possible by starting with tropinone

and using reversed order of the reacting steps). The ketal formation is shown by the scheme:

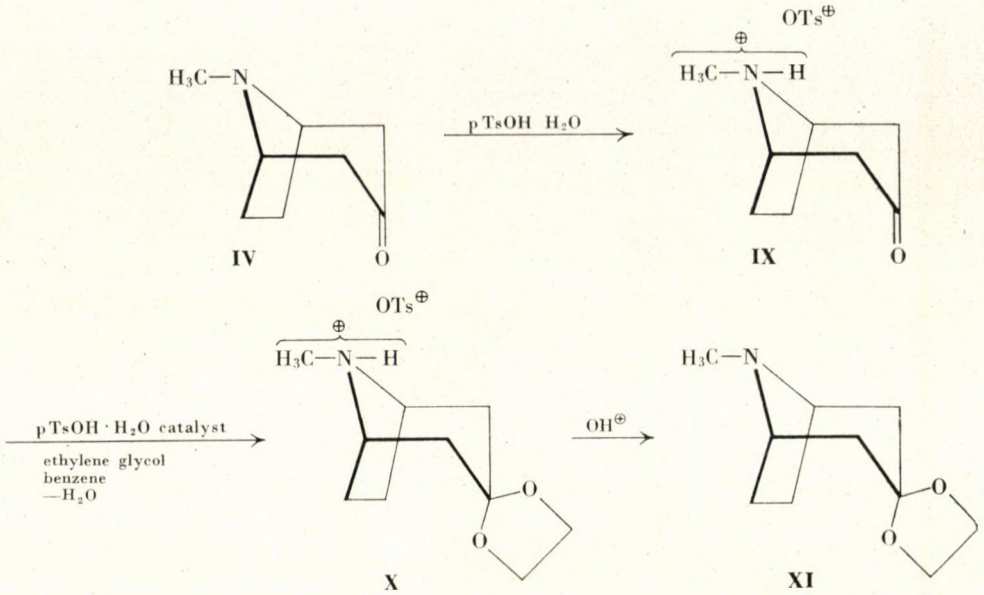

Accordingly, tropinone was converted to the *p*-toluenesulfonate salt with excess toluenesulfonic acid monohydrate, the excess being taken to act as acid catalyst in the next step. The reaction with ethylene glycol was performed in benzene solution by continuous removal of the water formed by azeotropic distillation. In this way tropinone ethylene ketal (**XI**) was obtained in 80% yield. Isolation of tropinone ethylene ketal (**XI**) in pure form, free of tropinone contaminations, necessitated the isolation of the tropinone ethylene ketal tosylate salt (**X**) intermediary product and its purification to remove any tropinone tosylate salt (**IX**). This purification can simply be effected by washing with acetone. Omission of this step resulted in each case in a contamination of the product (**XI**) by tropinone, as the two compounds could not be completely separated by fractional distillation.

Failure of the ketal forming reaction of N-ethoxycarbonylnortropinone is presumably due to solubility factors. Ethylene glycol and benzene give a heterogeneous system. Tropinone tosylate partially dissolves in ethylene glycol, while N-ethoxycarbonylnortropinone accumulates in the benzene phase and is out of contact with ethylene glycol.

In the next step, tropinone ethylene ketal was transformed with ethyl chloroformate to N-ethoxycarbonylnortropinone ethylene ketal (**XIII**). Alkaline hydrolysis of **XIII** in ethanol at elevated temperature yielded nortropinone ethylene ketal (**XIV**), which was hydrolyzed with 10% hydrochloric

acid in the concluding step of the reaction sequence to give the desired nortropinone in form of its hydrochloride salt.

The following scheme shows the reaction sequence with indication of the yields:

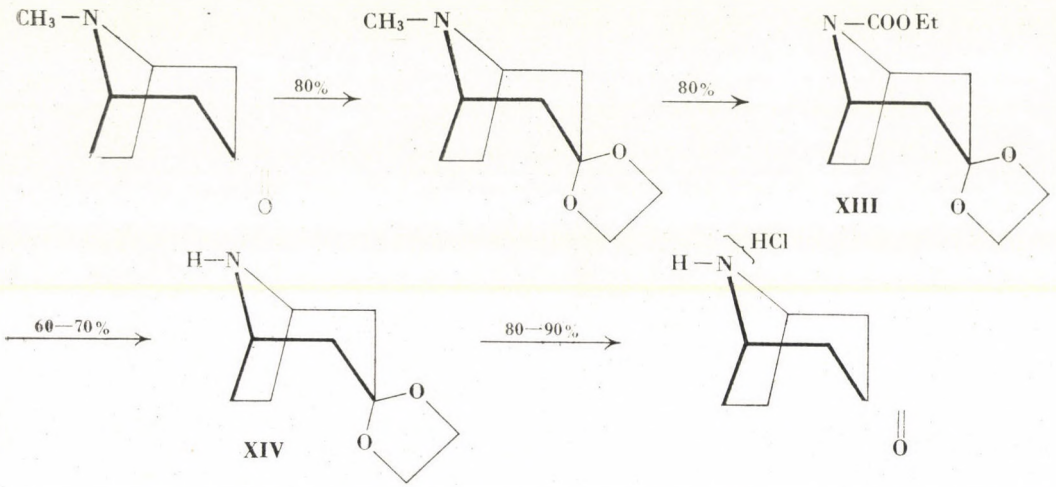

Other cyclic ketals prepared in this work are listed in Table I. These were obtained similarly to the ethylene ketal derivative. Tropinone glycerol ketal prepared by this method was found to be a mixture of two isomers. No attempt has been made to separate the isomers.

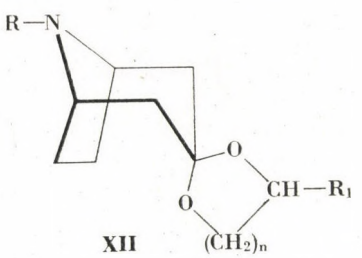

XII

Experimental

Tropinone ethylene ketal (XI; *cf.* Table I, No. 1)

349.3 g (1.84 moles) of p-toluenesulfonic acid monohydrate was added with stirring and cooling to a solution of 234.0 g (1.68 moles) of tropinone in 1 l of benzene. Subsequently 104.5 g (95 ml; 1.68 moles) of ethylene glycol was added and the mixture heated with stirring (bath temperature 120—130 °C) for 10—12 hrs. with continuous removal, by azeotropic distillation of the water formed (65—70 ml). The mixture was then allowed to cool, the crystals which deposited were collected by filtration, suspended in 1 l of acetone, stirred 1 hr. at room temperature and filtered. The dry product, tropinone ethylene ketal tosylate salt weighed

545 g (91%), m.p. 168—169 °C. It was dissolved in 11 times its weight of water and treated with an equivalent amount of NaOH solution with cooling. The base liberated was extracted with chloroform, the extract dried over anhydrous magnesium sulfate and the solvent removed in vacuum. The residue was fractionated in vacuum to give 242 g (79%) of tropinone ethylene ketal, b.p. 99—100 °C at 6 torr, a colourless, odourless liquid, stable to air on storage (neither colouration nor decomposition, in contrast to tropinone itself); $n_D^{20} = 1.4920$.

$C_{10}H_{17}NO_2$ (183.25). Calcd. C 65.55; H 9.35; N 7.64. Found C 65.13; H 9.82; N 7.61%.

The infrared spectrum possessed no $\nu C{=}O$ band, accordingly the product was free even of traces of tropinone. The following derivatives were prepared: methiodide (from acetone), m.p. 176—177 °C; tosylate (the intermediary product, *cf.* above), m.p. 168—169 °C; hydrochloride (from chloroform), m.p. 237—239 °C; picrate (from ethanol), m.p. 199—201 °C.

Table I

Cyclic ketals of tropinone **(XII)**

No.	R	R_1	n	B.p., °C/torr	M.p., °C
1	CH_3	H	1	99—100/6	—
2	COOEt	H	1	105—106/0.2	61
3	CH_3	CH_2OH	1	118—120/1	—
4	COOEt	$CH_2O{-}C{-}Ph$	1	199—202/0.08	88—90
5	CH_3	H	2	128—130/7	—
6	COOEt	H	2	122—123/2	—
7	H	H	1	118—122/5	—
8	H	H	2	97—101/4	—

Tropinone 1,3-propylene ketal (*cf.* Table I, No. 5)

139 g (1 mole) of tropinone was treated with 209 g of *p*-toluenesulfonic acid monohydrate in 500 ml of benzene as above, and the salt solution was heated with 91 g (86 ml) of 1,3-propanediol with stirring and heating for 10 hrs., until about 40 ml of water collected in the separator. The benzene was evaporated in vacuum, the residue treated with 50 g of NaOH, the free base extracted with chloroform, and the extract worked up as in the preceding case to give 85 g (44%) of the product, b.p. 128—130 °C at 7 torr; $n_D^{20} = 1.4972$.

$C_{11}H_{19}NO_2$ (197.28). Calcd. C 66.97; H 9.71; N 7.10. Found C 66.53; H 9.69; N 7.15%. The hydrochloride melted at 201—202 °C, the tosylate at 109—111 °C (from acetone).

Tropinone glycerol ketal (*cf.* Table I, No. 3)

It was prepared similarly to tropinone 1,3-propylene ketal in about 50% yield; the product had b.p. 118—120 °C at 1 torr.

The methotosylate melted at 156—158 °C (from acetone); the benzoate hydrochloride had m.p. 207 °C.

N-Ethoxycarbonylnortropinone ethylene ketal (XIII) (*cf.* Table I, No. 2)

100.0 g (0.55 mole) of tropinone ethylene ketal was dissolved in 130 ml of abs. benzene, a solution of 156 ml of ethyl chloroformate in 120 ml of benzene was added dropwise with stirring at reflux temperature, and the reaction mixture was stirred and refluxed until gas evolution (CH_3Cl) ceased. After standing overnight at room temperature, the mixture was filtered, the filtrate washed with three 40 ml portions of 10% aqueous acetic acid and two 40 ml portions of water, and dried. The solvent was removed in vacuum and the residue fractionated to give 105 g (80%) of the product, b.p. 105—106 °C at 0.2 torr. The distillate solidified on standing, m.p. 61 °C.

$C_{12}H_{19}NO_4$ (241.29). Calcd. C 59.75; H 7.89; N 5.90. Found C 60.06; H 7.76; N 6.05%.

N-Ethoxycarbonylnortropinone 1,3-propylene ketal (*cf.* Table I, No. 6)

It was prepared similarly to **XIII** in 60% yield; colourless liquid, b.p. 122—132° C at 2 torr.

N-Ethoxycarbonylnortropinone glycerol ketal benzoate (*cf.* Table I, No. 4)

Tropinone glycerol ketal benzoate was liberated from its hydrochloride salt and reacted with ethyl chloroformate as above. The product was obtained in 65% yield, b.p. 199—200 °C at 0.08 torr.

$C_{20}H_{25}NO_6$ (375.43). Calcd. C 63.99; H 6.71; N 3.73. Found C 63.99; H 7.10; N 3.50%.

Nortropinone 1,3-propylene ketal (*cf.* Table I, No. 8)

26.8 g (0.105 mole) of N-ethoxycarbonylnortropinone 1,3-propylene ketal was treated with a solution of 22.4 g (0.40 mole) of potassium hydroxide in 100 ml of ethanol at room temperature, and the mixture was subsequently refluxed for 7 hrs. After cooling 5.7 g of potassium carbonate was separated by filtration. The filtrate was neutralized to pH 6 with 1 : 3 hydrochloric acid, and the solvent removed in vacuo. The residue was treated with 80 ml of 10% NaOH solution and the free base extracted with three 100 ml portions of chloroform. The organic phase was dried over anhydrous sodium sulfate and evaporated. The residue (28.0 g) was fractionated in vacuum to give 12.1 g (63%) of the product, b.p. 97—101 °C at 4 torr. The fumarate salt had m.p. 192—193 °C (from ethanol).

$C_{11}H_{21}NO_6$ (299.33). Calcd. C 56.18; H 7.07; N 4.68%. Found C 55.90; H 7.42; N 4.59%.

Nortropinone ethylene ketal (XIV; *cf.* Table I, No. 7)

It was prepared similarly to the 1,3-propylene ketal (*cf.* preceding compound) but obtainable in higher yield; b.p. 118—122 °C at 5 torr. The hydrochloride salt was precipitated from chloroform–ether, m.p. 196—198 °C; the fumarate salt was prepared in ethanol, m.p. 194—196 °C.

$C_{13}H_{19}NO_6$ (285.30). C 54.73; H 6.71; N 4.91. Found C 54.94; H 7.02; N 5.13%.

Nortropinone hydrochloride (VII)

1.0 g (0.005 mole) of nortropinone ethylene ketal hydrochloride was treated with 20 ml of 12% HCl and kept at 85 °C for 1 hr. The solution was concentrated in vacuum to give a yellow oil, which crystallized on trituration with acetone. The crystals were filtered off at 0 °C, washed with acetone and dried to give a white crystalline product, m.p. 199—201 °C (lit. m.p. 201 °C [1]).

The infrared spectrum contained a $\nu C{=}O$ (ketone) band at 1725 cm^{-1} (no such band was detected in the starting material). Mixed m.p. with nortropinone ethylene ketal hydrochloride: 153—158 °C.

*

The authors are indebted to the United Works for Pharmaceutical and Dietetic Products for financial support of this work, to Dr. J. RÁKÓCZI, C. Sc. for his valuable comments, and to Dr. L. BUDA for the microanalyses.

REFERENCES

1. WILLSTÄTTER, R.: Ber. **29,** 1581 (1896)
2. POLONOVSKI, MA., POLONOVSKI MI.: Bull. Soc. chim. France **41,** 1190 (1927); Chem. Abstr. **22,** 429 (1928)
3. SHIMIZU, M., UCHIMARU, F.: Chem. and Pharm. Bull. (Tokyo) **9,** 300 (1961); Chem. Abstr. **56,** 10092 (1962)
4. FISCHER, J. G., MIKITE, GY.: Acta Chim. Acad. Sci. Hung. **68,** 253 (1971)
5. Neth. Application 6,510,033 (1966); Chem. Abstr. **65,** 3846 (1966)

János FISCHER
Gyula MIKITE } Budapest X., Kereszturi út 30—38.

Acta Chimica Academiae Scientiarum Hungaricae, Tomus 68 (3), pp. 267—276 (1971)

THERMAL DISSOCIATION OF UREA DERIVATIVES, I

Z. Csűrös, R. Soós, I. Bitter and Z. Bende

(Institute of Organic Chemical Technology, Technical University, Budapest)

Received January 9, 1970, revised June 25, 1970

The thermal dissociation of diphenylurea and its symmetrically substituted derivatives was studied in solvents of the aliphatic carboxylic acid and alcohol type. The decomposition was found to be a first order reaction in perchloric acid containing acetic acid or cyclohexanol; the formation of the activated complex takes place by means of intermolecular protonation. In cyclohexanol as solvent, consecutive reactions producing urethane should also be considered. The authors give the exact solution of the rate equation providing a useful guide for further investigations.

Introduction

In the production of aromatic isocyanates the formation of diarylureas is an inevitable side reaction. Even a high excess of phosgene cannot prevent the reaction of the primary product, carbamic acid chloride — in fact, isocyanate obtained from it by loss of hydrochloric acid — with the amine present, producing diarylureas. This process should be minimized, since diarylureas can be converted to isocyanate only very slowly even under vigorous conditions.

According to the literature data, treatment of N,N′-diarylureas with phosgene results in the formation of two moles of isocyanate and two moles of hydrochloric acid [1]. As demonstrated by the experiments carried out by Eckenroth [2], the reaction of N,N′-diphenylurea with phosgene takes place only at temperatures higher than 150 °C, *i.e.* after dissociation of the urea to aniline and phenylisocyanate; thus aniline and phosgene are the two compounds actually involved in the reaction.

$$C_6H_5-NH-CO-NH-C_6H_5 \rightleftharpoons C_6H_5NCO + C_6H_5NH_2$$

$$C_6H_5NH_2 + COCl_2 \rightleftharpoons C_6H_5NCO + 2HCl$$

The fact that on heating substituted arylureas decompose to isocyanate and amine is supported by several papers [3, 4]. Bennett [5] observed the formation of phenylisocyanate and obtained aniline hydrochloride in nearly quantitative yield on cooling the evaporated diphenylurea in the presence

of gaseous hydrochloric acid (this prevents recombination of the decomposition products). The experiments reported by IWAKURA [6] also prove the existence of two different decomposition products; the heating of di-*p*-phenethylureas in aliphatic alcohols results in the formation of the corresponding urethane, while the same procedure in acetic anhydride produces phenacetine, proving the formation of aniline.

Thus, the contribution of thermal dissociation to the process seems to be proved, however, the assumption of no direct reaction between arylureas and phosgene should yet be verified. First of all, the mechanism of the thermal dissociation should be elucidated, since the literature data regarding this subject are scarce and rather contradictory.

HOSHINO [7] and ELLINGTON [8] *et al.* studied the kinetics of dissociation in aliphatic fatty acids. In their opinion the activated complex is formed via tautomerism and subsequent proton migration.

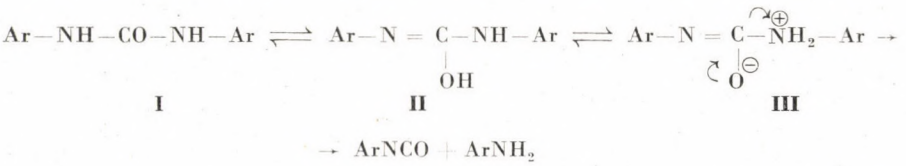

I **II** **III**

In carboxylic acid type solvents, recombination of the dissociated products cannot take place because of the formation of anilides in reactions with the isocyanate, and salt formation by the aniline:

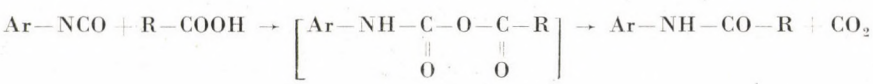

The formation of activated complex (**III**) seems likely, since — with one or more phenyl groups attached to the nitrogen atom — a conjugated system can develop, resulting in an increased strength of the bonds in the activated complex.

Tautomerism involves an intramolecular proton exchange, thus the basicity of nitrogen atoms in urea is the most important factor with respect to the occurrence of the reaction. According to the experiments carried out by ELLINGTON *et al.*, the activation energy of N,N′-dimethylurea is higher than that of N,N′-diphenylurea. This is evident in view of the resonance effect of the phenyl group in the tautomer formed from diphenylurea, accounting for the easier proton transfer in this case than in dimethylurea having a more basic nature; the more stable transition complex has a more pronounced promoting effect on the reaction. The activation energy of N,N′-dimethylurea is considerably lower than that of the corresponding symmetrical compound

and somewhat lower than that of N,N′-diphenylurea. Since here one of the nitrogens is a weaker, the other a stronger nucleophilic character than that observed in the symmetrical urea, in this case proton migration takes place more easily. On the other hand, the comparison of the activation energies with that of diphenylurea indicates overcompensation of the resonance effect, promoting the formation of tautomer (**II**) by easier proton uptake by the more basic nitrogen atom.

The authors' purpose was to investigate whether or not the explanation of the decomposition process in acidic solvents by intramolecular proton migration is acceptable.

$$R-COOH + Ar-NH-CO-NH-Ar \rightarrow R-C\overset{\ominus}{O}O + Ar-NH-\overset{\oplus}{C}=O + Ar-NH_2 \rightarrow$$
$$\xrightarrow{-H^{\oplus}} Ar-NCO + Ar-NH_2$$

Though HOSHINO [9] refers to the possibility of a reaction scheme involving general acid catalysis. MUKAIYAMA [10], studying the dissociation of various alkylureas in acids of different strength, found the sequence of the rate constants inconsistent with that of the acidities, thus the concept of general acid catalysis cannot be accepted. According to the latter author in view of the experimental conditions ensuring a minimum carboxylic acid to urea ratio of 50 : 1, the existence of an intermediate containing two carboxylic acid and one urea molecule can reasonably be assumed. One of the acid molecules behaves as a proton donor, the other being a proton acceptor:

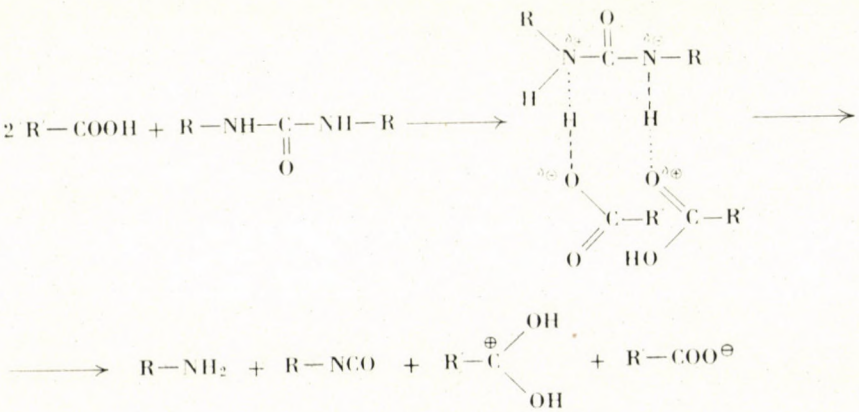

This concept is more or less applicable for interpretation of the solvent effect, though the low and high values of rate constants measured in benzoic acid and phenylacetic acid, respectively, can hardly be due to the slight difference in acidity between the two acids or to the greater space requirement

of the benzoic acid molecule. Also MUKAIYAMA suggested that the basicities of the nitrogen atoms in urea should be responsible for the substituent effect, which is thus governed by the proton acceptor and proton donor abilities of the nitrogens.

In our experimental work, the dissociation of symmetrically substituted diaryl ureas was investigated. In this case the nucleophilicity of the nitrogen atoms is identical, thus a kinetic study can decide whether protonation or deprotonation is the rate-determining process in the decomposition. Our experiments were carried out in solvents of the fatty acid and alcohol type in order to evaluate both of the above described mechanisms.

Experimental in acid solvent

A nearly identical method was used by all authors to follow the decomposition process in fatty acids, *viz.* the amount of carbon dioxide evolved in the reaction of the acid with the isocyanate formed was measured volumetrically or by a gravimetric method, determining the amount of barium carbonate precipitated after bubbling the gas through a barium hydroxide solution [7, 8, 9]. We found it easier to follow the reaction by measurement of the quantity of amine present, therefore a standardized perchloric acid solution in glacial acetic acid was used, in which the amine forms a perchlorate salt. The excess acid was back-titrated with tributylamine in benzene solution [11].

Upon plotting the logarithm of the actual concentration of urea as a function of time, a straight line was obtained in each case, its slope being independent of the initial concentration of urea and perchloric acid. This is consistent with the literature data, confirming the first order character of the dissociation process in acetic acid.

The results are summarized in Table I.

Strikingly, the value of the activation energy calculated from the measured data for diphenylurea is significantly lower than that reported by HOSHINO (36.2 kcal/mole). This can easily be understood when considering the stronger proton donor character of glacial acetic containing perchloric acid, with unchanged proton acceptor properties as compared to glacial acetic acid itself, thus the energetic conditions are more favourable for the formation of the activated complex. The insignificant differences in the rate constant indicate complete absence of acid catalytic effects on the dissociation process.

In order to demonstrate the solvent effect, a less acidic solvent — thus having more pronounced proton acceptor properties — was used instead of acetic acid. Cyclohexanol was chosen for this purpose. This alcohol has a sufficiently high boiling point, does not undergo decomposition at the temperature of the measurements and does not react with perchloric acid. N,N′-diphenyl-

urea was the only compound investigated in cyclohexanol containing perchloric acid; its decomposition was found to be a first order reaction. Experimental and calculated kinetic data are given in Table II.

Table I

R—NH—CO—NH—R	$C_{o,urea}$ mole/l	$C_{o,HClO_4}$ mole/l	$k \times 10^2$(min^{-1}) 100.0 C°	105.0 °C	108.0 C°	$E^{\ddagger}$ kcal/mole	$\Delta S^{\ddagger}$ e.u.
R = C_6H_5—	0.1852	0.1852	1.55	2.37	3.11	26.4	−1.4
	0.0934	0.1852	1.58	2.40	3.00		
	0.0698	0.1387	1.53	2.44	3.33		
	0.1267	0.1387	1.49	2.18	2.89		
	0.0942	0.0950	1.76	2.40	2.78		
	0.0474	0.0950	1.24	2.20	3.00		
	average of k		1.53	2.33	3.00		
R = p—$CH_3C_6H_4$—	0.1765	0.1765	0.960	1.63	2.09	32.5	13.7
	0.0880	0.1765	0.945	1.58	2.21		
	0.1300	0.1350	0.805	1.40	2.02		
	0.0650	0.1350	0.960	1.61	2.25		
	0.0880	0.0880	0.899	1.72	2.52		
	0.0440	0.0880	0.899	1.62	2.16		
	average of k		0.900	1.60	2.20		
R = p—ClC_6H_4—	0.1682	0.1685	1.65	2.61	3.83	27.0	0.5
	0.0840	0.1685	1.74	2.76	4.16		
	0.1250	0.1253	2.00	2.78	4.08		
	0.0625	0.1253	1.74	3.06	3.60		
	0.0840	0.0850	2.04	2.80	4.41		
	0.0600	0.0850	1.82	2.97	4.00		
	average of k		1.83	2.83	4.01		

The activation energy — contrary to the expectations — shows a slight increase. Though the strength of perchloric acid in cyclohexanol solution is not lower than that in acetic acid, protonation is somewhat restrained because of the greater space requirement of the attacking solvate cation. Also the great difference between the proton acceptor properties becomes levelled owing to the great space requirement of the cyclohexanol molecule. These factors may account for the practically unchanged value of activation energy. On the other hand, the rate of dissociation is lower in cyclohexanol than in acid solvents, though the permittivity of this alcohol is far greater than that of acetic acid. (This fact is also evidence against the concept of acid catalysis.)

Table II

C_0K (mole/l)	C_0, $HClO_4$ (mole/l)	t (°C)	$k \times 10^5$ (min^{-1})	average $t_{1/2}$ (min)	$E^{\ddagger}$ (kcal/mole)	$\Delta S^{\ddagger}$ e.u.
0.1350	0.1330		0.97	72		
0.0885	0.1000		0.92			
0.0715	0.0660	120.5	0.92			
0.1340	0.2660		0.96			
0.1000	0.2050		0.96	72		
0.0702	0.1595		0.945			
0.1240	0.1306		1.38			
0.0953	0.1101		1.33	53	27.5	−3.6
0.0667	0.0689	125.0	1.33			
0.1238	0.2550		1.41			
0.0953	0.1910		1.41	50		
0.0667	0.1350		1.34			
0.1382	0.1385		2.14			
0.1110	0.1020		2.14	32		
0.0728	0.0717	130.0	2.07			
0.1340	0.2660		2.14			
0.1000	0.2050		2.14	33		
0.0700	0.1385		2.18			

This must be due to one fact: in a carboxylic acid the greater number of proton donating molecules provides more frequent possibility for attack on the nitrogen atoms, *i.e.* the rate of proton uptake is higher.

Experiments in alcohol

Of the alcohol type solvents cyclohexanol was chosen; this has been used in the acidic experiments too, thus the comparison of the obtained results can be carried out. In this case the equation of the thermal dissociation of diphenylurea is the following:

$$C_6H_5-NH-CO-NH-C_6H_5 \underset{k_1'}{\overset{k_1}{\rightleftharpoons}} C_6H_5-NH_2 + C_6H_5-NCO \qquad (1)$$

$$C_6H_5-NCO + C_6H_{11}-OH \xrightarrow{k_2} C_6H_5NH-COOC_6H_{11} \qquad (2)$$

We assume that the rate of reaction between cyclohexanol and phenylisocyanate is far higher than that of the decomposition of diphenylurea ($k_2 \gg k_1$); thus reaction (1) is the rate-determining step.

Measurement of the amine formed was intended to be utilized for following the progress of dissociation. This was accomplished by means of titration

with perchloric acid in glacial acetic acid in non-aqueous medium. However, no commonly used indicator could be applied because of the presence of cyclohexanol. KRAUSZ [12] recently reported the use of dyes of the aminoanthraquinone type in non-aqueous titrations. "Cibacet blau F3R", a dispersion dye of the anthraquinone type was tested under the conditions of our experiments. A very sharp colour change from blue to red was obtained (base–acid) and so this indicator was used in the following.

Measurements were carried out at three different temperatures (122 °C, 130 °C and 138 °C) with various initial concentrations; in all the three cases the half-life time was found to *decrease* with decreasing initial concentrations (Table III). This indicates that the assumption of $k_2 \gg k_1$ is incorrect, *i.e.* the accumulation of isocyanate as well as the reverse reaction should be taken into account.

Table III

C_0K (mole/l)	$t_{1/2}$ (min)		
	122.5 °C	130.0 °C	138.0 °C
0.1300	—	155	80
0.1000	240	127	66
0.0900	218	—	—
0.0700	181	100	50
0.0500	150	84	42
0.0400	—	71	—
0.0300	110	59	32
0.0200	92	51	27

The rate equation can be given by the following general formula:

$A \underset{k_1'}{\overset{k_1}{\rightleftharpoons}} B + C$

$B + D \xrightarrow{k_2} E$

$$\frac{dB}{dt} = k_1 A - k_1' BC - k_2 BD$$

$k_2 D = k_2 D_0 = k_2'$
because $D \sim D_0$

A: momentary concentration of diphenylurea (mole/l)

B: momentary concentration of phenylisocyanate (mole/l)

C: momentary concentration of aniline (mole/l)

D: momentary concentration of cyclohexanol (mole/l)

By applying the steady-state principle, the concentration of phenylisocyanate can be expressed from the above equation, if $dB/dt = 0$, then

$$B = \frac{k_1 A}{k_1' C + k_2'}$$

substituting B into the following equation

$$\frac{dC}{dt} = k_1 A - k_1' BC ,$$

we obtain

$$\frac{dC}{dt} = \frac{k_1 k_2' A}{k_1' C + k_2'} .$$

If the decrease of urea concentration is represented by x, then $A = A_0 - x$, $C = x$ and the rate equation can be given as follows:

$$\frac{dC}{dt} = \frac{dx}{dt} = \frac{k_1 k_2' (A_0 - x)}{k_1' x + k_2'} .$$

After separation and integration of the above differential equation the following expression is obtained:

$$\left(A_0 + \frac{k_2'}{k_1'}\right) \ln \frac{A_0}{A_0 - x} - x = \frac{k_1 \cdot k_2'}{k_1'} t$$

From the integrated formula, the half-life time is

$$t_{1/2} = \frac{0.19 \cdot k_1'}{k_1 \cdot k_2'} A_0 + \frac{0.69}{k_1}$$

This relationship implies a decrease of half-life time with decreasing A_0; further on, the intercept of the straight line gives the half-life time of the reaction step with rate constant k_1 in the absence of other reverse reactions.

Supposing the value of k_1'/k_2' to be independent of the initial urea concentration (*i.e.* urea has no catalytic effect on any of the processes), the plot of the half-life time against the initial urea concentration should give a straight line, whose intercept yields the rate constant of thermal dissociation (Fig. 1).

Half-life times corresponding to a dissociation process taking place by means of first order reactions only, can be obtained from this figure. In our case these values — given in the order of increasing temperatures — are the following: 59, 32 and 17 min. The rate constants calculated from these data as well as the k_1'/k_2 values obtained from the intercepts are given in Table IV.

It can be seen that the calculated rate constants and those obtained in cyclohexanol solution of perchloric acid are in excellent agreement, thus the interpretation of the reaction steps is correct. The ratio of the rate constants (k_1'/k_2) for the reactions taking place between phenylisocyanate+aniline and cyclohexanol, respectively, was found to be about 10^3, considered to be correct by analogy with literature data.

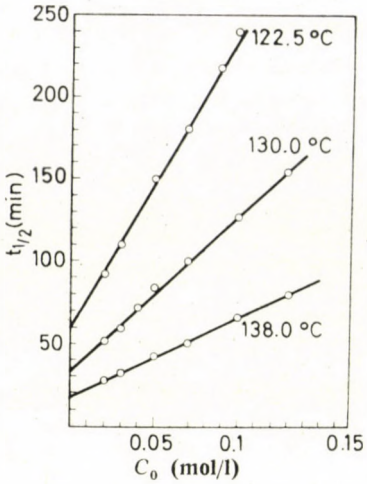

Fig. 1. Dissociation of diphenylurea in cyclohexanol solution; C_0: initial diphenylurea concentration. $t_{1/2}$: half-life time

Table IV

Temperature (°C)	120.5	122.5	125.0	130.0	138.0	$E^{\ddagger}$ (kcal/mole)
k_1 measured (min^{-1})	0.0095	0.0113*	0.0138	0.0214	0.0415*	27.5
k_1 calcd. (min^{-1})	—	0.0117	—	0.0215	0.0405	27.0
k_1'/k_2	—	1040	—	1040	1010	—

* Values calculated on the basis of the activation energy

Discussion

The experiments carried out in glacial acetic acid medium containing perchloric acid indicate that electron donating substituents (*e.g.* CH_3) decrease, while electron withdrawing groups (*e.g.* Cl) increase the rate constant of dissociation. (Investigation of urea derivatives containing nitro groups would be of much value, however, this has failed owing to the inadequate solubilities and analytical problems.) The substituent effects show that in acid solution the rate-determining step is not the intermolecular protonation of the nitrogen atom, but the substantially more hindered process of deprotonation. This is supported also by the rate constant obtained for N,N′-di-(*p*-tolyl)-urea which is the lowest of all values. If the basicities of the nitrogen atoms in urea are compared using the order of the basicity constants of the corresponding anilines, the following order is obtained: N,N′-di-*p*-tolyl- > N,N′-diphenyl- > N,N′-di-(*p*-chlorophenyl)-urea. The differences in basicity seem

to be blurred in the process of protonation, while in deprotonation these appear in a differentiated manner. This does not, however, preclude the possibility of a reverse behaviour in the case of substituents with extremely strong electron withdrawing character (*e.g.* NO_2)

The great differences in activation entropies can be interpreted by the fact that in diphenylurea the original molecule is forced into a coplanar state by conjugation, while in the activated complex an additional degree of freedom appears for internal rotation. The initial existence of this internal rotation is assumed in the di-*p*-tolyl and di-*p*-chlorophenyl derivatives; in the latter case it is due to the hindering effect of chlorine atoms on the conjugation of nitrogens with the rings. Further on, the development of the asymmetric structure of the activated complex is more restrained in the case of conjugation with the phenyl groups, and this fact may be responsible for the higher activation energy values. The observed 'compensation' effect may be due to the looser structure of the activated complex and the resulting higher entropy contribution by internal rotations and vibrations of low frequencies, in the case of higher activation energies.

As for the experiments carried out in alcohol, in the present paper only the possibilities and methods of evaluation were elucidated. Work is in progress to obtain more information on the observed effects.

REFERENCES

1. HENTSCHEL, W.: Ber. **17,** 1284 (1884)
2. ECKENROTH, H., WOLF, H.: Ber. **26,** 1483 (1893)
3. HOFFMANN, A. W.: Ber. **14,** 2725 (1881)
4. HABICH, A., LIMPRICHT, H.: Ann. **159,** 101 (1871)
5. BENNETT, W. B., SANDERS, J. H., HARDY, E. E.: J. Am. Chem. Soc. **75,** 2101 (1956)
6. IWAKURA, J., MAGAHUBO, K.: Bull. Tokyo Instr. Techn. **13/1,** 25 (1948)
7. HOSHINO, T., MUKAIYAMA, T., HOSHINO, H.: J. Am. Chem. Soc. **74,** 3097 (1952)
8. ELLINGTON, M., DANIELS, M., DANIELS, F.: J. Am. Chem. Soc. **79,** 829 (1957)
9. HOSHINO, T., MUKAIYAMA, T., HOSHINO, H.: Bull. Chem. Soc. Japan **25,** 392 (1952)
10. MUKAIYAMA, T., ÔZAKI, S., HOSHINO, T.: Bull. Chem. Soc. Japan **27,** 578 (1954)
11. GYENES, I.: Titrálások nemvizes közegben. Műszaki Könyvkiadó, Budapest, 1960
12. KRAUSZ, I., ENDRŐDI, M.: Magy. Kém. Foly. **73,** 133 (1967)

Zoltán CSŰRÖS
Rudolf SOÓS
István BITTER
Zoltán BENDE

Budapest XI., Műegyetem rkp. 3.

Acta Chimica Academiae Scientiarum Hungaricae, Tomus 68 (3), pp. 277—284 (1971)

PYRIMIDINES AND CONDENSED DERIVATIVES, II*

OXIDATION OF 2-(2-HYDROXYETHYLAMINO)-4(3*H*)-PYRIMIDINONES TO 2,3-DIHYDRO-3-HYDROXY-5(1*H*)-IMIDAZO[1,2-a]PYRIMIDINONES**

Gy. HORNYÁK and K. LEMPERT

(Institute of Organic Chemistry, Technical University, Budapest)

Received April 2, 1970

Oxidation of 2-(2-hydroxyethylamino)-6-methyl-4(3*H*)-pyrimidinone **(3)** by bichromate–sulfuric acid and chromium trioxide–acetic anhydride yields 2,3-dihydro-3-hydroxy-7-methyl-5(1*H*)-imidazo[1,2-a] pyrimidinone **(9)** and its 1-acetyl derivative **(10)**, respectively. On bromination of **3** by NBS, bromine is introduced into position **5**; oxidation of the resulting **6** by the above reagents yields **11** and **12**, the 6-bromo derivatives of **9** and **10**, respectively. **11** and **12** may also be obtained by NBS bromination of **9** and **10**, respectively.

For synthetic purposes larger quantities of *N*-(1,6-dihydro-4-methyl-6-oxo-2-pyrimidinyl)-glycine **(2)** were needed. This compound has previously been obtained by FELD'MAN and CHIH CHUNG-CHI by reacting 6-methyl-2-methylthio-4(3*H*)-pyrimidinone **(1)** in aqueous solution with glycine [3]. Considerable quantities of 6-methyluracil **(7)** are, however, formed owing to the accompanying hydrolysis of **1**, and the separation of the two products proved to be difficult. A possible alternative pathway for the preparation of **2**, oxidation of 2-(2-hydroxyethylamino)-6-methyl-4(3*H*)-pyrimidinone **(3)***** easily

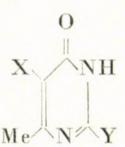

1: X = H, Y = SMe
2: X = H, Y = $NHCH_2COOH$
3: X = H, Y = $NHCH_2CH_2OH$
4: X = H, Y = $NHCH_2CHO$
5: X = Br, Y = SMe
6: X = Br, Y = $NHCH_2CH_2OH$

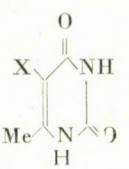

7: X = H
8: X = Br

* Part I: see [1].

** Based on a part of the Dr. Techn. Thesis of GY. HORNYÁK (Technical University, Budapest, 1967). The contents of this paper have been incorporated into a lecture delivered at a Meeting of the Hung. Chem. Soc. [2].

*** For proof of the tautomeric structures of the potentially tautomeric compound **3** and of compounds **5**, **6**, **9** and **11** to be discussed below, see [1].

obtainable by the reaction of **1** and 2-aminoethanol,* was, therefore, investigated.

Oxidation of **3** was attempted by potassium bichromate in sulfuric acid and by chromium trioxide in a mixture of acetic acid and acetic anhydride. As shown by the analytical results of the product, bichromate–sulfuric acid oxidation stops after the elimination of two hydrogen atoms, *i.e.* at the aldehyde stage. Since, according to its UV spectrum, the product (which could be isolated only somewhat circumstantially and in low yields) contained a conjugated double bond system in the pyrimidine ring, structure **4** was attributed to it. On the basis of the IR spectrum, according to which the compound contained but a *single*, *viz.* a lactam carbonyl group (at 1680 cm^{-1}), structure **4** had, however, to be rejected and, instead, the alternative structure **9** had to be accepted. Thus, the NH group of **4**, the primary oxidation product of **3**, was added intramolecularly to the aldehyde group situated favourably for this reaction to occur, and the resulting 2,3-dihydro-3-hydroxy-7-methyl-5(1*H*)-imidazo[1,2-a]pyrimidinone, containing only a masked aldehyde group, became insensitive to oxidation to such an extent that it was not oxidized further even by excess bichromate.

Intramolecular additions of cyclic NH groups to side chain carbonyl groups, leading to the formation of an additional ring, have already been observed (*cf. e. g.*: [4—6]).

Oxidation of **3** by chromium trioxide in a mixture of acetic acid and acetic anhydride led to a similar result. According to the analyses, however, the resulting product (**A**) contained an additional acetyl group as compared with **9**. In agreement with this **9** was obtained by acid hydrolysis of **A**.

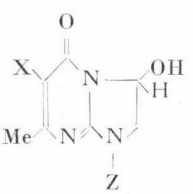

9: X = Z = H
10: X = H; Z = Ac
11: X = Br; Z = H
12: X = Br; Z = Ac

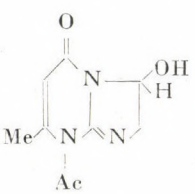

13

The IR spectrum of **A** has two amide I bands, at 1695 and 1680 cm^{-1}, respectively. These values, as well as the νOH band appearing at 3300 cm^{-1} and the *absence* of ester bands in the region 1300 to 1000 cm^{-1} unequivocally disprove **A** to be derived from **9** by acetylation at the hydroxyl group and re-

* This compound has previously been prepared by KAWAI by condensation of ethyl acetoacetate and *N*-(2-hydroxyethyl)-guanidine [14]; this synthesis, however, does not prove the structure of the product unequivocally.

veal it as an *N*-acetyl derivative (**10** or **13**). By the UV spectrum **10** was shown to be the correct structure because the spectrum (see Table I) was found to be very similar to those of the bicyclic *N*(2)-acylisocytosine derivatives **14**—**17** containing the same chromophore and prepared by structure proving syntheses [7, 8].

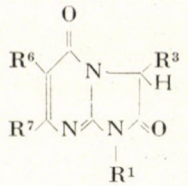

	R^1	R^3	R^6	R^7
14	Me	Me	Et	Me
15	n-Bu	H	H	Me
16	HOC_2H_4-	H	$-(CH_2)_4-$	
17	PhCH —	H	$-(CH_2)_4-$	

The UV spectra of the bicyclic *N*(2)-acylisocytosines are practically identical with those of non-acylated mono- and bicyclic isocytosines containing the same conjugated double bond system as the chromophore; this may be illustrated by the spectral data of compounds **9** and **11** also shown in Table I (for the spectra of numerous other mono- and bicyclic derivatives, see [1]). The similarity of the UV spectra of the acylated and non-acylated types manifests itself also in the values of $\Delta \log \varepsilon$: for the non-acylated mono- and bicyclic isocytosines containing a conjugated double bond system the value of $\Delta \log \varepsilon$ was found to fall between —0.24 and +0.18 [1]. The similarity of the spectra

Table I

UV Spectra of some imidazo[1,2-a]pyrimidines

Compound	Solvent	$\lambda_{max}(\log \varepsilon)$	$\Delta \log \varepsilon$
9	EtOH	226 (4.00); 290 (3.95)	—0.05
11	EtOH	230 (3.94); 304 (3.94)	0
10	EtOH	234 (3.88); 283 (4.00)	+0.12
12	EtOH	244 (3.92); 296 (4.08)	+0.16
14	buffer, pH = 2.1—10.3	239 (4.06); 285 (3.92) [7]	—0.14
15 [8]	EtOH	230 (4.07); 280 (3.94)*	—0.13
16 [8]	EtOH	236 (4.04); 282 (3.90)	—0.14
17 [8]	EtOH	236 (4.00); 282 (3.92)	—0.08

* Shoulder at 242 nm (3.74)

of acylated and non-acylated compounds emphasises our previous statement concerning the comparative insensitiveness of the UV spectra corresponding to the 2-amino-4(3*H*)-pyrimidinone chromophore towards structural variations [1].

Unsuccessful attempts were made to oxidize the hydroxyoxo compounds **9** and **10** to the corresponding dioxo derivatives by various oxidizing agents (manganese dioxide, hydrogen peroxide, *N*-bromosuccinimide). Only as a result of the reactions with NBS could defined products be obtained but, according to their analytical data and IR spectra, these proved to be monobromination products instead of oxidized derivatives.

The bromine atom introduced into **10** by NBS could first of all be proved *not* to be attached to the imidazolidine ring of the product **(B)** obtained, since **B** could also be prepared by the chromium trioxide–acetic anhydride oxidation of compound **C** (obtained from **3** by monobromination with NBS). In order to prove the bromine atom of **C** not to be attached to the hydroxyethylamino side chain, a structure proving synthesis of **C**, starting with **D** (the monobromination product of **1** obtained on bromination with bromine [9] or NBS) and 2-aminoethanol, seemed to be the most simple method. However, **C** could not be aminolyzed either with 2-aminoethanol or with other primary amines. On the other hand, acid hydrolysis of **C**, performed under rather vigorous conditions, furnished an already known [10] bromomethyluracil **(E)**, proving the correctness of our above statement. (On the other hand, acid hydrolysis of **D** also yielded **E**.)

While the transformations discussed in the preceding paragraph prove the bromine atoms of compounds **B**—**E** to be attached to identical positions, they do not prove their actual site of attachment. There are, namely, two active positions (C-5 and the methyl group) in 6-methyluracil **(7)** which might be attacked by bromine or NBS and, although compound **E** obtained on bromination of **7** is supposed [10] to be identical with 5-bromo-6-methyluracil **(8)**, this assumption has not been accurately proved.

In this connection the observation of Austrian authors should be mentioned on the one hand, according to which 3,4-dihydro-6-methyl-2(1*H*)-pyrimidinones are brominated at the methyl group [11] and, on the other, the opposing views concerning the structure of the product obtained by reacting **1** with *N*-chlorosuccinimide [12, 13].

In order to elucidate the problem accurately, the NMR spectrum of **D**, the bromination product of **1**, was examined. Since *two* methyl signals and *no* olefinic proton signal was found, **D** must be identical with **5** and, thus, **B**, **C** and **E** with **12**, **6** and **8**, respectively.*

* After completion of the present study, structure **8** was proved by Japanese authors for **E**, the product obtained on reacting **7** with NBS, by the same technique [15].

9 reacts with NBS similarly to **10**. Structure **11** for the product could be deduced from the observation that the product may also be obtained by acid hydrolysis of **12**.

In order to make possible the elucidation by spectroscopical methods (*cf.* [1]) of the actual tautomeric structures of some potentially tautomeric compounds described in the present paper, several related substances with 'fixed' structures were also prepared; the syntheses are described in Experimental.

Experimental*

2-(2-Hydroxyethylamino)-6-methyl-4(3*H*)-pyrimidinone (3)

A mixture of **1** (5.0 g; 32 mmoles), 2-aminoethanol (2.6 g; 42 mmoles), 2-ammonioethanol chloride (0.2 g) and dry n-propanol (40 ml) was refluxed for 48 hrs to yield, after standing overnight in a refrigerator, 4.7 g (87%) of **3**, colourless crystals, m.p. 204—205 °C (ethanol), lit. [14] m.p.: 204—205 °C.

IR (KBr): νNH + νOH: 3500—2850 with maxima at 3300 and 3100; Amide I: 1635 (broad). UV (ethanol): 224 (4.02); 290 (3.97).

2-(2-Benzylthio)-3,6-dimethyl-4(3*H*)-pyrimidinone

A mixture of 2-benzylthio-6-methyl-4(3*H*)-pyrimidinone [16] (11.6 g; 50 mmoles), potassium hydroxide (2.8 g; 50 mmoles), ethanol (100 ml) and methyl iodide (8.9 g; 63 mmoles) was allowed to stand for 6 hrs at room temperature, subsequently refluxed for 1 hr., and finally evaporated to dryness in vacuum. The oily residue was refluxed for 5 min. with 5% aqueous sodium hydroxide (60 ml) to yield, after being cooled to 0 °C, 9.5 g (77%) of 2-(2-benzylthio)-3,6-dimethyl-4(3*H*)-pyrimidinone, long colourless needles, m.p. 74—75 °C (aqueous acetone).

$C_{13}H_{14}N_2OS$ (246.3). Calcd. N 11.38; S 13.02. Found N 10.98; S 13.01%.

IR (KBr): Amide I: 1695, UV (ethanol): 289 (4.00), the spectral data proving the site of methylation unequivocally (*cf.* [1]).

2-(2-Hydroxyethylamino)-3,6-dimethyl-4(3*H*)-pyrimidinone

(a) A mixture of **3** (4.2 g; 25 mmoles), potassium hydroxide (1.4 g; 25 mmoles), ethanol (30 ml) and methyl iodide (7.1 g; 50 mmoles) was refluxed for 3 hrs. On cooling to room temperature crystals of potassium iodide separated which were filtered off. The mother liquor was allowed to stand overnight in a refrigerator to yield 2.4 g (52%) of 2-(2-hydroxyethylamino)-3,6-dimethyl-4(3*H*)-pyrimidinone; colourless needles, m.p. 186—187 °C (water).

$C_8H_{13}N_3O_2$ (183.2). Calcd. C 52.45; H 7.15; N 22.94. Found C 52.04; H 6.88; N 22.89%.

IR (KBr): νNH + νOH: 3280; Amide I: 1650, UV (ethanol): 228 (3.86), 289 (4.04), the spectral data proving the site of methylation unequivocally (*cf.* [1]).

(b) A mixture of 2-(2-benzylthio)-3,6-dimethyl-4(3*H*)-pyrimidinone (2.5 g; 10 mmoles), 2-aminoethanol (1.3 g; 22 mmoles), 2-ammonioethanol chloride (0.2 g) and dry ethanol (10 ml) was heated in a sealed tube for 15 hrs to 145—150 °C. The resulting solution was evaporated to dryness and the oily residue rubbed with ether (20 ml) to yield 1.1 g (60%) of a substance which by m.p., mixed m.p. and spectra was proved to be identical with the product prepared according to *(a)*.

2,3-Dihydro-1,6-dimethyl-2-thioxo-4(1*H*)-pyrimidinone

To a boiling solution of *N*-methylthiourea (4.5 g; 50 mmoles) in acetic acid (13 ml), diketene (4.3 g; 51 mmoles) was added by drops in about 5 min. After refluxing for further 20 min., water (5 ml) was added by drops. On standing 1 hr. in a refrigerator 2.5 g (32%) of

* M.p.'s are uncorrected.

the desired crystalline product separated, m.p. 268—270 °C (methanol). A m.p. of 235—245 °C (crude product?) is given in the literature [17].

IR (KBr): *v*NH: 3200—2900 with a maximum at 3080; Amide I: 1680. UV (ethanol): 218 (4.22), 270 (4.18); 290 (4.08), sh.

2-(2-Benzylthio)-1,6-dimethyl-4(1*H*)-pyrimidinone

A mixture of 2,3-dihydro-1,6-dimethyl-2-thioxo-4(1*H*)-pyrimidinone (7.8 g; 50 mmoles), dry ethanol (200 ml) in which metallic sodium (1.15 g; 50 mmoles) had previously been dissolved, and benzyl chloride (7.2 g; 57 mmoles) was refluxed for 3 hrs.

The oily residue, obtained on evaporation of the solvent, was rubbed with ether (20 ml) to yield 8.3 g (67%) of 2-(2-benzylthio)-1,6-dimethyl-4(1*H*)-pyrimidinone, colourless crystalline powder, m.p. 146—147 °C (acetone–petroleum ether).

$C_{13}H_{14}N_2OS$ (246.3). Calcd. N 11.38; S 13.02. Found N 11.57; S 12.95%.

IR (KBr): Amide I: 1650, UV (ethanol): 236 (4.46), the spectral data proving the presence of a cross-conjugated chromophore (*cf.* [1]), *i.e.* that the *N*-methyl groups in this and, thus, in the previous compound as well, are attached to N-1.

2-(2-Hydroxyethylamino)-1,6-dimethyl-4(1*H*)-pyrimidinone

A mixture of 2-(2-benzylthio)-1,6-dimethyl-4(1*H*)-pyrimidinone (4.9 g; 20 mmoles), 2-aminoethanol (1.3 g; 22 mmoles), 2-ammonioethanol chloride (0.2 g) and dry ethanol (30 ml) was refluxed for 10 hrs, and the residue, obtained on evaporation of the solvent, was rubbed with cold ether (10 ml) to yield 3.1 g (84%) of 2-(2-hydroxyethylamino)-1,6-dimethyl-4(1*H*)-pyrimidinone; colourless crystalline plates, m.p. 262—263 °C (aqueous acetone).

$C_8H_{13}N_3O_2$ (183.2). Calcd. N 22.94. Found N 22.70%.

IR (KBr): *v*NH + *v*OH: 3500—2800 with a maximum at 3270; Amide I: 1645. UV (ethanol): 213 (4.36); 264 (3.74), the spectral data again proving the presence of a cross-conjugated chromophore, *i.e.* the tautomeric structure of the product (*cf.* [1]).

1-Acetyl-2,3-dihydro-3-hydroxy-7-methyl-5(1*H*)-imidazo[1,2-a]pyrimidinone (10)

A suspension of **3** (4.8 g; 28 mmoles) in acetic acid (20 ml) was prepared and a mixture of chromium trioxide (2 g; 20 mmoles), acetic acid (20 ml) and acetic anhydride (10 ml) was added within about 30 min. by drops. The resulting solution was stirred for 1 hr. at room temperature and evaporated to dryness in vacuum. The greenish crystalline residue was extracted with acetone in a Soxhlet apparatus (about 10 hrs) and the acetonic solution evaporated to dryness in vacuum to give a crystalline residue of 1.3 g (22%) of almost pure **10**; colourless plates (from water), m.p. 190—191 °C.

$C_9H_{11}N_3O_3$ (209.2). Calcd. C 51.67; H 5.30; N 20.09. Found C 51.71; H 5.27; N 20.09%.

IR (KBr): *v*OH: 3300 (broad); Amide I: 1695 and 1680. UV: see Table I.

2,3-Dihydro-3-hydroxy-7-methyl-5(1*H*)-imidazo[1,2-a]pyrimidinone (9)

(a) By deacetylation of **10**: A mixture of **10** (0.2 g; 1 mmole), ethanol (3 ml) and 20% hydrochloric acid (2 ml) was refluxed for 30 min. and evaporated to dryness. The residue was dissolved in water (3 ml) and the solution neutralized by the addition of 5% aqueous sodium hydrogen carbonate solution. After standing for 3 hrs in a refrigerator 0.12 g (72%) of **9** separated gradually; colourless crystalline powder, m.p. 226—227 °C (d.) (from ethanol).

$C_7H_9N_3O_2$ (167.2). Calcd. C 50.30; H 5.43; N 25.14. Found C 50.33; H 5.40; N 25.19%.

IR (KBr): *v*OH + *v*NH: 3400—2400 with a maximum at 3200; Amide I: 1680. UV: see Table I.

(b) By oxidation of **3**: Aqueous sulfuric acid (3.9 ml of H_2SO_4 and 40 ml of water) was added by drops under continuous stirring within 15 min. to a mixture of **3** (4.2 g; 25 mmoles), potassium bichromate (5.3 g; 180 mmoles), acetic acid (2 ml) and water (120 ml), the reaction mixture being meanwhile slowly heated to its b.p. Refluxing was continued for further 30 min. The resulting dark green solution was neutralized with conc. ammonium hydroxide and treated with acetic acid until slightly acidic (pH = 5—6). The aqueous solution was concentrated to

approximately one third of its original volume in vacuum and allowed to cool to yield 2.7 g of a greyish crystalline product decomposing slowly at about 210 °C. A second crop of 2 g impure **9** (contaminated by chromium salts) was obtained by concentration of the mother liquor to half its original volume. By two successive crystallizations from water and ethanol, respectively, 0.4 g (9.7%) of pure **9** was obtained, m.p. 227 °C (d.).

Owing to the necessity of separating **9** from a considerable amount of inorganic salts and the slight solubility differences of **9** and its contaminants in water, method *(b)* cannot be recommended for the preparation of **9**.

5-Bromo-6-methyl-2-methylthio-4(3*H*)-pyrimidinone (5)

1 (1.56 g; 10 mmoles) was dissolved at 40 °C in a mixture of dioxane (30 ml) and water (10 ml). Under continuous stirring powdered *N*-bromosuccinimide (1.78 g; 10 mmoles) was added which dissolved immediately. After a few minutes crystals of **5** started to separate. Precipitation of the product was completed by further stirring for 1 hr. The product (1.4 g; 59%) was a colourless crystalline powder, m.p. 250—252 °C (d.) (from ethanol), lit. [9] m.p.: 255 °C, mixed m.p. with a sample prepared according to literature [9]: 250—252 °C.

IR (KBr): νNH: 3200—2500; Amide I: 1645.

NMR (DMSO-d_6): 2.55δ; 2.40δ (3—3 H).

5-Bromo-2-(2-hydroxyethylamino)-6-methyl-4(3*H*)-pyrimidinone (6)

3 (1.7 g; 10 mmoles) was dissolved in a warm mixture of dioxane (55 ml) and water (15 ml). At 40 °C, under continuous stirring powdered NBS (1.8 g; 10 mmoles) was added which dissolved immediately. The product was isolated as in the case of the previous preparation, the yield being 1.65 g (66%) of colourless crystalline needles, m.p. 236—8 °C (d.) (from water).

$C_7H_{10}BrN_3O_2$ (248.1). Calcd. C 33.90; H 4.06; Br 32.31; N 16.92. Found C 34.21; H 4.08; Br 32.44; N 16.63%.

IR (KBr): νOH + νNH: 3500—2600, with maxima at 3990, 3300, 3150 and 3095; Amide I: 1645. UV (ethanol): 229 (4.04); 304 (4.04).

5-Bromo-6-methyluracil (8)

(a) **5** (2.35 g; 10 mmoles) was refluxed for 10 hrs with 30% sulfuric acid (20 ml) to yield, on cooling, 1.5 g (73%) of **8**, crystalline powder, m.p. 247—249 °C (d.) (from water), lit. m.p.: 247 °C (d.) [10], 270—275 °C [15].

(b) **6** (0.5 g; 2 mmoles) was refluxed for 18 hrs with 30% sulfuric acid (4 ml) to yield, on cooling, 0.35 g (85%) of **8**, m.p. and mixed m.p. with the product obtained according to *(a)*: 247—249 °C (d.) (from water).

1-Acetyl-6-bromo-2,3-dihydro-3-hydroxy-7-methyl-5(1*H*)-imidazo[1,2-a]pyrimidinone (12)

(a) Powdered NBS (1.0 g; 5.5 mmoles) was added under continuous stirring to a solution of **10** (1.0 g; 5 mmoles) in a mixture of dioxane (36 ml) and water (4 ml). Stirring was continued for 1 hr. at room temperature and the solution evaporated to dryness in vacuum. The residue was boiled up with water (25 ml) to obtain 0.98 g (68%) of **12** as an insoluble crystalline residue, needles from ethanol, m.p. 216—217 °C.

IR (KBr): νOH: 3370 (broad); Amide I: 1700 and 1670. UV: see Table I.

(b) To a suspension of **6** (2.5 g; 10 mmoles) in a mixture of acetic acid (15 ml) and acetic anhydride (5 ml) a solution of chromium trioxide (0.7 g; 7 mmoles) in a mixture of acetic acid (30 ml) and acetic anhydride (20 ml) was added by drops at room temperature. Stirring was continued for 1 hr. and the resulting solution evaporated to dryness in vacuum. The crystalline residue was boiled up with water (20 ml) and the mixture allowed to stand overnight to yield 1.1 g (38%) of **12**, m.p. and mixed m.p. with the product prepared according to *(a)*: 216—217 °C (d.) (from ethanol).

6-Bromo-2,3-dihydro-3-hydroxy-7-methyl-5(1*H*)-imidazo-[1,2-a]pyrimidinone (11)

(a) A mixture of **12** (0.5 g; 1.7 mmoles), ethanol and 20% hydrochloric acid (4 ml each) was refluxed for 30 min. and evaporated to dryness in vacuum. The residue was dissolved in water (15 ml) and neutralized with 5% aqueous sodium hydrogen carbonate solution to yield 0.3 g (63%) of **11**, colourless crystalline powder, m.p. 234—236 °C (d.) (from water).

$C_7H_8BrN_3O_2$ (246.1). Calcd. C 34.17; H 3.28; Br 32.48; N 17.08. Found C 34.11; H 3.59; Br 32.58; N 16.93%.

IR (KBr): νNH + νOH: 3500—2600 with a maximum at 3270; Amide I: 1675. UV: see Table I.

(b) NBS (0.45 g; 2.5 mmoles) was added at 40 °C under continuous stirring to a mixture of **9** (0.4 g; 2.4 mmoles), dioxane and water (20 ml each). The NBS dissolved immediately and, after a few minutes, crystallization of the product started. Crystallization was completed by stirring for another hr. and allowing the reaction mixture to stand 2 hrs in a refrigerator to yield 0.42 g (71%) of **11**, m.p. and mixed m.p. with the product prepared according to *(a)*: 234—236 °C (d.) (from water).

IR, UV and NMR spectra were obtained in KBr pellets with an UR 10 spectrometer (Carl Zeiss, Jena), with a Spectromom 201 spectrometer (Magyar Optikai Művek,* Budapest), and at 60 MHz with a JNM—C—60 spectrometer (Japan Electron Optics Laboratory, Tokyo), respectively. The UV spectra have previously been published [18].

*

The authors express their gratitude to Miss K. Ófalvi, Mrs. S. Viszt-Simon and Mrs. I. Zauer-Csüllög for the microanalyses, to Dr. L. Láng and Mr. M. Vörös for the UV and to Dr. P. Sohár for the IR and the NMR spectra.

REFERENCES

1. Á gai, B., Hornyák, Gy., Láng, L., Lempert, K., Sohár, P.: Per. Polytechn. [Budapest], Ser. Chem. Engng., (In press)
2. Ágai, B., Hornyák, Gy., Lempert, K.: Lecture delivered at the Meeting of the Hung. Chem. Soc., Pécs, August 24, 1967
3. Feld'man, I. Kh., Chih Chung-Chi: Zhur. Obshch. Khim. **30,** 3832 (1960); Chem. Abstr. **55,** 21136 (1961)
4. Zondler, H., Pfleiderer, W.: Chem. Ber. **99,** 2984 (1966)
5. Doleschall, G., Hornyák, Gy., Hornyák-Hámori, M., Lempert, K., Wolfner, A.: Acta Chim. Acad. Sci. Hung. **53,** 385 (1967)
6. Singh, H., Singh, S.: Tetrahedron Letters **1970,** 585; *cf.* Alper, H., Alper, A. E.: J. Org. Chem. **35,** 835 (1970); Alper, H.: Chem. Communications **1970,** 383
7. Prokof'ev, M. A., Antonovich, E. G., Shvachkin, Yu. P.: Vestnik. Moskow. Univ. **12,** No. 3, Ser. Mat., Mekh., Astron., Fiz., Khim. No. 3, 199 (1957); Chem. Abstr. **52,** 9145 (1958)
8. Ágai, B., Hornyák, Gy., Lempert, K.: Unpublished results
9. Barrett, H. W., Goodman, J., Dittmer, K.: J. Am. Chem. Soc. **70,** 1753 (1948)
10. Matsukawa, T., Ohta, B.: Yakugaku Zasshi (J. Pharm. Soc. Japan) **70,** 134 (1950); Chem. Abstr. **44,** 5886 (1950)
11. Zigeuner, G., Hamberger, H., Blaschke, H., Sterk, H.: Monatsh. Chem. **97,** 1408 (1966)
12. West, R., Barrett, H. W.: J. Am. Chem. Soc. **76,** 3146 (1954)
13. Carbon, J. A.: J. Org. Chem. **25,** 1731 (1960)
14. Kawai, S.: Sci. Papers Inst. Phys. Chem. Research (Tokyo) **16,** Nos. 306—9, 24 (1931); Chem. Abstr. **25,** 5665 (1931)
15. Sasaki, T., Ando, M.: Bull. Chem. Soc. Japan **41,** 2215 (1968)
16. Dodson, E. R., Peterson, R. M., Seyler, J. K.: J. Am. Chem. Soc. **72,** 3281 (1950)
17. Lacey, R. N.: J. Chem. Soc. [London] **1954,** 831
18. Láng, L. (Ed.): Absorption Spectra in the Ultraviolet and Visible Region, Vols. VII—XIV, Publishing House of the Hungarian Academy of Sciences, Budapest, 1966—1970

Gyula Hornyák
Károly Lempert } Budapest XI., Gellért tér 4.

* Hungarian Optical Works.

INDEX

Printed in Hungary

A kiadásért felel az Akadémiai Kiadó igazgatója — Műszaki szerkesztő: Várhelyi Tamás

A kézirat nyomdába érkezett: 1970. XII. 28. — Terjedelem: 9,75 (A/5) ív, 56 ábra

71.70932 Akadémiai Nyomda, Budapest — Felelős vezető: Bernát György

ACTA CHIMICA

ТОМ 68—ВЫП. 3

РЕЗЮМЕ

Изучение селективности мембранных электродов иодистого серебра

З. ПУХОНЬ, К. ТОТ и Э. ПУНГОР

Изучалась селективность иодистых мембранных электродов в присутствии различных анионов, дающих с серебром либо осадок, либо комплекс, а также различных ионов металлов, образующих комплексы с иодидом. Результаты подтверждают теоретические соображения относительно расчета константы селективности.

Было доказано, что иодо-комплексы металлов ведут себя по отношению к иодистому электроду так же, как и циано-комплексы по отношению к цианидному электроду. Последний вопрос исследуется дальше.

Критическое рассмотрение констант стабильности некоторых комплексов лантанидов с α-гидроксикарбоксильными кислотами

А. ГЕРГЕЙ и И. НАДЬПАЛ

На основе экспериментальных данных из литературных источников с помощью метода приведенных кривых пересматривались критически константы стабильности следующих равновесных систем: Nd(III)-метилпропилгликолят, Yb(III)-изобутилметилгликолят, -изопропилметилгликолят и -диэтилгликолят, Er(III)-α-гидроксициклогексанкардоксилат и Sm(III)-манделат. Заново с помощью метода приведенных кривых выбиралась область кривых образования, подходящая для развития комплексов типа MA. На основе метода наименьших квадратов из данных участков кривых рассчитывалось точное значение констант стабильности и обсуждались критически литературные данные.

Теоретические спектры магнитного резонанса систем типа AA′A″ . . . XX′X″ . . . случай кажущейся простоты

А. РОККЕНБАУЕР и Л. РАДИЧ

Исследованы теоретические спектры магнитного резонанса систем типа AA′A″ . . . XX′X″ . . . = $A_n^+X_m^+$ в предельном случае, когда взаимодействие частиц A между собой является сильным по сравнению со взаимодействием между частицами A и X, а взаимодействием частиц X между собой можно пренебречь (предельный случай сильного взаимодействия). Наши рассчеты применимы для описания как ЯМР, так и ЭПР спектров. Мы изучали условия, ведущие к появлению спектров кажущейся простоты, когда спектры систем $A^+X_m^+$ идентичны со спектрами системы A_nX_m, содержащей магнетически эквивалентные частицы. Было установлено, что системы типа $A^+X_m^+$ обладают спектрами кажущейся простоты только тогда, когда точечная группа симметрии подсистемы A_n^+ является абелевой: в этом случае наблюдается только среднее значение констант взаимодействия I_{AX}. Но когда точечная группа подсистемы A_n^+ не является абелевой, получаются более

сложные спектры из вырожденных уровней подсистемы A_n^+, и такого рода спектры дают дополнительные информации к определению констант взаимодействия I_{AX}.

Мы рассчитали теоретические спектры нескольких сильно взаимодействующих систем $A^+X_m^+$ и дали новую интерпретацию спектров протонного резонанса нескольких фосфоро-азотных соединений.

Отличие между частями A и X в спектрах систем $A_3^+X_3^+$ и $A_4^+X_4^+$ также объясняется тем, что точечная группа симметрии не является абелевой.

Гидрирование оксосоединений, I

Гидрирование и электрогидрирование ацетона в кислых средах. Экспериментальная часть

ДЬ. ХОРАНИ, Ш. САБО, Я. ШОЛТ и Ф. НАДЬ

Изучалось гидрирование и электрогидрирование ацетона в кислых средах (1 *N* $HClO_4$) на платиновом порошке и платинированной платине, соответственно, с помощью волюмометрического, гальвано- и потенциостатического методов. Было установлено, что в изученных экспериментальных условиях продуктом как гидрирования, так и электрогидрирования является пропан.

Исследовались с термодинамической точки зрения условия появления изопропилового спирта в продуктах электрогидрования ацетона.

Было установлено, что при потенциостатических исследованиях уменьшение силы тока, сопровождаемое появлением изопропилового спирта не обязательно следует рассматривать как процесс старения.

Снятие кривых заряда показало, что ацетон не влияет на адсорбцию водорода.

Окисление на окисно-никелевом электроде, III.

Определение скорости окисления электрохимическим методом

ДЬ. ВЕРТЕШ, ДЬ, ХОРАНИ и Ф. НАДЬ

Определялась скорость окисления спиртов на окисно-никелевом электроде. Принимая во внимание то, что между потенциалом электрода и количеством окиси-гидроокиси никеля (III), эффективным с точки зрения окисления, не наблюдается однозначной зависимости, был разработан косвенный метод определения скорости окисления. Метод исходит из следующего основного принципа: при разряжении электрода одновременно с субстратом и с током, определенной силы скорость реакции может быть определена на основе определенных при различных силах тока полных времен разряда — после восстановления всего количества NiOOH.

Было установлено, что скорость окисления этанола на окисно-никелевом электроде пропорциональна количеству окиси-гидроокиси никеля(III), находящемуся в данный момент на электроде.

Изучение адсорбционных явлений на платиновом электроде с помощью метода радиоактивной индикации, VII

Одновременное изучение адсорбции и электрогидрирования фенил-уксусной кислоты

ДЬ. ХОРАНИ и Ф. НАДЬ

1. При электрогидрировании фенилуксусной кислоты измерялись одновременно скорость гидрирования и адсорбция субстрата.

2. Было установлено, что между покрытием и скоростью — согласно ожиданиям — существует соответствующая зависимость — пропорциональность.

Использование модифицированного деметилирования по фон Брауну, I

Гриньяровская реакция аминокетонов, получение тропан-3-олов замещенных в положении 3

Й. Г. ФИШЕР и ДЬ. МИКИТЕ

Получение 2-этоксикарбонил-нортропинона позволяло синтезировать с помощью реакции Гриньяра соединения тропан-3-ола, замещенные в положении 3, которые не могут быть синтезированы другим путем, например, реакцией Гриньяра, исходя из тропинона. Было установлено, что карбаминокислая эфирная часть молекулы не изменяется во время реакции. Были получены новые результаты относительно гриньяровской реакции тропинона и N-этоксикарбонил-нортропинона, а именно была установлена ее стереоспецифичность. Гидроксильная группа в продукте реакции занимает аксиальное простанственное расположение.

Использование модифицированного деметилирования по фон Брауну, II

Новый способ получения нортропинона

Й. Г. ФИШЕР и ДЬ. МИКИТЕ

Из тропинона с хорошим выходом был получен нортропинон через этиленкеталь тропинона. Из последнего получался этиленкеталь нортропинона на основе модифицированного деметилирования по фон Брауну. При кислом гидролизе (10%-ая HCl) почти с количественным выходом образуется нортропинон. Циклические кетали тропинона и нортропинона, в отличии от основных соединений, являются совершенно стабильными.

Термическая диссоциация карбамидов, I

З. ЧЮРЁШ, Р. ШОШ, И. БИТТЕР и З. БЕНДЕ

Изучалась термическая диссоциация дифенилкарбамида и его симметрично замещенных производных в растворителях типа алифатических карбоновых кислот и спиртов. Было установлено, что в хлорной кислоте с добавками уксусной кислоты и циклогексанола разложение представляет собой процесс первого порядка, и промежуточный комплекс образуется за счет межмолекулярного присоединения протона, в то время как в циклогексаноле необходимо также считаться и с последовательной реакцией образования уретана. Точное решение уравнения скорости является основой для дальнейших исследований.

Примидины и их конденсированные производные, II

Окисление 2-(2-гидроксиэтиламино)-4(3*H*)-пиримидинонов до 2,3-дигидро-3-гидрокси-5(1*H*)-имидазо [1,2-а] пиримидинонов

ДЬ. ХОРНЯК и К. ЛЕМПЕРТ

Окисление 2-(2-гидроксиэтиламино)-6-метил-4(3*H*)-пиримидинона (3) бихроматом в серной кислоте или трехокисью хрома в уксусном ангидриде приводит к образованию 2,3-дигидро-3-гидрокси-7-метил-5(1*H*)-имидазо [1,2-а]-пирамидинона (9) или его 1-ацетилпроизводному (10), соответственно. Соединение 3 бромируется в положении 5 с помощью N-бромсукцинимида. Окисление продукта этой реакции с помощью вышеупомянутых реагентов приводит к образованию 6-бромзамещенных 9 или 10, соответственно (11 и 12, соответственно). Соединения 11 и 12 могут быть также получены бромированием 9 и 10 с помощью N-бромсукцинимида.

The Acta Chimica publish papers on chemistry in English, German, French and Russian.

The Acta Chimica appear in volumes consisting of four parts of varying size, 4 volumes being published a year.

Manuscripts should be addressed to

Acta Chimica
Budapest 112/91 Műegyetem

Correspondence with the editors should be sent to the same address.

The rate of subscription is $ 16.00 a volume.

Orders may be placed with "*Kultúra*" Foreign Trade Company for Books and Newspapers (Budapest I., Fő utca 32. Account No. 43-790-057-181) or with representatives abroad.

Les Acta Chimica paraissent en français, allemand, anglais et russe et publient des mémoires du domaine des sciences chimiques.

Les Acta Chimica sont publiés sous forme de fascicules. Quatre fascicules seront réunis en un volume (4 volumes par an).

On est prié d'envoyer les manuscrits destinés à la rédaction à l'adresse suivante:

Acta Chimica
Budapest 112/91 Műegyetem

Toute correspondance doit être envoyée à cette même adresse.

Le prix de l'abonnement est de $ 16.00 par volume.

On peut s'abonner à l'Entreprise pour le Commerce Extérieur de Livres et Journaux «*Kultúra*» (Budapest I., Fő utca 32. Compte-courant No. 43-790-057-181) ou à l'étranger chez tous les représentants ou dépositaires.

«*Acta Chimica*» издают трактаты из области химической науки на русском, французском, английском и немецком языках.

«*Acta Chimica*» выходят отдельными выпусками разного объема. 4 выпуска составляют один том. 4 тома публикуются в год.

Предназначенные для публикации рукописи следует направлять по адресу:

Acta Chimica
Budapest 112/91 Műegyetem

По этому же адресу направлять всякую корреспонденцию для редакции.

Подписная цена — $ 16.00 за том.

Заказы принимает предприятие по внешней торговле книг и газет «*Kultúra*» (Budapest I., Fő utca 32. Текущий счет № 43-790-057-181) или его заграничные представительства и уполномоченные.

Reviews of the Hungarian Academy of Sciences are obtainable at the following addresses:

ALBANIA

Drejtorija Qëndrone e Përhapjes dhe Propagandimit të Librit
Kruga Konferenca e Pazes
Tirana

AUSTRALIA

A. Keesing
Box 4886, GPO
Sydney

AUSTRIA

GLOBUS
Höchstädtplatz 3
A — 1200 Wien XX

BELGIUM

Office International de Librairie
30, Avenue Marnix
Bruxelles 5
Du Monde Entier
5, Place St. Jean
Bruxelles

BULGARIA

HEMUS
11 pl Slaveikov
Sofia

CANADA

Pannonia Books
2, Spadina Road
Toronto 4, Ont.

CHINA

Waiwen Shudian
Peking
P. O. B. 88

CZECHOSLOVAKIA

Artia
Ve Směčkách 30
Praha 2
Poštovní Novinová Služba
Dovoz tisku
Vinohradská 46
Praha 2
Mad'arská Kultura
Václavské nám. 2
Praha 1
SLOVART A. G.
Gorkého
Bratislava

DENMARK

Ejnar Munksgaard
Nörregade 6
Copenhagen

NLAND

Akateeminen Kirjakauppa
Keskuskatu 2
Helsinki

FRANCE

Office International de Documentation e t Librairie
48 rue Gay Lussac
Paris 5

GERMAN DEMOCRATIC REPUBLIC

Deutscher Buch-Export und Import
Leninstraße 16
Leipzig 701
Zeitungsvertriebsam.
Fruchtstraße 3—4
1004 Berlin

GERMAN FEDERAL REPUBLIC

Kunst und Wissen
Erich Bieber
Postfach 46
7 Stuttgart S.

GREAT BRITAIN

Blackwell's Periodicals
Oxenford House
Magdalen Street
Oxford
Collet's Subscription Import Department
Dennington Estate
Wellingborough, Northants.
Robert Maxwell and Co. Ltd.
4 — 5 Fitzroy Square
London W. 1

HOLLAND

Swetz and Zeitlinger
Keizersgracht 471—487
Amsterdam C.
Martinus Nijho
Lange Voorhout 9
The Hague

INDIA

Hind Book House
66 Babar Road
New Delhi 1

ITALY

Santo Vanasia
Via M. Macchi 71
Milano
Libreria Commissionaria Sansoni
Via La Marmora 45
Firenze

JAPAN

Kinokuniya Book-Store Co. Ltd.
826 Tsunohazu 1-chome
Shinjuku-ku
Tokyo
Maruzen and Co. Ltd.
P. O. Box 605
Tokyo-Central

KOREA

Chulpanmul
Phenjan

NORWAY

Tanum-Cammermeyer
Karl Johansgt 41 — 43
Oslo 1

POLAND

RUCH
ul. Wronja 23
Warszawa

ROUMANIA

Cartimex
Str. Aristide Briand 14—18
Bucureşti

SOVIET UNION

Mezhdunarodnaya Kniga
Moscow G—200

SWEDEN

Almquist and Wiksell
Gamla Brogatan 26
S—101 20 Stockholm

USA

F. W. Faxon Co. Inc.
15 Southwest Park
Westwood Mass. 02090
Stechert Hafner Inc.
31. East 10th Street
New York, N. Y. 10003

VIETNAM

Xunhasaba
19, Tran Quoc Toan
Hanoi

YUGOSLAVIA

Forum
Vojvode Mišića broj 1
Novi Sad
Jugoslovenska Knjiga
Terazije 27
Beograd

10. VI. 1971

Index: 26.007

ACTA CHIMICA

ACADEMIAE SCIENTIARUM HUNGARICAE

TOMUS 68 FASCICULUS 4

AKADÉMIAI KIADÓ, BUDAPEST

1971

ACTA CHIM. ACAD. SCI. HUNG.

ACTA CHIMICA

A MAGYAR TUDOMÁNYOS AKADÉMIA KÉMIAI TUDOMÁNYOK OSZTÁLYÁNAK IDEGEN NYELVŰ KÖZLEMÉNYEI

SZERKESZTI

LENGYEL BÉLA

TECHNIKAI SZERKESZTŐK

DEÁK GYULA és HARASZTHY-PAPP MELINDA

Az Acta Chimica német, angol, francia és orosz nyelven közöl értekezéseket a kémia tudományok köréből.

Az Acta Chimica változó terjedelmű füzetekben jelenik meg, egy-egy kötet négy füzetből áll. Évente átlag négy kötet jelenik meg.

A közlésre szánt kéziratok a szerkesztőség címére (Budapest 112/91 Műegyetem) küldendők.

Ugyanerre a címre küldendő minden szerkesztőségi levelezés. A szerkesztőség kéziratokat nem ad vissza.

Megrendelhető a belföld számára az „Akadémiai Kiadó"-nál (Budapest V., Alkotmány utca 21. Bankszámla 05-915-111-46), a külföld számára pedig a „Kultúra" Könyv- és Hírlap Külkereskedelmi Vállalatnál (Budapest I., Fő utca 32. Bankszámla: 43-790-057-181) vagy annak külföldi képviseleteinél és bizományosainál.

Die Acta Chimica veröffentlichen Abhandlungen aus dem Bereiche der chemischen Wissenschaften in deutscher, englischer, französischer und russischer Sprache.

Die Acta Chimica erscheinen in Heften wechselnden Umfanges. Vier Hefte bilden einen Band. Jährlich erscheinen 4 Bände.

Die zur Veröffentlichung bestimmten Manuskripte sind an folgende Adresse zu senden:

Acta Chimica
Budapest 112/91 Műegyetem

An die gleiche Anschrift ist auch jede für die Redaktion bestimmte Korrespondenz zu richten. Abonnementspreis pro Band: $16.00.

Bestellbar bei dem Buch- und Zeitungs-Außenhandels-Unternehmen »*Kultúra*« (Budapest I., Fő utca 32. Bankkonto No. 43-790-057-181) oder bei seinen Auslandsvertretungen und Kommissionären.

Acta Chimica Academiae Scientiarum Hungaricae, Tomus 68 (4), pp. 285—296 (1971)

EQUILIBRIA OF α-AMINO-ACID COMPLEXES OF TRANSITION METAL IONS, IV

STABILITY CONSTANTS, ENTHALPY AND ENTROPY CHANGES OF THE ALANINE, PHENYLALANINE AND TYROSINE COMPLEXES

A. GERGELY, I. NAGYPÁL and B. KIRÁLY

(Institute of Inorganic and Analytical Chemistry, L. Kossuth University, Debrecen)

Received January 1, 1970

The stability constants of the phenylalanine and tyrosine complexes of the $3d^5$—$3d^{10}$ transition metal ions have been determined pH-metrically at 20, 25, 30 and 35 °C. It was found that in these systems the value of log K_1/K_2 is always smaller than for the corresponding alanine complexes.

The values of the formational enthalpy of the $3d^6$—$3d^{10}$ transition metal ion complexes with alanine, phenylalanine and tyrosine have been determined both from the temperature dependence of the stability constants and calorimetrically. The data obtained with these two independent methods agree within 0.2—1.0 Kcal/mole.

The sum of ΔH_1 and ΔH_2 for the Co(II), Ni(II) and Zn(II) phenylalanine and tyrosine complexes is in general smaller than for the corresponding alanine complexes. At times, however, the difference in ΔH_2 and ΔH_1 for the former complexes is comparatively larger than for the alanine complexes. This is more pronounced for the tyrosine complexes than for the phenylalanine chelates. It was concluded from the experimental data that in the aromatic amino-acid complexes the stability is determined partly by back-coordination. This phenomenon is more pronounced for tyrosine complexes.

The primary factor determining the stability of the Cu(II) complexes of the aromatic amino acids is the Jahn–Teller effect.

Introduction

The equilibrium conditions of transition metal complexes of phenylalanine and tyrosine have been studied by several authors during recent years. From a comparison of the stability constants of the Cu(II)-alanine and Cu(II)-phenylalanine systems, IZATT *et al.* [1] found that the log K_2 values were almost identical. However, the value of log K_1/K_2 was smaller for the phenylalanine complex than for the alanine chelate. This was all the more striking since values of 10.04 and 9.38 were obtained for pK_2 at 20 °C for alanine and phenylalanine, respectively. This experimental observation was explained by back-coordination.

The thermodynamic parameters of the alanine and phenylalanine complexes of Cu(II) and Ni(II) were determined calorimetrically by ANDERSON *et al.* [2—4], under precisely defined conditions. Although the results obtained were very similar to the previous data, no interpretation of this interesting phenomenon was given.

More recently, SIMEON and WEBER [5] carried out equilibrium studies from a consideration of the stereospecific effects of the phenylalanine and ala-

nine ligands. According to ANDERSON *et al.* [2—4] the MA_2 type complexes of phenylalanine are relatively more stable than the corresponding chelates of alanine; SIMEON and WEBER obtained a similar result for Cu(II), but that for Ni(II) did not entirely support the observation.

Apart from the earlier studies relating to the phenylalanine and tyrosine complexes [6] systematic experiments were carried out by SYTCHEV and MIKHAL [7] in addition to the above mentioned authors. For the phenylalanine and tyrosine complexes of Fe(II)—Zn(II) (with the exception of some systems) these authors obtained the result that $K_2 > K_1$. However, they did not interpret this surprising experimental result.

The data of the authors cited above disagree at times. They do draw attention, however, to the fact that the stability determining factors for the aromatic amino-acid complexes may be different from those for aliphatic amino-acid chelates.

Several authors have dealt with the thermodynamic conditions of the $3d^5$—$3d^{10}$ transition metal alanine complexes [1—4, 6, 8, 9]. However, with the exception of the Cu(II) and Ni(II) phenylalanine chelates [2—4], data on formational enthalpies and entropies relating to the transition metal aromatic amino-acid complexes are not available in the literature. The values of the stability constants largely call for a re-examination. Hence, because of the missing equilibrium data, there is no possibility for an interpretation of the factors determining stability.

In an earlier publication [10] we determined pH-metrically the thermodynamic data of the $3d^5$—$3d^{10}$ transition metal alanine complexes. It was shown that if the pH is measured under carefully defined conditions, the enthalpy and entropy changes may be determined with satisfactory accuracy via the stability constants. At the same time the data available in the literature relating to the alanine complexes were critically re-examined.

The aim of this work, in accordance with the above, is the study of the factors determining the stability of the phenylalanine and tyrosine complexes. To this end, the stability constants and formational enthalpy and entropy values of the phenylalanine and tyrosine complexes were determined. The latter were determined both form the temperature dependence of the stability constants and calorimetrically. At the same time a calorimetric study was made on the alanine complexes.

Experimental

Reanal chemicals of p.a. quality were used. Alanine and phenylalanine were purified by recrystallisation from a 1 : 1 mixture of water–ethanol; tyrosine from water. The concentrations of metal chloride solutions were checked gravimetrically. The concentrations of phenylalanine and tyrosine in both pH-metric and calorimetric measurements were 5×10^{-3} M. The ligand to metal ratio in the pH-metric measurements was 3 : 1, and in the calorimetric measurements 2 : 1. Every solution contained 5×10^{-2} M KCl.

For the measurements of pH a Radiometer PHM-4 type apparatus was used. The standardization of the instrument and the measurements were carried out as previously reported [10]. The method of IRVING *et al.* [11] was used to eliminate the error arising from the diffusion potential differences.

The calorimetric measurements were carried out as in a previous publication [12] with the apparatus constructed by us. In the present case, however, the bridge-voltage applied was 2.5 V. Accordingly, one scale division on the galvanometer corresponded to a temperature change of 8×10^{-5} °C.

Calculations

The protonation constants and the formation curves were calculated from the pH-metric titration data in the normal manner. For the calculation of the accurate constants, that $\bar{n}$ region was selected with our curve-reduction method [13, 14], in which the formation of MA_3 and hydrolysis do not play a part. Following this, the constants were calculated applying the least-squares principle [10]. The values of the formational enthalpy were calculated using the van't Hoff equation, likewise with the least-squares principle, via the constants obtained at different temperatures.

The enthalpies of formation were determined from the calorimetric data too by a method reported earlier [12]. The heat change corresponding to hydrogen ion dissociation was obtained in a separate process. From a knowledge of the latter, the hydrogen ion concentration and the stability constants, and hence the concentration changes, ΔH_1 and ΔH_2 could be calculated.

Results and discussion

The formation curves of the phenylalanine and tyrosine complexes at different temperatures may be seen in Figs 1 and 2.

Because of the hydrolysis already occurring at $\bar{n} \sim 0.5$ the studies of the Mn(II) complexes were carried out only at 25 °C. For the Cu(II) complexes the individual formation curves (as may be seen in the Figures) are well separated from each other. However, for the phenylalanine and tyrosine complexes of Co(II), Ni(II) and Zn(II) the changes are smaller. Consequently, only the formation curves obtained at 20 and 35 °C are depicted in the Figures.

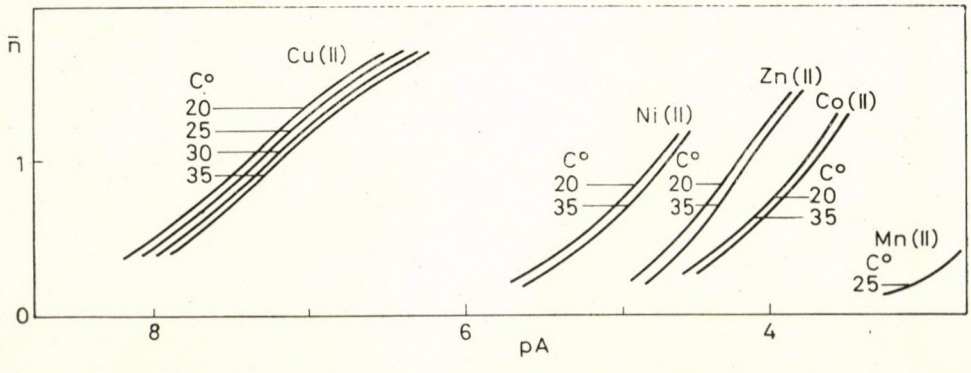

Fig. 1. Formation curves at different temperatures for the Cu(II), Ni(II), Zn(II), Co(II) and Mn(II) phenylalanine systems

The solubilities of the phenylalanine and tyrosine complexes differ substantially from each other. Tyrosine dissolves much more poorly than phenylalanine, but the behaviour of the metal–ligand systems is in contrast to this. Thus, for the Co(II) and Ni(II) phenylalanine systems the MA_2 complexes precipitate at $\bar{n} \sim 1.2$, and for the Cu(II) and Zn(II) phenylalanine systems at $\bar{n} \sim 1.8$. (The separation of a precipitate for the individual complexes begins in the pH range 6—8.5.) At the same time there is no precipitation at all in

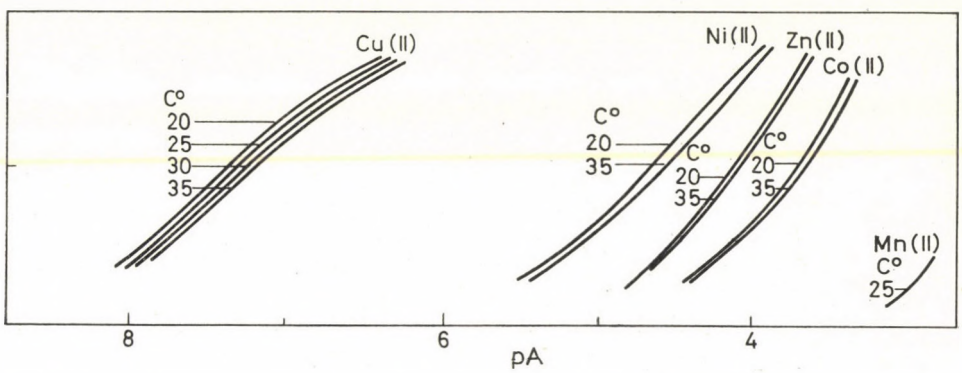

Fig. 2. Formation curves at different temperatures for the Cu(II), Ni(II), Zn(II), Co(II) and Mn(II) tyrosine systems

the pH range studied of the corresponding tyrosine complexes. We shall return to the interpretation of this phenomenon later. It must be noted here, however, that the ensuing change in solubility, mainly for the Co(II) and Zn(II) tyrosine complexes forming at higher pH values, may be connected with the induced dissociation of the phenolic hydroxyl group or with its participation in the complex equilibrium. This suggestion is supported by the fact that, form our calculations with the curve-reduction method, for all the tyrosine complexes we may reckon with the formation of MA_n type complexes in general only up to $\bar{n} = 1.0$—1.5.

The values of the stoichiometric stability constants obtained for the phenylalanine and tyrosine complexes are given in Tables I and II.

The calculated errors in the stability constants in Tables I and II (with the same limitation as already reported [10]) are in general 0.01 log K. This systematic deviation in the same way is present at every temperature. Hence, the accuracy of the enthalpy of formation is determined only by the scatter of log K.

The thermodynamic stability constants obtained as reported [10] for the Ni(II) and Cu(I) phenylalanine systems are given in Table III together with the data of ANDERSON *et al.*

Considering that ANDERSON *et al.* obtained $pK_2 = 9.31$ compared with our 9.26, the difference in the stability constants is 0.02—0.08, a good agreement. Considering also that our results for the alanine complexes agree with the most accurate literature data, all the constants obtained by us for the phenylalanine and tyrosine complexes may qualify as being of sufficient accuracy.

Our own and the literature constants for the phenylalanine and tyrosine complexes are given in Tables IV and V.

Table I

Stoichiometric stability constants of the Mn(II), Co(II), Ni(II), Cu(II) and Zn(II) complexes of phenylalanine at 20, 25, 30 and 35 °C

		20 °C	25 °C	30 °C	35 °C
Phenyl-alanine	pK_2	9.20	9.08	8.97	8.85
	pK_1	2.09	2.09	2.09	2.09
Mn(II)	log K_1	—	2.4	—	—
	log K_2	—	2.3	—	—
Co(II)	log K_1	4.05	4.03	4.03	4.00
	log K_2	3.47	3.44	3.41	3.39
	log K_1/K_2	0.58	0.59	0.62	0.61
Ni(II)	log K_1	5.13	5.11	5.08	5.05
	log K_2	4.36	4.32	4.32	4.27
	log K_1/K_2	0.77	0.79	0.76	0.78
Cu(II)	log K_1	7.90	7.82	7.78	7.73
	log K_2	6.92	6.84	6.74	6.69
	log K_1/K_2	0.98	0.99	1.04	1.04
Zn(II)	log K_1	4.31	4.29	4.28	4.24
	log K_2	4.09	4.06	4.00	4.00
	log K_1/K_2	0.22	0.22	0.28	0.24

The data in Tables IV and V refer to different ionic strengths but it is still possible to evaluate the accuracy of the constants. Considering the different ionic strengths, the data of SIMEON and WEBER for the phenylalanine complexes differ from our own data by 0.2 log K which may be considered fairly good agreement. However, the constants determined by SYTCHEV and MIKHAL [7] at times differ by one order of magnitude from our data. This is more pronounced for the comparison of the stability constants of the tyrosine complexes, but for the Co(II) and Ni(II) phenylalanine systems they also found that $K_2 > K_1$, which for these systems in such an extent has no justification. Since

no such error is involved in the calculation procedure employed, it presumably reflects the experimental error in their data.

In the calorimetric work we measured 8—10 points. In the metal ion–ligand systems the measurement interval was selected, taking into account that

Table II

Stoichiometric stability constants of the Mn(II), Ni(II), Co(II), Cu(II) and Zn(II) complexes of tyrosine at 20, 25, 30 and 35 °C

		20 °C	25 °C	30 °C	35 °C
Tyrosine	pK_3	10.21	10.14	10.01	9.94
	pK_2	9.16	9.05	8.94	8.82
	pK_1	2.12	2.12	2.12	2.12
Mn(II)	log K_1	—	1.5	—	—
	log K_2	—	3.5	—	—
Co(II)	log K_1	3.92	3.93	3.93	3.92
	log K_2	3.48	3.45	3.42	3.38
	log K_1/K_2	0.44	0.48	0.51	0.54
Ni(II)	log K_1	5.03	5.02	4.99	4.97
	log K_2	4.29	4.25	4.23	4.17
	log K_1/K_2	0.74	0.77	0.76	0.80
Cu(II)	log K_1	7.79	7.75	7.71	7.65
	log K_2	6.88	6.82	6.74	6.66
	log K_1/K_2	0.91	0.93	0.97	0.99
Zn(II)	log K_1	4.15	4.16	4.19	4.20
	log K_2	4.13	4.11	4.06	4.01
	log K_1/K_2	0.02	0.05	0.13	0.19

Table III

Thermodynamic stability constants of the Ni(II) and Cu(II) phenylalanine complexes at 25 °C

Metal	log K_1	log K_2	log K_1/K_2	Reference
Ni(II)	5.56	4.66	0.90	[3]
	5.46	4.53	0.93	this work
Cu(II)	8.25	7.13	1.12	[3]
	8.18	7.00	1.18	this work

MA and MA_2 type complexes for the Co(II), Ni(II) and Zn(II)–ligand systems form up to $\bar{n} \sim 1.2$, and for Cu(II) up to 1.5.

From among the calorimetric titration results, the data obtained for the alanine–metal ion systems are given in Table VI.

Table IV

Comparison of pH-metrically determined stability constants of the Co(II), Ni(II), Cu(II) and Zn(II) phenylalanine complexes with literature data

Metal	t °C	Ionic strength (M)	log K_1	log K_2	log K_1/K_2	Ref.
Co(II)	25	0.01	4.00	4.08	−0.08	[9]
	25	0.05	4.02	3.43	0.59	this work
Ni(II)	20	0.37	5.19	4.47	0.72	[8]
	25	0.01	4.73	5.29	−0.56	[9]
	20	0.05	5.13	4.36	0.77	this work
Cu(II)	20	0.37	8.03	7.11	0.92	[8]
	25	0.01	7.38	6.86	0.52	[9]
	20	0.05	7.90	6.91	0.99	this work
Zn(II)	20	0.37	4.41	4.09	0.32	[8]
	25	0.01	4.58	4.45	0.13	[9]
	20	0.05	4.31	4.09	0.22	this work

Table V

Comparison of pH-metrically determined stability constants of the Co(II), Ni(II), Cu(II) and Zn(II) tyrosine complexes with literature data

Metal	t °C	Ionic strength (M)	log K_1	log K_2	log K_1/K_2	Reference
Co(II)	25	0.01	4.1	4.0	0.1	[9]
	25	0.05	3.93	3.45	0.48	this work
Ni(II)	25	0.01	4.9	5.6	−0.7	[9]
	25	0.05	5.02	4.25	0.77	this work
Cu(II)	25	0.01	7.0	7.5	−0.5	[9]
	25	0.05	7.75	6.82	0.93	this work
Zn(II)	25	0.01	4.6	4.7	−0.1	[9]
	25	0.05	4.16	4.11	0.05	this work

Table VI

Calorimetric and pH-metric titration results for the alanine–metal ion systems

$C_{Alanine} = 0.01\ M$

Alanine			Co(II)–alanine			Ni(II)–alanine		Zn(II)–alanine		Cu(II)–alanine		
ml	pH	$-Q$ cal/l	ml	pH	$-Q$ cal/l	pH	$-Q$ cal/l	pH	$-Q$ cal/l	ml	pH	$-Q$ cal/l
1.0	9.287	2.56	0.3	6.665	3.24	5.696	4.00	6.441	2.65	0.4	3.562	8.33
1.5	9.520	2.99	0.6	7.035	3.20	5.952	3.95	6.670	2.69	0.8	3.730	8.11
2.0	9.719	2.82	0.9	7.281	2.73	6.203	3.93	6.904	2.82	1.2	3.931	8.96
2.5	9.898	2.48	1.2	7.492	2.82	6.435	4.01	7.102	2.52	1.6	4.165	7.43
3.0	10.071	2.48	1.5	7.669	2.99	6.636	3.97	7.271	2.99	2.0	4.435	7.34
3.5	10.262	2.44	1.8	7.852	2.73	6.836	4.10	7.434	2.82	2.4	4.737	7.51
4.0	10.480	2.39	2.1	8.019	2.82	7.017	3.84	7.593	2.86	2.8	5.062	6.74
4.5	10.735	2.13	2.4	8.186	3.16	7.212	4.01	7.739	2.90	3.2	5.416	6.74
			2.7	8.361	2.90	7.419	3.97			3.6	5.791	6.87
										4.0	6.299	7.04

With phenylalanine and tyrosine similar results were obtained but the data for the Co(II) and Zn(II) systems were not too accurate. This is explained by the following reasons: because of the poor solubility of these two ligands, we used 0.005 *M* solutions. At the same time, the formation of the complexes is in general accompanied by a smaller heat change than that of the corresponding alanine chelates. Thus, in the alanine titration, for an addition of 0.3 ml of alkali the galvanometer deflection was 18 scale divisions on average, and 32 for Co(II)–alanine. The corresponding values for phenylalanine and Co(II)–phenylalanine were 10 and 14 scale divisions. As the combined error in the measurement and the evaluation was about 2 scale divisions, this means a greater relative error (with a similarly small heat change) for the Co(II) and Zn(II) complexes of phenylalanine and tyrosine. For the Ni(II) and Cu(II) phenylalanine and tyrosine complexes, where the same amount of added alkali gave an average galvanometer deflection of 20 or 36 scale divisions, naturally the measurement is substantially more accurate.

The satisfactory accuracy of the enthalpy changes calculated *via* the constants determined at different temperatures for the alanine complexes has already been proved [10]. The available literature data for the Ni(II) and Cu(II) phenylalanine systems are given in Table VII together with our own results. The data in Table VII determined by ANDERSON *et al.* refer to zero ionic strength. Since the error given by the authors for the individual complex formation processes is $\pm$ (0.2—0.8) Kcal/mole, the agreement with our values appears satisfactory.

The enthalpy and entropy changes of the Co(II), Ni(II), Cu(II) and Zn(II) complexes of alanine, phenylalanine and tyrosine are given in Table VIII, together with the data calculated calorimetrically and on the basis of the temperature dependence of the stability constants.

From the data in Table VIII it may be concluded that the enthalpy changes for the Ni(II) and Cu(II) phenylalanine and tyrosine complexes obtained by the two methods agree well with each other. In the distribution of the heat

Table VII

Enthalpies and entropies of formation of the Ni(II) and Cu(II) phenylalanine complexes

Ni(II) phenylalanine

Method	$-\Delta H_1$ Kcal/mole	$-\Delta H_2$ Kcal/mole	ΔS_1 e. u.	ΔS_2 e. u.	Ref.
calorimetric	3.2	3.3	13.8	10.0	[3]
calorimetric	2.7	1.9	15*	14*	this work
temp. dep. of log K	2.2	2.3	16*	12*	this work

Cu(II) phenylalanine

Method	$-\Delta H_1$	$-\Delta H_2$	ΔS_1	ΔS_2	Ref.
calorimetric	5.3	6.4	19.8	13.7	[2]
calorimetric	4.7	6.9	20*	9*	this work
temp. dep. of log K	4.6	6.4	21*	10*	this work

* calculated from the thermodynamic stability constants

effects between ΔH_1 and ΔH_2, however, at times larger deviations are observed. We have already pointed out one possible cause of this for the calorimetric measurement [12]. For the Co(II) and particularly the Zn(II) phenylalanine and tyrosine complexes there is a more significant deviation between the enthalpy changes obtained by the two methods. As a result of the previously detailed reasons, therefore, we believe the data obtained for the two latter systems from the temperature dependence of the stability constants to be the more suitable. On the basis of the data obtained with the two independent methods, the error may be put at 0.2—1.0 Kcal/mole.

On the basis of the formational enthalpies and entropies, and of the stability constants determined by us for the alanine, phenylalanine and tyrosine complexes, the following conclusions may be drawn as to the factors determining the stability of the aromatic amino-acid–metal complexes:

1. From Table VIII it is clear that there is no significant difference in the sum of the entropy and enthalpy changes for the Cu(II) complexes of, in turn, alanine, phenylalanine and tyrosine. (The calorimetrically obtained data for the Cu(II)–tyrosine system form an exception.) At the same time, the val-

Table VIII

Enthalpies and entropies of formation of the alanine, phenylalanine and tyrosine complexes determined calorimetrically and from the temperature dependence of the stability constants

Ligand	Co(II)				Ni(II)			
	$-\Delta H_1$	$-\Delta H_2$	ΔS_1	ΔS_2	$-\Delta H_1$	$-\Delta H_2$	ΔS_1	ΔS_2
	Kcal/mole	Kcal/mole	e. u.	e. u.	Kcal/mole	Kcal/mole	e. u.	e. u.
Alanine	2.0	2.3	13	8	3.4	3.9	14	7
	1.3*	2.3*	15*	9*	3.6*	3.8*	13*	8*
Phenylalanine	1.1	2.2	15	8	2.2	2.3	16	12
	1.5*	0.3*	14*	15*	2.7*	1.9*	15*	14*
Tyrosine	−0.2	2.7	19	6	1.7	3.1	17	9
	−0.6*	1.7*	20*	11*	2.0*	2.8*	16*	10*
	Cu(II)				Zn(II)			
Alanine	4.7	6.0	22	10	2.3	1.7	13	13
	4.9*	5.5*	21*	13*	1.5*	2.8*	17*	10*
Phenylalanine	4.6	6.4	21	10	1.8	2.8	13	9
	4.7*	6.9*	20*	9*	0.9*	1.7*	17*	13*
Tyrosine	4.0	6.0	21	11	−1.5	3.5	24	7
	5.9*	6.6*	16*	10*	1.4*	2.6*	14*	6*

calorimetric results determined at 27 °C

ues of $\log K_2$ for the Cu(II)–phenylalanine and tyrosine systems are almost identical with that of the alanine complex (*cf.* Table IX). With regard to the values of pK_2 (alanine: 9.72; phenylalanine: 9.08; tyrosine: 9.05), this means a significant increase of stability for the Cu(II) aromatic amino-acid complexes. On the other hand, from the data of the thermodynamic changes it can only be concluded that, similarly to the aliphatic amino-acid–Cu(II) complexes [15], the most important factor determining stability is the Jahn–Teller effect. Consequently, the presence of the aromatic ring is not reflected in the entropy changes. At the same time, taking into consideration the error in ΔH_1 and ΔH_2 explained above, the back-coordination assumed by IZATT *et al.* [1] can be neither excluded nor verified. However, if it plays a part at all, this can only be of a very small extent for the Cu(II)–phenylalanine and tyrosine systems.

2. The sum of ΔH_1 and ΔH_2 for the Co(II), Ni(II) and Zn(II)–phenylalanine and tyrosine complexes is in general smaller than that for the corresponding alanine complexes. (The data obtained by the two methods for the Zn(II)–tyrosine system differ significantly from each other. Consequently, the possibility of drawing conclusions in this case is rather limited.) On the other hand, the values of the entropy changes are generally larger than for the alanine complexes.

From the stability constants in Table IX for the alanine, phenylalanine and tyrosine systems it is clear that, despite the differences in pK already referred to, the values of log K_2 for the phenylalanine and tyrosine complexes agree

Table IX

Stability constants of the alanine, phenylalanine and tyrosine complexes at 25 °C, $I = 0.05$ M

Ligand	log K_1				log K_2			
	Co(II)	Ni(II)	Cu(II)	Zn(II)	Co(II)	Ni(II)	Cu(II)	Zn(II)
Alanine	4.35	5.46	8.17	4.60	3.51	4.47	6.78	4.07
Phenylalanine	4.02	5.11	7.83	4.28	3.43	4.32	6.83	4.06
Tyrosine	3.93	5.02	7.75	4.16	3.45	4.25	6.82	4.11

with those of the alanine complexes. On the basis of the entropy changes, this comparative increase in stability for the aromatic amino-acid complexes may be ascribed (at least in part) to the aromatic structure. The neutral MA_2 type complexes are less hydrated, or rather the water structure is changed to a greater extent, than the alanine complexes.

3. Altough the sum of the enthalpy changes for the Co(II), Ni(II) and Zn(II)–phenylalanine and tyrosine complexes is smaller than that for the corresponding alanine complexes, there is a considerable difference in the distribution. With regard to the indicated possibilities of error, the ratio $\Delta H_2/\Delta H_1$ is generally larger for the former complexes than for the latter. This phenomenon may be explained in part by the assumption of back-coordination. The probability of this is supported by the difference in solubility (described above) of the alanine and tyrosine chelates. This experimental finding, together with the data obtained for the enthalpy changes, is most probably explained as follows: as a consequence of the phenolic hydroxyl group, back-coordination for the tyrosine complexes is more significant than for the phenylalanine complexes. By this means the complex molecules will be more polar and the solubility will be increased.

Thus, it may be stated that the bonding in the MA_2 type aromatic amino acid complexes is relatively more covalent. This is reflected in the comparatively greater enthalpy change accompanying the formation of MA_2. Another

factor determining stability, in addition to the foregoing, is the greater entropy change that can be ascribed to the presence of the aromatic ring. These effects are more pronounced for the tyrosine complexes than for the phenylalanine chelates.

*

We acknowledge the partial collaboration of Mr. I. Sóvágó in the experimental work and in the calculations.

REFERENCES

1. Izatt, R. M., Warthall, I. W., Anderson, K. P.: J. Phys. Chem. **65,** 1914 (1961)
2. Anderson, K. P., Greenhalgh, W. O., Izatt, R. M.: Inorg. Chem. **5,** 2106 (1966)
3. Anderson, K. P., Newell, D. A., Izatt, R. M.: Inorg. Chem. **5,** 62 (1966)
4. Anderson, K. P., Greenhalgh, W. O., Butler, E. A.: Inorg. Chem. **6,** 1056 (1967)
5. Simeon, V., Weber, O. A.: Croat. Chem. Acta, **38,** 161 (1966)
6. Stability Constants of Metal-Ion Complexes (Special Publication No. 17). The Chemical Society, London, 1964.
7. Sytchev, A. Ya., Mikhal, P. K.: Biochimija **27,** 25 (1962)
8. Stack, W. F., Skinner, H. A.: Trans. Faraday Soc. **63,** 1136 (1967)
9. Raju, E. V., Mathur, H. B.: J. Inorg. Nucl. Chem. **30,** 2188 (1968)
10. Gergely, A., Király, S., Nagypál, I., Mojzes, J.: Magy. Kém. Foly. **76,** 452 (1970) Acta Chim. Acad. Sci. Hung. **67,** (2) 133—143 (1971)
11. Irving, H. M., Miles, M. G., Pettit, L. D.: Anal. Chim. Acta **38,** 475 (1967)
12. Gergely, A., Nagypál, I., Sóvágó, I.: Magy. Kém. Foly. **76,** 550 (1970); Acta Chim. Acad. Sci. Hung. **67,** (3) 241—250 (1971)
13. Nagypál, I., Gergely, A.: Magy. Kém. Foly. **75,** 50 (1969)
14. Nagypál, I., Gergely, A., Jékel, P.: J. Inorg. Nucl. Chem. **31,** 3447 (1969)
15. Sharma, V. S., Mathur, H. B., Biswas, A. B.: J. Inorg. Nucl. Chem. **26,** 382 (1964)

Arthur Gergely
István Nagypál
Bálint Király
Debrecen 10, Hungary.

Acta Chimica Academiae Scientiarum Hungaricae, Tomus 68 (4), pp. 297—311 (1971)

MECHANISM OF ADSORPTION INDICATION, VIII

AZO DYES AS ADSORPTION INDICATORS. EFFECT OF SUBSTITUENTS ON THE MECHANISM OF ADSORPTION INDICATION

L. LÉGRÁDI

(Nitrochemical Works, Fűzfőgyártelep)

Received January 22, 1970

Revised manuscript received April 27, 1970

In this paper 46 azo compounds are listed, suitable for use as adsorption indicators. Most of these compounds have not been described in the literature as yet. The ions determined by means of argentometric titration against the listed indicators, the conditions of application, as well as the principle for the indicating action are given. The acid–base or the surface precipitation principle or both of them can be applied for the majority of azo adsorption indicators. The effect of substituents on argentometric applications of these indicators are discussed in detail.

In the practice, several azo dyes are in use as adsorption indicators. In this paper the well-known azo compounds are listed and divided into groups, together with several azo compounds prepared especially for our studies on their indication mechanism. Our purpose was the investigation of the principle of action of azo dyes showing adsorption indicator character, of the conditions of applicability of an azo compound as an adsorption indicator, as well as of the effects of substituents on applicability.

In Table I there are 22 compounds listed, known as indicator bases working in accordance with the acid–base principle. Regarding the application of these indicators in argentometry, *o*-ethyl- and *p*-ethoxy-α-naphthyl red were used for detailed illustration [3—7]. In a recent paper the mechanism of adsorption indication by indicator bases working on the acid–base principle was discussed [10, 11]. Preparation and investigation of a great number of indicators have been carried out in order to determine the effect of substituents. Azobenzene was used as a parent compound, this is neither an acid–base indicator, nor an adsorption one. After attachment of an amino group to the benzene ring in *p*-position to the azo group, *p*-aminoazobenzene was obtained, suitable for use as both an acid–base and an adsorption indicator. The other 21 compounds listed are essentially derivatives of *p*-aminoazobenzene. Thus the presence of an amino group in *p*-position to the azo group is a necessary and sufficient condition for obtaining an acid–base or adsorption indicator from an azo compound. Of course, this indicating effect should be improved by attachment of other substituents, too.

Attachment of an other substituent of $+M$ action in *p*-position to the azo-nitrogen is advantageous, resulting in an increased difference between the

Acta Chim. Acad. Sci. Hung. 68, 1971

Table I

Azo bases as adsorption indicators

No.	Indicator	pK	Ions to titrate	Colour change			pH in precip. titr.	Ref.
				in solution		in precipitation titration		
				alkaline	acid			
1.	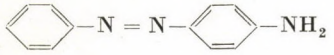	2.5	Br^-, I^-, SCN^-	yellow	orange	from orange red to yellow	4—5	
2.	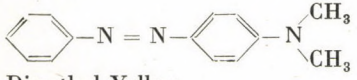 Dimethyl Yellow	3.4	Br^-, I^-, SCN^-	yellow	red	brown to orange	4—5	
3.	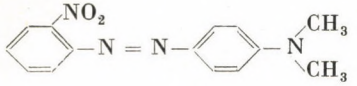	2.5	Cl^-, Br^-, I^-, SCN^-	orange	dark orange	red to orange	4—5	
4.	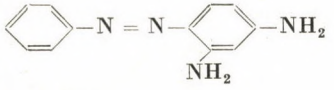	4.8	Br^-, I^-	yellow	orange	orange to yellow	4—6	
5.	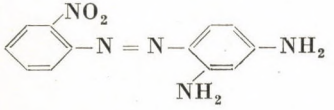	2.1	Br^-, I^-, SCN^-	yellow	orange	orange to yellow	4—5	
6.	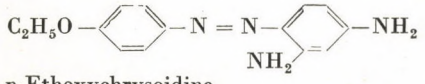 *p*-Ethoxychrysoidine	4.5	Br^-, I^-, SCN^-	yellow	red	red to yellow	5—6.5	[1]
7.	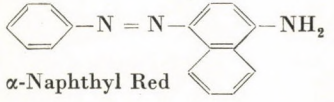 α-Naphthyl Red	4.3	Br^-, I^-	yellow	red	purple to orange	4—5	[2]

8. 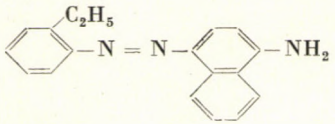 *o*-Ethyl-α-naphthyl Red	2.6	Br^-, I^-, SCN^-	yellow	pink	purple to orange	3—5	[3, 4, 5]
9. 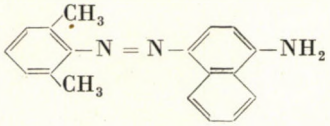	3.0	Cl^-, Br^- I^-	yellow	orange red	red to orange	3—5	
10. 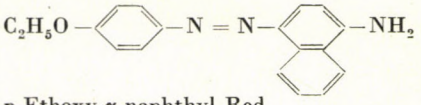 *p*-Ethoxy-α-naphthyl Red	3.6	Br^-, I^-, SCN^-	yellow	violet	violet to yellow	4—6	[6, 7]
11. 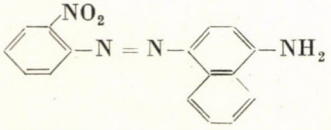	3.5	Br^-, I^-	brown-ish yellow	red	purple to orange red	3—5	
12. 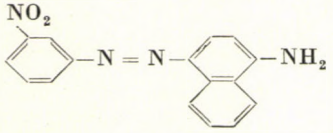	3.5	Br^-, I^-	brown-ish yellow	red	purple to orange red	3—5	
13. 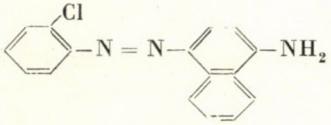	3.5	Br^-, I^-, SCN^-	yellow	red	red to orange	3—5	

Table I (continued)

No.	Indicator	pK	Ions to titrate	Colour change		pH in precip. titr.	Ref.
				in solution		in precipitation titration	
				alkaline	acid		
14.	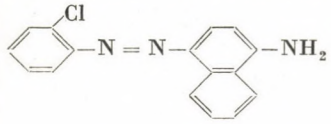	3.3	Br^-, I^-, SCN^-	orange yellow	orange red	red to orange	3—5	
15.	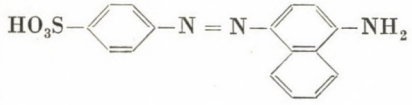	4.6	Br^-, I^-	yellow	violet	red to orange	4—5	
16.	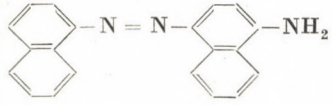	2.5	Br^-, I^-, SCN^-	orange	purple	blue violet to orange	3—5	
17.	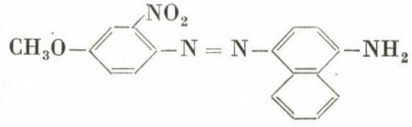	3.9	Cl^-, Br^-, I^-	orange	purple	blue to orange brown	3—5	[8]
18.	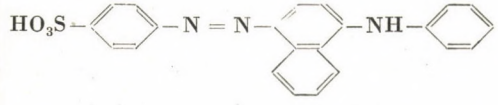		Cl^-, Br^- I^-, SCN^-			blue or green to orange	3—5	[9]
19.	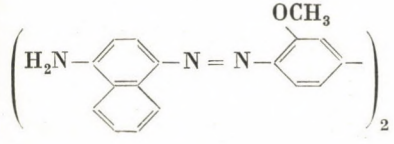	2.9	Cl^-, Br^-, I^-	red	blue	blue to violet	3—6	

20.	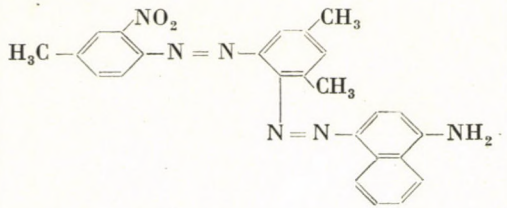	—	Br^-, I^-, SCN^-	water: claret | claret; ethanol: claret | blue	violet blue to orange red	5—6
21.	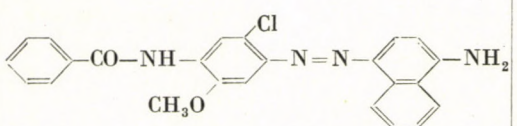	2.5	Cl^-, Br^-, I^-, SCN^-	orange	dark orange	violet blue to grey	3—5
22.	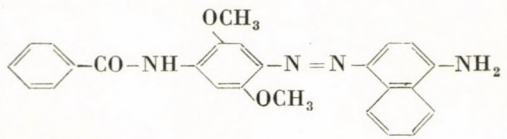	2.8	Br^-, I^-, SCN^-	orange	blue	blue to orange	3—5

wavelengths of acid and alkaline absorption maxima of the indicator, thus the colours will be more distinct and easier to observe.

The favourable effect of alkyl groups on the adsorption indicator properties can be seen by comparison of Compounds 7, 8 and 9. Compound 7 is α-naphthyl red, suitable for titration of bromide and iodide ions, showing but a weak colour change. Compound 8 is *o*-ethyl-α-naphthyl red, showing better colour change in the titration of bromide, iodide and thiocyanate ions. Compound 9 contains two alkyl groups in *o*-position to the azo-nitrogen, and can be used for the titration of chloride, bromide, iodide and thiocyanate ions. Thus, the presence of an alkyl group in *o*-position to the azo-nitrogen is advantageous for the adsorption indicator properties.

The nitro group produces the greatest effect when present in *p*-position to the azo-nitrogen. By the substitution of a nitro group into *p*-aminoazobenzene or α-naphthyl red in *p*-position indicator acids listed in Table II come into being. The presence of a nitro group in *o*-position to the azo-nitrogen shows advantageous effect on the adsorption indication in Compounds 3, 5 and 17, while there is no effect in Compound 11.

Dimethyl yellow is suitable for the titration of bromide, iodide and thiocyanate ions only, however, after introduction of a nitro group into *o*-position, it can be used for the determination of chloride ions, too. Similarly, attachment of a nitro group to *p*-methoxy-α-naphthyl red in *o*-position makes it suitable for the titration of chloride ions. Chrysoidine can be used for the titration of iodide and bromide ions only, however, introduction of a nitro group in *o*-position provides a possibility for the determination of thiocyanate ions, too. Nitro groups in *m*-position to the azo-nitrogen show no effect on adsorption indication.

The presence of a sulfo group makes the basic dyes water-soluble, without affecting the colour change. Its position with respect to the azo-nitrogen has no importance regarding the nature of the indicators. In some cases the presence of the sulfo group makes the azo compound a surface precipitation indicator; this, when being an acid–base indicator too, will work on the acid–base principle, together with the surface precipitation one, in argentometric titrations. The introduction of a sulfo group into dimethyl yellow will result in methyl orange, having a better colour change than the former one, in adsorption indication. In Compound 18 the presence of a sulfo group is also advantageous, while in Compound 15 this was not observed.

The presence of a halogen atom in the dye molecule — represented by Compounds 13 and 14 — shows no advantageous effect on the acid–base or adsorption indicator properties.

The best titration results with indicator bases working on the acid–base principle were obtained in the case of iodide ions; bromide ions produced somewhat poorer results. The colour change is sometimes weak for thiocyanate

ions, poor if any, for the chloride ion and indicator bases cannot be used in the titration of cyanide ions.

Table II contains azo indicator acids commonly used or prepared by us, suitable for use as adsorption indicators. The azo indicator acids usable as adsorption indicators can be divided into three groups on the basis of their operation. The first group contains compounds having a basic amino group in addition to the acidic nitro group. Their action has been illustrated on the example of *p*-nitro-α-naphthyl red [12]. Compounds 1—3 in Table II are of such nature. Compounds 4—7 belong to the second group. In general, they contain nitro and hydroxyl groups. Their mechanism of adsorption indication was elucidated on the example of Compound 5 [4-(4'-nitrophenylazo)-1-naphthol] [13]. Indicators in the third group are characterized by the presence of carboxyl or sulfo groups in addition to the nitro and hydroxyl groups. 2-(4'-Nitrophenylazo)-1-naphthol-4-sulfonic acid is a typical compound, used for illustration of their indication mechanism [14]. In this latter case also adsorption–desorption processes take part in the mechanism of adsorption indication, while in indicator acids of groups 1—2, this occurs at higher ion excess only.

The indicators listed in Table II are acid–base indicators except for Compound 10; Compounds 3 and 6 work in alcohol only. Compounds 5, 7, 11 and 15 are universal argentometric indicators, equally suitable for titration of chloride, bromide, iodide, cyanide and thiocyanate ions. There is no order of preference for ions in the application, as observed for the basic dyes. Here every ion has equal chances and, in general, it is the nature of the dye molecule which determines the ions measurable by argentometric titration. Argentometric titration of the cyanide ion should be carried out in the presence of an indicator acid almost exclusively. Of the halogen ions, iodide ion can be titrated in the presence of an indicator acid in most cases. This can be attributed to the fact that the silver iodide precipitate provides the most favourable conditions for the adsorption–desorption processes, important for the mechanism of indication and thus for the production of a colour change, too. In contrast to the basic dyes always showing the best colour change for iodide ions and the weakest for chloride ions, the behaviour of these compounds cannot be predicted, and sometimes they give better colour change for bromide or chloride ions than for iodide ion.

The amphoteric adsorption indicators form a special group of azo adsorption indicators. The term amphoteric refers to the nature of the adsorption indicator only, irrespective of their behaviour in acid–base titrations. Amphoteric adsorption indicators are compounds behaving simultaneously as indicator acids and bases in adsorption indication. An excess of silver ions will make the indicator base to change its colour to a lighter one in acid or neutral medium, while the colour of the indicator acid will change to a darker shade in neutral or alkaline medium under such conditions. The dark colour,

Table II

Azo indicator acids as adsorption indicators

No.	Indicator	pK	Ions to titrate	Colour change			pH in precip. titr.	Ref.
				in solution		in precipitation titration		
				alkaline	acid			
1.	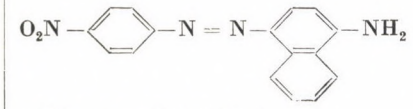 *p*-Nitro-α-naphthyl Red	—	Br^-, I^-, SCN^-	water: purple ethanol: purple	colour-less red	yellow to blue or green	9—10	[12]
2.	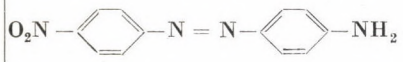	12.0	I^-	orange	orange red	yellow to orange	6—7	
3.	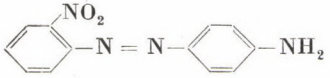	—	I^-, CN^-	water: yellow ethanol: yellow	yellow red	yellow to orange	8—10	
4.	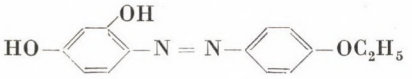	12.0	Cl^-, Br^-, I^-, SCN^-	orange	orange red	orange to red	8—10	
5.	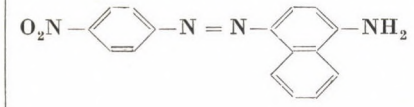	9.6	Cl^-, Br^-, I^-, SCN^-	yellow	violet	red to blue	8—9	[13]
6.	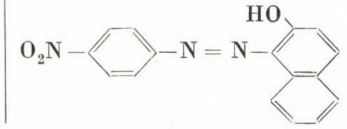	—	I^-, CN^-	water-insoluble ethanol: red	violet	orange to orange red	8—10	

7.	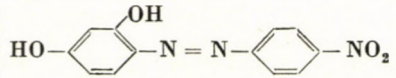 Azoviolet	12.0	Cl^-, Br^-, I^-, CN^-, SCN^-	yellow	violet	orange to violet or blue	6—10	
8.	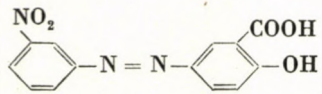 Alizarin Yellow GG	11.1	Br^-, I^-	yellow	orange	yellow to orange	7—8	
9.	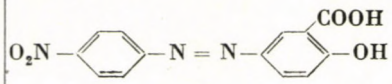 Alizarin Yellow R	11.1	I^-	yellow	orange	yellow to orange	7—8	
10.	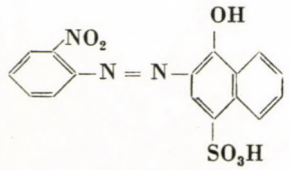	—	I^-, SCN^-	orange	orange	yellow to greenish yellow	9—10	[14]
11.	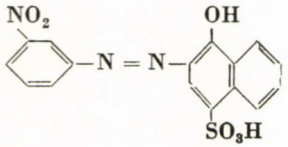	—	I^-, Br^-, Cl^-, CN^-, SCN^-	orange	orange	yellow to red	6—9	[14]
12.	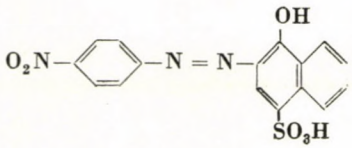	7.6	Cl^-, Br^-, I^-, CN^-	orange	purple	red to blue or green	9—10	[14]

Table II (continued)

No.	Indicator	pK	Ions to titrate	Colour change		pH in precip. titr.	Ref.
				in solution		in precipitation titration	
				alkaline	acid		
13.	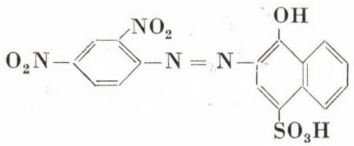	9.3	Cl^-, Br^-, I^-, CN^-	orange	blue	red to blue	9—10	[14]
14.	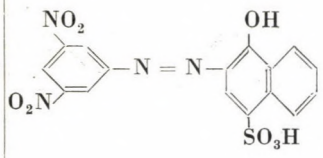	7.3	Cl^-, Br^-, I^-, SCN^-	yellow	red	yellow to violet or green	7—9	[14]
15.	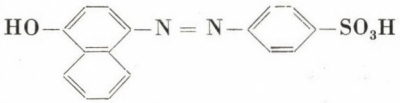 Tropeolin OOO	8.2	Cl^-, I^-, CN^-, SCN^-	yellow	red	yellow to purple	6—7	
16.	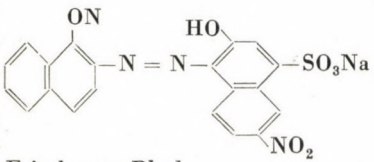 Eriochrome Black	6.3	Cl^-, Br^-, I^-	red	blue	greyish red to green blue to violet grey	6—7 8—10	[15]

due to the quinoidal structure, is not identical in the acid and alkaline media as produced by different structural changes. Thus the existence of an amphoteric adsorption indicator does not involve the presence of both acidic and basic functional groups in the azo dye. In general, attachment of a sulfo group to an azo indicator base will not alter its indicator base character, though it will increase its solubility and change the range of its colour change. Amphoteric azo adsorption indicators prepared from indicator acids by attachment of a basic group are listed in Table III.

The next group of azo adsorption indicators contains azo compounds acting as surface precipitation indicators. These are listed in Table IV. Compound 1 of this table is not an acid–base indicator. The only difference between this compound and metanil yellow is the presence of a chlorine atom in *o*-position, eliminating the indicator character of the molecule. However, it acts as a surface precipitation indicator, similarly to fluorescein and its derivatives [17]. Compound 2 differs from metanil yellow in the position of its sulfo group with respect to the azo-nitrogen, it being in *p*-position instead of *m*-position. Similarly to metanil yellow, it is an indicator base, however, it cannot be used as an adsorption indicator on the basis of acid–base principle, since the colour change will take place only after the addition of a significant excess of the reagent.

Finally, there are azo compounds which act on more than one principle as precipitation indicators. These are summarized in Table V. Of these indicators, Compounds 1 and 2 work equally well on the acid–base and surface precipitation principles, while Compounds 3 and 4 show poor colour change as surface precipitation indicators. The compounds listed in Table V are indicator bases with surface precipitation properties, owing to the presence of sulfo or carboxyl groups. No surface precipitation indicators could be prepared from azo indicator acids.

In addition to the listed compounds, several other well-known azo dyes were investigated and found to be unsuitable for use as adsorption indicators. The water-insoluble azo pigments Hansascharlach RN (C. I. 12120), Permanentrot R extra (C. I. 12085), Hansagelb G (C. I. 11680) could not be used as adsorption indicators. Of these pigments only the ice red or para red (C. I. 12070) was found to be suitable for titration of iodide and cyanide ions (Table II, Compound 6). Since it is insoluble in water, it was dissolved in alcohol and made alkaline before use. Of the basic azo dyes, Diaminbraun (C. I. 22311) and Basic Brown (C. I. 21000) could not be used as adsorption indicators. This is due to the fact that these compounds are not acid–base indicators. Direct azo dyes Dihanyl Brown (C. I. 35005), Dihanyl Orange (C. I. 22130), Direktschwarz RW (C. I. 30245), and Direkttiefschwarz EW (C. I. 30235) could not be used as being no acid–base indicators. Of the azo chromic mordant dyes, Alizarinchromechtgelb (C. I. 14095), Chromolangelb GRK (C. I. 13900),

Table III

Amphoteric azo adsorption indicators

No.	Indicator	pK	Ions to titrate in		Colour change			pH	Ref.
			acid	alkaline	in solution		in precipitation titration		
			medium		acid	base			
1.	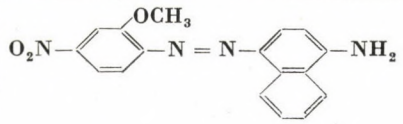	—	I^-, Br^-	Cl^-, Br^-, I^-, SCN^-	pink	purple	violet to orange yellow to blue	6—7 9—10	[8]
2.	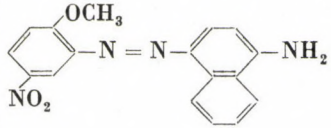	3.1	I^-, Br^-	CN^-	red	yellow	purple to orange pink to violet	4—5 9—10	[8]

Table IV

Azo compounds as surface precipitation indicators

No.	Indicator	pK	Ions to titrate	Colour change			pH	Ref.
				in solution		in precipitation titration		
				acid	base			
1.	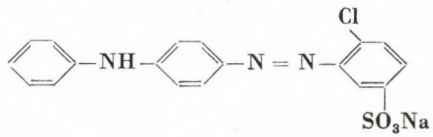	—	Cl^-, Br^-, I^-, SCN^-	orange	orange	orange to pink	4—5	
2.	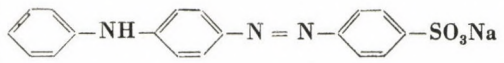 Tropeolin OO	2.2	Cl^-, Br^-, I^-, SCN^-	red	yellow	yellow to pink	6—7	[16]

Table V

Azo adsorption indicators acting on mixed principle

No.	Indicator	pK	Ions to titrate	Colour change			pH	Ref.
				in solution		in precipitation titration		
				acid	base			
1.	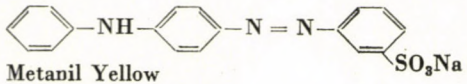 Metanil Yellow	1.7	Cl^-, Br^-, I^-, SCN^-			yellow to pink	6—7	[16]
			Cl^-, Br^-, I^-, SCN^-	red	yellow	blue to orange	3—4	[18]
2.	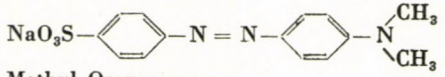 Methyl Orange	3.7	Cl^-, Br^-, I^-, SCN^-			yellow to orange	6—7	[19]
			Br^-, I^-, SCN^-	red	orange	red to orange	4—5	
3.	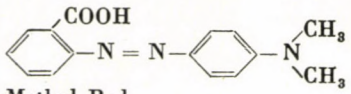 Methyl Red	5.3	Br^-, I^-, SCN^-			orange to orange red	6—7	
			Br^-, I^-, SCN^-	red	yellow	red to orange	4—5.5	
4.	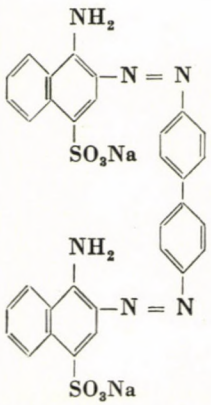 Congo Red	4.0	Br^-, I^-, SCN^-			red to purple	6—7	
			Br^-, I^-, SCN^-	blue	red	blue to red	4—5	[20, 21]

Neolangrün BL (C. I. 13425) are not adsorption indicators. Tropeolin O was the only well-known azo acid–base indicator which was not found to be a suitable adsorption indicator.

General aspects for use of azo compounds as adsorption indicators

The above examples show that azo compounds act as adsorption indicators mainly on the basis of the acid–base principle. This requires, in general, adequately different absorption maxima of the acidic and alkaline forms of the compound. There are some exceptions, too, which are not acid–base indicators but still act as adsorption indicators. It can be stated that the majority of the azo acid–base indicators are satisfactory adsorption indicators, with some exceptions, of course. For example, a change in the position of the sulfo group from *m*-position to *p*- one in metanil yellow results in unaltered acid–base indicator properties but it will follow the surface precipitation principle when operating as an adsorption indicator.

Of the azo acid–base indicators, both the indicator bases and indicator acids can be utilized as adsorption indicators, in neutral and acid or neutral and alkaline media, respectively. In the indicator base the amino group in *p*-position to the azo group is an important substituent. Advantageous effects are obtained by substituents of $+M$ action in *o*- or *p*-position and by alkyl or nitro groups in *o*-position. In the indicator acids the most important substituent is the nitro or hydroxyl group in *p*-position with respect to the azo group.

According to the above discussion, the azo compounds acting as adsorption indicators can be divided into the following groups:

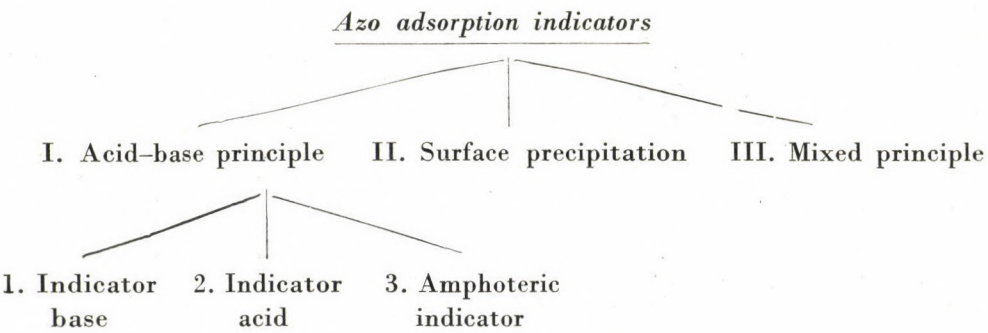

REFERENCES

1. SCHULEK, E., RÓZSA, P.: Z. anal. Chem. **115**, 185 (1938);
PUNGOR, E., SCHULEK, E.: Z. anal. Chem. **150**, 116 (1956)
2. TANDON, K. N., MEHROTRA, R. C.: Anal. Chim. Acta **26**, 589 (1962); **27**, 15, 198 (1962)
3. LÉGRÁDI, L.: Magy. Kém. Foly. **70**, 27 (1964); Acta Chim. Acad. Sci. Hung. **42**, 107 (1964)
4. LÉGRÁDI, L.: Magy. Kém. Foly. **70**, 61 (1964)

5. LÉGRÁDI, L.: Magy. Kém. Foly. **70,** 271 (1964)
6. LÉGRÁDI, L.: Magy. Kém. Foly. **70,** 405 (1964); Acta Chim. Acad. Sci. Hung. **47,** 103 (1966)
7. LÉGRÁDI, L.: Magy. Kém. Foly. **74,** 359 (1968)
8. LÉGRÁDI, L.: Magy. Kém. Foly. **74,** 56 (1968)
9. MEHROTRA, R. C.: J. Indian Chem. Soc. **25,** 519, 523, 527, 541 (1948)
10. LÉGRÁDI, L.: Magy. Kém. Foly. **75,** 72 (1969)
11. LÉGRÁDI, L.: Magy. Kém. Foly. **75,** 77 (1969)
12. LÉGRÁDI, L.: Magy. Kém. Foly. **73,** 525 (1967)
13. LÉGRÁDI, L.: Magy. Kém. Foly. **74,** 61 (1968)
14. LÉGRÁDI, L.: Magy. Kém. Foly. **74,** 64 (1968)
15. LÉGRÁDI, L.: Magy. Kém. Foly. **75,** 372 (1969)
16. KOLTHOFF, I. M.: Z. anal. Chem. **70,** 395 (1927); **71,** 235 (1927)
17. PUNGOR, E., KONKOLY THEGE, I.: Talanta, **10,** 1211 (1963)
18. PUNGOR, E., HOLLÓSNÉ-ROKOSINYI, E.: Magy. Kém. Foly. **63,** 28 (1957)
19. TANDON, K. N.: Ph. D. Thesis, University of Agra, 1963
20. MEHROTRA, R. C.: Anal. Chim. Acta **2,** 36 (1948)
21. TANDON, K. N., MEHROTRA, R. C.: Anal. Chim. Acta **27,** 97 (1962)

László LÉGRÁDI; Fűzfőgyártelep, Hungary.

Acta Chimica Academiae Scientiarum Hungaricae, Tomus 68 (4), pp. 313—318 (1971)

SEPARATION OF TRACES OF ELEMENTS BY PRECIPITATION, VIII

SORPTION OF LANTHANIDES AND SCANDIUM ON IRON(III) HYDROXIDE IN A CARBONATE MEDIUM

E. UPOR and GY. NAGY

(Mecsek Ore Mining Enterprise)

Received January 23, 1970

The sorption of the lanthanide metals and scandium on iron hydroxide was studied in a Na_2CO_3 medium. It was found that as a result of the hydrolytic decomposition of the relatively low stability carbonate complexes, the sorption of the light lanthanides is complete at a Na_2CO_3 concentration of 0.2 *M*, but the sorption of the heavy lanthanides is only approximately complete. With increase of the Na_2CO_3 concentration or of the atomic number the sorption decreases. Scandium behaves similarly to the heavy lanthanide metals. The sorption passes through a minimum in the pH range 9—11. Lu^{3+}, Yb^{3+} and Sc^{3+} can be separated with 2 *M* Na_2CO_3 from Fe^{3+} and to a certain extent from the other lanthanide metals too. Every lanthanide metal ion can be separated from uranium, but only the first members of the series can be separated from thorium and zirconium.

Introduction

It is well known that the carbonates of the lanthanide metals are sparsely soluble compounds [1]. In addition to the poorly soluble normal carbonates of composition $Ln_2(CO_3)_3$, however, more soluble anionic complexes also exist [2, 3]. The compositions of these complexes were reported to be $[Ln(CO_3)_3]^{3-}$ and $[Ln(CO_3)_4]^{5-}$. From the rather limited amount of papers the following are known on their properties.

1. The stabilities of the complexes are not high; log K_n for the $[Ln(CO_3)_3]^{3-}$ complex is 1.89 for Nd and 1.94 for Eu [2]. (K_n is the stepwise stability constant; $n = 3$.) Numerical values have been determined for only a few of the metal ions.

2. The stabilities and solubilities of the complexes increase with atomic number [2, 3]. The solubility in 2 *M* Na_2CO_3 solution varies between 0.09 and 0.10 m*M*.

3. The solubility increases monotonously with increasing carbonate concentration. The solubility in $(NH_4)_2CO_3$ is smaller by an order of magnitude than in alkali metal carbonates [4, 5].

4. Solubility differences for individual lanthanide metals permit a certain degree of separation.

As has been found for other systems too, the solubility of a complex ion in itself does not determine to what extent it can remain in solution in the pre-

sence of a precipitate (*e.g.* a metal hydroxide) capable of sorption. From earlier studies [6] we found that with 0.1 *M* Na_2CO_3 in the presence of $Fe(OH)_3$ each lanthanide metal (if present in small amount) goes practically completely into the precipitate. In this way the separation of uranium from the lanthanide metals can be achieved.

In this paper we report the results of further investigations into the effects exerted on the sorption of the lanthanide metals by some important factors. Because of its chemical similarity to the lanthanide metals we also report here the experimental results for scandium.

Experimental

In our experiments 50 mg of iron(III) and various amounts of lanthanide metals were precipitated in a volume of 50 ml with a solution of Na_2CO_3. To prevent possible variations arising from ageing, the precipitates were filtered off after 30 minutes. In the study of the dependence of sorption on pH, the pH was changed by the addition of HCl or NaOH. To obtain fixed pH values we applied 10 ml each of H_3BO_3 + NaOH (pH 9.4) or glycine + NaOH (pH > 10) buffer mixtures (0.2 *M* H_3BO_3 and the required amount of NaOH, or 0.1 *M* glycine and the required amount of NaOH). When the pH had been approximately adjusted previously, the capacity of the buffer solution proved sufficient to maintain the desired pH values even in 1 *M* Na_2CO_3. pH was measured with a RADELKISZ OP-401/1 pH-titrimeter using a combined calomel-glass electrode. From a consideration of analytical practice, in the experiments we used the two most important temperatures, 25 and 80 °C.

In general, to ascertain the extent of sorption the filtrate was analyzed since in the majority of experiments this contained the smaller amount of the ion to be determined. The determination was carried out with arsenazo III photometrically [7] or by isotopic tracing and measurement of γ-activity. Because of the high salt concentration, it was necessary in the case of the arsenazo III analysis to make checks from time to time using an internal standard method, or to perform separations by dibutylphosphate extraction. The following isotopes were used for the tracing: ^{141}Ce, ^{147}Nd, ^{143}Sm, ^{152}Eu, ^{153}Gd, ^{160}Tb, ^{170}Yb, ^{174}Lu and ^{45}Sc. The activities of solutions were measured with a 20th Century Electronics 1363-D 100-channel amplitude analyzer with a GAMMA ND-118 pick-up and an NZ-111-BP NaI(Tl) hollow crystal of 15 ml useful volume. The activities used were chosen so that 1% of them should be at least commensurable with the background.

Results

As we have already referred to in the introduction, at 25 and 80 °C with 0.1 *M* Na_2CO_3 in the pH range 7—13 each lanthanide metal and scandium precipitates quantitatively (> 99%) with $Fe(OH)_3$. This is true between wide concentration limits.

However, we obtained a different result by changing the Na_2CO_3 concentration. In Tables I and II are the results of experiments made at fixed pH's of 9.4 and 10.9. It can be seen from the results that the sorption decreases with increasing carbonate concentration and at higher concentrations becomes quite small for the heavy lanthanide metals. The sorption is more at pH 10.9 than at 9.4.

The pH-dependence of the sorption was studied over a wide pH range. As can be seen in Fig. 1 the curves pass through a minimum and the sorption at pH 12 is already complete in 1.0 *M* Na_2CO_3. The section of the curve be-

tween pH 9 and pH 11 is qualitatively similar to the sorption curves of Zr^{4+} and UO_2^{2+}.

The effect of temperature is not significant; the values measured at 25 and 80 °C agree within the limits of experimental error.

The relative extent of sorption under the conditions of incomplete sorption is not independent of the lanthanide ion concentration. For example,

Table I

Sorption of lanthanides and scandium on $Fe(OH)_3$ from a Na_2CO_3 solution at pH 9.4

(50 mg Fe^{3+}; 0.01—100 μg Ln^{3+}; 25 °C; in 50 ml volume)

Na_2CO_3 *M*	Ce^{3+}	Nd^{3+}	Sm^{3+}	Gd^{3+}	Tb^{3+}	Ho^{3+}	Yb^{3+}	Lu^{3+}	Sc^{3+}
	% sorption								
0.1	100	100	100	100	100	100	100	99	99
0.2			100			95	92		
0.5	100	100	97	93	90	87	60	50	50
1.0	100	98	91	80	68	62	40	44	25
2.0	99	96	89				<5	<5	<5

Table II

Sorption of lanthanides and scandium on $Fe(OH)_3$ from a Na_2CO_3 solution at pH 10.9

(The experimental conditions are the same as in Table I)

Na_2CO_3 *M*	Ce^{3+}	Nd^{3+}	Sm^{3+}	Eu^{3+}	Gd^{3+}	Tb^{3+}	Ho^{3+}	Yb^{3+}	Lu^{3+}	Sc^{3+}
	% sorption									
0.1	100	100	100	100	100	100	100	100	97	98
0.2	100	100	100	100			95			90
0.5	100	100	99	99	98	93	85	65	45	50
1.0	100	97	94	94		69	62	45	28	30
2.0								15	11	12

the sorption of 10 μg Sm^{3+} at 80 °C at pH 10.5 is 91%, whereas that of 10 mg is only 74%; that of 10 μg Yb^{3+} is 39%, but that of 10 mg is only 7%. According to our studies, the Freundlich isotherm is valid between wide limits of concentration (at least three orders of magnitude) (*cf.* Fig. 2). The value of the exponent, $1/n$, is 0.87 for Sc^{3+} and 0.89 for Yb^{3+}; that is, the relative extent of sorption decreases with increasing concentration.

The mechanism of sorption was examined. Similarly to the case with other complex ions (uranyl carbonate, or cobalt(II), zinc(II) and other ammine complexes) [8, 9], it was observed here too that the complex decomposes and by means of hydrolytic sorption only the central cation goes into the precipitate (Table III).

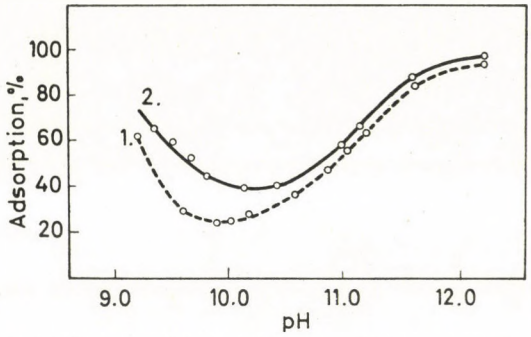

Fig. 1. Dependence on pH of the sorption of Sc^{3+} and Yb^{3+} on $Fe(OH)_3$ from a Na_2CO_3 solution (50 mg Fe^{3+}; 1 μg Sc^{3+} or Yb^{3+}; in 50 ml volume; 25 °C. $CO_3^{2-} + HCO_3^-$ concentration· 1.0 *M*. The pH was controlled by changing the ratio of these, or with NaOH. Filtration after 30 min). 1. Sc^{3+}; 2. Yb^{3+}

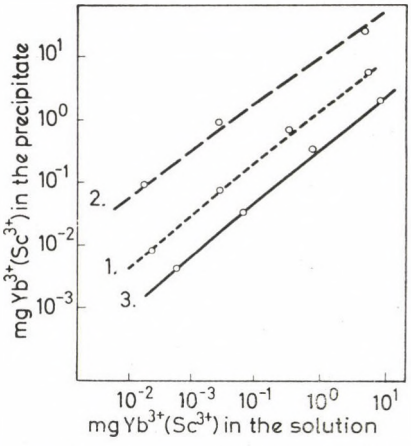

Fig. 2. Freundlich isotherms for the adsorption of Sc^{3+} and Yb^{3+} on $Fe(OH)_3$ from a Na_2CO_3 solution (50 mgFe^{3+}; in 50 ml volume). 1. Yb^{3+}; 0.5 *M* Na_2CO_3; pH 10.5; 25 °C 2. Yb^{3+}; 0.2 *M* Na_2CO_3; pH 10.6; 25 °C 3. Sc^{3+}; 1.0 *M* Na_2CO_3; pH 10.6; 80 °C

Table III

Sorption of Ln^{3+} and CO_3^{2-} on $Fe(OH)_3$ from a carbonate medium
(50 mg Fe^{3+}; 0.5 *M* Na_2CO_3; 80 °C)

Studied ion	Bound Ln mmole	Bound CO_2 mmole	CO_2/Ln
Gd^{3+}	0.46	0.06	0.13
Dy^{3+}	0.34	0.05	0.14
Er^{3+}	0.25	0.03	0.12
Yb^{3+}	0.30	0.04	0.11
Sc^{3+}	0.95	0.04	0.04
Y^{3+}	0.50	0.03	0.06

Conclusions. Separation possibilities

In addition to the very few data mentioned in the introduction, the results of the sorption experiments also prove that the stabilities of the carbonate complexes of the lanthanide metals are relatively small. The increase of stability with atomic number is also signified by the decrease of the extent of sorption on iron hydroxide. In this connection too we observe that the properties of the heavy lanthanide metals lie close to those of thorium.

It is well known that in a carbonate medium Th^{4+} exerts a desorbing effect on UO_2^{2+} [10]. The explanation of this is to be found in the greater stability of the $[UO_2(CO_3)_3]^{4-}$ complex ion in addition to the good bonding ability for CO_2^{3-} (poor for OH^-) of $Th(OH)_4$.

Since the stability of the carbonate complex of thorium is greater than those of the corresponding lanthanide complexes, in accordance with expectations it was found that thorium does not exert a desorbing effect during the sorption of the lanthanide metals.

It can be seen from the experimental results that the sorption of Sc^{3+} is similar to those of heavy lanthanide metals, *e.g.* Yb^{3+} and Lu^{3+}; this is in agreement with the picture formed in connection with the analysis of scandium.

From the data reported here and from our earlier work, in the presence of $Fe(OH)_3$ as carrier, the possibilities of the separation of lanthanides from other ions forming carbonate complexes are the following.

1. All the lanthanide metals and scandium can be separated from uranium with 0.1 *M* Na_2CO_3 at pH 9—11. Under such conditions only a small percentage of the uranium remains in solution, while the lanthanide metals go quantitatively into the precipitate. The separation can be made complete from large amounts of uranium by repeated precipitation and by utilization of the desorbing effect of added thorium [10].

2. The lanthanide metals and scandium can be separated from zirconium with 0.2 *M* Na_2CO_3 at pH 9.0—9.4. The separation is not quantitative since 10—30% of the zirconium (depending on its concentration) remains in the precipitate. By repeated precipitation, however, only a few per cent of the zirconium remains in the precipitate while merely for the last members of the lanthanide series is there a loss of a few per cent. The separation is thus of limited efficiency. The separation from the light lanthanide metals is quantitative and so can be used for example in the case of their determination. In other cases it may be used depending on the concentration conditions and on the requirements of the separation.

3. The separation from thorium is much more pronounced. With 0.75 *M* Na_2CO_3 at 25 °C at pH 9.2—9.6 more than 90% of the thorium remains in the solution and so may be separated by repeated precipitation from lanthanum and from the first members of the cerium group (Pr^{3+}, Nd^{3+}, Ce^{3+}). Since

the thorium distribution between the precipitate and the solution is greater at Na_2CO_3 concentrations lower than this (*e.g.* with 0.5 *M* Na_2CO_3 more than 50% is to be found in the precipitate), thorium is quite inseparable from the heavy lanthanides and only very imperfectly from the ions in the middle of the series.

4. According to the values reported in Table I, scandium, ytterbium and lutetium can be separated from La^{3+}, Ce^{3+} and Nd^{3+}, and to a decreasing extent with increase of the atomatic number, from some of the other lanthanide metals. This separation may be utilized, for example, in the determination of the Sc^{3+}, Yb^{3+} and Lu^{3+} content of lanthanide compounds by a neutron activation method. In this case the separation may even be improved (in accordance with the Freundlich isotherms) by the addition of an inactive carrier which does not interfere in the analysis.

5. Sc^{3+}, Yb^{3+} and Lu^{3+} can evidently be separated from iron by this technique.

Further studies must be carried out for the analytical application of the listed possibilities (except the uranium–lanthanide metal separation).

REFERENCES

1. Ryabchikov, D. I., Ryabuhin, V. A.: Analiticheskaya khimia redkozemelnih elementov i ittriya. Izd. Nauka, Moscow, 1966
2. Yatsimirakii, K. S., Kostromina, N. A., Shcheka, Z. A., Davidenko, N. K., Kriss, E. E., Yermolenko, V. I.: Khimia komplexnih soyedyinyii redkozemelnih elementov. Izd. Naukova Dumka, Kiev, 1966
3. Head, E. L., Holley, C. E.: Rare Earth Research, Vol. II, p. 51. Gordon and Breach, New York, 1964
4. Taketatsu, T.: Bull. Chem. Soc. Japan **36**, 549 (1963)
5. Ryabchikov, D. I., Senyvin, M. M., Sklyarenko, Yu. S.: Khimia radioelementov i radiatsionnih prevrashchenyi, p 75. Moscow, 1959
6. Upor, E., Nagy, Gy.: Acta Chim. Acad. Sci. Hung. **52**, 235 (1967)
7. Mohai, M., Upor, E.: Magy. Kém. Foly. **74**, 270 (1968)
8. Upor, E.: Acta Chim. Acad. Sci. Hung. **51**, 119 (1967)
9. Upor, E.: Acta Chim Acad. Sci. Hung. **64**, 17 (1970)
10. Upor, E., Nagy, Gy.: Magy. Kém. Foly. **73**, 20 (1967)

Endre Upor; Pécs, 39-es Dandár út 3/a
Gyula Nagy; Pécs, Páfrány-u 27.
Hungary.

Acta Chimica Academiae Scientiarum Hungaricae, Tomus 68 (4), pp. 319—337 (1971)

SOME REMARKS ON THE CALCULATION OF ACTIVATION ENTROPIES ON BASIS OF THE THEORY OF ABSOLUTE REACTION RATES

Gy. VARSÁNYI

(Department of Physicai Chemistry, Technical University, Budapest and Central Research Institute for Chemistry, Hungarian Academy of Sciences, Budapest)

Received January 8, 1970

It has been shown that the usual method for calculating the activation entropy on the basis of the theory of absolute reaction rates often leads to false results. The method has been discussed in detail and a correction diagram has been supplied on the basis of the frequency and anharmonicity coefficient of the critical normal vibration. The practical use of the method has been demonstrated in some classical examples.

Introduction

According to the theory of absolute reaction rates [1, 2], the reaction rate is determined by the decomposition of the activated complex. The reaction rate per volume is defined as:

$$v = \nu' x^{\ddagger} \tag{1}$$

where ν' denotes the decomposition frequency of the activated complex (to products) and $x^{\ddagger}$ stands for the concentration of the complex. The fundamental assumption of this theory is that the starting materials are in equilibrium with the activated complex. The correctness of this assumption has been questioned by several authors. However, since the possibility of equilibrium cannot be denied in the case of most reactions, we shall consider this basic criterion of the theory as accepted. This concept leads to further presumptions of equilibrium: the existence of a simultaneous equilibrium between starting materials and the activated complex, as well as between the activated complex and the products:

$$\Sigma A_i \rightleftharpoons X^{\ddagger} \rightleftharpoons \Sigma B_i \tag{2}$$

Naturally, a macroscopic reaction cannot be observed at equilibrium, therefore, due to the dynamic character of the equilibrium, our considerations are concerned with the rate of *exchange reactions*.

According to the theory of absolute reaction rates, the concentration of the activated complex, $x^{\ddagger}$, may be expressed from the equilibrium constant written for the left-hand side of equilibrium (2)

$$x^{\ddagger} = K^{\ddagger} \Pi a_i = \frac{F^{\ddagger}}{\Pi F_i} \Pi a_i \, e^{-\frac{\Delta E_0^{\ddagger}}{RT}} \tag{3}$$

where a_i stands for the concentrations of the starting compounds, F denotes the appropriate thermal partition functions, and $\Delta E_0^{\ddagger}$ is the activation energy at the absolute zero.*

Instead of the corresponding vibrational degree of freedom, EYRING [1] separated a translational partition function from the partition function $F^{\ddagger}$ of the activated complex in the co-ordinate direction of the decomposing bond:

$$f_{cr} = \frac{(2\pi m \mathbf{k}T)^{1/2}}{h} y \tag{4}$$

where y denotes the path of one of the preformed dissociation products of the activated complex relative to the other, at the end of which the products are formed. The application of formula (4) is justified if this path is potential-free, what has been assumed by the authors due to the flatness of the top of the activation barrier. According to Formula (1), ν is the reciprocal of the time interval during which the end-products are formed. Thus the product of y and ν' is, of necessity, an average velocity component of the complex in the direction of bond elongation:

$$y\nu' = \left(\frac{\mathbf{k}T}{2\pi m}\right)^{1/2}. \tag{5}$$

Considering Eqs (3), (4), and (5) instead of Eq. (1) one obtains:

$$v = \frac{\mathbf{k}T}{h} \frac{F^*}{\Pi F_i} \Pi a_i e^{-\frac{\Delta E_0^{\ddagger}}{RT}} = \frac{\mathbf{k}T}{h} K^* \Pi a_i \tag{6}$$

where F^* is the partition function of the activated complex, apart from that referring to the separated degree of freedom, while K^* is an equilibrium constant where the contribution of the separated vibrational degree of freedom is not taken into consideration in the thermodynamic potential of the activated complex.

The correctness of the theory seems to be supported by the fact that when applied to the conditions of the earlier collision theory, the expression of the reaction rate [3], derived from the collision number was obtained. This requires that the separated translational degree of freedom would be ascribed to the vibrational degree of freedom of the forming bond and not to that of the decomposing one. The complete expression of the normal translational and rotational partition functions can be obtained. In the latter, when defining the moment of inertia of

* When discussing the theory of absolute reaction rates, most authors neglect the dimension of the equilibrium constant $K^{\ddagger}$ or fail to point out a rather important fact: instead of the partition functions ($F_{tr} = \mathbf{D}V$, with V as the volume of the system) the equilibrium constant contains the factors $\mathbf{D}/N_A$, where N_A is the Avogadro number so the thus defined translational partition function is not dimensionless as the other partition functions but has a dimension of mole/volume. Thus the dimension of the complete equilibrium constant is $(\text{mole/volume})^{1-m}$, where m is the molecularity of the reaction. Consequently, $x^{\ddagger}$ is actually obtained as a concentration.

the activated complex, the internuclear distance in the diatomic complex was considered equal to the sum of the two atomic radii.

If the single vibrational degree of freedom is described by Eq. (4), one obtains the rate expression of the collision theory with the only deviation that $\Delta E_0^{\ddagger}$ replaces the experimental activation enthalpy, $\Delta H^{\ddagger}$.

The so-called *universal frequency factor*, $\frac{\mathbf{k}T}{h}$, in Eq. (6) may also be interpreted by considering the vibrational partition function of the normal vibration concentrated at the decomposing bond for an extremely low frequency when it is equal to $\frac{\mathbf{k}T}{h\nu}$. If, in addition, it is assumed that due to this vibration the activated complex decomposes already at the maximum internuclear distance of the first vibration period, frequency ν' can be identified with the vibrational frequency, ν. This consideration also leads to Eq. (6).

In the theory of absolute reaction rates, Eq. (6) has been supplemented with a probability factor smaller than 1, called the *transmission coefficient.* This factor, denoted by $\varkappa$, was interpreted by EYRING as the probability of the complex decomposing into the products and not back into the starting compounds. This implies that the life-time of the activated complex is equal to $\frac{1}{\nu'}$, for if it does not decompose with frequency ν' to the products, then it must decompose to the starting materials. The interpretation of $\varkappa$ involves further difficulties, if $\frac{\mathbf{k}T}{h\nu}$ is regarded as the partition function of the normal vibration concentrated at the decomposing bond because decomposition to the starting materials requires the rupture of a different bond. If Eq. (6) is referred to the latter, equilibrium constant K^* will not be identical with the original one. It seems more unambiguous to define $\varkappa$ as ν'/ν, in other words, as the ratio of the cleavage and vibration frequencies of the bond being ruptured. The transmission coefficient is the probability that the activated complex decomposes to the products during a single vibrational period and *does not remain intact.* The probability of decomposition to the starting materials may be characterized by another $\varkappa$, denoting a process from the right to the left.

Determination of the activation entropy

On the basis of Eq. (6), the reaction rate constant is

$$k = \varkappa \frac{\mathbf{k}T}{h} K^* . \tag{7}$$

According to thermodynamics,

$$K^* = e^{-\frac{\Delta\mu^*}{RT}} \tag{8}$$

$\Delta\mu^*$ is the excess free energy of the activated complex relative to the starting materials, disregarding, however, the vibrational contribution of the decomposing bond. The state * has in general no physical reality except when the activated complex contains only two atoms because the contribution of only one of the three vibrational degrees of freedom of the decomposing bond is not taken into account, and the rotational degree or degrees of freedom resulting upon decomposition are not taken into consideration either. Separating again the free energy into two appropriate terms we obtain

$$k = \varkappa \frac{\mathbf{k}T}{h} e^{\frac{\Delta S^*}{R}} e^{-\frac{\Delta H^*}{RT}}. \tag{9}$$

On the basis of Eq. (9), one cannot calculate the activation entropy from the pre-exponential factor of the Arrhenius equation, for ΔH^* is not equivalent to $\Delta H^\ddagger$, which can be calculated from the temperature dependence of the rate constant. Still, in practice, the activation entropy is calculated from Eq. (9), by taking into consideration the real activated state instead of the state * and taking the transmission coefficient equal to 1:

$$k = \frac{\mathbf{k}T}{h} e^{\frac{\Delta S^\ddagger}{R}} e^{-\frac{\Delta H^\ddagger}{RT}} \tag{10}$$

from which the pre-exponential factor is

$$A = \frac{\mathbf{k}T}{h} e^{\frac{\Delta S^\ddagger}{R}}. \tag{11}$$

Let us examine whether this procedure is justified. From statistical mechanics:

$$\Delta\mu^\ddagger = \Delta\mu^* - RT \ln f_{cr} \tag{12}$$

where f_{cr} is the partition function of the critical normal vibration. $\Delta\mu^*$ can be replaced by $\Delta\mu^\ddagger$ if f_{cr} is close to 1, which is true if the frequency is high. In this case, however, f_{cr} cannot be considered equal to $\frac{\mathbf{k}T}{h\nu}$ neither can the transmission coefficient be taken for 1, since a bond with a high vibrational frequency is by no means likely to decompose during a single vibrational period.

The vibrational partition function can be substituted for $\frac{\mathbf{k}T}{h\nu}$ if the frequency is rather low, *i.e.* when the value of the transmission coefficient may also approach unity. But then f_{cr} is considerably higher than 1, consequently, $\Delta\mu^*$ cannot be replaced by $\Delta\mu^{\ddagger}$.

Calculation of the partition function f_{cr}

The partition function of a harmonic vibration can be given in an explicit form. However, assumption of harmonic vibration contradicts to the presumption that the bond will decompose owing to vibration. This supports the assumption of anharmonicity, which has been taken into account by the quadratic expression for the vibrational energy. Accordingly the anharmonic vibrational energy with respect to the zero-energy state is

$$E = h\nu\, v\, [1-x(v+1)]. \tag{13}$$

By taking the first derivative of the total vibrational energy with respect to v and putting the differential coefficient equal to zero by the usual method, one obtains $\frac{1-x}{2x}$ for the quantum number v_D, corresponding to the dissociation level. Inserting this into Eq. (13), the dissociation energy with respect to the zero energy state will be:

$$D = \frac{h\nu}{4x}(1-x)^2. \tag{14}$$

In the anharmonic vibrational partition function, however, the series of levels cannot be interrupted at the dissociation level, but instead it should be continued by a one-dimensional translational series. The translational partition function is the area below a half Gauss curve, with its tail joining the envelope curve of Boltzmann factors plotted as a function of the vibrational quantum numbers. Fig. 1 shows the anharmonic partition function for $x = 0.03$ and $x = 0.1$ at 600 K if the frequency amounts to 50 cm^{-1}. The two parts of the curves fit if:

$$\exp(-av_D^2) = \exp\left\{-\frac{h}{\mathbf{k}T}\, v_D\, [1-x(v_D+1)]\right\} \tag{15}$$

Substituting the value of v_D expressed by the anharmonicity coefficient one obtains

$$a = \frac{h\nu}{\mathbf{k}T}\, x. \tag{16}$$

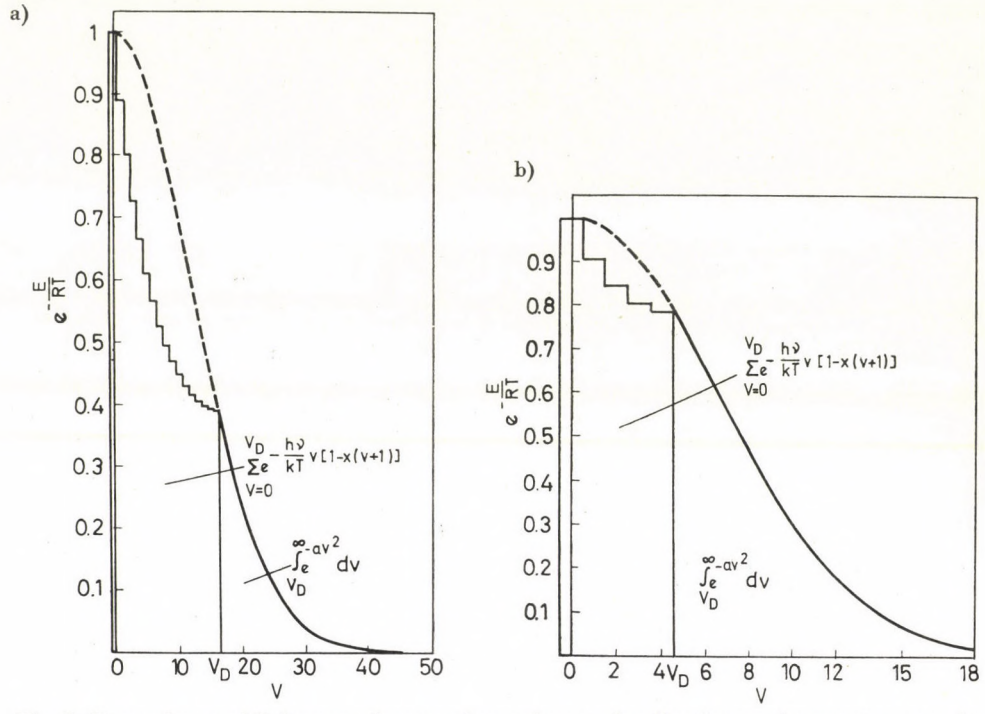

Fig. 1. Dependence of Boltzmann factors of an anharmonic vibration on the quantum number at 600 K and 50 cm^{-1} for anharmonicity coefficients a) $x = 0.03$ and b) $x = 0.1$

To determine the area below the tail of the Gauss curve, a supplementary diagram has been constructed by plotting the graphical integral of e^{-y^2} from y^* to infinity against the exponential corresponding to the * state (Fig. 2). This exponential is the Boltzmann factor corresponding to the dissociation level. If the area read from the supplementary diagram is divided by $\sqrt{a}$, one obtains the contribution to the partition function beyond dissociation. This contribution must be added to the sum of the Boltzmann factors pertaining to all vibrational levels:

$$f_{anh} = \sum_{v=0}^{v_D} \exp\left\{-\frac{hvv}{\mathbf{k}T}[1 - x(v+1)]\right\} + \frac{1}{\sqrt{a}} \int_{v_D}^{\infty} e^{-v^2}\, dv\,. \qquad (17)$$

The Gauss curve corresponds to potential-free translation. The fit to the partition function of the anharmonic vibration is, however, precise, for the potential energy of the vibration also decreases to zero up to the dissociation level. In a harmonic case, the vibrational energy is equally distributed to kinetic and potential energies. The dissociation energy calculated from the potential minimum is $D' = h\nu/4x$, which is exactly one half of the total harmonic vibrational energy* in state $v + 1/2 = 1/2x$.

* Accordingly, the anharmonic vibrational energy $E = h\nu[v + 1/2 - x(v + 1/2)^2]$ is distributed into kinetic and potential energies as follows: $T = h\nu/2\,(v + 1/2)$ and $V = h\nu/2\,(v + 1/2) - h\nu\, x(v+1/2)^2$. In the state of $v+1/2 = 1/2x$, the potential energy decreases to zero.

In possession of the concrete anharmonic partition functions, one may examine the manner in which they differ from $\frac{kT}{h\nu}$ applied in Eq. (10), as well as the amount of normal affinity contribution of the critical bond per one degree of freedom. Fig. 3 gives the $\frac{kT}{h\nu}$ to f_{cr} ratio as a function of the nor-

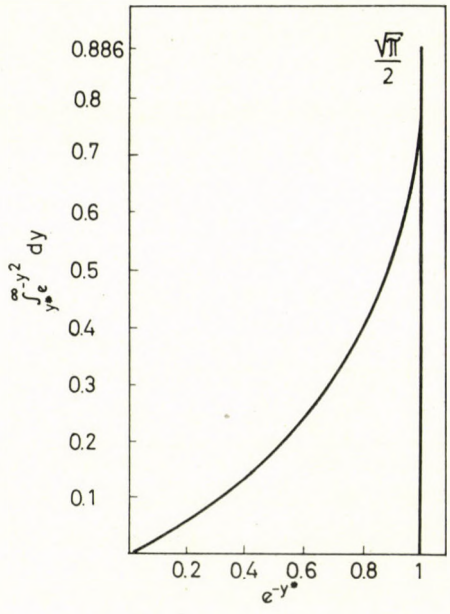

Fig. 2. Dependence of the one-dimensional translational partition function fitting that of an anharmonic vibration on the Boltzmann factor pertaining to the dissociation energy

mal vibration frequency corresponding to the critical bond at 300 K, while Fig. 4 shows the value of $-\Delta\mu_{cr}/RT$ also as a function of frequency. As may be seen, in the case of high frequencies, the partition function greatly differs from $\frac{kT}{h\nu}$ while in the range of low frequencies, the normal affinity contribution becomes significant. In the case of different anharmonicities, the shape of the curve plotted in Fig. 3 appears to be quite specific in the range of low frequencies. The reason is that in the case of maximum anharmonicity ($x = 0.1$), the curve shows a steep rise towards low frequencies and intersects the curve for harmonic vibration. In an anharmonic case, the rise of the vibrational partition function is less steep towards low frequencies than for harmonic vibrations, since the limit of the harmonic partition function is $\frac{kT}{h\nu}$, while that of the anharmonic partition function, where the contribution of potential-free trans-

lation becomes more and more significant with decreasing frequencies, shows a value of $\frac{1}{2}\left(\frac{\pi \mathbf{k}T}{h\nu x}\right)^{1/2}$, *i.e.* it is a lower-order hyperbola. At moderately low frequencies the anharmonic partition function is higher than the harmonic, for the energy levels converge, *i.e.* the decrease of Boltzmann factors is not purely exponential. With slight anharmonicity ($x = 0.01$), this tendency is observable

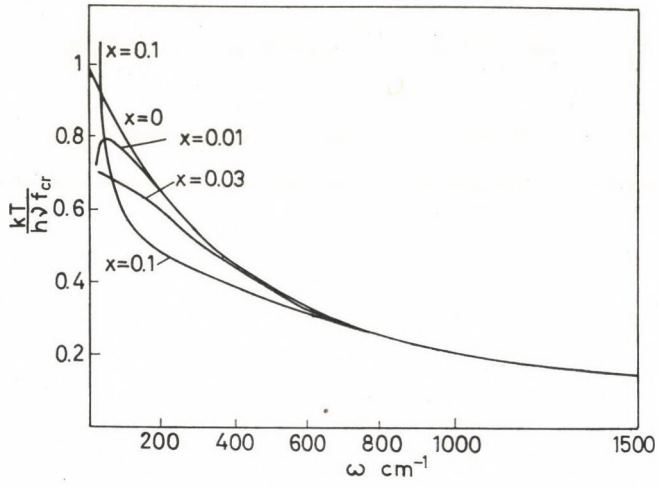

Fig. 3. Dependence of $(\mathbf{k}T/h\nu) : f_{cr}$ on the wave number ω at 300 K

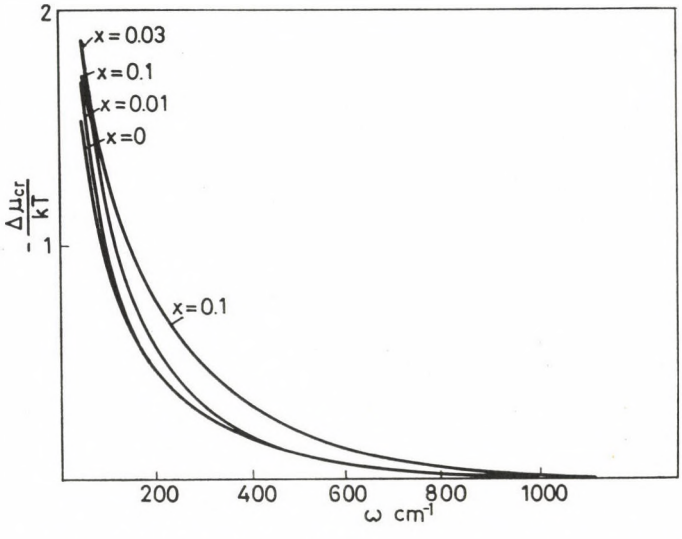

Fig. 4. Dependence of $-\Delta\mu_{cr}/RT$ on the wave number at 300 K

only at 100 cm^{-1}, that is why the local maximum of the curve develops at this point. It must be noted, however, that towards still lower frequencies, after reaching a minimum, this curve will also show an abrupt rise.

Correction for the calculation of activation entropy

As seen from the above considerations, the separation of the partition function for one degree of freedom in the form $\frac{kT}{h\nu}$ from $F^{\ddagger}$ given in Eq. (3) is a weak point of the theory. If this is not done, instead of Eq. (9), one may write:

$$k = \varkappa \nu K^{\ddagger} = \varkappa \nu \, e^{\frac{\Delta S^{\ddagger}}{R}} \, e^{-\frac{\Delta H^{\ddagger}}{RT}} . \tag{18}$$

On the basis of this the pre-exponential factor is:

$$A = \varkappa \nu \, e^{\frac{\Delta S^{\ddagger}}{R}} . \tag{19}$$

If the quotient of exponentials containing the activation entropies derived from Eqs (19) and (11) is denoted by q_S,

$$q_S \equiv e^{\frac{\Delta S_c}{R}} = \frac{kT}{h\nu\varkappa} \tag{20}$$

where ΔS_c is the correctional entropy term. Let us denote the activation entropy calculated from Eq. (11) by $\Delta S^{\ddagger}$; then the activation entropy calculated without neglections is:

$$\Delta S^{\ddagger} = \Delta S^{\ddagger\prime} + \Delta S_c = \Delta S^{\ddagger\prime} + R \ln q_S . \tag{21}$$

Determination of the transmission coefficient

In the case of a diatomic activated complex, the frequency quotient of the decomposition and the vibration of the decomposing bond, defined earlier as $\varkappa$, is equal to N_D/N, where N_D is the number of molecules with at least the dissociation energy and N is the total number of molecules. According to statistical mechanics:

$$\frac{N_D}{N} = \frac{1}{f} \int_D^{\infty} e^{-\frac{E}{RT}} dE . \tag{22}$$

Provided that the energy levels are equidistant and the partition function f can also be substituted for an integral we have

$$\frac{N_D}{N} = e^{-\frac{D}{RT}}. \tag{23}$$

Neither of the conditions holds, however, for an anharmonic vibration, therefore, in general:

$$\frac{N_D}{N} = \frac{1}{f_{anh}} \int_{\nu_D}^{\infty} e^{-av^2}\, dv \tag{24}$$

(f_{anh} has been given in Eq. (17)).

With an activated complex containing several atoms, the energy may fluctuate between several vibrational degrees of freedom. For this case, the probability of decomposition, identified here with $\varkappa$, has been calculated, among others, by HINSHELWOOD [4] with the following formula:

$$\varkappa = \frac{\left(\frac{D}{RT}\right)^{3n-7}}{(3n-7)!} e^{-\frac{D}{RT}} \tag{25}$$

with n denoting the number of atoms in the complex (in a linear complex, $3n$—6 must be taken into account instead of $3n$—7). Evidently, the case of a diatomic complex is also included in Eq. (25). Considering that the vibration of the decomposing bond is necessarily anharmonic, one should write Eq. (24) here too, instead of the exponential, and $\frac{D}{RT}$ should be replaced by an appropriately modified quantity in the numerator. It can be established, however, that Formula (25) may be used only if $\frac{D}{RT} > 3n$—7*. In this case, however, convergence of the vibrational levels is so slight that Eq. (24) may actually be replaced by the exponential given in Eq. (25). At the same time, the numerator of the expression may be left in its original form.

At frequencies corresponding to $\frac{D}{RT} < 3n$—7, the value of $\varkappa$ can be determined from the specific feature of the relationship (25), that its logarithm

* If $\frac{D}{RT}$ were not greater than $3n - 7$, further increase in the number of atoms or degrees of freedom would decrease the probability of bond decomposition. It can be also deduced that if $\frac{D}{RT} = 3n - 7$, Eq. (25) reaches a maximum and approaches 0 with decreasing frequency. This has no physical meaning.

shows a slight slope as a function of $\frac{D}{T}$, so the curve may be easily interpolated between the first calculated point and $\varkappa = 1$, which corresponds to $\nu = 0$. Figs 5a, 5b and 5c show the negative logarithm of $\varkappa$ as a function of the reduced frequency $\frac{\nu}{T}$ at different anharmonicity factors. Fig. a is valid for triato-

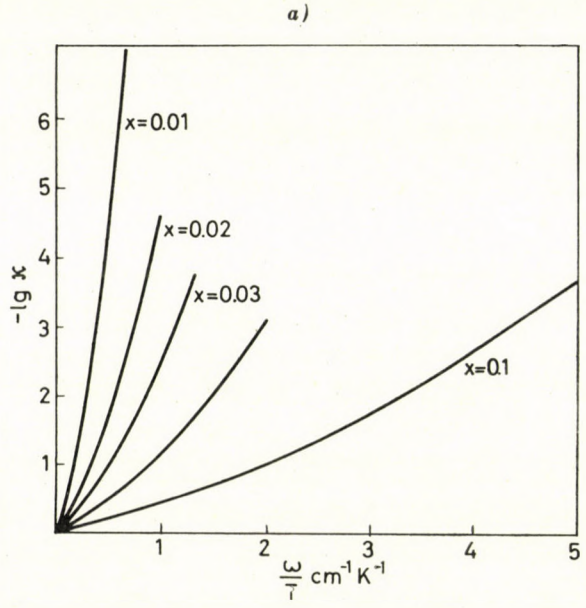

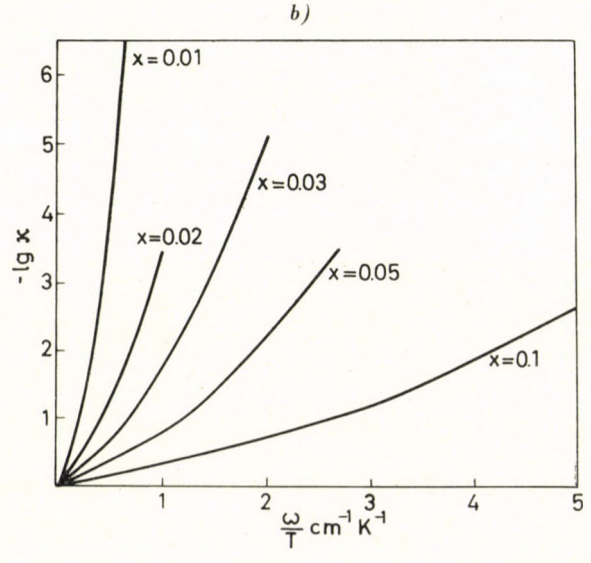

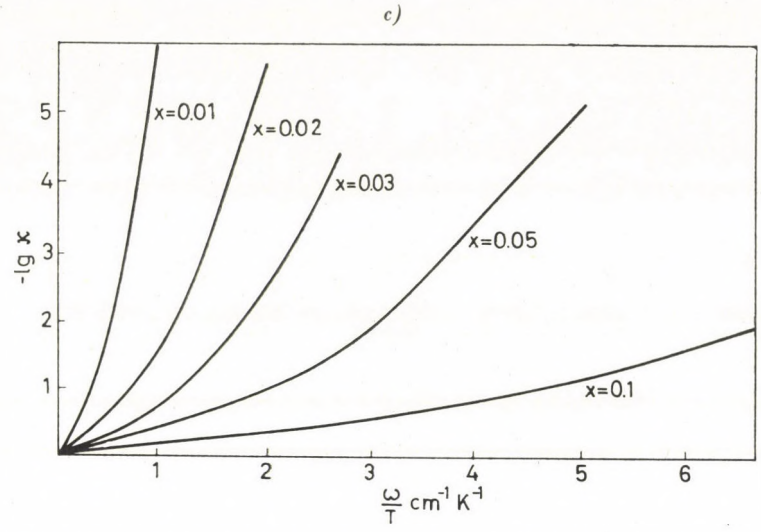

Fig. 5. Dependence of the negative logarithm of the transmission coefficient calculated from Eq. (25) on the reduced wave number ω/T for a) linear triatomic, b) non-linear tetra-atomic and c) hexa-atomic activated complex

mic linear activated complex, Fig. b holds for a non-linear tetra-atomic, and Fig. c for a non-linear hexa-atomic activated complex.

These diagrams were used in preparing Figs 6a, 6b and 6c, which leads to the value ΔS_c in Eq. (20), as a function of the reduced frequency, under

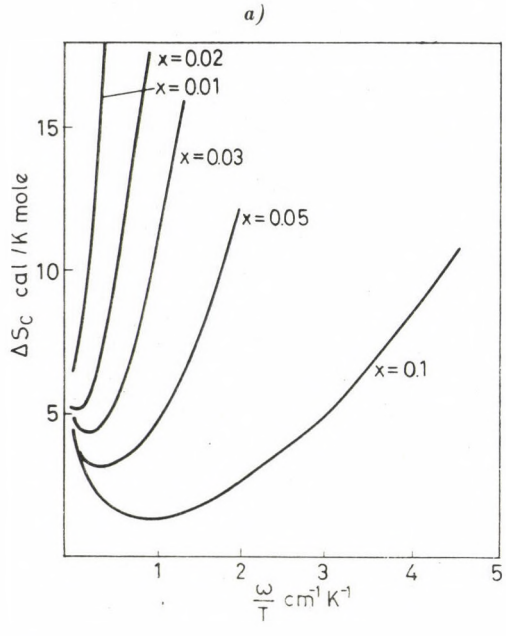

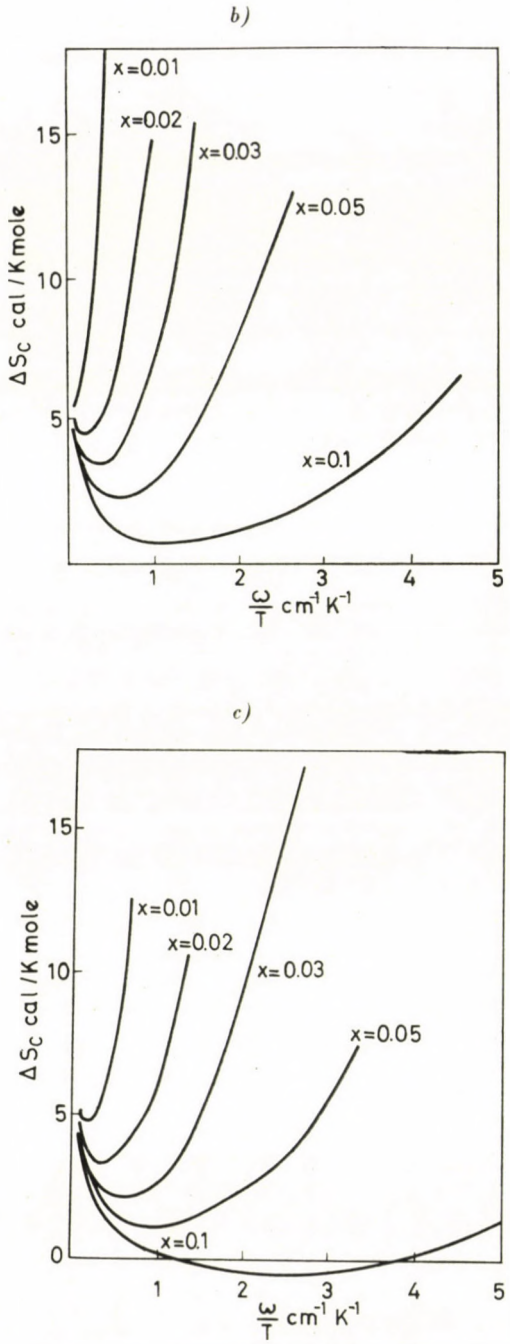

Fig. 6. Correction of the activation entropy calculated from Eq. (11) as a function of the reduced wave number for a) linear triatomic, b) non-linear tetra-atomic and c) hexa-atomic activated complex

conditions similar to the above. It can be seen that *e.g.* in the case of a hexa-atomic activated complex with an anharmonicity factor of $x = 0.1$, at reduced frequencies 1.2 and 3.8 cm^{-1} K^{-1}, the entropy correction is zero, in other words, the activation entropy calculated from Eq. (11) happens to be correct. Otherwise, in case of less anharmonic vibrations, a substantial mistake may arise with an order of magnitude of 10 cal/K.mole in the calculated activation entropy.

Estimation of the critical frequency and the anharmonicity coefficient

Table I summarizes the vibration frequencies and anharmonicity factors of some diatomic molecules. Some data of molecules in the excited electronic states are also shown in order to illustrate the energy conditions of the activated state.

These data draw attention to the following: 1. Electronic excitation substantially decreases the frequency. 2. The anharmonicity factor generally

Table I

Molecules	Excitation energy kcal/mole	Frequency cm^{-1}	Anharmonicity coefficient
AlH	0	1575	0.080
AlH($^1\Pi$)	153.5	850	
BaH	0	1323	0.017
C=C	0	1856	0.008
C=C($^3\Pi_g$)	115.2	1107	0.035
Cl_2	0	565	0.007
Cl_2($^3\Pi$)	52.6	239	0.023
H_2	0	4395	0.027
H_2($^1\Pi_u$)	287.7	2443	0.027
H_2($^1\Sigma_{+u}$)	263.5	1357	0.015
H_2^+	0	2297	0.027
HCl	0	2990	0.017
HI	0	2310	0.017
I_2	0	215	0.003
I_2($^3\Pi_{1u}$)	34.1	44	0.023
LiH	0	1406	0.016
LiH (exc.)	76.2	234	
NaCl	0	315	0.004
OH	0	3735	0.022
OD	0	2721	0.016

runs opposite to the number of electrons contained in the bond. 3. The anharmonicity factor of molecules containing hydrogen substantially increases with excitation. 4. The frequency of H_2^+ with one electron is approximately one half of that of H_2 containing two electrons. 5. The frequency of the entirely ionic NaCl is about 40% of the value calculated from HOOKE's law on the basis of a single covalent bond.

Conclusions on the frequencies of bonds occurring in the activated complex may be drawn from some classical examples. Relying on the fundamental study of BODENSTEIN [6] on the decomposition of HI, according to Formula (11), —10.7 cal/K.mole is obtained for the activation entropy of the process. EYRING [7] suggests that the activated complex is trapezoidal H_2I_2 molecule. On this basis, the translational and rotational contributions to the activation entropy may be calculated. This calculation is specified in Table II. (The data in brackets refer to an activated complex in which the bond lengths have extended by 20%). Supposing that the activation entropy calculated from Formula (11) is correct, according to the data given in the table, the vi-

Table II

Compound	HI	$H_2I_2^{\ddagger}$	$\Delta^{\ddagger}$
$\mathbf{D}/N_A$	5.92×10^{6}	1.672×10^{7}	
S_{tr}(cal/K.mole)	35.94	38.00	—33.88
I_A (kg m^2)	0	5.395×10^{-47}	
		(8×10^{-47})	
I_B(kg m^2)	4.216×10^{-47}	7.46×10^{-45}	
		$(1.05\times10^{-44}$	
I_C (kg m^2)	4.216×10^{-47}	7.515×10^{-45}	
		(1.05×10^{-44})	
F_r	58.2	7.90×10^{4}	
		(1.347×10^{5})	
S_r (cal/K.mole)	10.06	25.38	5.26
		(26.44)	(6.32)
S_{tr} + Sr(cal/K.mole)	46.00	63.38	—28.62
		(64.44)	(—27.56)

brational entropy contribution of the activated complex must be some 17 cal/K.mole. Fig. 7 showing the vibrational entropy contribution as a function of the reduced frequency has been plotted to estimate the contributions. The reduced frequency of HI vibration at the temperature of measurements 556 K exceeds 4 cm^{-1} K^{-1}, which has practically no entropy contribution. One cannot assume all covalent bonds in the trapezoidal H_2I_2 at such bond

angles. The most probable conformation is an $H_2^+I_2^-$ ion pair. The complex has six normal vibrations, five inplane and one out-of-plane. The five inplane vibrations may be classified as follows: 1. N—H stretching, 2. I—I stretching, 3. H_2^+—I_2^- stretching, 4. libration of H_2^+ in the plane, 5. translational-like motion back and forth of H_2^+ along the molecular axis. Out-of-plane vibration

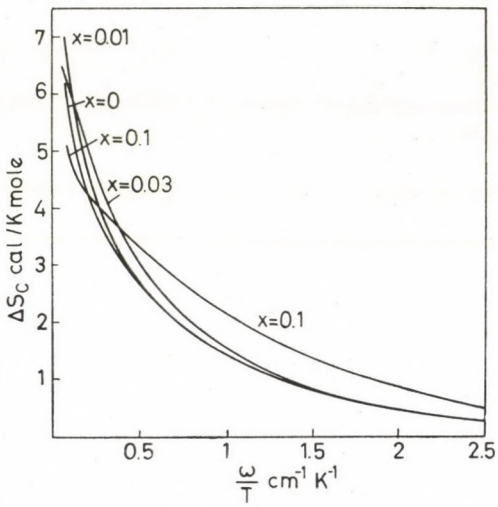

Fig. 7. Entropy contribution of a single vibrational degree of freedom as a function of the reduced wave number

is a libration of H_2^+ perpendicular to the plane. The reduced frequency of vibration 1 is around 4 and has no entropy contribution. The reduced frequency of vibration 2 is approximately 0.15 ($S = 5.5$ cal/K.mole), of vibration 3 about 0.4 ($S = 3.5$ cal/K.mole), of vibration 4 approximately 2 ($S = 0.5$ cal/K.mole), of vibration 5 approximately 0.2 (5 cal/K.mole), and that of the out-of-plane vibration is approximately 0.2 ($S = 5$ cal/K.mole). The contribution of vibrational entropy is, according to the above calculations, 19.5 cal/K.mole more than would be obtained by using Formula (11). The critical vibration here is the inplane vibration 3, that is, the $H_2^+ - I_2^-$ stretching. Due to the ionic character of the bond and the coupling to vibration 4, the vibrational frequency may be estimated as 200—250 cm^{-1} (reduced frequency: 0.4) and its anharmonicity coefficient as 0.03—0.05. On the basis of Fig. 6b, compared with Formula (11), the correction of the entropy is approximately 3 cal/K.mole, which is in conformity with the above considerations. Thus, the probable activation entropy is -8 cal/K.mole and the vibrational entropy of the activated complex is 19.5 cal/K.mole.

As another classical example, the measurements by BLADES and MURPHY [8] on the decomposition of ethylvinylether at 500 °C can be mentioned. Ac-

cording to Formula (11), the activation entropy was calculated as −10.2 cal/K.mole. This suggested that the activated complex was a cyclic formation. The process being a unimolecular reaction, there is no change of translational entropy and the negative activation entropy can only be explained by the cessation of internal rotational degrees of freedom. In vinylethylether, the internal rotation of two groups may be realized: the rotation of the CH_3 group around the O—C axis, and that of the three methyl hydrogens round the C—C axis. The reduced moments of inertia are approximately 4×10^{-46} kgm^2, and 5.5×10^{-47} kgm^2 resp. Accordingly, the entropy contributions are 8.6 and 4.7 cal/K.mole, respectively. No considerable change of the rotational entropy can be expected from the deformation of the entire molecule. It may be calculated that in the case of five atoms of similar mass, in a U-formation, the product of the three principal moments of inertia is about one and a half times that obtained from the W-formation. This gives about 0.4 cal/K.mole for the rotational entropy difference. According to the above changes, an entropy decrease of 13 cal/K.mole is obtained for the activation. If we accepted the decrease in entropy calculated from Formula (11) to be 10 cal/K.mole, we would obtain no more than 3 cal/K. mole for the vibrational entropy contribution of the activated complex. Evidently, this is an impossibly low value. The process assumed is the following:

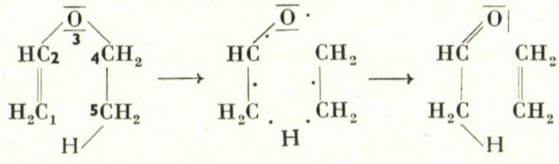

Vinylethylether has 33 normal vibrations, 4 of which are skeletal vibrations, 3 inplane skeletal bending modes, 2 out-of-plane skeletal vibrations (one of

Table III

Vibration	Reduced frequency $cm^{-1}K^{-1}$		Entropy contribution cal/K.mole	
O·C stretching	0.7	(1.0)	2.0	(1.5)
C—O·C bending	0.2	(0.3)	5.0	(3.5)
O·C—C bending	0.3	(0.4)	3.5	(3.0)
Inphase out-of-plane vibration of C_2H_4 groups	0.2	(0.3)	5.0	(3.5)
C_2H_4 libration	0.2	(Internal rotation)	5.0	
CH_2 rocking (C_3)	0.8	(Internal rotation)	2.0	
			22.5	(11.5)

this is the internal rotation of the $C-CH_3$ group), 8 CH stretchings and 16 CH bending vibrations (one of these is the internal rotation of the CH_3 group). Table III shows the reduced frequencies and entropy contributions of the low frequency vibrations of the activated complex. The reduced frequencies and entropy contributions of the corresponding vibration in the starting material are given in brackets.

No considerable change can be expected in the frequencies of the rest of the normal vibrations, i.e. also the entropy contribution of the decreased frequency is negligible. The table shows the vibrational contribution to the activation entropy to be approximately 11 cal/K.mole, while that calculated from Formula (11) is 3 cal/K.mole. The critical vibration is probably the O·C stretching whose anharmonicity coefficient is obviously very low, which explains the entropy correction of about 8 cal/K.mole. According to the above, the correct activation entropy of the reaction is only −2 cal/K.mole.

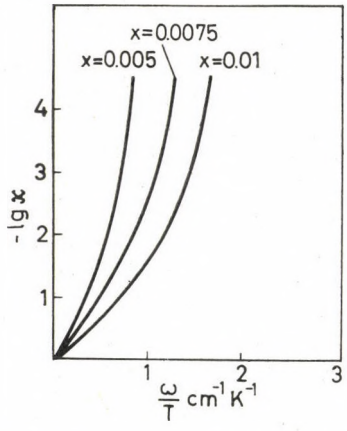

Fig. 8. Dependence of the negative logarithm of the transmission coefficient on the reduced wave number for a thirteen-atom-activated complex

According to Eqs (21) and (20), the transmission coefficient may be calculated as 0.018 from the entropy correction of 8 cal/K. mole. On the basis of Eq. (25), at a reduced frequency of 0.7 $cm^{-1} K^{-1}$ such a transmission coefficient will correspond to an anharmonicity coefficient $x = 0.007$ (Fig. 8). According to Table I, such an anharmonicity coefficient may be expected in stretchings with no hydrogen participation.

In summary of the above, the following procedure may be suggested for the calculation of the activation entropy: 1. As first approach, let us calculate the activation entropy ($\Delta S^{\ddagger\prime}$) according to Eq. (11). 2. Let us give the most probable configuration of the activated complex. 3. Then estimate the principal moments of inertia and normal frequencies of the complex. 4. On this basis, calculate from Fig. 7 the activation entropy. 5. If this approximately corre-

sponds to the result calculated from Formula (11), let us check whether or not the entropy correction is negligible, according to Fig. 6. 5/a. If, on the basis of the normal frequencies and Fig. 7, the activation entropy proves to be higher than that calculated from Formula (11), examine whether the reduced frequency of the critical normal vibration and its estimated anharmonicity coefficient explain, according to Fig. 6, the deviation from the entropy found. If either on the basis of 5 or 5/a, the deviation is not greater than 1—2 cal/K.mole, both the assumed configuration of the activated complex and the assumed rate-determining step may be considered as acceptable.

REFERENCES

1. EYRING, H.: J. Chem. Phys. **3,** 107 (1935)
2. GLASSTONE, S., LAIDLER, K. J., EYRING, H.: The Theory of Rate Processes. McGraw-Hill, New York, 1941
3. LAIDLER, K. J.: Chem. Kinetics. McGraw-Hill, New York, 1960
4. HINSHELWOOD, C. N.: Proc. Roy. Soc. **A 113,** 230 (1927)
5. HERZBERG, G.: Molecular Spectra and Molecular Structure, I. Van Nostrand, 1950
6. BODENSTEIN, H.: Z. phys. Chem. **29,** 295 (1899)
7. WHEELER, A., TOPLEY, B., EYRING, H.: J. Chem. Phys. **4,** 178 (1936)
8. BLADES, A. T., MURPHY, G. W.: J. Am. Chem. Soc. **74,** 1039 (1952)

György VARSÁNYI; Budapest XI., Budafoki út 8.

Acta Chimica Academiae Scientiarum Hungaricae, Tomus 68 (4), pp. 339—344 (1971)

INVESTIGATION OF ADSORPTION PHENOMENA ON PLATINIZED Pt ELECTRODES BY TRACER METHODS, VIII

NEW OBSERVATIONS CONNECTED WITH THE POTENTIAL DEPENDENCE OF THE ADSORPTION OF ACETIC ACID AND SULFURIC ACID

Gy. HORÁNYI, E. M. RIZMAYER and F. NAGY

(Central Research Institute for Chemistry of the Hungarian Academy of Sciences, Budapest)

Received January 8, 1970

It was found that a relation of the form $f(c) \cdot F(E)$ can be written to a good approximation for the dependence of adsorption on concentration and potential for acetic acid and sulfuric acid (similarly as for hydrochloric acid).

In the studied cases more or less well separated sections occur in the potential dependence of the adsorption.

In an earlier communication [1] it was shown that for the dependence on the potential (E) and concentration (c) of the adsorption of chloride ions, to a good approximation an equation of the type

$$\Gamma = f(c) \cdot F(E) \tag{1}$$

is valid; that is, the adsorption is given by the product of two functions of one variable each.

We arrived essentially at the same conclusion from our earlier studies [2, 3] connected with the adsorption of acetic acid and sulfuric acid, but on the basis of the fact that with increase of concentration at each potential the adsorption approached different limiting values this finding was so formulated that the maximum adsorbed amount is a function of the potential.

Similarly, in connection with the study of the adsorption of chloride ions we came to the conclusion that $F(E)$ can be given to a good approximation in the form

$$F(E) = \frac{A \cdot 10^{b_1(E-E_{01})}}{1+10^{b_1(E-E_{01})}} + \frac{B \cdot 10^{b_2(E-E_{02})}}{1+10^{b_2(E-E_{02})}} . \tag{2}$$

Our earlier studies with sulfuric acid and acetic acid covered concentrations of only 10^{-3}—10^{-4} M. The potential was varied in large, 100 mV steps and so from the data arising from these measurements it was possible to draw only limited conclusions on the validity of Eq. (1) and no conclusions at all on Eq. (2). Thus, to answer the question, there was a need for further measurements; we report on these in the present communication.

Experimental

Studies were made in the apparatus and with the method reported earlier [4]. The greatest concentration used in the case of sulfuric acid was 10^{-1} M, and for acetic acid 10^{-2} M. As an illustration of the possibilities and accuracy of measurement, in Table I are given the overall count rates (I_t) measured at 700 mV and the count rate (I_Γ) proportional to the adsorbed amount as determined from I_t according to reference [2], in the cases of several measurements.

Table I

Count rates measured at 700 mV with various electrodes and specific activities

c (M)	I_t (cpm)	I_Γ (cpm)
	Sulfuric acid	
10^{-2}	108,000	94,000
10^{-1}	19,700	9,300
	Acetic acid	
10^{-4}	200,000	198,000
2×10^{-3}	45,000	43,000
5×10^{-5}	241,000	240,000
5×10^{-3}	91,000	82,000
5×10^{-2}	14,000	7,000

As may be seen from the Table, the accuracy of measurement deteriorates considerably at high concentration. The count rate proportional to the adsorption is generally smaller at higher concentrations because the increase of concentration could in general be achieved only with the simultaneous decrease of the specific activity. For the study of the validity of Eq. (1), the count rate arising from the adsorbed material measured at different potentials at each concentration were divided by the count rate observed at 700 mV. These quantities (Γ_r) are given as a function of the potential in Figs 1 and 2 for acetic acid and sulfuric acid, respectively. For the sake of clarity, only the points measured for certain concentrations are given.

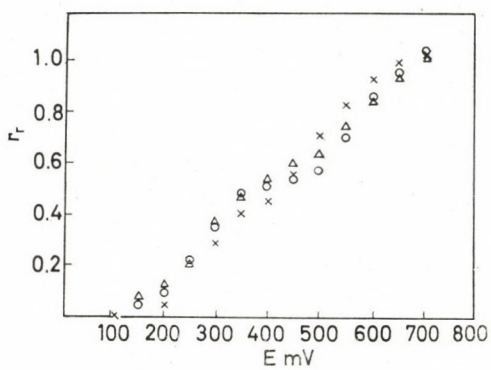

Fig. 1. Dependence of Γ_r on the potential at various concentrations of acetic acid. △ 5×10^{-5} M; × 5×10^{-3} M; ○ 10^{-2} M

It may be seen from the Figures that the potential dependence of Γ_r is scarcely affected by concentration changes of almost five and three orders of magnitude, respectively, for sulfuric acid and acetic acid. It would not be a significant mistake if a single curve were drawn through the points, and so it must be accepted that Eq. (1) is valid in these cases too. In the following the question arises as to the form of the function $F(E)$. This question will be treated separately for the two acids.

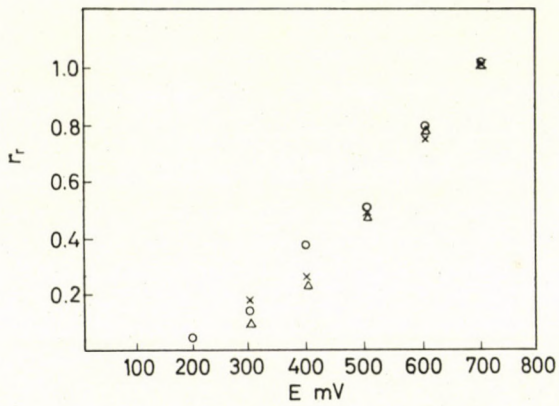

Fig. 2. Dependence of Γ_r on the potential at various concentrations of sulfuric acid. ○ 10^{-6} *M*; △ 10^{-4} *M*; × 10^{-1} *M*

Adsorption of acetic acid

The potential dependence of the adsorption of acetic acid at a concentration of 5×10^{-3} *M* is shown in Fig. 3 (curve 1). The individual points were measured at 50 mV intervals on freshly prepared electrodes pre-treated by anodic and cathodic polarization (20—30 mA).

This curve apparently differs from those reported earlier [3] in which the relatively flat section at potentials between 300 and 500 mV is missing. The reason for this, the change of the potential in too large steps, has already been mentioned. Apart from this, it must also be noted that the nature of this section depends to a large extent on the life-history of the electrode and on such factors as are at present insufficiently understood. In the case of the study of the adsorption of chloride ions, it was shown that changes occur in the nature of the potential dependence of the adsorption with the ageing of the electrode and with its use [1]. Substantially the same is observed in the case of acetic acid too.

For the characterization of the potential dependence of adsorption, $\frac{d\Gamma_r}{dE} - E$ curves were used. Curve 2 of Fig. 3 was drawn on the basis of the $\frac{\Delta\Gamma_r}{\Delta E}$ values calculated from the measured data corresponding to curve 1.

For the sake of comparison we also show the $\frac{\Delta\Gamma_r}{\Delta E}$ curve (curve 3) determined in a study of the adsorption of chloride ions and reported in an earlier communication.

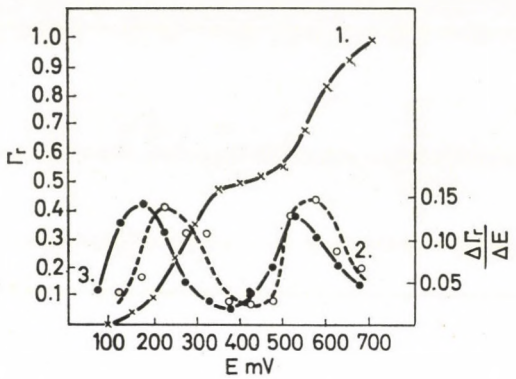

Fig. 3. Dependence of Γ_r (curve 1) and $\Delta\Gamma_r/\Delta E$ (curve 2) on the potential at an acetic acid concentration of 5×10^{-3} M. Potential dependence of $\Delta\Gamma_r/\Delta E$ in the case of chloride ions (curve 3)

From curves 2 and 3 it appears that there is no substantial difference in behaviour between the two adsorbed materials. In both cases two maxima occur. The positions of the maxima correspond to the values of E_{01} and E_{02} in Eq. (2) (if E_{01} and E_{02} are far enough from each other, and in the present case this is so).

Without engaging in too far-reaching conclusions, we may state that the adsorption of acetic acid is probably of the same type as that of chloride ions, *i.e.* it can be described by a potential dependence of the same form as Eq. (2).

It appears that the constants A and B in the two cases are of approximately the same magnitude. The difference would be primarily in the values of E_{01} and E_{02}.

From the comparison of several measurements, however, it is clear that there is a considerable scatter, especially in the value of E_{02}. What makes the measurements rather difficult is that acetic acid is adsorbed quite weakly, and so the impurities present even in low concentration exert a displacement effect. For this reason we believe that there is only the possibility of establishing the above-mentioned tendencies from our measurements.

We cannot say too much either regarding the form of the function $f(c)$. We can establish that at concentrations above 10^{-3} M the adsorption depends but slightly on the concentration. As already mentioned, in our experiments the increase of concentration was effected by adding inactive acetic acid in several steps to the labelled acetic acid present in low concentration. Naturally,

during this, the specific activity too decreased which, in the case of unchanged adsorption, results in the proportional decrease of the count rate.

The results of a measurement series carried out at 700 mV are given in Table II.

It may be seen from the data in the Table that the count rate for concentrations above 2×10^{-3} M is almost inversely proportional to the concentration, that is the adsorption already changes only slightly with concentration.

Table II

c (M)	I_Γ (cpm)
10^{-4}	295,000
2×10^{-3}	41,000
10^{-2}	9,400
5×10^{-2}	2,000

Adsorption of sulfuric acid

Phenomena agreeing essentially with the observations for acetic acid were found in the case of sulfuric acid too. The values of Γ_r determined at a sulfuric acid concentration of 10^{-1} N are given in Fig. 4. The $\frac{\Delta\Gamma_r}{\Delta E}$—$E$ curve relating to these is drawn with a dashed line.

The potential dependence of the adsorption was also studied for 10^{-1} N sulfuric acid without perchloric acid as background electrolyte. The corresponding curves are shown in Fig. 5. (In this case the potential refers to a 1

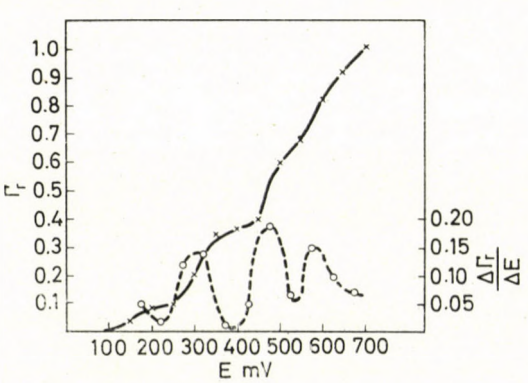

Fig. 4. Potential dependence of Γ_r and $\Delta\Gamma_r/\Delta E$ at a sulfuric acid concentration of 10^{-1} N in a 1 N perchloric acid background solution

atmosphere hydrogen electrode immersed into 10^{-1} N sulfuric acid solution.) There is no substantial difference between the values observed with and without perchloric acid.

A comparison of Figs 3, 4 and 5 shows that the difference between acetic acid and sulfuric acid lies in the appearance of a third peak. This means the

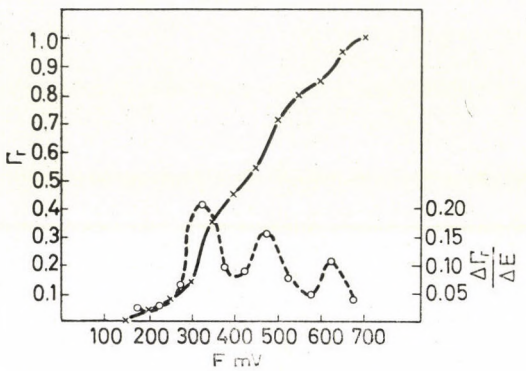

Fig. 5. Potential dependence of Γ_r and $\Delta\Gamma_r/\Delta E$ at a sulfuric acid concentration of 10^{-1} N without perchloric acid background solution

occurrence of a third term in Eq. (2). Here too the experimental uncertainty is too large for us to attempt the determination of the form of the function in addition to the revealed tendencies.

The presented experimental results in all cases indicate that on platinum more or less separated sections appear in the potential dependence of the adsorption.

For the evaluation of the phenomena it is probably necessary to develop a new model of adsorption. However, this can only be done after the acquisition of more experimental results.

REFERENCES

1. Solt, J., Horányi, Gy., Nagy, F.: Magy. Kém. Foly. **76,** 636 (1970)
2. Horányi, Gy., Solt, J., Nagy, F.: Magy. Kém. Foly. **73,** 561 (1967)
3. Solt, J., Horányi, Gy., Nagy, F.: Magy. Kém. Foly. **74,** 52 (1968)
4. Solt, J., Horányi, Gy., Nagy, F.: Magy. Kém. Foly. **73,** 414 (1967)

György Horányi
Edit M. Rizmayer
Ferenc Nagy
Budapest II., Pusztaszeri út 59—67.

Acta Chimica Academiae Scientiarum Hungaricae, Tomus 68 (4), pp. 345—358 (1971)

APPROACH OF THE EQUALIZED ELECTRONEGATIVITY BY MOLECULAR PARAMETERS

S. SZŐKE

(Central Research Institute for Chemistry, Hungarian Academy of Sciences)

Received January 23, 1970

The mean electronegativities which are satisfactory approximations for the equalized ones can be brought into close relation with the simplest molecular parameters. The force constants of diatomic molecules or of single isolated bonds can be expressed by means of the equalized electronegativities, bond orders, bond strengths and interatomic distances.

Using the force constant relationship, the equalized electronegativity can be applied for the construction of empirical potential energy functions.

Similarly, a simple relationship can be observed between the electronegativities, vibrational force constants, and quantum-chemical two-center (molecular or bond) repulsion integrals.

The potential energy functions of di- and polyatomic molecules can be determined with the necessary accuracy even in our days — in most cases only by parameters of empirical character. The empirical parameters are established by spectroscopic measurements. We very seldom encounter solutions in which the application of parameters other than those of spectroscopic origin are tried for the calculation of energy levels.

Electronegativity was introduced into theoretical chemistry by PAULING; this is the energy by which an atom attracts an electron or electrons belonging to another atom, for establishing a bond. His scale is based on thermochemical data but, to a certain extent, he met difficulties in correct dimensioning. The first interpretation which proved to be satisfactory was given by MULLIKEN, relating this concept to two parameters of energy dimensions, the electron affinity and the ionization potential. In the definition given by MULLIKEN already parameters for the actual valence state occur.

The dimensional problem was finally solved by ICZKOWSKI and MARGRAVE, who showed that if either ionization potential or electron affinity are considered, the energy change involves also a change in the charge. According to these authors, the potential must be accepted as a dimension (energy/charge meaning potential). The concept that electronegativity — although its numerical values are determined by the atomic structure — is reasonable only when associated with a chemical bond, takes its origin from the work of HINZE and JAFFÉ. Similarly to the ionization potential or electron affinity,

electronegativity, too, connected with atomic orbitals combined to molecular orbitals.

Like the covalent atomic radii, this is a typical 'atoms in the molecules' property determining a concept — the bond length — which has no sense in atomic aspects.

Equalized electronegativity

In connection with the chemical bond and the formation of molecules we have to consider the equalization of electronegativities. The electronegativity of the atoms forming a chemical bond must become equal, otherwise equilibrium could not exist. The concept of equalized electronegativity was introduced by SANDERSON [1] into the valence theory and was later extended to orbital electronegativities.

According to PRITCHARD [2] equalization is, however, not perfect, because if the interactions between electrons are also taken into consideration, the electronegativity values for the constituent atoms are not perfectly equal but deviate on the two atoms by some $\pm 5\%$ from a calculated mean value.

Quantum-chemical approximation of electronegativity

The principles laid by HINZE and JAFFÉ [3] as well as by HINZE, WHITEHEAD and JAFFÉ [4] are the starting point for a number of theoretical works; their results are referred to in most semi-empirical procedures of quantum chemistry.

For calculating equalized electronegativities one of the most frequently used possibilities is the iterative procedure elaborated by PRITCHARD and SUMNER [5]; in this SCF procedure the Coulomb integral α_q is replaced by the electronegativities of π-orbitals. Subscript q refers to the occupancy of the orbitals, and electronegativity can be considered as a function of the occupancies. In every cycle of the calculations the overlap integrals and α_q-s are to be adjusted to the occupancies calculated in the former cycle, until we obtain SCF series of charge distributions. The mean electronegativity of the system $-C=N-$, $[C(t_1t_2t_3\,\pi);\ N(t_1^2t_2t_3\pi)]$ according to the PAULING scale, is 2.75, in the MULLIKEN system 6.82; by the iterative procedure we get for the carbon atom 6.50 and for the nitrogen 7.13; the deviation from the mean value is thus about $\pm 5\%$ [6].

The principles of the quantum chemical approach and methodology of the neutral atomic electronegativity were elaborated by MULLIKEN [6, 7], ICZKOWSKI and MARGRAVE [8], HINZE and JAFFÉ [9], HINZE, WHITEHEAD and JAFFÉ [3], KLOPMAN [10, 11], JÖRGENSEN [12], PRITCHARD [13], PRIT-

CHARD and SKINNER [14], BAIRD and SICHEL [15], BAIRD, SICHEL and WHITEHEAD [16]. The expression

$$x_A = I_A^v + A_A^v \tag{1}$$

given by MULLIKEN, where x_A is the electronegativity of the atom A, I_A^v and A_A^v are the ionization potential and electron affinity, respectively, forms the basis of a number of quantum-chemical procedures, mainly of those which are in extended use also at present (PPP, EH, CNDO and others).

The approach of equalized electronegativity by molecular parameters

A number of theoretical and spectroscopic parameters serve for the characterization of the chemical bond and, accordingly, the chemical bond can be classified from several points of view. The classification has been performed on the basis of the separated atom configurations [17]; this method has a number of advantages, *e.g.* it requires only integer and half integer bond orders, which can be given by the following simple formula

$$N = 1/2\,(\Sigma q_b - \Sigma q_{ab}) \tag{2}$$

where N is the bond order; q_b is the occupancy of bonding and q_{ab} that of the antibonding orbitals.

Some of the molecular parameters can be determined on the basis of various spectra. With the aid of these it is intended to elucidate the qualitative properties of the bond.

The strength of the bond was earlier referred to as the dissociation energy belonging to the vibrational quantum number: $v = 0$. Since the energy state of the dissociated products is not always known exactly MULLIKEN [18] suggested either the vibrational frequency or the reciprocal bond distance instead. As to the vibrational frequency, its connection with the vibrational force constant is well known, and thus the possibility arises that some ratio of the dissociation energies and interatomic distances be used as parameter in the most characteristic expression for the bond strength.

There is a characteristic relationship between the two above mentioned quantities within a given type of molecule; we found the following expression valid:

$$\bar{k}_e = d\varepsilon \bar{D}_e^{1/2} r_e^{-1} \tag{3}$$

where $\bar{k}_e$ is the force constant reduced to unit bond order, $\varepsilon = (x_A x_B)^{1/2}$ is the mean value of the electronegativities of the atoms forming the bond, D_e is the dissociation energy similarly reduced to unit bond order; r_e is the in-

teratomic distance. Eq. (3) can be written in the following form:

$$\varepsilon = \frac{\bar{k}_e}{d} \frac{r_e}{\bar{D}_e^{1/2}} \tag{4}$$

or taking the bond order into consideration,

$$\varepsilon = \frac{k_e}{d} \left[\frac{r_e^2}{DN} \right]^{1/2} . \tag{5}$$

Eq. (5) can be regarded as an approach by molecular parameters of the equalized electronegativity established [19, 20] by quantum-chemical methods; thus the electronegativity shows essentially the relationship existing between the two quantities $(D_e/r_e^2)^{1/2}$ and k_e, characterizing the bond strength.

Some examples for the validity of Eq. (3)

The criterion for the validity of Eqs (3) and (5), respectively, is, within a given molecule type, a good approximate agreement of the d constants. In the following tables the dissociation energies are given in Kcal/mole, the force constants in mdyn/Å, the interatomic distances in Å, and the atomic electronegativity values are taken from PAULING. The electronegativities of PAULING have their limitations; that they can be successfully used in approximate cases is due to the fact that the single values reflect a relatively good mutual ratio, offering a more or less appropriate basis for comparison.

Of course, all electronegativity scales give schematic values, therefore when checking on the maximal errors of d ($\pm 10\%$), besides the uncertainty of the dissociation energy data, we must be well aware of this fact.

Table I shows the parameters of the alkali metals and alkali hydrides, as well as the corresponding d constants of Eq. (3); these constants characterize the $ss\sigma$ bond, and their average value is 0.137 ± 0.001 and 0.15 ± 0.002, respectively.

The dissociation energy data referred to in Table I were taken from the monograph of GAYDON [21]. The interatomic distances and force constants in the paper were taken from the parameter values of COTTRELL [22] compiled mainly on the basis of HERZBERG's data.

Table II gives the parameters characterizing the hydrides of group **Va, VIa** and **VIIa** elements. In these molecules bonds of the $ps\sigma$ type can be found. Values of the d constant were given only for those diatomic molecules, for which realistic basic parameter values could be obtained.

Table I

Parameters of group **Ia** *hydrides and group* **Ia** *homonuclear molecules*

a)

	k_e (mdyn/Å)	r_e (Å)	$\frac{(x_1x_2)^{1/2}}{\varepsilon}$	D_e (Kcal/mole)	d
LiH	1.026	1.596	1.448	58	0.148
NaH	0.781	1.887	1.376	47	0.156
KH	0.561	2.244	1.296	43	0.148
KH	0.561	2.244	1.296	43	0.148
RbH	0.545	2.376	1.296	41	0.150
CsH	0.467	2.494	1.212	42	0.148

Average: 0.151

b)

	k_e (mdyn/Å)	r_e (Å)	$\frac{(x_1x_2)^{1/2}}{\varepsilon}$	D_e* (Kcal/mole)	d
Li_2	0.255	2.672	1.0	25	0.136
Na_2	0.172	3.078	0.9	17.3	0.141
K_2	0.099	3.923	0.8	11.8	0.140
Rb_2	0.082	4.200	0.8	10.8	0.131
Cs_2	0.069	4.420	0.7	10.4	0.135

* Dissociation energies taken from GAYDON [21]

Table II

Parameters of group **Va, VIa** *und* **VIIa** *hydride molecules*

	k_e	r_e	ε	D_e	d
NH	6.030	1.038	2.51	84.0	0.272
PH	3.257	1.433	2.10	71.0	0.264
OH	7.792	0.971	2.71	103.0	0.275
SH	4.193	1.350	2.29	82.3	0.272
FH	9.655	0.917	2.90	135.0	0.263
ClH	5.157	1.257	2.51	102.2	0.260
BrH	4.117	1.414	2.42	86.5	0.259
IH	3.142	1.604	2.29	70.5	0.262

The average d value for these molecules is 0.266 ± 0.005. The dissociation energies were taken from the monograph of VEDENEYEV [23]. The parameters of group **IIa, IIIa** and **IVa** hydrides are listed in Table III. Bond types $sp\sigma$ and $sps\sigma$ are assumed in these molecules. Beryllium has two $sp\sigma$ hybridized electrons, carbon has four.

Table III

Parameters of group **IIa, IIIa, IVa** *hydride molecules*

	k_e	r_e	ε	D_e	d
BH	3.044	1.232	2.05	70.0	0.219
AlH	1.620	1.646	1.78	67.0	0.183
BeH	2.263	1.343	1.78	54.0	0.235
MgH	1.275	1.731	1.59	46.0	0.204
CaH	0.977	2.002	1.45	42.4	0.207
SrH	0.854	2.145	1.45	38.0	0.202
CH	4.482	1.120	2.29	80.0	0.245
SiH	2.39	1.521	1.94	75.1	0.216

Table IV

Orbital configurations of period I hydrides

LiH	$1\sigma^2$	$2\sigma^2$			$x^1\Sigma^+$
BeH	$1\sigma^2$	$2\sigma^2$	3σ		$x^2\Sigma^+$
BH	$1\sigma^2$	$2\sigma^2$	$3\sigma^2$		$x^1\Sigma^+$
CH	$1\sigma^2$	$2\sigma^2$	$3\sigma^2$	1π	$x^2\Pi r$
NH	$1\sigma^2$	$2\sigma^2$	$3\sigma^2$	$1\pi^2$	$x^3\Sigma^-$
OH	$1\sigma^2$	$2\sigma^2$	$3\sigma^2$	$1\pi^3$	$x^2\Pi i$
FH	$1\sigma^2$	$2\sigma^2$	$3\sigma^2$	$1\pi^4$	$x^1\Sigma^+$

The data for covalent homo- and heteronuclear molecules are given in Table IX together with dissociation energies taken from VEDENEYEV. The electron configurations for the diatomic hydrides of atoms in the first period are shown in Table IV according to CADE and HUO [24]. Graduality in the number of electrons implies graduality in the atomic distances, force constants and dissociation energies too.

In Table V the electronegativities equalized according to Eq. (5) are compared with the geometrical means of atomic electronegativities. The deviations average about $\pm 2\%$.

Table V

a) *Equalized parameters calculated from molecular parameters*
b) *The geometric means of the* PAULING *values*

Molecules	*a*	*b*
NH	2.45	2.51
PH	2.12	2.10
OH	2.55	2.71
SH	2.24	2.29
FH	2.93	2.90
ClH	2.57	2.57
BrH	2.36	2.36
IH	2.32	2.32

d values of molecular ions

The validity of Eq. (3) is most convincingly justified by the constancy of the *d* values for molecular ions.

The molecular ions are formed by removal of a bonding or an antibonding electron. If a bonding electron is removed the force constant, the dissociation energy and the reciprocal interatomic distance will diminish; if an antibonding electron is removed, these characteristic values will increase. It is very regrettable that the cases occurring in the literature are not always so unequivocal and it is very hard to decide whether it is an experimental error or an anomaly (most often in the dissociation energy).

When a bonding electron is removed, the bond order decreases by 0.5, in the opposite case it increases by the same value. In this manner, bond orders of integer or half integer values are obtained for the molecules. The H_2^+, HF, HO^+ and HCl^+ molecular ions have a bond order of 0.5 while MgH^+ and BeH^+ have a bond order of 1. A rather marked change can be observed in the HF^+, where the force constant decreases from 9.655 to 4.99 [25]. A similar situation occurs with OH^+ where we obtain 4.88 mdyn/Å for the force constant instead of the value of 7.79 in OH. Between the force constants of BeH and BeH^+ the deviation is not so considerable (2.263 and 2.640 mdyn/Å). At the same time the dissociation energy rises from 53 to 75 Kcal/mole [21]. The bond strength has changed remarkably because the two hybrid electrons have perturbed each other in BeH. In the BeH^+, ionization has changed neither the bond order nor the equalized electronegativity. It has been assumed that equilibrium is regained by the rearrangement of energy values. We call attention to the fact that some of these parameter values cannot be regarded as finally accepted;

we also have to expect changes mainly in the atomic but also in the orbital electronegativities. The bond orders based upon the separated atomic orbital configurations determined by MULLIKEN are suitable to our purposes, since the dissociation energy leading to separate atoms serves as one of the basic parameters.

Table VI

Parameters of hydride molecular ions

	k_e	r_e	D_e	ε	N	d
BeH	2.263	1.334	53^{V}	1.78	1.0	0.235
BeH^+	2.64	1.310	75^{V}	1.78	1.0	0.224
BH	3.044	1.232	70	2.05	1.0	0.219
BH^+	3.23	1.215	30	2.05	0.5	0.247
CH	4.482	1.120	$80^{V,G}$	2.29	1.0	0.245
CH^+	4.11	1.130	$84^{V,G}$	2.29	1.0	0.221
OH	7.792	0.971	$102^{V,G}$	2.71	1.0	0.275
OH^+	4.88	1.03	111^{G}	2.71	0.5	0.244
FH	9.655	0.917	$135^{V,G}$	2.90	1.0	0.263
FH^+	4.99	1.08	106^{V}	2.90	0.5	0.255
AlH	1.62	1.646	$67^{V,G}$	1.78	1.0	0.183
AlH^+	1.76	1.59	67	1.78	1.0	0.192
H_2	5.733	0.74	104	2.1	1.0	0.198
H_2^+	1.567	1.06	61	2.1	0.5	0.143

Some calculated data for a few molecular ions are shown in Table VI, demonstrating in these cases that when the molecule releases a bonding or an antibonding electron, the d values remain nearly constant while all the basic parameters change.

Empirical potential energy functions and mean electronegativities

For the empirical potential energy functions the following relation and similar ones are known from the literature [26]:

$$U(r) = D_e\left[1 - e^{-(k/aD)^{1/2} f(r)}\right] \tag{6}$$

where $U(r)$ is the potential energy, and a is 1 or 2; $f(r)$ is a function of the interatomic distances. With mean electronegativities, we obtain:

$$U(r) = D_e\left[1 - e^{-\gamma f(r)}\right] \tag{7}$$

and

$$\gamma = d\left[\frac{x_A x_B}{D}\right]^{1/2}. \tag{8}$$

If Eq. (7) is rearranged to the following form

$$\frac{D_e - U(r)}{D_e} = \bar{D}(r) = e^{-\gamma f(r)} \tag{9}$$

and if the PAULING electronegativity is replaced by the MULLIKEN one, we obtain

$$\bar{U}(r) = \exp\left[-d' If(r)\right] \exp\left[d' Af(r)\right]. \tag{10}$$

In the above equation,

$$I = \left[\frac{I_A I_B}{D}\right]^{1/2} \quad \text{and} \quad A = \left[\frac{A_A A_B}{D}\right]^{1/2}$$

I_A is the ionization potential; A_A is the electron affinity.

The force constant equation and molecular terms

The parameters occurring in the force constant equation have their quantum chemical equivalents and, consequently, the force constants can be expressed by the terms used in quantum chemistry. With regard to the fact that we need molecular parameters, only terms (integrals) of two centers (atoms) can be used for replacing the spectroscopic parameters.

The connection between the dissociation energy and the resonance integral (two-center exchange integral) was given first by MULLIKEN [6, 7]. PEARSON [27] and KLOPMAN [10] calculated bond and dissociation energies on the basis of the approximation

$$D_e = 2\beta. \tag{11}$$

The reciprocal interatomic distances represent essentially the repulsion energy between the bonding electrons. According to POPLE, this energy in bonds is approximated most simply by the expression e^2/r (in these equations e is the charge of the electron). In the derivation of POPLE, the point charge approximation can be extended to any single electron pair bond. According to KLOPMAN, when s electrons are bonding, the formula

$$\gamma_\sigma = e^2/\sqrt{r^2 + \varrho(x) + \varrho(y)} \tag{12}$$

is suggested for the repulsion term (where γ_σ is the repulsion term and ϱ is the radius of s orbitals). According to KLOPMAN and BRATOŽ [28], the values of the covalent atomic radii agree with the radii of s orbitals; this means that when applying Eq. (12) in Eq. (3) the proportionality constant d increases to 1.5 times its value and approaches the d's of the bonds coupled by p-electrons [19].

If we insert β or γ terms into the force constant relationship (5), the relation remains valid with the same restrictions as in the approximation from which the applied parameter has been taken. Replacing the mean electronegativity by the mean value of the SCF Coulomb terms, the force constant can be approached as follows

$$k = d\alpha\beta^{1/2}\gamma. \tag{13}$$

This relation is only suitable for the demonstration of analogies. In the most simple cases it shows the connection between the individual quantum chemical repulsive and attractive terms, and the force constants and other spectroscopic characteristics.

If, however, we wish to obtain values for the force constants or the potential energy levels (with which the former are in close connection) in good approximation to the experimental data, we cannot be satisfied with such simple terms as those used in Eq. (13). Therefore one of the two-center repulsion integral approximations of MATAGA and NISHIMOTO [29], or OHNO [30], should be inserted into the originally given force constant relationship, for the repulsion term e^2/r recommended by POPLE

$$\gamma = e^2/(r+a)$$
$$\gamma = \frac{e^2}{\sqrt{r^2+a^2}} \tag{14}$$

where a is an expression containing ionization potentials and electron affinities of the atoms forming the bond, which can be traced back to the MULLIKEN electronegativities [29, 30].

Similarly, the equation $D_e = 2\beta$ must also be corrected by an expression which, according to the derivation of MULLIKEN, PEARSON, SICHEL and WHITEHEAD [6, 12, 27, 32], contains elements of the bond order (occupancy) matrix and the overlap integrals.

Eq. (13) in the above form is restricted to single electron pair bonds.

Atomic orbital exponents and electronegativities

A number of authors have investigated the relationship between electronegativities and effective atomic charges [33, 34, 36, 37].

The connection between the SLATER orbital exponents and PAULING's electronegativity scale becomes clear when in the first rows of the periodic

table two corresponding values are referred to each other. The ratios thus obtained can be seen in Table VII. In the second row the ratio of the two data is 0.65. In the third period we do not get such a perfect constant, nevertheless, the ratio of the two values is suitable for demonstrating the numerical parallelism of the two concepts.

Table VII

	Li	Be	B	C	N	O	F	Average
I_a	0.65	0.975	1.30	1.625	1.95	2.275	2.6	
I_b	1.00	1.50	2.00	2.50	3.00	3.50	4.00	
I_c	0.65	0.65	0.65	0.65	0.65	0.65	0.65	0.65
	Na	Mg	Al	Si	P	S	Cl	
II_a	2.20	2.85	3.50	4.15	4.80	5.45	6.10	
II_b	0.90	1.20	1.50	1.80	2.10	2.50	3.00	
II_c	2.44	2.38	2.33	2.31	2.29	2.18	2.03	2.28

I_a Orbital exponents.
II_a Effective nuclear charge data from SLATER.
I_b, II_b Electronegativity data from PAULING.
I_c, II_c Ratio of rows *a* and *b*.

Table VIII

Orbital exponents of elements in the second period according to SLATER *(I) and* SANTRY–SEGAL *(II)*

	Na	Mg	Al	Si	P	S	Cl
I	0.73	0.95	1.17	1.38	1.60	1.82	2.03
II	0.92	1.23	1.56	1.89	2.19	2.52	2.82
III	0.90	1.20	1.50	1.80	2.10	2.50	3.00
II/III	1.02	1.04	1.05	1.04	1.04	1.01	0.94

III: PAULING electronegativities

In Table VIII the numerical values for the period are shown with the difference that the orbital exponents are given according to SANTRY and SEGAL who included into the calculation also the electrons of *d*-orbitals [36]. The ratio of their orbital exponents and electronegativities is 1.014 ± 0.02.

The two valence theory parameters must be in close connection; the energy of attraction between a given atom and the electrons of another atom is in correlation with the energy of interaction with its own electrons. The scales of the single characteristics cannot be calculated simply and at the same time also reliably enough, therefore the parallelism often remains concealed.

The attraction and repulsion terms involved in the operators can be brought into correlation with the potential energy functions *via* the force constant relationship.

The electronegativity and ionization potentials as well as the core and repulsion integrals in the semi-empirical methods of quantum chemistry are well defined characteristics of the chemical bond.

The one-center repulsion integral term and electronegativity

The MULLIKEN electronegativity scale rests upon a more exact basis than that given by PAULING. In spite of this, the construction of a system extensible to the whole periodic table has been unsuccessful, owing to the fact that the ground state electron affinities can be calculated only with considerable error [8, 9].

The same difficulty emerged in the semi-empirical quantum chemical calculations when one-center repulsion integrals were to be determined. Using the P.P.P. method, a number of authors have avoided the electron affinity by deriving the one-center repulsion energy term from the easily calculable C-atom term, multiplying it by the ratio of the corresponding SLATER $2p$-orbital exponents. PAOLONI has shown that the repulsion terms are proportional to these orbital exponents [39]:

$$\gamma_{AA} = k\xi_A \tag{15}$$

where γ_{AA} and ξ_A are the one-center repulsion terms, and the SLATER orbital exponent, respectively. The repulsion term belonging to the atom A may be derived from the data for the C-atom according to the following relation:

$$\gamma_{AA} = \gamma_{CC} \frac{\xi_A}{\xi_C} . \tag{16}$$

On the basis of Table VII, it is evident that the ratio of electronegativities and orbital exponents is nearly constant in the first rows of the periodic table, and is a perfect constant (0.65) in the second period.

On the basis of this, Eq. (16) can be re-written in the following form by the aid of the electronegativities:

$$\gamma_{AA} = \gamma_{CC} \frac{P_A}{P_C} \tag{17}$$

where P_A, P_C are PAULING electronegativities.

Table IX

Parameters of homonuclear molecules

	k_e	r_e	ε	D_{ij}	d
O_2	11.76	1.207	3.5	58.5	0.265
S_2	4.96	1.889	2.5	50.9	0.263
F_2	4.45	1.435	4.0	36.0	0.266
P_2	5.56	1.894	2.1	38.7	0.268
Cl_2	3.28	1.988	3.0	58.0	0.280
C_2	9.51	1.312	2.3	72.0	0.294
Br_2	2.46	2.284	2.8	45.5	0.298
I_2	1.72	2.667	2.5	35.6	0.308
N_2	22.96	1.094	3.0	75.0	0.322
B_2	3.58	1.589	2.0	69.0	0.342

Average: 0.289

Parameters of heteronuclear molecules

	k	r_e	ε	D	N	d
BN	8.328	1.281	2.45	92	2.0	0.321
CN	16.850	1.172	2.74	178	2.5	0.330
SiN	7.291	1.574	2.32	104	2.5	0.308
NO	15.96	1.151	3.24	150	2.5	0.292
BO	13.65	1.208	2.64	184	2.5	0.295

REFERENCES

1. Sanderson, R. T.: Science **114,** 670 (1951)
2. Sanderson, R. T.: Chemical Periodicity. Reinhold Publishing Co., New York, 1960
3. Hinze, J., Whitehead, M. A., Jaffé, H. H.: J. Am. Chem. Soc. **85,** 148 (1963)
4. Pritchard, H. O.: J. Am. Chem. Soc. **85,** 1876 (1963)
5. Pritchard, H. O., Sumner, F. H.: Proc. Roy. Soc. (London) **A 235,** 136 (1956)
6. Mulliken, R. S.: J. Chem. Phys. **3,** 573 (1935)
7. Mulliken, R. S.: J. Chem. Phys. **2,** 782 (1934)
8. Iczkowski, P. P., Margrave, J. L.: J. Am. Chem. Soc. **83,** 3547 (1961)
9. Hinze, J., Jaffé, H. H.: J. Am. Chem. Soc. **84,** 540 (1962)
10. Klopman, G.: J. Am. Chem. Soc. **86,** 1463 (1964)
11. Klopman, G.: J. Am. Chem. Soc. **86,** 4550 (1964)
12. Jörgensen, C. K.: Orbitals in Atoms and Molecules. Academic Press, New York, 1962
13. Pritchard, H. O., Skinner, H. A.: Trans. Faraday Soc. **49,** 1254 (1953)
14. Pritchard, H. O., Skinner, H. A.: Chem. Revs. **55,** 745 (1955)
15. Baird, N. C., Whitehead, M. A.: Theoret. Chim. Acta (Berlin) **2,** 259 (1964)
16. Baird, N. C., Sichel, J. M., Whitehead, M. A.: Theoret. Chim. Acta (Berlin) **11,** 38 (1968)
17. Herzberg, G.: Molecular Spectra and Molecular Structure. D. Van Nostrand Company, Inc., Princeton, 1950

18. MULLIKEN, R. S.: J. Intern. Quant. Chem. **1,** 1 (1967)
19. SZŐKE, S.: Acta Chim. Acad. Sci. Hung. **51,** 183 (1967)
20. SZŐKE, S.: Acta Chim. Acad. Sci. Hung. **58,** 399 (1968)
21. GAYDON, A. G.: Dissociation Energies and Spectra of Diatomic Molecules. Chapman and Hall Ltd., London, 1968
22. COTTRELL, T. L.: The Strengths of Chemical Bonds. Butterworths Scientific Publications, London, 1958
23. VEDENEYEV, V. I.: Bond Energies, Ionization Potentials and Electron Affinities. Edward Arnold, Ltd., London, 1966
24. CADE, P. E., HUO, W. M.: J. Chem. Phys. **47,** 614 (1967)
25. MORAN, T. F., FRIEDMAN, H.: Chem. Phys. **40,** 860 (1964)
26. LIPPINCOTT, E. R., SCHROEDER, R.: J. Chem. Phys. **23,** 1099 (1955)
27. PEARSON, R. G.: J. Chem. Phys. **17,** 969 (1949)
28. BRATOŽ, S., DAUDEL, R., ROUX, M., ALLAVENA, M.: Rev. Mod. Phys. **32,** 412 (1960)
29. MATAGA, N., NISHIMOTO, K. Z.: Phys. Chem. (Frankfurt) **13,** 140 (1967)
30. OHNO, K.: Theoret. Chim. Acta (Berlin) **2,** 219 (1964)
31. POPLE, J. A.: Proc. Phys. Soc. (London) **A 68,** 81 (1955)
32. BAIRD, N. C., WHITEHEAD, M. A.: Can. J. Chem. **44,** 1933 (1966)
33. BELLUGUE, J., DAUDEL, R.: Rev. Sci. **84,** 541 (1946)
34. COULSON, C. A.: Proc. Roy. Soc. (London) **A 207,** 63 (1951)
35. PRITCHARD, H. O., SKINNER, H. A.: Chem. Rev. 735, 1955
36. TOWNES, C. H., DAILEY, P. B.: J. Chem. Phys. **17,** 782 (1949)
37. GORDY, W.: J. Chem. Phys. **14,** 305 (1946)
38. SANTRY, D. J., SEGAL, G. A.: J. Chem. Phys. **47,** 158 (1957)
39. PAOLONI, G.: Nuovo Cimento **4,** 410 (1956)

Sándor SZŐKE; Budapest II., Pusztaszeri út 59/67

Acta Chimica Academiae Scientiarum Hungaricae, Tomus 68 (4), pp. 359—370 (1971)

UNTERSUCHUNG DER IONISATION VON METALLEN UND METALLIONENNEUTRALISATION MIT DER ROTIERENDEN RING-SCHEIBENELEKTRODE, VII

ABHÄNGIGKEIT DER ANODISCHEN AUFLÖSUNG DES KUPFERS VON DER KONZENTRATION DER CHLORIDIONEN

L. Kiss, J. Farkas und A. Kőrösi

(Lehrstuhl für Physikalische Chemie und Radiologie der Eötvös Loránd Universität, Budapest)

Eingegangen am 28. Januar 1970.

Die anodische Auflösung von Kupfer in 1,0 n H_2SO_4 + x n HCl($x = 6{,}7 \cdot 10^{-3}$—$8{,}7 \cdot 10^{-2}$) wurde mittels der rotierenden Ring-Scheibenelektrode untersucht. Es wurde festgestellt, daß die Geschwindigkeit des Vorganges in dem untersuchten Konzentrationsbereich durch die Diffusion der Kupfer(I)-Komplexe von der Elektrodenoberfläche in das Innere der Lösung bestimmt wird. Bei einem bestimmten, von der Chloridionenkonzentration der Lösung und der Drehzahl der Elektrode abhängigen Wert der anodischen Stromdichte wird ein CuCl-Film auf der Elektrodenoberfläche abgeschieden. Die mit der Abscheidung dieser Schicht zusammenhängenden Erscheinungen wurden gedeutet.

In unserer vorangegangenen Mitteilung [1] wurde über Ergebnisse berichtet, welche bei der Untersuchung der anodischen und spontanen Auflösung von Kupfer erhalten wurden. Diese Untersuchungen wurden bei konstanter Chloridionenkonzentration, in 5 n H_2SO_4 + 1 n HCl bzw. in 1 n HCl-Lösungen durchgeführt. In der vorliegenden Arbeit wird darüber berichtet, inwiefern die Chloridionenkonzentration der Lösung die Geschwindigkeit der anodischen Auflösung beeinflußt.

Beim anodischen Auflösungsvorgang von Kupfer in chloridionenhaltiger Lösung entstehen Kupferkomplexe [2, 3], wobei an der Oberfläche des Kupfers bzw. in der unmittelbaren Nähe der Oberfläche (innerhalb der Diffusionsschicht) folgende Vorgänge verlaufen können:

$$Cu + Cl^- \rightleftharpoons CuCl + e \qquad \text{(I)}$$

$$CuCl + Cl^- \rightleftharpoons CuCl_2^- \qquad \text{(II)}$$

$$\vdots$$

$$CuCl_{j-1}^{(j-2)-} + Cl^- \rightleftharpoons CuCl_j^{(j-1)-} \qquad \text{(j)}$$

$$\vdots$$

Aus den in der vorangegangenen Mitteilung beschriebenen Ergebnissen ging hervor, daß die Geschwindigkeit des Vorganges durch die Diffusion der gebildeten chloridhaltigen Kupferkomplexe in das Innere der Lösung bestimmt wird, falls die Lösung genügend indifferente Elektrolyten enthält und die Konzentration der Chloridionen genügend hoch ist. Demgemäß kann sich für die Vorgänge (I)—(j) ein Gleichgewicht einstellen. Es soll bemerkt werden,

daß der Vorgang (I) in zwei Stufen verlaufen kann: als erste Stufe erfolgt die Adsorption des Chloridions und dann erst die Elektronenübertragung. Bei der anodischen Polarisation der Elektrode kann der durch die Elektrode fließende Strom auf folgende Weise geschrieben werden:

$$i = i_1 + i_2 + \ldots + i_j + \ldots \tag{1}$$

i_1 = Diffusionsgeschwindigkeit des CuCl von der Elektrodenoberfläche in das Innere der Lösung, in Stromdichteeinheiten,
i_2 = analoge Größe für $CuCl_2^-$,
i_j = analoge Größe für $CuCl_j^{(j-1)-}$.

Werden die Diffusionskoeffizienten der Komplexe mit verschiedener Anzahl von Chloridliganden als identisch angenommen und enthält die Lösung keine kupfer(I)haltige Komplexe, so ergeben sich zwischen den Teilstromstärken und den Konzentrationen der einzelnen Komplexe folgende Zusammenhänge:

$$i_1 = X_1 [CuCl] \tag{2}$$

$$i_2 = X_1 [CuCl_2^-] = X_1 K_2 [CuCl][Cl^-] \tag{3}$$

$$\vdots$$

$$i_j = X_1 [CuCl_j^{(j-1)-}] \tag{4}$$

$$\vdots$$

wo X_1 die in [1] angeführte Bedeutung besitzt und K_2 die Stabilitätskonstante des Komplexes $CuCl_2^-$ ist. Da hinsichtlich des Elektrodenvorgangs (1) Gleichgewicht herrscht, kann [CuCl] als Funktion des Elektrodenpotentials angegeben werden:

$$[CuCl] = \frac{k''_{a_1}}{k'_{k_1}} [Cl^-] \exp\left\{\frac{F\varphi}{RT}\right\} \tag{5}$$

wo k''_{a_1} und k'_{k_1} die Geschwindigkeitskonstanten des Vorgangs (I) in Richtung des oberen bzw. unteren Pfeiles sind bei $\varphi = 0$ (φ ist der Potentialunterschied zwischen der Vergleichselektrode und der untersuchten Elektrode). Die übrigen Bezeichnungen sind die üblichen.

Aufgrund von Gl. (2)—(5) ist

$$i_1 = X_1 \frac{k''_{a_1}}{k'_{k_1}} [Cl^-] \exp\left\{\frac{F\varphi}{RT}\right\} \tag{6}$$

$$i_2 = X_1 \frac{k''_{a_1}}{k'_{k_1}} K_2 [Cl^-]^2 \exp\left\{\frac{F\varphi}{RT}\right\} \tag{7}$$

$$\vdots$$

$$i_j = X_1 \frac{k''_{a_1}}{k'_{k_1}} \frac{\beta j}{K_1} [Cl^-]^j \exp\left\{\frac{F\varphi}{RT}\right\} \tag{8}$$

$$\vdots$$

K_1 und K_2 = Stabilitätskonstanten der Komplexe CuCl bzw. $CuCl_2^-$, β_j = Komplexprodukt des Komplexes $CuCl_j^{(j-1)-}$. Aufgrund von Gl. (1)—(4) und (6)—(8) ist

$$i = X_1 \frac{k''_{a_1}}{k'_{k_1}} \exp\left\{\frac{F\varphi}{RT}\right\} \sum_{j=1}^{n} \frac{\beta j}{K_1} [Cl^-]^j \tag{9}$$

wo n die maximale Koordinationszahl ist. Aus Gl. (9) ergibt sich, falls $[Cl^-]$ = konst., die Gleichung (1) der vorangegangenen Mitteilung. In diesem Fall ist

$$k'_{a_1} = k''_{a_1} \sum_{j=1}^{n} \frac{\beta j}{K_1} [Cl^-]^j . \tag{10}$$

Wird φ aus Gl. (9) ausgedrückt:

$$\varphi = \frac{RT}{F} \ln \frac{k'_{k_1}}{k''_{a_1}} - \frac{RT}{F} \ln X_1 - \frac{RT}{F} \ln \sum_{j=1}^{n} \frac{\beta j}{K_1} [Cl^-]^j + \frac{RT}{F} \ln i \tag{11}$$

so erhält man einen Ausdruck, der im wesentlichen mit dem in der Literatur [5] für ähnliche Fälle abgeleiteten Ausdruck übereinstimmt. Aus Gl. (9) und (11) geht hervor, daß die Reaktionsordnung des Anodenvorganges — bezogen auf das Chloridion — mit steigender Cl^--Konzentration von 1 bis n zunehmen kann. Demgemäß verschiebt sich die Polarisationskurve bei ansteigender Cl^--Konzentration in Richtung der negativen Potentiale. Aus Gl. (5) ist ersichtlich, daß die CuCl-Konzentration bei anodischer Polarisation in der Nähe der Elektrodenoberfläche zunimmt. Bei genügend positivem Potential kann die Konzentration des in Wasser schlecht löslichen CuCl so hoch werden, daß es in Form des festen Salzes auf der Oberfläche abgeschieden wird [3, 6—8]. Gemäß Gl. (5) ist das Potential φ_t, bei dem die Abscheidung von CuCl beginnt (falls keine übersättigte Lösung gebildet wird)

$$\varphi_t = \varphi' - \frac{RT}{F} \ln [Cl^-] \tag{12}$$

wo

$$\varphi' = \frac{RT}{F} \ln \frac{k'_{k_1} [CuCl]_t}{k''_{a_1}}$$

und $[CuCl]_t$ die Sättigungskonzentration des Kupfer(I)-chlorids in der gegebenen Lösung ist. φ_t verschiebt sich also mit dem Logarithmus der Cl^--Konzentration linear in Richtung der negativen Potentiale und es ist

$$\frac{\partial \varphi_t}{\partial \ln [Cl^-]} = -\frac{RT}{F} .$$

Wird an der Elektrodenoberfläche festes CuCl abgeschieden, so ist die Konzentration des Kupfer(I)-chlorids an der Oberfläche konstant gleich $[CuCl]_t$. Demzufolge ist die Geschwindigkeit des anodischen Lösungsvorganges unter Teilnahme von Cu(I) (falls auch im weiteren nur Cu(I)-haltige Komplexe entstehen) gemäß Gl. (2)—(5) und (9)

$$i_t = X_1 [CuCl]_t \sum_{j=1}^{n} \frac{\beta j}{K_1} [Cl^-]^{j-1} . \tag{13}$$

Wie auch aus Gl. (13) hervorgeht, ist zum Erreichen von $[CuCl]_t$ eine um so höhere Stromdichte notwendig, je höher die Chloridionenkonzentration ist. Ähnliche Folgerungen können auch aus Gl. (11) und (12) gezogen werden, da ja, wie diese Gleichungen erkennen lassen,

$$\left| \frac{\partial \varphi_t}{\partial \ln [Cl^-]} \right| < \left| \frac{\partial \varphi}{\partial \ln [Cl^-]} \right| \tag{14}$$

ist.

Demzufolge kann bei genügend hohen Cl^--Konzentrationen die Abscheidung von festem CuCl an der Elektrodenoberfläche selbst im Fall von relativ positiven Potentialen (hohen Stromdichten) nicht erwartet werden. Diese Erscheinung wurde durch SMOLJANINOV [8] bei dem anodischen Lösungsvorgang von Kupfer in Salzsäure beobachtet: in 1,0 n Salzsäure bei 0 und 20 °C bildete sich bei genügend hohen Stromdichten ein Kupfer(I)-chlorid-Film auf der Kupferanode, während diese Erscheinung in 7,0 n Salzsäure nicht auftrat. Wir möchten bemerken, daß der erwähnte Verfasser sich zum Mechanismus bzw. zum geschwindigkeitsbestimmenden Vorgang der untersuchten Erscheinungen überhaupt nicht äußerte. Bei den in unseren eigenen Untersuchungen verwendeten Stromdichten fanden wir, daß in 0,1 n Salzsäure bei Zimmertemperatur kein Kupfer(I)-chlorid an der Elektrodenoberfläche abgeschieden wurde [1].

Versuchsergebnisse und ihre Deutung

Die Wirkung der Chloridionenkonzentration auf die anodische Auflösung des Kupfers wurde mit der rotierenden Ring-Scheibenelektrode untersucht. In den Versuchen wurden in erster Reihe die anodischen Polarisationskurven bei verschiedenen Chloridkonzentrationen sowie die die am Ring meßbaren Grenzströme bestimmt. Das experimentelle Verfahren, die Vorbereitung der Elektrode und die Qualität der verwendeten Reagenzien entsprachen dem in [9] und [10] beschriebenen. Die Messungen wurden bei Zimmertemperatur, in 1,0 n H_2SO_4 + x n HCl, unter Stickstoffatmosphäre durchgeführt.

Der Wert von x lag zwischen den Grenzen $6{,}7 \cdot 10^{-3}$ und $8{,}7 \cdot 10^{-2}$. Die angegebenen Potentialwerte beziehen sich in sämtlichen Fällen auf die 1,0 n Kalomelelektrode. Die sichtbare Oberfläche der Scheibenelektrode war 0,25 cm²; die angegebenen Stromstärken beziehen sich auf diese Fläche. Zum Registrieren der Potential–Zeit bzw. Grenzstrom–Zeit-Zusammenhänge wurde der Polarograph Radelkis OH-102 benützt.

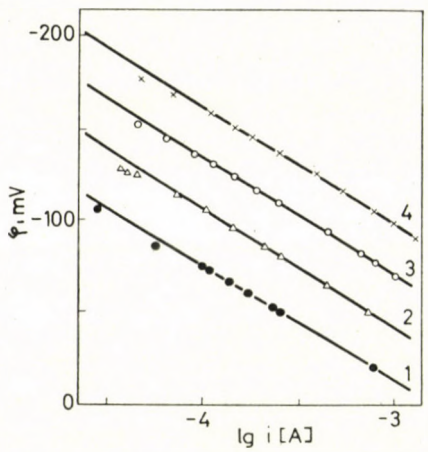

Abb. 1. An der Kupferscheibenelektrode gemessene Polarisationskurven in 1 n H_2SO_4 + + x n HCl. $f = 3070$ Min^{-1}. 1. $x = 6{,}67 \cdot 10^{-3}$; 2. $x = 2{,}00 \cdot 10^{-2}$; 3. $x = 4{,}00 \cdot 10^{-2}$; 4. $x = 7{,}33 \cdot 10^{-2}$

In Abb. 1 sind die an der Kupferscheibenelektrode bei verschiedenen Chloridkonzentrationen bestimmten Polarisationskurven dargestellt, bei einer Drehzahl der Scheibe von 3070 Min^{-1}. Die Abhängigkeit der Polarisationskurven von der Drehzahl im untersuchten Konzentrationsbereich war in völliger Übereinstimmung mit der in [1] beschriebenen Abhängigkeit. Aus Abb. 1 geht hervor, daß der Zusammenhang φ–lg i eine Gerade mit dem Neigungswinkel von 60 mV ergibt, d.h. der Grenzstrom der Chloridionen ist wesentlich höher als i [5]. Demgemäß ist die Bedingung erfüllt, daß die Konzentration der Chloridionen an der Elektrodenoberfläche praktisch unabhängig von dem durch die Elektrode fließenden Strom ist. Die Erfüllung dieser Bedingung wird durch die in der vorangegangenen Mitteilung beschriebenen Abhängigkeit der Polarisationskurve von der Drehzahl der Elektrode bestätigt. Die letzten Meßpunkte der Polarisationskurven in Abb. 1 bei hohen Stromdichten konnten im allgemeinen nur durch rasche Potentialmessung nach dem Einstellen der Stromstärke bestimmt werden, da sich das Potential mit der Zeit in positiver Richtung verschiebt.

In Abb. 2 ist — aufgrund der Angaben der Polarisationskurven — der Logarithmus der durch die Kupferscheibenelektrode fließenden anodischen Stromstärke in Abhängigkeit vom Logarithmus der Chloridkonzentration, bei konstantem Elektrodenpotential und konstanter Drehzahl dargestellt. Hier ergeben sich keine Geraden; im untersuchten Konzentrationsbereich

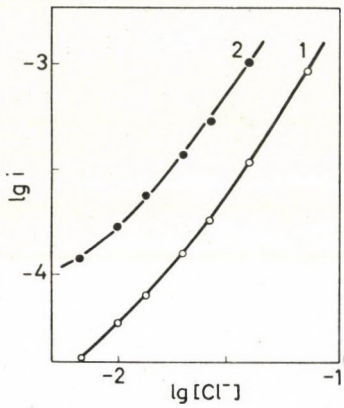

Abb. 2. Abhängigkeit des Logarithmus der durch die Kupferscheibenelektrode fließenden anodischen Stromstärke vom Logarithmus der Chloridionenkonzentration. $f = 3070$ Min^{-1}. 1. $\varphi = -100$ mV; 2. $\varphi = -70$ mV

verändert sich die Richtungstangente der Kurve, d.h. — gemäß Gl. (9) — die auf das Chloridion bezogene scheinbare Ordnung der Reaktion mit dem Anstieg der Chloridkonzentration von 1,0 auf 1,67. Demgemäß werden unter den gegebenen Bedingungen im wesentlichen nur CuCl- und $CuCl_2^-$-Teilchen von der Elektrodenoberfläche wegtransportiert.

In Abb. 3 ist der an der aus Kohlenstoffpaste hergestellten Ringelektrode meßbare Oxydationsgrenzstrom i_h des Cu(I)-haltigen Komplexes in Abhängigkeit von der anodischen Stromstärke i durch die Scheibenelektrode, bei verschiedenen Chloridkonzentrationen dargestellt. Bei geringen Stromdichten sind i_h und i proportional, wie auch in unseren früheren Arbeiten [1] gefunden wurde. Bei einem bestimmten, von der Chloridionenkonzentration abhängigen Wert der Stromstärke biegt die Gerade jedoch ab und verläuft im weiteren parallel zur Abszisse. Bei Steigerung der anodischen Polarisation der Scheibenelektrode nimmt demgemäß der Grenzstrom i_h, d.h. die Konzentration der Cu(I)-haltigen Komplexe nach dem Erreichen eines bestimmten Wertes i_{h_t} nicht weiter zu.

Ähnliche Kurven werden erhalten, wenn die Drehzahl der Elektrode f bei einer gegebenen Chloridionenkonzentration verändert wird (Abb. 4).

Diese Erscheinung kann damit erklärt werden, daß die Sättigungskonzentration des CuCl bei derjenigen Stromstärke i_t erreicht wird, die dem Abbiegen der Geraden in die Horizontale entspricht. Bei dieser Stromstärke beginnt

also die Abscheidung des festen Salzes. In Abb. 3 und 4 kann beobachtet werden, daß meistens noch ein Meßpunkt vor dem Beginn der horizontalen Strecke vorliegt, bei dem $i_h > i_{h_t}$ ist. Dieser Meßpunkt kann nur dann bestimmt werden, wenn die Kurve i_h—i von geringen Stromstärken in Richtung zu hohen

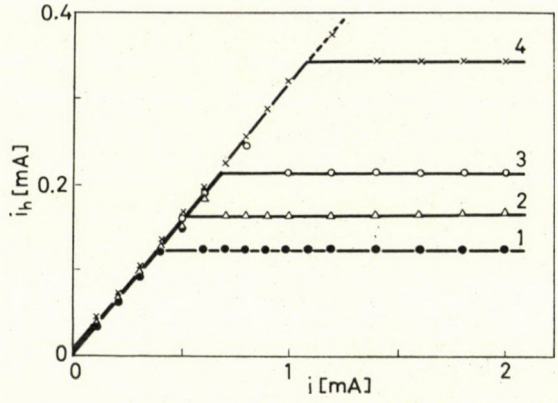

Abb. 3. An der Kohlenpastenringelektrode gemessener Oxydationsgrenzstrom i_h in Abhängigkeit von der durch die Kupferscheibenelektrode fließenden anodischen Stromstärke i. An der Ringelektrode eingestelltes Potential $\varphi_R = +600$ mV. $f = 2120$ Min^{-1}. Zusammensetzung der Lösung: 1,0 n H_2SO_4 + x n HCl. 1. $x = 2{,}66 \cdot 10^{-2}$; 2. $x = 4{,}00 \cdot 10^{-2}$; 3. $x = 5{,}33 \cdot 10^{-2}$; 4. $x = 8{,}66 \cdot 10^{-2}$

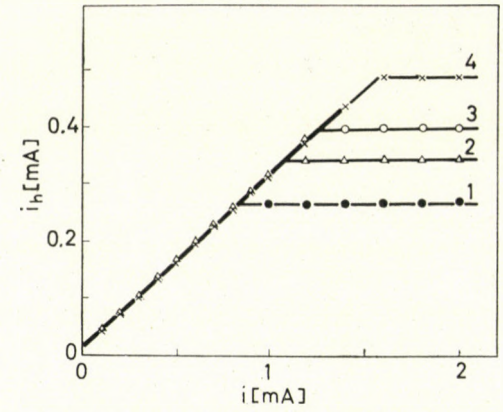

Abb. 4. Zusammenhang i_h—i bei verschiedenen Drehzahlen der Elektrode in 1,0 n H_2SO_4 + + $8{,}66 \cdot 10^{-2}$ n HCl. $\varphi_R = +600$ mV. 1. $f = 1040$; 2. $f = 2120$; 3. $f = 2870$; 4. $f = 4780$ Min^{-1}

Stromstärken aufgenommen wird. Er entspricht der Tatsache, daß die Abscheidung des festen CuCl aus übersättigter Lösung beginnt. Demzufolge wird der wirkliche Wert von i durch den Schnittpunkt der schrägen und horizontalen Strecken der Kurve i_h—i angezeigt.

Aus Abb. 5 und 6 ist ersichtlich, daß — in Übereinstimmung mit Gl. (13) — ein linearer Zusammenhang zwischen i_t bzw. i_{h_t} und $[Cl^-]$ bei konstan-

ter Drehzahl der Elektrode besteht, während bei konstanter Chloridionenkonzentration i_t bzw. i_{h_t} proportional der Quadratwurzel der Drehzahl der Elektrode ($f^{1/2}$) verändert werden. Der Wert von i_t ist jedoch nicht nur von der Chloridionenkonzentration und von der Drehzahl der Elektrode abhängig,

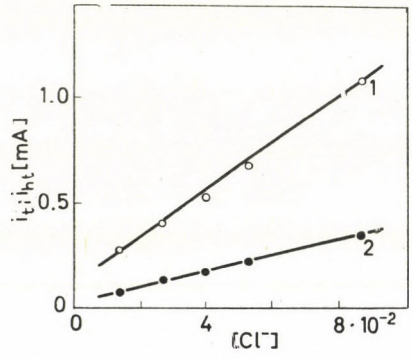

Abb. 5. Abhängigkeit von i_t (Kurve 1) und von i_{h_t} (Kurve 2) von der Konzentration der Chloridionen. $f = 2120$ Min^{-1}

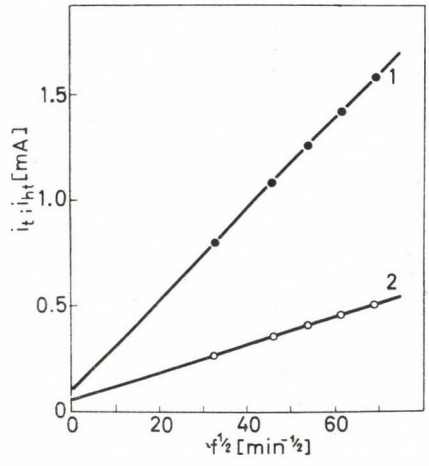

Abb. 6. Abhängigkeit von i_t (Kurve 1) und von i_{h_t} (Kurve 2) von der Quadratwurzel der Drehzahl der Elektrode. HCl-Konzentration der Lösung: $8{,}66 \cdot 10^{-2}$ n

sondern auch von der Temperatur [8], da die Sättigungskonzentration $[CuCl]_t$ temperaturabhängig ist.

Im weiteren wurde untersucht, welche Vorgänge an der Oberfläche der Kupferscheibenelektrode beim Einschalten von Stromstärken oberhalb i_t verlaufen. In Abb. 7 ist eine bei diesen Untersuchungen erhaltene, charakteristische Kurvenschaar beispielshalber dargestellt. Kurve *a* zeigt die zeitliche Veränderung der an die Scheibe angeschlossenen Stromstärke. Der eingeschaltete Strom i ist wesentlich höher als i_t, $i \simeq 5\, i_t$. Die dabei erfolgende Verände-

rung des Potentials der Scheibenelektrode wird durch Kurve *b* angezeigt. Der Verlauf dieser Kurve φ–t kann auf folgende Art gedeutet werden: beim Einschalten des anodischen Stroms steigt die Konzentration des CuCl an der Elektrodenoberfläche an. Beim Erreichen des Potentials, welcher Punkt α entspricht, wird die Lösung an der Oberfläche der Elektrode derart übersättigt, daß die Abscheidung der CuCl-Schicht auf der Elektrode beginnt. Dadurch wird die Übersättigung behoben und das Potential wird etwas nega-

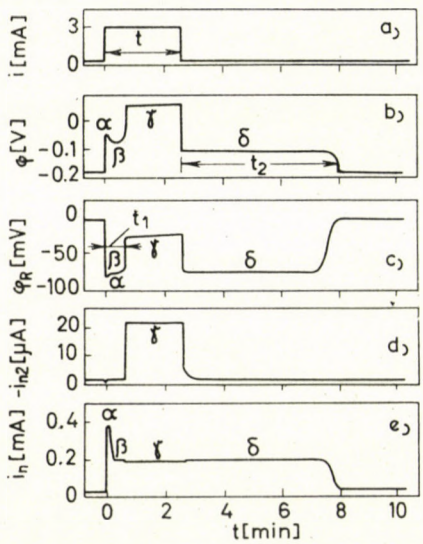

Abb. 7. Veranschaulichung der Vorgänge nach dem Abscheiden von festem CuCl. Zusammensetzung der Lösung: 1,0 n H_2SO_4 + 4,00 · 10^{-2} n HCl. $f = 2120$ Min^{-1}. *a:* Zeitliche Veränderung der durch die Kupferscheibenelektrode fließenden Stromstärke. *b:* Veränderung des Potentials der Kupferscheibenelektrode während der gleichen Zeitdauer. *c:* Veränderung des stromfreien Potentials der Kohlenpastenringelektrode während der gleichen Zeitdauer. *d:* An der Kohlenpastenringelektrode gemessener kathodischer Strom ($\varphi_R = -100$ mV). *e:* An der Kohlenpastenringelektrode gemessener anodischer Grenzstrom ($\varphi_R = +600$ mV)

tiver (Strecke β). Nach dem Aufbau des CuCl-Films wird die Stromdichte an den frei gebliebenen Teilen der Oberfläche hoch, folglich verschiebt sich das Potential in positiver Richtung und ein neuer Elektrodenvorgang, namentlich die Auflösung des Kupfers in zweiwertiger Form, wird ermöglicht (Strecke γ). Nach dem Ausschalten des anodischen Stroms verschiebt sich das Potential der Kupferscheibenelektrode in negativer Richtung, und das Potential der Elektrode φ_t wird bis zum Auflösen der CuCl-Schicht an der Elektrode durch die Sättigungskonzentration $[CuCl]_t$ bestimmt (Strecke δ).

Diese Vorstellung wird auch durch Kurven *c*, *d* und *e* unterstützt. Kurve *c* zeigt die zeitliche Veränderung des an der Kohlenringelektrode gemessenen Potentials φ_R. Das Potential des Ringes wird durch das Redoxsystem Cu(I)/Cu(II) eingestellt. Demzufolge verändert sich φ_R mit steigender Cu(I)-Konzen-

tration in negativer Richtung (Strecken α, β), bei dem Entstehen von Cu(II) (Strecke γ) in positiver Richtung und nimmt endlich nach dem Ausschalten des Stromes denjenigen Wert an, der der Strecke β entspricht. Daß in der Strecke γ tatsächlich Cu(II)-Ionen gebildet werden, wird durch Kurve *d* bewiesen. Hier wurde an der Ringelektrode ein Potential von −100 mV (bezogen auf 1 n Kalomelelektrode) eingestellt. Bei diesem Potential werden Cu(II)-Ionen

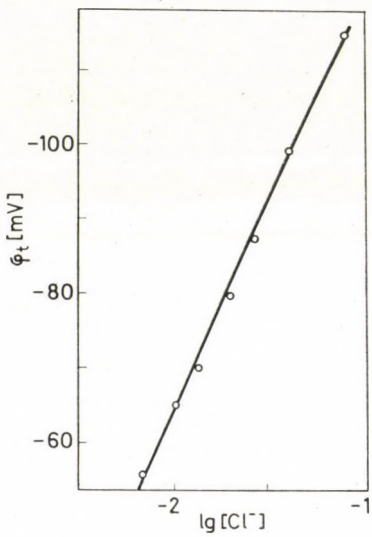

Abb. 8. Abhängigkeit des der Strecke in Abb. 7b entsprechenden Potentials φ_t vom Logarithmus der Chloridionenkonzentration der Lösung

zu Cu(I)-Ionen reduziert, dagegen wird Cu(I) nicht zu metallischem Kupfer reduziert. Wie ersichtlich, kann am Ring nur während der Strecke γ ein kathodischer Strom ($-i_{h_2}$) gemessen werden, d.h. nur ist diesem Zeitraum entstehen Cu(II)-Ionen in verhältnismäßig großen Mengen. (Es soll bemerkt werden, daß $-i_{h_2}$ kein Grenzstrom ist, da bei dem Potential, bei welchem der Grenzstrom erreicht wäre, auch Cu(I) schon reduziert wird.)

Kurve *e* zeigt den an dem Kohlenpastenring gemessenen Oxydationsgrenzstrom i_h. In Übereinstimmung mit der obengenannten Vorstellung weist i_h bei α ein Maximum auf und ist in den Strecken β, γ und δ praktisch unverändert.

Aus der Strecke δ der Kurve *b* kann also der Wert von φ_t bestimmt werden. In Abb. 8 ist der auf diese Art bestimmte Wert von φ_t in Abhängigkeit von Logarithmus der Chloridionenkonzentration dargestellt. In Übereinstimmung mit Gl. (12) ergibt sich eine Gerade, jedoch beträgt der Neigungswinkel anstelle von 59 mV bei der gegebenen Versuchsreihe 57 mV.

Unsere Versuchsergebnisse zeigen also, daß die Bildung des CuCl-Films auf der Kupferscheibenelektrode während der Strecke β erfolgt und die Dicke

des Films während der Strecke γ langsamer zunimmt. Für die Dicke des Films ist die Länge der Strecke δ (der Zeitraum t_2) charakteristisch. Die Menge des an der Oberfläche der Elektrode gebildeten CuCl ist der für die Bildung verbrauchten Ladungsmenge Q proportional:

$$Q = (i - i_t)\, t_1 \tag{15}$$

i = durch die Elektrode fließende Stromstärke ($i > i_t$), t_1 = vom Einschalten des Stroms i verflossene Zeit bis zum Beginn der Strecke γ (siehe Abb. 7c); der Wert von i_t ist durch Gl. (13) gegeben. Die Geschwindigkeit der Entfernung der CuCl-Schicht von der Elektrodenoberfläche ist also i_t und die Zeitdauer der Entfernung beträgt t_2, folglich muß folgende Gleichheit bestehen:

$$(i - i_t)\, t_1 = i_t\, t_2 \tag{16}$$

Aufgrund von (16) und (13) ist

$$\frac{t_1}{t_2 + t_1} = X_1(a + b[\mathrm{Cl}^-]) \tag{17}$$

wo

$$a = \frac{[\mathrm{CuCl}]_t}{i} \quad \text{und} \quad b = \frac{[\mathrm{CuCl}]_t\, K_2}{i}\,.$$

Folglich verändert sich bei konstantem i $t_1/(t_2+t_1)$ linear mit der Chloridionenkonzentration und der Logarithmus von $t_1/(t_2+t_1)$ verändert sich ebenfalls linear mit dem Logarithmus der Drehzahl der Elektrode. In letzterem Fall muß der Neigungswinkel der Geraden 1/2 betragen. Aus Abb. 9 und 10 ist ersichtlich, daß die Versuchsergebnisse mit Gl. (17) im Einklang stehen. Aus Gl. (15) bzw. (16) kann die auf der Oberfläche gebildete Menge von CuCl berechnet werden.

Unsere Versuchsergebnisse bestätigen also, daß die Geschwindigkeit der anodischen Auflösung von Kupfer in den untersuchten, chloridionenhaltigen

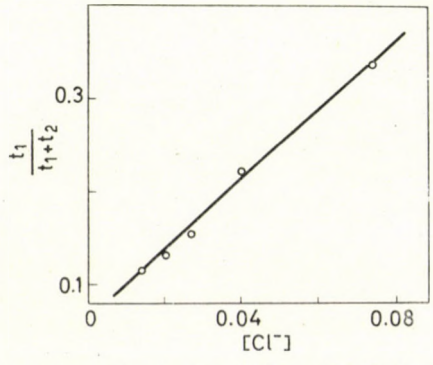

Abb. 9. Zusammenhang zwischen $t_1/(t_2 + t_1)$ und der Chloridionenkonzentration der Lösung

Lösungen durch die Diffusion der entstehenden Kupferkomplexe in das Innere der Lösung bestimmt wird. In Übereinstimmung mit den Literaturangaben wurde festgestellt, daß bei entsprechenden Bedingungen eine poröse CuCl-Schicht an der Anode gebildet wird [3, 6—8]. Nach der Ausbildung der CuCl-Schicht entstehen neben den Cu(I)-haltigen Komplexen auch Cu(II)-Ionen [7].

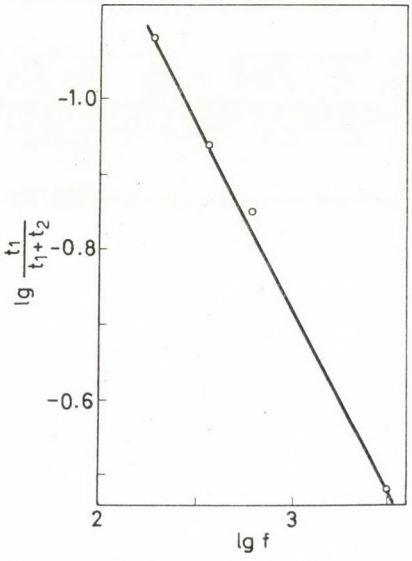

Abb. 10. Zusammenhang zwischen $\lg t_1/(t_2 + t_1)$ und $\lg f$

LITERATUR

1. Kiss, L., Farkas, J., Kőrösi, A.: Magy. Kém. Foly. **76,** 569 (1970); Acta Chim. Acad. Sci. Hung. **67,** 179 (1971)
2. Náray-Szabó, St., Szabó, Z.: Z. phys. Chem. **A 166,** 228 (1933)
3. Stephenson, L., Bartlett, J. H.: J. Electrochem. Soc. **101,** 571 (1954)
4. Beck, M.: Chemie von Komplex-Gleichgewichten (Ung.). Akadémiai Kiadó, Budapest 1965. p. 17.
5. Krawtzow, V. I.: Elektrodnije prozessi v rastworach kompleksow metallow. p. 116. Izd. LGU, 1969.
6. Cooper, R. S.: J. Electrochem. Soc. **103,** 307 (1956)
7. Cooper, R. S., Bartlett, J. H.: J. Electrochem. Soc. **105,** 109)1958)
8. Smolyaninov, I. S.: Izv. Voronezhskogo Gos. Ped. Inst. **47,** 18 (1964)
9. Kiss, L., Farkas, J.: Magy. Kém. Foly. **76,** 389 (1970); Acta Chim. Acad. Sci. Hung. **66,** 395 (1970)
10. Kiss, L., Kőrösi, A., Farkas, J.: Magy. Kém. Foly. **73,** 551 (1967); Ann. Univ. Sci. Budapest **9,** 3 (1967)

László Kiss
József Farkas
Antal Kőrösi
Budapest VIII., Puskin u. 11—13.

Acta Chimica Academiae Scientiarum Hungaricae, Tomus 68 (4), pp. 371—385 (1971)

UMWANDLUNGEN DER NETZWERKSTRUKTUR IN DER OBERFLÄCHENSCHICHT VON SILIKATGLÄSERN

S. DOBOS

(Forschungsgruppe für anorganische Chemie der Ungarischen Akademie der Wissenschaften, Budapest)

Eingegangen am 30. Januar 1970

Bei der Ausbildung der Oberflächenschicht von Glas muß neben dem diffusionsbestimmten Ionenaustausch und der Ablösung des Silikatnetzwerkes an der Grenzfläche Schicht–Wasser recht oft auch mit einer Strukturumwandlung des Silikatnetzwerkes gerechnet werden. Diese Strukturänderung kann durch eine Umordnung des Raumnetzes oder durch die Änderung der Zahl der >Si—O—Si< Bindungen erfolgen. Die Strukturänderung kann aufgrund der Konzentrationsverteilung der Komponenten in der Oberflächenschicht und gegebenenfalls aufgrund der zeitlichen Veränderung der Ablösungsgeschwindigkeit des Silikatnetzwerkes erkannt werden.

Das Wesen der Strukturumwandlung in der Oberflächenschicht des untersuchten Glases mit der Einwaagezusammensetzung 20 Mol% K_2O, 12 Mol% SrO, 68 Mol% SiO_2, besteht wahrscheinlich in der Umordnung des Raumnetzes, weshalb das Silikatnetzwerk chemisch widerstandsfähiger und zugleich für die Ionendiffusion durchlässiger wird.

Bei wiederholten Schmelzversuchen von Gläsern der genannten Zusammensetzung erhielten wir in einigen Fällen ein Glas, dessen Oberflächenschicht ohne Strukturänderung ausgebildet wurde, in anderen Fällen dagegen ein Glas, bei dem die Oberflächenschichtbildung mit einer Strukturänderung verbunden erfolgte. Mittels IR-spektroskopischen und DTA-Messungen wurde festgestellt, daß die Erklärung für dieses gegensätzliche Verhalten der mit der gleichen Einwaagezusammensetzung und unter nahezu identischen Bedingungen hergestellten Gläser in ihrer unterschiedlichen Struktur zu suchen ist.

Durch Anwendung des zweiten Fickschen Gesetzes auf die Diffusionsvorgänge, welche die Oberflächenschicht von Silikatgläsern ausbilden, leiteten BOKSAY, BOUQUET und DOBOS [1, 2] eine Gleichung für die Verteilung der Alkaliionen in der Oberflächenschicht ab. Im Zeitpunkt t ist der Molenbruch n der Alkaliionen in der Oberflächenschicht

$$n = e^{-(a/D)y} \frac{1}{\sqrt{\pi}} \int_{-\infty}^{s} e^{-p^2} dp - \frac{1}{\sqrt{\pi}} \int_{-\infty}^{r} e^{-p^2} dp + 1 - e^{-(a/D)y} \qquad (1)$$

wo a die Ablösungsgeschwindigkeit des Silikatnetzwerkes, D die Diffusionskonstante des Alkaliions, y die Tiefenkoordinate der Schicht,

$$s = \frac{y - at}{\sqrt{4Dt}}, \qquad r = -\frac{y + at}{\sqrt{4Dt}}$$

und p ein Integrationsparameter ist.

Wenn die Vorgänge, welche die Oberflächenshicht ausbilden, stationär werden, nimmt Gl. (1) folgende einfache Form an (Abb. 1):

$$n = 1 - e^{-(a/D)y}. \tag{2}$$

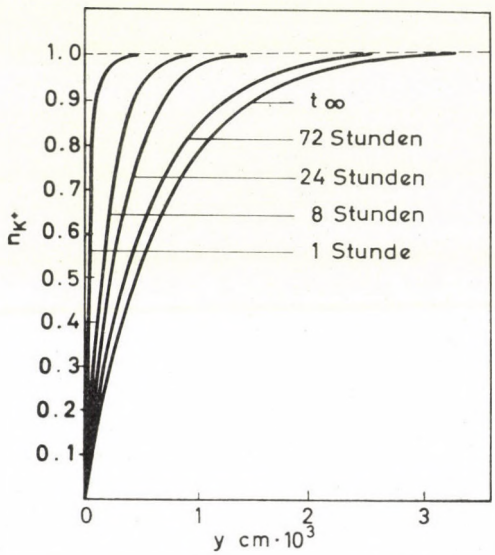

Abb. 1. Veränderung des Molenbruches der Kaliumionen in Abhängigkeit von der Tiefenkoordinate der Schicht nach verschiedenen Lagerungszeiten in Wasser bei Gläsern vom Typ P

In der Ableitung der Gleichung wurde die Lösungsgeschwindigkeit a des Silikatnetzwerkes sowie der Diffusionskoeffizient D als konstant angenommen. Die Gültigkeit der Gleichung wurde durch Bestimmung der Alkaliionenverteilung in der Oberflächenschicht eines Glases mit der Zusammensetzung 20 Mol% K_2O, 12 Mol% SrO, 68 Mol% SiO_2 bewiesen.

Strukturänderungen des Silikatnetzwerkes im Laufe der Ausbildung der Oberflächenschicht

Unseren Erfahrungen gemäß zeigt die Alkaliionenverteilung der Oberflächenschicht bei einfachen Silikatgläsern mit hohem Alkaligehalt im allgemeinen einen von Gl. (1) und (2) abweichenden Charakter: das Kriterium, daß der Diffusionskoeffizient und die Ablösungsgeschwindigkeit des Netzwerkes konstant sind, ist nur in Ausnahmefällen erfüllt.

Es ist leicht einzusehen, daß der Diffusionskoeffizient in der Schicht nur dann konstant sein kann, wenn die Struktur des Silikatnetzwerkes entlang der Gesamttiefe der Schicht unverändert ist. Ändert sich die Struktur, so ändert sich auch der Wert von D und folglich weicht der Charakter der Alkaliionen-

verteilung von der einfachen Form gemäß Gl. (1) bzw. (2) ab. Eine zeitliche Veränderung der Ablösungsgeschwindigkeit des Netzwerkes zeigt ebenfalls eine Strukturänderung des Netzwerkes in der Oberflächenschicht an. Inwiefern die Konzentrationsverteilung der Komponenten (z.B. Alkaliionen) in der Oberflächenschicht durch die Änderung der Netzwerkstruktur modifiziert wird, bzw. wie diese Änderung auf die Lösungsgeschwindigkeit einwirkt, wird durch die Art und den zeitlichen Verlauf der Strukturänderung bestimmt.

Bevor wir versuchen, die möglichen Strukturänderungen zu umreißen, muß definiert werden, was unter einer unveränderten Struktur verstanden werden soll. Das Netzwerk der Schicht wird als unverändert betrachtet, wenn die Zahl und räumliche Anordnung der $\geqslant$Si—O—Si$\leqslant$ Bindungen im SiO_2-Raumnetz im Vergleich zum kompakten Glas unverändert sind. Auch die Zahl und Anordnung der an das Raumnetz angeschlossenen $\geqslant$Si—$\overline{O}$ Gruppen müssen unverändert bleiben. Streng genommen bedeutet natürlich der Ionenaustausch bereits an und für sich eine geringfügige Änderung der Struktur, da die Nichtberücksichtigung der abweichenden Größe und polarisierenden Wirkung des an die Stelle des Alkaliions tretenden Partners nur mit Vernachlässigungen möglich ist.

Formell können zwei große Gruppen der möglichen Strukturumwandlungen angenommen werden:

In die erste Gruppe gehören diejenigen Vorgänge, bei denen die Zahl der $\geqslant$Si—O—Si$\leqslant$ und $\geqslant$Si—$\overline{O}$ Bindungen unverändert bleibt und nur ihre räumliche Anordnung verändert wird. Die Wahrscheinlichkeit solcher Änderungen ist infolge des thermodynamisch metastabilen Zustands der kompakten Glasphase sehr hoch. Die Neigung des Raumnetzes zur Stabilisierung kann in dem durch Dealkalisation gestörten System leichter befriedigt werden. Diese »spontane« Umlagerung der Struktur, welche durch die Dealkalisation der Schicht sterisch erleichtert wird und durch den Restalkaliionengehalt, durch verunreinigende Fremdionenspuren sowie durch das vorhandene Wasser katalysiert werden kann, stellen wir uns so vor, daß die Zahl der $\geqslant$Si—O—Si$\leqslant$ und $\geqslant$Si—$\overline{O}$ Bindungen dadurch nicht berührt, sondern lediglich ihre räumliche Anordnung in Richtung des niedrigeren Energiezustands verändert wird. Ob nun ein derartiger Ordnungsvorgang die Diffusion der Alkaliionen erleichtern oder erschweren wird, kann kaum eindeutig vorausgesagt werden; dagegen erscheint es höchstwahrscheinlich, daß dieser Vorgang den chemischen Widerstand des Netzwerkes steigern und folglich seine Lösungsgeschwindigkeit in Wasser oder in einem anderen Reagens verringern wird.

In die zweite Gruppe der Strukturumwandlungen des Netzwerkes könnten jene Vorgänge eingereiht werden, bei denen sich die Zahl der $\geqslant$Si—O—Si$\leqslant$ und $\geqslant$Si—$\overline{O}$ Bindungen im Netzwerk verändert. Solche Änderungen können sich in erster Linie durch Reaktionen zwischen dem Netzwerk und den von außen in die Schicht eindiffundierten Komponenten abspielen. So kann z.B.

der Angriff des Wassers zur Hydrolyse eines Teiles der ≥Si—O—Si≤ Bindungen führen:

$$\geq Si—O—Si\leq + H_2O = 2\ (\geq SiOH)$$

Offensichtlich wird die Diffusion der Ionen in der Schicht durch die obige Reaktion erleichtert. Zugleich wird die Ablösungsgeschwindigkeit des Netzwerkes erhöht. Die ≥Si—O—Si≤ Bindungen können auch durch andere Reagenzien gespalten werden. Die Hydrolyse kann auch mit gleichzeitiger Umlagerung der Struktur kombiniert verlaufen.

Im entgegengesetzten Sinn verläuft die Kondensation der ≥Si—OH Gruppen; ihre Wahrscheinlichkeit ist keineswegs gering, wenn wir z. B. an die spontane Alterung von Kieselsäuregelen oder an die pH-abhängige Polymerisation von Solen denken:

$$\begin{matrix} \geq SiO-O-H \\ \vdots \quad\ \vdots \\ H-O-Si\leq \end{matrix} \xrightarrow{-H_2O} \geq Si-O-Si\leq$$

Der Wasseraustritt wird durch starke Elektronenakzeptoren (z. B. Hydroxoniumionen) erleichtert. Spielt sich die Kondensation allein ab, ist sie also nicht mit einer gleichzeitigen Strukturumlagerung kombiniert, so gelangen wir zu einer Struktur, in der die Diffusion der Alkaliionen langsamer wird. Auch die Geschwindigkeit der Auflösung des Netzwerkes nimmt infolge der Kondensation ab. Eine — der Kondensation ähnliche — Verdichtung der Struktur könnte auch durch Einwirkung von Kationen mit kleineren Ionenradien und hohen Ladungen verlaufen.

Die beiden, rein formell unterschiedenen Vorgangsgruppen, nämlich die räumliche Umlagerung der Struktur und die Änderung der Zahl der Brückensauerstoffatome, verlaufen in Wirklichkeit wahrscheinlich in jedem Fall mehr oder weniger miteinander kombiniert.

Unter Berücksichtigung der genannten möglichen Vorgänge können z. B. folgende Teilvorgänge bei der Ausbildung der Oberflächenschicht im Laufe der Reaktion von Glas mit Wasser unterschieden werden:

1. Ionenaustausch zwischen den Alkaliionen des Glases und den Wasserstoffionen des Wassers, wobei das Wasserstoffion in mehr oder weniger hydratiertem Zustand in das Glas eintritt. Der Vorgang wird durch die Diffusion der Partner des Ionenaustausches bestimmt.

2. Eine eventuelle Änderung der Netzwerkstruktur der Schicht.

3. Die Ablösung des Netzwerkes der Schicht an der Grenzfläche Schicht–Wasser.

Es ist leicht einzusehen, daß bei gleichzeitigem Verlauf aller drei Vorgänge der Ionenaustausch am schnellsten ist; ihm folgt die Änderung der Struktur und zuletzt die Auflösung des Netzwerkes.

Auch liegt es auf der Hand, daß keine Strukturänderung auftritt, wenn die Geschwindigkeit dieser Änderung geringer ist als die Geschwindigkeit der Ablösung des Netzwerkes; in diesem Fall ist die Ablösungsgeschwindigkeit des Netzwerkes konstant.

Ist die Geschwindigkeit der Netzwerkänderung kommensurabel höher als die Auflösungsgeschwindigkeit des Netzwerkes, so nimmt die letztere zeitlich ab oder zu, je nach dem, ob die Strukturänderung eine mehr oder weniger widerstandsfähige Struktur ergibt. Diesen Fall kann man sich wie folgt vorstellen: die mögliche Strukturänderung ist an einer bestimmten Stelle A der Schicht noch nicht beendet, wenn die Front der Ablösung diese Stelle erreicht. Wegen der höheren Geschwindigkeit der Strukturänderung ist jedoch diese Änderung in der nächsten, tiefer liegenden Stelle B bereits mehr fortgeschritten als wenn die Ablösungsfront diese Stelle erreicht. Das Wasser greift also an den zwei Stellen unterschiedliche Strukturen an, folglich sind die Ablösungsgeschwindigkeiten an den Stellen A und B verschieden.

Verändert sich die Struktur sehr schnell im Vergleich zur Ablösungsgeschwindigkeit, so zeigt sich eine konstante Ablösungsgeschwindigkeit des Netzwerkes, abgesehen von einer äußerst kurzen Anlaufperiode, die gegebenenfalls mit den zur Verfügung stehenden Meßverfahren gar nicht nachgewiesen werden kann.

Aus dem Gesagten folgt, daß eine Änderung der Ablösungsgeschwindigkeit des Netzwerkes ein sicheres Anzeichen der Strukturänderung ist, während eine konstante Ablösungsgeschwindigkeit kein genügendes Kriterium für eine unveränderte Struktur darstellt. Ein sicheres Urteil ermöglicht nur die Bestimmung der Verteilung der Alkaliionenkonzentration in der Schicht.

In der vorliegenden Arbeit und in unseren weiteren Arbeiten werden Oberflächenschichten behandelt, deren Ausbildung unter Strukturänderung verläuft, wobei Beispiele für einige Grundtypen der möglichen Vorgänge angegeben werden.

Experimenteller Teil

Unsere Untersuchungen beruhen auf dem Verfahren, welches zur Bestimmung der Verteilung der Alkaliionenkonzentration in der Oberflächenschicht entwickelt wurde [1, 3]. Die Glasprobe (Länge 6—7 cm, Durchmesser 0,1—0,3 cm, Oberfläche 4—6 cm^2), vorangehend in einem dichtgeschlossenen Reagenzrohr über Magnesiumperchlorat als Trocknungsmittel gelagert, wurde mit Hirschleder poliert und durch Waschen mit Cyclohexan entfettet. Die Oberflächenschicht wurde in Polyäthylengefäßen, in 400 ml Wasser bei 40 $\pm$ 0,2 °C ausgebildet, wobei — um die Rückwirkung der aus dem Glas herausgelösten Reaktionsprodukte zu vermeiden — das Wasser so oft gewechselt wurde, daß die Konzentration der Alkaliionen im Wasser den Wert von $5 \cdot 10^{-4}$ Grammionen/Liter nicht überschritt. Aus dem flammenphotometrisch bestimmten Alkaligehalt der aus dem Wasser genommenen Proben wurde die Herauslösungsgeschwindigkeit der Alkaliionen aus dem Glas und aus dem photometrisch bestimmten Silikatgehalt dieser Proben die Geschwindigkeit der Ablösung des Silikatnetzwerkes berechnet.

Die auf dem Glasstab ausgebildete Oberflächenschicht wurde in 5—20 Schritten mit 1%iger Fluorwasserstoffsäurelösung stufenweise abgelöst. Dies erfolgte jeweils in 17 $\pm$ 0,1 ml

Lösung, in Proberöhren aus Polyäthylen, unter gleichmäßiger Bewegung des Glasstabes. Die Temperatur der Fluorwasserstoffsäurelösung betrug 20 $\pm$ 0,2 °C, die Dauer der Behandlung beider einzelner Fraktionen jeweils 2 . . . 10 $\pm$ 0,05 Minuten. Die Fluorwasserstoffsäurelösungen, welche die einzelnen Schichtfraktionen enthielten, wurden in zwei Teile geteilt, wobei aus dem einen Teil der Silikatgehalt der Schichtfraktion photometrisch, aus dem anderen Teil der Alkali- und Erdalkaligehalt, gegebenenfalls noch weitere Komponenten bestimmt wurden. Die Gesamtzeit zum Ablösen der ganzen Oberflächenschicht lag zwischen 10 und 100 Minuten, während der Vorgang der Ausbildung der Schicht im allgemeinen 1 bis 30 Tage benötigte. Nach den Berechnungen von BOUQUET [4] beeinflußt die Ablösung mit Fluorwasserstoffsäure zwar die Verteilung der Alkaliionenkonzentration der Schicht, die gerade bestimmt werden soll, jedoch ist der dadurch verursachte Fehler um vier Größenordnungen geringer als der zu bestimmende Wert, sodaß die Rückwirkung des Meßvorganges (der Ablösung mit Fluorwasserstoffsäure) vernachlässigt werden kann. In Anbetracht dessen, daß die stufenweise Ablösung der Oberflächenschicht bei um 20 °C niedrigerer Temperatur verläuft als die Ausbildung der Schicht und auch ihre Dauer wesentlich kürzer ist, kann angenommen werden, daß die aufgrund der stufenweisen Ablösung erhaltenen Angaben die Struktur widerspiegeln.

Durch Ablösen mit Fluorwasserstoffsäure unter den genannten Bedingungen kann die Ablösungsgeschwindigkeit des Netzwerkes in Fluorwasserstoffsäure (vorzugsweise in Einheiten Grammatom Si $\cdot$ cm^{-2} min^{-1}) in den verschiedenen Abschnitten der Schicht berechnet werden. Diese Ablösungsgeschwindigkeit (im weiteren mit $v_{HF,\,Si}$ bezeichnet) ist für die Struktur des Silikatnetzwerkes charakteristisch. Ändert sich das Silikatraumnetz im Laufe der Ausbildung der Schicht nicht, so muß die Ablösungsgeschwindigkeit in allen Abschnitten der Schicht identisch sein und mit der Ablösungsgeschwindigkeit des kompakten Glases in Fluorwasserstoffsäure übereinstimmen. (Aus später anzuführenden Gründen wird diese Erwartung in der Praxis nur annähernd erfüllt.) Verändert sich die Struktur des Netzwerkes während der Ausbildung der Oberflächenschicht, so muß sich die Ablösungsgeschwindigkeit entlang der Tiefenkoordinate der Schicht auf charakteristische Weise verändern. Neben der Verteilung der Alkaliionenkonzentration in der Schicht liefert also die Bestimmung von $v_{HF,Si}$ weitere Möglichkeiten zum Anzeigen eventueller Strukturänderungen, wobei gegebenenfalls auch gewisse Schlüsse bezüglich der Art dieser Änderungen gezogen werden können.

In unserer Arbeit wird die Alkaliionenkonzentration der einzelnen Abschnitte der Schicht bezogen auf den Si-Gehalt des Schichtabschnittes angegeben:

$$c_{K^+} = \frac{\text{Grammion } K^+}{\text{Grammatom Si}} ,$$

und die Verteilung wird nicht als Funktion der geometrischen Tiefenkoordinate, sondern als Funktion der Netzwerksilikat-Koordinate angegeben, wobei letztere die Zahl der Grammatome Silicium in einem Prisma der Schicht mit der Grundfläche von 1 cm^2 und der Dicke y ist [1].

Die Silikat-Koordinate wird mit g bezeichnet:

$$g = \sum_{i=1}^{k}{}' \mathrm{Si}_i ,$$

wo Si_i die Zahl der Grammatome Silicium in den einzelnen Schichtfraktionen, bezogen auf 1 cm^2 ist. Die Dimension von g ist also Grammatom $\cdot$ cm^{-2}.

Versuchsmodell

Die Möglichkeit der Strukturumwandlungen während der Ausbildung der Schicht wird in erster Linie durch den Ionenaustausch geschaffen, besonders wenn die im Ionenaustausch teilnehmenden Partner von verschiedener Größe sind; hierauf haben bereits BOKSAY, BOUGQUET und DOBOS im Zusammenhang mit natriumoxydhaltigen Gläsern hingewiesen [1, 3]. Dagegen erklären sie die Tatsache, daß die Oberflächenschichten bei ihrem Modellglas

mit der Zusammensetzung 20 Mol% K_2O, 12 Mol% SrO und 68 Mol% SiO_2 die Gleichungen (1) und (2) erfüllen, d.h. daß diese Oberflächenschicht ohne Strukturänderung gebildet wurde, mit der ähnlichen Größe des Kalium- und Hydroxoniumions.

Sechs Schmelzversuche des obengenannten kaliumoxydhaltigen Glases mit unveränderter Einwaagezusammensetzung ergaben in vier Fällen Gläser, bei denen die Verteilung der Alkaliionenkonzentration der Oberflächenschicht Gl. (1) und (2) nicht erfüllte, ihre Netzwerkstruktur wurde also im Laufe der Ausbildung der Oberflächenschicht verändert.

Diese Tatsache muß als überraschend bezeichnet werden, da unseres Wissens nach der einzige Unterschied zwischen den sechs Schmelzversuchen darin bestand, daß das verwendete BDH SiO_2 bei jenen zwei Gläsern, die keine Strukturveränderung aufwiesen, bzw. bei den vier Gläsern, die eine Strukturveränderung zeigten, aus verschiedenen Lieferungen stammte.

In der gegenwärtigen Arbeit wurden die letzteren Gläser als Modell verwendet. Sie werden im weiteren als Typ P_2 bezeichnet, während die Gläser, die keine Strukturänderung aufweisen, als Typ P_1 bezeichnet werden.

Versuchsergebnisse

In Abb. 2 sind die Versuchsergebnisse mit dem Modell aus P_2-Glas dargestellt. Das Glas wurde zwecks Ausbildung der Schicht 20 Tage lang bei 40 °C in Wasser gelagert. Kurve I zeigt die Konzentrationsverteilung der Kaliumionen, Kurve II ist das auf graphischem Wege hergestellte Differential von Kurve I, Kurve III ist die Ablösungsgeschwindigkeit des Netzwerkes in Fluorwasserstoffsäure. Beim Vergleich von Kurve I mit den Kurven in Abb. 1 fällt ihr unterschiedlicher Charakter sofort auf. Welche Aufklärung bieten nun die Meßdaten hinsichtlich der Art der Strukturumwandlung?

Verfolgen wir die Änderung der Parameter vom kompakten Glas bis zur wäßrigen Phase, in der Abbildung also von rechts nach links. Bei dem Übertritt aus dem kompakten Glas in die Oberflächenschicht nimmt die Konzentration der Kaliumionen ab, ähnlich wie bei dem P_1-Glas, in dessen Oberflächenschicht der Molenbruch der Kaliumionen gemäß den Kurven in Abb. 1 abnimmt. Der Konzentrationsgradient nimmt in der Schicht des P_1-Glases in Richtung vom kompakten Glas zur wäßrigen Phase monoton von Null bis zum Wert a/D zu. Der Verlauf des Konzentrationsgradienten für die Schicht im stationären Zustand wird durch das Differential der Gl. (2) nach y beschrieben:

$$\frac{dn}{dy} = \frac{a}{D} e^{-(a/D)y} . \qquad (3)$$

Gegenüber dieser monotonen Änderung wird bei dem P_2-Glas der Anstieg des Konzentrationsgradienten um $g \simeq 5 \cdot 10^{-5}$ Grammatom Si · cm^{-2} mäßiger, durchläuft dann ein Maximum und nimmt bis zur Grenze der wäßrigen Phase ab. Wenn die Diffusion der Kaliumionen selbst durch einen immer mäßiger ansteigenden und sogar abnehmenden Konzentrationsgradienten

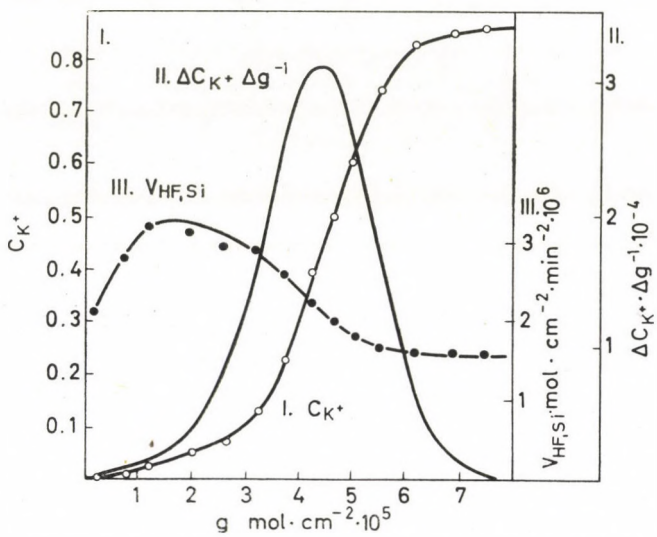

Abb. 2. Veränderung der Kaliumionenkonzentration (I), des Gradienten der Kaliumionenkonzentration (II) und der Ablösungsgeschwindigkeit des Netzwerkes in Fluorwasserstoffsäure (III) in Abhängigkeit von der durch den Silikatgehalt der Schicht ausgedrückten Tiefenkoordinate bei P_2-Glas

aufrechterhalten werden kann, so ist das nur dadurch möglich, daß der Weg der Alkaliionen in Richtung der Schicht–Wasser-Grenzfläche über eine solche Struktur führt, in welcher der Diffusionskoeffizient des Kaliumions dauernd höher wird, d.h. die Schicht wird in Richtung der Schicht–Wasser-Grenzfläche stets lockerer und für das Kaliumion durchlässiger.

Untersuchen wir nun den Verlauf der Ablösungsgeschwindigkeit mit Fluorwasserstoffsäure. Zunächst soll aber die Netzwerkablösungsgeschwindigkeit mit Fluorwasserstoffsäure bei der Schicht von P_1-Glas, die ohne Strukturänderung gebildet wurde, kurz behandelt werden. Aus der unveränderten Netzwerkstruktur sollte — wie bereits erwähnt wurde — folgen, daß jeder Punkt der Schicht mit der gleichen Geschwindigkeit in Fluorwasserstoffsäure gelöst wird. Demgegenüber verhält sich aber die Ablösungsgeschwindigkeit Abb. 3 entsprechend, d.h. sie nimmt vom kompakten Glas zur Grenzfläche der wäßrigen Phase hin monoton zu. Unserer Meinung nach dürfte diese Erscheinung damit zu erklären sein, daß der pH der Fluorwasserstoffsäurelösung in der Reaktionszone der Schicht–Wasser-Grenzfläche davon abhängig ist, wieviel

Kaliumionen aus der Schicht — infolge des Austausches mit Wasserstoff- bzw. Hydroxoniumionen — abwandern. Wird durch die Fluorwasserstoffsäurelösung ein Schichtabschnitt angegriffen, der näher zum kompakten Glas liegt, also mehr Kaliumionen enthält, so nimmt der pH in der Reaktionszone zu, die Dissoziation des Fluorwasserstoffs nimmt zu, folglich ist hier die Ablösungsgeschwindigkeit des Silikatnetzwerkes geringer als in der Schichtstrecke mit niedrigeren Kaliumionenkonzentrationen.

Die Netzwerkablösungsgeschwindigkeit in der Oberflächenschicht des P_2-Glases (Kurve III in Abb. 2) nimmt von rechts nach links, d.h. vom kom-

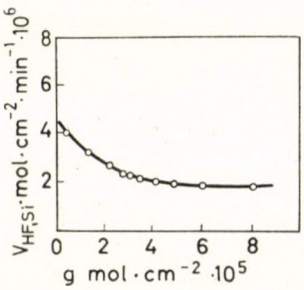

Abb. 3. Veränderung der Ablösungsgeschwindigkeit des Netzwerkes in Fluorwasserstoffsäure in Abhängigkeit von der durch den Silikatgehalt der Schicht ausgedrückten Tiefenkoordinate bei P_1-Glas

pakten Glas in Richtung zur wäßrigen Phase hin anfangs zu, ähnlich wie beim P_1-Glas, danach aber wird der Anstieg mäßiger, die Kurve durchläuft einen Inflexionspunkt, dann ein Maximum und nimmt dann ab. Es handelt sich bei dieser Kurve vermutlich um die Resultierende von mindestens zwei Effekten, und zwar muß gegenüber der die Ablösungsgeschwindigkeit steigernden Wirkung der nach links abnehmenden Kaliumionenkonzentration in Grenzflächennähe mit einer allmählichen Änderung der Netzwerkstruktur gerechnet werden, welche die chemische Widerstandsfähigkeit des Netzwerkes erhöht. Wird die Ablösungsgeschwindigkeit mit Fluorwasserstoffsäure in Abhängigkeit vom Logarithmus der Kaliumionenkonzentration in der Schicht dargestellt (Abb. 4), so erhält man bei Glas P_1 eine Gerade, welche den funktionellen Zusammenhang zwischen der Kaliumionenkonzentration und der Ablösungsgeschwindigkeit mit Fluorwasserstoff zu unterstützen scheint. Bei dem P_2-Glas zeigt jedoch die Abweichung der Kurve von der Geraden an, daß die Netzwerkablösungsgeschwindigkeit außer der Kaliumionenkonzentration auch noch von anderen Faktoren abhängig ist.

In Abb. 5 ist die zeitliche Veränderung der Austrittsgeschwindigkeit der im Laufe der Ausbildung der Oberflächenschicht in die wäßrige Phase austretenden Kaliumionen (Kurve I) und der Ablösungsgeschwindigkeit des Netz-

werkes $v_{H_2O,Si}$ (Kurve II) dargestellt. Die Geschwindigkeit der Ablösung des Netzwerkes ist nicht konstant, sie nimmt anfangs stürmisch und dann langsamer ab, wodurch angezeigt wird, daß in der Grenzschicht eine solche Strukturänderung vor sich geht, welche die chemische Widerstandsfähig-

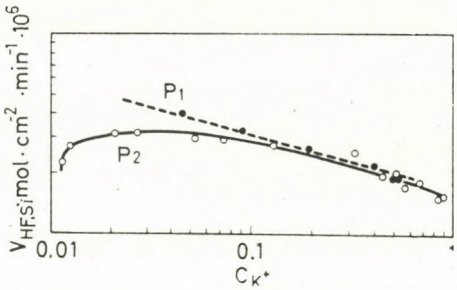

Abb. 4. Veränderung der Ablösungsgeschwindigkeit des Netzwerkes in Fluorwasserstoffsäure in Abhängigkeit von der Kaliumionenkonzentration der Schicht bei P_1- und P_2-Glas

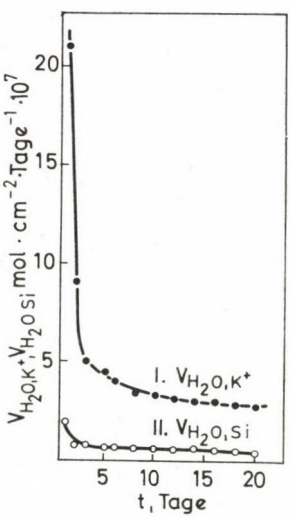

Abb. 5. Veränderung der Austrittsgeschwindigkeit der Kaliumionen (I) und der Ablösungsgeschwindigkeit des Netzwerkes (II) in Abhängigkeit von der Zeitdauer des Lagerns in Wasser bei P_2-Glas

keit des Netzwerkes an der jeweiligen Grenzfläche der Schicht stets erhöht. Aus der Tatsache, daß die Austrittsgeschwindigkeit der Komponenten selbst am 20. Tage nicht konstant ist, kann gefolgert werden, daß die Oberflächenschicht noch keineswegs im stationären Zustand vorliegt. Im stationären Zustand muß nämlich, wie leicht einzusehen ist, die Gleichung

$$\frac{v_{H_2O,K^+}}{v_{H_2O,Si}} = \frac{c_{K^+,Gl}}{c_{Si,Gl}} \tag{4}$$

gelten, wo $c_{K+,Gl}$ die Kaliumionenkonzentration und $c_{Si,Gl}$ die Siliziumkonzentration im kompakten Glas ist. Die zeitliche Veränderung des Verhältnisses der Austrittsgeschwindigkeiten ist in Abb. 6 dargestellt; die gestrichelte Gerade zeigt den Wert von $c_{K+,Gl}/c_{Si,Gl}$ an. Auch am 20. Tag zeigt das Geschwindig-

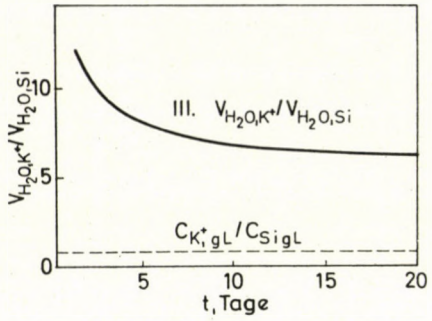

Abb. 6. Verhältnis der Austrittsgeschwindigkeit der Kaliumionen und der Ablösungsgeschwindigkeit des Netzwerkes in Abhängigkeit von der Lagerungszeit in Wasser bei P_2-Glas

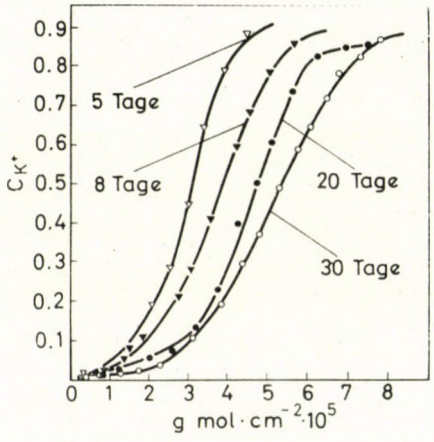

Abb. 7. Veränderung der Kaliumionenkonzentration in Abhängigkeit von der durch den Silikatgehalt der Schicht ausgedrückten Tiefenkoordinate bei P_2-Glas

keitsverhältnis einen vom stationären Zustand wesentlich abweichenden Wert und die geringe Steilheit der Kurve unterstützt die Annahme, daß der stationäre Zustand nur nach sehr langer Zeit erreichbar ist. Diese langsame Annäherung an den stationären Zustand unterscheidet das Verhalten des P_2-Glases ebenfalls vom Verhalten des P_1-Glases, bei welchem die Vorgänge, welche die Oberflächenschicht ausbilden, nach dem achten Tag stationär wurden [1].

Wir haben bisher über unsere Beobachtungen im Zusammenhang mit Schichten berichtet, welche im Laufe von 20tägiger Lagerung in Wasser gebildet wurden. In Abb. 7 sind die Verteilungskurven der Kaliumionenkonzentration in Schichten nach 5-, 8-, 20- und 30tägiger Lagerung in Wasser

dargestellt. Die betreffenden Kurven der Netzwerkablösungsgeschwindigkeit in Fluorwasserstoffsäure sind in Abb. 8 gezeigt. Qualitativ ihrer Form nach sind die Kurven einander ähnlich und die Front der einzelnen Vorgänge verschiebt sich mit zunehmender Lagerungsdauer in Wasser nach innen. Darüber hinausgehende Schlüsse dürften aus den Kurven wohl kaum zu ziehen sein, jedoch möchten wir darauf aufmerksam machen, daß die Kurven der Netzwerkablösungsgeschwindigkeit mit zunehmender Zeitdauer der Lagerung von einem

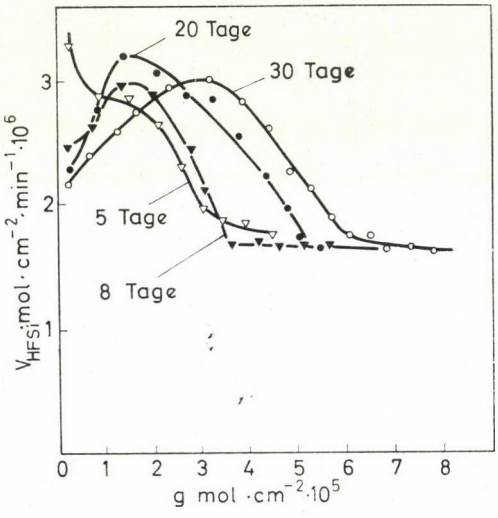

Abb. 8. Veränderung der Ablösungsgeschwindigkeit des Netzwerkes in Fluorwasserstoffsäure in Abhängigkeit von der durch den Silikatgehalt der Schicht ausgedrückten Tiefenkoordinate nach verschiedenen Zeitdauern der Lagerung in Wasser bei P_2-Glas

stets niedrigeren Niveau starten. Dies scheint darauf hinzuweisen, daß die Strukturumwandlung des Netzwerkes ein zeitlich langsamer Vorgang ist. Bei der Schicht, welche durch 5tägige Lagerung in Wasser gebildet wurde, ist dieser Anfangswert so hoch, daß das Maximum in Richtung des Schichtinneren ganz verschwindet.

Schlußfolgerungen

Aufgrund der Versuchsergebnisse kann auf folgende Strukturumwandlungen in der Oberflächenschicht des P_2-Glases gefolgert werden:

1. Die Strukturänderung ergibt einen Anstieg der chemischen Widerstandsfähigkeit, der Stabilität des Netzwerkes; der Beweis dafür ist der Verlauf der Ablösungsgeschwindigkeit in Fluorwasserstoffsäure.

2. Die Strukturumwandlung ist langsam, ihre Geschwindigkeit ist kommensurabel mit der Geschwindigkeit der Ablösung des Netzwerkes in Wasser;

der Beweis dafür ist die Änderung der Ablösungsgeschwindigkeit in Wasser während der Lagerung in Wasser.

3. Die Tatsache, daß die Ablösungsgeschwindigkeit des Netzwerkes in Wasser zeitlich abnimmt, bestätigt die Behauptung in Punkt 1.

4. Die Strukturumwandlung, die stabilisierend auf das Netzwerk wirkt, erleichtert zugleich die Diffusion der Kaliumionen; dies wird durch die festgestellte Änderung des Konzentrationsgradienten der Kaliumionen in der Oberflächenschicht bestätigt.

Aufgrund der Aussagen in 1.—4. und unserer Hypothesen bezüglich der Umwandlungsmöglichkeiten der Netzwerkstruktur halten wir es für wahrscheinlich, daß das Wesen der Umwandlung in einer räumlichen Umordnung des Silikatnetzes besteht. Es ist jedoch keineswegs auszuschließen, daß dabei $\gtrless$Si—O—Si$\lessgtr$ Bindungen gespalten werden bzw. neue $\gtrless$Si—O—Si$\lessgtr$ Bindungen entstehen, sodaß im Endergebnis auch das Verhältnis der $\gtrless$Si—O—Si$\lessgtr$ und $\gtrless$Si—$\overline{\text{O}}$ Bindungen verändert werden kann.

Die Ursache der Strukturumwandlung

Bei der Reproduktion der Schmelzen von Gläsern mit der Einwaagezusammensetzung $20\ K_2O \cdot 12\ SrO \cdot 68\ SiO_2$ erhielten wir — wie bereits bemerkt wurde — in zufallsartiger Weise manchmal P_1-Glas, dann wieder P_2-Glas. Die Proben aus ein und derselben Schmelze waren stets von demselben Typ, also entweder P_1- oder P_2-Gläser.

Die Erscheinung muß als äußerst interessant bezeichnet werden, zumal wir versuchten, die Schmelzen stets unter identischen Verhältnissen durchzuführen, obwohl bemerkt werden muß, daß wir die Schmelztemperatur nur mit einer Genauigkeit von 1350 ± 50 °C reproduzieren konnten.

Die Ursache der Strukturumwandlung kann auch in den Verunreinigungen des zum Wässern verwendeten Wassers liegen. Da wir das Wasser aus einer kupfernen Destillationsanlage gewannen, dachten wir an die Wirkung der Verunreinigungen von Kupferionen. Dieser Verdacht wurde auf die Beobachtungen von FISCHER und HECKEL gegründet, wonach Spuren von Schwermetallionen die Korrosion von Gläsern wesentlich vermindern können [5].

Deshalb führten wir Wässerungen mit destilliertem Wasser durch, aus welchem die Kupferionenverunreinigungen mit dem Oxycelluloseverfahren von SCHULEK und Mitarbeitern [6] entfernt worden waren. Die Strukturänderung erfolgte dennoch. Andererseits untersuchten wir die Ausbildung der Oberflächenschicht in 0,01 *m* Kupferacetatlösung und fanden überhaupt keinen Unterschied im Vergleich zu den Ergebnissen mit reinem Wasser. Wir untersuchten auch die Kupferionenverteilung in der Oberflächenschicht und fanden, daß die Gesamtmenge der Kupferionen in der ersten Schichtfraktion an-

gesammelt war, folglich können diese Ionen die im Inneren der Schicht verlaufende Strukturänderung keineswegs verursachen.

Es scheint eher wahrscheinlich, daß die Erklärung der Strukturumwandlung bei der Ausbildung der Oberflächenschicht des P_2-Glases in den Eigenheiten dieses Glases selbst zu suchen ist. Es könnte angenommen werden, daß — trotz unserer Bestrebung, identische Schmelzbedingungen aufrechtzuerhalten — infolge unkontrollierbarer Wirkungen, das Glas während des Schmelzens für das Verhalten gemäß Typ P_1 bzw. P_2 präformiert wird. Deshalb wurden

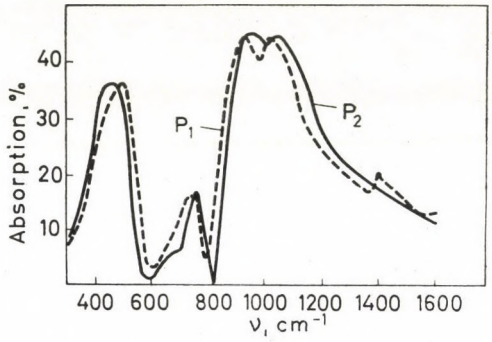

Abb. 9. IR-Absorptionsspektren von P_1 und P_2-Gläsern

IR-spektroskopische bzw. DTA-Untersuchungen der P_1- und P_2-Gläser durchgeführt.

Für IR-spektroskopische Zwecke wurde das Glas zu Pulver gemahlen und in einer Konzentration von 0,2% geprüft. Es wurde ein Perkin-Elmer Spektrograph Typ 225 mit Kaliumjodidpastille angewendet. Die Messungen wurden im Wellenzahlenbereich 300—1600 cm^{-1} durchgeführt, wo sich die Banden der Si—O—Si Bindungen befinden. Wie aus Abb. 9 hervorgeht, weisen besonders die Maxima der Si—O—Si Banden bei 470 cm^{-1} und 870 cm^{-1} wesentliche Unterschiede auf, je nachdem, ob es sich um P_1-Glas oder P_2-Glas handelt. (Es soll bemerkt werden, daß die IR-Spektren von Gläsern desselben Typs, die aus verschiedenen Schmelzen stammten, untereinander eine recht gute Übereinstimmung zeigten.)

Die DTA-Kurven der Gläser wurden im Temperaturbereich von 25—1300 °C mit einer Mettler Vakuumthermowaage aufgenommen. (Einwaage 15 mg, Temperaturprogramm 6 °C/Minute, Empfindlichkeit 100 μV.) Gemäß Abb. 10 weichen die DTA-Kurven der beiden Glastypen charakteristisch voneinander ab. (Die Übereinstimmung der DTA-Kurven von Gläsern desselben Typs, jedoch aus verschiedenen Schmelzen, war verhältnismäßig gut.)

Es kann also festgestellt werden, daß P_1- und P_2-Gläser unterschiedliche Strukturen besitzen; die Ursache des abweichenden Verhaltens bei der Ausbil-

dung der Oberflächenschicht liegt also in dieser unterschiedlichen Strukturpräformation.

Um zu entscheiden, weshalb bei der Glasschmelze — selbst bei verhältnismäßig gleichen Bedingungen — Gläser mit abweichender Struktur gebildet werden, scheint es zweckmäßig, Untersuchungen in zwei Richtungen durchzuführen. Einerseits sollten die Verunreinigungen des Glases hinsichtlich ihrer

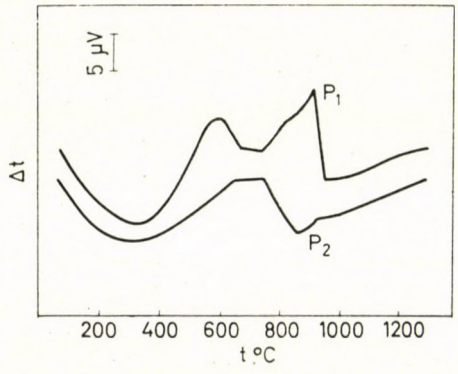

Abb. 10. DTA-Kurven von P_1 und P_2-Gläsern

Wirkung sorgfältig geprüft werden, andererseits soll die Schmelze des Glases unter streng kontrollierten Bedingungen, zweckmäßig in der thermoanalytischen Waage selbst, unter Verfolgung der beim Schmelzen und während dem Abkühlen verlaufenden Vorgänge durchgeführt werden. Aus unseren Vorversuchen in diesen Richtungen ergab sich bis zur Zeit kein einheitlich auswertbares Bild.

LITERATUR

1. Boksay, Z., Bouquet, G., Dobos, S.: Physics and Chemistry of Glasses **8** 140 (1967)
2. Boksay, Z., Bouquet, G., Dobos, S.: Physics and Chemistry of Glasses **9** 69 (1968)
3. Bouquet, G., Dobos, S., Boksay, Z.: Ann. Univ. Sci. Budapest, Sect. Chim. **6,** 5 (1964)
4. Bouquet, G.: Doktorsdissertation, Budapest 1966
5. Fischer, J., Heckel, E.: Glastechn. Ber. **35,** 8 (1962)
6. Schulek, E., Remport-Horváth, Zs., Lasztity, A.: Talanta **10,** 621 (1963)

Sándor Dobos; Budapest VIII., Múzeum-krt. 6—8.

Acta Chimica Academiae Scientiarum Hungaricae, Tomus 68 (4), pp. 387—396 (1971)

STUDY OF THE VAPOUR-LIQUID EQUILIBRIUM IN PROPIONIC ACID–CARBON TETRACHLORIDE MIXTURES

J. Liszi

(Department of Electrochemical Research, Hungarian Academy of Sciences, and Department of Physical Chemistry, University of Veszprém, Veszprém)

Received January 30, 1970

From a study of the vapour–liquid equilibrium of propionic acid–carbon tetrachloride, it was found that the given system behaves approximately as if it were an ideal mixture of dimeric propionic acid and carbon tetrachloride. The calculated vapour–liquid equilibrium values were checked against data determined experimentally at 30, 40, 50, 60 and 70 °C.

In our earlier work [1] binary mixtures of propionic acid and apolar substances were studied. The extent of association of propionic acid was determined from the dielectric properties in the liquid phase at 20 °C. The results showed that propionic acid was almost completely dimerized in the studied mixtures which, to a good approximation, could be considered as ideal binary mixtures of dimeric propionic acid and the apolar substance. In the present work we examine the extent to which the above mentioned result can be used to describe the vapour–liquid equilibrium in propionic acid–carbon tetrachloride mixtures. With this aim the equilibrium data were determined at 30, 40, 50, 60 and 70 °C. The experimental results are compared with the values calculated from the above approximation.

1. The thermodynamic model

The propionic acid–carbon tetrachloride mixtures are treated as ideal ternary mixtures of the type A–A_2–B. This means that the nominally two-component (propionic acid and carbon tetrachloride) mixtures are considered as ideal ternary mixtures of monomeric propionic acid (A), dimeric propionic acid (A_2) and carbon tetrachloride (B). The following relations are valid between the partial pressures of the components, nominal and actual:

$$P_{\text{prop}} = P_1 + P_2 \tag{1}$$

$$P_B = P_3. \tag{2}$$

The total pressure is

$$P_t = P_1 + P_2 + P_3 = P_{\text{prop}} + P_B. \tag{3}$$

The nominal mole fraction of carbon tetrachloride in the vapour phase can be calculated from the partial pressure with the following relation:

$$y_B = \frac{y_3}{1+y_2} = \frac{P_3}{P_t+P_2} . \tag{4}$$

The actual mixture is considered as an ideal ternary mixture which means that the Raoult Law is accepted as valid for the ternary mixture:

$$P_i = x_i P_i^0 . \tag{5}$$

A relation similar to Eq. (4) is valid between the nominal mole fraction of carbon tetrachloride in the liquid phase and the actual mole fraction:

$$x_B = \frac{x_3}{1+x_2} . \tag{6}$$

For the above relations to be applied to the system studied, the composition of the A–A_2–B type ternary mixture must be known. Table I contains the values of the association equilibrium constant referring to the liquid phase,

$$K = \frac{x_2}{x_1^2} \tag{7}$$

expressed in mole fractions for pure propionic acid as a function of the temperature. In the last two columns of the Table are liquid phase mole fractions relating to pure propionic acid of the monomeric and dimeric forms (x_1^0 and x_2^0). These latter data were calculated from Eq. (7) using the relation:

$$x_1^0 + x_2^0 = 1 . \tag{8}$$

Table I

True composition of pure propionic acid as a function of temperature

t °C	K	x_1^0	x_2^0
8	3040*	0.0180	0.9810
20	1804**	0.0232	0.9760
21	1450*	0.0256	0.9744
31	868*	0.0334	0.9666
41	526*	0.0427	0.9573
51	332*	0.0535	0.9465
60	225***	0.0644	0.9356
70	149***	0.0785	0.9215

The data denoted by * and ** are to be found in references [2] and [1], respectively. The values denoted by *** were calculated with the equation

$$\log K = -3.7712 + \frac{2039.9}{T} \tag{9}$$

determined from the first six rows of the Table. The data of Table I show that even at 70 °C the amount of monomeric propionic acid in pure propionic acid does not reach 8%. This permits the conclusion, in agreement with the earlier dielectric studies [1], that to a first approximation propionic acid can be considered as dimeric propionic acid. If this approximation is permitted, then the equilibrium vapour pressure of propionic acid is almost identical with the equilibrium vapour pressure of dimeric propionic acid:

$$P^0_{\text{prop}} \simeq P^0_2. \tag{10}$$

From similar considerations:

$$x_2 + x_3 \simeq 1 \tag{11}$$

($x_1 \sim 0$). Hence the total pressure of the mixture:

$$P_t \simeq x_2 P^0_2 + x_3 P^0_3. \tag{12}$$

From relations (6) and (11) the nominal mole fraction of carbon tetrachloride in the liquid phase is

$$x_B \simeq \frac{1 - x_2}{1 + x_2}. \tag{13}$$

The calculation of the vapour–liquid equilibrium data is made using the above approximations. x_2, the actual mole fraction of dimeric propionic acid in the liquid phase, is calculated with relation (13) from the given nominal mole fraction, $x_B \cdot P_2$, the partial pressure of dimeric propionic acid, is determined from relations (5) and (10) using the known value of x_2. Relation (11) furnishes x_3, the actual mole fraction of carbon tetrachloride. With x_3 known, Eqs (2) and (5) give P_3, the partial pressure of carbon tetrachloride in the ternary mixture. The total pressure can be calculated from relation (12). With the partial pressures and the total pressure known, the nominal mole fraction of carbon tetrachloride in the vapour phase is calculated from Eq. (4).

2. Experimental data and check on the applied model

In our experiments the nominal composition of the vapour phase and the total pressure of the system were measured as a function of the nominal mole fraction of carbon tetrachloride. The apparatus used has been described in an earlier paper [3]. The determination of concentration was performed via the index of refraction in the case of propionic acid–carbon tetrachloride mixtures. Measurements were made with mixtures at 30, 40, 50, 60 and 70 °C. The results are given in Tables II—VI and Figs 1—10. The first column in the Tables

Table II

Vapour–liquid equilibrium data for propionic acid–carbon tetrachloride mixtures at 30 °C

$\sigma_y = 0.005$; $\sigma_{pt} = 3$ torr

x	y_B^m	P_t^m torr	y_B^c	P_t^c torr
0.000	0.000	6	0.000	6
0.091	0.795	25	0.802	25
0.165	0.885	41	0.889	39
0.191	0.902	40	0.905	43
0.201	0.915	44	0.910	45
0.265	0.920	50	0.927	51
0.272	0.928	51	0.938	55
0.282	0.948	62	0.941	57
0.341	0.951	61	0.954	64
0.343	0.950	67	0.955	65
0.345	0.956	70	0.958	65
0.352	0.958	62	0.956	66
0.401	0.964	72	0.964	72
0.410	0.965	77	0.966	73
0.415	0.968	71	0.966	73
0.420	0.970	72	0.967	74
0.435	0.965	73	0.969	76
0.450	0.975	75	0.971	77
0.455	0.972	79	0.971	78
0.495	0.970	85	0.975	82
0.512	0.971	81	0.977	84
0.630	0.986	94	0.986	95
0.782	0.981	108	0.993	107
0.952	0.995	119	0.999	118
1.000	1.000	121	1.000	121

contains the nominal mole fraction of carbon tetrachloride in the liquid phase. In the second column is the experimentally determined mole fraction of carbon tetrachloride in the vapour phase, and in the third column is the measured total pressure. The fourth column shows the calculated mole fraction in the

Table III

Vapour–liquid equilibrium data for propionic acid–carbon tetrachloride mixtures at 40 °C

$\sigma_y = 0.004$; $\sigma_{pt} = 4$ torr

x_B	y_B^m	P_t^m torr	y_B^c	P_t^c torr
0.000	0.000	10	0.000	10
0.018	0.440	15	0.435	17
0.051	0.694	26	0.691	29
0.102	0.816	44	0.825	46
0.149	0.869	58	0.879	61
0.172	0.890	68	0.896	68
0.203	0.918	73	0.914	76
0.237	0.929	83	0.928	85
0.274	0.939	90	0.940	95
0.325	0.948	101	0.952	107
0.326	0.947	104	0.953	107
0.364	0.958	113	0.960	115
0.380	0.962	113	0.962	119
0.382	0.963	115	0.963	119
0.426	0.965	124	0.969	128
0.552	0.983	147	0.981	150
0.582	0.980	153	0.983	155
0.627	0.984	160	0.986	162
0.681	0.986	175	0.989	170
0.683	0.987	169	0.989	170
1.000	1.000	208	1.000	208

vapour phase, and the fifth column the calculated total pressure. For each measurement series the mean square differences between the calculated and the measured results are also given. The continuous lines in the Figures are the calculated values and the circles are the measured results.

The presented results show that the vapour–liquid equilibrium data of a propionic acid–carbon tetrachloride mixture can be described by the approximation formulae introduced in the first part of this paper. In the description of these data, the role of monomeric propionic acid is disregarded. The propion-

Table IV

Vapour–liquid equilibrium data for propionic acid–carbon tetrachloride mixtures at 50 °C

$\sigma_y = 0.008$; $\sigma_{pt} = 2$ torr

x_B	y_B^m	P_t^m torr	y_B^c	P_t^c torr
0.000	0.000	18	0.000	18
0.046	0.602	40	0.621	43
0.102	0.796	69	0.794	71
0.248	0.902	133	0.918	132
0.297	0.941	150	0.935	150
0.376	0.952	174	0.953	175
0.438	0.964	192	0.964	193
0.467	0.966	202	0.968	201
0.505	0.982	213	0.972	211
0.526	0.980	216	0.974	217
0.539	0.976	219	0.975	220
0.550	0.980	221	0.977	223
0.783	0.990	274	0.992	271
1.000	1.000	306	1.000	306

Table V

Vapour–liquid equilibrium data for propionic acid–carbon tetrachloride mixtures at 60 °C

$\sigma_y = 0.008$; $\sigma_{pt} = 3$ torr

x_B	y_B^m	P_t^m torr	y_B^c	P_t^c torr
0.000	0.000	32	0.000	32
0.051	0.582	69	0.582	69
0.165	0.834	140	0.836	140
0.316	0.914	212	0.923	215
0.355	0.930	225	0.934	232
0.365	0.927	234	0.937	236
0.374	0.923	238	0.939	240
0.400	0.933	246	0.945	250
0.411	0.938	252	0.948	255
0.454	0.950	267	0.956	271
0.476	0.952	274	0.959	278
0.481	0.958	279	0.960	280
0.570	0.980	305	0.972	309
0.813	0.980	376	0.991	375
1.000	1.000	413	1.000	413

Table VI

Vapour–liquid equilibrium data for propionic acid–carbon tetrachloride mixtures at 70 °C

$\sigma_y = 0.009$; $\sigma_{pt} = 4$ torr

x_B	y_B^m	P_t^m torr	y_B^c	P_t^c torr
0.000	0.000	49	0.000	49
0.047	0.555	96	0.549	99
0.112	0.739	160	0.757	161
0.150	0.795	191	0.813	194
0.175	0.820	208	0.840	215
0.181	0.838	216	0.845	219
0.225	0.860	250	0.878	253
0.276	0.900	285	0.904	290
0.301	0.915	305	0.914	306
0.355	0.925	328	0.931	340
0.414	0.937	370	0.946	375
0.470	0.952	400	0.956	405
0.485	0.956	409	0.959	412
0.523	0.962	426	0.964	431
0.540	0.961	435	0.967	439
0.550	0.962	440	0.968	444
0.551	0.963	442	0.968	444
0.625	0.971	478	0.976	477
0.674	0.978	495	0.981	497
0.732	0.982	514	0.985	519
0.827	0.991	550	0.992	552
0.880	0.992	570	0.995	570
1.000	1.000	605	1.000	605

ic acid–carbon tetrachloride system behaves as if it were an ideal mixture of dimeric propionic acid and carbon tetrachloride.

In the evaluation of the results, however, the following considerations cannot be neglected. With increasing concentration of carbon tetrachloride the association equilibrium is so displaced that the relative amount of monomeric propionic acid increases compared with that of the dimer. This phenomenon implies that with the increase of x_B the approximation should gradually lose its validity. At the same time, however, with the increase of x_B the partial pressure of carbon tetrachloride contributes more and more decisively to the total pressure of the system. As a result of these two contrasting effects the approximation gives satisfactory results over the entire concentration range.

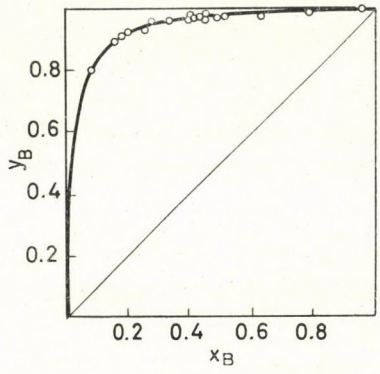

Fig. 1. Vapour phase nominal mole fraction of carbon tetrachloride as a function of the liquid phase nominal mole fraction at 30 °C

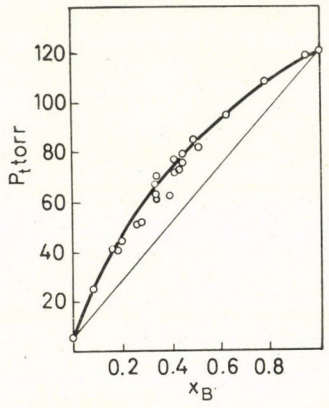

Fig. 2. Equilibrium total pressure of propionic acid–carbon tetrachloride mixtures as a function of the liquid phase nominal mole fraction of carbon tetrachloride at 30 °C

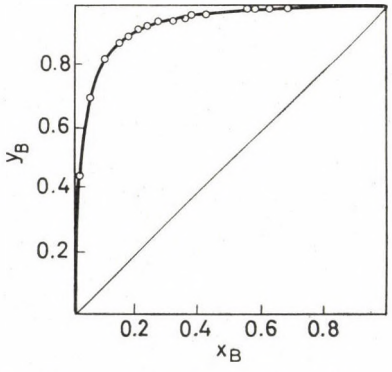

Fig. 3. Vapour phase nominal mole fraction of carbon tetrachloride as a function of the liquid phase nominal mole fraction at 40 °C

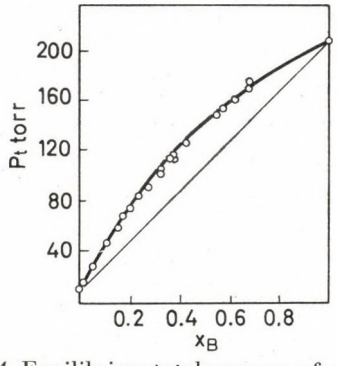

Fig. 4. Equilibrium total pressure of propionic acid–carbon tetrachloride mixtures as a function of the liquid phase nominal mole fraction of carbon tetrachloride at 40 °C

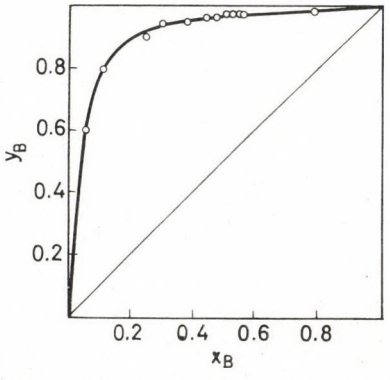

Fig. 5. Vapour phase nominal mole fraction of carbon tetrachloride as a function of the liquid phase nominal mole fraction at 50 °C

Thus from an examination of the association properties of propionic acid it appears that this carboxylic acid may be modelled more simply than formic or acetic acids. In the case of formic acid chain association occurs [4], while for acetic acid the monomeric molecules, which have a strongly dipolar character, do not permit the application of an ideal mixture model [3].

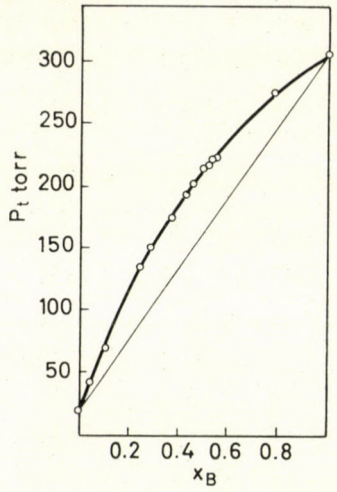

Fig. 6. Equilibrium total pressure of propionic acid–carbon tetrachloride mixtures as a function of the liquid phase nominal mole fraction of carbon tetrachloride at 50 °C

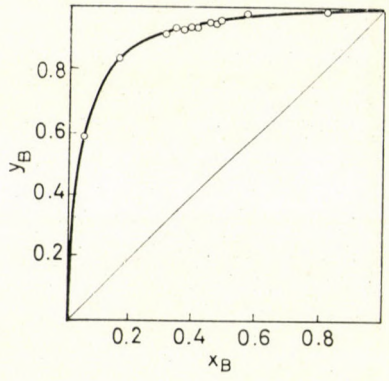

Fig. 7. Vapour phase nominal mole fraction of carbon tetrachloride as a function of the liquid phase nominal mole fraction at 60 °C

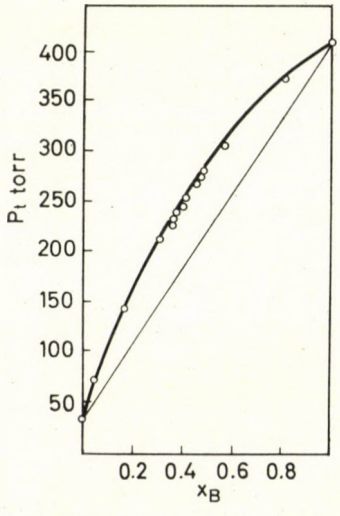

Fig. 8. Equilibrium total pressure of propionic acid–carbon tetrachloride mixtures as a function of the liquid phase nominal mole fraction of carbon tetrachloride at 60 °C

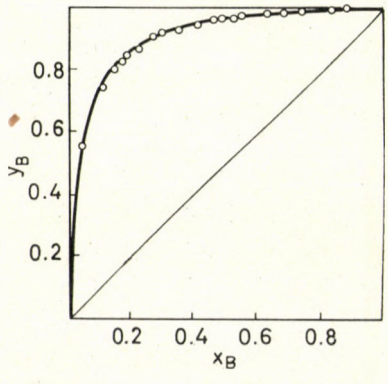

Fig. 9. Vapour phase nominal mole fraction of carbon tetrachloride as a function of the liquid phase nominal mole fraction at 70 °C

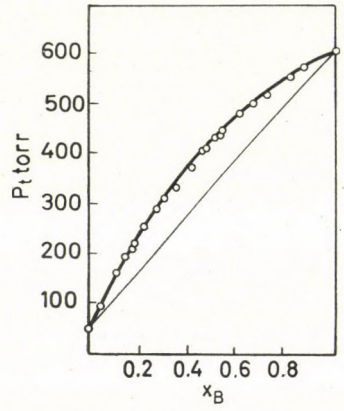

Fig. 10. Equilibrium total pressure of propionic acid–carbon tetrachloride mixtures as a function of the liquid phase nominal mole fraction of carbon tetrachloride at 70 °C

The reported results are based in part on the scientific student circle work of I. FÜLÖP, who presented a lecture on this theme at the 9th National Conference of Scientific Student Circles.

List of symbols

A — monomeric propionic acid
A_2 — dimeric propionic acid
B — carbon tetrachloride
K — association equilibrium constant (in mole fractions) referring to the liquid phase
P — pressure
T — absolute temperature
x — mole fraction in the liquid phase
y — mole fraction in the vapour phase
σ — square mean difference of the differences between the measured and calculated values

Lower indices

B — carbon tetrachloride in the nominal mixture
prop — propionic acid in the nominal mixture
i — general component
t — total
pt — referring to the total pressure
y — referring to the vapour phase mole fraction
1 — monomeric propionic acid in the actual mixture
2 — dimeric propionic acid in the actual mixture
3 — carbon tetrachloride in the actual mixture

Upper indices

m — measured (experimental) data
c — calculated data
0 — pure substance

REFERENCES

1. LISZI, J.: Acta Chim. Acad. Sci. Hung. (In press.)
2. PIMENTAL, C. C., MCCLELLAN, A. L.: The Hydrogen Bond. Freeman, San Francisco and London 1960
3. LISZI, J.: Magy. Kém. Foly. **75**, 452 (1969)
4. CHAPMAN, D.: J. Chem. Soc. 225 (1956)

János LISZI; Veszprémi Vegyipari Egyetem, Veszprém, Hungary.

Acta Chimica Academiae Scientiarum Hungaricae, Tomus 68 (4), pp. 397–402 (1971)

ANWENDUNG VON AMIDCHLORIDEN IN RINGSCHLUSSREAKTIONEN, II

SYNTHESE VON THIENO(2,3-d)-4(3H)-PYRIMIDINONEN

Z. CSŰRÖS, R. SOÓS, J. PÁLINKÁS und I. BITTER

(Lehrstuhl für organisch-chemische Technologie, Technische Universität, Budapest)

Eingegangen am 9. Januar 1970

Ausgehend aus 2-Amino-3-carbäthoxy-4,5-dimethylthiophen und Dimethylformamidchlorid wurde N,N-Dimethyl-N'-[(3-carbäthoxy-4,5-dimethyl)-2-thienyl]-formamidinhydrochlorid hergestellt. Das auf diese Weise gewonnene trisubstituierte Amidin wurde mit Ammoniak, aliphatischen und aromatischen primären Aminen, Hydrazin und Alkylendiaminen cyclisiert. Dadurch wurden 5,6-Dimethylthieno(2,3-d)-4(3H)-pyrimidinone und die bisher noch nicht beschriebenen Alkylen-bis-3,3'-5,6-dimethylthieno(2,3-d)-4(3H)-pyrimidinone erhalten.

In einer früheren Mitteilung [1] berichteten wir über ein Verfahren zur Herstellung von 4(3H)-Chinazolinonderivaten. Dieses neue Verfahren wurde zur Herstellung von Thieno(2,3-d)-4(3H)-pyrimidinonen herangezogen.

Das Thieno(2,3-d)-4(3H)-pyrimidinon und seine Derivate sind — ähnlich wie 4(3H)-Chinazolinone — Stoffe mit therapeutischer Wirkung. Eine Verbindung dieser Art wurde zuerst durch BAKER und Mitarbeiter [2] als Komponente des Thiophen-Isosteren der gegen Malaria wirksamen Hydrangea-Alkaloide hergestellt. Das Endprodukt wurde aus 2-Aceto-3-methylthiophen über einen äußerst verwickelten Weg mit einer Ausbeute von 4% erhalten.

SCHWEDOW und Mitarbeiter [3] erhielten das Thieno(2,3-d)-4(3H)-pyrimidinon aus 2-Amino-3-carbalkoxythiophen und Formamid durch Kochen bei 200—210 °C.

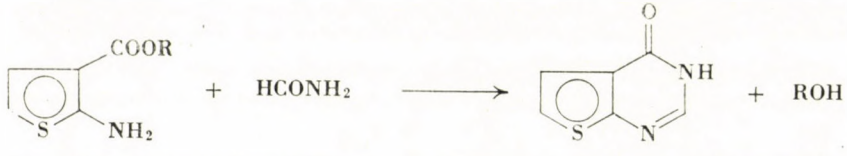

Im wesentlichen dasselbe Verfahren wurde durch ROBBA und Mitarbeiter [4] beschrieben; daneben berichten sie auch über eine neue Synthese, in der das Produkt aus 2-Amino-3-carboxamidothiophen mit Ameisensäure erhalten wird.

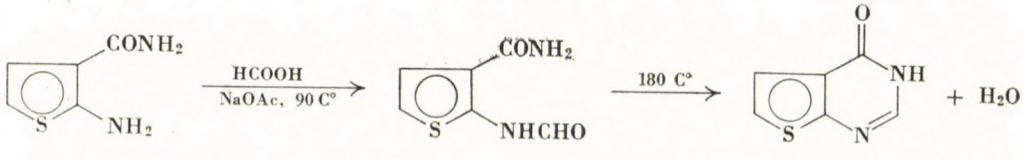

Den Ausgangsstoff, 2-Amino-3-thiophencarbonsäureamid, erhielten sie durch Kondensation von Thioacetaldehyd mit Cyanamid.

RIED und GIESSE [5, 6] stellten außer den nichtsubstituierten Verbindungen auch die 5- bzw. 6-Alkylverbindungen her, wobei die entsprechenden 2-Amino-3-carbalkoxythiophenderivate mit Iminoester, Amidinen, Amidoximen bzw. aktivierten Nitrilen in Reaktion gebracht wurden. Bei den verschiedenen 2-, 5- und 6-Substituenten erhielten sie in 1—16stündigen Reaktionen bei 120—160 °C Ausbeuten von 12—47%.

Im Vergleich zu den genannten Verfahren besitzt unser Verfahren mehrere Vorteile. Das Thieno(2,3-d)-4(3H)-pyrimidinon wird meist bei niedrigen Temperaturen und kurzen Reaktionszeiten mit guten Ausbeuten erhalten. Außerdem ist es möglich, die N-substituierten Derivate unmittelbar herzustellen.

Der erste Schritt der Synthese ist die Herstellung des Amidinsalzes. Das N,N-Dimethyl-N'-[(3-carboxy-4,5-dimethyl)-2-thienyl]-formamidinhydrochlorid **(III)** wurde aus Dimethylformamidchlorid **(I)** und dem als Ausgangsstoff gewählten 2-Amino-3-carbäthoxy-4,5-dimethylthiophen **(II)** gewonnen

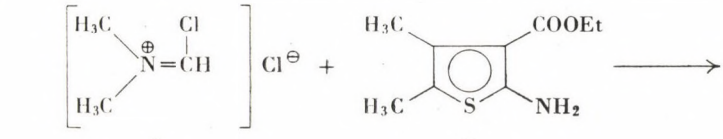

I II

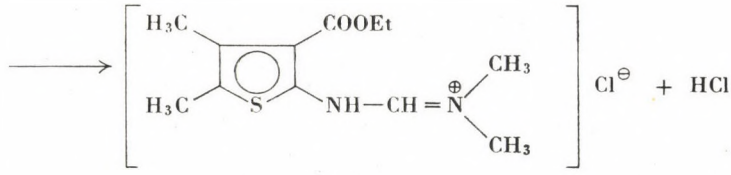

III

Die Komponenten wurden bei Zimmertemperatur in Chloroform in äquimolarem Verhältnis in Reaktion gebracht. Das Produkt wurde durch Eindampfen der Lösung gewonnen.

Das Amidinsalz bleibt in kristalliner oder öliger Form zurück. Aus dem öligen Rückstand wird das kristalline Amidinhydrochlorid durch Verreiben mit Dioxan erhalten.

Im zweiten Schritt der Synthese wird der Ringschluß zum Thieno(2,3-d)-4(3H)-pyrimidinon **(IV)** durchgeführt.

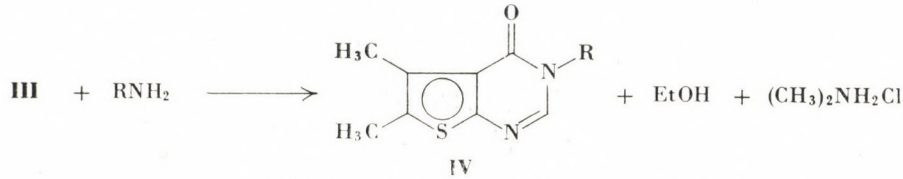

IV

R = H, NH_2, Methyl, Butyl, Benzyl, *p*-Toluyl

Als Ringschlußreagens wurden Ammoniak, aliphatisches Amin, Aralkylamin, aromatisches Amin bzw. Hydrazin verwendet. Das Amidinsalz und das Amin wurden in äquimolarem Verhältnis in Alkohol in Reaktion gebracht. Die Reaktion verläuft bereits bei Zimmertemperatur, kann jedoch durch Erwärmen beschleunigt werden.

Zwecks Identifizierung der Produkte wurden einige Thieno(2,3-d)-4(3H)-pyrimidinone auch nach dem Verfahren von RIED und GIESSE [5, 6] hergestellt. Die N-substituierten Derivate wurden aus der Ausgangsverbindung durch Alkylierung erhalten. Die Schmelzpunkte und IR-Spektren der nach den beiden Verfahren hergestellten Stoffe waren völlig identisch. In Einklang mit den Ergebnissen von ROBBA und Mitarbeiter [4, 7, 8] wurde festgestellt, daß die Spektren der Thieno(2,3-d)-4(3H)-pyrimidinone und der entsprechenden 4(3H)-Chinazolinone einander recht ähnlich sind; was besonders für die charakteristischen Schwingungen gilt.

Als Beispiel wird das IR-Spektrum des 3-Butyl-5,6-dimethyl-thieno-(2,3-d)-4(H)-pyrimidinons vorgeführt.

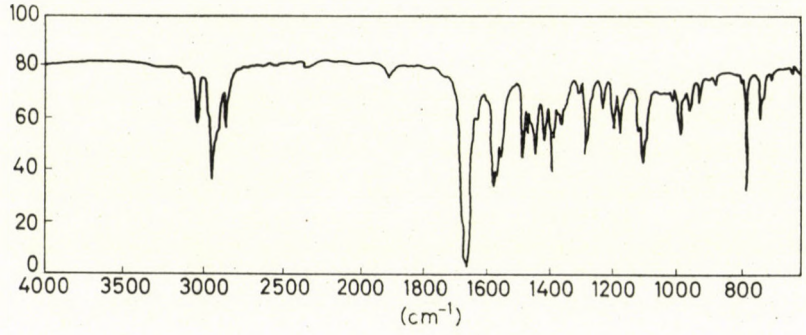

Abb. 1

Zwischen 1500 und 1700 cm^{-1} befinden sich zwei starke Banden. Die stärkere ist die Lactamcarbonyl-Bande, die schwächere die Valenzschwingung des aromatischen Kerns, die mit anderen Banden, u.a. vermutlich mit der Bande der Bindung >C=N—, zusammen erscheint.

Die den Lactamcarbonyl-Gruppen der synthetisierten Verbindungen entsprechenden Wellenzahlen sind in Tab. I angegeben.

Wurde Alkylendiamin als Ringschlußreagens verwendet, so gelangten wir zu den bisher noch nicht beschriebenen Alkylen-bis-3,3'-thieno(2,3-d)-4(H)-pyrimidinonen **(V)**.

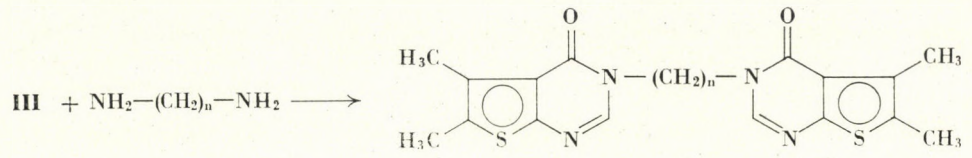

V

$n = 2, 4, 6$

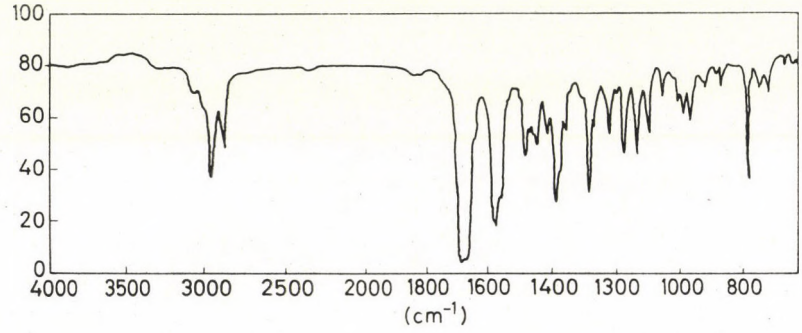

Abb. 2

Die Komponenten wurden in äquimolarem Verhältnis in Alkohol in Reaktion gebracht. Nach kurzem Sieden wurde das Produkt durch Filtrieren isoliert. Interessanterweise konnte das aminoalkylierte Derivat selbst mit Diaminüberschuß nicht erhalten werden. Diese Versuchsergebnisse sind in Übereinstimmung mit den bei der Herstellung von bis-4(3H)-Chinazolinonen beobachteten Befunden [1].

Bei der Untersuchung der Spektren der bis-Verbindungen wurde festgestellt, daß sie den Spektren der entsprechenden Thieno(2,3-d)-4(3H)-pyrimidinonen sehr ähnlich sind.

Als Beispiel wird das IR-Spektrum des Hexylen-bis-3,3'-5,6-dimethylthieno(2,3)-4(3H)-pyrimidinons gezeigt.

Zwischen 1500 und 1700 cm^{-1} befinden sich auch hier zwei starke Banden. Die stärkere Lactamcarbonyl-Bande befindet sich bei 1683 cm^{-1}.

Die wichtigsten Angaben der synthetisierten Verbindungen sind in Tab. I zusammengefaßt; Hinweise auf das angewendete Verfahren sind ebenfalls angegeben.

Die synthetisierten Verbindungen wurden durch Elementaranalyse, gegebenenfalls durch Mischschmelzpunkte und Molekulargewichtsbestimmungen, sowie durch IR-Spektroskopie identifiziert. Die IR-Spektren wurden mit KBr-Pastillen auf dem Perkin-Elmer Spektrograph Typ 237 aufgenommen.

Tabelle I

Verbindung	Verfahren	Schmelzpunkt °C	Ausbeute %	>C=O cm^{-1}	Analyse					
					berechnet %			gefunden %		
					C	H	N	C	H	N
5,6-Dimethylthieno(2,3-d)-4(3H)-pyrimidinon (P) [5, 6]	a	273—4	95,1	1670	53,33	4,44	15,55	53,08	4,29	15,34
3-Methyl-P	a	144—6	84,9	1671	55,56	5,15	14,43	55,90	5,26	14,69
3-Butyl-P	b	141—2	92,3	1665	61,01	6,78	11,86	59,71	6,85	11,70
3-Benzyl-P	b	133—4	96,1	1670	66,66	5,18	10,36	66,30	5,31	10,12
3-p-Toluyl-P	c	200—2	77,1	1689	66,66	5,18	10,36	55,32	5,31	10,52
3-Amino-P	d	181—2	92,1	1672	49,23	4,61	21,53	49,29	4,65	21,60
Äthylen-bis-3,3'-P	e	321—3	93,6	1671	57,97	5,31	13,52	57,53	5,46	13,34
Hexylen-bis-3,3'-P	e	218—9	94,0	1683	59,72	5,88	12,67	59,81	5,70	12,46

Experimenteller Teil

1) (I) Dimethylformamidchlorid [1]
2) (II) 2-Amino-3-carbäthoxy-4,5-dimethylthiophen [9]
3) (III) N,N-Dimethyl-N'-[(3-carbäthoxy-4,5-dimethyl)-2-thienyl]-formamidinhydrochlorid

13 g (0,1015 Mol) Dimethylformamidchlorid werden in 150 ml abs. Chloroform gelöst. Eine Lösung von 19,9 g (0,1 Mol) 2-Amino-3-carbäthoxy-4,5-dimethylthiophen in Chloroform wird langsam zugegeben, wobei die Temperatur nicht über 40 °C steigen soll. Die Lösung wird auf dem Wasserbad eingedampft. Das Produkt wird getrocknet. Bleibt das Produkt in Form eines öligen Rückstandes zurück, so wird es mit wenig Dioxan verrieben und die abgeschiedenen Kristalle werden filtriert und getrocknet.

26,6 g (94,7%). Schmelzpunkt: 147—150 °C.

4) (IVa) 5,6-Dimethylthieno(2,3-d)-4(3H)-pyrimidinon (a)

29,05 g (0,1 Mol) N,N-Dimethyl-N'-[(3-carbäthoxy-4,5-dimethyl)-2-thienyl]-formamidinhydrochlorid werden in 100 ml Äthylalkohol gelöst und die Lösung wird mit Ammoniak gesättigt. Nach 6stündigem Stehen wird die Lösung am Wasserbad eingedampft, der Rückstand mit wenig Wasser und Alkohol gewaschen und getrocknet.

17,1 g (95,1%). Schmelzpunkt: 273—274 °C.

5) (IVb) 3-Butyl-5,6-dimethylthieno(2,3-d)-4(3H)-pyrimidinon (b)

29,05 g (0,1 Mol) N,N-Dimethyl-N'-[(3-carbäthoxy-4,5-dimethyl)-2-thienyl]-formamidinhydrochlorid werden in 100 ml Äthylalkohol gelöst. 7,31 g (0,1 Mol) Butylamin werden zugefügt. Die Lösung wird 1 Stunde lang im Sieden gehalten und anschließend eingedampft. Der kristalline Rückstand wird mit wenig Wasser und Alkohol gewaschen und getrocknet.

21,8 g (92,3%). Schmelzpunkt: 141—142 °C.

6) (IVc) 3-p-Toluyl-5,6-dimethylthieno(2,3-d)-4(3H)-pyrimidinon (c)

29,05 g (0,1 Mol) N,N-Dimethyl-N'-[(3-carbäthoxy-4,5-dimethyl)-2-thienyl]-formamidinhydrochlorid werden in 100 ml Äthylalkohol gelöst. 10,7 g (0,1 Mol) *p*-Toluidin werden zugegeben. Die Lösung wird 3 Stunden lang im Sieden gehalten, anschließend abgekühlt und mit

der doppelten Menge Wasser versetzt. Der abgeschiedene Niederschlag wird filtriert, mit Wasser und wenig Alkohol gewaschen und getrocknet.

20,8 g (77,1%). Schmelzpunkt: 200—202 °C.

7) (IVd) 3-Amino-5,6-dimethylthieno(2,3-d)-4(3H)-pyrimidinon (d)

29,05 g (0,1 Mol) N,N-Dimethyl-N'-[(3-carbäthoxy-4,5-dimethyl)-2-thienyl]-formamidinhydrochlorid werden in 100 ml Äthylalkohol gelöst. 3,2 g (0,1 Mol) Hydrazinhydrat werden zugegeben. Nach 24stündigem Stehen wird der abgeschiedene Niederschlag filtriert, mit wenig Wasser und Alkohol gewaschen und getrocknet.

17,9 g (92,1%). Schmelzpunkt: 181—182 °C.

8) (V) Hexylen-bis-3,3'- 5,6-dimethylthieno(2,3-d)-4(3H)-pyrimidinon (e)

29,05 g (0,1 Mol) N,N-Dimethyl-N'-[(3-carbäthoxy-4,5-dimethyl)-2-thienyl]-formamidinhydrochlorid werden in 100 ml Äthylalkohol gelöst. 5,53 g (0,05 Mol) Hexamethylendiamin werden zugegeben. Die Lösung wird 1 Stunde lang im Sieden gehalten und anschließend abgekühlt. Der abgeschiedene Niederschlag wird filtriert, mit wenig Wasser und Alkohol gewaschen und getrocknet.

20,8 g (94,2%). Schmelzpunkt: 218—219 °C.

LITERATUR

1. Csűrös, Z., Soós, R., Pálinkás, J., Bitter, I.: Acta Chim. Acad. Sci. Hung. **63,** 215 (1970)
2. Baker, B. R., Joseph, J. P., Schaub, R. E., McEvoy, F. J., Williams, J. H.: J. Org. Chem. **18,** 138 (1953)
3. Schwedow, W. J., Ryzhkowa, V. K., Grinew, A. N.: Isobret. Prom. Obrastsy, Towarnye Snaki, **43,** (5) 24 (1966)
4. Robba, H., Lecomte, J. M.: Compt. Rend. **C 264,** 207 (1967)
5. Ried, W., Giesse, R.: Liebigs Ann. Chem. **713,** 143 (1968)
6. Ried, W., Giesse, R.: Angew. Chem. **80,** 122 (1968)
7. Robba, M., Lecomte, J. M., Cugnon de Sevricourt, M.: Compt. Rend. **C 266** (2) 128 (1968)
8. Robba, M., Lecomte, J. M., Legven, Y.: Compt. Rend. **C 266,** (25) 1706(1968)
9. Gewald, K., Schinke, E., Böttcher, H.: Ber. **99,** 94 (1966)

Zoltán Csűrös
Rudolf Soós
János Pálinkás
István Bitter

Budapest XI., Műegyetem-rakpart 3.

Acta Chimica Academiae Scientiarum Hungaricae, Tomus 68 (4), pp. 403—410 (1971)

BENZAZEPINES, IV*

SYNTHESIS OF DIHYDRO-[1,5]BENZOTHIAZEPINES BY THE REACTION OF *o*-AMINOBENZENETHIOL WITH α,β-UNSATURATED KETONES

O. HIDEG-HANKOVSZKY and K. HIDEG

(Pharmacological Institute of the University Medical School, Pécs)

Received January 23, 1970

The synthesis of disubstituted dihydro-[1,5]benzothiazepines by the reaction of *o*-aminobenzenethiol with the appropriate α,β-unsaturated ketones (*e.g.* pyridylacrylophenones, pyridylacrylonaphthones and 2-heteroarylidenetetralin-1-ones) is reported. The position of the double bond is also discussed.

The first synthesis of dihydro-[1,5]benzothiazepines by the reaction of *o*-aminobenzenethiols with some α,β-unsaturated ketones was reported by MUSHKALO [1], RIED and MARX [2] and STEPHENS and FIELD [3].

Our investigations in the benzothiazepine series have been extended to include other α,β-unsaturated compounds, such as β-methyl-vinyl-pyridyl ketones, heterocyclic acrylophenones, pyridylacrylonaphthones and 2-arylidenetetralin-1-ones (**IV**). The unsaturated ketone compounds are partly unknown, but they have been synthesized in our experiments according to the usual routes for chalcones, *e.g.* by condensation of an aldehyde with the appropriate ketone; the catalyst employed was alkali hydroxide in aqueous ethanol.

The ketone compound (**II**) is allowed to react with an equimolar amount of *o*-aminobenzenethiol (**I**). The first step is a nucleophilic attack by the sulfhydryl group on the β-carbon atom of the double bond, followed by condensation of the carbonyl group with the aromatic primary amine to give a seven-membered ring system.

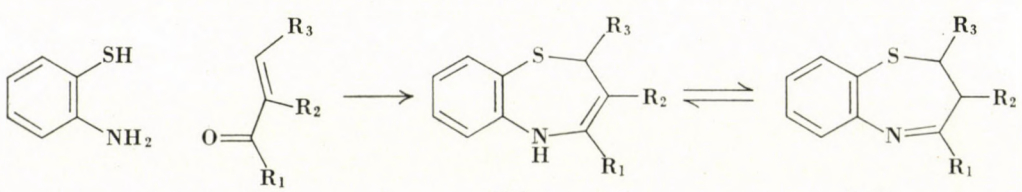

I **II** **III/a** **III/b**

In the formed dihydro-compound the double bond can be a C=C (**III/a**) or C=N (**III/b**) bond, depending on the electron-withdrawing effect of the substituents present. When R_1=CH_3 and R_2=*p*-methoxyphenyl, the double

* Part III: K. HIDEG, H. O. HANKOVSZKY, Acta Chim. Acad. Sci. Hung. **57**, 213 (1968).

bond is Δ^3 and NH stretching can be observed at 3320 cm^{-1}, while C=N stretching cannot be detected. The double bond preferably assumes a position in conjugation with the aromatic ring. The other compounds have the structure **III/b** (2,3-dihydro-2,4-disubstituted[1,5]benzodiazepines) supported by the presence of the C=N stretching (1650 cm^{-1}) and absence of the NH stretching frequencies in their IR spectra.

If the ketonic component is a 2-arylidenetetralin-1-one (**IV**), the compound produced has a new ring system (12-aryl-10,11,12,12a-tetrahydronaphtho[1',2'-e]benzo[b][1,4]thiazepine (**V**):

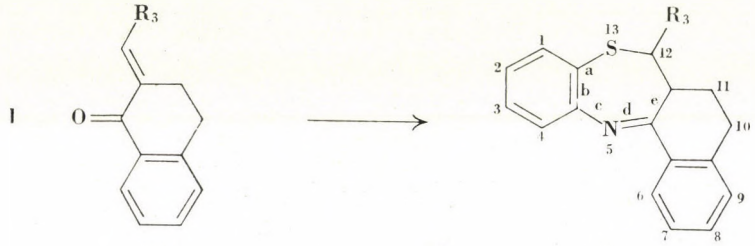

IV **V**

The dihydrothiazepines (**III**) can be reduced with complex metal hydrides to the tetrahydro derivatives (**VI**).

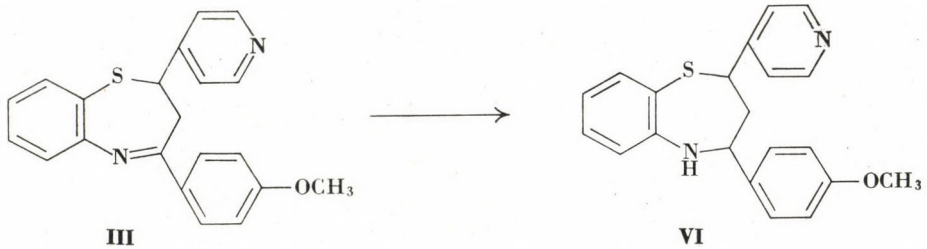

III **VI**

The hydrochlorides and alkylpyridinium salts of **III** and **VI** have also been prepared.

The compounds prepared are listed in Table I.

Experimental

All m.p.'s were determined on a Boetius Melting Point Apparatus and are uncorrected. The IR spectra were obtained with a Beckman Model IR-4 spectrophotometer

The α,β-unsaturated ketones were synthesized by the reactions of ketones with aldehydes in the presence of alkali.

2,3-Dihydro-2-(4-pyridyl)-4-(4-methoxyphenyl)-[1,5]benzothiazepine (No. 8)

A solution of 23.9 g (0.1 mole) of 4-methoxy-β-(4-pyridyl)acrylophenone and 12.5 g (0.1 mole) of *o*-aminobenzenethiol in 100 ml of xylene was refluxed in an apparatus equipped with a water separator adapter for 3 hrs.; during this time 1.8 ml (0.1 mole) of water was collected.

On cooling, a yellow solid (31.8 g; 92%) precipitated. A sample was recrystallized from xylene to give a bright yellow substance, m.p. 43—44 °C; the IR spectrum did not reveal any NH stretching at 3350—3000 cm^{-1}, but C=N at 1650 cm^{-1} (m) was observable.

Dihydrochloride

The base was dissolved in ethanol–acetone and acidified with ethanolic hydrochloric acid (1 : 1) to pH 5; the yellow dihydrochloride precipitated. A sample was recrystallized for analysis to give m.p. 135—136 °C.

Monomethiodide (No. 9)

A solution of 0.01 mole of the base in acetone was mixed with 3 ml of methyl iodide and refluxed for 3 hrs. The precipitated solid was filtered off and dried (3.5 g; 70%). The recrystallized sample had m.p. 118—120 °C.

Reduction

Reduction of No. 8 to 2,3,4,5-Tetrahydro-2-(4-pyridyl)-4-(4-methoxyphenyl)-[1,5]-benzothiazepine dihydrochloride

(a) With $NaBH_4$

3.5 g (0.01 mole) of No. 8 was dissolved in 100 ml of abs. ethanol, 5 g of $NaBH_4$ suspended in 50 ml of abs. ethanol was added in small portions, and the mixture was refluxed for 10 hrs. The complex was decomposed by water, the alcohol removed in vacuum and the oily residue extracted with chloroform (3×100 ml). The chloroform solution was dried over anhydrous Na_2SO_4 and the solvent evaporated.

The solid was recrystallized from aqueous ethanol to give a bright yellow substance (3.0 g; 85%), m.p. 214—216 °C; IR analysis: 3225 cm^{-1} (m) (NH).

$C_{21}H_{20}N_2OS$ (348.47). Calcd. C 72.38; H 5.79; N 8.04; S 9.20. Found C 72.84; H 5.54; N 8.00; S 9.09%.

Dihydrochloride

A solution of the base in 100 ml of acetone was acidified with alcoholic hydrochloric acid, when a yellow solid precipitated. A sample recrystallized for analysis had m.p. 143—145 °C.

$C_{21}H_{20}N_2OS \cdot 2HCl$ (421.39). Calcd. C 59.85; H 5.26; N 6.65; S 7.61; Cl 16.83. Found C 59.26; H 4.85; N 7.08; S 7.40; Cl 16.77%.

(b) With $LiAlH_4$

To a solution of 0.01 mole of No. 8 in 100 ml of abs. ether there was added 3 g of $LiAlH_4$ suspended in 100 ml abs. ether, and the mixture was refluxed for 3 hrs. After decomposition of the complex in the usual manner, the etheral layer was separated, and dried over anhydrous Na_2SO_4. The ether was evaporated and the residual solid dissolved in acetone, acidified, and worked up as before. The product had m.p. 143—146 °C.

12-(2,4-dichlorophenyl)-11,12,12a-tetrahydronaphtho-[1',2'-e]benzo[b][1,4]thiazepine (No. 18)

2-(2,4-dichlorobenzylidene)-tetralin-1-one (30.3 g; 0.1 mole) and 12.5 g (0.1 mole) of *o*-aminobenzenethiol were refluxed in 100 ml of xylene for 4 hrs. The solution was cooled and the precipitated solid filtered off (26.5 g; 65%), m.p. 148—152 °C. The recrystallized sample melted at 151—152 °C.

Table I

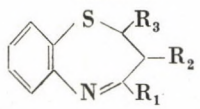

No.	R_1	R_2	R_3	B.p., °C/mm or M.p., °C	Formula (Molecular weight)	Analysis, %					
						C	H	N	Hlg	S	CH_3
						Calcd./Found					
1.	$-CH_3$	H	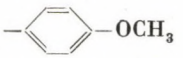	202—210/0.3	$C_{17}H_{17}NOS$ (283.39)	72.05 71.98	6.05 6.18	4.94 4.93	—	11.32 11.28	10.95 10.84
				153—154	$C_{17}H_{17}NOS \cdot HCl$ (319.85)	63.84 63.58	5.67 5.77	4.38 4.79	11.08 11 15	10.03 10.03	9.70 9.45
2.		H		124—125	$C_{20}H_{16}N_2S$ (316.43)	75 92 75.78	5.10 4.93	8.85 8.58	—	10.13 9.91	—
				149—150	$C_{20}H_{16}N_2S \cdot 2HCl$ (389.35)	61.70 61.80	4.66 4.73	7.19 7.13	18.21 18.27	8.23 8.53	—
3.		H		55— 57	$C_{20}H_{14}Cl_2N_2S$ (385.31)	62.34 62.13	3.67 3.59	7.27 7.40	18.40 18.20	8.32 8.25	—
4.	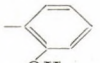	H	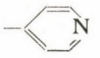	140—141	$C_{20}H_{16}N_2OS$ (332.43)	72.26 72.02	4.85 4.62	8.43 8.53	—	9.65 9.76	—
				143—144	$C_{20}H_{16}N_2OS \cdot 2HCl$ (405.35)	59.26 59.09	4.47 4.48	6.91 6.91	17.50 17.47	7.91 7.81	—
5.	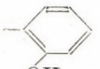	H	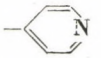	195—196	$C_{21}H_{19}IN_2OS$ (474.36)	53.18 53.39	4.04 4.08	5.90 5.73	26.75 26.22	6.76 7.05	—

6.	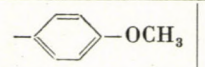	H		121—122	$C_{21}H_{18}N_2OS \cdot 2HCl$ (419.37)	60.15 59.99	4.81 4.66	6.68 7.02	16.91 16.55	7.64 7.42	7.40 7.60
7.	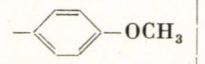	H	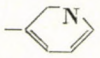	138—140	$C_{21}H_{18}N_2OS \cdot 2HCl$ (419.37)	60.15 59.94	4.81 5.06	6.68 6.86	16.91 16.52	7.64 7.66	7.40 7.48
8.	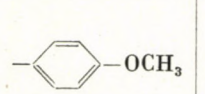	H	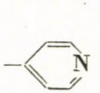	43— 44 135—136	$C_{21}H_{18}N_2OS$ (346.45) $C_{21}H_{18}N_2OS \cdot 2HCl$ (419.37)	72.81 72.60 60.15 59.85	5.24 4.92 4.81 4.73	8.09 7.80 6.68 6.42	— 16.91 16.79	9.25 9.32 7.64 7.55	8.96 9.12 7.40 8.00
9.	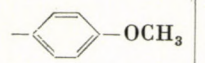	H	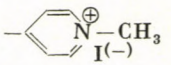	118—120	$C_{22}H_{21}IN_2OS$ (488.39)	54.10 54.15	4.33 4.30	5.73 6.42	25.99 26.10	6.57 6.72	6.35 6.75
10.		H	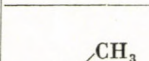	113—114 145—147	$C_{22}H_{20}N_2OS$ (360.48) $C_{22}H_{20}N_2OS \cdot 2HCl$ (433.40)	73.31 73.12 60.97 60.81	5.59 5.43 5.12 5.29	7.77 7.69 6.46 6.79	— 16.36 16.58	8.89 9.05 7.40 7.40	8.61 8.61 7.16 6.98
11.	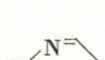	H	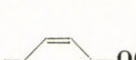	33— 34 118—119	$C_{21}H_{18}N_2O$ (346.45) $C_{21}H_{18}N_2O \cdot 2HCl$ (419.37)	72.81 73.22 60.15 60.08	5.24 5.44 4.81 4.71	8.09 7.91 6.68 6.94	— 16.91 16.80	9.25 9.03 7.64 7.55	8.96 9.12 7.40 7.80
12.	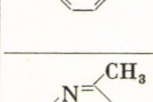	H	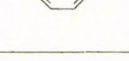	112—113	$C_{22}H_{20}N_2OS \cdot HCl$ (396.94)	66.57 66.78	5.33 5.12	7.05 6.92	8.93 9.07	8.07 7.97	7.82 7.54
13.	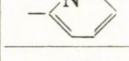	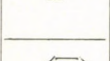	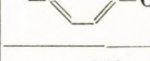	186—187	$C_{29}H_{23}NS$ (417.57)	83.42 83.67	5.55 5.73	3.35 3.43	—	7.68 7.50	—
14.	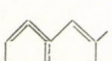	H	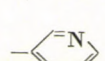	47— 49 133—135	$C_{24}H_{18}N_2S$ (366.48) $C_{24}H_{18}N_2S \cdot 2HCl$ (439.41)	78.66 78.85 65.60 65.26	4.95 5.13 4.59 4.69	7.64 7.48 6.37 6.45	— — 16.14 16.12	8.75 8.60 7.30 7.08	— —

Table I (continued)

No.	R_1	R_2	R_3	B.p., °C/mm or M.p., °C	Formula (Molecular weight)	Analysis, %					
						C	H	N	Hlg	S	CH_3
						Calcd./Found					
15.		H	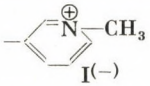	204—205	$C_{25}H_{21}IN_2S$ (508.43)	59.06 59.15	4.16 4.08	5.51 5.59	24.96 24.83	6.30 6.49	—
16.		H	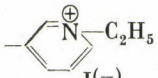	180—181	$C_{26}H_{23}IN_2S$ (522.45)	59.77 59.69	4.44 4.58	5.36 5.16	24.29 24.64	6.14 6.39	—
17.	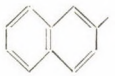	H		46— 57	$C_{24}H_{18}N_2S$ (366.48)	78.66 78.71	4.95 4.76	7.64 7.90	—	8.75 8.72	—
			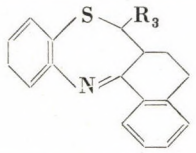								
18.			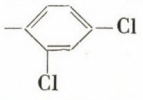	151—152	$C_{23}H_{17}Cl_2NS$ (410.37)	67.32 66.82	4.18 4.38	3.41 3.17	17.28 17.35	7.81 8.04	—
19.			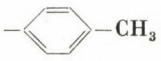	184—186	$C_{23}H_{21}NS$ (343.49)	80.43 80.24	6.16 6.31	4.08 4.14	—	9.33 9.65	—

20.		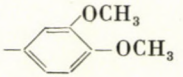	187—188	$C_{25}H_{23}NO_{22}S$ (401.54)	74.74 74.56	5.77 5.22	3.49 3·36	—	7.98 8.21	15.46 15.39
21.			173—174	$C_{21}H_{17}NS_2$ (347.50)	72.59 72.64	4.93 4.62	4.03 4.04	—	18.45 18.38	—
22.		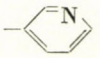	171—173	$C_{22}H_{18}N_2S \cdot 2HCl$ (415.39)	63.61 63.78	4.85 4.55	6.75 6.70	17.07 16.99	7.72 7.52	—
23.		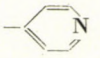	128—129	$C_{22}H_{18}N_2S \cdot 2HCl$ (415.39)	63.61 63.38	4.85 5.07	6.75 6.72	17.07 16.78	7.78 8.02	—
24.	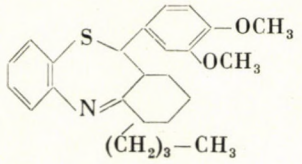		95— 96	$C_{25}H_{31}NO_2S$ (409.60)	73.31 73.10	7.63 7.91	3.42 3.64	—	7.83 7.62	15.15 15.19

We thank Mrs. M. Ott, Mrs. A. Halász and Miss T. Huszár for the analyses and for the synthesis of some intermediates.

REFERENCES

1. Mushkalo, L. K.: Zh. Obshch. Khim. **28,** 507 (1958)
2. Ried, W., Marx, W.: Chem. Ber. **90,** 2683 (1957)
3. Stephens, W. D., Field, L.: J. Org. Chem. **24,** 1576 (1959)

Olga Hideg-Hankovszky
Kálmán Hideg
Pécs, Szigeti út 30, Hungary.

Acta Chimica Academiae Scientiarum Hungaricae, Tomus 68 (4), pp. 411—419 (1971)

INVESTIGATION OF THE RHEOLOGICAL PROPERTIES OF GLUTEN, III

THE ROLE OF HYDROPHOBIC BONDS IN THE RHEOLOGICAL PROPERTIES OF GLUTEN

R. LÁSZTITY

(Department of Food Chemistry, Technical University, Budapest)

Received January 23, 1970

Although no suitable methods are available for the direct experimental detection of hydrophobic bonds present in the gluten complex, numerous indirect observations point to the importance of hydrophobic bonds in determining the rheological properties. The most important findings are:

1. The rheological properties of glutens hydrated with water containing higher aliphatic hydrocarbons (heptane to undecane), exhibit a significant deterioration as compared to the control gluten. This effect increases with increasing chain length.

2 The cohesivity of glutens, hydrated with water containing higher aliphatic fatty acids or alcohols decreases strongly with increasing molecular weight of the alcohol or fatty acid added.

3. The simultaneous presence of urea and aliphatic hydrocarbons hinders gluten formation to a higher degree than urea alone.

It has been pointed out in earlier communications [1, 2] that bonds between the fractions forming the gluten complex and their interactions play an important role in determining the rheological properties of gluten.

While great attention has been paid in wheat protein research to disulfide bonds, and a few attempts have been made at clarifying the role of hydrogen bonds, practically no studies were undertaken in connection with the hydrophobic bonds.

Only during the recent decade did protein chemists begin to investigate the importance of hydrophobic bonds (interaction of the non-polar groups of proteins in aqueous medium). Several theoretical problems relevant to this theme have been solved, as evidenced by the review by SCHERAGA [3]. It has been proved or assumed for several proteins that hydrophobic bonds play an important role in determining the structure (ribonuclease, β-lactoglobulin, etc.).

Gluten proteins contain several amino acids which possess hydrophobic side chains (alanine, leucine, phenylalanine, isoleucine, valine, proline). Moreover, taking into consideration that the hydrophobic parts of longer polar side chains (*e.g.* in the case of lysine and glutamic acid) may also interact, there can be no doubt about the potential possibility of the formation of hydrophobic bonds.

Dough and gluten formation proceed in aqueous media. Owing to the fact that an interaction of the non-polar groups with water is 'unfavourable'

from the thermodynamic viewpoint, the thermodynamic tendency points towards a linkage of the non-polar groups with each other (with a consequent weakening of the interaction between these groups and water). This problem is dealt with in the review by KAUZMAN [4]. In general, the formation of hydrophobic bonds is an endothermic process, *i.e.* the change in thermodynamic potential is negative since the effect of the change in entropy ($T\Delta S$) exceeds that of the change in enthalpy (ΔH). Up to a certain temperature limit, the strength of hydrophobic bonds increases with increasing temperature, so that hydrophobic bonds are of particular importance from the viewpoint of thermal stability of proteins.

The solubility of gliadin in non-polar solvents, and the influence of the latter on solubility are also indicative of the possible importance of the role of hydrophobic bonds. All this shows convincingly that a study of the hydrophobic bonds is unavoidably necessary for the understanding of factors which influence the structure and rheological properties of gluten proteins.

Up to now wheat protein research paid little attention to this problem. Only the observation might perhaps be mentioned that the rheological properties of doughs are changed already by small quantities of certain aliphatic hydrocarbons [5—8].

In earlier studies [9] concerned with the effect of certain hydrocarbons on the formation and rheological properties of dough, we found an increase in the development time and stability of the dough, while its extensibility became slightly poorer. Owing to the complexity of the system, no unequivocal conclusions could be drawn. It was presumed, however, that there is a relationship between the effect of hydrocarbons and the hydrophobic bonds of the protein skeleton of gluten.

Though several papers discussing the theoretical aspects of hydrophobic bonding appeared in recent years, the comparison with experimental data, the verification by measurements, *i.e.* experimental techniques are at the initial stage, and are restricted primarily to model substances [10, 11, 12, 13].

In a recent work, GRATZER and DOTY [11] report the extremely high stability of the L-polyalanine helix in aqueous media. This high stability is explained by BIXON *et al.* [14], among others, by the stabilizing effect of hydrophobic bonds. Other authors [15—17] attribute importance to hydrophobic bonds in determining the stability of glutamic acid–leucine polypeptides. From the experimental point of view, research [18, 19], aimed at studying the bonding of various organic compounds to proteins and their interaction with proteins is of interest.

Indirect methods have been used primarily also in the present work. The effect of compounds has been studied, which are able to interact with the hydrophobic groups of the gluten complex, and through these groups can

interact with the existing hydrophobic bonds. Moreover, the relationship between the amount of amino acids with hydrophobic side chains and the rheological properties of the gluten complex has been studied.

Materials and methods

148 flour samples were used for the investigations. These samples were made by laboratory milling of wheat species or milling mixtures produced in the period from 1963 to 1968. The samples were selected so as to give an overall characterization of Hungarian wheats and flours from the viewpoint of baking quality, species and place of cultivation.

Gluten was prepared as described in earlier publications [20, 2]. Similarly, the relaxation of wet gluten was measured in the same way as described earlier [20]. Relaxation time and relaxation constant, too, were calculated by this method.

The amino acid composition was determined after performic acid oxidation and hydrolysis with hydrochloric acid, by paper chromatography, using the butanol process [21, 22].

Results and discussion

1. *Relationship between the amount of amino acids with hydrophobic side-chains and the rheological properties of gluten*

In research work carried out up to the present, the amount of proline and other amino acids with hydrophobic side-chains has been scarcely studied in connection with the rheological properties of gluten. However, in consideration of the fact that the total quantity of these amino acids may amount to more than 30 per cent of the gluten proteins, their importance in the development of gluten structure and gluten properties is indubitable.

A mathematical-statistical evaluation was made from data available on the amino acid composition and the rheological characteristics of gluten. On the basis of this evaluation, it has been established that the strictest correlation between amino acid composition and rheological properties will be obtained if the total amount of proline, leucine and isoleucine is considered. The numerical data are given by the following equations and correlation coefficients:

$$t_r = 75.74 - 0.194\ H - 0.044\ H^2 \text{ and}$$

$$K = 89.37 - 0.267\ H - 0.053\ H^2$$

$$r_{t_r} = 0.501 \text{ and } r_K = 0.482$$

where

$H = 10\ h - 228$,

t_r is the relaxation time (sec),

K is the relaxation constant (g),

h is the proline + leucine + isoleucine content (in per cent).

The relationship found can be represented by a second order curve with a maximum (*cf.* Figs 1 and 2). The correlation is not very strict, but nevertheless, it is definitely significant even at a reliability level of 1 per cent.

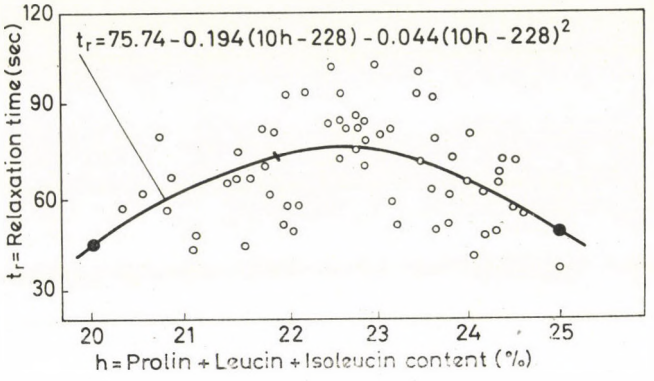

Fig. 1

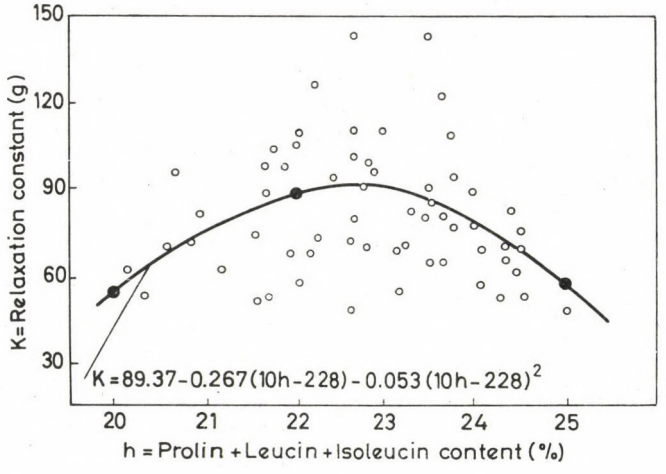

Fig. 2

As concerns the explanation of the relationship, primarily the role of the hydrophobic bonds must be considered, which may be partly intramolecular, and partly intermolecular. It is reasonable to assume that such bonds participate in the formation of those parts of the gluten structure which, after the hydratation of gluten practically do not remain hydrated, do not participate in the swelling, and ensure that swelling remains limited, and no peptization occurs.

The negative effect after a given optimum quantity is due most probably to the following reasons. At a too high proportion of amino acids with hydro-

phobic side-chains, the amount of the other amino acids decreases, and together with this, the number of those primary or secondary bonds which are also of importance from the viewpoint of the rheological properties of gluten. Indeed, this explanation is supported by results obtained for the rheological properties of glutens modified chemically [2].

2. *Effect of hydrocarbons on the rheological properties of gluten*

These tests were carried out as follows. Dehydrated gluten was contacted with water containing a known amount of hydrocarbons. After hydratation and swelling, the hydrated mass was worked mechanically, until a continuous, homogeneous substance was obtained. The excess solution was removed, and the relaxation test was performed as described earlier. The experimental results are shown in Table I.

The data in Table I show that the rheological properties of gluten are affected unfavourably by the presence of higher aliphatic hydrocarbons. When tested organoleptically, gluten becomes less stretchable and crumbly. In the case of pentane and hexane, an increase in the relaxation time and in the force necessary to cause a deformation of identical degree can be observed, particularly with glutens of poorer quality.

The pronounced changes which can be detected even at the relatively low concentrations used, definitely indicate an interaction between the hydrocarbons and the proteins of gluten. As concerns the character of this interaction, on the basis of thermodynamical considerations one can assume that a linkage is formed between the hydrocarbons and the hydrophobic side chains

Table I

Effect of hydrocarbons on the rheological properties of gluten

No.	Relaxation time (sec)					
	Control	Pentane	Hexane	Heptane	Octane	Undecane
	0.03 mole/100 g of gluten					
1	102	106	101	94	82	65
2	95	95	96	82	76	72
3	88	91	82	71	66	50
4	73	72	70	72	68	53
5	69	65	63	58	55	48
6	62	65	60	55	54	45
7	58	60	62	59	51	45
8	53	48	49	44	40	37
9	43	44	40	38	37	35
10	38	45	40	38	40	41

of proteins. In the case of pentane and hexane, a weaker bond is formed, extending or rather protecting those hydrophobic nuclei which in the course of hydratation, osmotic water uptake and swelling, and peptization prevent the aggregates from unlimited swelling and disintegration. When higher hydrocarbons are added, the interaction may become stronger due to the higher affinity, so that existing interactions between side chains may cease, *i.e.* existing hydrophobic bonds may be ruptured, and replaced by bonds between the added hydrocarbon and the side chains. This situation is analogous to that assumed for the rupture of the hydrogen bonds by urea. The two analogous processes are illustrated by the following scheme:

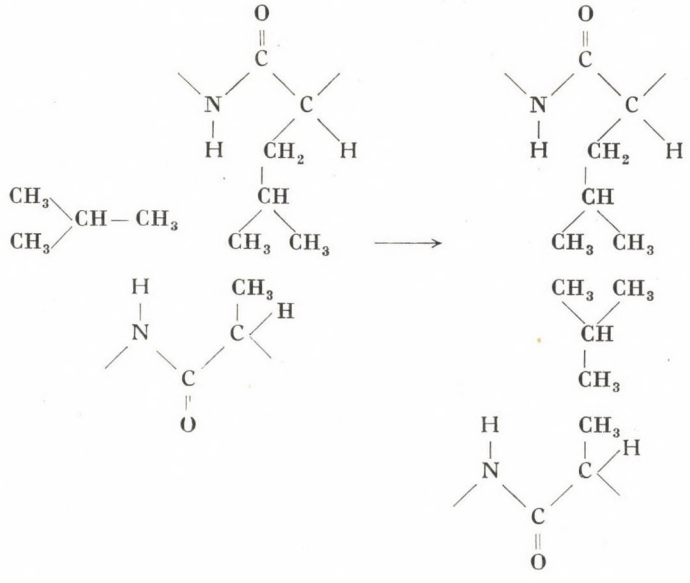

3. *Effect of fatty acids on the rheological properties of gluten*

The procedure was the same as in the preceding series of experiments with the difference that part of the fatty acids was present in the aqueous medium as an emulsion.

The rheological properties of the glutens under these conditions are summarized in Table II.

The data in the table show an interesting pattern. The changes in rheological properties are different depending on the acid and the gluten. In the case of formic and acetic acid, the peptizing effect predominates, which brings about rapid deterioration of the rheological properties. With acids of increasing carbon atom number, up to and including valeric acid, an increase in relaxation time can be observed, while palmitic and stearic acid already cause a slight deterioration of rheological properties.

For the explanation of the observed changes it is assumed that, similarly to pentane and hexane, fatty acids with 3—5 carbon atoms, bring about hydrophobization. On the other hand, the decreasing relaxation time observed with higher fatty acids indicates that the interaction of more strongly hydrophobic compounds with proteins may result in the rupture of existing hydrophobic bonds.

Table II

Effect of fatty acids on the rheological properties of gluten

No.	Relaxation time (sec)								
	Acid added: 0.01 molar solution (emulsion)								
	Control	Formic	Acetic	Propionic	Butyric	Valeric	Palmitic	Oleic	Stearic
1	102	39	40	56	72	85	80	b	75
2	95	47	30	50	68	80	82	b	71
3	88	39	28	52	59	69	79	b	80
4	73	48	a	41	48	53	63	b	65
5	69	41	a	44	50	60	62	b	58
6	62	42	a	48	47	50	52	b	47
7	58	29	a	32	39	40	52	b	49
8	52	a	a	30	30	42	48	b	41
9	43	a	a	27	30	40	42	46	30
10	38	a	a	25	28	32	32	57	28

a = not measurable (sticky, spreading mass)
b = not measurable (crumbling, disintegrating mass)

Unsaturated oleic acid does not fit at all into the series. Oleic acid causes a change similar in character to a very high degree of thermal denaturation. Presumably, this is caused by the interaction of oleic acid with a preferred side chain.

4. *Effect of aliphatic alcohols on the rheological properties of gluten*

In order to examine the effect of aliphatic alcohols, the process of gluten formation and the properties of the gluten formed were studied in 0.01 molar aqueous alcoholic medium (solution or emulsion). The rheological properties of the glutens are summarized in Table III.

The data listed in the table show that with the exception of methanol and ethanol which have a slight peptizing effect, the cohesivity of gluten diminishes and its rheological properties deteriorate with increasing number of carbon atoms in the alcohol. In view of the fact that solutions of identical molar con-

centration were used in each case, this effect on gluten may be ascribed to the increasing hydrophobic character of the side chain. The interaction of the hydrophobic side chain is believed to be similar to that assumed in the case of hydrocarbons or fatty acids.

Table III

Effect of aliphatic alcohols on the rheological properties of gluten

No.	Aliphatic alcohols (0.01 molar aqueous solution or emulsion)	Rheological properties of gluten	
		Penetration (in 0.1 mm)	Organoleptic characterization
1	Methanol	201	soft, inelastic, cohesive
2	Ethanol	190	soft, cohesive
3	Propanol-1	112	elastic
4	Butanol-1	103	tough, elastic
5	Pentanol-1	98	elastic
6	Hexanol-1	125	crumbling
7	Heptanol-1	179	crumbling
8	Octanol	211	crumbling

5. *Effect of hydrocarbons on the formation of gluten in the presence of urea*

In earlier works concerned with the role of hydrogen bonds, the effect of the addition of increasing amounts of urea on the rehydration of dry gluten and on gluten formation has been studied. These experiments were now repeated with the difference that various hydrocarbons were added to the urea solution (0.03 mole per 1 g of gluten). The experimental results show that under these conditions, the absence of gluten formation or a considerable decrease in the amount of gluten formed is observed already at a lower urea concentration. The results are plotted in Figs 3 and 4.

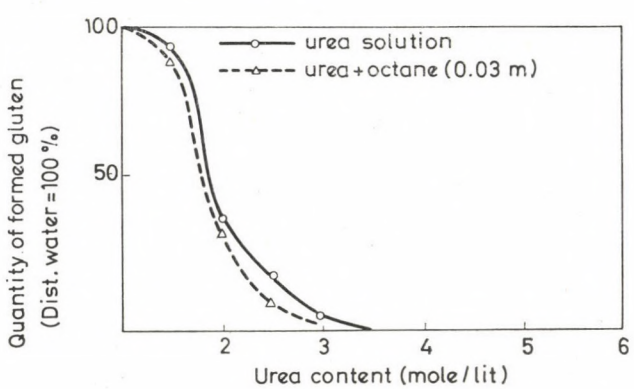

Fig. 3

The observed behaviour can be explained by assuming that the combined addition of urea and hydrocarbons hinders not only the formation of intermolecular hydrogen bonds but also the formation of the corresponding hydrophobic bonds as a result of the interaction between hydrocarbons and nonpolar protein side chains.

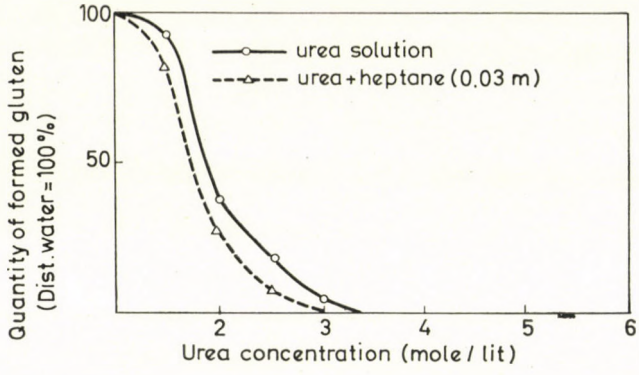

Fig. 4

REFERENCES

1. LÁSZTITY, R.: Die Nahrung **11,** 3 (1968)
2. LÁSZTITY, R.: Acta Chim. Acad. Sci. Hung. **62,** 75 (1969)
3. SCHERAGA, H. A.: "Noncovalent Bonds", in H. Neurath: The Proteins, Vol. I. 2nd Ed. Academic Press, New York, 1963
4. KAUZMAN, F.: Advances in Protein Chemistry **14,** 1 (1959)
5. MUELLER, H. G., HLYNKA, I., KUZMINA, F. D.: Cereal Chem. **41,** 303 (1965)
6. PONTE, J. C., TITCOMBE, S. T., COTTON, R. N.: Cereal Chem. **41,** 205 (1964)
7. PONTE, J. C., TITCOMBE, S. T., DE STEFANIS, V. A., COTTON, R. N.: Cereal Chem. **43,** 475 (1966)
8. PONTE, J. C., DE STEFANIS, V. A., TITCOMBE, S. T., COTTON, R. N.: Cereal Chem. **44,** 211 (1967)
9. LÁSZTITY R.: III. Internat. Kongr. Internationale Probleme der modernen Getreidechemie und Getreideverarbeitung. Bergholz-Rehbrücke, 1967
10. SCHERAGA, A. H., STEINBERG, I. Z.: J. Am. Chem. Soc. **84,** 2829 (1962)
11. GRATZER, W. E., DOTY, P.: J. Am. Chem. Soc. **85,** 1193 (1963)
12. WETTLAUFER, D. N.: Fed. Proc. **21,** 408 (1962)
13. SINGER, S. J.: Advances in Protein Chemistry **17,** 1 (1962)
14. BIXON, M., SCHERAGA, A. H., LIPSOM, S.: Biopolymers **12,** 28 (1963)
15. MILLER, W. G., NYLUND, B. E.: J. Am. Chem. Soc. **87,** 3542 (1965)
16. SMIPP, R. L., MILLER, W. G., NYLUND, B. E.: J. Am. Chem. Soc. **87,** 3547 (1965)
17. HANSCH, O., FUCHS, K., LAWRENCE, C. L.: J. Am. Chem. Soc. **87,** 5770 (1965)
18. IWASA, J., FUJITA, F., HANSCH, C.: J. Med. Chem. **8,** 150 (1965)
19. FUJITA, T., IWASA, J., HANSCH, C.: J. Am. Chem. Soc. **86,** 5175 (1965)
20. LÁSZTITY, R. Acta Chim. Acad. Sci. Hung. **53,** 169 (1967)
21. DÉVÉNYI, T., GERGELY, J.: Amino acids, peptides, proteins (in Hungarian). Budapest, 1963
22. LÁSZTITY, R. (Ed.): Laboratory practice in food chemistry (in Hungarian). Budapest.

Radomir LÁSZTITY; Budapest XI., Műegyetem rkp. 3.

Acta Chimica Academiae Scientiarum Hungaricae, Tomus 68 (4), pp. 421—424 (1971)

FLAVONOIDS, XXI*. INVESTIGATIONS ON SUBSTITUTED CHALCONE AZIRIDINES

PREPARATION OF N-SUBSTITUTED-3-AMINOFLAVANONES

(PRELIMINARY COMMUNICATION)

R. Bognár, Gy. Litkei and P. Szigeti

(Institute of Organic Chemistry, L. Kossuth University, Debrecen 10)

Received November 30, 1970

In a previous paper we have reported on the reactions of 2'-OR-chalcone epoxides (R = CH_2—C_6H_5; CH_2—C_6H_4—*p*—NO_2; CH_3) [1]. Our investigations have now been extended to studies on the preparation and conversions of some 2'-OR-chalcone aziridines (**II, III**) unknown so far.

The aziridines were prepared by allowing the substituted chalcones **Ia, Ib** and **Ic** to react with cyclohexylamine in the presence of iodine [2]; *cis*- and *trans*-1-cyclohexyl-2-(*p*-R'-phenyl)-3-(2'-OR-benzoyl)-ethyleneimine (**IIa, IIIa; IIb, IIIb** and **IIc, IIIc**) were then isolated from the reaction mixture by fractional crystallization. The aziridines **IIc, IIIc** were also prepared from the chalcone dibromide **IVc** with cyclohexylamine [3].

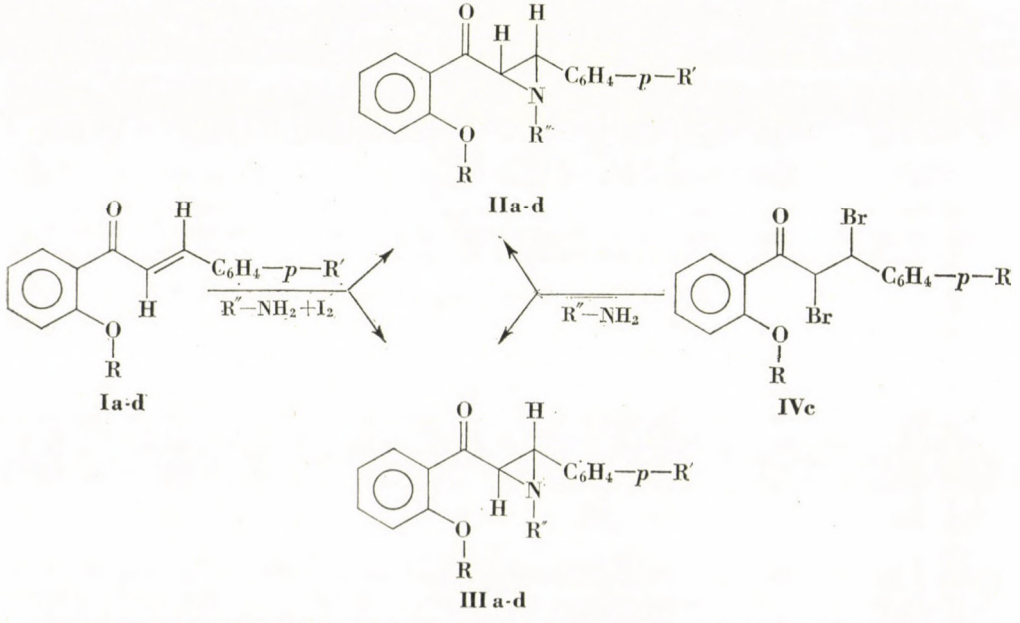

a: R = $CH_2C_6H_5$; R' = H; b: R = CH_2—O—CH_3; R' = H; c: R = $CH_2C_6H_5$; R' = Cl; d: R = $CH_2C_6H_5$; R' = NO_2

* Part XX: Acta Chim. Acad. Sci. Hung., in press.

The chalcone **Id** and benzylamine gave in the presence of iodine *cis*- and *trans*-1-benzyl-2-(*p*-nitrophenyl)-3-(2'-benzyloxybenzoyl)-ethyleneimine (**IId, IIId**).

The structures and stereochemistry of the aziridines obtained were determined by analysis, IR and UV spectroscopy [4]. Some data are given in Table I.

Table I

Aziridine derivatives

Yield, %	M.p., °C	Calcd.			Found			νCO [cm^{-1}]	λ_{max} mμ (log ε)
		C	H	N Cl	C	H	N Cl		
IIa 21	118—119				82.0	6.7	3.37	1688	252 (4.02); 311 (3.68)
		82.0	7.0	3.40					
IIIa 41.5	90— 92				81.9	6.7	3.38	1650	254 (4.13); 311 (3.78)
IIb 12.5	98— 99				75.9	7.4	3.61	1670	251 (3.96); 302 (3.55)
		75.9	7.4	3.84					
IIIb 34	100—102				75.9	7.3	3.84	1660	257 (4.15); 300 (3.72)
IIc 41.5	125 -127				75.8	6.2	3.14	1680	254 (3.69); 311 (3.40)
		75.5	6.3	3.14					
IIIc 38.5	120—122				75.5	6.1	3.18	1649	260 (3.96); 312 (3.58)
IId 21.5	125—126				75.1	5.3	5.97	1675	259 (4.14); 293 (4.10)
		75.0	5.1	6.05					
IIId 48	107—109				74.9	5.2	6.10	1658	266 (4.22); 289 (4.22)

The *cis*- or *trans*-aziridines were allowed to react with dry HCl in ether. Under similar conditions, the analogous *trans*-2'-OR-chalcone epoxides (R = $-CH_2-C_6H_5$; CH_2-O-CH_3) yield dihydroflavonol [1, 5], or the α-hydroxy-β-chloro derivatives (chlorohydrins); the aziridines give a mixture of the hydrochlorides of α-chloro-β-R''-amino- and α-R''-amino-β-chloro derivatives. In the course of these reactions, the formation of flavanone derivatives could not be detected.

Formation of *cis*- or *trans*-aziridines from 2'-acetoxy chalcone (**Ie**), or 2'-hydroxychalcone (**If**) with cyclohexylamine, in the presence of iodine, could not be observed, however, after treatment of the reaction mixture with dry HCl in ether, 3-cyclohexylaminoflavanone hydrochloride (**V**; R'' = C_6H_{11}) and 2-benzalcoumaranone (**IX**) were isolated from the reaction mixture by fractional crystallization.

The reactions of 2'-acetoxychalcone dibromide (**IVe**) with cyclohexylamine and subsequent treatment of the reaction mixture with HCl in ether gave the flavanone derivative (**V**; R'' = C_6H_{11}) in a yield of 15%.

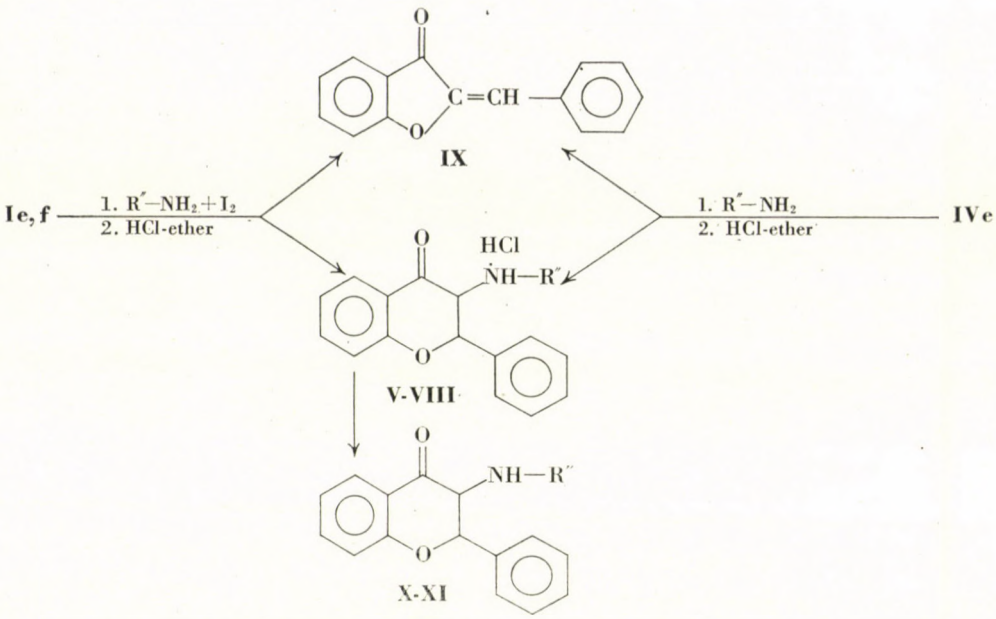

e: R = $COCH_3$; R' = H; f: R = R' = H; **V**: R" = C_6H_{11}; **VI**: R" = $CH_2C_6H_5$; **VII**: R" = *n*-C_4H_9; **VIII**: R" = i-C_4H_9; **X**: R" = C_6H_{11}; **XI**: R" = $CH_2C_6H_5$

Table II

3-R"-aminoflavanone derivatives

Yield., %	M.p., °C	Calcd. C	Calcd. H	Calcd. N Cl	Found C	Found H	Found N Cl	ν_{CO} [cm^{-1}]	λ_{max} mμ (log ε)
V 26.5	179—180	70.5	6.7	3.92 9.92	70.3	6.6	4.01 9.89	1705	252 (4.00) 326 (3.53)
VI 36.5	157—158	72.2	5.5	3.84 9.75	71.6	5.7	3.84 9.68	1699	220 (4.27) 256 (4.08) 326 (3.61)
VII 23	163—165	68.8	6.6	4.23 10.07	68.8	6.6	4.14 9.71	1700	252 (3.96) 326 (3.53)
VIII 27	171—173	68.8	6.6	4.24 10.07	68.7	6.8	4.20 9.99	1700	252 (3.96) 325 (3.56)
X 78	98—100	78.5	7.1	4.37	78.9	6.8	4.43	1693	217 (4.39) 253 (3.98) 325 (3.57)
XI 78	94— 96	80.5	5.8	4.26	80.4	5.8	4.22	1695	222 (4.23) 252 (3.96) 323 (3.53)

Under similar circumstances 2'-hydroxychalcone (**If**) and benzylamine, or *n*-butylamine, or isobutylamine yielded the flavanone derivatives (**VI**—**VIII**; R'' = $CH_2C_6H_5$; *n*-C_4H_9; *i*-C_4H_9).

When 3-cyclohexylamino- (**V**; R'' = C_6H_{11}) or 3-benzylaminoflavanone hydrochloride (**VI**; R'' = $CH_2C_6H_5$) were allowed to react with a calculated volume of alkali, the products were 3-cyclohexylamino- (**X**; R'' = C_6H_{11}) or 3-bezylaminoflavanone (**XI**; R'' = $CH_2C_6H_5$).

Some data of the prepared derivatives are given in Table II.

*

Our thanks are due to Mr. Z. DINYA, Mrs. É. D. RÁKOSI and Mr. S. SZABÓ for the analyses, and to Mrs. S. HAJNAL for her valuable technical assistance.

REFERENCES

1. BOGNÁR, R., STEFANOVSKY, J.: Tetrahedron **18,** 143 (1962); BOGNÁR, R., LITKEI, GY.: Magy. Kém. Foly. **68,** 269 (1962)
2. SOUTHWICK, P. L., CRISTMAN, D. R.: J. Am. Chem. Soc. **74,** 1886 (1952)
3. CROMWELL, N. H., BABSON, R. D., HARRIS, C. E.: J. Am. Chem. Soc. **65,** 312 (1943)
4. CROMWELL, N. H., BABURY, R. E., ADELFANG, J. L.: J. Am. Chem. Soc. **82,** 4241 (1960)
5. ENEBÄCK, C.: Soc. Sci. Fennica Comm. Phys.-Math. **28,** 1 (1963)

Rezső BOGNÁR
György LITKEI
Pál SZIGETI

Szerves Kémiai Intézet,
Debrecen 10, Hungary.

The chemistry of functional groups. Ed. by S. Patai. *The chemistry of the carbon–nitrogen double bond*, pp. 794 + xiii

Interscience Publishers, a division of John Wiley and Sons, London, 1970.

The new volume of the well-known series "The Chemistry of the Functional Groups" deals with the carbon–nitrogen double bond. As pointed out in the Preface of the series "The emphasis is laid on the functional group treated and on the effects which it exerts on the chemical and physical properties, primarily in the immediate vicinity of the group in question, and secondarily on the behaviour of the whole molecule."

The first, introductory chapter (written by C. SANDORFFY) deals with general and theoretical aspects of the azomethine group. The next chapter (Methods of formation of the carbon–nitrogen double bond, by SHLOMO DAYAGI and YAIR DEGANI) is devoted to the formation of the azomethine group, either from groups present in the molecule, or by introducing the new group directly or indirectly. The next three chapters (Analysis of azomethines, by D. J. CURRAN and S. SIGGIA; The optical rotatory dispersion and circular dichroism of azomethins, by R. BONNETT; Basic and complex-forming properties, by J. W. SMITH) describe the characterization and characteristics of the carbon–nitrogen double bond. Five chapters deal with the reactions, transformations and rearrangements which the azomethine group can undergo, either alone or in conjunction with other reagents (Additions to the azomethine group, by KAORU HARADA; Cycloaddition reactions of carbon–nitrogen double bonds, by Jean-Pierre ANSELME; Substitution reactions at the azomethine carbon and nitrogen atoms, by R. J. MORATH and G. W. STACY; *Syn-anti* isomerization and rearrangements, by C. G. MCCARTY; Cleavage of the carbon–nitrogen double bond, by A. BRUYLANTS and Mrs. E. FEYTMANTS DE MEDICIS.) The next two chapters are devoted to the electrochemistry (by H. LUND) and photochemistry (by G. WETTERMARK) of the carbon–nitrogen double bond. The last chapters describe the chemistry of imidoyl halides (by R. BONNETT) and quinonediimines (by K. T. FINLEY and L. K. J. TONG) containing carbon–nitrogen double bond too.

The authors of the present volume similarly to those of the former ones did not aspire "to give an encyclopedic coverage of their subject, but to concentrate on the most important recent developments and mainly on material that has not been adequately covered by reviews or other secondary sources by the time of writing of the chapter . . .".

This new volume of the series, as has been becoming customary, is excellently edited and, appearing in a tasteful presentation, will be of great value to readers interested in this field of organic chemistry.

GY. DEÁK

E. S. STERN and C. J. TIMMONS:

Gillam and Stern's Introduction to Electronic Absorption Spectroscopy in Organic Chemistry, pp. 277 + VI

Edward Arnold Ltd., London, 1970.

Almost a generation of organic chemists have obtained their first introduction to UV-visible spectroscopy from GILLAM and STERN's book. It is therefore an event that this classic is republished in a completely rewritten form. The organization of the book remains the same as in the second edition, but the subject matter has been brought up to date, spectra are presented on linear wavenumber scale and wavenumbers and wavelengths are both given in the Tables.

The book consists of the following chapters: I. Introduction; II. The determination and presentation of absorption spectra: III. General principles and simple examples of the assignments of bands; IV. The selective absorption of molecules containing one functional group; V. Conjugated chromophores; VI. Benzenoid absorption; VII. Aromatic heterocyclic compounds; VIII. Application of absorption spectrophotometry to qualitative analysis; IX. The spectrophotometric determination of organic compounds; X. Ultraviolet absorption spectroscopy applied to problems of molecular structure; three appendices: a short bibliography, the use of solvents, and some data of temperature effects. A Table of four place logarithms and of reciprocals and an Author and Subject Index complete the volume.

The book is written primarily for the organic chemist; although the results of quantum-mechanical calculations are referred to, quantum-mechanical theory is not needed to understand and use the book. Examples of elementary calculations and rules are generously used to give easier understanding to the less physico-chemically minded. The amount of information on the various groups of compounds is enormous in relation to the size of the book and the organization of the Tables and the short discussions on the subjects make the information usable even to beginners.

The reviewer finds it especially important that steric effects are discussed and the importance of scale projection diagrams and other aids are stressed.

The book will be an excellent companion for postgraduate students and for practising organic chemists who are trying to obtain additional information about their compounds or who want to use electronic absorption spectroscopy as an analytical tool.

M. VAJDA

INDEX

ERRATUM

Integrated Rate-Equations in Chemical Kinetics

P. J. Robinson, *Acta Chim.* **66,** 407 (1970)

The following typographical errors have occurred in Table I of the above paper:

(a) The first line should refer to $m \neq 1$, not $m = 1$.

(b) The third expression for f (for $m = n = 0.5$) should have $+$ not $-$ in the denominator.

(c) In the last expression for f (for $m = n = 1.5$) the second term in the square brackets should be $a\sqrt{[B]/[A]}$ not $a\sqrt{[A]/[B]}$.

ACTA CHIMICA

ТОМ 68 — ВЫП. 4.

РЕЗЮМЕ

Равновесия коплексов ионов переходных металлов с α-аминокислотами, IV

Константы стабильности, энтальпии и энтропии образования комплексов аланина, фенилаланина и тирозина

А. ГЕРГЕЙ, И. НАДЬПАЛ и Б. КИРАЙ

pH-Метрически определялись константы стабильности комплексов между ионами переходных металлов с электронной структурой $3d^5$–$3d^{10}$ и фенилаланином и тирозином при температурах 20, 25, 30 и 35°C. Было найдено, что в этих системах величина $10g\ K_1/K_2$ всегда ниже величины для соответствующих комплексов аланина.

Энтальпии образования комплексов между ионами переходных металлов с электронной структурой $3d^6$ — $3d^{10}$ и аланином, фенилаланином и тирозином определялись как на основе температурной зависимости констант стабильности, так и калориметрическим путем. Расхождение между величинами, полученными двумя различными методами, не превышает $\pm 0{,}2 \div 1{,}0$ ккал/моль.

Сумма ΔH_1 и ΔH_2 в случае комплексов Co(II), Ni(II) и Zn(II) с фенилаланином и тирозином обычно ниже тех самых величин для соответствующих комплексов аланина. Разность же величин ΔH_1 и ΔH_2 в некоторых случаях относительно выше для первых перечисленных систем, нежели для комплексов. Это гораздо значительнее проявляется в случае комплексов с тирозином, нежели в случае хелатных комплексов фенилаланина.

На основе экспериментальных данных было установлено, что стабильность комплексов ароматических аминокислот обусловлена также обратной координацией. В случае тирозина это явление проявляется гораздо сильнее.

Основным фактором, определяющим стабильность комплексов Cu(II) с ароматическими аминокислотами, является эффект Джана-Теллера.

Механизм адсорбционной индикации, VIII

Азо-красители как адсорбционные индикаторы. Влияние заместителей на механизм адсорбционной индикации

Л. ЛЕГРАДИ

Приводятся 46 азосоединений, которые могут быть использованы в качестве адсорбционных индикаторов. Большая часть соединений еще неизвестна в литературе. Приводятся ионы, в аргентометрическом титровании которых отдельные соединения могут быть использованы, приводятся условия применения, а также принципы, на которых основано действие индикаторов. Большинство азо-адсорбционных индикаторов действует по кислотно-основному принципу, кроме того по принципу поверхностной адсорбции на осадке, а также на основе обоих принципов. Подробно обсуждается роль заместителей индикаторов при использовании их в аргентометрическом титровании.

О некоторых вопросах разделения следов элементов осаждением, VIII

Сорбция редкоземельных металлов и скандия на гидроокиси железа(II) в карбонатных средах

Э. УПОР и ДЬ. НАДЬ

Изучалась сорбция редкоземельных металлов и скандия на гидроокиси железа в среде Na_2CO_3. Было установлено, что, вследствие гидролитического разложения карбонатных комплексов со сравнительно низкой стабильностью, при концентрации Na_2CO_3, равной 0,2 М сорбция легких лантанидов является полной и сорбция тяжелых лантанидов — почти полной. С увеличением концентрации Na_2CO_3, а также порядкового номера лантанидов их сорбция уменьшается. Поведение скандия подобно поведению тяжелых лантанидов. В интервале $pH = 9 \div 11$ кривая сорбции проходит через минимум. Lu^{+3}, Yb^{+3} и Sc^{+3} могут быть отделены от Fe^{+3} и в некоторой степени от других редкоземельных металлов с помощью 2М Na_2CO_3. Все редкоземельные металлы могут быть отделены от урана, но от тория и циркония разделяются лишь первые члены ряда.

Некоторые замечания к расчету энтропии активации на основе теории абсолютных скоростей реакций

ДЬ. ВАРШАНИ

Было показано, что величины энтропии активации, рассчитанные обычным путем, часто оказываются фальшивыми на основе теории абсолютных скоростей реакций. Подробно обсуждается метод расчета, и приводится диаграмма для поправки, опирающейся на критические частоты нормальных колебаний и на коэффициент ангармоничности. Применимость метода иллюстрируется некоторыми классическими примерами.

Изучение адсорбционных явлений на платиновом электроде с помощью метода радиоактивной индикации, VIII

О некоторых новых наблюдениях относительно зависимости адсорбции уксусной и серной кислот от потенциала

ДЬ. ХОРАНИ, Э. РИЗМАЙЕР и Ф. НАДЬ

Было установлено, что зависимость адсорбции уксусной и серной кислот от потенциала и концентрации — подобно случаю соляной кислоты — может быть описана в виде $f(c)F(E)$.

В изученных случаях зависимость адсорбции от потенциала может быть разделена на более или менее явно ограниченные участки.

Подход к выравненным электроотрицательностям с помощью молекулярных параметров

Ш. СЁКЕ

Средняя электроотрицательность, являющаяся хорошим приближением к выравненным электроотрицательностям, может быть связана с помощью простой зависимости с фундаментальными молекулярными параметрами.

Силовые постоянные двухатомных молекул или отдельных изолированных связей могут быть выражены с помощью величин выравненных электроотрицательностей, энергий связи, порядков связей и межатомных расстояний.

Используя уравнения силовых постоянных, выравненные электротрицательности могут быть использованы как молекулярные параметры для построения эмпирических зависимостей потенциальной энергии.

Была найдена также простая зависимость между электроотрицательностями с одной стороны, а с другой стороны и силовыми постоянными колебательного движения, а также двухцентровыми интегралами квантовой химии, относящимися к молекуле или к связи.

Изучение ионизации металлов и восстановления ионов металлов с помощью вращающегося дискового электрода с кольцом, VII

Зависимости анодного растворения меди от концентрации хлористых ионов

Л. КИШ, Й. ФАРКАШ и А. КЕРЕШИ

С помощью вращающегося дискового электрода с кольцом изучалось анодное растворение меди в растворах 1,0 *н* H_2SO_4 + X*н* HCl ($X = 6{,}7 \cdot 10^{-3}$—$8{,}7 \cdot 10^{-2}$ *н*). Установлено, что скорость ионизации меди в указанных растворах определяется диффузией комплексных ионов Cu(I) с поверхности электрода в глубину раствора. На поверхности электрода, при определенной плотности тока, зависящей от скорости вращения электрода и от концентрации хлористых ионов осаждается слой CuCl. Были объяснены явления, сопровождающие процесс осаждения этого слоя.

Структурные превращения в скелете поверхностного слоя силикатных стекол

Ш. ДОБОШ

При образовании поверхностного слоя стекла, наряду с ионным обменом, контролируемым диффузией, а также растворением силикатного скелета на границе раздела фаз поверхностный слой — вода, часто необходимо считаться и со структурными превращениями в силикатном скелете поверхностного слоя. Структура силикатного скелета может изменяться вследствие перегруппировок в пространственной сетке или вследствие изменения числа связей $\geqslant Si—O—Si \leqslant$. Эти изменения могут быть обнаружены на основе распределения компонентов в поверхностном слое, а в некоторых случаях на основе изменения скорости растворения силикатного скелета во времени.

Структурные изменения в скелете поверхностного слоя иллюстрируются образцом с исходным составом K_2O — 20 мол.%, Sr O — 12 мол.% и SiO_2 — 68 мол.%. Сущность этих изменений связана с перегруппировками в пространственной сетке, что приводит к повышению химической стойкости силикатного скелета и к повышению проницаемости по диффузии ионов.

Повторным плавлением стекла с исходным составом 20 K_2O—12 SrO—68 SiO_2 может быть получено стекло как с измененной, так и с неизменной структурой скелета поверхностного слоя. На основе ИК спектроскопических и ДТА исследований было установлено, что такое противоречивое поведение можно приписать различной структуре стекол, образующихся при сравнительно одинаковых условиях плавления и из одинакового исходного состава.

Изучение равновесия пар — жидкость в смеси пропионовая кислота — четыреххлористый углерод

Я. ЛИСИ

При изучении равновесия пар — жидкость в системе пропионовая кислота — четыреххлористый углерод было найдено, что последняя, в первом приближении, представляет собой идеальную смесь димера пропионовой кислоты с четыреххлористым углеродом. Расчетные параметры равновесия пар — жидкость проверялись экспериментально при 30, 40, 50, 60 и 70° С.

Использование хлористых амидов в реакциях циклизации, II

Синтез тиено(2,3-d)-4(3H)-пиримидинонов

З. ЧЮРЕШ, Р. ШОШ, Й. ПАЛИНКАШ и И. БИТТЕР

Исходя из 2-амино-3-карбетокси-4,5-диметилтиофена и хлористого диметилформамида, был получен солянокислый N,N-диметил-N'-[(3-карбетокси-4,5-диметил)-2-тиенил]-формамидин. Полученный трехзамещенный амидин подвергался циклизации с аммиаком, алифатическими и ароматическими аминами, гидразином и алкилендиаминами. Таким образом были получены 5,6-диметил-тиено(2,3-d)-4/3H)-пиримидиноны, а также неописанные до сих пор в литературе алкилен-бис-3,3'-5,6-диметил-тиено(2,3-d)-4/3H/-пиримидиноны.

Бензазепины, IV

Синтез дигидро-[1,5]бензтиазепинов на основе реакции о-аминобензотиола с α,β-ненасыщенными кетонами

О. ХИДЕГ-ХАНКОВСКИЙ и К. ХИДЕГ

Приводится синтез дизамещенных дигидро-[1,5]-бензтиазепинов на основе реакции о-аминобензотиола с соответствующими α,β-ненасыщенными кетонами (напр., пиридилакрилофеноны, пиридилакрилонафтоны и 2-гетероарилиден-тетралин-1-оны). Обсуждается также положение двойной связи.

Изучение реологических свойств клейковины, III

Роль гидрофобных связей в формировании реологических свойств клейковины

Р. ЛАСТИТИ

Несмотря на то, что наличие гидрофобных связей в комплексах клейковины еще не было доказано экспериментально, однако, на основе многочисленных косвенных наблюдений, полученных соответствующими методами, была установлена роль гидрофобных связей формировании реологических свойств клейковины. Наиболее важными заключениями являются следующие:

1. Реологические свойства клейковины, гидратированной водой, содержащей алифатические углеводороды с большим числом углеродных атомов (гептан—ундекан), значительно ухудшаются по сравнению с контрольной клейковиной. Влияние увеличивается с удлинением цепи.

2. Когезия клейковины, гидратированной водой, содержащей алифатические жирные кислоты или спирты, с большим числом углеродных атомов, падает с увеличением молекулярного веса добавленных кислот или спиртов.

3. Совместное присутствие карбамида и алифатического углеводорода в большей степени препятствует образованию клейковины, нежели одиночный раствор карбамида с той же самой концентрацией.

Printed in Hungary

A kiadásért felel az Akadémiai Kiadó igazgatója — Műszaki szerkesztő: Várhelyi Tamás

A kézirat nyomdába érkezett: 1971. I. 20. — Terjedelem: 12 (A/5) ív, 68 ábra

71.71054 Akadémiai Nyomda, Budapest — Felelős vezető: Bernát György

The Acta Chimica publish papers on chemistry in English, German, French and Russian.

The Acta Chimica appear in volumes consisting of four parts of varying size, 4 volumes being published a year.

Manuscripts should be addressed to

Acta Chimica
Budapest 112/91 Műegyetem

Correspondence with the editors should be sent to the same address.

The rate of subscription is $16.00 a volume.

Orders may be placed with "*Kultúra*" Foreign Trade Company for Books and Newspapers (Budapest I., Fő utca 32. Account No. 43-790-057-181) or with representatives abroad.

Les Acta Chimica paraissent en français, allemand, anglais et russe et publient des mémoires du domaine des sciences chimiques.

Les Acta Chimica sont publiés sous forme de fascicules. Quatre fascicules seront réunis en un volume (4 volumes par an).

On est prié d'envoyer les manuscrits destinés à la rédaction à l'adresse suivante:

Acta Chimica
Budapest 112/91 Műegyetem

Toute correspondance doit être envoyée à cette même adresse.

Le prix de l'abonnement est de $16.00 par volume.

On peut s'abonner à l'Entreprise pour le Commerce Extérieur de Livres et Journaux «*Kultúra*» (Budapest I., Fő utca 32. Compte-courant No. 43-790-057-181) ou à l'étranger chez tous les représentants ou dépositaires.

«*Acta Chimica*» издают трактаты из области химической науки на русском, французском, английском и немецком языках.

«*Acta Chimica*» выходят отдельными выпусками разного объема. 4 выпуска составляют один том. 4 тома публикуются в год.

Предназначенные для публикации рукописи следует направлять по адресу:

Acta Chimica
Budapest 112/91 Műegyetem

По этому же адресу направлять всякую корреспонденцию для редакции.

Подписная цена — $16.00 за том.

Заказы принимает предприятие по внешней торговле книг и газет «*Kultúra*» (Budapest I., Fő utca 32. Текущий счет № 43-790-057-181) или его заграничные представительства и уполномоченные.

Reviews of the Hungarian Academy of Sciences are obtainable at the following addresses:

ALBANIA

Drejtorija Qändrone e Pärhapjes
dhe Propagandimit të Librit
Kruga Konferenca e Päzes
Tirana

AUSTRALIA

A. Keesing
Box 4886, GPO
Sydney

AUSTRIA

GLOBUS
Höchstädtplatz 3
A-1200 Wien XX

BELGIUM

Office International de Librairie
30, Avenue Marnix
Bruxelles 5
Du Monde Entier
5, Place St. Jean
Bruxelles

BULGARIA

HEMUS
11 pl Slaveikov
Sofia

CANADA

Pannonia Books
2, Spadina Road
Toronto 4, Ont.

CHINA

Waiwen Shudian
Peking
P. O. B. 88

CZECHOSLOVAKIA

Artia
Ve Smečkách 30
Praha 2
Poštovní Novinová Služba
Dovoz tisku
Vinohradská 46
Praha 2
Mad'arská Kultura
Václavské nám. 2
Praha 1
SLOVART A. G.
Gorkého
Bratislava

DENMARK

Ejnar Munksgaard
Nörregade 6
Copenhagen

FINLAND

Akateeminen Kirjakauppa
Keskuskatu 2
Helsinki

FRANCE

Office International de Documentation
et Librairie
48, rue Gay Lussac
Paris 5

GERMAN DEMOCRATIC REPUBLIC

Deutscher Buch-Export und Import
Leninstraße 16
Leipzig 701
Zeitungsvertriebsamt
Fruchtstraße 3—4
1004 Berlin

GERMAN FEDERAL REPUBLIC

Kunst und Wissen
Erich Bieber
Postfach 46
7 Stuttgart S.

GREAT BRITAIN

Blackwell's Periodicals
Oxenford House
Magdalen Street
Oxford
Collet's Subscription import
Department
Dennington Estate
Wellingsborough. Northants.
Robert Maxwell and Co. Ltd.
4—5 Fitzroy Square
London W. 1

HOLLAND

Swetz and Zeitlinger
Keizersgracht 471—487
Amsterdam C
Martinus Nijhof
Lange Voorhout 9
The Hague

INDIA

Hind Book House
66 Babar Road
New Delhi 1

ITALY

Santo Vanasia
Via M. Macchi 71
Milano
Libreria Commissionaria Sanso
Via La Marmora 45
Firenze

JAPAN

Kinokuniya Book-Store Co. Ltd.
826 Tsunohazu 1-chome
Shinjuku-ku
Tokyo
Maruzen and Co. Ltd.
P. O. Box 605
Tokyo-Central

KOREA

Chulpanmul
Phenjan

NORWAY

Tanum-Cammermeyer
Karl Johansgt 41—43
Oslo 1

POLAND

RUCH
ul. Wronia 23
Warszawa

ROUMANIA

Cartimex
Str. Aristide Briand 14—18
Bucureşti

SOVIET UNION

Mezhdunarodnaya Kniga
Moscow G—200

SWEDEN

Almquist and Wiksell
Gamla Brogatan 26
S—101 20 Stockholm

USA

F. W. Faxon Co. Inc.
15 Southwest Park
Westwood Mass. 02090
Stechert Hafner Inc.
31. East 10th Street
New York, N. Y. 10003

VIETNAM

Xunhasaba
19, Tran Quoc Toan
Hanoi

YUGOSLAVIA

Forum
Vojvode Mišića broj 1
Novi Sad
Jugoslovenska Knjiga
Terazije 27
Beograd

25. VI. 1971 **Index: 26.007**